Vol. 198, July 15, 1987
Complete in one issue

ISSN 0003-2670

ANALYTICA CHIMICA ACTA

International journal devoted to all branches of analytical chemistry

ELSEVIER

ANALYTICA CHIMICA ACTA

International journal devoted to all branches of analytical chemistry
Revue internationale consacrée à tous les domaines de la chimie analytique
Internationale Zeitschrift für alle Gebiete der analytischen Chemie

PUBLICATION SCHEDULE FOR 1987

	J	F	M	A	M	J	J	A	S	O	N	D
Analytica Chimica Acta	192	193	194	195	196	197	198	199	200	201	202	203

Scope. *Analytica Chimica Acta* publishes original papers, short communications, and reviews dealing with ever aspect of modern chemical analysis both fundamental and applied.

Submission of Papers. Manuscripts (three copies) should be submitted as designated below for rapid an efficient handling:

Papers from the Americas to: Professor Harry L. Pardue, Department of Chemistry, Purdue University, We Lafayette, IN 47907, U.S.A.

Papers from all other countries to: Dr. A. M. G. Macdonald, Department of Chemistry, The University, P.O. Box 36 Birmingham B15 2TT, England. Papers dealing particularly with computer techniques to: Professor J. T. Cler Universität Bern, Pharmazeutisches Institut, Baltzerstrasse 5, CH-3012 Bern, Switzerland.

Submission of an article is understood to imply that the article is original and unpublished and is not bein considered for publication elsewhere. Upon acceptance of an article by the journal, authors will be asked to transf the copyright of the article to the publisher. This transfer will ensure the widest possible dissemination c information.

Papers in English, French and German are published. There are no page charges. Manuscripts should conform i layout and style to the papers published in this Volume. See inside back cover for "Information for Authors".

Reprints. Fifty reprints will be supplied free of charge. Additional reprints (minimum 100) can be ordered. A order form containing price quotations will be sent to the authors together with the proofs of their article.

Publication. *Analytica Chimica Acta* appears in 12 volumes in 1987. The subscription for 1987 (Vols. 192–203) Dfl. 2700.00 plus Dfl. 300.00 (p.p.h.) (total approx. US $1463.40). All earlier volumes (Vols. 1–191) except Vol 23 and 28 are available at Dfl. 243.00 (US $118.54), plus Dfl. 18.00 (US $8.78) p.p.h., per volume.

Our p.p.h. (postage, packing and handling) charge includes surface delivery of all issues, except to subscribers i the U.S.A., Canada, Australia, New Zealand, P.R. China, India, Israel, South Africa, Malaysia, Thailand, Singapor South Korea, Taiwan, Pakistan, Hong Kong, Brazil, Argentina and Mexico, who receive all issues by air deliver (S.A.L. — Surface Air Lifted) at no extra cost. For Japan, air delivery requires 50% additional charge; for all othe countries airmail and S.A.L. charges are available upon request.

Subscription. Subscription should be sent to: Elsevier Science Publishers B.V., Journals Department, P.O. Bo 211, 1000 AE Amsterdam, The Netherlands. Tel: 5803 911, Telex: 18582, to which requests for sample copies ca also be sent.

Claims for issues not received should be made within three months of publication of the issues. If not they canno be honoured free of charge.

Readers in the U.S.A. and Canada can contact the following address: Elsevier Science Publishing Co. Inc., Journ Information Center, 52 Vanderbilt Avenue, New York, NY 10017, U.S.A., Tel: (212) 916-1250, for furth information, or a free sample copy of this or any other Elsevier Science Publishers journal.

Advertisements. Advertisement rates are available from the publisher on request.

0003-2670/87/$03.5

Printed in The Netherlands

ANALYTICA CHIMICA ACTA

International journal devoted to all branches of analytical chemistry

bstracted, Indexed in: Anal. Abstr.; Biol. Abstr.; Chem. Abstr.; Curr. Contents Phys. Chem. Earth Sci.; fe Sci.; Index Med.; Mass Spectrom. Bull.; Sci. Citation Index; Excerpta Med.)

OL. 198 **CONTENTS** **JULY 15, 1987**

(Continued overleaf)

(Contents continued)

ANALYTICA CHIMICA ACTA
VOL. 198 (1987)

ANALYTICA CHIMICA ACTA

International journal devoted to all branches of analytical chemistry

ELSEVIER Amsterdam–Oxford–New York–Tokyo

Anal. Chim. Acta, Vol. 198 (1987)

Analytica Chimica Acta, 198 (1987) 1—12
Elsevier Science Publishers B.V., Amsterdam — Printed in The Netherlands

OPTICAL SENSORS: AN ION-SELECTIVE OPTRODE FOR POTASSIUM

OTTO S. WOLFBEIS* and BERNHARD P. H. SCHAFFAR

Analytical Division, Institute of Organic Chemistry, Karl-Franzens University, A-8010 Graz (Austria)

(Received 3rd March 1987)

SUMMARY

A new type of sensor (called ion-selective optrode) for the continuous determination of electrolytes is presented that can be exploited in optical and fibre-optic sensors. It is based on the ability of certain fluorescent dyes to respond to an electrical potential at the interface between a lipid phase and an aqueous phase. The potential is created by addition of a neutral ion-carrier, and its magnitude is measured with an appropriate potential-sensitive dye. An opto-sensor for potassium is described. A lipid bilayer is formed on a glass support by applying the Langmuir-Blodgett film technique. A lipid-soluble rhodamine dye is incorporated into this layer together with valinomycin as the ion-carrier. When exposed to potassium ion solutions in the 0.01—100 mM range, fluorescence intensity is continuously diminished. It is shown that two kinds of response towards potassium solutions occur: one is selective for this ion, but the other is unselective, being evident with other metal ions. The unselective response can be compensated for by a reference optrode. The signal change of the ion-selective optrode depends on the nature of the layer and the concentrations of dye and valinomycin. The relationship between $\Delta I/I$ (i.e., the reduction in intensity relative to the total signal) and the logarithmic analyte concentration is linear over a wide range, typically 0.01—10 mM. The selectivity factor over sodium varies from 2.5 to 5.

The development of optical sensors (called optrodes by linguistic analogy to electrodes) is a fast-growing area of research because of some unique features of optosensors, in particular fibre-optic sensors. They have been discussed in several reviews [1—7]. Their small size and lack of sensitive liquid-liquid junctions, the possibility of conducting remote analyses via long fibres, and their biocompatibility appear to be most attractive features of optosensors.

Several quite different principles have so far been applied for optical sensing purposes. Thus, measurements of the intensity of transmitted light [8], reflected light [9], and fluorescence as a result of ground-state protolytic equilibria [10, 11] have been used, mainly for measurement of pH values. The determination of the efficiency of dynamic fluorescence quenching which occurs in the first excited state [10, 12] has been exploited widely to measure oxygen and related quenchers. Further sensing principles are based on the measurement of the efficiency of electronic energy transfer [13], fluorescence decay time [14], phosphorescence [15], and chemiluminescence [16].

0003-2670/87/$03.50

Aside from these concepts, which rely on some sort of indicator chemistry immobilized at the end of fibres or on solid supports, simple bare-ended fibres without a particular reagent phase at their surface have also been used for measurement of the intrinsic absorption or fluorescence of an analyte. This kind of "sensor" has been developed mainly in the context of remote sensing of trace analytes, but the principle is the same as in conventional photometry or fluorimetry of coloured or fluorescent molecules. Such sensors are unselective and will not be considered further here.

Practically all electrolyte sensors known so far rely on principles that are an extension of traditional indicator chemistry. Once a suitable indicator has been found, it can be immobilized on a support to give, upon interaction with a metal ion, a coloured or fluorescent chelate [17]. Alternatively, an immobilized fluorophore may be dynamically quenched by the analyte [18]. Often, the indicators are chosen so as to be fairly selective for the analyte of interest. As a result, practically all known electrolyte sensors are quite different from each other with respect to indicator and, therefore, spectra and immobilization techniques.

Recently, however, a more generally applicable approach has been made by preparing a reagent phase that responds to sodium, but conceivably may also be applied to potassium and other electrolytes by making use of other ionophores [19]. The components of such a reagent phase are an anionic fluorophore electrostatically bound to copper(II)/polyethyleneimine and a sodium-selective ionophore immobilized on silica. In the absence of sodium, fluorescence is quenched by copper ion; when sodium is added, it forms a cationic complex which forms ion-pairs with some of the fluorophore, causing it to fluoresce.

The availability of ion-carriers with high selectivity for a certain metal ion is due to their general use in ion-selective electrodes [20]. Because ion-carriers provide an excellent means for improving the selectivity of otherwise identical sensors, it appeared promising to apply this selection principle to optical sensors. This was expected to result in a sensing material in which only the ion-carrier need be changed, whereas its fabrication can remain very similar and the optical system can remain the same. Ion-carriers are known to be capable of creating a potential at electrode surfaces that can be measured by potentiometry. Recently, optical indicators that respond to potential changes have become available [21—23]. This provided the possibility of measuring potentials by an optical rather than an electrochemical method. The present paper deals with the first sensor for which the working principle is based on optical measurement of a potential created by an ion-carrier at the lipid/water interface by means of a potentiometric indicator.

EXPERIMENTAL

Chemicals

Distilled water as received was twice-distilled again, first over potassium permanganate. The alkali and alkaline earth chloride solutions were of the

highest available quality (Suprapur, Merck), containing $<10^{-3}$% of each of the other ions. The phosphates, acetates, and sulphates were of usual analytical-reagent quality (Merck). Both buffered and unbuffered solutions were investigated. The former were prepared by adding 1 ml of a 0.3 M phosphate buffer (either sodium or potassium phosphate) to 1 l of either sodium or potassium standard solutions, thus making the final buffer concentration 0.3 mM. This is distinctly below the molarity range of the alkali metal ions tested (1–10 mM). When alkali metal solutions with molarities below 1 mM were investigated, no buffer was added. The pH of the buffered solutions was 6.70 ± 0.03. Arachidic acid (saturated C_{20} acid; Sigma) was used as received.

The ion-selective dye (the C_{18}-ester of rhodamine B; RhoB/C18), which has spectral properties similar to rhodamines, but which is excellently soluble in lipids and almost insoluble in water, was prepared as described by Keller et al. [24]. It is now commercially available, as are the other potential-sensitive dyes mentioned in the text (Lambda Probes & Diagnostics, A-8053 Graz, Austria).

Optical instrumentation

The absorption spectra of the solutions in 1 × 1-cm cuvettes were run on a Perkin-Elmer Lambda-5 spectrophotometer. Fluorescence spectra were run on a Aminco SPF-500 fluorimeter equipped with either a 250-W xenon or 220-W tungsten halogen lamp. For ion-sensing purposes, the excitation and emission wavelengths were set to 540 and 620 nm, respectively; the bandpasses were 15–20 nm on each monochromator. For the measurement of the response of the sensing membranes, aqueous solutions of the various electrolytes were pumped through a flow-through cell, with the sensing layer exposed to the aqueous phase, and fluorescence was collected through the glass support. To get rid of considerable stray light, the optical

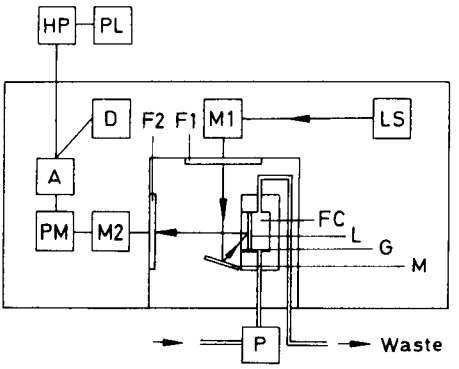

Fig. 1. Optical arrangement for measurement of fluorescence from Langmuir-Blodgett films: LS, light source; M_1, excitation monochromator; F_1, primary filter transmissive to light below 580 nm; M, mirror; G, glass slide with membrane layer L; FC, flow-through cell; F_2, secondary filter transmissive to light above 590 nm; M_2, emission monochromator; PM, photomultiplier; A, amplifier; D, display; HP, desk calculator; PL, plotter; P, peristaltic pump.

arrangement shown in Fig. 1 was chosen, and fluorescence was collected at 620 nm rather than at the emission maximum (590 nm).

Membrane preparation

Glass slides (50 × 12 mm, 1 mm thick) were first chemically modified to make the surface hydrophobic. For this purpose, they were treated with a 1:1 mixture of concentrated sulphuric and nitric acids for at least several days, washed with distilled water to remove the acid and dried over phosphorus pentoxide under reduced pressure at 120°C. Surface modification was accomplished by reaction with dichlorodimethylsilane (a 5% solution in toluene) for 24 h at room temperature, and rinsing with toluene and acetone. This provides a glass with a silylated surface that should not be touched.

Langmuir-Blodgett (LB) films were obtained by the usual technique [25, 26]: A water-filled trough (30 × 10 cm) was covered with 0.2—1.0 ml of a toluene solution containing the desired amount of indicator, lipid and carrier. In some types of sensors, only valinomycin and RhoB/C18 were used to fabricate LB layers. The toluene was left for evaporation (5—10 min) and a pressure of 22 mN m^{-1} was applied to the thin lipid film spread over the water surface. Then, a monolayer was adsorbed onto the glass slide by immersing it once slowly (4 cm min^{-1}) into the aqueous phase; the bilayer was formed when the slide was drawn back.

Glass slides prepared by this technique have dye-labelled lipid layers on both sides. Because sensing is possible only on one side of the glass, the other would only provide a considerable fluorescence background. Therefore, the LB layer was removed from one side by cleaning it carefully with acetone-soaked wadding. Before exposure to sample solutions in the flow-through cell, the sensors were washed for 5 min with distilled water until a constant fluorescence signal was obtained.

Again, the sensing surface of the glass thus obtained should not be touched. The quality of a homogeneously covered glass can easily be checked by gently breathing onto the cold glass surface: the LB surface loses its transparency, while the untreated surface remains almost clear. Attention has to be paid to prevent the LB trough from contamination by valinomycin.

RESULTS

Choice of membrane composition

Fluorescent probes, sensitive to potentials formed at various interfaces, have been used for rapid monitoring of potential fluctuations, mainly from a biophysical point of view [21—23], and numerous cyanine dyes have been recommended as giving good response (typically 5—8% signal change in biomembranes). It was found here, however, that indocarbocyanines and thiadicarbocyanines are of limited practical utility for optosensors because of their photochemical instability and minute Stokes losses (in the order of 10—20 nm). Rhodamines, in contrast, display outstanding photostability and

favourable spectral properties in having long-wave excitation and emission maxima as well as acceptable Stokes shifts. Because rhodamines have been reported to respond to changes in potential [27, 28], it was decided to use rhodamine B in place of the cyanine dyes.

The LB technique was considered to be ideal for the design of an ion-selective optrode (ISO) because it provides highly reproducible layers of well defined thickness and because it allows the dye to be placed exactly at the lipid/water interface, i.e., the site where the potential is created. Bilayers were favoured over monolayers because they are more easily prepared and give a higher fluorescence signal.

A limitation is the poor solubility of rhodamine B in lipids. Therefore it had to be chemically modified by introducing a lipid chain into the cationic dye. One of the ways to accomplish this is esterification of its carboxy group with 1-octadecanol to give an ester (RhoB/C18) that is soluble in lipids and toluene, but almost insoluble in water. This ester was incorporated into the LB layers prepared from arachidic acid, with valinomycin incorporated as the ion-carrier. The ester is not washed out into the aqueous sample because of its C-18 anchor group. A cross-section of such a bilayer is shown in Fig. 2. It is evident that valinomycin, because of its size, acts as a heavy perturber of ordered lipid membranes.

Membrane properties

As with rhodamine B, the spectral properties of RhoB/C18 in the membrane are slightly different from the spectra run in methanol. Table 1 summarizes the spectral data in methanol, toluene, and in the LB membrane. It can be seen from these data that RhoB/C18 when incorporated in the bilayer membrane has spectral data similar to those in toluene, indicating that it is surrounded by a lipid phase, and not by a protic or polar phase.

Another characteristic difference in the spectra of the dye in solution and in the LB layer is the breadth of the band. Band narrowing of both the excitation and emission bands has been observed for various dyes [29] in

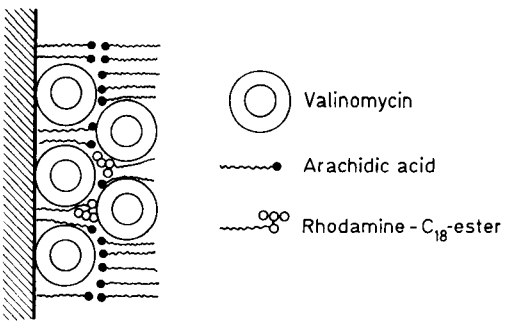

Fig. 2. Schematic cross-section of an arachidic acid bilayer with valinomycin and rhodamine B/C18 ester incorporated.

TABLE 1

Absorption and emission maxima of rhodamine B and rhodamine B octadecyl ester (RhoB/C18) in methanol, toluene and in lipid bilayers

Dye	Solvent	Maximum (nm)		Stokes loss
		Absorption	Emission	
Rhodamine B	Methanol	545	572	27
Rhodamine B	Toluene	560	582	22
Rhodamine B	Lipid bilayer	554	580	26
RhoB/C18	Methanol	554	578	24
RhoB/C18	Toluene	567	590	23
RhoB/C18	Lipid bilayer	567	592	25

thin layers. This was also found in this work for styryl dyes such as 4-(4'-dimethylaminostyryl)-quinolinium methiodide. Typically, the full width at half maximum (FWHM) for the excitation and emission bands are, respectively, 55 and 48 nm in solution and 22 and 22 nm in the arachidic acid LB layer. Interestingly, no significant band narrowing was found with the rhodamine dye.

Membrane response to electrolytes

In a first series of experiments, it was verified that the presence of the salts studied here (with or without valinomycin) did not have any effect on the emission characteristics of the dye in fluid solution. The same was true for the absorption spectra. When the dye was incorporated into the lipid bilayer, however, the fluorescence changes described in the following sections were found. The effects of electrolytes on the absorption properties of the dye in LB layers could not be studied because of the low absorptivity, which was calculated to be in the order of 0.0008 l mol^{-1} cm^{-1} for the arachidic acid-containing bilayers, and even lower for stained valinomycin bilayers. High levels of scattered light around the analytical wavelengths also prevented the acquisition of fluorescence excitation spectra.

The response of a sensor bilayer prepared from arachidic acid, valinomycin and RhoB/C18 towards potassium, sodium and ammonium ion is shown in Fig. 3A. A decrease of maximally −14% is observed when the concentration of potassium ion increases from zero to 10 mM. Ammonium and sodium ions interfere to some extent in that the signal of 10 mM ammonium chloride corresponds to 0.5 mM K^+, and 10 mM Na^+ correspond to 0.07 mM K^+. Typical response times for 90% of the final value are 1.5 min for a bilayer.

To confirm that the observed effects are indeed due to the presence of an ion-carrier, bilayers were prepared from arachidic acid and RhoB/C18 without valinomycin. Both sodium and potassium, in varying concentrations, produce a weak decrease in fluorescence intensity, as can be seen in Fig. 3B, whilst calcium remains inert. The effect is the same for the chlorides and

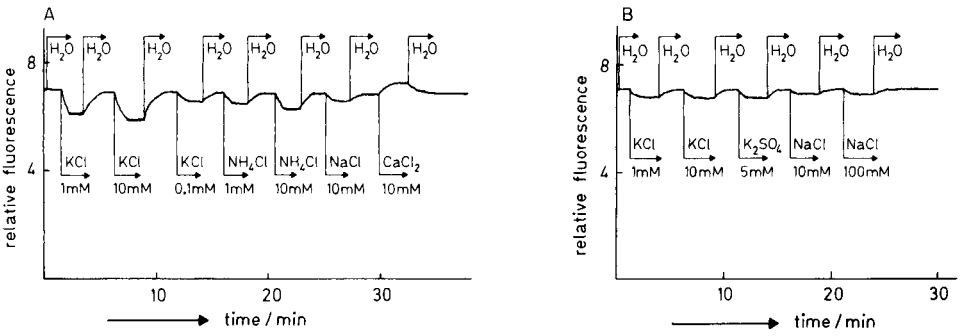

Fig. 3. Fluorescence responses of arachidic acid bilayers with and without valinomycin: (A) membrane prepared from 0.5 ml of a solution of 0.45 mg of arachidic acid, 1.0 mg of valinomycin and 0.022 mg of rhodamine B ester in 10 ml of toluene spread over a 300-cm^2 water surface; (B) membrane prepared from 1.0 ml of a solution of 1.0 mg of arachidic acid and 0.02 mg of rhodamine B ester in 10 ml of toluene spread over a 300-cm^2 water surface.

sulphates and will later be referred to as the unselective effect. Comparison of Fig. 3A and 3B shows that only with potassium ion is there a significant decrease in intensity. This is strong evidence that it is indeed the incorporation of valinomycin that accounts for the selectivity for potassium.

The lipid-to-valinomycin ratio was varied over the 40:1 to 0:1 (mol/mol) range. The most distinctive signal changes were observed at a ratio of 7:3 in the bilayer. Lower carrier concentrations gave smaller signal changes, whereas at higher levels the signal change was not improved.

Selectivity

The selectivity for potassium is most distinct when membranes are formed from valinomycin and RhoB/C18 alone, i.e., when no arachidic acid is present (Fig. 4). Typical selectivity data are $1:10^{2.5}$—$1:10^{3.5}$ over sodium for

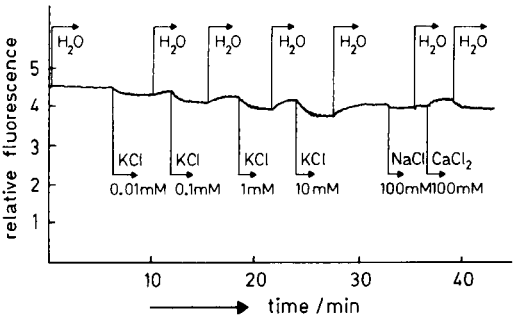

Fig. 4. Response of an LB-layer-based ion-selective optrode prepared from valinomycin and rhodamine C_{18}-ester without arachidic acid. The high selectivity for potassium over sodium and a slight leaching of the dye are apparent.

arachidic acid bilayers, but $1:10^5$ for pure valinomycin (plus RhoB/C18) sensor layers. The selectivity over ammonium ion (not shown in Fig. 4) is less satisfactory ($1:10^2$ for the pure valinomycin layer).

In order to prove whether the anions have any interfering effect, various alkali sulphates and phosphates were also tested and found to give the same signal changes as the respective chlorides. This demonstrates that the anions do not act as fluorescence quenchers and do not perturb the membranes. Similarly, changes in pH from 6.5 to 7.5 (buffer concentration 0.3 mM phosphate) did not produce a change in the fluorescence emission intensity. However, at pH values of 10 and 4 considerable signal changes were observed.

As can be seen from Figs. 3A and 4, all monovalent cations cause a decrease in the fluorescence intensity of the sensing membrane. Bivalent cations, in contrast, had an unusual effect in that they caused a weak signal enhancement. The effect is more distinct in Fig. 3A than in Fig. 4.

The dye/valinomycin ratio was varied from 1:5 to 1:20 in tests to establish the conditions for the best response towards K^+. At ratios of 1:20, the fluorescence was very poor and could hardly be detected, but the relative signal change was maximal (−20% for 10 mM K^+). At a ratio of 1:5, the measured intensity was about 3.5 times greater, but the relative signal change was only −13%. An acceptable compromise is a ratio 1:10, with a signal change of −16% for 10 mM K^+.

Relation between signal change and analyte concentration

The plot of signal change ($\Delta I/I$) versus log [K^+] (Fig. 5) shows that there is a linear relationship over a fairly wide concentration range. The slope varies greatly with the kind of LB layer used for the sensor. Linearity over the whole concentration range holds better for LB layers prepared from valinomycin and dye alone; for those also containing arachidic acid, the slope is better but the linear range is more limited. At potassium concentrations below 1 mM, the decrease in $\Delta I/I$ is much greater than would be expected in case of a linear relation.

The relation between −log [K^+] and $\Delta I/I$ can be described over a wide concentration range by a linear equation of the type

$$-\log [K^+] = f(100\ \Delta I/I) + k \qquad (1)$$

Typical values for slope f and intercept k for the various membrane types are, respectively, −0.22 to −0.42 and 4.0 to 5.2 for the arachidic acid membranes, and −0.30 to −0.40 and 5.5 to 7.5 for valinomycin LB layers.

Standard solutions of potassium ion were passed over the sensing membrane containing valinomycin and the rhodamine B C18-ester without arachidic acid (Fig. 4) and the signal changes were recorded. The data were used to re-calculate the K^+ concentrations with the help of Eqn. 1. The results, summarized in Table 2, show that the precision over the $10^{-2}-10^{-4}$ M concentration range is acceptable (considering that this is the first potential-sensitive optrode).

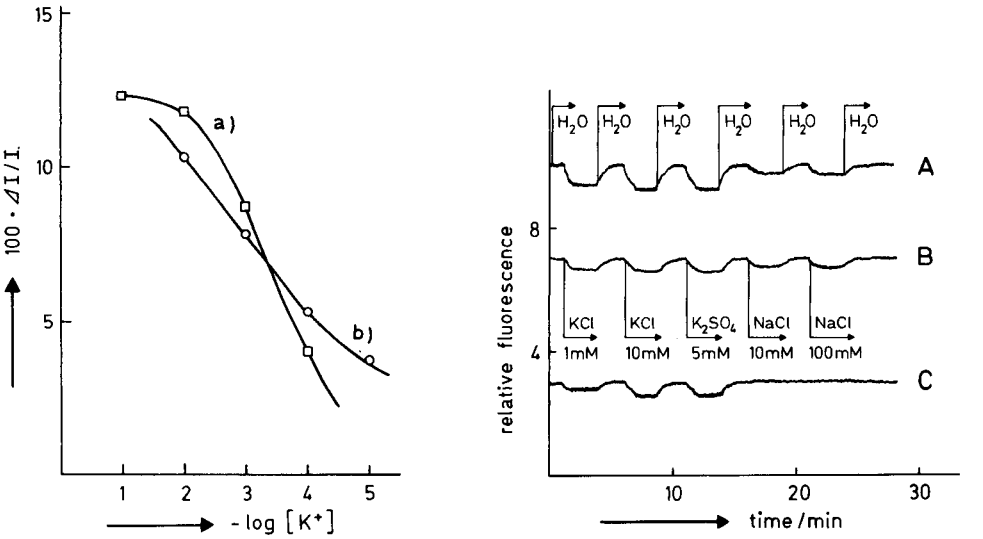

Fig. 5. Plots of 100 $\Delta I/I$ vs. $-\log [K^+]$ for the valinomycin membranes with (a) and without (b) arachidic acid.

Fig. 6. (A) Response of the LB bilayer from arachidic acid, valinomycin and RhoB/C18; (B) response of the LB bilayer as in (A), but without valinomycin; (C) difference curve demonstrating that interferences by Na^+ can be eliminated by the two-sensor technique.

TABLE 2

Comparison of experimental potassium concentrations with values calculated from Eqn. 1, with k = 6.1 and f = −0.39. The data given were obtained with the sensor described for Fig. 4

$-\log [K^+]$ (experimental)	100 $\Delta I/I$ (%)	$-\log [K^+]$ (calc. from Eqn. 1)
2.0	10.4	2.0
3.0	7.8	3.1
4.0	5.3	4.0
5.0	3.7	4.7

Sensitivity and precision

Potassium could be detected in the 0.01 mM–100 mM concentration range with various kinds of sensing layers. While the ISOs can have a dynamic range of more than four decades, the precision remains poor because of the small signal change of maximally −20%. It is obvious from Fig. 5 that the valinomycin membrane containing arachidic acid is more sensitive in the 0.5 mM range than the membrane without arachidic acid because of the better slope. Assuming an experimental error of ±1% in the determination of

$\Delta I/I$, a precision of ±4 mM for both types of sensors is to be expected in the clinically interesting 5-mM range. This is certainly too poor for practical purposes. In order to give a significant precision of ±0.5 mM in this range, a resolution of ±0.1% in the determination of the signal change is required, which was achieved with the fluorimeter used and may also be achieved when a less expensive opto-electronic instrument is developed.

Membrane stability

Owing to its good solubility in lipid phases, the indicator is normally not washed out by the aqueous sample solutions. Freshly prepared bilayer membranes show practically no wash-out (Fig. 3A), but after several days the dye leaches out at a rate of approximately 5% per hour (Fig. 4). While no photodecomposition was obvious during the illumination of the sensing membrane in the fluorimeter, a considerable loss in fluorescence intensity was observed when the membrane were re-used after one week.

DISCUSSION

Electrochemical sensors for electrolytes (the ion-selective electrodes, ISEs) have had outstanding success in the past 20 years. Our interest in optical sensors made it obvious that the selectivity of ion-carriers could be exploited in the design of an ion-selective optrode. This seemed feasible in view of the known ability of certain indicators (usually a fluorophore having a strongly changed dipole moment in the first excited singlet state) to respond to electrical potential. Because such a potential is formed at the membrane/water interface, the preparation of well-defined and very thin lipid layers was considered to be a promising approach. Because of the thin layer, the potential per cm is very large at the interface. A potentiometric dye placed at this site would therefore respond strongly to potential changes. If placed remotely from the interface, the dye would respond much less sensitively, but rather produce a considerable fluorescence background.

The Langmuir-Blodgett (LB) technique was considered to give particularly well-defined sensing layers because the technique is well established. Initial experiments on ISOs based on the potentiometric approach were done by chemical immobilization of indicators on PVC or related materials [7, 30] and it was soon recognized that a careful control of experimental conditions was necessary to obtain reproducible results. Even though it was found that LB films can have considerably different properties from one preparation to the other, the reproducibility is somewhat better at the moment than in the case of other techniques for preparing suitable membranes.

The absence of any spectral changes in solution indicates that it is indeed an effect that occurs at the interface between the lipid and the aqueous sample solution. When the responses of LB layers with and without valinomycin are compared, it is evident that the well-defined selectivity towards potassium ion is caused by the neutral ion-carrier. However, it is

obvious that processes other than the creation of a potential occur and also give rise to changes in fluorescence intensity. This is obvious from Fig. 3 where all monovalent cations give signal changes, but when valinomycin is present, the selectivity for potassium is quite distinct. Thus, one has to differentiate between two kinds of response towards electrolytes: the first effect is a slight decrease in total fluorescence intensity when the sensing layer is exposed to monovalent cations; the second effect is a decrease in intensity that is practically caused by potassium ion alone. The total effect that is observed with the potassium sensor presented here is therefore the sum of a selective and an unselective response. In order to obtain a signal that is independent of unselective interferences by alkali ions, it is necessary to work with two different sensors, one containing valinomycin and the other without it (Fig. 6).

Langmuir-Blodgett layers prepared from valinomycin and dye only in a molar ratio of 10:1, display the best response, because the unselective effect of cations remains small, and the potassium-selective effect is well defined in the 0.1—10 mM range. This is favourable in view of the ca. 5 mM concentration of potassium ion in human blood. The two-sensor technique appears less feasible in this case because of the lack of a suitable reference optrode.

It is of interest to discuss the results in relation to a recent concept for an intrinsic biosensor suggested by Krull et al. [31] who described the fluorescence properties of a phosphatidyl membrane labelled with 1-anilinonaphthalene sulphonate (ANS). Monolayers rather than bilayers were studied and showed only a very feeble fluorescence. The membranes were sensitive to supported structures and were perturbed by incorporating phloretin or valinomycin as probes to give a signal decrease after incorporation into the phosphatidyl-ANS monolayers. Unfortunately, the response towards potassium ion (or any other electrolyte) was not studied, so that no further comparisons can be made. ANS was considered to be a good probe for membrane interior hydrophobicity and order, but might be difficult to keep inside a lipid membrane when it is exposed to an aqueous environment because of its water solubility.

An attractive alternative to the ISO described here will be the extension of the principle to fibre-optic sensors. Because of the weak signal that can be expected when the sensing membrane is placed at the distal end of the fibre, it will be useful to make the sensing layer itself the external optical phase of a fibre, i.e., by attaching the LB layer directly onto the fibre core. This, in combination with the evanescent wave technique [32] will result in a sensor suitable for remote detection as well as improved signal-to-noise ratio.

In conclusion, a new type of optical sensor has been presented that is based on the measurement of a potential created at the sensor/sample interface, by using a potentiometric dye. The principle has been shown to be applicable to a potassium sensor, but appears useful for sensing any other kinds of electrolyte for which a suitable ion-carrier is available.

The assistance of Dr. A. Leitner (Institut für Experimentalphysik) in preparing the Langmuir-Blodgett layers is highly appreciated. B. P. H. S. thanks the AVL-List GesmbH. for a stipend.

REFERENCES

1 T. Hirschfeld, T. Deaton, F. Milanovich and S. Klainer, Opt. Eng., 22 (1983) 527.
2 D. W. Lübbers and N. Opitz, Sensors & Actuators 4 (1984) 641.
3 J. I. Peterson and G. G. Vurek, Science, 224 (1984) 123.
4 T. Hirschfeld, J. B. Callis and R. B. Kowalski, Science, 226 (1984) 312.
5 O. S. Wolfbeis, Trends Anal. Chem., 4 (1985) 184.
6 W. R. Seitz, Anal. Chem., 56 (1985) 16A.
7 O. S. Wolfbeis, Z. Anal. Chem., 325 (1986) 387.
8 M. J. Goldfinch and C. R. Lowe, Anal. Biochem., 138 (1984) 430.
9 G. F. Kirkbright, R. Narayanaswami and N. A. Welti, Analyst, 109 (1984) 1025 (and references therein).
10 J. L. Gehrich, D. W. Lübbers, N. Opitz, D. R. Hansmann, W. W. Miller, J. K. Tusa and M. Yafuso, IEEE Trans. Biomed. Eng., 33 (1986) 117.
11 H. Offenbacher, O. S. Wolfbeis and E. Fürlinger, Sensors & Actuators, 9 (1986) 73.
12 O. S. Wolfbeis, H. E. Posch and H. K. Kroneis, Anal. Chem., 57 (1985) 2556 (and references therein).
13 D. M. Jordan, D. R. Walt and F. P. Milanovich, Anal. Chem., 59 (1987) 437.
14 J. Pusterhofer, M. Lippitsch, M. J. P. Leiner and O. S. Wolfbeis, Oxygen Sensor with the Decay Time as the Information Carrier, Abstract of the Contributions at the 2nd Symposium on Quant. Luminescence Spectrometry in Biomed. Sci., Ghent, Belgium, May 11—14, 1987.
15 H. Kautsky and G. O. Müller, Naturwissenschaften, 29 (1941) 150; Z. Naturforsch., Teil A, 2 (1947) 167.
16 T. M. Freeman and W. R. Seitz, Anal. Chem., 53 (1981) 98.
17 L. A. Saari and W. R. Seitz, Anal. Chem., 55 (1983) 667.
18 E. Urbano, H. Offenbacher and O. S. Wolfbeis, Anal. Chem., 56 (1984) 427.
19 Z. Zhujun, J. L. Mullin and W. R. Seitz, Anal. Chim. Acta, 184 (1986) 251.
20 U. Oesch, D. Amman and W. Simon, Clin. Chem., 32 (1986) 1448.
21 A. S. Waggoner and A. Grinvald, Ann. NY Acad. Sci., 309 (1977) 217.
22 P. Fromherz and R. Kotulla, Ber. Bunsenges. Phys. Chem., 88 (1984) 1106.
23 H. Windisch, W. Müller and H. A. Tritthart, Biophys. J., 48 (1985) 877.
24 P. M. Keller, S. Pearson and W. Snipes, J. Cell Sci., 28 (1977) 167.
25 K. B. Blodgett and I. Langmuir, Phys. Rev., 51 (1937) 964.
26 G. G. Roberts, Adv. Phys., 34 (1986) 475.
27 G. V. Murvanidze, I. I. Severina and V. P. Skulachev, Dokl. Akad. Nauk SSSR, 261 (1981) 1252.
28 T. Aiuchi, T. Daimatsu, K. Nakaya and Y. Nakamura, Biochim. Biophys. Acta, 685 (1982) 289.
29 F. W. Deeg and C. Brauchle, J. Chem. Phys., 85 (1986) 4201.
30 O. S. Wolfbeis and P. Hochmuth, unpublished results, 1984/85.
31 U. J. Krull, Ch. Bloore and G. Gumbs, Analyst, 111 (1986) 259.
32 J. T. Ives, W. M. Reichert, J. N. Lin, V. Hlady, D. Reinecke, P. A. Suci, R. A. VanWagenen, K. Newby, J. Herron, P. Dryden and J. D. Andrade, in M. Martellucci (Ed.), Optical Fibre Sensors, M. Nijhoff—W. Junk, New York, 1987.

Analytica Chimica Acta, 198 (1987) 13—23
Elsevier Science Publishers B.V., Amsterdam — Printed in The Netherlands

THE TOTAL FLUORESCENCE OF HUMAN URINE

MARC J. P. LEINER, MICHAEL R. HUBMANN and OTTO S. WOLFBEIS*

Analytical Division, Institute of Organic Chemistry, Karl-Franzens University, A-8010 Graz (Austria)

(Received 16 January 1987)

SUMMARY

The total fluorescence of human urine was measured at various excitation and emission wavelengths and is presented in 3-dimensional form. Despite the complexity of the composition of urine, 3—5 distinct fluorescence maxima can be observed. Effects of pH were studied and tentative assignments as to the species responsible for the peaks were made. Most likely, however, the peaks observed do not result from a single fluorescent urinary metabolite, but rather from several species having similar spectral properties and being present in comparable concentrations.

Human urine is composed of numerous organic substances [1], but only some of them are fluorescent [2]. Urine has frequently been reported to display a blue-green fluorescence [3] that can change in case of pathological urine. Surprisingly, the fluorescence of urine has not received particular attention in the past, although various attempts have been made to isolate and identify fluorescent substances.

More recently, it was realised that, in comparison with normal urine, additional fluorescent substances are present in uremic urine. Consequently, powerful chromatographic methods have been exploited to separate fluorescent compounds. The obtained fractions were examined under various excitation and emission wavelengths [4—8]. Despite these efforts, only a few of the fluorescent compounds have been identified with respect to their chemical structure.

So far, all studies on fluorescent metabolites in human urine have been done with high-performance liquid chromatography (h.p.l.c.) and fluorescence detection at fixed wavelengths, thus only parts of the total fluorescence were recorded. For a complete description, the fluorescence intensity has to be presented as a function of all excitation and emission wavelengths. A 3-dimensional spectrum is therefore required to describe the fluorescence completely. The data obtained may be presented mathematically by a so-called excitation/emission matrix [9], as an isometric presentation of the 3-dimensional spectrum as shown in Fig. 1, or as a contour map (Figs. 2—4 and 6), which may be termed a fluorescence topogram.

In this paper, the total fluorescence of human urine is described, along

0003-2670/87/$03.50

with tentative assignments of peaks and prominent shoulders. The work here is a continuation of previous studies on the 3-dimensional fluorescence of biological liquids such as serum [10, 11] and low-density lipoproteins [12].

EXPERIMENTAL

Urines were obtained from fasting and healthy men (age 20—40 years) in the morning. For the acquisition of the data in the ultraviolet (u.v.) region, urines were diluted 1:800 for spectrophotometry and 1:100 for fluorimetry with phosphate buffer (20 mmol l^{-1}, pH 7.00). The pH was checked with a pH meter (a combined glass electrode) calibrated against standard buffers of pH 4.00, 7.00 and 9.00 (Merck). The resulting solutions (n = 20) showed absorption maxima at 227 ± 1.4 nm and 287.4 ± 0.9 nm, with absorbances ranging from 0.2 to 0.6 at 228 nm and 0.05 to 0.25 at 287 nm. The 287-nm absorption band was occasionally found as a shoulder only.

For the acquisition of the topograms in the short-wave visible region, urines were diluted 1:20 for photometry and 1:40 for fluorimetry with phosphate buffer (20 mM, pH 7.00). There were no absorption maxima evident in the 350—500 nm range, and absorbances did not exceed 0.25 at 350 nm (the lowest excitation wavelength), dropping to lower absorbances with increasing wavelengths. At 450 nm, absorbances did not exceed 0.1. For the acquisition of the topograms in the long-wave visible region, urines were diluted 1:10 with 1 M hydrochloric acid.

Fluorescence spectra were scanned on an Aminco SPF-500 spectrofluorimeter in 1 × 1-cm quartz cells at room temperature. Bandpasses were 8 nm throughout, in both excitation and emission. The spectra were not corrected with respect to the response of the photomultiplier tube (an R-777 type), the gratings (600 lines mm^{-1}, blazed at 300 nm in excitation and at 500 nm in emission) or the light source (a 250-W high-pressure xenon lamp). The elements of the excitation/emission matrix were acquired with 10-nm increments of both the emission and the excitation wavelengths.

The digitized fluorescence intensity data were stored on a Hewlett-Packard 9815A desk calculator and then transferred to a Univac 1100/81 computer (EDV-Zentrum der Universität Graz). Fluorescence emission curves were reconstituted from the data points with a smooth curve based on a modified cubic curve fit for equally spaced points. The contour plots of the spectra were drawn with a Hewlett-Packard plotter (type 7221S). Data processing was done with home-made software. The 3-dimensional representation shown in Fig. 1 was achieved with the SURFACE program developed by Kalcher [13].

RESULTS

The ultraviolet region of the 3-dimensional presentation of the total fluorescence of human urine is shown in Fig. 1. Unfortunately, this kind of

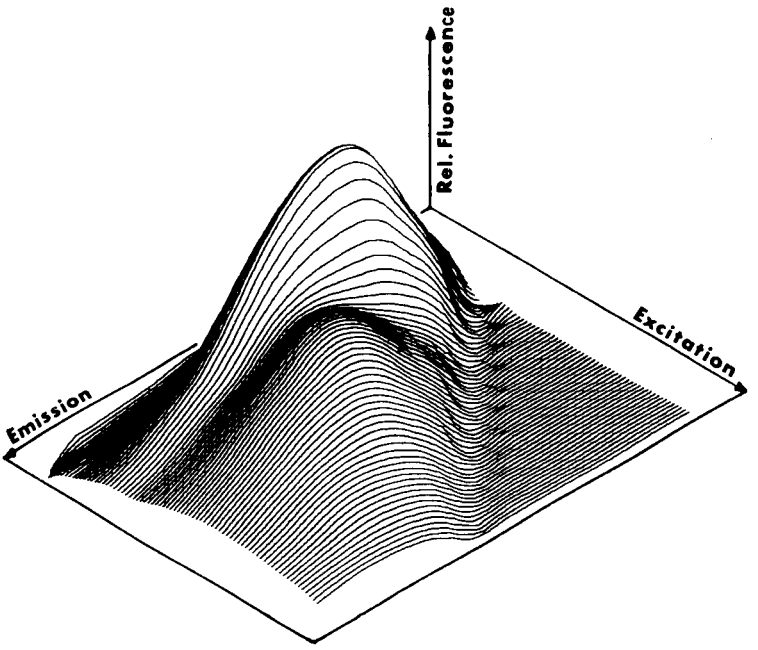

Fig. 1. Isometric projection of the total fluorescence of human urine in the ultraviolet region. pH 7.00, dilution 1:1000. The corresponding contour plot is given in Fig. 2.

representation depends on the perspective, and peaks as well as shoulders may remain hidden. Connection of data points with the same fluorescence intensity (i.e., same height) by contour lines results in a topographic presentation of the 3-dimensional plot (Figs. 2—6). Because such topograms always present a top view, they can be compared more easily with other topograms obtained similarly.

The total fluorescence was divided into three spectral regions. The first region comprises the u.v.-excitable fluorescence (Fig. 2), covering the excitation wavelength range from 250 to 400 nm and displaying two broad peaks. The second region (Fig. 3) covers the 400—500-nm excitation range, resulting in blue-green and green emissions. The relative intensity is smaller than the u.v.-excitable emissions and only one broad single peak with at least two shoulders are recognizable. The third region comprises the red emissions resulting from the presence of porphyrins in urine (Fig. 4). This region exhibits the least fluorescence intensity. The fluorescence maxima will subsequently be referred to as peaks 1—5. No differences were found between topograms acquired in phosphate and Tris buffer.

The ultraviolet part (Fig. 2) shows the most intense fluorescence and exhibits two peaks. Peak 1 is very broad and composed of fluorescences from two or more species. In contrast to the fairly constant excitation maximum at 288.5 ± 0.9 nm, which agrees with the absorption maximum of urine, the emission maximum at 379.1 ± 5.8 nm (extremes 370 and 390 nm) varies

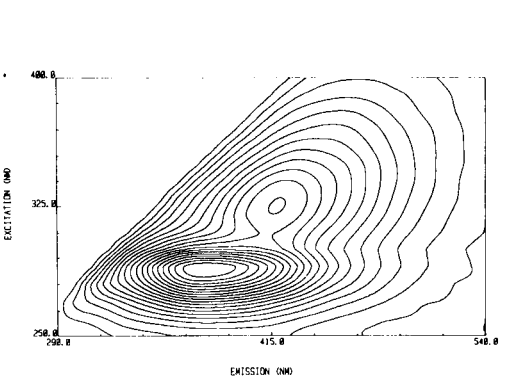

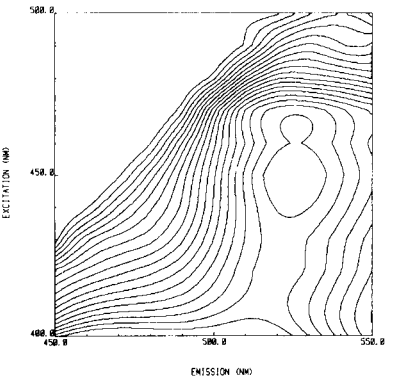

Fig. 2. Fluorescence topogram of the ultraviolet region for human urine. Contour lines from 5 to 95% (in 5% increments) of the highest peak. pH 7.00, dilution 1:1000.

Fig. 3. Fluorescence topogram of the short-wave visible region for human urine. Contour lines as in Fig. 2. pH 7.00, dilution 1:40.

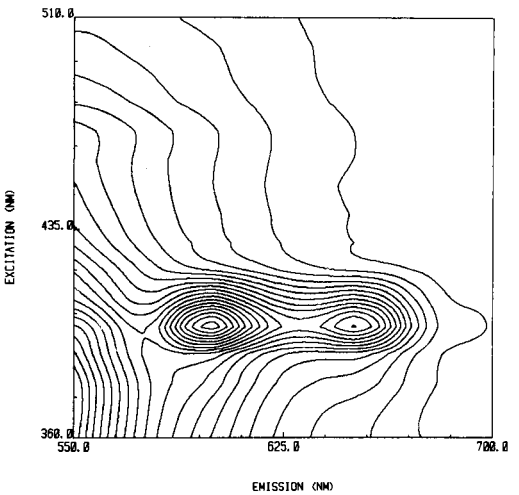

Fig. 4. Fluorescence topogram of the long-wave visible region of human urine. Contour lines as in Fig. 2. Dilution 1:10, solvent 1 M hydrochloric acid.

considerably from sample to sample. Peak 2 has an excitation maximum of 324.3 ± 3.2 nm (extremes 320 and 331 nm) and an emission maximum at 418.9 ± 2.6 nm (extremes 414 and 423 nm). Additionally, there are shoulders evident at about 280/315 nm and 370/455 nm.

The short-wave visible part (Fig. 3) is somewhat less characteristic in showing three maxima at 450/525 nm (peak 3), 465/525 nm (peak 4) and 420/525 nm (peak 5). Two shoulders were located at 430/460 nm and 490/535 nm. Peaks 3, 4 and 5 were occasionally found to be blurred by the

strong fluorescence resulting from peak 2 so that they appeared as shoulders only. In other words, this part of the topogram varies much more from sample to sample than the ultraviolet part.

The long-wave visible part (Fig. 4) shows two distinct maxima at 400/600 nm (peak 6) and 400/650 nm (peak 7) in the topograms for urine in 1 M hydrochloric acid. When acquired in pH 7.00 buffer solution, the peaks are badly diminished only. Although their relative intensities are small, they can easily be recognized. In many cases, these emissions formed shoulders only.

The pH dependence of location and intensity of peaks was also studied. Figure 5 shows the effect of pH on the intensities measured at 3 peaks. The shape of the 290/380-nm curve is similar to that found with many indoles [14] in that there is fluorescence quenching outside the pH 2—11 range and, in the case of tryptophan (Trp) and related amines, a slight pH dependence between pH 8 and 10. The agreement of the pH-dependence curve at 325/400 nm and the curve of pyridoxic acid [15] is less significant, probably owing to the large number of urinary metabolites fluorescing at this wavelength. For the riboflavins, the agreement of the pH-dependence curve for urine (measured at 450/525 nm) with the published curve [16] is excellent.

DISCUSSION

The main purpose of this study was to explore fluorescence topography of human urine as a new variant of pattern recognition methods in analytical biochemistry, clinical chemistry and, eventually, diagnosis. This aim can be achieved by computer programs without knowledge of the species contributing to the total fluorescence [17]. Nevertheless, correlation of peak maxima data with chemical compounds present in urine would be essential for meaningful interpretation of pathological deviations.

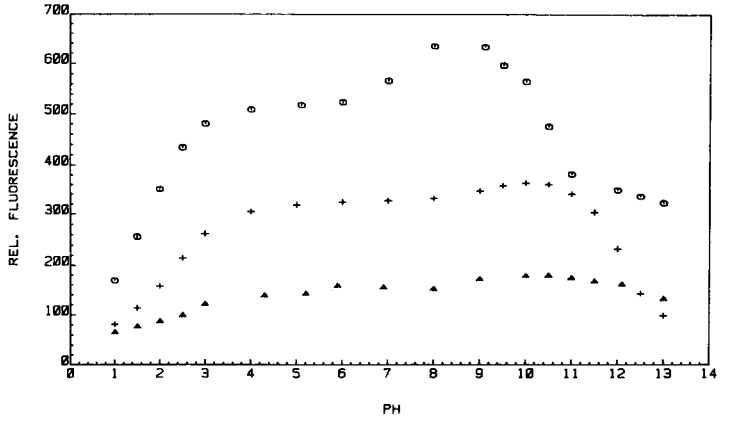

Fig. 5. Plots of fluorescence intensity of human urine vs. pH at characteristic excitation/emission combinations: (+) at 290/380 nm; (△) at 325/420 nm; (○) at 450/525 nm.

Assignment of peaks

Among the manifold substances occurring in urine, only those having high values for the product $\epsilon c \phi_f$ will form a peak or shoulder in the total fluorescence. Here, ϵ is the molar absorptivity of the substance at the relevant excitation wavelength, c is its concentration and ϕ_f is its quantum yield.

The emission of peak 1 in Fig. 2 extends far into the visible region and is most probably caused by several species. Table 1 summarizes a number of metabolites which have spectral properties in agreement with the data of peak 1 and are also present in significant concentrations. The data show that indoxyl sulphate ("urinary indicane") is most probably a major species responsible for peak 1; it is present in rather high concentration and its spectral maxima match the peak data best. Von dem Borne has already attributed the blue fluorescence of urine to indoxyl-type compounds [18].

The two skatole sulphates as well as indolyl-3-acetate may also contribute to the short-wave part (290/360—370 nm) of the peak. The assignment to an indole-derived species is supported by the pH-dependence curve which is typical for an indole (Fig. 5). Nevertheless, there are additional fluorescent species likely to be present which contribute to the background but do not form a peak of their own.

Wachter et al. [19] reported the fluorescence excitation and emission maxima of a number of urinary metabolites after electrophoretic separation. The spectral data indicate that any of the species investigated can make contributions to the short-wave fluorescence as long as it is present in sufficiently high concentration and its fluorescence efficiency is high. Unfortunately, no relative fluorescence yields were given. Similarly, MacNeil et al. [20] and Mills et al. [21] characterized a series of indole-type urinary metabolites and found their spectra to have excitation maxima in the 285—312-nm range, and emission maxima in the 347—360-nm range, a fact that again points to the contribution of indoles to the short-wave part of peak 1. Rosano et al. [22], by setting the wavelengths of the h.p.l.c. detector to 300/350 nm, were able to quantify 5-hydroxyindole-3-acetic acid (the major metabolite of

TABLE 1

Fluorescent species in human urine that may contribute to the 290/380-nm peak, along with published excitation and emission maxima (at pH 7.00), and approximate amount of daily excretion

Species	Excitation/emission maxima[a] (nm)	Approx. daily excretion[b] (μmol)
Indoxyl sulphate	290/380	300.0
Indolyl-3-acetate	290/360	32.3
Skatol-5-sulphate	290/370	11.0
Skatol-6-sulphate	290/360, 370	21.0
5-Hydroxyindole-3-acetate	300/345—355	24.0
5-Hydroxytryptophan	295/340	—

[a]Data from ref. 2. [b]Data from ref. 1.

serotonine), which is an important marker in detecting cancerous tumours and neurological disorders. Excretion ranged from 1.1 to 7.0 mg per day, whilst in patients with diagnosis of cancerous tumours the level was higher by a factor of ten or more. Similar results were obtained by others [23].

Peak 2, located at 325/420 nm, is also characteristic of topograms of healthy fasting subjects. The fluorescent species present in urine that may be responsible for this maximum are compiled in Table 2. Only four metabolites could be found with spectral data sufficiently in agreement with the peak maximum. It is, however, most likely that various other species with peak maxima different from those of peak 2 contribute to the total emission at the peak. Thus, Mabuchi and Nakahashi [4] demonstrated in a careful h.p.l.c. study, that a number of endogeneous fluorescent metabolites can be detected in normal urine when the fluorescence detector is adjusted to wavelengths of 322/415 nm, i.e., close to the maximum of peak 2. Eighteen major components were found, with most significant contributions from about five species which, however, could not be identified. Similarly, Graffeo and Karger [24] assayed indole-3-acetic acid, 5-hydroxytryptophan, serotonine, tryptamine and indole-3-acetic acid by a h.p.l.c. method with fluorescence detection at about this wavelength. Abnormal excretion of blue-fluorescent lipids was detected in urine of patients with neuronal ceroid lipofuscinosis [25].

The data given in Table 2 show that 4-pyridoxic acid is the most likely candidate for the species responsible for peak 2, because it is the most strongly fluorescent species and its spectral data agree well with the peak maximum. This assumption is corroborated to some extent by the dramatic increase in the intensity of peak 2 after administration of a vitamin B_6 tablet (200 mg of pyridoxalium chloride; Neurobion forte, Merck) in the evening before the urine sample was taken. Figure 6 shows the relevant topogram. The peak for pyridoxic acid, which is the major (40—50%) metabolite of the vitamin, is dramatically enhanced in this case so that it overrides all other species, even at a dilution of 1:12 500. One day later, the topographic pattern of the urine of the same subject was found to be normal again.

TABLE 2

Fluorescent species identified in human urine that may contribute to the 325/420 nm peak, along with published excitation and emission maxima (at pH 7.00) and approximate amount of daily excretion

Species	Excitation/emission maxima[a] (nm)	Approx. daily excretion[b] (μmol)
4-Pyridoxic acid	317/420—425	4.1
Xanthine	315/435	40.0
3-Hydroxyanthranilic acid	320/415	50.0
5-Hydroxyanthranilic acid	340/430	—

[a]From ref. 2. [b]From ref. 1.

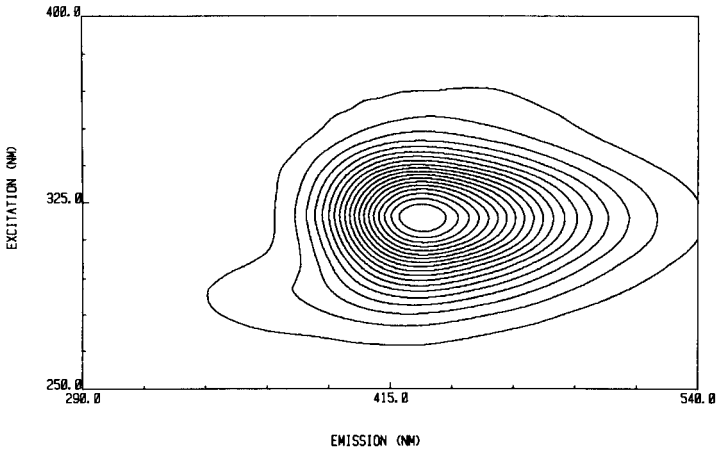

Fig. 6. Fluorescence topogram of a human urine in the ultraviolet region 12 h after administration of 200 mg vitamin B_6. Contour lines as in Fig. 2. pH 7.00, dilution 1:12 500 (!).

Pyridoxic acid has been recognized as one of the major fluorescent metabolites in urine and was assayed fluorimetrically at 350/450 nm [26]. It was, however, noted that at these wavelengths other substances interfered, a fact that supports the assumption that there are contributions of materials other than pyridoxic acid to peak 2.

Peaks 3, 4 and 5, located at 450/525 nm, 465/525 nm and 420/525 nm, are most likely due to the presence of riboflavin or one of its urinary metabolites or a combination thereof. For riboflavin, spectral maxima ranging from 436 to 455 nm have been reported for excitation, and from 510 to 531 nm for emission [2]. The data for 7-α-hydroxyriboflavin and 8-α-hydroxyriboflavin are given as 437/525 nm and 445/535 nm, respectively. The excretion of riboflavin is age-dependent, ranging from 0.2 to 2.5 μmol per day [27]. Apart from riboflavin, Ohkawa et al. [28] detected the two above-mentioned hydroxyriboflavins in human urine under 440-nm excitation and 530-nm detection after h.p.l.c. separation, and also mentioned the presence of hydroxyethylflavin. Because no other substances were found with spectral data in agreement with the maxima of peak 3, it may be concluded that the peak was most likely caused by riboflavin and its primary metabolites. This assignment is further supported by the pH-dependence curve of the 450/525-nm emission (Fig. 5) which is similar to, but not identical with, the pH-dependence curve of pure riboflavin [16]. The differences can be attributed to a fluorescence background having pH characteristics different from riboflavins.

Peaks 5 and 6 are rather weak in intensity. Because it was assumed that they result from porphyrins which are known to be most strongly fluorescent in acidic solution, the topograms were acquired in 1 M hydrochloric acid (Fig. 4). The two peaks found they agree well with published data for both

uroporphyrin and coproporphyrin. Literature values are 405/596, 619 and 653 nm (three emission maxima) for uroporphyrin, and 400—405/595, 618, 652 and 671 nm (four emission maxima) for coproporphyrin, both in 2 M hydrochloric acid [2]. The excretion rate is 0.2 and 0.47 μmol per day, respectively [1, 29, 30]. Significantly enhanced levels are found in cases of inherited porphyrias and induced porphyrinurias. Other porphyrins are also present in urine, but their concentrations are vanishingly small [29].

Assignment of shoulders

The 280/315-nm shoulder has not so far been assigned definitively to a single species. Hanai and Hubert [5] analyzed normal and cancerous urine by a combination of h.p.l.c. and fluorescence and identified, among others, the following fluorescent species when the wavelengths were set to 280/315 nm: dopamine, 5-hydroxytryptophan, tryptophan, 5-hydroxyindole-3-acetic acid, 4-hydroxy-3-methoxyphenylacetic acid and 3-methoxymandelic acid. Characteristic concentration changes were found in urines of cancer patients and newborn babies. Tyrosine and vanillylmandelic acid are further species fluorescing at this wavelength, being present in urine in concentrations of 100—140 μmol per day [1] and ca. 29 μmol per day [31], respectively. They all may be responsible for the 280/315-nm shoulder.

The 370/455-nm shoulder may be formed by one or more of the species listed in Table 3. The three kynurenines and the two pterins appear to be the main species; they are known to fluoresce much more intensely than both folic acid and xanthurenic acid. Hausen et al. [32] and others [33] monitored the concentration of neopterin (a tumour marker) in human urine at approximately the same wavelengths (353/438) as observed for the shoulder in Fig. 2 (370/455); they found excretion rates between 113 and 163 μmol neopterin per mol of creatinine (age- and sex-dependent).

During a study on porphyrines in urine, this 460-nm emission has also been

TABLE 3

Fluorescent species in human urine that may contribute to the 370/455-nm shoulder, along with published excitation and emission maxima (at pH 7.00, unless otherwise specified) and approximate amount of daily excretion

Species	Excitation/emission maxima[a] (nm)	Approx. daily excretion[b] (μmol)
Kynurenine	370/490[c]	14.0
Biopterin	370/450	8.9
Neopterin	353/438	1.8
5-Hydroxykynurenine	375/460[c]	—
3-Hydroxykynurenine	365/460[c]	27.0
Folic acid	365/450	0.21
Xanthurenic acid	350/460[c]	15.0

[a]From ref. 2. [b]From ref. 1. [c]At pH 11.

detected by others [30]; it was stated that "this peak is produced by an unknown substance, present in all urine specimens examined", and that "some normal specimens contain a high concentration of this substance". So far, no suggestions can be made concerning the 430/460-nm and 490/535-nm shoulders.

Conclusions

Because the total fluorescence of human urine can be resolved into a few peaks and shoulders, fluorescence topography appears to have the potential of becoming a useful method for pattern recognition and rapid screening of urine. The time to acquire a 150 × 150-nm matrix is about 20 min, and commercially available instrumentation (e.g., from Perkin-Elmer, Baird, SLM Aminco) will contribute to a wider utilization of the method.

Fluorescence topography may also be combined with separation techniques such as chromatography. By using size-exclusion chromatography and thin-layer chromatography, only one strongly fluorescent substance was found in uremic urine and normal urine [6]. It was stated, however, that "methods with greater resolution . . . may produce different results". The present work clearly demonstrates that numerous fluorophores are present in urine.

A severe limitation may result from the fact that the pattern of urine topograms varies much more from one sample to another than serum topograms which, in contrast, are fairly constant in the case of healthy persons. While this finding is not surprising (type and amount of metabolites are largely determined by nutrition, sex and age), it can limit the utility of the method for practical purposes.

Attempts have been made to make topography suitable for quantitative analysis of multicomponent mixtures [34]. This, however, requires a knowledge of the fluorescence spectra of all species contributing to the overall fluorescence. Apart from the metabolites listed in the Tables, it is likely that there will be a large variety of unidentified components that remain hidden in the background. This makes quantitative analysis by published methods very difficult, if not impossible.

REFERENCES

1 Wissenschaftliche Tabellen Geigy, Vol. 1: Körperflüssigkeiten, 8th edn., CIBA-Geigy AG, Basle, 1983.
2 O. S. Wolfbeis, in S. G. Schulman (Ed.), The fluorescence of organic natural products, Molecular luminescence spectroscopy. Methods and applications, Vol. 1, Wiley, New York, 1985, pp. 167–370.
3 P. W. Danckwortt and J. Eisenbrand, Luminescenz-Analyse im filtrierten ultravioletten Licht, Akad. Verlags-Ges., Leipzig, 1964, p. 162 (and references therein).
4 H. Mabuchi and H. Nakahashi, Clin. Chem., 29 (1983) 675.
5 T. Hanai and J. Hubert., J. Liq. Chromatogr., 7 (1984) 1627.
6 H. A. Schwertner, Nephron, 31 (1982) 209.
7 E. D. Bell and W. I. P. Mainwaring, Clin. Chim. Acta, 35 (1971) 83.
8 W. E. Lindup, Clin. Chem., 29 (1983) 2122 (and references therein).

9 I. M. Warner, G. Patonay and M. P. Thomas, Anal. Chem., 57 (1985) 463A.
10 O. S. Wolfbeis and M. Leiner, Anal. Chim. Acta, 167 (1985) 203.
11 M. J. P. Leiner, R. J. Schaur, G. Desoye and O. S. Wolfbeis, Clin. Chem., 32 (1986) 1974.
12 E. Koller, O. Quehenberger, G. Jürgens, O. S. Wolfbeis and H. Esterbauer, FEBS Lett. . 198 (1986) 229.
13 K. Kalcher, Comput. Chem., 6 (1982) 39.
14 J. W. Bridges and R. T. Williams, Biochem. J., 107 (1968) 22.
15 J. W. Huff and W. A. Perlzweig, J. Biol. Chem., 155 (1944) 345.
16 R. Kuhn and G. Moruzzi, Ber. Dtsch. Chem. Ges., 67 (1934) 988.
17 M. J. P. Leiner, Ph.D. thesis, University of Graz, 1984.
18 G. A. K. von dem Borne, Ned. Tijdschr. Geneeskd., 82 (1938) 1808.
19 H. Wachter, K. Grassmayr, W. Gütter, A. Hausen and G. Sallaberger, Mikrochim. Acta, Part I, (1972) 861.
20 J. D. MacNeil, M. Häusler, R. W. Frei and O. Hutzinger, Anal. Biochem., 45 (1972) 100.
21 M. H. Mills, M. G. King, N. G. Keats and R. A. MacDonald, J. Chromatogr., 377 (1986) 350.
22 T. G. Rosano, J. M. Meola and T. A. Swift, Clin. Chem., 28 (1982) 207.
23 V. Skrinska and Sh. Hahn, J. Chromatogr., 311 (1984) 380.
24 A. P. Graffeo and B. L. Karger, Clin. Chem., 22 (1976) 184.
25 T. Ohashi, Y. Eto, K. Maekawa, S. Yamaguchi, K. Goto, J. Obata, K. Kumagai, H. Onoe and S. Yanagishita, Brain Dev., 7 (1985) 227.
26 S. K. Reddy, M. S. Reynolds and J. M. Price, J. Biol. Chem., 233 (1958) 691.
27 V. J. Gatautis and H. K. Naito, Clin. Chem., 27 (1981) 1672.
28 H. Ohkawa, N. Ohishi and K. Yagi, J. Biol. Chem., 258 (1983) 5623.
29 W. E. Schreiber, V. A. Raisys and R. F. Labbé, Clin. Chem., 29 (1983) 527.
30 Ch. Sobel, C. Cano and R. E. Thiers, Clin. Chem., 20 (1974) 1397.
31 G. M. Anderson, F. C. Teibel and D. J. Cohen, Clin. Chem., 31 (1985) 819.
32 A. Hausen, D. Fuchs, K. König and H. Wachter, J. Chromatogr., 227 (1982) 61.
33 P. Mura, C. Tallineau, D. Reiss and A. Piriou, J. Liq. Chromatogr., 7 (1984) 2289.
34 I. M. Warner, J. B. Callis, E. R. Davidson and G. D. Christian, Clin. Chem., 22 (1976) 1483.

Analytica Chimica Acta, 198 (1987) 25—36
Elsevier Science Publishers B.V., Amsterdam — Printed in The Netherlands

SPECTROPHOTOMETRIC DETERMINATION OF TOTAL CYANIDE IN WASTE WATERS IN A FLOW-INJECTION SYSTEM WITH GAS-DIFFUSION SEPARATION AND PRECONCENTRATION

ZHAOHAI ZHU and ZHAOLUN FANG*

Institute of Forestry and Soil Science, Academia Sinica, P.O. Box 417, Shenyang (Peoples' Republic of China)

(Received 20th August 1986)

SUMMARY

An automated flow-injection system with gas-diffusion separation and preconcentration and spectrophotometric detection is described for the determination of total cyanide in waste waters. An unstable red intermediate product of the reaction of cyanide with isonicotinic acid and 3-methyl-1-phenyl-2-pyrazolin-5-one is used instead of the conventional blue final product to improve the efficiency. A novel combination of a gas-diffusion separator with the sampling valve enables efficient on-line separation, preconcentration and sampling of cyanide. The sampling frequency is 40 h^{-1} and the detection limit is 0.006 $\mu g\ ml^{-1}$ (3σ) when a 2-ml sample is taken and a preconcentration factor of 3.5 is achieved. The relative standard deviation is 1.4% (n = 22) at the 0.5 $\mu g\ ml^{-1}$ level. Results obtained with the proposed method are in good agreement with the standard manual spectrophotometric method. Interference studies show that in the presence of 1,10-phenanthroline, most potential interferents present in appreciable amounts do not interfere, but the interference from cobalt is not overcome in this system.

The importance of cyanide determination in environmental samples can hardly be overemphasized. Stringent control of cyanide in industrial effluents demands automation so that determinations can be conducted preferably at intervals of a few minutes for extended periods. Recently, this has been the subject of numerous published papers [1—10]. These include air-segmented continuous flow systems [1] and flow-injection systems [3—10] using optical [7, 10] and electrochemical detection [3—6, 8, 9]. Most of these systems deal only with the automated determination of free cyanide and have to be preceded by a tedious manual distillation procedure if the concentration of total cyanide which includes complexed cyanide is desired. As complexed cyanide is undoubtedly a serious potential hazard, the value of an automated system will be much lower if the distillation process is not incorporated in the system

Pihlar and Kosta [2] described an automated system which included the distillation process but a preliminary manual pretreatment with ultraviolet radiation was necessary to decompose strongly bound metal cyanide complexes. The system was used to determine total cyanide at a sampling fre-

0003-2670/87/$03.50

quency of 60 h^{-1}. However, the introduction of nitrogen into the distillation unit and its subsequent removal by means of a debubbler resulted in a rather complicated system. Okumoto et al. [6] developed a flow-injection system with a gas-diffusion separator and a cyanide-selective electrode flow-through detector. They claimed a detection limit of 0.1 $\mu g\ ml^{-1}$ with a sampling frequency of 40 h^{-1}; but apparently no attempt was made to determine total cyanide.

An efficient on-line gas-diffusion system which can achieve separation of free cyanide and all of the complexed cyanide excepting cobalt cyanide is described in this paper. The teflon microporous membrane diffusion unit forms a part of the flow-injection loop and preconcentration can be effected simultaneously during the distillation, enhancing the sensitivity for the determination.

Spectrophotometric methods for cyanide determination have an advantage over electrochemical detection in having fewer memory effects and freedom from electrostatic interferences, yet the spectrophotometric methods with acceptable sensitivities and precisions presently available [11, 12] require prolonged reaction periods of over half an hour, making them relatively unsuitable for automation by a flow-injection system. Nevertheless, Rios et al. [10] succeeded in developing a flow-injection method for the determination of free cyanide using pyridine/barbituric acid as the colour-developing reagent. Owing to the slow reaction, a 476-cm coil immersed in a 35°C water bath had to be used for the colour development, resulting in a relatively low sampling frequency of 20 h^{-1}. Even so, the sensitivity was worse than that of manual procedures.

The isonicotinic acid/3-methyl-1-phenyl-2-pyrazolin-5-one spectrophotometric method is one of the most widely used procedures for cyanide determination following distillation [11]. The method is sensitive and relatively selective and has been recommended as a standard procedure in China. Yet the operation is long and tedious and requires considerable skill from the operator. The colour reaction is slow, requiring an incubation period of 40 min even at elevated temperatures; this renders it almost impossible to adapt the procedure for flow injection analysis (f.i.a.) without a drastic loss of sensitivity. However, it was observed that a red intermediate product appears immediately after the mixing of the reagent with a sample containing cyanide. The colour fades rapidly with the development of the final blue product. In this paper, use is made of the unstable red intermediate product to develop a fast flow-injection method, which takes advantage of the reproducible timing and precisely controlled mixing conditions inherent in a flow-injection system to achieve fast but sensitive results. Combination of this reaction with on-line gas-diffusion resulted in the production of a fully automated system for total cyanide determination capable of handling 40 samples per hour at sub-$\mu g\ ml^{-1}$ levels.

EXPERIMENTAL

Reagents

All reagents were of reagent grade and deionized water was used throughout.

The 1,10-phenanthroline solution was prepared by dissolving 20 g of 1,10-phenanthroline in 200 ml of 2 mol l^{-1} hydrochloric acid. Chloramine-T (0.1%)/buffer solution was prepared by mixing one volume of aqueous 1% (w/v) chloramine-T solution with nine volumes of 0.25 mol l^{-1} potassium dihydrogenphosphate/0.25 mol l^{-1} disodium hydrogenphosphate solution (pH 6.7). Isonicotinic acid/pyrazolone solution was prepared by dissolving 18.4 g of isonicotinic acid 6.0 g of sodium hydroxide and 0.13 g of 3-methyl-1-phenyl-2-pyrazolin-5-one in 250 ml of water, resulting in a 0.6 mol l^{-1} isonicotinic acid/3 mmol l^{-1} pyrazolone solution.

A 10.0 μg ml^{-1} cyanide stock solution was prepared and standardized by a conventional titration procedure [11] and working solutions were made by diluting this stock to 0.10, 0.20, 0.40, 0.60, 0.80 and 1.00 μg ml^{-1} with 1 g l^{-1} sodium hydroxide solution, just before use.

Apparatus

A Bifok-FIA-05 flow injection analyzer equipped with a Gilson 8-channel peristaltic pump and a single-channel injection valve (L100-1) was used. The 40-place autosampler (FIA-07) was modified by adding a timer to synchronize the action of the autosampler and the valve. A FIAstar 5023 spectrophotometer with an 18-μl flow cell was used as the detector, the absorbance output being recorded with a Kipp and Zonen BD-41 chart recorder.

A Tecator type-II Chemifold comprising two three-way connectors was used to construct the manifold. The gas-diffusion unit was made from PVC plates the detailed dimensions of which are shown in Fig. 1. Identical grooves were machined accurately on the two plates and teflon microporous membranes reinforced with nylon net were sandwiched in-between them.

Procedure

The pH of waste-water samples was adjusted to 11.5—13.0 by adding sodium hydroxide pellets during collection, and filtered if necessary. Samples were loaded into plastic sample cups on the autosampler. The automated system was set up as shown in the flow diagram (Fig. 2A). The volume of sample taken for each determination was controlled by the duration of the sampling period of the FIA-07 autosampler when the pick-up probe was in its lower position. The sample was acidified by merging with a flow of 2 mol l^{-1} hydrochloric acid and heated while passing through the 600-cm teflon coil (0.8 mm i.d.) inserted in a thermostated (60°C) water bath. 1,10-Phenanthroline was added to the acid to assist the dissociation of stable metal cyanide complexes. The liberated hydrogen cyanide diffused through the teflon membrane of the separator and was

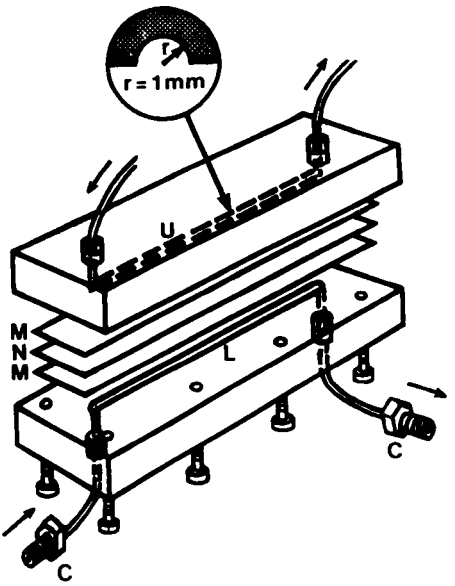

Fig. 1. Gas-diffusion unit: M, microporous teflon membrane; N, nylon net support; C, connectors to injection valve; U, upper groove for sample donor stream; L, lower groove for acceptor solution (length 9 cm, volume 135 μl) which also acts as sampling loop for injection valve.

absorbed by the acceptor solution (0.025 mol l^{-1} NaOH) enclosed in the sample loop of the injection valve. Normally a 50-s sampling period was used, during which about 2 ml of sample was introduced into the distillation system creating a 3.5-fold preconcentration in the sample loop. A longer period would naturally increase the preconcentration factor but at the expense of a lower sampling frequency. At the end of the sampling stage, the sampling probe was automatically lifted to its upper position under control of the autosampler and wash water was aspirated into the sample line. Simultaneously, the next sample was moved automatically to its sampling position but no sample was aspirated until the beginning of the next sampling stage. In the system studied, the wash period (i.e., the time interval between two sampling stages) was 40 s. At the end of the wash period, the sampling probe was restored to its lower position to begin another sampling cycle; 110 s after the beginning of the first sampling stage, the front of the sample zone reached the gas-diffusion unit. The injection valve was controlled by an extra timer so that it had already moved over from its injection position to its collecting position 1 s in advance, waiting for acceptance of the liberated gas. The distilled hydrogen cyanide could then diffuse through the membrane into the acceptor solution in the sample loop. This collecting (preconcentration) stage lasted for a period of 60 s, i.e. 10 s longer than the sampling period; this was found to be sufficient to allow the somewhat

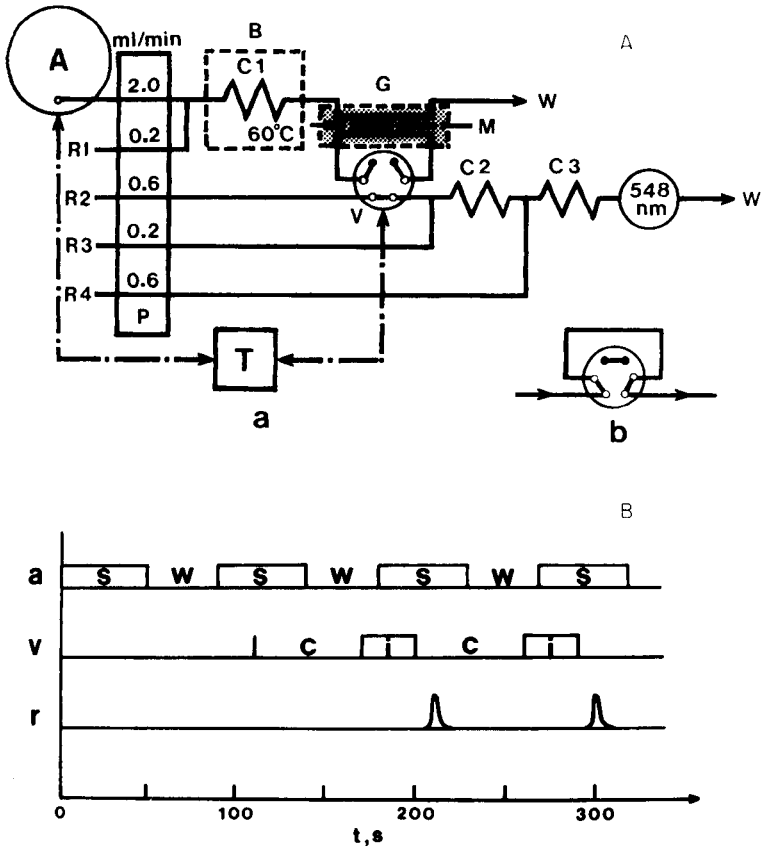

Fig. 2. (A) Automated flow-injection system for total cyanide determination: A, autosampler; P, peristaltic pump; B, thermostated water bath; G, gas-diffusion unit (cf. Fig. 1); T, timer; V, injection valve; C1, C2, C3, mixing coils with tube lengths 600 cm, 60 cm and 90 cm, respectively (tube i.d. for C1 is 0.8 mm, C2, C3, 0.5 mm); W, waste; R1, 1,10-phenanthroline acid solution; R2, 0.025 mol l^{-1} NaOH; R3, chloramine-T buffer solution; R4, isonicotinic acid/pyrazolone solution. (a) Valve in sampling/preconcentrating position; (b) valve in injection position. (B) Sequence of operation for the automated system in (A): a, autosampler; v, injection valve; r, recorder; s, sampling period; w, wash period; c, collecting period; i, injection period.

dispersed sample zone to pass through the gas-diffusion unit completely. This was checked by replacing the sample with a dye solution and observing the effluent through transparent tubing at the outlet of the gas-diffusion unit. At the end of the collecting stage, which was 170 s after the start of the sampling stage, the valve was actuated and the preconcentrated sample was injected into a sodium hydroxide carrier and merged with the chloramine-T and isonicotinic acid/pyrazolone reagents downstream. The valve remained in the injection position for 30 s, after which it was automatically restored to the collecting position. Then, 40 s after the sample had been injected, a peak was recorded, i.e., the first peak appeared about 210 s after the

beginning of the sampling stage; but thereafter a new sample peak would appear every 90 s, giving a sampling frequency of about 40 s h^{-1} (see Fig. 2B).

Continuous recordings were made by the chart recorder. A standard series in the range 0.1 μg ml^{-1} cyanide was run with samples, and the peak absorbances were used for evaluation. A typical recording of a standard series is shown in Fig. 3.

RESULTS AND DISCUSSION

Characteristics of colour-forming species in the isonicotinic acid/pyrazolone method for cyanide

The isonicotinic acid/pyrazolone method, which is used quite extensively as a manual procedure, utilizes the blue final product with peak absorbance at 638 nm as the colour-forming and measured species. The molar absorptivity is 1.0×10^5 l mol^{-1} cm^{-1} [13] and the sensitivity is acceptable for most cyanide determinations. However, colour development for 40 min at 25—35°C is necessary to reach a stable state (see Fig. 4). Preliminary experiments with a flow-injection system based on this reaction with measurement at 638 nm produced a sensitivity one order of magnitude lower than the manual method even when very long reaction coils were used. Thus the adaptation of such a reaction to f.i.a. did not seem to be very promising. However, it was observed that immediately after the introduction of the reagent into the sample solution a red intermediate product with peak absorbance at 548 nm was formed which faded rapidly, gradually being transformed into the final blue product. No attempt was made to identify the red product; according to the literature [14], the blue product is a condensation compound of one molecule of isonicotinic acid with two molecules of pyrazolone, so the red product might be an intermediate product consisting of one molecule of isonicotinic acid and one molecule of pyrazolone which is gradually transformed to the blue product on further condensation.

A study of the kinetic properties was conducted by pumping suitable proportions of the sample and reagent solutions and merging them shortly before entry into the flow cell of the spectrophotometer as described for Fig. 4. The flow was stopped and wave-length scans in the 400—700 nm region were made at repeated intervals. The result is shown in Fig. 5. Some distortion in the recordings was inevitable owing to the relatively slow scan speed of the monochromator (30 s for full wavelength region) compared to the rate of change in absorbance, yet the study produced adequate evidence of the favourable characteristics of the red intermediate product for use in a flow-injection system. The product was not stable for any period of time; the absorbance increased rapidly to a maximum and then dropped steadily, yet the maximum absorbance occurred only 35 s after merging of the reactants compared to 40 min for the final product. When optimum reagent concentrations were adopted as for the conventional manual method, the

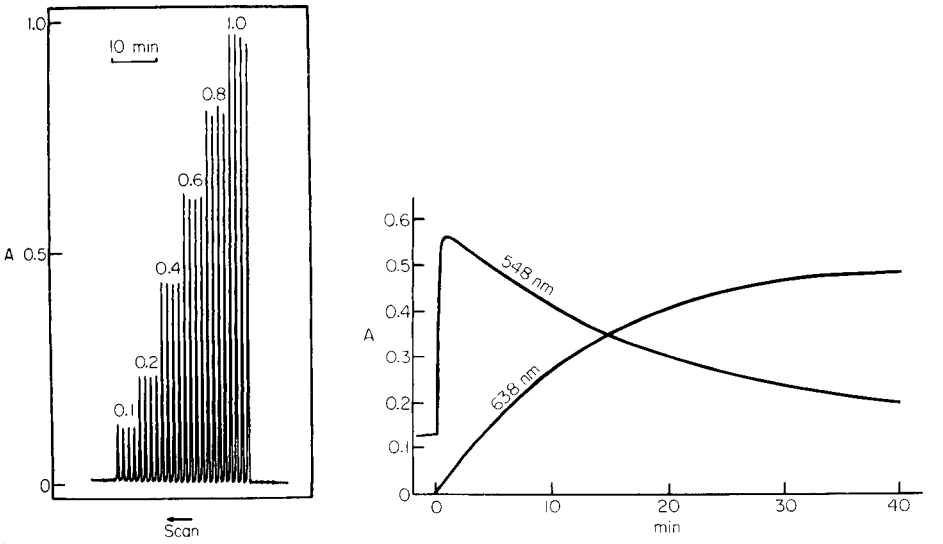

Fig. 3. Recorded tracings for a series of 0—1.00 μg ml^{-1} cyanide standard solutions, from the flow-injection system in Fig. 2A.

Fig. 4. Stop-flow time/absorbance recordings at 548 nm and 638 nm, monitoring the formation of the red and blue products, respectively, from 1 μg ml^{-1} cyanide against a reagent blank. The time scale is in minutes after the moment of stopping the flow. The recording for the 548-nm measurement does not begin from zero because of the time difference between the mixing of sample and reagent and the actual measurement; this phenomenon does not occur for the 638-nm measurement because the formation of the blue product is much slower. Reagent concentrations were optimized for the red product (see text).

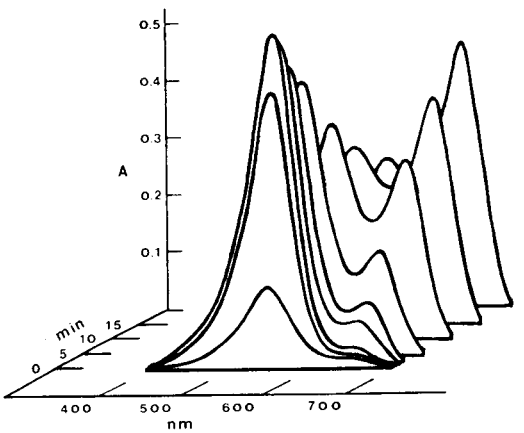

Fig. 5. Absorption spectra obtained during colour development from 1 μg ml^{-1} cyanide, scanned at predetermined intervals. Scan speed, 10 nm s^{-1} ; reagent concentrations optimized for red product (see text).

highest molar absorptivity for the red product was 40% lower than that of the blue product. Attempts to improve the sensitivity of the red product through optimization of reaction conditions resulted in only a marginal improvement in the molar absorptivity (4.6×10^4 l mol^{-1} cm^{-1}), yet omission of the dimethylformamide stabilizer lowered the molar absorptivity of the blue product (3.3×10^4 l mol^{-1} cm^{-1}). A flow-injection system could readily be designed by controlling the flow rate and length of the reaction coil so that when the section of sample zone containing the maximum concentration of the analyte passes through the flow cell, the reaction producing the red product is also at the optimum stage.

The gas-diffusion separation/preconcentration/sampling unit

On-line gas diffusion separation has been used quite successfully in a number of flow-injection systems for the determination of volatile species since the pioneering work by Baadenhuijsen and Seuren-Jacobs [15]. A similar separator has been used by Okumoto et al. [6] for the gas-diffusion separation of hydrogen cyanide. The gas diffusion unit used in the present work was relatively easy to make. But because of insufficient efficiency (ca. 30%) in the transport of the hydrogen cyanide through the membrane when continuously flowing donor and acceptor streams were used, there was considerable loss in sensitivity even when the donor/acceptor stream ratio was large. As a lower detection limit was desired, it was decided to introduce a completely stationary acceptor solution in the groove of the diffusion unit which also formed a part of the sample loop of the injection valve. This combination of the gas diffusion unit with the sampling valve could produce a certain extent of preconcentration during the separation. It was shown that, by using a 50-s sampling period totalling 2 ml of 0.5 μg ml^{-1} cyanide sample and a groove capacity of about 135 μl, a 3.5-fold enhancement in sensitivity could be achieved compared to the peak signal obtained by using a 1:1 donor/acceptor stream ratio. The combination of gas-diffusion unit with the sampling valve could be readily modified to produce a new type of integrated microconduit [16].

Optimization of reaction conditions and flow parameters

Because a detectable species which is different from that of the original isonicotinic acid/pyrazolone method was used in the flow-injection determination, the optimum reaction conditions were expected also to be different. Thus a detailed study on the reaction conditions was conducted with the flow-injection manifold in Fig. 6. The total flow rate of carrier and reagent streams and the coil lengths were designed so that the residence time for the sample would coincide with the optimum colour development time obtained in the kinetic studies.

Under fixed concentrations of isonicotinic acid (0.26 mol l^{-1}) and pyrazolone (1.3 mmol l^{-1}) at pH 7.4, variation in the chloramine-T concentration was found to have a great influence on the peak absorbance of a 1 μg ml^{-1}

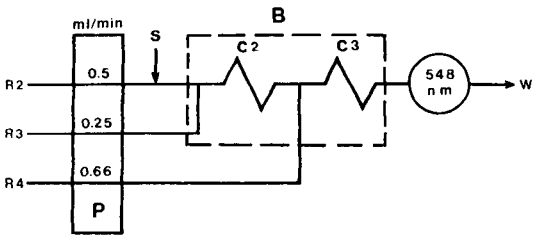

Fig. 6. Manifold used for the optimization of reaction conditions. Sample volume 150 μl; symbols as in Fig. 2A.

cyanide standard (Fig. 7A). The curve shows a maximum at 0.10% (w/v) chloramine-T concentration (9 mmol l^{-1} in coil C2) and decreases quite steeply at both higher or lower concentrations. Therefore a concentration of 0.10% was chosen for further studies. The concentrations of isonicotinic acid and pyrazolone were not critical above a concentration of 0.6 mol l^{-1} (0.26 mol l^{-1} in final stream) and 3 $mmol^{-1}$ (1.3 mmol l^{-1} in final stream), respectively. Concentrations of 0.6 mol l^{-1} isonicotinic acid and 3 mmol l^{-1} pyrazolone were used in the system.

Studies on the optimum pH range, by using standard Clark and Lubs buffer solutions, yielded the results shown in Fig. 7B. Optimum response was obtained in the range pH 6.4—7.4; between these values, variations in absorbance obtained for a 1 μg ml^{-1} cyanide standard solution were less than 2%. This is somewhat easier to control than the narrower range of pH 6.3—6.6 for the original isonicotinic acid/pyrazolone method [13]. Dimethylformamide (DMF) was used in the original isonicotinic acid/pyrazolone method mainly to stabilize the final product; as this final product was of no concern in the flow-injection system, DMF was abandoned.

The optimization of parameters were completed under ambient conditions of 20 ± 5°C. The reaction rate was found not to be very sensitive to temperature changes; a variation of 0.005 in absorbance (1.3% variation) was caused

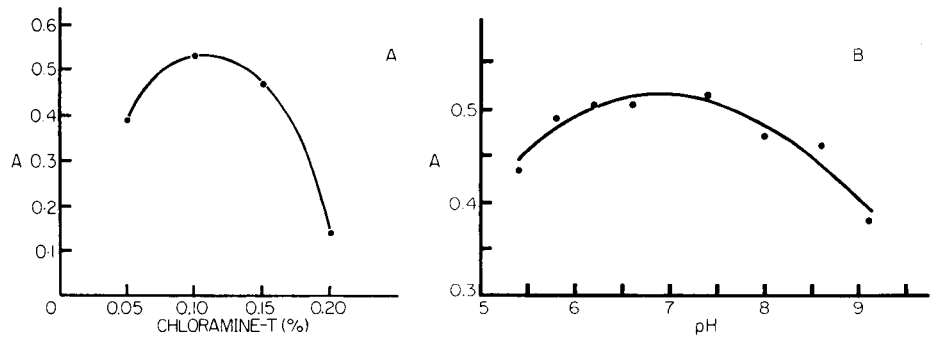

Fig. 7. Influence of chloramine-T concentration (A) and pH (B) on peak response for 1 μg ml^{-1} cyanide. Concentrations of other reagents are described in the text.

by a 1°C change in temperature for a 0.5 μg l^{-1} cyanide standard solution, therefore no attempt was made to control the reaction temperature by thermostating.

Interference studies

In cyanide determinations, interferences from metals capable of forming strongly bound cyanide complexes are well documented in the literature [17]. Although most of the interferences can be eliminated by a distillation process in acidic medium, some ions such as cobalt and copper still pose serious problems even with a distillation pretreatment. These phenomena were confirmed for the flow-injection system in Fig. 2A and Fig. 6, with and without the gas-diffusion separation. When the former system was used, certain complexing agents were found to be useful in minimizing the interfering effects from these ions, with 1,10-phenanthroline being the most effective. The results obtained by using 1,10-phenanthroline as the complexing agent and the system including gas diffusion are shown in Table 1. Most of the recoveries were acceptable, including those obtained when small amounts of nickel, copper and iron(II) were present, but the interference from cobalt remained serious. Hence the results obtained will exclude the amount of cyanide which is complexed with cobalt.

Limit of detection, precision and accuracy

When the system shown in Fig. 2A is used with a sampling period of 50 s (sampling frequency 40 h^{-1}), the detection limit was 6 μg l^{-1} cyanide, estimated as 3 times the standard deviation (n = 21) for a blank solution. The precision obtained for a 0.5 μg ml^{-1} cyanide standard was 1.4% relative standard deviation (n = 22).

The accuracy of the method was tested by the determination of total cyanide waste water samples collected from electroplating factories both with the flow-injection method and the standard manual isonicotinic acid/pyrazolone method [11]. The results (Table 2) show that the results obtained by the two methods agree quite well, giving a correlation coefficient of 0.9996.

Conclusion

The unstable red intermediate product of the isonicotinic acid/pyrazolone method was used successfully for the determination of total cyanide (excluding cobalt cyanide) in waste water samples by flow injection analysis. This provides yet further evidence of the feasibility of using flow-injection systems to utilize unstable reaction products in quantitative analysis. Exploration of the wealth of information in the chemical literature would undoubtedly yield many more selective and sensitive reactions which have never been used in quantitative analysis because of their instability. The potential of f.i.a. in this field is vast.

The combination of on-line gas-diffusion separation with preconcentra-

TABLE 1

Interferences from various ions on 0.5 μg ml^{-1} cyanide in the system in Fig. 2A with 1,10-phenanthroline present

Ion	Concentrations (μg ml^{-1})			Ion	Concentrations (μg ml^{-1})		
	Interferent	Cyanide	Recovery (%)		Interferent	Cyanide	Recovery (%)
Br^-	10	0.49	98	NO_2^-	10	0.50	100
I^-	10	0.48	96	Cd^{2+}	10	0.52	104
SCN^-	2	0.50	100	Cu^{2+}	10	0.42	84
S^{2-}	5	0.50	100	Zn^{2+}	10	0.50	100
	10	0.46	92	Ni^{2+}	1	0.48	96
Phenol	10	0.48	96	Co^{2+}	1	0.09	18
Hydroquinone	100	0.50	100	Fe^{3+}	100	0.49	98
Formaldehyde	1	0.47	94	Fe^{2+}	10	0.40	80
SO_3^{2-}	10	0.49	98	Pb^{2+}	10	0.49	98
$S_2O_3^{2-}$	100	0.51	102	Hg^{2+}	1	0.50	100

TABLE 2

Comparison of results from the analysis of five waste water samples by the flow-injection method and a standard manual procedure

Method	Total cyanide (μg ml^{-1})				
Standard	16.1	6.5	0.71	0.07	0.02
Flow-injection	15.5	6.7	0.68	0.04	0.03

tion in a sampling valve opens up new possibilities in the development of more selective and sensitive methods for f.i.a. The gas-diffusion unit and the sampling valve might be integrated into one compact unit following the integrated microconduit concept of Růžička and Hansen [16], and further work is being done on these lines.

REFERENCES

1 R. A. Durst, Anal. Lett., 10 (1977) 961.
2 B. Pihlar and L. Kosta, Anal. Chim. Acta, 114 (1980) 275.
3 B. Pihlar, L. Kosta and B. Hristovski, Talanta, 26 (1979) 805.
4 H. Ma, L. Jin and H. Yan, Kexue Tongbao (Science Bulletin), 28 (1983) 1145.
5 T. P. Lynch, Analyst, 109 (1984) 421.
6 C. Okumoto, M. Nagashima, S. Mizoiri, M. Kazama and K. Akiyama, Eisei Kagaku, 30 (1984) 7.
7 P. Linares, M. D. Luque de Castro and M. Valcarcel, Anal. Chim. Acta, 161 (1984) 257.
8 P. W. Alexander, P. R. Haddad and M. Trojanowicz, Anal. Chem., 56 (1984) 2417.
9 H. Cui, Z. Zhu and Z. Fang, Huanjing Huaxue, 3 (1984) 48.
10 A. Rios, M. D. Luque de Castro and M. Valcarcel, Talanta, 31 (1984) 673.
11 The Environment Protection Bureau of the Chinese Ministry of City and Countryside

Construction and Environment Protection, Methods for Environmental Monitoring and Analysis, Technical Standard Press, Beijing, 1983, p. 94.
12 F. J. Welcher (Ed.), Standard Methods of Chemical Analysis, 6th edn., Van Nostrand, Princeton, NJ, 1963.
13 A. Watanabe, I. Ito and A. Hirakoba, Bunseki Kagaku, 26 (1977) 505.
14 The Environment Protection Bureau of the Chinese Ministry of City and Countryside Construction and Environment Protection, Standard Methods for Monitoring and Analysis of Pollution Sources (Waste Gases), Technical Standard Press, Beijing, 1983, p. 60.
15 H. Baadenhuijsen and H. E. H. Seuren-Jacobs, Clin. Chem., 25 (1979) 443.
16 J. Růžička and E. H. Hansen, Anal. Chim. Acta, 161 (1984) 1.
17 K. Ishii, T. Iwamoto and K. Yamanishi, Bunseki Kagaku, 22 (1973) 448.

Analytica Chimica Acta, 198 (1987) 37—44
Elsevier Science Publishers B.V., Amsterdam — Printed in The Netherlands

DETERMINATION OF ACETALDEHYDE BY FLOW INJECTION ANALYSIS WITH SOLUBLE OR IMMOBILIZED ALDEHYDE DEHYDROGENASE

ALA'DDIN M. ALMUAIBED and ALAN TOWNSHEND*
Department of Chemistry, University of Hull, Hull HU6 7RX (Great Britain)
(Received 22nd December 1986)

SUMMARY

Acetaldehyde (0.18—7.7 $\times 10^{-4}$ M) in water is determined by using a double injection technique with the soluble enzyme or with a mini-column of aldehyde dehydrogenase immobilized on cyanogen-activated Sepharose 4B. The NADH produced is monitored spectrophotometrically. The sample throughput is ca. 40 h^{-1}, and the immobilized enzyme is stable for at least a month. Ethanol up to 5% (v/v) does not interfere.

Various methods including spectrophotometry [1—3], a continuous flow procedure [4], automated distillation in connection with fluorimetry [5], and gas chromatography [6] have been reported for acetaldehyde determinations. Some spectrophotometric methods have drawbacks such as lack of sensitivity [1] and simplicity [2]. The continuous flow method is based on spectrophotometric detection of a blue colour when a solution of acetaldehyde, a secondary amine and sodium nitroprusside are mixed together. The method suffers from a low sampling rate and needs a modified sampler to prevent loss of acetaldehyde by volatilization.

Several enzymatic methods have been suggested for the determination of acetaldehyde [7—12]. Many [7—9] are based on the oxidation of reduced nicotinamide adenine dinucleotide (NADH) catalyzed by yeast alcohol dehydrogenase (ADH). The methods are not accurate at low concentrations of aldehyde because they involve the measurement of a small decrease in the large NADH absorbance, and the sensitivity is greatly decreased by the presence of large concentrations of ethanol. Other enzymatic methods involve the oxidation of acetaldehyde to acetate catalyzed by aldehyde dehydrogenase (AlDH) in the presence of NAD^+ [10—12]:

$$CH_3CHO + NAD^+ + OH^- \rightleftharpoons CH_3COO^- + H^+ + NADH$$

The NADH formed can be monitored spectrophotometrically at 340 nm or spectrofluorimetrically.

Recently, acetaldehyde has been determined by a flow-injection procedure based on the use of soluble aldehyde dehydrogenase (AlDH) [13].

0003-2670/87/$03.50

The method has drawbacks such as the high cost and rapid consumption of the enzyme, which justify attempts to immobilize the enzyme for use in the flow system. In this paper, therefore, two flow-injection systems are compared for acetaldehyde determination based on either immobilized AlDH or on-line injection of soluble enzyme. A double injection valve technique is used for the latter procedure, as an alternative method to the merging zones method reported by Lazaro et al. [13], for economizing on enzyme consumption. Both methods are simple, sensitive and reproducible, but the method based on the immobilized enzyme is more economic.

EXPERIMENTAL

Chemicals

Distilled deionized water was used throughout. Aldehyde dehydrogenase (potassium-activated from bakers yeast, EC. 1.2.1.5.; 20.6 U mg^{-1} solid), NAD^+ (free acid; 98%) and cyanogen bromide-activated Sepharose 4B were obtained from the Sigma Chemical Co. Acetaldehyde (May and Baker) was used to prepare an aqueous 4% (v/v) acetaldehyde solution which was standardized by iodometric back-titration [14]. The stock solution was kept in a refrigerator. Sodium pyrophosphate was used in the buffer solution, adjusted with sodium hydroxide to give the required pH [15].

Immobilization of aldehyde dehydrogenase

The AlDH was immobilized on cyanogen bromide-activated Sepharose 4B by the procedure described for α-chymotrypsin [16], in which 0.3 g of the activated Sepharose was added to 2.5 ml of 0.1 M sodium hydrogencarbonate containing 2 mg of AlDH. The mixture was gently stirred at 4°C for 24 h. A 0.05-g portion of glycine was added to the slurry, which was gently stirred for 12 h at 4°C, and filtered through a G-3 porosity sintered glass filter. The Sepharose-bound enzyme was washed in turn with 50 ml of water, 0.1 M sodium hydrogen carbonate and 0.5 M sodium chloride, and 100 ml of water. The resulting immobilized enzyme was packed into a glass column (2 × 25 mm). The beads were stored at 4°C in 1 ml of sodium pyrophosphate buffer, pH 7.0, containing 1×10^{-4} M dithiothreitol.

Apparatus and procedures

The absorbance was measured at 340 nm with an LKB Ultrospec II spectrophotometer connected to a Perkin-Elmer 56 chart recorder. The two injection valves were Rheodyne RH-5020 rotary valves (Anachem). The manifold and reaction coil tubing was 0.5 mm i.d. teflon. The pump was a Gilson Minipuls 2 (Anachem).

The manifolds used for acetaldehyde determination by the injected soluble enzyme technique and with the immobilized enzyme are shown in Figs. 1 and 2, respectively. Acetaldehyde solution (30 μl) was injected into the carrier stream, which was 0.15 M potassium chloride/9×10^{-4} M NAD^+/6×10^{-3} M 2-mercaptoethanol (for the immobilized enzyme only)/0.04 M

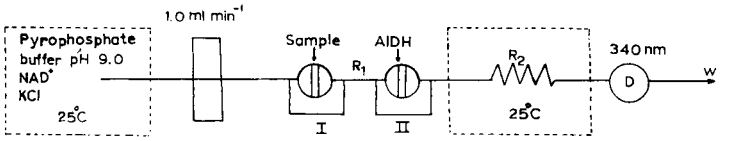

Fig. 1. Manifold for acetaldehyde determination: R_1, shortest possible connection (here 5 cm); R_2, 50-cm coil; D, detector; W, waste.

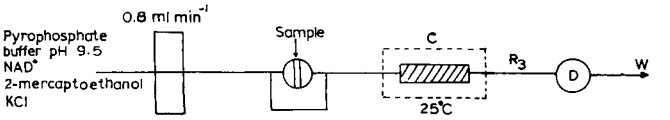

Fig. 2. Manifold for acetaldehyde determination: C, aldehyde dehydrogenase immobilized on cyanogen bromide-activated Sepharose 4B in a glass tube (2 × 25 mm); R_3, shortest possible connection (here 10 cm); W, waste.

sodium pyrophosphate. The carrier solution was adjusted to pH 9.0 (soluble enzyme) or pH 9.5 (immobilized enzyme) with sodium hydroxide solution. Soluble enzyme (0.08 U in 20 μl) in the pH 9.0 pyrophosphate buffer was injected by the second valve exactly 10 s after injection of the acetaldehyde (Fig. 1).

RESULTS

The double-injection and enzyme-immobilization techniques

The usual way to economize on the use of a reagent in flow injection analysis is to apply the merging-zones technique [17, 18] in which small volumes of sample and reagent are injected into different flow streams in such a way that when the streams combine, the samples and reagent zones merge. This has the advantage that diffusional mixing is no longer necessary, but the disadvantage that much of the sample is diluted. An alternative to this procedure is to join the two injectors in series in a single flow stream. As the sample zone, injected first, arrives at the second injection valve, the reagent is injected. Accurate timing of injections is required. Such a method was used in this investigation.

The effect of time between injections (5—20 s) was studied for the soluble enzyme system. It was found that any time between 10 and 15 s had no significant effect on the peak height for acetaldehyde, therefore 10 s was selected for use.

It has been reported that aldehyde dehydrogenase can be immobilized on glass beads by the carbodimide method [19]. Initially, therefore, attempts were made to immobilize it on controlled-pore glass by this method, but the resulting preparation had no activity. Instead, the dehydrogenase was immobilized on cyanogen bromide-activated Sepharose 4B by the procedure described for α-chymotrypsin [16] to give an active product.

Optimization

The effect of pH on the activity of the soluble and immobilized enzymes was examined by using sodium pyrophosphate buffer over the pH range 5.7—11.7. The results are shown in Fig. 3. Maximum activity was at ca. pH 9.0 for the soluble enzyme and pH 9.5—10 for the immobilized enzyme, compared to values of pH 8—10 [13] and 9.2 [20] found previously for the soluble enzymes; pH 9.0 and pH 9.5, therefore, were selected for further studies of the free and immobilized enzyme, respectively.

The effect of flow rate was studied over the range 0.6—2.0 ml min^{-1}. The results given in Fig. 4 show that slower flows result in greater absorbances, as would be expected because the acetaldehyde is in contact with the enzyme for longer periods. Thus 0.8 ml min^{-1} and 1.0 ml min^{-1} were selected for determinations with the immobilized and soluble enzyme, respectively.

Aldehyde dehydrogenase is somewhat heat-labile. Heating to >55°C causes rapid loss of activity [20]. The effect of temperature on the activity of both enzymes was studied. The results are shown in Fig. 5, on the basis of which 25°C was chosen for subsequent work. The immobilized enzyme column was replaced with a fresh one for further studies after these experiments.

The length of R_1 (Fig. 1) was the minimum required to connect the two injection valves. The length of R_3 (Fig. 2), likewise, was as short as possible to minimize dispersion of the NADH produced. The effect of the length of coil R_2 (Fig. 1) was investigated over the range 50—200 cm. It was found that the absorbance decreased slightly as the length of tube increased, attributed to dispersion. Thus 50 cm was selected for further studies.

Potassium ions play an important role in the activation of aldehyde

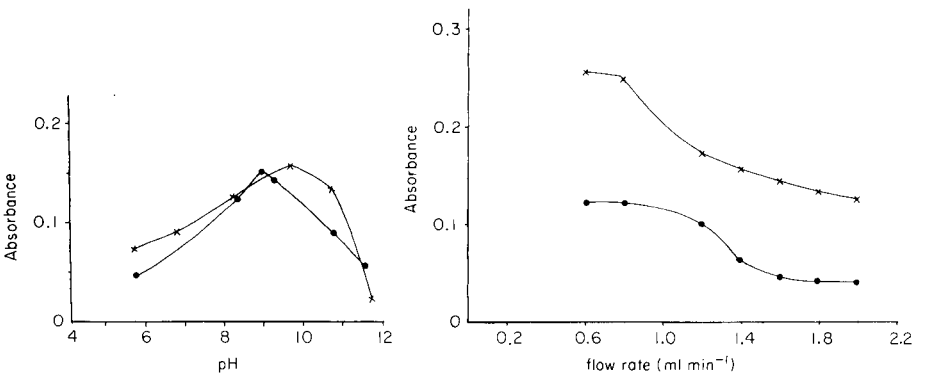

Fig. 3. Effect of pH on the activity of the enzyme: (•) soluble; (×) immobilized. (18 μg ml^{-1} acetaldehyde in both cases.)

Fig. 4. Effect of flow rate on the absorbance: (•) soluble enzyme, 12.0 μg ml^{-1} acetaldehyde; (×) immobilized enzyme, 24 μg ml^{-1} acetaldehyde.

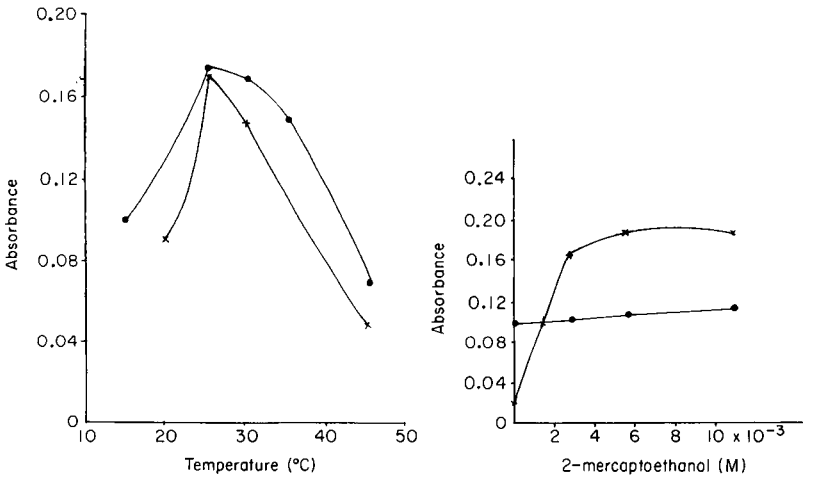

Fig. 5 Effect of temperature on activity of the enzyme: (•) soluble; (×) immobilized. (18 μg ml^{-1} acetaldehyde in both cases.)

Fig. 6. Effect of 2-mercaptoethanol concentration on the activity of the enzyme: (•) soluble, 12.0 μg ml^{-1} acetaldehyde; (×) immobilized, 18 μg ml^{-1} acetaldehyde.

dehydrogenase. Two mechanisms of activation by potassium ions have been proposed, one in which the ion binds to and forms an essential part of the catalytic structure of the active site [21], and the other in which the ion induces or stabilizes the active conformation [22]. In the present work, a study of the effect of different concentrations of potassium chloride on the activity of the soluble and immobilized enzymes confirmed that potassium was essential for enzyme activation. The absorbance increased swiftly with increasing concentration of potassium chloride up to 0.15 M in both systems, but there was no significant change in the range 0.15—0.5 M.

It has been reported that the addition of a thiol such as glutathione, thioglycollate or cysteine is essential for the activity of the potassium-activated enzyme from yeast [23]. This was not mentioned or used by Lazaro et al. [13]. It has been suggested that the thiol group might bind inhibiting heavy metals [23], act as a link between enzyme and co-enzyme [24] or form a bond between enzyme and oxidized co-enzyme subject to cleavage by the substrate [25]. The effect of different concentrations of 2-mercaptoethanol [12] on the activity of soluble and insoluble enzyme was investigated over the range 1.4—11 × 10^{-3} M. It was found that mercaptoethanol had no effect on the activity of the soluble enzyme but was essential for activation of the immobilized enzyme. In the latter system, the absorbance increased with increasing concentration of mercaptoethanol in the carrier stream up to 4 × 10^{-3} M, above which the absorbance approached a plateau. The results are shown in Fig. 6 for a fresh column of enzyme. Interestingly, after the column had been activated in this way, it could be

used satisfactorily for ca. 40 samples without the need to add mercaptoethanol.

Naturally, NAD^+ has a significant effect on the absorbance [13], therefore the effect of different concentrations of NAD^+ over the range $1.5—12 \times 10^{-4}$ M was investigated in both systems. The absorbance for 18 μg ml^{-1} (4×10^{-4} M) acetaldehyde increased with increasing NAD^+ concentration until it became constant at 6×10^{-4} M in both systems. Therefore 9×10^{-4} M was used for further studies. The absorbance increased with increasing amount of soluble enzyme up to 0.02 U, above which any increase had no significant effect on the peak height; 0.08 U was selected for further work.

The effect of different concentrations of ethanol on the activity of immobilized aldehyde dehydrogenase was investigated. Ethanol up to 5% (v/v) had no effect on the peak heights for 18 μg ml^{-1} acetaldehyde.

Analytical performance

When solutions of acetaldehyde prepared in 0.04 M sodium pyrophosphate buffer, pH 9.0 (soluble enzyme) or pH 9.5 (immobilized enzyme), were injected into the manifold shown in Figs. 1 or 2, linear calibration graphs were obtained over the range 6—31 μg ml^{-1} ($14—70 \times 10^{-5}$ M, r = 0.999, n = 12) and 6—37 μg ml^{-1} ($14—84 \times 10^{-5}$ M, r = 0.999, n = 14) with the soluble and immobilized enzyme, respectively. The sample throughput and detection limit (2 × noise) were 45 h^{-1} and 30 ng (in 30 μl) for the soluble enzyme and 40 h^{-1} and 20 ng (in 30 μl) for the immobilized enzyme. Figure 7 shows calibration graphs and peaks for acetaldehyde

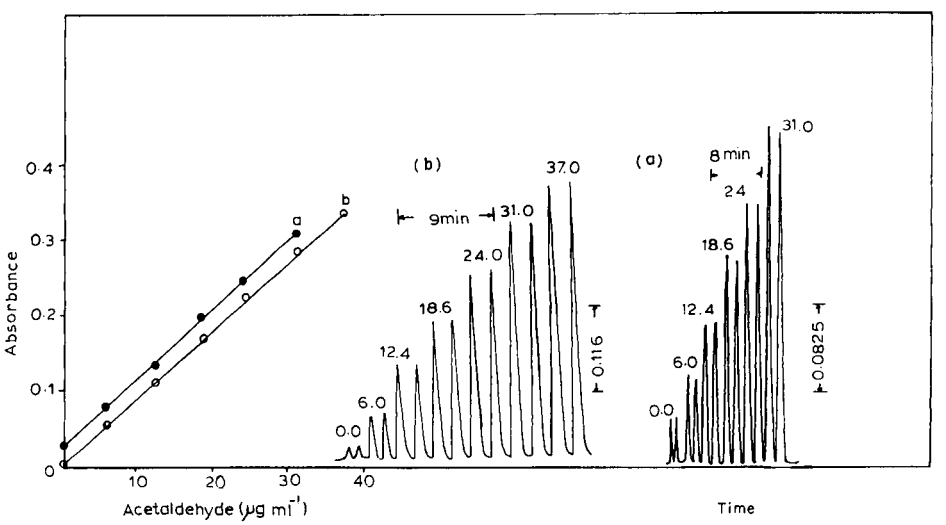

Fig. 7. Calibration graphs and peaks for acetaldehyde: (a) soluble enzyme; (b) immobilized enzyme. Numbers on the peaks are μg ml^{-1} acetaldehyde.

determination by both methods. The soluble enzyme method has a higher blank value than the immobilized enzyme method. This might be due to some impurities such as NADH which are present in the soluble enzyme.

Aldehyde dehydrogenase immobilized in cyanogen bromide-activated Sepharose 4B showed high stability. The same column could be used at 25°C for a month without any loss in activity. The column was kept in the pH 7.0 pyrophosphate buffer at 4°C when not in use.

Conclusions

In comparison with the soluble enzyme flow-injection method for acetaldehyde reported recently [13], the methods described offer a number of advantages such as a longer linear range (0.6—34 μg ml^{-1}, compared with 1—8 μg ml^{-1}). The use of immobilized aldehyde dehydrogenase makes the determination of acetaldehyde more economic and simpler than with the soluble enzyme, and the blank signal is smaller.

A. M. Almuaibed thanks the Iraqi Government (Ministry of Higher Education and Scientific Research), University of Salahalddin, for financial support.

REFERENCES

1 D. I. Belkin, G. V. Kravchenko and M. Ya. Rozkin, Zh. Anal. Khim., 31 (1980) 1022.
2 G. P. Arsenault and W. Yaphe, Anal. Chem., 38 (1966) 503.
3 S. Flamerz and W. A. Bashir, Anal. Chem., 54 (1982) 1734.
4 A. T. Taylor and M. E. Northmore, Automation in Analytical Chemistry, Technicon Symposia, Vol. VII, Medical Inc., New York, 1971, pp. 263, 1667.
5 A. R. Stowell, K. E. Crow, R. M. Greenway and R. D. Batt, Anal. Biochem., 84 (1978) 384.
6 M. A. Korsten, S. Matsuzaki, S. Feinman and C. S. Lieber, N. Engl. J. Med., 292 (1975) 386.
7 E. Racker, in S. P. Colowick and N. O. Kaplan (Eds.), Methods in Enzymology, Vol. III, Academic, New York, 1957, p. 295.
8 H. Holzer, E. Holzer and G. Schulz, Biochem. Z., 326 (1955) 385.
9 E. Bernt and H. U. Bergmeyer, in H. U. Bergmeyer (Ed.), Methods of Enzymatic Analysis, 2nd edn., Vol. 3, Verlag Chemie, Weinheim, 1974, p. 1506.
10 S. Black, Arch. Biochem. Biophys., 34 (1951) 86.
11 S. Black, in S. P. Colowick and N. O. Kaplan (Eds.), Methods in Enzymology, Vol. I, Academic, New York, 1955, p. 508.
12 F. Lundquist, in H. U. Bergmeyer (Ed.), Methods of Enzymatic Analysis, 2nd edn., Vol. 3, Verlag Chemie, Weinheim, 1974, p. 1509.
13 F. Lazaro, M. D. Luque de Castro and M. Valcárcel, Anal. Chim. Acta, 185 (1986) 57.
14 A. E. Parkinson and E. C. Wagner, Ind. Eng. Chem., 6 (1934) 433.
15 D. D. Perrin and B. Dempsey, Buffers for pH and Metal Ion Control, Chapman and Hall, London, 1974, p. 142, Table 10.31.
16 J. Porath, K. Aspberg, H. Drevin and R. Axen, J. Chromatogr., 86 (1973) 53.
17 J. Mindegaard, Anal. Chim. Acta, 104 (1979) 185.
18 H. Bergamin F°, E. A. G. Zagatto, F. J. Krug and B. F. Reis, Anal. Chim. Acta, 101 (1978) 17.
19 Chi-Yu Lee, J. Solid-Phase Biochem., 3 (1978) 71.

20 E. Racker, J. Biol. Chem., 177 (1949) 883.
21 C. H. Suelter, Science, 168 (1970) 789.
22 H. J. Evans and G. J. Sorger, Ann. Rev. Plant Physiol., 17 (1966) 17.
23 A. O. M. Stoppani and C. Milsten, Biochem. J., 67 (1957) 406.
24 J. Vaneys and N. O. Kaplan, Biochem. Biophys. Acta, 23 (1957) 574.
25 E. Racker, Physiol. Rev., 35 (1955) 1.

Analytica Chimica Acta, 198 (1987) 45—51
Elsevier Science Publishers B.V., Amsterdam — Printed in The Netherlands

FLOW-INJECTION AMPLIFICATION FOR THE SPECTROPHOTOMETRIC DETERMINATION OF IODIDE

A. AL-WEHAID and A. TOWNSHEND*
Chemistry Department, University of Hull, Hull HU6 7RX (Great Britain)
(Received 12th November 1986)

SUMMARY

A flow manifold is described in which iodide (0.05—15 $\mu g\ ml^{-1}$) in a 50-μl sample is oxidized by bromine water to iodate, most of the excess of bromine is reduced by formic acid, and the iodate is reacted with more iodide to form triiodide, which is determined spectrophotometrically. Six-fold amplification is achieved. The relative standard deviation is ca. 1%).

Many methods have been proposed for determining traces of iodide. In flow injection analysis, iodide has been determined by spectrophotometry [1—4] and amperometry [5—7] and with an ion-selective electrode [8]. Of the spectrophotometric procedures, Deguchi et al. [1, 2] used iodide catalysis of the cerium(IV)/arsenic(III) reaction, Miyazaki et al. [3] applied fluorescein as a reagent in the presence of an oxidant, and Kamson [4] utilized the reaction with iodate.

The sensitivity of iodide determinations can be increased six-fold compared to its determination by direct oxidation to iodine if iodide is first oxidized to iodate (usually with bromine water) which, in turn is reduced by adding an excess of iodide in an acidic medium:

$$I^- + 3Br_2 + 3H_2O \rightarrow IO_3^- + 6Br^- + 6H^+;\ IO_3^- + 5I^- + 6H^+ \rightarrow 3I_2 + 3H_2O$$

Unconsumed bromine can be removed by boiling, by bromination of phenol or, most commonly, by reduction with formic acid before the excess of iodide is added. This is the so-called Leipert reaction [9].

In this paper, the advantages of flow injection analysis (simplicity, high precision, rapidity and low reagent consumption) are combined with the benefits of amplification for the spectrophotometric determination of iodide.

EXPERIMENTAL

The flow-injection manifold used is shown in Fig. 1. Two Ismatec Mini S820 peristaltic pumps were used to deliver the reagents and water carrier stream. Iodide samples were introduced via a Rheodyne RH-5020 injection valve (Anachem) with a 50-μl sample volume. Teflon tubing (0.5 mm i.d.)

0003-2670/87/$03.50

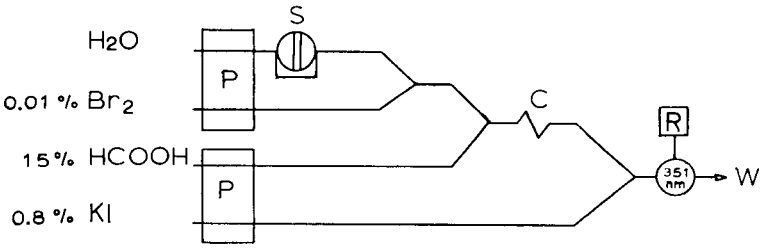

Fig. 1. Manifold for iodide determination; P, pump; S, sample injector; C, 100-cm coil; R, recorder; W, waste. The recommended flow rates are 0.50 ml min^{-1} for the water (sample) stream, 0.50 ml min^{-1} for the bromine solution, 0.3 ml min^{-1} for the formic acid solution, and 0.6 ml min^{-1} for the potassium iodide solution.

was used for the manifold. The triiodide formed was measured at 351 nm in a Cecil CE 373 spectrophotometer provided with an 18-μl flow cell and connected to a chart recorder.

All reagents were AnalaR (BDH) and distilled/deionized water was used throughout. Bromine (99.5%) was used to prepare the bromine solutions by dissolution in water. Formic acid solutions were prepared by dilution of the 90% (w/v) acid with water. A stock solution of 1000 μg ml^{-1} (7.88×10^{-3} M) iodide was prepared by dissolving exactly 1.308 g of potassium iodide in water, and diluting to exactly 1 l. Working standards were prepared by appropriate dilution with water to cover the range 0—5 μg ml^{-1} iodide (0—3.9×10^{-5} M). The 0.8% (w/v) potassium iodide solution was prepared daily in water.

RESULTS AND DISCUSSION

Effect of variables

In the first stages of this work, iodide samples were injected directly into a stream of bromine solution using the manifold in Fig. 1 without the water channel. Better sensitivity was achieved when iodide samples were injected into a water stream which later merged with a bromine solution (Fig. 1). The faster mixing thus achieved allowed a shorter manifold to be used, so that dispersion was less and sensitivity was increased. The excess of bromine was removed by merging with a formic acid stream. Merging with a potassium iodide stream then produced triiodide (I_3^-) which was monitored spectrophotometrically.

In order to optimize the method, two main features were investigated: one was the peak-height absorbance produced on injecting an iodide sample, the other was the reduction of the bromine water by formic acid to ensure that the background signal produced on mixing with the final iodide stream is reasonably small. The background reaction was investigated first, to establish conditions that would give a small background absorbance but allow maximum sensitivity for iodide. In all the following experiments, the flow

rate was 0.35 ml min^{-1} in the sample channel and 0.5 ml min^{-1} in each of the other channels.

The background absorbance depends mainly on two factors, time (i.e., flow rate and coil length) and formic acid concentration. For example, when 0.01% bromine solution at 0.5 ml min^{-1} merges with 5% formic acid at 0.5 ml min^{-1}, the background absorbance decreases as the length of coil C (Fig. 1) increases, i.e., as the reaction time increases (Fig. 2). The background absorbance also decreases as the formic acid concentration increases at fixed flow rates and coil length (Fig. 3). The background absorbance must be diminished to a reasonable level so that the signal can be backed off. This can be done by increasing either the coil length or formic acid concentration at fixed flow rates. The first option will cause more dispersion of injected samples; for example, with 10 μg ml^{-1} iodide samples at fixed (30%) formic acid concentration, the use of a 75-cm or 100-cm coil gave a peak-height absorbance of 0.54, but use of a 200-cm coil decreased this absorbance to 0.51. Therefore a 100-cm bromine reduction coil was selected.

The effect of bromine water concentration was evaluated at a 0.5 ml min^{-1} flow rate for injections of a 50 μg ml^{-1} iodide solution (50 μl). The same absorbance (ca. 2.5) was achieved in the range 0.01—0.1% (v/v) bromine solution, therefore 0.01% was used subsequently. The use of a coil to increase the time for iodide oxidation was also investigated. There was a slight decrease in peak height as the coil length was increased from 5 to 100 cm but it was very much less than would be expected from dispersion alone

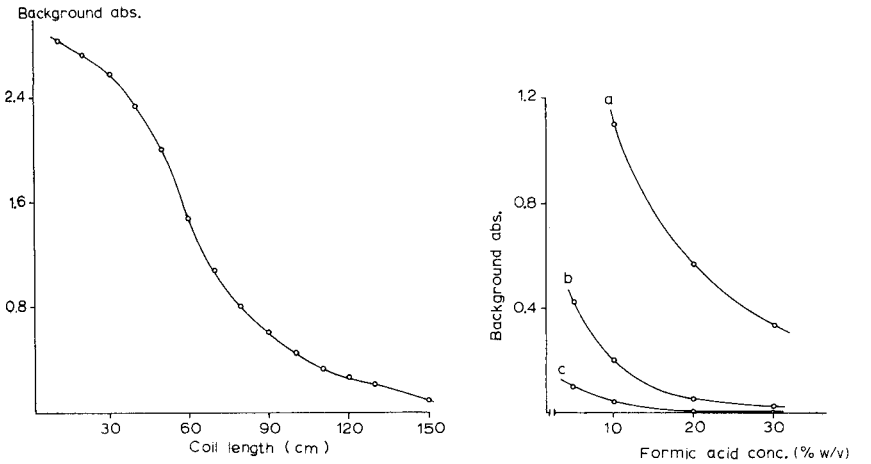

Fig. 2. Effect of bromine reduction coil length on background absorbance. (5% formic acid, 0.01% bromine, 0.7% potassium iodide solutions.)

Fig. 3. Effect of formic acid concentration on background absorbance for different reduction coil lengths: (a) 50; (b) 100; (c) 150 cm. (0.01% bromine, 0.7% potassium iodide solutions.)

(which was shown to cause a 20% decrease in peak height as the coil length increased from 50 to 100 cm in this manifold). The effects of increased oxidation time and dispersion were almost in balance, so that there was no overall increase in sensitivity; therefore an additional coil was not incorporated at this point. The effect of formic acid concentration was also evaluated. Under the conditions used, $\geqslant$15% (v/v) formic acid concentrations gave similar results for 10 μg ml^{-1} iodide, as well as a low background absorbance of ca. 0.1 (Fig. 3); lower concentrations of formic acid (5—10%, w/v) gave gradually decreased absorbances. The concentration of potassium iodide added in the final stage was examined in the range 0.1—1.0% (w/v); the measured absorbances increased gradually over this range and maximum absorbance for 50 μg ml^{-1} iodide was found with 0.8—1.0% (w/v) potassium iodide. The reaction between iodate and iodide is rapid and therefore takes place quickly after merging. Including a coil of 30—60-cm length after the merging point caused a decrease of about 30% in peak height; thus the minimum distance between the merging point and the detector (ca. 25 cm) gave the maximum peak-height absorbance.

The flow rate in each channel shown in Fig. 1 was studied individually to obtain the best overall flow rate in terms of sensitivity, sampling rate and reagent consumption. When the other three flow rates were 0.5 ml min^{-1}, increasing the sample stream flow rate from 0.1 to ca. 0.7 ml min^{-1} resulted in an increase in sensitivity (curve a, Fig. 4) and sample throughput but the sensitivity decreased at higher flow rates. The general form of curve (a) was unexpected, therefore a simpler set-up consisting of a pump, injection valve, two water streams meeting at a T-junction and a spectrophotometer was assembled, and a blue dye was injected into one stream in order to investigate this effect in more detail. When the sample stream flow rate was increased gradually up to 1.6 ml min^{-1}, and the flow rate in the other channel was kept constant at 0.5 ml min^{-1}, again there was an increase in the peak height absorbance as the flow rate increased. The peak shapes obtained during these experiments are shown in Fig. 5. At low flow rates in the sample channel, the peaks are drawn out, but become narrower and higher as the flow rate increases. When the sample channel flow rate was kept constant and the flow rate of the merging stream was increased, the peak height progressively decreased (Fig. 5). The change in peak height in both experiments is shown in Fig. 6. The reasons for these effects are illustrated in Fig. 7. When the flows in both channels are similar, reproducible and fast mixing is achieved in the T-piece (Fig. 7c). As the sample channel flow rate decreases, however, its flow into the exit stream is restricted, leading to the drawn-out peaks (Fig. 7a).

Figure 4 (curves b and c) shows the effects of changing the flow rates of the formic acid and potassium iodide streams. The maximum peak-height absorbance is achieved with a flow rate of ca. 0.6 ml min^{-1} for the potassium iodide stream (curve c). The sensitivity decreases as the flow rate of the formic acid stream increases (curve b).

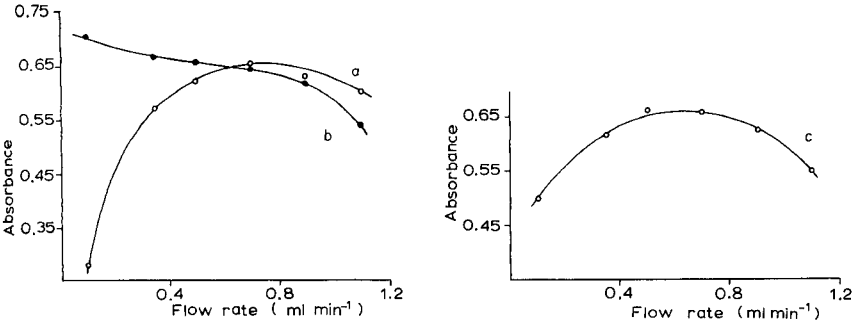

Fig 4. Effect of flow rates on peak-height absorbance for 10 μg ml^{-1} iodide: (a) sample stream; (b) formic acid stream; (c) potassium iodide stream. (Concentrations as in Fig. 1; other streams held at 0.5 ml min^{-1}.)

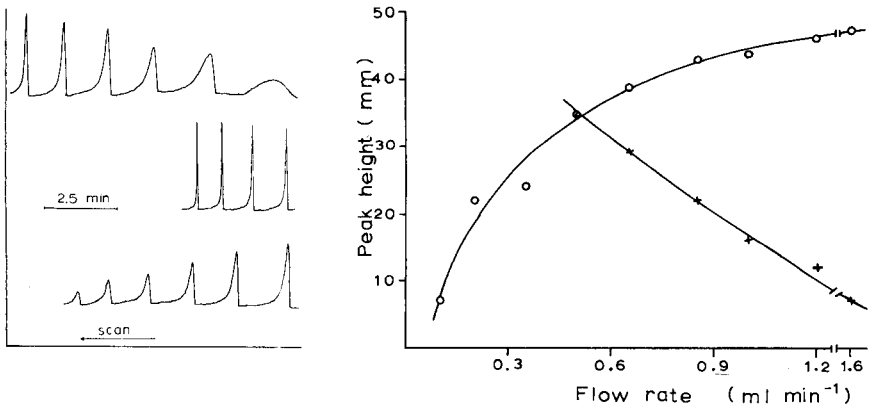

Fig. 5. Peaks obtained for methylene blue with increasing flow rate in the sample stream (top rows, second row follows on from first row) and in the merging stream (bottom row). Flow rate increases from right to left; values are given in Fig. 6. The manifold used is outlined in Fig. 7.

Fig. 6. Effect of flow rate in: (○) sample stream, (×) merging stream. (Flow rate in other stream is 0.5 ml min^{-1}.)

The effect of using a buffer solution with pH values covering the range 5.9—8.0 and prepared by mixing appropriate volumes of 0.1 M potassium dihydrogenphosphate and 0.1 M sodium hydroxide [10], in place of the water stream, was also investigated. There was no difference in absorbance over that pH range from that achieved by use of the water carrier. The conditions given in Fig. 1 are those recommended on the basis of all the above results. The background absorbance under these conditions was 0.09.

Analytical performance

The calibration peaks for iodide in the range 1—5 μg ml^{-1} (0.7—3.9

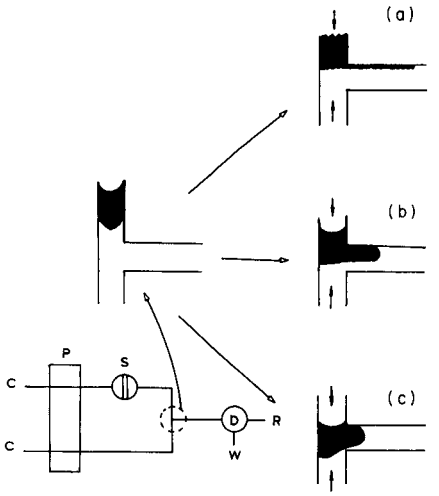

Fig. 7. Diagram illustrating the effect of increasing sample flow rate on mixing of dye sample with merging stream (at 0.5 ml min^{-1}) at a T-junction. Sample flow rates: (a) 0.1 ml min^{-1}; (b) 0.2 ml min^{-1}; (c) 0.5 ml min^{-1}. The manifold used is also shown.

$\times 10^{-5}$ M) obtained under the recommended conditions were of similar shape to those shown centrally in Fig. 5. The calibration graph was linear up to at least 5 μg ml^{-1} iodide with a correlation coefficient (6 points) of 1.00. The least-squares calibration equation is: peak-height absorbance = 5.99×10^{-2} [μg I^- ml^{-1}] + 1.19×10^{-3}. The detection limit (2 $\times$ noise) is 50 ng ml^{-1} (3.9×10^{-7} M) and the sample injection rate is 52 h^{-1}. The relative standard deviation is 1.1% for 5 μg ml^{-1} iodide and 0.53% for 15 μg ml^{-1} iodide (both 10 injections). The overall dispersion of the system was 3.9.

An interference study showed that sodium, copper, iron(II) and chloride ions had no effect at the 100 μg ml^{-1} level on the response of 5 μg ml^{-1} iodide. Azide ions interfered seriously at this level, causing a peak height absorbance of 0.60 for a 5 μg ml^{-1} iodide solution compared to 0.29 for iodide alone, and gave a peak in the absence of iodide. Thiocyanate ions had the opposite effect, and at 100 μg ml^{-1} gave a negative peak equivalent to the background absorbance.

Conclusions

A useful amplification procedure has been achieved by taking advantage of flow injection. Three reactions take place in sequence in the manifold to achieve six-fold amplification, without complete removal of the excess of bromine. Further work is continuing, including the use of a solid-phase oxidant to replace the bromine channel, and thus make the formic acid channel superfluous. Eventually, attempts to cycle the system will be made, so that the iodine formed is recycled, to achieve 36-fold or 216-fold amplification.

REFERENCES

1 T. Deguchi, A. Tanaka, I. Sanemasa and H. Nagai, Bunseki Kagaku, 32 (1983) 23.
2 A. Tanaka, M. Miyazaki and T. Deguchi, Anal. Lett., 18 (1985) 695.
3 M. Miyazaki, N. Okubo, K. Hayakawa and T. Umeda, Chem. Pharm. Bull., 32 (1984) 3702.
4 O. F. Kamson, Anal. Chim. Acta, 179 (1986) 475.
5 K. W. Pratt and D. C. Johnson, Anal. Chim. Acta, 148 (1983) 87.
6 D. MacKoul, D. C. Johnson and K. G. Schick, Anal. Chem., 56 (1984) 436.
7 H. Ma and H. Yan, K'o Hsueh T'ung Pao, 27 (1982) 959.
8 J. Slanina, W. A. Lingerak and F. Bakker, Anal. Chim. Acta, 117 (1980) 91.
9 T. Leipert, Mikrochem., Pregl Festschrift, (1929) 266.
10 D. D. Perrin and B. Dempsey, Buffers for pH and Metal Ion Control, Chapman and Hall, London, 1974, p. 139.

Analytica Chimica Acta, 198 (1987) 53—61
Elsevier Science Publishers B.V., Amsterdam — Printed in The Netherlands

SPECTROSCOPIC STUDY OF THE ALUMINIUM/LUMOGALLION SYSTEM IN THE PRESENCE OF NON-IONIC SURFACTANTS

J. L. CARRIÓN DOMINGUEZ and M. DE LA GUARDIA CIRUGEDA*

Department of Analytical Chemistry, Faculty of Chemistry, University of Valencia, Burjasot, Valencia (Spain)

(Received 30th July 1986)

SUMMARY

The effects of different non-ionic ethylene oxide condensate surfactants on the fluorescence and the molecular absorption of the aluminium/lumogallion system are reported. Ethylene oxide condensates with fatty alcohols give higher micellar enhancement factors than tert-octylphenols or nonylphenols; ethylene oxide/propylene oxide copolymers provide only a 50% increase in the fluorescence of the complex. The aluminium/lumogallion seems to form mixed micelles with the fatty alcohol condensates; the strong complex/micelle interaction provides increased absorbance of the complex at 500 nm and higher fluorescence enhancement, allowing the detection of 0.11 $\mu g\ l^{-1}$ aluminium.

Among the analytical applications of surface-active agents [1], it is well known that micellar media can provide bathochromic and hyperchromic effects in the spectrophotometry of many metal chelates, so that more sensitive determinations become possible. Such increases in sensitivity are obtained in the presence of cationic and non-ionic surfactants at concentrations greater than the critical micellar concentration (c.m.c.). In the presence of anionic surfactants, a high ionic strength is required to achieve these phenomena [2].

In the case of fluorescent compounds, the use of micellar media can permit more sensitive determinations of organic molecules [3, 4], as well as metal ions through the formation of fluorescent chelates [5—7]. This fluorescence enhancement by the micellar microenvironment can be interpreted in terms of protection of the excited singlet state of the fluorogenic molecule from non-fluorescent deactivations [3, 4].

In the presence of ionic surfactants, it seems that the increased sensitivity is due to electrostatic interactions between the hydrophilic radicals of the monomers which form the micelles having a positive or a negative charge, and the charged metal complexes [4—8]. The interaction of a metal complex with uncharged micelles is not specific, because electrostatic interactions do not exist. However, there exists a certain selectivity for each system in terms of steric factors, and because of competitive interaction between the free ligand and the complex with the micelles [9]. The solubilization of the

0003-2670/87/$03.50

complex and/or of the ligand in the micelle is due to Van der Waals interactions. These are of the dipole-dipole type with formation of hydrogen bonds between hydroxyl groups of the ligand and the ether groups of an oxyethylenated chain [7]. To obtain better sensitivity for the fluorescence or the absorption of a complex, the micelles must be of a certain size and shape, i.e., the choice of surfactant [10—12] is a decisive factor in achieving higher sensitivity of the determinations. Under certain conditions, the interaction with the micelles will be more favourable with the ligand and in others with the complex. Previous studies [9] have shown that the metal ion/ligand mole ratio and the concentration as well as the nature of the surfactant, can have remarkable effects on sensitization of the systems.

In order to establish the conditions in which the spectrophotometric determination of metal complexes are sensitized and the characteristics which the surfactants should possess for this purpose, the present study is concerned with the influence of the nature and the condensation degree of different non-ionic ethylene oxide condensate surfactants on the fluorescence and on the absorption of the aluminium/lumogallion system, previously described by Ishibashi and Kina [13].

EXPERIMENTAL

Apparatus and reagents

A Shimadzu RF-520 double-beam spectrofluorimeter with 1-cm pathlength cells was used for recording the fluorescence spectra. The absorption spectra were recorded with a Shimadzu UV-240 double-beam spectrophotometer, equipped with 1-cm path length cells.

The aluminium solution (10 mg l^{-1}) was prepared by dissolving 0.1760 g of $AlK(SO_4)_2 \cdot 12H_2O$ (Merck; analytical-reagent grade) in water, adding 1% (v/v) sulphuric acid and diluting to 1 l with water. A 10^{-3} M solution of lumogallion (ICN Pharmaceuticals; analytical-reagent grade) was prepared by dissolving 34 mg in 100 ml of water. An acetic/acetate buffer of pH 5 was used. Aqueous 15% (w/v) solutions of the following non-ionic surfactants and polyethylene glycols were used: (a) the nonylphenol ethylene oxide condensates, Nemol K-36, K-1032, K-1035, K-2030 and K-3030 (Massó and Carol), with average numbers of ethylene oxide molecules of 7.2, 13.4, 17.8, 25.8 and 36.4, respectively, characterized by nuclear magnetic resonance (n.m.r.) [14] and u.v. spectroscopy [15]; (b) the tert-octylphenol ethylene oxide condensates, Triton X-114, X-100 and X-405 (Fluka) with average condensation degrees of 7.8, 10.2 and 44.2, respectively, characterized by n.m.r. and u.v. spectroscopy [16]; (c) the ethylene oxide/propylene oxide condensates, Genapol PF-10, PF-20 and PF-40 (Hoechst) with average molecular weights of 2080, 2420 and 2840, respectively, and ethylene oxide/propylene oxide mole ratios of 0.23, 0.57 and 1.01, respectively, determined by n.m.r. [17], as well as Genapol PF-80 (Hoechst) with an average molecular weight of 8100 and 80% ethylene oxide; (d) the ethylene oxide/fatty alcohols condensates,

Dehscoxid 650, 728 and 729 (Tensia Surfac), containing 4.5, 8.5 and 23 moles of ethylene oxide, respectively, according to the manufacturer specifications; and (e) polyethylene glycols PEG-200, PEG-400 and PEG-600 (ICI Pharma), with average condensation degrees of 4.05, 8.55 and 11.5, respectively, determined by the hydroxyl index obtained experimentally [18, 19], as well as PEG-6000 (ICI Pharma) with an average molecular weight between 5800 and 6800, according to the manufacturer's specifications.

General procedures

Fluorimetric study. In order to study the influence of the nature and the degree of condensation of different non-ionic surfactants on the fluorescence of the aluminium/lumogallion complex, calibration curves were prepared; for this, aliquots (0—0.3 ml) of a 10 mg l^{-1} aluminium solution were placed in 25-ml volumetric flasks, and 10 ml of distilled water, 0.25 ml of 10^{-3} M of lumogallion solution and 1.25 ml of acetate buffer pH 5 were added. These solutions were heated at 75°C for 60 min; when they were cool, 2.5 ml of an aqueous 15% (w/v) solution of the surfactant studied was added and the solution was diluted to volume with distilled water. The emission spectra were recorded at the maximum excitation wavelength of each system, against a distilled water blank; 10-nm slits were used for both excitation and emission. The sensitivity of the spectrofluorimeter was adjusted for a solution containing 80 μg l^{-1} aluminium in the absence of surfactant, prepared as described above. The fluorescence was measured an hour after the solutions had been prepared.

Spectrophotometric study. The absorbances of the solutions, prepared as described above, were measured at 500 nm against a water blank. Solutions with greater concentrations were also prepared in order to study the effect of the surfactant concentrations on the absorbances.

Determination of the c.m.c. In order to determine the c.m.c. of the surfactants studied in the presence of the aluminium/lumogallion complex, solutions were prepared as described above, containing 80 μg l^{-1} aluminium, 10^{-5} M lumogallion and surfactant concentrations between 4×10^{-3} and 0.1% (w/v). The c.m.c. of the surfactants was also determined in the same medium in the absence of the complex. In the method used, the average weight of 25 drops of each solution was obtained from five series of measurements. As the surface tension is proportional to the weight of a known volume of solution, if all the experimental conditions are kept constant, the c.m.c. can be evaluated from the break in the plot of this average weight versus the concentration of surfactant.

In order to achieve monomer/micelle equilibrium, all the measurements were made 24 h after preparation of the solutions, in the same session, and at a constant temperature of 20°C.

RESULTS AND DISCUSSION

Study of the fluorescence

Influence of surfactant concentration. The influence of the concentration of different surfactants and polyethylene glycols on the fluorescence intensity of solutions containing 80 $\mu g\ l^{-1}$ aluminium and 10^{-5} M lumogallion can be observed in Fig. 1; the c.m.c. for each system considered is also indicated.

In the presence of Nemol K-1032, Triton X-100 and Dehscoxid 728, the fluorescence increases at surfactant concentrations close to the c.m.c., although higher concentrations are required to achieve maximum enhancement. The fluorescence intensities of the system stabilize at a surfactant concentration of 1% (w/v) for Nemol K-1032 and Triton X-100, and for greater concentrations of Dehscoxid 728, providing then the same type of variation in the fluorescence with surfactant concentration as that observed in the presence of PEG-6000 and Genapol PF-80. These gradual increases are attributable

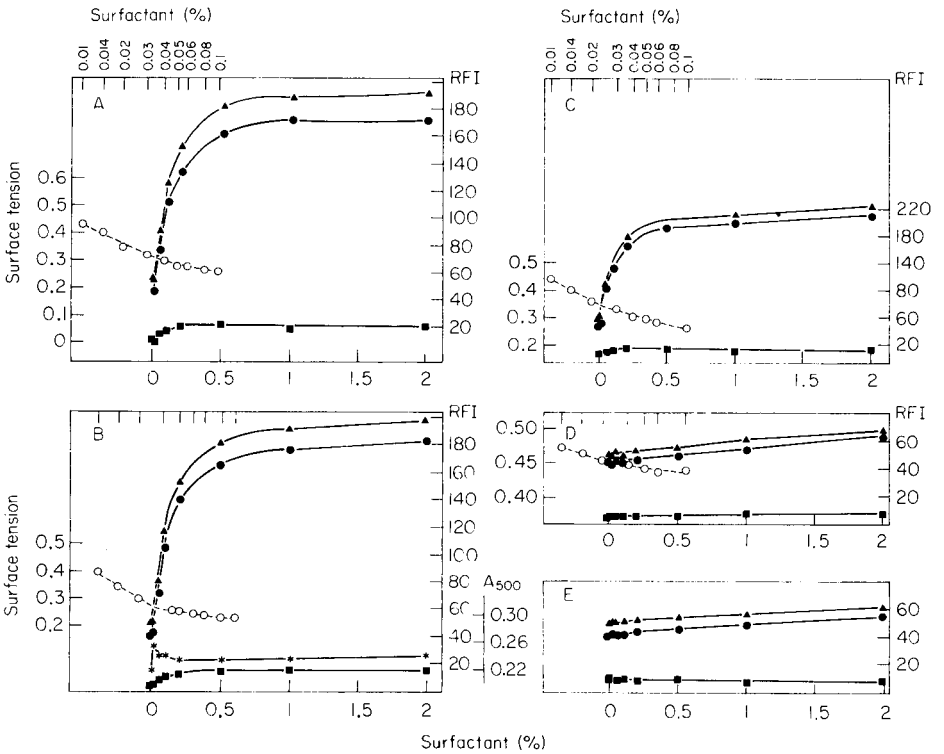

Fig. 1. Influence of the concentration of different surfactants and PEGs on the relative fluorescence intensity (RFI) of aluminium/lumogallion solutions: (A) Nemol K-1032; (B) Triton X-100; (C) Dehscoxid 728; (D) Genapol PF-80; (E) PEG-6000. Curves: (○) surface tension values in presence of the complex; (▲) fluorescence of the aluminium/lumogallion complex; (■) lumogallion fluorescence; (●) net fluorescence of aluminium/lumogallion complex. (*) Absorbance of the aluminium/lumogallion complex at 500 nm.

to the increased viscosity produced at the higher concentrations. As can be seen in Fig. 1(A—E) the complex and the ligand compete in their interaction with the micelles. The ligand requires a surfactant concentration only slightly higher than the c.m.c. to achieve optimum interaction with the micelles, whereas the complex requires a significantly higher concentration to give maximum fluorescence. The viscous effect at high surfactant concentrations is not appreciable for lumogallion alone. In all cases, the increase in fluorescence of the complex is much higher than that of the lumogallion alone.

For solutions containing Genapol PF-80, there is a slight increase in fluorescence at concentrations higher than the c.m.c. (Fig. 1D). The ligand does not interact with the micelles to any significant extent. In the case of increasing concentration of PEG-6000, the slight increase in the fluorescence of the complex can be ascribed to increased solution viscosity, and there is no variation in the fluorescence of the ligand.

Based on these results, a 1.5% (w/v) surfactant concentration was chosen to study further effects on the fluorescence of the aluminium/lumogallion complex.

The c.m.c. values obtained in the presence and in the absence of the complex are compared in Table 1. There was no appreciable change in c.m.c. values for Nemol K-1032, Triton X-100 and Genapol PF-80. For Dehscoxid 728, the c.m.c. was lower in the presence of the complex, suggesting that mixed micelles were formed.

Influence of temperature. The variation of the slope of aluminium calibration graphs prepared with 10^{-5} M lumogallion and 1.5% (w/v) Triton X-100 as a function of the temperature is presented in Fig. 2. The fluorescence intensity of the system reaches a maximum at 25°C and gradually decreases at higher temperatures. This variation with temperature can be interpreted on the basis of an optimum size and structure of the micelle [4] for maximal complex/micelle interaction, but increasing the temperature decreases the viscosity of the medium. The micellar microenvironment then deteriorates which may lead to quenching by increased molecular collisions.

Influence of the nature and degree of condensation of the surfactant. Calibration graphs were plotted for each of the systems studied. The calibration equations and the detection limits (calculated as three times the standard

TABLE 1

Values of the c.m.c. of different surfactants in the absence and presence of the aluminium/lumogallion complex

Surfactant	Molecular weight	C.m.c. (M)		Relative difference (%)
		Without complex	With complex	
Nemol K-1032	830	4.69×10^{-4}	4.45×10^{-4}	5.1
Triton X-100	660	4.07×10^{-4}	4.07×10^{-4}	0
Dehscoxid 728	580	7.41×10^{-4}	4.14×10^{-4}	44.1
Genapol PF-80	8100	2.35×10^{-5}	1.35×10^{-5}	42.6

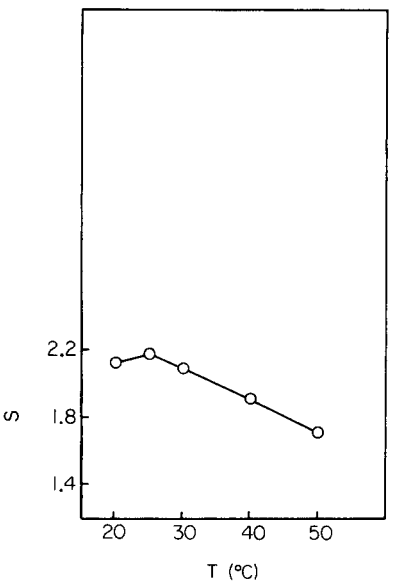

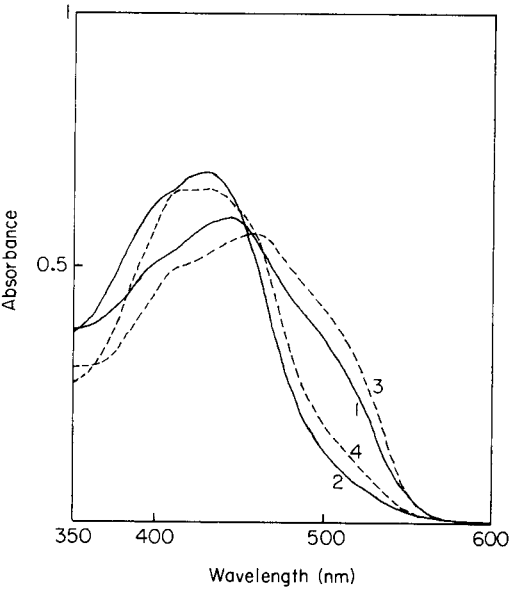

Fig. 2. Influence of the temperature on the fluorescence intensity of the aluminium/lumogallion complex in presence of Triton X-100. S, slope of calibration graph.

Fig. 3. Visible absorption spectra: (1) aluminium/lumogallion; (2) lumogallion; (3) aluminium/lumogallion and Triton X-100; (4) lumogallion and Triton X-100.

deviation of the blank from 12 measurements) are indicated in Table 2, as well as the micellar enhancement factors (MEF). These factors were calculated as the ratio of the slopes of the calibration plots with and without addition of surfactant. The maximum excitation wavelength was 470 nm in all cases. The micellar media provided a hypsochromic displacement of the maximum emission wavelength, which did not occur in the presence of the polyethylene glycols (Table 2).

It can be seen that the chemical nature of the surfactant has a notable influence on the sensitization of the fluorescence. Thus the ethylene oxide/fatty alcohol condensates gave higher enhancement factors than the tert-octylphenols or the nonylphenols; the ethylene oxide/propylene oxide condensates provided consistently lower enhancement factors. Within the same family of surfactants, despite the fact that a surfactant concentration greater than the c.m.c. was used in all cases, no systematic variation of the MEF with the degree of condensation was noted. The detection limits found (Table 2) did not differ significantly for different kinds of surfactant.

These results confirm that the nature of the surfactant is the most significant factor influencing the packaging of the molecules of the complex in the micelles [9, 11] and thus the interaction of the hydroxyl groups of the complex with the ethylene oxide molecules of the monomer constituents of the

TABLE 2

Micellar enhancement of the fluorescence of the aluminium/lumogallion system by non-ionic surfactants[a]

Surfactant	λ_{ex} (nm)	λ_{em} (nm)	Calibration equation	r^2	*MEF*	Detection limit ($\mu g\ l^{-1}$)
—	470	570	$I_F = 4.37 + 0.56\ c$	0.999	—	0.35
Nemol K-36	470	555	$I_F = 29.8 + 2.03\ c$	0.999	3.63	0.27
Nemol K-1032	470	555	$I_F = 23.0 + 2.18\ c$	0.999	3.89	0.25
Nemol K-1035	470	555	$I_F = 24.6 + 2.06\ c$	0.9999	3.68	0.13
Nemol K-2030	470	555	$I_F = 23.6 + 2.18\ c$	0.9999	3.89	0.18
Nemol K-3030	470	555	$I_F = 23.8 + 2.09\ c$	0.999	3.73	0.16
Triton X-114	470	555	$I_F = 21.5 + 1.58\ c$	0.99	2.82	1.73
Triton X-100	470	555	$I_F = 21.3 + 2.29\ c$	0.999	4.09	0.13
Triton X-405	470	555	$I_F = 21.0 + 2.12\ c$	0.9999	3.79	0.16
Dehscoxid 650	470	555	$I_F = 25.3 + 2.18\ c$	0.999	3.89	0.28
Dehscoxid 728	470	555	$I_F = 14.4 + 2.54\ c$	0.999	4.54	0.11
Dehscoxid 729	470	555	$I_F = 19.1 + 2.26\ c$	0.9999	4.04	0.21
Genapol PF-10	470	560	$I_F = 13.0 + 0.82\ c$	0.999	1.46	0.55
Genapol PF-20	470	565	$I_F = 12.9 + 0.77\ c$	0.9999	1.38	0.65
Genapol PF-40	470	565	$I_F = 12.3 + 0.84\ c$	0.999	1.50	0.32
Genapol PF-80	470	570	$I_F = 9.79 + 0.75\ c$	0.9999	1.34	0.20
PEG-200	470	570	$I_F = 7.92 + 0.58\ c$	0.99	1.04	0.44
PEG-400	470	570	$I_F = 9.54 + 0.56\ c$	0.999	1	0.32
PEG-600	470	570	$I_F = 8.55 + 0.60\ c$	0.999	1.07	0.22
PEG-6000	470	570	$I_F = 8.10 + 0.65\ c$	0.999	1.16	0.23

[a] I_F, fluorescence intensity; c, concentration in $\mu g\ l^{-1}$; r^2, correlation coefficients; MEF, micellar enhancement factor.

micelles [7]. The ethylene oxide/propylene oxide condensates gave very low enhancement factors; this could be attributed to the small hydrophobic portion of the molecules, which makes the micellar structure different from that formed by the other surfactants. The notable increase in fluorescence observed with the nonylphenols and the tert-octylphenols can be explained by the interaction between the aromatic rings present in both the complex and surfactant. The aluminium/lumogallion complex probably forms part of the structure of the micelles of fatty alcohol condensates with the formation of mixed micelles. The strong complex/micelle interaction could be responsible for the highest enhancement factors found.

Spectrophotometric study

The influence of the surfactant concentration on the net absorption (at 500 nm) of solutions containing up to 2% (w/v) Triton X-100 in the presence of 0.3 mg l^{-1} aluminium and 3.75×10^{-5} M lumogallion is indicated in Fig. 1B.

In the vicinity of the c.m.c., there is an increase in absorbance, but at greater surfactant concentrations, the readings decrease and then become constant for >0.2% (w/v) Triton X-100.

The calibration equations for solutions containing 0—120 $\mu g\ l^{-1}$ aluminium, 10^{-5} M lumogallion and 1.5% of each of the surfactants tested are listed in Table 3. In all cases except for Dehscoxid 728, the presence of surfactant decreases the absorbances slightly compared to the aluminium/lumogallion system alone. The visible absorption spectra for 0.3 mg l^{-1} aluminium and 3.75×10^{-3} M lumogallion alone and in the presence of 0.1% Triton X-100, as well as the spectra in the absence of aluminium, are shown in Fig. 3. There is a bathochromic shift in the maximum wavelength from 430 nm to 445 nm when the complex forms, and the shift is more pronounced in the micellar medium, but the surfactant does not have any significant effect on the net absorbance of the system at 500 nm.

These results suggest that the sensitization of the fluorescence is due to an increase in the fluorescence quantum yield because the excited singlet state is protected by the micellar microenvironment, and not to an increase in the amount of radiation absorbed. The formation of mixed micelles among the monomers of Dehscoxid 728 and the aluminium/lumogallion complex, increases the absorbance of the complex, which provides an additional increase in fluorescence in this particular medium.

TABLE 3

Calibration data for the aluminium/lumogallion system in presence of non-ionic surfactants, based on absorbance at 500 nm

Surfactant	Calibration equation[a]	r^2	ΔS[b] (%)
—	$A = 0.040 + 8.60 \times 10^{-4} c$	0.99	—
Nemol K-1032	$A = 0.060 + 8.22 \times 10^{-4} c$	0.9999	−4.4
Nemol K-1035	$A = 0.054 + 7.82 \times 10^{-4} c$	0.999	−9.0
Nemol K-2030	$A = 0.052 + 8.10 \times 10^{-4} c$	0.99	−5.7
Nemol K-3030	$A = 0.057 + 7.47 \times 10^{-4} c$	0.99	−13.0
Triton X-100	$A = 0.056 + 7.85 \times 10^{-4} c$	0.99	−8.7
Triton X-405	$A = 0.046 + 7.85 \times 10^{-4} c$	0.99	−8.7
Dehscoxid 728	$A = 0.117 + 1.65 \times 10^{-3} c$	0.999	+91.4
Dehscoxid 729	$A = 0.050 + 8.33 \times 10^{-4} c$	0.9999	- 3.0
Genapol PF-40	$A = 0.050 + 8.22 \times 10^{-4} c$	0.999	−4.3
Genapol PF-80	$A = 0.048 + 8.72 \times 10^{-4} c$	0.99	+1.4
PEG-200	$A = 0.051 + 8.38 \times 10^{-4} c$	0.999	−2.5
PEG-400	$A = 0.052 + 7.88 \times 10^{-4} c$	0.99	−8.4
PEG-600	$A = 0.046 + 8.38 \times 10^{-4} c$	0.999	−2.5
PEG-6000	$A = 0.048 + 8.25 \times 10^{-4} c$	0.99	−4.0

[a]Concentrations (c) in $\mu g\ l^{-1}$. [b]Change in slope relative to the system without surfactant.

Conclusions

The presence of non-ionic surfactants at concentrations higher than the c.m.c. leads to sensitization of the fluorescence of the aluminium/lumogallion system. The complex/micelle interaction predominates over the ligand/micelle interaction, in contrast to what was observed for the aluminium/morin system in analogous micellar media [9, 10]. This sensitization depends on the nature of the surfactant and especially on the rigidity of its interaction with the complex. The formation of mixed micelles between the molecules of the complex and the monomers of ethylene oxide with fatty alcohols is suggested by the fact that only these surfactants provide an increase in the absorbance of the complex. This increase, linked to the enhancement in the fluorescence quantum yield, provides the maximum enhancement factors.

REFERENCES

1 W. L. Hinze, in K. L. Mittal (Ed.), Solution Chemistry of Surfactants, Vol. 1, Plenum, New York, 1979, p. 79.
2 J. H. Callahan and K. D. Cook, Anal. Chem., 56 (1984) 1632.
3 H. Singh and W. L. Hinze, Anal. Lett., 15 (1982) 221.
4 N. J. Turro, M. Grätzel and A. M. Braun, Angew. Chem. Int. Ed. Engl., 19 (1980) 675.
5 G. J. Klopf and A. D. Cook, Anal. Chim. Acta, 162 (1984) 293.
6 A. Sanz-Medel and J. J. Garcia-Alonso, Anal. Chim. Acta, 165 (1984) 159.
7 B. A. Mulley and A. D. Metcalf, J. Pharm. Pharmacol., 8 (1956) 774.
8 A. T. Pilipenko, T. A. Vasil'Chuk and A. T. Volkova, Z. Anal. Khim, 38 (1983) 855.
9 L. Braco, J. L. Carrión, C. Abad and M. de la Guardia, J. Mol. Struct., 143 (1986) 489.
10 J. Medina, M. de la Guardia and F. Hernandez, Analyst, 108 (1983) 1386.
11 A. Sanz-Medel, M. M. Fernandez, M. de la Guardia and J. L. Carrión, Anal. Chem., 58 (1986) 2161.
12 K. Kina and N. Ishibashi, Microchem. J., 19 (1974) 26.
13 N. Ishibashi and K. Kina, Anal. Lett., 5 (1972) 637.
14 J. L. Carrión, M. de la Guardia and J. Medina, Quim. Anal., 2(4) (1983) 271.
15 M. de la Guardia, J. L. Carrión and J. Medina, Anal. Chim. Acta, 155 (1983) 113.
16 J. L. Carrión, S. Sagrado and M. de la Guardia, Anal. Chim. Acta, 185 (1986) 101.
17 J. L. Carrión and M. de la Guardia, Quim. Anal., 6(1) (1986) 76.
18 PNE 55-731. Instituto Nacional de Racionalización y Normalización Madrid (1981).
19 M. Galdú, Tesis de licenciatura, Valencia, 1985.

Analytica Chimica Acta, 198 (1987) 63—69
Elsevier Science Publishers B.V., Amsterdam — Printed in The Netherlands

MICRODETERMINATION OF RIBOFLAVIN AND RIBOFLAVIN 5′-PHOSPHATE BY A CATALYTIC PHOTOKINETIC METHOD

T. PÉREZ-RUIZ*, C. MARTINEZ LOZANO and V. TOMÁS

Department of Analytical Chemistry, Faculty of Sciences, University of Murcia, Murcia (Spain)

(Received 19th November 1986)

SUMMARY

The method is based on the rate of photoreduction of both compounds by EDTA, which is a linear function of the concentration of riboflavin and riboflavin 5′-phosphate at low concentrations. The rate is monitored spectrophotometrically by the formation of ferroin, which is generated after reduction of iron(III) by the 1,5-dihydro form of the riboflavins in the presence of 1,10-phenanthroline. Linear calibration graphs are obtained between 3×10^{-8} and 9.6×10^{-7} M. The method is successfully applied to the determination of vitamin B_2 in pharmaceuticals, foods and rat tissues.

Vitamin B_2 is the general term for the isoalloxazine derivative which can exist as riboflavin, flavin mononucleotide (FMN) or flavin adenine dinucleotide (FAD); FMN and FAD are protein-bound and the latter is usually the most abundant in natural products. Vitamin B_2 is a dietetically important compound and many reports on its determination in various materials have been published. Fluorimetric methods [1—3] are considered to be the most sensitive for riboflavin, and measurements can be made by measuring the natural fluorescence of the vitamin, or of lumiflavin, which is derived from riboflavin by irradiation with light and enhances the intensity. Spectrophotometric methods [1] measure the absorbance at 267 or 444 nm. Electrochemical methods [4—8] and high-performance liquid chromatography [9—14] have also been used. Semi-automated systems based on some of these methods have been reported [15—17].

Here, a sensitive catalytic photokinetic method is described for the determination of riboflavin and riboflavin 5′-phosphate. It is based on the generation of the 1,5-dihydro form of the B_2 vitamins by photochemical reactions between riboflavin or FMN and EDTA. The reduced forms, RFH_2 and $FMNH_2$, reduce iron(III) in the presence of 1,10-phenanthroline to ferroin, which is measured by spectrophotometry. The proposed method is more sensitive than the common fluorimetric procedure, but is less so than methods based on laser fluorimetry [18] or anodic adsorptive stripping voltammetry [7, 8]. The new method is specific for riboflavin and FMN in multivitamin preparations.

0003-2670/87/$03.50

EXPERIMENTAL

Reagents and equipment

The reagents were of analytical grade; doubly distilled water was used for the preparation of solutions and all dilutions. Standard solutions (1×10^{-4} M) of riboflavin or riboflavin 5′-phosphate were prepared by dissolving the compounds, previously dried and stored in the dark in a desiccator over phosphorus(V) oxide, in 0.02 M acetic acid. Working standards were prepared daily from these solutions as required by dilution with water.

The light source was a halogen lamp (Sylvania 24 V, 250 W). The illumination device has already been described [19]. The absorbance was measured with a Pye-Unicam SP8-200 spectrophotometer equipped with 10-mm glass cells.

Procedure

The sample must always be prepared in diffuse light and the solutions added should be previously thermostatted to about 25°C. To a 25-ml volumetric flask, add 1 ml of 2 M acetate buffer, pH 5.5, 5 ml of 0.1 M EDTA, 2 ml of 0.001 M iron(III) [as iron(III) ammonium sulphate], 1 ml of 1% 1,10-phenanthroline solution and an appropriate volume of riboflavin or FMN solution (standard or sample) to give a final concentration between 0.03 and 1.0 μM. Dilute to the mark with water and transfer to the reaction cell, maintained at 25 ± 0.5°C. Wait for 1 min, switch on the halogen lamp of the photolysis device and irradiate for 15 min. Transfer a portion of the irradiated solution to the spectrophotometer cell and measure the absorbance at 510 nm.

RESULTS AND DISCUSSION

Under anaerobic conditions over a wide pH range, photoreduction of riboflavin (RF) or FMN by EDTA is accomplished in a matter of seconds with a source of white light, the products being RFH_2 (or $FMNH_2$), ethylenediaminetriacetic acid, formaldehyde and CO_2 [20—23]. The basic rate equation for the reactions is given by

$$-d[A]/dt = \sum_{\lambda} \phi I_{abs}$$

where A represents riboflavin or riboflavin 5′-phosphate (FMN), ϕ is a constant and I_{abs} is the intensity of absorbed radiation, which can be obtained by application of the Lambert-Beer law:

$$-d[A]/dt = \sum_{\lambda} \phi I_0 [1 - \exp(-2.3\epsilon l[A])]$$

where ϵ is the molar absorptivity, l is the path length, λ refers to a photochemically active wavelength incident on the sample, and I_0 is the incident intensity of radiation at the relevant wavelength. When the absorbance of

the photoactive component is small ($\leqslant 0.05$), a simplified form is obtained by a Taylor-series expansion of the exponential term:

$$-d[A]/dt = \sum_{\lambda} \phi I_0 \epsilon l[A]$$

This means that the rate of the photochemical reaction is a linear function of the instantaneous concentration of riboflavin or FMN. This is the basis for the photochemical kinetic method [24].

The products of the photoreduction of riboflavin and FMN by EDTA are strong reductants [4, 25] and react rapidly with oxidants with reconversion to riboflavin and FMN, respectively. When an oxidant such as iron(III) is added to a solution of riboflavin (or FMN), EDTA (H_2Y^{2-}) and 1,10-phenanthroline (phen) at pH 5.5 (acetate buffer) and this is irradiated, iron reacts with H_2Y^{2-} to form the FeY^- complex, RFH_2 or $FMNH_2$ (AH_2) are formed as described above, and the reaction then is

$$AH_2 + 2FeY^- + 6phen + 2H^+ \rightarrow A + 2Fe(phen)_3^{2+} + 2H_2Y^{2-}$$

The cycle is repeated until no iron(III) remains. It is very well known that the reduction of FeY^- and the reaction between iron(III) and 1,10-phenanthroline is rapid, whereas the photoreduction of riboflavin or FMN is much slower, thus the photochemical reaction is the rate-determining step. The influence of the variables on the rate of photogeneration of the Fe(II)-phenanthroline complex was studied in order to develop a kinetic method for the determination of riboflavin or FMN.

Effect of reaction variables

The influence of pH on the rate of the photochemical reactions is shown in Fig. 1. The dependence of $Fe(phen)_3^{2+}$ yield on the initial concentrations of EDTA and 1,10-phenanthroline were then studied with an irradiation time of 15 min at pH 5.5. For both riboflavin and FMN (0.33 μM), the yields

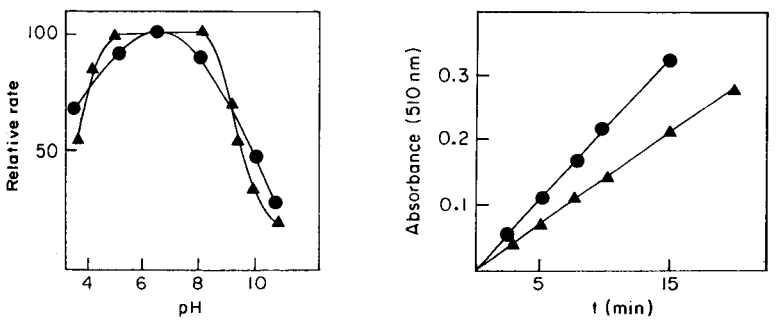

Fig. 1. Rate of photoreduction as a function of pH: (•) riboflavin; (▲) riboflavin 5′-phosphate.

Fig. 2. Influence of irradiation time on the yield of $Fe(phen)_3^{2+}$: (▲) open to atmosphere; (•) in absence of oxygen. Conditions: pH 5.5, 1.6×10^{-2} M EDTA, 2×10^{-3} M phen, 0.33 M riboflavin or FMN.

rapidly increased and reached maximal values with $1-3 \times 10^{-2}$ M EDTA (at constant 2×10^{-3} M phen) and with $1.7-6 \times 10^{-3}$ M 1,10-phenanthroline (at constant 1.6×10^{-2} M EDTA). The iron(III) concentration was varied from 3×10^{-5} to 2×10^{-4} M while the other variables were maintained constant. No change in the rate of formation of ferroin was detected. Therefore 8×10^{-5} M iron(III) is the recommended concentration. The rate of the overall redox process is slightly affected by temperature changes in the range 20—40°C. A temperature of 25 ± 0.5°C was selected. Under aerobic conditions, the 1,5-dihydroflavin generated reduces iron(III) and oxygen. However, as the rate of reduction of oxygen is much slower than that of iron(III), the former is not significant while iron(III) remains in the solution. Thus it is possible to work with solutions open to the atmosphere.

For each illumination and at a fixed concentration of riboflavin or FMN, the concentration of ferroin formed is a linear function of the irradiation time (Fig. 2). Thus greater sensitivity is obtained at longer irradiation times. Illumination for 15 min was chosen as a compromise between sensitivity and duration of the analysis. The recommended conditions, therefore are 2×10^{-2} M EDTA, 8×10^{-5} M Fe(III), 2×10^{-3} M 1,10-phenanthroline and pH 5.5 (acetate buffer), at 25 ± 0.5°C, with an irradiation time of 15 min.

Determination of riboflavin and riboflavin 5'-phosphate

Under the recommended conditions, the calibration graph of absorbance vs. molarity was linear for riboflavin and FMN in the range 0.03—1 μM. The relative standard deviation for the determination of 0.2 μM analyte was 1.3% for riboflavin and 0.8% for FMN ($n = 10$). The limits of detection and quantitation [26] were 7.6×10^{-3} μM and 2.2×10^{-2} μM for riboflavin and FMN, respectively.

The method is more sensitive if bathophenanthroline is used instead of 1,10-phenanthroline. Riboflavin and FMN can then be determined in the range 0.016—0.5 μM. With a longer irradiation time (20 min) and working in deaerated conditions, the lower limit is decreased to 6×10^{-9} M.

The method is very selective. The only interferents observed were oxidants and reductants that, under the recommended conditions, can oxidize ferroin or reduce the Fe(III)—EDTA complex; they must be previously destroyed. The effect of other vitamins is shown in Table 1.

TABLE 1

Tolerance of the riboflavin procedure to other vitamins

Vitamin	Tolerable mole ratio[a]
Thiamine (B_1); biotin (H)	1000[b]
Ascorbic acid (C)[c]	500
Pyridoxine (B_2); cyano cobalamin (B_{12})	200
Nicotinamide; pantothenic acid	100

[a]Smallest amount that caused an error of 2.5% in the determination of 0.33 μM riboflavin. [b]Maximum tested. [c]Previously destroyed by oxidation.

TABLE 2

Determination of riboflavin and riboflavin 5'-phosphate in pharmaceutical preparations

Sample[a]	Source	(mg)	Amount found (mg)	
			Photokinetic[b]	Fluorimetric[c]
Riboflavin				
Protovit	Roche	1	0.98 ± 0.04	1.01
Apiroserum dextrobergone	Ibys	0.6	0.59 ± 0.03	0.58
Polybion C	Merck	15	15.1 ± 0.03	14.90
Becozyme	Merck	4	3.98 ± 0.03	4.02
Riboflavin 5'-phosphate				
Organzyme	Bama	8	7.70 ± 0.03	7.68

[a]Composition of samples. *Protovit:* riboflavin 1 mg; thiamine, 2 mg; nicotinamide, 10 mg; pyridoxine, 1 mg; biotin, 0.1 mg; ascorbic acid, 50 mg; dexpanthenol, 10 mg; retinol, 5000 I.U.; ergocalciferol, 1000 I.U.; saccharin, 5 mg; and water, 1 g. *Apiroserum dextrobergone:* riboflavin, 0.6 mg; thiamine, 0.5 mg; nicotinamide, 0.5 mg; pyridoxine, 0.3 mg; glucose, 5 mg; sodium chloride, 0.85 mg; water, 100 g. *Polybion C:* riboflavin, 15 mg; thiamine, 15 mg; nicotinamide, 50 mg; calcium pantothenate, 25 mg; pyridoxine, 10 mg; biotin, 0.15 mg; cyanocobalamin, 10 μg; ascorbic acid, 300 mg; saccharin, 15 mg; excipient, 5 g. *Becozyme:* riboflavin, 4 mg; thiamine, 10 mg; pyridoxine, 4 mg; nicotinamide, 40 mg; biotin, 0.5 mg, cyanocobalamin, 8 μg; panthenol, 6 mg; water, 2 mg. *Organzyme B:* riboflavin phosphate, 8 mg; thiamine, 20 mg; pyridoxine, 10 mg; calcium pantothenate, 25 mg; nicotinamide, 50 mg; cyanocobalamin, 25 μg; biotin 0.2 mg; excipient 0.5 g. [b]Average of four determinations ± s.d. [c]Average of two determinations.

TABLE 3

Determination of vitamin B_2 in foods

Sample	(mg/100 g)	Vitamin B_2 found (mg/100 g)	
		Photokinetic[a]	Fluorimetric[b]
Whole milk	—	0.13 ± 0.02	0.14
Baby milk 1	0.60	0.58 ± 0.04	0.61
Baby milk 2	0.47	0.49 ± 0.02	0.47
White bread	—	0.19 ± 0.02	0.18
Wholemeal (fortified)	0.79	0.75 ± 0.03	0.76
Enriched cornflour	1.50	1.49 ± 0.02	1.46

[a]Average of four determinations ± s.d. [b]Average of two determinations.

Application to real samples

The method was tested by analyzing pharmaceuticals, foods and animal tissues. For pharmaceutical preparations, the sample (containing water-soluble vitamins) was dissolved in water and a suitable aliquot was used. Table 2 summarizes the results obtained together with the nominal contents and the data obtained by the official spectrofluorimetric method [27].

TABLE 4

Determination of total flavins in rat tissues

Tissue	Total flavins found ($\mu g\ g^{-1}$)	
	Photokinetic[a]	Lumiflavin fluorescence method[b]
Heart	12.11 ± 0.04	12.40
Kidney	27.90 ± 0.06	28.01
Liver	25.22 ± 0.04	24.8

[a]Average of four determinations ± s.d. [b]Average of two determinations.

For foods, 5 g of the sample (milk, bread or cornflour) was weighed into a 100-ml beaker and 25 ml of 0.1 M hydrochloric acid was added. The suspension was heated and, after cooling, filtered. The solution was transferred to a volumetric flask and the recommended procedure was applied. The results (Table 3) were in good agreement with the nominal contents and with those obtained by fluorimetry [27].

The flavins were quantitatively extracted from animal tissues by the "warm-water extraction method" [28]. The suspension obtained was filtered and the filtrate hydrolyzed with 0.2 M hydrochloric acid in an autoclave at 120°C for 2 h. After diluting with water in a 100-ml volumetric flask, an aliquot of the solution was used. Table 4 shows the results obtained which are in excellent agreement with those found by the lumiflavin method [28].

REFERENCES

1 R. Strohecker and H. M. Henning, Vitamin Assay, Tested Methods, Verlag Chemie, Weinheim, 1965, pp. 98—123.
2 W. H. Sebrell and R. S. Harris, The Vitamins, Vol. 5, Academic, New York, 1967.
3 J. Koziol, in D. McCormick and L. Wright (Eds.), Methods in Enzymology, Vol. XVIII, Part B, Academic, London, 1971, pp. 253—285.
4 M. Brezina and P. Zuman, Polarography in Medicine, Biochemistry and Pharmacy, Interscience, London, 1958, pp. 389—394.
5 I. E. Davidson, in W. F. Smith (Ed.), Polarography of Molecules of Biological Significance, Academic, London, 1979, pp. 133—134.
6 T. M. Florence, J. Electroanal. Chem., 97 (1979) 219.
7 J. Wang, D. B. Luo, P. A. M. Farias and J. S. Mahmoud, Anal. Chem., 57 (1985) 158.
8 H. Sawamoto, J. Electroanal. Chem., 186 (1985) 257.
9 C. Y. W. Ang and F. A. Moseley, J. Agric. Food. Chem., 28 (1980) 483.
10 R. P. Kwok, W. P. Rose, R. Tabor and T. S. Pattison, J. Pharm. Sci., 70 (1981) 1014.
11 E. A. Woodcock, J. J. Warthesen and T. P. Labuza, J. Food Sci., 47 (1982) 545.
12 D. J. Mauro and D. I. Wetzel, J. Chromatogr., 299 (1984) 281.
13 N. Ichinose, K. Adachi and G. Schwedt, Analyst, 110 (1985) 1505.
14 N. Ichinose and K. Adachi, Analyst, 111 (1986) 391.
15 D. C. Egberg and R. H. Potter, J. Agric. Food Chem., 23 (1975) 815.
16 O. Pelletier and R. Madere, J. Assoc. Off. Anal. Chem., 60 (1977) 140.
17 D. C. Egberg, J. Assoc. Off. Anal. Chem., 62 (1979) 1041.
18 N. Ishibashi, T. Ogawa, T. Imasaka and M. Kunitake, Anal. Chem., 51 (1979) 2096.

19 F. Sierra, C. Sánchez-Pedreño, T. Pérez-Ruiz and C. Martinez Lozano, Anal. Chim. Acta, 78 (1975) 277; 94 (1977) 129.
20 J. R. Merkel and W. J. Nickerson, Biochim. Biophys. Acta, 14 (1954) 303.
21 B. Holmstrom, Photochem. Photobiol., 3 (1964) 97.
22 K. Enns and W. Burgess, J. Am. Chem. Soc., 87 (1965) 5766.
23 V. Massey, M. Stankovich and P. Hemmerich, Biochemistry, 17 (1978) 1 (and references therein).
24 R. J. Lukasiewicz and J. M. Fitzgerald, Anal. Lett., 2 (1969) 159.
25 E. Knobloch, in D. McCormick and L. Wright (Eds.), Methods in Enzymology, Vol. XVIII, Part B, Academic, London, 1971, pp. 305—381.
26 ACS Committee on Environmental Improvement, Anal. Chem., 52 (1980) 2242.
27 Official Methods of Analysis, 13th edn., Association of Official Analytical Chemists, Washington, 1980, p. 743.
28 K. Yagi, in D. McCormick and L. Wright (Eds.), Methods in Enzymology, Vol. XVIII, Part B, Academic, London, 1971, pp. 290—296.

Analytica Chimica Acta, 198 (1987) 71—79
Elsevier Science Publishers B.V., Amsterdam — Printed in The Netherlands

OPTIMIZATION OF PHOTOPLATE EVALUATION IN SPARK-SOURCE MASS SPECTROMETRY

X. D. LIU, P. VAN ESPEN and F. ADAMS*
Department of Chemistry, University of Antwerp (U.I.A.), B2610 Wilrijk (Belgium)
(Received 28th May 1986)

SUMMARY

In spark-source mass spectrometry with photoplate detection, errors caused by densitometric measurements and the linearization of the blackening data are very important for the ultimate accuracy achieved. Two methods are described for the determination of the linearization parameters in the Hull equation by least-squares optimization of the known abundance ratio of isotope pairs.

Because of its multi-element capability and excellent detection limits, spark-source mass spectrometry (SSMS) is a well established technique for the analysis of high-purity metals and alloys. Many studies have been devoted to improving the precision of the analysis either with photoplate or electrical detection [1—4]. Random variations in the spark plasma and the often considerable heterogeneity in the distribution of trace elements in the samples are considered to be the most important sources of errors. For measurements with ion-emulsion (photoplate) detection, the errors caused by the densitometric evaluation and linearization of the data are also believed to have a great effect on accuracy. In the literature, there is general agreement that the optimum achievable precision is about 2—3% for electrical detection or 5—10% for photoplate detection. The higher errors for the latter mode are directly the result of errors in densitometry and in the evaluation of the photoplate response.

Several empirical formulae of variable complexity have been reported for calculating the ion intensity from the transmission data of the photoplate [5]. Accuracy associated with plate evaluation is strongly dependent on the method used for linearization. The Hull equation [6] has been selected in this laboratory and in others, as it offers fair accuracy while requiring only two variables for linearization of the plate response. In this paper, a method is described for evaluating the two linearization parameters in the Hull formula, i.e., the slope of the characteristic curve γ, and the saturation blackening T_s from the information available in the mass spectra. The results are compared with those obtained by another less elaborate approach based on the simpler equation proposed by Seidel [5].

0003-2670/87/$03.50

EXPERIMENTAL

The measurements were done with a double-focussing spark-source mass spectrometer (JMS-01, BM-2; JEOL, Tokyo) with Mattauch-Herzog geometry, equipped with an automatic spark control system. The conducting samples to be examined were cut into electrodes (about 1 mm thick, 2 mm wide and 15 mm long) without further sample preparation. If the samples were non-conducting, they were mixed with pure graphite powder and pressed as electrodes. Before analysis, sample electrodes were presparked for about one hour, in order to remove the possible contaminants from the surface as well as to decrease the memory effects from previous runs.

The experimental spark parameters must be selected carefully to ensure stable sparking. Typical slit settings were: main slit 25 μm, α-slit 0.8 mm, β-slit 1.5 mm. A relatively wide β-slit was used to eliminate to some extent the discrimination effect on the sensitivity of ions with various mass, at the expense of a slight deterioration of the mass resolution to ca. 4000 [7]. Illford Q2 ion-sensitive photoplates were used as the ion detector. For high-purity samples, fourteen exposures were recorded on the plate in the range 5×10^{-4}—600 nC, increasing in steps of a factor 3 in exposure; for samples with impurities at a higher level, the increasing steps were 2 and the highest exposure was reduced accordingly.

The plates were developed at low temperature (8°C) as described by Franzen and Schuy [2]. This resulted in less fogging at high exposures compared to the standard development at room temperature. The transmission profiles of the mass lines were stored on a magnetic tape with the aid of a microprocessor-controlled densitometer. Data reduction was done by a VAX 11/780 computer, using the program described by Pilate and Adams [8]. The transmission data were converted to ion intensities by using the approach of Hull, and the transmission profile was integrated.

If no suitable matrix isotope was available for use as the internal standard, at least one relatively homogeneously distributed element in each sample was accurately determined by atomic absorption spectrometry (AAS) and used as the internal standard.

METHOD FOR LINEARIZATION

The Hull approach for linearization is described by the equation

$$I = K[(1.0 - T)/(T - T_s)]^{\gamma} \quad (1)$$

where I is the ion intensity corresponding to a measured transmission T, K is a proportionality constant, T_s is the saturation transmission and γ is the slope of the calibration plot or characteristic plot. If γ is set to unity and T_s to zero, Hull's equation becomes Seidel's equation. Commonly, there is a tendency to obtain smaller γ parameters for higher ion masses.

First, it is worthwhile to illustrate the importance of the parameters γ and

T_s in the linearization process. In Fig. 1, transmission as a function of the relative ion intensity is plotted for selected values of both parameters. The parameter γ has opposite effects on both sides of the transmission 0.5, which has a corresponding ion intensity of 1 (Fig. 1a); above this transmission, a small value of γ produces an increase in ion intensity but below it the intensity is decreased. In contrast, the parameter T_s has little influence on the weak mass lines with transmission above 0.7 but becomes increasingly important for more intense lines (Fig. 1b).

Owing to the simultaneous and integrating detection capability of photoplate SSMS, the blackening of the isotopes of some multi-isotopic elements is available in the mass spectra. This feature can be used conveniently to test the correctness of any linearization procedures applied. The linearization procedure can be considered to be successful when the measured isotope ratios are equal, within the error estimates, to the corresponding ratios of natural isotopic abundance. However, the impurities may be distributed inhomogeneously and the coulometer readings may be unreliable [9, 10]; hence when isotope ratios are used as a check on linearization, it is desirable to compare the intensities of the isotope pairs from single exposures.

In the converse argument, comparison of the isotope ratios of homogeneously distributed elements between different exposures can be put to use for calibration of exposures. Because of the limited dynamic range of the photographic emulsion, isotope pairs with an abundance ratio of between say 1.5 to 3.0 are preferable. The integrating nature of the photographic detection system then prevents the occurrence of errors caused by unstable spark plasmas and also those resulting from sample heterogeneities. In fact, then only the errors arising from densitometry and from non-uniform response of the photoplate need be considered.

These principles might be used in a straightforward way as follows. First, the linearization parameters are set at $\gamma = 1$ and $T_s = 0$ and the parameter γ is evaluated by calculating the quotient of the logarithms of the natural isotopic abundance ratio and the experimentally obtained ratio of peak areas:

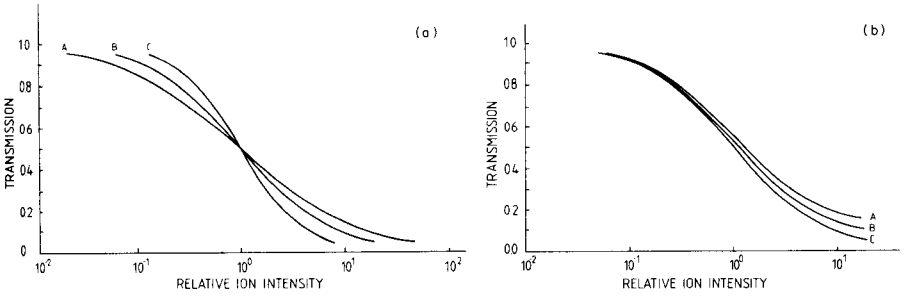

Fig. 1. Calibration curves obtained by using the equation of Hull: (a) T_s = 0.00 and γ = 1.3 (A), 1.0 (B) and 0.7 (C); (b) γ = 1.0 and T_s = 0.10 (A), 0.05 (B) and 0.00 (C).

γ = ln (isotopic abundance 1/isotopic abundance 2)/ln (peak area of isotope 1/peak area of isotope 2) (2)

Unfortunately, there are some problems in applying this equation. First, the saturation transmission cannot be calculated from Eqn. 2. Secondly, the non-linear response of the photoplate within the intensity range needed for integrating a single mass peak prevents the use of the Hull formula through the application of the average or maximum peak transmissions. Indeed, with the non-linear nature of the transformation process, this simplification would lead to different values of γ as found for different isotope pairs. Hence, whenever peak profiles and not peak maxima are measured, the procedure must be applied to the transmission data on a point-by-point basis before peak integration and background subtraction. It must be concluded that straightforward application of Eqn. 2 is inappropriate for calculating parameter γ. It can only be used to judge in hindsight to what extent the experimentally found isotopic ratio of a particular isotope pair approximates the natural abundance ratio.

In subsequent paragraphs, two procedures are described for plate calibration in which the linearization parameters are found by optimizing the isotopic abundance ratios of many isotope pairs simultaneously by using the entire measured profile of each mass line. The isotopic pairs are selected pairwise from single exposures, thus circumventing the complexity caused by other sources of error which are not associated directly with the ion emulsion detection. Optimum linearization parameters are then selected by least-squares optimization.

Isotopic abundance ratio method. Given natural isotopic abundances in the sample, the mean deviation (Dev) defined by the following equation can be used as a criterion for the quality of linearization.

$$\mathrm{Dev} = \left\{ [\sum_i (R_{\mathrm{exp}} - R_{\mathrm{nat}})^2] / (n-1) \right\}^{1/2} \tag{3}$$

where R_{exp} is the experimentally found isotope abundance ratio of a given isotope pair, R_{nat} is the corresponding natural isotope abundance ratio, and n is the number of isotope pairs selected. A minimum value of Dev is calculated by iterative non-linear least-squares optimization of the parameters in the Hull equation. The method is implemented in the Fortran program OPTIMA.

Stage intensity ratio method. Theoretically, if the linearization is done properly, the ratio of the intensities on the stages with different exposures, called the stage intensity ratio (R), should be the same for all the isotopes of a given element (i.e., the difference of these ratios should approach zero when other error sources are excluded. Therefore, a mean difference (Dif) is taken as the criterion for the quality of linearization in this method:

$$\mathrm{Dif} = \left\{ \sum_{\text{element } i} \sum_{\text{stage } k} \sum_{\text{isotope } j} [(R_1 - R_2)/(R_1 + R_2)/2]^2 \right\}^{1/2} \tag{4}$$

where $R_1 = I_{k,j,i}/I_{k',j,i}$ and $R_2 = I_{k,j',i}/I_{k',j',i}$, with $k \neq k'$ and $j \neq j'$. $I_{k,j,i}$ is the intensity of a line on stage k for isotope j of the element i. Thus, R_1 and R_2 are the stage intensity ratios of two isotopes of an element on different stages of the plate. This method is implemented in program OPTIMB.

The advantage of the stage intensity ratio method over the isotopic abundance ratio method is that it does not require the use of the natural isotopic abundance ratios.

The input information of the OPTIMA program is the identification number of the photoplate and the stage numbers, the position and the natural isotopic abundances of at least five isotope lines and the location on the plate where the corresponding backgrounds should be measured. For OPTIMB, the isotopic abundances are not required and the element symbol and the nominal mass are supplied. With this input information, each mass line can be identified on the bulk storage device which contains the results of point-by-point scanning microdensitometry of the photoplate. The integration range for each line is found automatically, with between 60 and 120 data points used for densitometry measurements every single micrometer on a high-resolution photoplate. The background correction is done after linearization by simultaneously applying the Hull equation to background intervals of the plate and subtracting the resulting ion intensity from the measured ion intensity for each data point. The integration over the peak profile thus corresponds to the net peak area after linearization. It is a more precise evaluation of the peak than either the method based on maximum transmission or the application of the half-height peak-width correction described by Schuy and Franzen [11].

Several precautions must be taken in selection of the isotopes: (1) the mass line must be interference-free; (2) the background of the line should be at an acceptable level, e.g., with >85% transmission; (3) the calibration mass lines selected should cover as wide a portion of the mass range as possible; and (4) spectral lines with various maximum blackening should be selected in order to cover the dynamic range of transmission as well as possible.

RESULTS AND DISCUSSION

The effect of parameters γ and T_s

The characteristics of plate linearization as described may be illustrated by the following example on the analysis of ultrapure indium metal reported elsewhere [12]. The twelve isotope pairs summarized in Table 1 were used.

The deviation (Dev) defined in Eqn. 3 was calculated with program OPTIMA for each possible combination of γ and T_s within the range $\gamma = 0.35$ to 1.00 in increments of 0.05 and $T_s = 0.00$ to 0.11 in increments of 0.01 for these twelve isotope pairs. As is shown in Fig. 2, where —Dev is plotted against γ and T_s, the minimum deviation corresponds to Dev = 0.0784 for $\gamma = 0.55$ and $T_s = 0.06$. The combination of $\gamma = 1.0$ and $T_s =$

TABLE 1

Isotope pairs used for optimizing γ and T_s in an indium sample

Stage exposure	Isotope, with maximum transmission in brackets
10 nC	^{206}Pb(0.60); ^{208}Pb(0.35); ^{207}Pb(0.64); ^{205}Pb(0.35)
32 nC	^{119}Sn(0.25); ^{124}Sn(0.34); ^{112}Sn(0.38); ^{124}Sn(0.34); ^{121}Sb(0.38); ^{123}Sb(0.52); ^{206}Pb(0.28); ^{208}Pb(0.14); ^{207}Pb(0.33); ^{208}Pb(0.14)
64 nC	^{119}Sn(0.12); ^{124}Sn(0.20); ^{122}Sn(0.24); ^{124}Sn(0.20); ^{121}Sb(0.23); ^{123}Sb(0.27)
128 nC	^{122}Sn(0.15); ^{124}Sn(0.12); ^{121}Sb(0.12); ^{123}Sb(0.16)

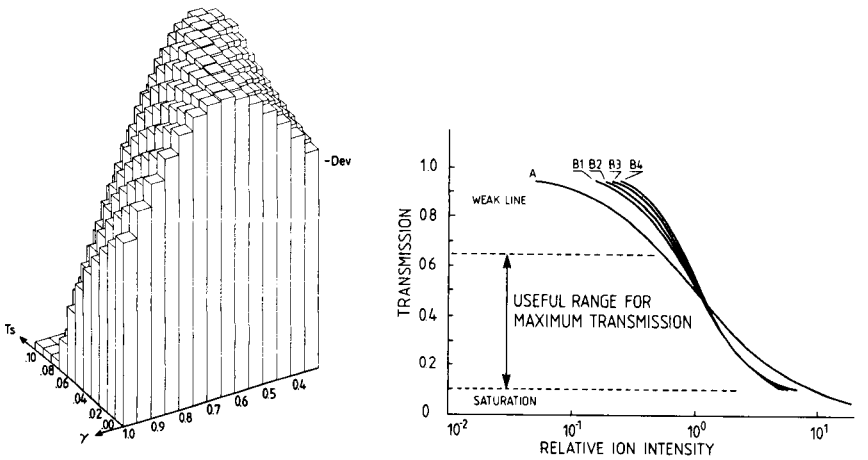

Fig. 2. Graphical presentation of the negative deviations from the Hull equation as a function of T_s and γ, for the 12 isotope pairs listed in Table 1.

Fig. 3. Calibration curves calculated from the Hull equation with optimized γ and T_s of Fig. 2: (B1) T_s = 0.02 and γ = 0.65; (B2) T_s = 0.04 and γ = 0.60; (B3) T_s = 0.06 and γ = 0.55; (B4) T_s = 0.08 and γ = 0.50; (A) T_s = 0.00 and γ = 1.00 (Seidel).

0.00 which corresponds to Seidel's equation yields a deviation of 0.1541 or twice as much as the optimum obtained with the Hull approach. Because the combination of γ = 1.0 and T_s = 0.0 is away from the top area, the Seidel equation cannot yield results of the same quality as the Hull approach using well chosen linearization parameters.

It is also apparent from the tridimensional plot in Fig. 2 that the optimum result of linearization is not strictly defined: several other combinations of γ and T_s provide an acceptable result compared to the optimum (e.g., the conditions with γ = 0.50 and T_s = 0.08, γ = 0.55 and T_s = 0.05 to 0.07, γ = 0.60 and T_s = 0.03 to 0.05, and finally γ = 0.65 and T_s between 0.01 and 0.03). The resulting calibration curves for a few of these optimum par-

ameters are shown in Fig. 3. The shape of the response surface in Fig. 2 depends on the boundary conditions chosen for optimization. Indeed, γ predominantly influences the shape of the linearization function at both high and low transmission values whereas the influence of T_s is largest at low transmissions (see Fig. 1). Therefore, the experimental data chosen for linearization should cover the same range of transmission values as those to be used in the actual analysis.

The dynamic range of the ion intensity is usually 50 to 1000, which corresponds to a transmission range between 0.65 and 0.10 for maximum peak transmission. Only the mass lines that fall within the dynamic range are adopted for the calculation. It can be seen that the four curves shown in Fig. 3 coincide very well in the range of transmission 0.65—1.00, while they diverge outside this range. Considering that the ion intensity of the mass lines is the integration of the entire profile, the divergences in the range of transmission 0.65—1.0 can have a significant influence on the ion intensities. However, this influence is much reduced when the integration limits on both sides of a peak are defined as say 10 or 20% of the maximum intensity.

In routine applications, it is not necessary to calculate Dev for all combinations of γ and T_s as shown here for illustration. The speed of the optimization process is increased by using a subroutine from the CERN library (code D509). First, T_s is fixed to incremental values (e.g. 0.00, 0.02, 0.04 ... 0.14), for which γ is optimized and Dev is calculated. The combination of γ and T_s with the smallest Dev is then used as the starting point for a new optimization until the progress in Dev becomes less than a preset control value. Though OPTIMA and OPTIMB are approaches of a quite different nature, their results are fairly consistent.

Improvements in precision

The linearization methods based on the isotope abundance and stage intensity ratios have been applied extensively in routine analysis. It was observed that the parameter γ as found by both methods is smaller when it is calculated from high mass isotopes such as tin, antimony and lead than from low mass elements up to cadmium. This indicates that results could be improved by running separate linearizations for different mass ranges. A drawback would be the increase in complexity encountered.

Results for an indium analysis are presented in Tables 2 and 3 as an example. By using stage intensity ratios, an optimum of $\gamma = 0.72$ and $T_s = 0.02$ was obtained for this example; the corresponding data for the isotopic abundance ratios were 0.68 and 0.02. The improvement in precision in comparison with results based on the Seidel formula are summarized in Table 2 for six elements which were known to be homogeneously distributed in the material. The mean relative standard deviation for the ion intensities is improved from 0.15 to 0.08. The improvement in accuracy of isotope abundance ratios is shown for the same elements in Table 3. The average deviation between the natural abundance ratio and the result after Hull

TABLE 2

The relative standard deviation of the intensities of isotope mass lines

Isotope	Relative standard deviation		Isotope	Relative standard deviation	
	Seidel	Hull		Seidel	Hull
^{110}Cd	0.12	0.16	^{123}Sb	0.28	0.09
^{111}Cd	0.14	0.10	^{203}Tl	0.02	0.08
^{118}Sn	0.07	0.11	^{205}Tl	0.16	0.05
^{119}Sn	0.29	0.09	^{206}Pb	0.19	0.09
^{122}Sn	0.14	0.02	^{207}Pb	0.09	0.09
^{124}Sn	0.16	0.01	^{208}Pb	0.16	0.06
^{121}Sb	0.19	0.03	^{209}Bi	0.14	0.09
			Mean	0.154	0.076

TABLE 3

Comparison of the experimentally obtained and the natural isotopic abundance ratio

Isotope pair	Table value	Experimental value[a]	
		Seidel	Hull
Pb(206/207)	1.044	1.32 (25)	1.27 (22)
Pb(206/208)	0.4512	0.393 (13)	0.474 (5)
Pb(207/208)	0 4321	0.296 (31)	0.374 (13)
Sn(119/122)	1.818	2.14 (18)	1.90 (5)
Sn(122/124)	1.444	1.77 (22)	1.64 (14)
Sn(122/124)	0.7946	0.814 (3)	0.846 (7)
Sb(121/123)	1.339	1.427 (7)	1.31 (2)
Cd(110/111)	0.972	1.05 (8)	1.02 (5)
Cu(63/65)	2.235	2.46 (10)	2.10 (6)
Zn(64/66)	1.758	2.05 (17)	1.78 (1)
Zn(64/68)	2.630	3.39 (29)	2.62 (0)
Zn(66/68)	1.498	1.65 (10)	1.47 (2)
Mean		16%	7%

[a]The relative deviation (%) from the table value is given in parentheses.

linearization is 7% compared with 16% for linearization based on the Seidel formula. Figure 4 shows a plot of the isotope ratio as a function of the true ratio for both approaches to linearization. It shows a general tendency to overestimate when the Seidel approach is used.

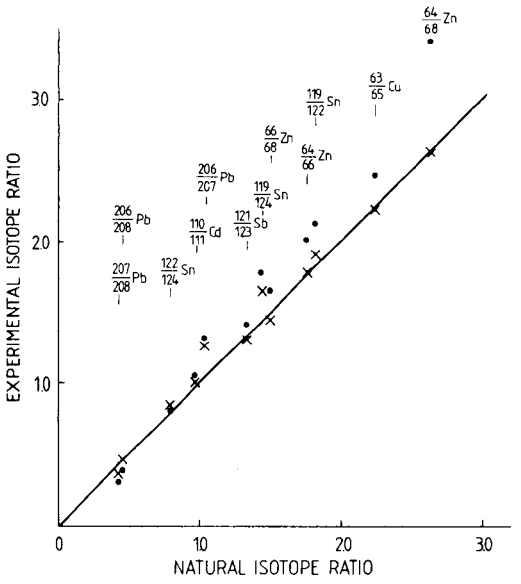

Fig. 4. Experimental isotope abundance ratio obtained by using the equations of Hull (X) and Seidel (•), as a function of the natural abundance ratio.

Thanks are due to the Nationaal Fonds voor Wetenschappelijk Onderzoek, Belgium for financial support.

REFERENCES

1 R. K. Skogerboe, A. T. Kashuba and G. H. Morrison, Anal. Chem., 40 (1968) 1096.
2 J. Franzen and K. D. Schuy, Fresenius' Z. Anal. Chem., 225 (1967) 295.
3 G. D. Nicholls, A. L. Graham, E. Williams and M. Wood, Anal. Chem., 39 (1967) 584.
4 E. Van Hoye, F. Adams and R. Gijbels, Bull. Soc. Chim. Belg., 84 (1975) 595.
5 P. R. Kennicott, in A. J. Ahearn (Ed.), Trace Analysis by Mass Spectrometry, Academic, New York, 1979, p. 179.
6 C. W. Hull, Proc. 10th Mass Spectrometry Conference, New Orleans, 1962, p. 404.
7 L. Vos and R. Van Grieken, Int. J. Mass Spectrom. Ion Phys., 51 (1983) 63.
8 A. Pilate and F. Adams, Anal. Chim. Acta, 122 (1980) 57.
9 E. Van Hoye, R. Gijbels and F. Adams, Talanta, 23 (1976) 369.
10 S. R. Taylor, Geochim. Cosmochim. Acta, 35 (1971) 1187.
11 K. D. Schuy and J. Franzen, Fresenius' Z. Anal. Chem., 225 (1967) 260.
12 X. D. Liu, J. Verlinden and F. Adams, Bull. Soc. Chim. Belg., 95 (1986) 309.

Analytica Chimica Acta, 198 (1987) 81—86
Elsevier Science Publishers B.V., Amsterdam — Printed in The Netherlands

INTERFERENCES IN INVERSE ZEEMAN-CORRECTED ATOMIC ABSORPTION SPECTROMETRY CAUSED BY ZEEMAN SPLITTING OF MOLECULES

G. WIBETOE and F. J. LANGMYHR*

Department of Chemistry, University of Oslo, P.O. Box 1033, Blindern, 0315 Oslo 3 (Norway)

(Received 3rd November 1986)

SUMMARY

Orthophosphoric acid was vaporized in the graphite furnace of an inverse Zeeman-corrected atomic absorption spectrometer and the performance of the background corrector system was studied at some analyte lines in the wavelength region where the species PO is known to have strong band systems. The investigation revealed cases of both over- and under-compensation probably caused by Zeeman splitting of PO rotational lines.

Among the different types of non-specific absorption that have to be compensated for in electrothermal atomic absorption spectrometry (a.a.s.), the structured background of line-rich electronic excitation spectra of molecules are probably the most difficult to deal with. When the conventional continuous background corrector is used, the average background over the band-pass of the monochromator is likely to differ from the background at the analyte emission line. If the emission line of the analyte element coincides with a rotational line of a molecular spectrum, an undercompensation error is introduced; in cases of non-coincidence, an overcompensation error is likely to occur.

In those instances where the background is measured very close to the analyte emission line, as is the case with the Smith-Hieftje and several direct Zeeman background-corrector systems, incorrect analytical results may also be encountered. Kurfürst [1], applying direct Zeeman a.a.s., has described a case of overcompensation caused by a structured background.

Even when the measurement of the background is made exactly at the analyte wavelength, as is the case with the inverse Zeeman correction system, a correct measurement of background is not guaranteed. With this system, the background signal alone and the analyte-plus-background signals are measured either in two different polarization planes (parallel and transverse to the magnetic field), or with and without a magnetic field applied to the atomization cell. Massmann [2] has pointed out that molecules exhibiting Zeeman splitting may have different background values when measured in

0003-2670/87/$03.50

the two orthogonal polarization planes, or when measured with and without the magnetic field applied.

If the absorption rotation line of a molecule showing Zeeman splitting is close to or overlaps an analyte emission line, an over- or under-compensation may occur as for an adjacent atomic absorption line. For the latter type of lines, 22 cases of overcompensation have been found in inverse Zeeman a.a.s. [3—5]. In these instances, the matrix element absorption lines are situated close to the analyte absorption lines. Whether a negative, positive or no error is experienced in inverse Zeeman a.a.s. depends on the degree of overlap of the unsplit absorption matrix line (no magnetic field applied) with the analyte emission line compared to the σ-component overlap with the same emission line.

A survey of the literature showed only two cases of interference caused by Zeeman splitting of molecules. One case is reported by Massmann [2] who found that the background in an acetylene/air flame, when measured at the 306.8-nm bismuth line, differed in the two orthogonal polarization planes. He assumed that the resulting negative error was due to the Zeeman splitting of an OH rotational line. A second case was recently described by Carnrick et al. [6]. During inverse Zeeman electrothermal a.a.s. measurements of cadmium at the 326.1-nm line, these authors found an overcompensation which they believed to be caused by the splitting of a PO line.

The present paper reports on the performance of an inverse Zeeman background corrector during measurements of some elements which have lines in the wavelength range where PO exhibits band systems. PO has two strong band systems in the ultraviolet region, the β-system in the range 319.8—358.7 nm and the γ-system in the region 228.0—275.0 nm [7]. Both systems involve the ground state in the transitions $^2\Sigma—^2\Pi$ which should form the basis of absorption of radiation. In these transitions, the PO molecule shows Zeeman splitting; this splitting is considerable for low rotational quantum numbers (J) and decreases with increasing J-values [8]. Phosphate is often present in samples analyzed by a.a.s. and in the presence of this matrix the use of a conventional deuterium background corrector has led to overcompensation errors [9—11]. However, in these particular instances, the errors could be removed by doing the measurements with a Zeeman background corrector.

EXPERIMENTAL

Equipment and chemicals

The a.a.s. measurements were made with a Perkin-Elmer (P-E) model 5000 Zeeman spectrometer and a P-E HGA-400 graphite furnace. Time-resolved absorption data, i.e., both the analytical signal corrected for background and the background signal itself, were collected and displayed with the P-E 3600 Data System and an Anadex DP-9500 B Printer. The graphite tubes were of the pyrolitically coated type; the atomization cells were

purged with argon (≥ 99.9% by volume). Solutions were transferred to the furnace with plastic-tipped micropipettes. The hollow-cathode and electrodeless lamps were all from Perkin-Elmer.

The acids were of Suprapur quality (Merck). A 1% (w/v) lanthanum solution was prepared by dissolving lanthanum(III) oxide (Suprapur, Merck) in the minimum amount of nitric acid.

Measurements

From 20% (w/v) orthophosphoric acid, 5-μl portions were transferred to the graphite furnace and were atomized according to the furnace parameters given in Table 1.

TABLE 1

General furnace parameters for studying the performance of the inverse Zeeman background corrector for orthophosphoric acid at different element lines. Maximum power or 1-s ramp time were used at the atomization step as indicated in the text

Step	1	2	3
Temp. (°C)	120	400	2000
Ramp (s)	10	10	1 (0)
Hold (s)	20	20	3 (4)
Read (s)	—	29	—[a]
Int. flow	—	—	gas stop

[a]Read step.

RESULTS AND DISCUSSION

Figure 1 shows the absorbance profiles of the analyte and background signals as obtained for the three main palladium lines at 247.6, 244.8 and 276.3 nm. The signals in Fig. 1A and B were obtained with maximum power and 1-s ramp time, respectively, in the atomization step. The background profiles are very much alike at the three wavelengths (curves 1—3), still the signals are overcompensated at the 247.6-nm line and undercompensated at the 244.8-nm line; at the 276.3-nm line no compensation error occurs.

The atomization steps with maximum power (Fig. 1A) and with 1-s ramp time (Fig. 1B) seem to produce several absorbing species (maybe also species in different excited vibrational levels). Only the species evaporating after about 1 s with maximum power, or 3 s with 1-s ramp time, are subject to background compensation error at two of the three palladium lines.

Persson and Frech [12] used high-temperature equilibrium calculations in a study of the atomization of orthophosphoric acid in a graphite furnace. Their calculations showed that volatile phosphorus monoxide and dioxide are formed below 1800 K ($P_{O_2} \leq 10^{-13}$ atm.) and that P_2 is the dominating species above 1600 K; their experiments revealed that PO was still present at 2500 K.

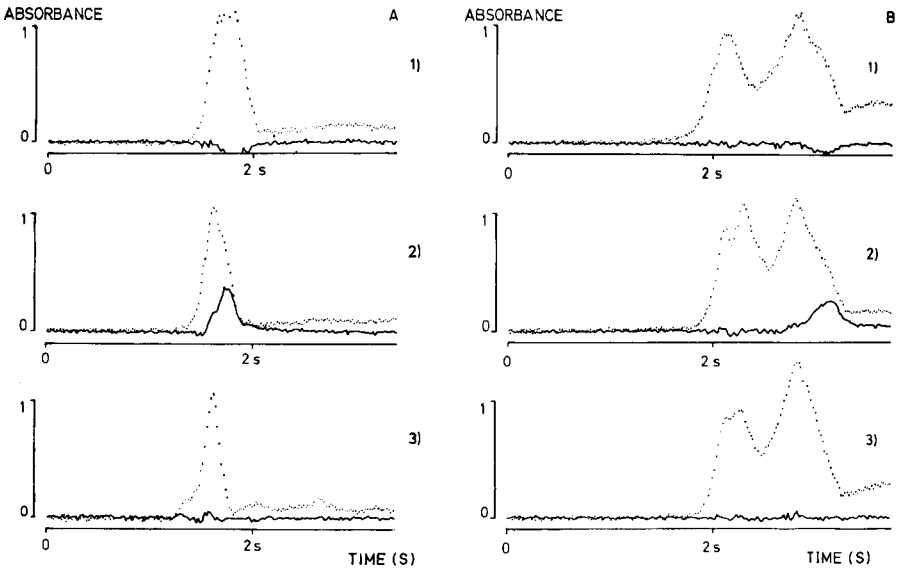

Fig. 1. Absorbance profiles of 5 μl of 20% (w/v) phosphoric acid as measured at different palladium lines: (1) 247.6 nm, (2) 244.8 nm, (3) 276.3 nm. Maximum power (A) and 1-s ramp time (B) were used in the atomization step. The solid and dashed curves are the analyte signal corrected for background and the background signal, respectively. For experimental conditions see Table 1; slit width 0.2 nm.

It seems most likely that the present background errors were caused by Zeeman splitting of a rotational line of the PO molecule. This assumption is supported by the work of Massmann et al. [13] who recorded the absorption spectrum of PO in an air/acetylene flame with a spectrometer of very high resolution; from this study, it is seen that the 247.642-nm and 244.791-nm palladium lines are situated close to PO rotational lines.

For the actual determination of palladium in phosphoric acid, the interferences discussed above should not represent any problems. When the pyrolysis temperature is raised to 800°C, the matrix is volatilized, as is apparent from the absence of any background signal during the subsequent atomization step and the absence of the above compensation errors. However, in other matrices, PO may still be present after a pyrolyzing step of 800°C or higher. For instance, when 1% lanthanum was present in orthophosphoric acid, the correction errors were increased when the acid was measured according to the furnace parameters given in Table 1 and the interferences were still present after a pyrolysis step of 800°C.

Two other analyte lines in the wavelength range of the PO γ-system were found to give compensation errors when 5-μl portions of 20% orthophosphoric acid were atomized with the furnace parameters listed in Table 1. The background signals at the 244.2-nm copper and the 247.3-nm iron lines

showed similar form and height as those observed at the palladium lines, the negative correction errors also appeared at the same times as for the palladium lines.

A background compensation error was also found in the region of the PO β-system. As can be seen from Fig. 2, phosphoric acid gives an overcompensation error at the 325.8-nm indium line. For comparison, the signals at the 326.1-nm cadmium line are also given; the overcompensation at this line has already been described by Carnrick et al. [6]. In Fig. 2, both overcompensations appear at the same time as for the palladium lines, the errors again probably being caused by the splitting of a PO rotational line.

The interference at the indium line can be avoided by applying a higher temperature of pyrolysis.

Conclusions

In electrothermal a.a.s., it is in general difficult to predict the cases in which interference from structured molecular compounds will occur. The molecular species present are seldom known, detailed spectroscopic data are lacking for many molecules, and the various background corrector systems may behave differently towards the species present. With the inverse Zeeman background corrector, the situation is still more complicated because the possible Zeeman splitting has to be taken into account.

The recent studies of background compensation errors in inverse Zeeman-corrected measurements have demonstrated that interferences caused by Zeeman splitting of molecular species also have to be considered. The many

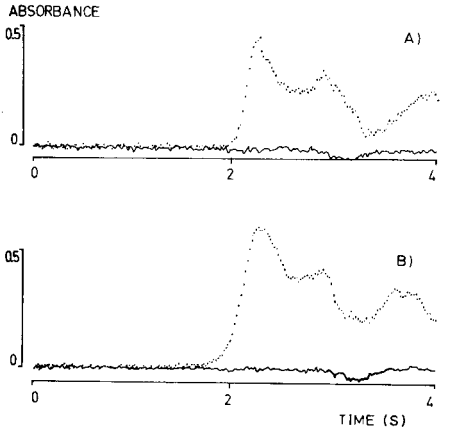

Fig. 2. Absorbances profiles of 5 μl of 20% (w/v) phosphoric acid measured at the 326.1-nm cadmium line (A) and the 325.8-nm indium line (B). The solid and dashed curves are the analyte signal corrected for background, and the background signal, respectively. For experimental conditions see Table 1; ramp time 1 s, slit width 0.7 nm.

types of matrices encountered in analytical atomic absorption spectrometry may reveal other interferences of the present type; the extent of this interference cannot be stipulated and will require more systematic studies.

REFERENCES

1 U. Kurfürst, Fresenius' Z. Anal. Chem., 315 (1983) 304.
2 H. Massmann, Talanta, 29 (1982) 1051.
3 G. Wibetoe and F. J. Langmyhr, Anal. Chim. Acta, 165 (1984) 87.
4 G. Wibetoe and F. J. Langmyhr, Anal. Chim. Acta, 176 (1985) 33.
5 G. Wibetoe and F. J. Langmyhr, Anal. Chim. Acta, 186 (1986) 155.
6 G. R. Carnrick, W. Barnett and W. Slavin, Spectrochim. Acta, Part B, 41 (1986) 991.
7 R. W. B. Pearse and A. G. Gaydon, The Identification of Molecular Spectra, 3rd edn., Chapman & Hall, London, 1963.
8 G. Herzberg, Spectra of Diatomic Molecules, 2nd edn., D. Van Nostrand, New York, 1950.
9 F. J. Fernandez and R. Giddings, At. Spectrosc., 3 (1982) 61.
10 V. Voellkopf and Z. Grobenski, At. Spectrosc., 5 (1984) 115.
11 G. R. Carnrick, D. C. Manning and W. Slavin, Analyst, 108 (1983) 1297.
12 J. A. Persson and W. Frech, Anal. Chim. Acta, 119 (1980) 75.
13 H. Massmann, Z. El Gohary and S. Gücer, Spectrochim. Acta, Part B, 31 (1976) 399.

Analytica Chimica Acta, 198 (1987) 87—101
Elsevier Science Publishers B.V., Amsterdam — Printed in The Netherlands

LA MATRICE EAU DE MER ET LE SIGNAL DU CUIVRE EN SPECTROMETRIE D'ABSORPTION ATOMIQUE SANS FLAMME
Partie 1: Etude de l'Influence des Principaux Composants

J. Y. CABON et A. LE BIHAN*

Université de Bretagne Occidentale, UA CNRS 322 (Chimie, électrochimie et photochimie moléculaires), 6, Avenue V. Le Gorgeu, 29287 Brest-Cedex (France)

(Reçu le 27 novembre 1986)

SUMMARY

(Copper signals from seawater matrices in electrothermal atomic absorption spectrometry. Part 1: study of the effects of principal inorganic ions.)

The effects of the main inorganic ions of seawater (Na^+, Mg^{2+}, Ca^{2+}, Cl^-, SO_4^{2-}), and of nitrate as modifier, on the electrothermal atomic absorption spectrometric signal of copper are studied. Sodium chloride, sulfate or nitrate, magnesium chloride or nitrate, and calcium chloride can cause serious interferences. Thermal treatment at about 700°C prevents the interference of $MgCl_2$ by its hydrolysis. Ashing can be done without loss of copper at higher temperatures in the presence of sulfate salts (1300°C) and nitrate salts (1200°C) than in the presence of chloride salts (1100°C). This is ascribed to the stabilising effect of oxides and sulfides. A study of the influence of two-component matrices, MCl-MNO_3 or MCl-MSO_4, on the atomization signal of copper confirms this stabilizing effect which adds to the decrease in interference connected with removal of chloride in acidic medium.

RESUME

L'étude de l'influence des principaux composés inorganiques de l'eau de mer (Na^+, Mg^{2+}, Ca^{2+}, Cl^-, SO_4^{2-}) et du nitrate, sur le signal du cuivre mesuré par spectrométrie d'absorption atomique sans flamme est réalisée. Les trois sels de sodium (NaCl, Na_2SO_4, $NaNO_3$), le chlorure et le nitrate de magnésium, et le chlorure de calcium provoquent des interférences conséquentes. La calcination à une température voisine de 700°C permet d'éliminer l'interférence du chlorure de magnésium qui est hydrolysé. La calcination peut être effectuée sans perte de cuivre à température plus élevée (1300°C) en milieu sulfate qu'en milieu nitrate (1200°C) et en milieu chlorure de sodium (1100°C). Ceci traduit l'effet stabilisateur de l'oxyde de sodium et plus particulièrement du sulfate (sulfure) de sodium. L'étude de l'influence des matrices à deux composants, MCl-MNO_3 ou MCl-MSO_4, sur le signal d'atomisation du cuivre confirme cet effet stabilisateur qui s'ajoute à la diminution d'interférence liée au départ de chlorure en milieu acide.

La spectrométrie d'absorption atomique sans flamme n'étant pas encore [1] une méthode absolue, un dosage ne peut être effectué que par comparaison avec une courbe d'étalonnage réalisée dans un milieu aussi semblable que possible à celui étudié, ou par une méthode d'addition standard. L'emploi de cette méthode implique que soit vérifiée la constance des inter-

0003-2670/87/$03.50

férences et donc d'avoir une connaissance aussi exacte que possible de leurs causes. De même, cette méthode est d'autant plus sensible aux erreurs de correction [2, 3] liées à la présence d'absorptions non-spécifiques que les concentrations à déterminer sont plus proches de la limite de détection. L'atténuation maximum des absorptions non-spécifiques doit donc être recherchée en évitant les pertes de métal et les contaminations.

Des études théoriques assez nombreuses concernant les phénomènes de production d'atomes neutres conduisent à une compréhension des interférences [4—8] en présence d'une matrice simple et relativement peu concentrée, ce qui ne correspond pas au cas de l'eau de mer (Tableau 1). Pour ce milieu, la complexité des phénomènes engendrés par la matrice apparaît [10] lorsque l'on considère les résultats des études effectuées à l'occasion de la mise au point de méthodes de dosage direct. Dans le cas du cuivre, seuls Segar et Cantillo [11] annoncent un dosage direct en l'absence de modificateur. Les études réalisées ultérieurement n'ont qu'approché la gamme de sensibilité nécessaire pour des milieux non pollués (10^{-8}—10^{-7} M) et ce, en utilisant des modificateurs: NH_4NO_3 [12, 13], Na_2O_2 [14] ou l'acide ascorbique [15, 16]. Aucune étude systématique des effets liés à la présence simultanée des interférants potentiels n'a été réalisée.

Une prévision théorique des signaux et de leur évolution dans un tel mélange ne pourrait être obtenue que si l'on disposait de tous les paramètres, y compris l'état de surface du four [17], permettant d'accéder à une bonne connaissance du milieu au moment de l'atomisation du métal, ainsi que de données précises concernant les phénomènes tant physiques que chimiques intervenant en phase gazeuse après l'atomisation. Ce n'est en général pas le cas, aussi, avons-nous cherché à établir, à partir de résultats obtenus dans des conditions expérimentales éventuellement utilisables pour un dosage dans le milieu marin, un schéma explicatif des phénomènes observés. En un premier temps, nous avons étudié l'influence sur le signal du cuivre 10^{-6} M des principaux composés minéraux présents dans l'eau de mer (Na^+, Mg^{2+}, Ca^{2+}, Cl^-, SO_4^{2-}) ainsi que celle de l'anion nitrate fréquemment utilisé comme modificateur de matrices.

TABLEAU 1

Composition en ions majoritaires d'une eau de mer type [9]

Ion	Na^+	Mg^{2+}	Ca^{2+}	K^+	Cl^-	SO_4^{2-}	HCO_3^-
Concentration (M)	0,47	0,053	0,01	0,01	0,55	0,028	0,0024

PARTIE EXPERIMENTALE

Les concentrations en cuivre et sels étudiés, le volume d'échantillon injecté et le débit de gaz utilisé ont été choisis de telle sorte que le signal du métal tant en mode hauteur de pic qu'en mode intégration surface soit suffisamment important pour qu'un suivi de ses variations puisse être effectué,

sans que les valeurs soient entachées d'erreurs importantes de corrections. De même les courbes présentées dans la partie quantitative de l'étude correspondent aux variations de surface du massif d'atomisation qui sont nettement plus reproductibles que les hauteurs de pic plus sensibles à l'état de surface du four.

Les solutions de sels de sodium, magnésium et calcium (produits pour analyse) sont préparées par dilution dans de l'eau ultrapurifiée à l'aide du système MQ-Millipore alimenté en eau par le système Milliro-Millipore. Les acides utilisés sont des produits Suprapur (Merck).

Le spectromètre d'absorption atomique utilisé est un Perkin-Elmer Zeeman 3030 muni d'un passeur d'échantillons AS-60X. La lampe au cuivre est une lampe Intensitron (15 mA). Certaines matrices n'absorbant pas à 324,7 nm, la volatilisation des sels est observée à 220 nm en utilisant une lampe à hydrogène (25 mA).

L'échantillon (10 μl) est introduit dans un four de graphite à revêtement pyrolytique (Perkin-Elmer). Le débit de gaz (azote Air-Liquide, qualité U) est fixé à 50 ml min^{-1}. Le séchage est réalisé à 120°C. La montée en température à 2700°C s'effectue en 1 s soit à partir de la température de séchage soit à partir de la température de calcination.

Etant donné l'agressivité de certains sels ou acides, il est nécessaire de contrôler périodiquement l'état des parois du four par passage d'une solution standard.

RESULTATS ET DISCUSSION

Etude des variations du signal du cuivre pour un composé CuX

En l'absence de matrice et pour une concentration en métal inférieure à 10^{-6} M, la température de sortie du signal sa forme et sa surface ne sont pas fonction de l'anion (chlorure, nitrate, sulfate) auquel il est associé. Ceci indique qu'au cours du traitement thermique, une même espèce se forme, ce qui est cohérent avec le mécanisme proposé, notamment par Chung [18]:

$$CuO_{(s)} \rightarrow Cu_{(s)} \rightarrow Cu{-}Cu_{(g)} \rightarrow Cu^{0}_{(g)}$$

L'espèce $Cu{-}Cu_{(g)}$ diatomique, n'apparaissant qu'aux basses températures de calcination. La formation de l'oxyde peut provenir, soit de l'hydrolyse de CuX, soit des atomes d'oxygène adsorbés sur le graphite [19]. En revanche, les courbes des Figs. 1, 3, 5 réalisées en présence de matrice MX (M:Na, K, Ca, Mg) 10^{-1} M en anion X mettent en évidence que pour un même anion X, les caractéristiques du signal d'atomisation du cuivre sont fonction du cation M et réciproquement.

Les causes des variations de ces caractéristiques sont à rechercher dans les changements de température de départ de l'élément, et dans la variation des espèces chimiques présentes avant et pendant l'atomisation. Une variation de la température de départ de l'élément coïncide avec une variation

de la température des parois et du mélange gazeux du four, entraînant un déplacement des équilibres qui conduisent à l'apparition d'atomes neutres du métal [4] ainsi d'ailleurs qu'à un changement de leur durée de vie dans le four [20, 21]. Czobik et Matousek [6] ont ainsi montré que l'effet de transport ou de distillation [22] induisait dans le cas du plomb en présence de chlorure de sodium, une sortie anticipée du métal, associée à une augmentation de la hauteur du pic. An contraire, Slovak et Dočekal [23] ont mis en évidence un effet de "miniplateforme" en présence de matrice réfractaire induisant pour le cuivre et le fer un départ à température plus élevée, associé aussi à une augmentation de la hauteur de pic. Cet effet de "miniplateforme", légèrement différent de l'effet d'occlusion qui n'est à considérer que pour une mesure en hauteur de pic [24], ne peut comme lui se traduire que par un départ du métal à des températures plus élevées [25], c'est-à-dire par une augmentation du signal. Aucun de ces effets ne peut donc expliquer seul une diminution du nombre d'atomes neutres.

En ce qui concerne les espèces chimiques stabilisées avant l'atomisation, l'existence de concentrations importantes en espèces susceptibles de s'associer au métal favorise d'autant plus la formation de nouveaux composés que les réactions envisageables à la surface du graphite du four (hydrolyse, réduction) ou de la phase gazeuse (O_2, CO . .) sont défavorisées par la dispersion du métal dans la matrice. Cet effet, dès lors que la matrice MX existe sous forme fondue en même temps que le métal, ne dépend pas de la température de volatilisation de MX. Il participe à l'explication de la stabilisation des espèces CuX:CuCl [26], Cu_2S [27], Cu_2O [28] alors que c'est l'atomisation du métal réduit qui est prévisible [8, 18]. Il peut entraîner des départs de métal non-mesurés car selon leur stabilité, la température et la composition du milieu gazeux, les espèces vaporisées sous forme CuX sont ensuite plus ou moins dissociées puis transformées en atomes neutres.

La stabilisation de CuX en phase gazeuse par les atomes X est à la base des études qui sont actuellement considérées comme expliquant les phénomènes d'interférence [4, 8, 29] bien que quelques incertitudes subsistent notamment quant aux pressions partielles d'oxygène dans le four [30, 31]. La pression partielle des atomes X à proximité immédiate du métal dépend, dans ce cas notamment, de la température de vaporisation de la matrice MX et de sa constante de dissociation. Ceci explique que pour ce type d'effet, ce soit le couple M et X qu'il faille considérer [32] et non le cation ou l'anion isolé.

Interférence des chlorures

L'interférence chlorure dans le cas du cuivre a été notamment étudiée par Churella et Copeland [14] qui concluent pour NaCl, $MgCl_2$ et $CaCl_2$ à des phénomènes d'occlusion, par Smeyers-Verbeke et al. [33] et par Matsusaki [34] qui attribue un rôle prépondérant à la formation de chlorure métallique en solution. Slavin et al. [29] confirment les travaux de L'vov [35] qui avance le rôle prédominant des associations en phase gazeuse.

Nous avons représenté sur les Figs. 1 et 2 l'influence de différents chlorures sur le signal du cuivre pour une montée en température de 120 à 2700°C en 1 s. Les absorptions non spécifiques mesurées à 220 nm sont également reportées permettant de suivre le départ de la matrice, les matrices $MgCl_2$ et $CaCl_2$ n'absorbant pas à 324,7 nm (Fig. 1). La Fig. 2 traduit quantitativement les interférences rencontrées pour des teneurs inférieures à 10^{-1} M. Dans cette étude, les variations d'interférences sont considérées comme quantitativement traduites par les variations du rapport de l'absorbance de la solution étudiée à celle d'une solution 10^{-6} M de chlorure de cuivre en milieu acide chlorhydrique 10^{-3} M, prise comme référence. Les courbes obtenues mettent en évidence un ordre d'atténuation du signal qui correspond aux pressions de vapeur des chlorures métalliques [36]. Le chlorure de magnésium provoque l'interférence la plus importante et le chlorure de calcium la moins élevée.

Appliqués au cas de l'eau de mer, ces résultats expliquent un effet très important de NaCl (pour 0,5 M ≈ 80% d'interférence) mais aussi de $MgCl_2$ (85% d'interférence) en dépit d'une teneur dix fois moindre. $CaCl_2$ et KCl présents à 10^{-2} M ont aussi un effet non-négligeable: 20—35% d'atténuation du signal à leur concentration respective.

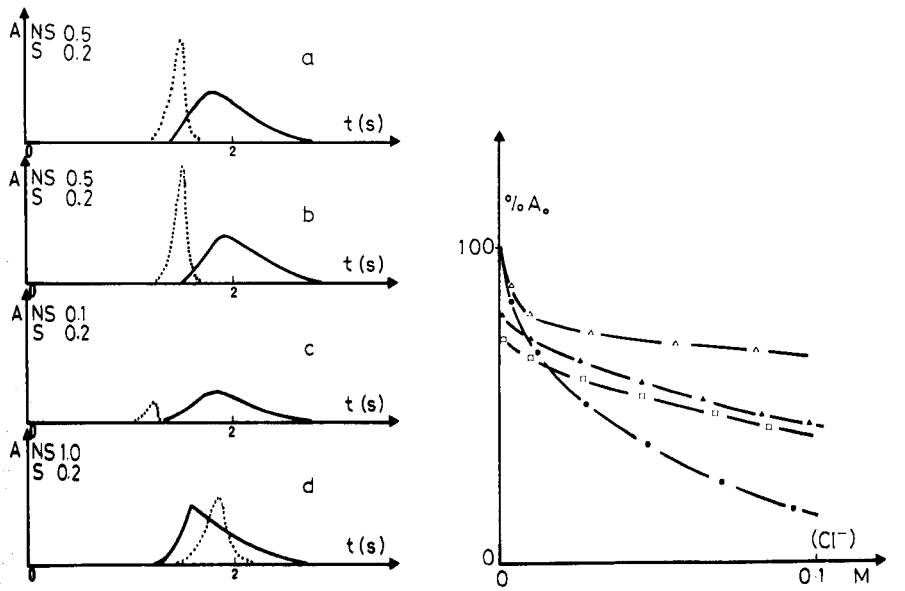

Fig. 1. Influence de différents chlorures sur le signal d'atomisation du cuivre (10^{-6} M) (—): (a) NaCl 0,1 M; (b) KCl 0,1 M; (c) $MgCl_2$ 0,5 M; (d) $CaCl_2$ 0,05 M. (· · ·) Matrices observées à 220 nm.

Fig. 2. Influence de la concentration en chlorure sur la surface du pic d'atomisation du cuivre (10^{-6} M): (▲) NaCl; (□) KCl; (●) $MgCl_2$; (△) $CaCl_2$.

Pour les composés MX étudiés, l'apparition du chlore en phase gazeuse n'est a priori conséquente [37] qu'après leur volatilisation. Dans ces conditions la modification et l'atténuation du pic en présence de chlorure de calcium dont la température de volatilisation est la plus élevée sont une illustration de la stabilisation de CuCl en phase liquide associée à un phénomène type distillation. C'est effectivement dans ce cas que l'interférence est la plus faible, la distillation se produisant alors que la pression partielle de chlore en phase gazeuse n'est pas encore importante puisque $CaCl_2$ n'est pas vaporisé.

Interférences des nitrates

Bien que les concentrations en nitrates dans l'eau de mer ne situent pas cette espèce parmi les interférents naturels potentiels, leur emploi fréquent comme modificateur et le fait qu'ils constituent un moyen d'accès à l'étude de l'interférence des oxydes, nous ont amené à considérer leur influence sur le signal. Yasuda et Kakiyama [26] ont montré que la décomposition des nitrates métalliques produisait NO_2 puis NO dans le four, Eklund et Holcombe [28] précisent que le métal est alors transformé en son oxyde. Ils indiquent dans leurs résultats, obtenus sur filament en état stationnaire, une augmentation de la sensibilité du dosage du cuivre en présence de nitrate de calcium et une atténuation en présence des nitrates de sodium et de potassium.

Nous avons répresenté sur les Figs. 3 et 4, l'influence des différents nitrates sur le signal du cuivre. Les absorptions non-spécifiques mesurées à 220 nm permettant de suivre le départ de la matrice sont également reportées (Fig. 3). Si l'on admet le mécanisme décrit par Yasuda et Kakiyama [26], le premier pic de la matrice peut être attribué aux espèces nitrées issues de la décomposition du nitrate dans le cas de Na, K et Mg. Le dernier pic (ou massif pour le calcium) correspond comme nous l'avons montré pour le nitrate de sodium [38] au départ de l'oxyde. Les courbes de la Fig. 4 traduisent quantitativement ces interférences. Elles montrent que jusqu'à une teneur de 5.10^{-2} M, seul le nitrate de magnésium, qui est liquide dès 95°C et se décompose à 330°C [36] provoque une atténuation (environ 20%) du signal, attribuable à la sublimation du nitrate de cuivre vers 220°C [39]. Ce fait souligne que le nitrate de magnésium ne doit être utilisé comme modificateur qu'avec précaution.

Le nitrate de calcium, dont CaO est le produit résultant, n'induit pas d'atténuation dans la gamme de concentration étudiée en raison de sa volatilisation à une température supérieur à celle du métal (Fig. 3d) et de la trop faible augmentation de la pression d'oxygène liée à sa décomposition [8]. Le même raisonnement peut être tenu pour MgO, il explique l'existence du palier pour des concentrations en nitrate de magnésium supérieures à 3.10^{-2} M (Fig. 4).

En revanche, bien que n'interférant pas jusqu'à 5.10^{-2} M, les nitrates de sodium et de potassium provoquent des atténuations du signal à partir de

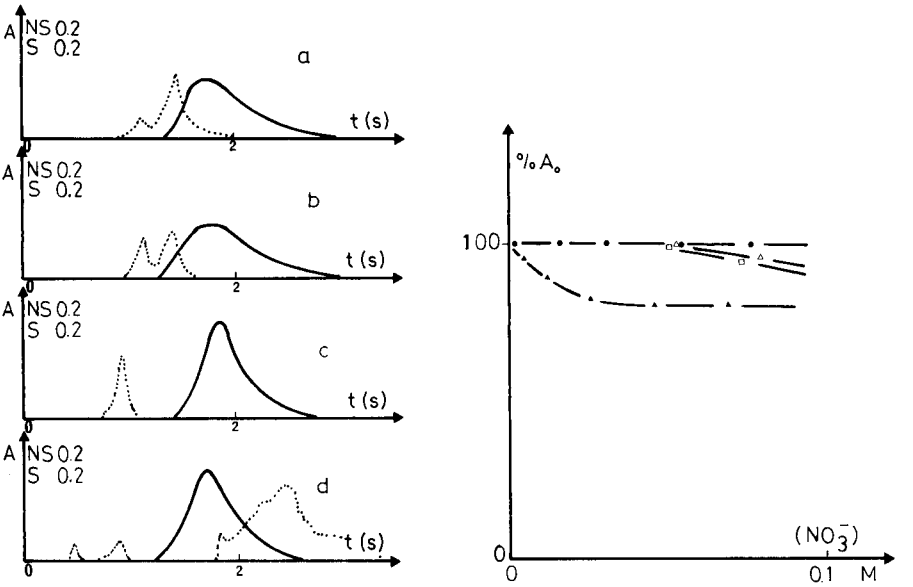

Fig. 3. Influence de différents nitrates sur le signal d'atomisation du cuivre (10^{-6} M) (—): (a) $NaNO_3$ 0,1 M; (b) KNO_3 0,1 M; (c) $Mg(NO_3)_2$ 0,05 M; (d) $Ca(NO_3)_2$ 0,05 M. (···) Matrices observées à 220 nm.

Fig. 4. Influence de la concentration en nitrate sur la surface du pic d'atomisation du cuivre (10^{-6} M): (△) $NaNO_3$; (□) KNO_3; (▲) $Mg(NO_3)_2$; (●) $Ca(NO_3)_2$.

cette concentration. Nous avons vérifié que ces atténuations sont identiques à celles mesurées en présence de NaOH ou KOH 5.10^{-2} M. Ceci indique que ce sont en fait les oxydes de sodium et de potassium, se volatilisant juste avant le départ du métal, qui provoquent l'interférence et non les oxydes d'azote. La pression d'oxygène étant déjà, indépendamment de la présence de matrice, importante dans cette zone [8], il est logique de considérer que cette interférence est liée à la stabilisation de l'oxyde de cuivre en phase matrice liquide. Aux concentrations rencontrées dans l'eau de mer, seul l'oxyde de sodium issu d'une modification de la matrice par un traitement à l'acide nitrique, serait susceptible d'entraîner une atténuation conséquente du signal (≈20%) pour $NaNO_3$ 0,5 M.

Interférence des sulfates

Smeyers-Verbeke et al. [32] notent une faible interférence positive du sulfate de magnésium (+40%) et une interférence nulle des sulfates de sodium et potassium sur le signal de cuivre. Eklund et Holcombe [28] indiquent, sur filament, une dépression importante pour les sulfates de sodium et potassium (voisine de 100%). Ils considèrent que les espèces prédominantes formées sont l'oxyde MO, SO_2 et O_2. Dans une précédente publication, Cabon et al. [38] avaient montré qu'au moins dans le cas du

sulfate de sodium (et dans le cas d'une montée lente en température) la matrice résultante, correspondait au sulfure de sodium. Une simple addition d'eau acidifiée par l'acide nitrique dans le four après une calcination de sulfate de sodium vers 1000°C confirme cette donnée car elle se traduit par un dégagement d'acide sulfhydrique et un retour à une matrice type oxyde de sodium lors de l'atomisation suivante. Enfin, il est à signaler que Suzuki et Ohta [27] expliquent un mécanisme d'élimination d'interférence par la thiourée, dans le cas du cuivre notamment, par la formation de Cu_2S qu'ils ont identifié par spectre de rayons-X.

Nous avons représenté sur la Fig. 5 l'influence de différents sulfates sur le signal d'atomisation du cuivre, et les absorptions non-spécifiques mesurées à 220 nm. Le pic non-spécifique apparaissant pour $MgSO_4$ et le premier pic lié à $CaSO_4$ sont attribués aux oxydes de soufre. Ces courbes mettent en évidence une forme tout à fait caractéristique du signal non-spécifique obtenu pour les sulfates de sodium et de potassium. Parallèlement l'accroissement de la hauteur du pic spécifique, à surface égale peut atteindre 400%. Pour ces deux matrices, le départ de métal se situe après un délai nettement plus important que dans le cas du signal obtenu en l'absence de matrice, les maximums sont eux aussi décalés mais beaucoup plus faiblement. Dans le cas du signal reporté en présence de sulfate de magnésium, la forme du massif indique un départ du métal dans deux conditions différentes. Ce signal pourrait correspondre à un départ sous la forme induite par la matrice MgO suivi d'un signal type Cu_2S lié à la présence d'une matrice MgS. Le second départ présente un maximum très décalé en température, par rapport au signal repéré en l'absence de matrice. Le sulfate de calcium, aux teneurs auxquelles il peut être introduit (10^{-2} M) n'a pas d'effet très important sur le signal d'atomisation du cuivre.

Il est à noter qu'ainsi que le montrent les courbes de la Fig. 6, la forme caractéristique du signal du cuivre n'apparaît en présence de Na_2SO_4 que progressivement et à partir de teneurs en sulfate supérieures à 4.10^{-3} M. Il n'est donc pas a priori possible d'exclure qu'en ce qui concerne la forme du massif, il puisse s'agir d'un phénomène type occlusion. Du point de vue quantitatif, les courbes de la Fig. 7 mettent en évidence que ni le sulfate de calcium ni celui de magnésium ne provoquent d'atténuation de la surface mesurée. Par contre, et bien qu'en hauteur de pic, un accroissement conséquent soit constaté, les sulfates de potassium et de sodium provoquent une interférence négative qui atteindrait dans le cas du dernier 50% aux teneurs susceptibles de se rencontrer dans une eau de mer où l'on utiliserait l'acide sulfurique 0,25 M comme modificateur pour chasser les ions chlorure. Sur un autre plan, l'emploi d'une solution étalon de métal stabilisée en milieu acide sulfurique 0,5 M peut, ainsi que le montrent les courbes de la Fig. 6, induire une erreur conséquente si le dosage est effectué par la méthode des additions standards en mode hauteur de pic.

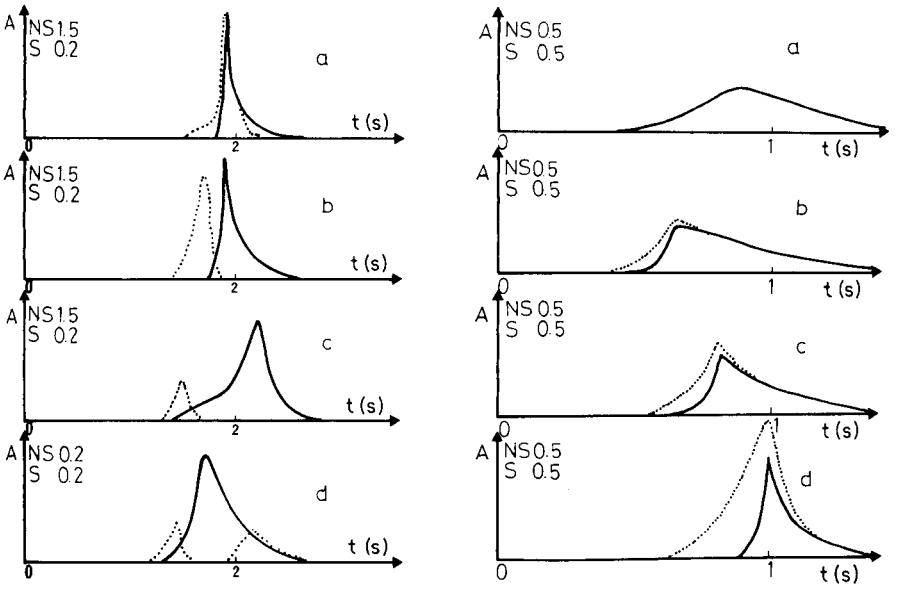

Fig. 5. Influence de différents sulfates sur le signal d'atomisation du cuivre (10^{-6} M) (—): (a) Na_2SO_4 0,1 M; (b) K_2SO_4 0,1 M; (c) $MgSO_4$ 0,1 M; (d) $CaSO_4$ 0,01 M. (···) Matrices observées à 220 nm.

Fig. 6. Influence de la concentration en Na_2SO_4 sur le signal d'atomisation du cuivre (10^{-6} M) (—): (a) eau MQ; (b) Na_2SO_4 0,004 M; (c) Na_2SO_4 0,008 M; (d) Na_2SO_4 0,05 M. (···) Matrices observées à 324,7 nm. Délai de lecture 1s.

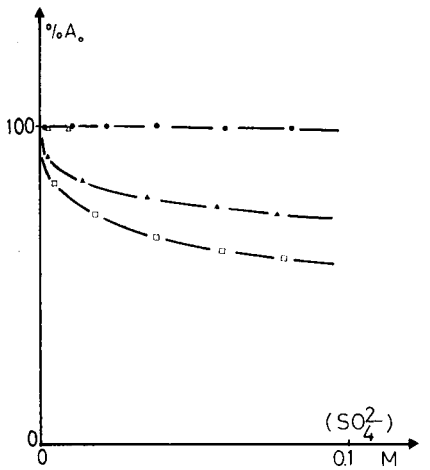

Fig. 7. Influence de la concentration en sulfate sur la surface du pic d'atomisation du cuivre (10^{-6} M): (▲) Na_2SO_4 0,1 M; (□) K_2SO_4 0,1 M; (●) $MgSO_4$ (0,1 M); (△) $CaSO_4$ 0,01 M.

Effet du traitement thermique

Effets de la calcination sur l'interférence chlorure. Les courbes de la Fig. 8A montrent les variations de l'atténuation du signal du cuivre après une calcination de 20 s à différentes températures. En l'absence de matrice, une perte de métal apparaît au-dessus de 1150°C. En présence de chlorure de calcium, aucune modification de l'atténuation n'apparaît jusqu'à une température légèrement inférieure à 1100°C. Nous retrouvons pour la calcination du chlorure de sodium, la variation présentée par Segar et Cantillo [11] qui s'expliquerait par un départ au-dessus de 800°C d'une partie de l'interférent NaCl, la décroissance ultérieure s'expliquant par les pertes de chlorure métallique à ce stade. Ces courbes mettent en évidence qu'il n'est pas envisageable d'éliminer cette interférence chlorure de sodium par simple calcination.

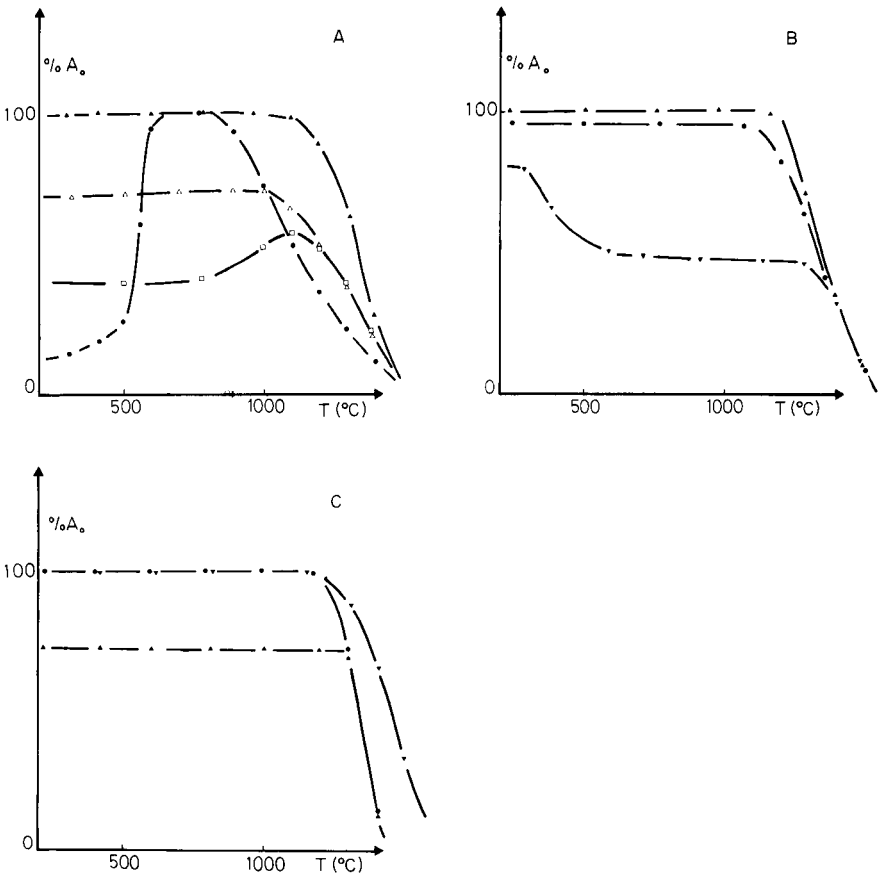

Fig. 8. Influence de la température de calcination (t = 20 s) sur la surface du pic d'atomisation du cuivre (10^{-6} M) en différentes milieux (A): (▲) eau MQ; (□) NaCl 0,1 M; (△) $CaCl_2$ 0,05 M; (●) $MgCl_2$ 0,05 M. (B): (●) $NaNO_3$ 0,1 M; (▼) $Mg(NO_3)_2$ 0,05 M; (▲) $Ca(NO_3)_2$ 0,05 M. (C): (▲) Na_2SO_4 0,1 M; (▼) $MgSO_4$ 0,1 M; (●) $CaSO_4$ 0,01 M.

En revanche, dans le cas du chlorure de magnésium, dès 200°C, la surface du pic croît jusqu'à retrouver pour 600°C une atténuation nulle qui subsiste jusqu'à 800°C. Au delà de cette température, les pertes de métal redeviennent sensibles. Erspamer et Niemczyk [40] lors d'une comparaison des graphites pyrolytique et non-pyrolytique ont mis en évidence la décomposition en trois espèces de $MgCl_2$. Ils estiment que celle se vaporisant la dernière ne peut être MgO mais pourrait être $MgCl_x$. Kantor et Bezur [41] concluent, en se référant à l'hydrolyse par adsorption d'électrolytes neutres sur charbon actif, à l'hydrolyse partielle de $MgCl_2$ tout comme Slavin et al. [29]. Pour notre part, nous avons constaté en cours de calcination la disparition totale du pic repéré à 220 nm attribué à $MgCl_2$ et la suppression de l'interférence. L'augmentation de l'interférence au-dessus d'une certaine température de calcination confirme qu'il existe un départ du cuivre, sans doute sous forme Cu_3Cl_3 [26], associé à la volatilisation de la matrice $MgCl_2$ non encore hydrolysée. Le fait qu'après une première calcination de $MgCl_2$ à 800°C, il soit alors possible de calciner à 1100°C pendant 20 s sans perte de cuivre confirme cette proposition.

Effet de la calcination sur l'interférence nitrate. Nous avons reporté sur la Fig. 8B les courbes montrant les variations de l'interférence provoquée par les différents nitrates après calcination à différentes températures. Elles confirment la perte de nitrate du cuivre dès 200°C en présence de nitrate de magnésium et l'interférence faible mais non-négligeable du nitrate de sodium qui reste inchangée même lorsque les oxydes d'azote ont été chassés par calcination. Il est compréhensible que l'existence de nitrate de magnésium fondu [36], stable à la température de sublimation de $Cu(NO_3)_2$ [39], favorise la perte de métal tandis que les interférences de $NaNO_3$ et $Ca(NO_3)_2$ (Fig. 4) sont en fait celles provoquées par NaO_x et CaO.

Influence de la calcination sur l'interférence sulfate. Les courbes de la Fig. 8C réalisées en présence de 10^{-1} M de sulfate de sodium et de magnésium, ou 10^{-2} M de sulfate de calcium, indiquent que la calcination n'a aucun effet sur cette interférence si l'on travaille en intégration de surface. On note par contre que la hauteur du pic du signal croît d'environ 20% lorsque l'on calcine au-dessus de 500°C le sulfate de magnésium sans que l'on parvienne à une forme de massif correspondant à un seul pic assimilable à Cu_2S. Ceci confirme que MgO et MgS subsistent après calcination dans les conditions employées. Dans le cas de Na_2SO_4, les pertes de métal à haute température de calcination n'apparaissent qu'au-dessus de 1300°C (alors qu'en présence de NaO_x elles sont sensibles dès 1200°C) au moment où la matrice Na_2S se volatilise. La présence de cette espèce permet donc bien de maintenir le métal jusqu'à température plus élevée dans le four. Une telle stabilisation n'est obtenue ni par le sulfate de magnésium ni par celui de calcium.

Les résultats des études réalisées en présence d'un seul sel démontrent que pour l'eau de mer, l'anion interférent prépondérant sera le chlorure sans qu'il soit possible de négliger les sulfates dont l'importance au moment

de l'atomisation et de la calcination s'accroît s'ils sont, à ce moment, associés à l'ion sodium.

Etude de l'interférence dans des matrices à deux composants MCl-M(NO_3) et MCl-M(SO_4)

Afin de réaliser cette étude à quantité constante de métal dans le four, nous avons été amenés à faire évoluer le rapport des deux anions de la matrice par addition d'acide nitrique ou sulfurique. Nous avons d'abord vérifié par addition d'acide chlorhydrique que l'adjonction de protons à la solution n'a aucun effet spécifique sur l'interférence. Comme nous avons démontré [38] la quantitativité de l'élimination du chlorure dans le cas de NaCl par addition de quantité d'acide nitrique ou sulfurique correspondant à la stoechiométrie de la réaction, il est justifié de considérer que les matrices MCl-HNO_3 (ou H_2SO_4) se comportent comme des mélanges MCl-MNO_3 ou MCl-MSO_4 dans lesquels la somme des concentrations des deux anions ainsi que la teneur en métal sont constantes.

Etude de l'interférence chlorure-nitrate. Les courbes de la Fig. 9A, réalisées pour raison d'homogénéité en milieu initial 0,1 M en chlorure, font apparaître que pour les chlorures de sodium et de magnésium, dès un rapport $[NO_3^-]/[Cl^-]$ voisin de 1, l'élimination de l'interférence est presque totale. Le phénomène ne peut toutefois être considéré comme la simple élimination de l'interférence liée à la présence des chlorures car les courbes obtenues traduisent des interférences nettement plus faibles, avant ce rapport 1, que celles qui devraient être trouvées aux teneurs de NaCl et $MgCl_2$ restantes (cf. Fig. 2) et ce, d'autant qu'il aurait pu paraître logique d'y additionner l'interférence résultant du nitrate de sodium ou du nitrate de magnésium apparu (Fig. 4). Dans le cas du chlorure de magnésium, il est possible que cette minimisation de l'interférence soit liée à une hydrolyse facilitée du sel mais ce type d'explication ne peut convenir pour le chlorure de sodium. Nous proposons de considérer que dans ce cas, dès les premières additions de nitrate, une partie du chlorure de cuivre se transforme en oxyde qui est stabilisé par la présence de la matrice oxyde de sodium. Des essais effectués par addition de soude indiquent le même effet, ce qui confirme l'importance de la présence d'oxyde de sodium.

La courbe représentée dans le cas du chlorure de calcium met en évidence, après une phase durant laquelle l'interférence diminue rapidement, l'apparition d'un palier correspondant à 15% d'interférence qui subsiste jusqu'à un rapport $[NO_3^-]/[Cl^-]$ peu différent de 2 qui correspond à l'élimination totale du chlorure, vérifiée à 220 nm. Comme dans le cas du chlorure de sodium, l'addition de nitrate se traduit par une minimisation de l'interférence supérieure à celle qui résulte de la simple élimination de $CaCl_2$. Etant donné la température de fusion de CaO (2580°C) ce produit peut être considéré comme exclu du milieu lors du départ du cuivre qui commence vers 1150°C. Dans ces conditions il semble que l'augmentation supplémentaire du signal soit attribuable au seul départ du métal sous forme d'oxyde.

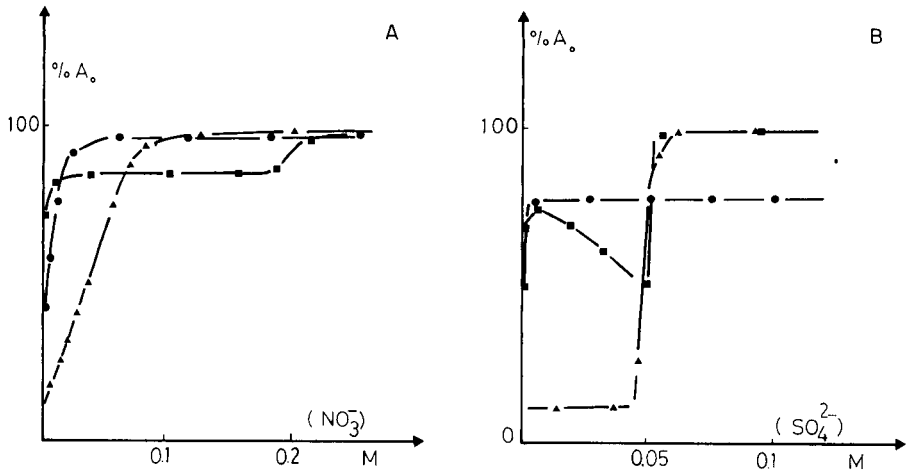

Fig. 9. Influence de la concentration en HNO_3 (A) ou en H_2SO_4 (B) sur la surface du pic d'atomisation du cuivre (10^{-6} M): (•) NaCl 0,1 M; (▲) $MgCl_2$ 0,05 M, (■) $CaCl_2$ 0,05 M.

Sur un plan plus pratique, il faut remarquer que l'interférence du chlorure de magnésium n'étant éliminée que pour un rapport $[NO_3^-]/[Cl^-]$ voisin de 1, toute concentration de nitrate moindre induit des variations conséquentes de l'interférence en fonction du temps et de la température de calcination (Fig. 8A) ou du volume d'échantillon injecté, voire de la salinité de l'échantillon.

Etude de l'interférence chlorure-sulfate. Les courbes de la Fig. 9B sont réalisées par addition d'acide sulfurique à un milieu initial 0,1 M en chlorure. Dans les trois cas étudiés, dès que le rapport $[SO_4^{2-}]/[Cl^-]$ est voisin de 0,5, l'interférence atteint la valeur prévisible correspondant à une matrice MSO_4 0,05 M. Il est par contre facile de remarquer que la courbe correspondant à $MgCl_2$ n'a pas la croissance que justifierait l'élimination de ce chlorure (Fig. 2) et que dans le cas de $CaCl_2$ après une atténuation très rapide de l'interférence, celle-ci recommence à croître nettement jusqu'au voisinage du rapport $[SO_4^{2-}]/[Cl^-] = 0,5$. Nous n'avons pas d'explication à proposer pour ces phénomènes, le comportement de ces deux chlorures apparaissant d'après les études déjà effectuées [29, 40, 41] extrêmement complexe.

Dans le cas du chlorure de sodium, l'addition d'acide sulfurique se traduit dès 10^{-2} M, c'est-à-dire dès qu'apparaît nettement la forme caractéristique du pic du cuivre en présence de Na_2SO_4 (Fig. 6), par l'accès à la valeur minimum de l'interférence et ce, bien qu'il reste encore une concentration en NaCl élevée (9.10^{-2} M). Il est possible d'en déduire que la formation de Cu_2S dans une matrice Na_2S stabilise suffisamment le cuivre pour éviter que l'interférence chlorure apparaisse et ceci même pour une phase gazeuse riche en chlorure. Par ailleurs, la valeur maximum du signal n'est pas atteinte car l'interférence liée à la présence de sulfate de sodium (Fig. 7) se substitue à celle du chlorure.

La remarque faite au paragraphe précédent sur l'élimination de l'inter-

férence de $MgCl_2$ qui doit être totale pour que n'existe plus de risque de variation du signal lié aux conditions de calcination, reste valable.

Conclusion

Cette première partie de l'étude a mis en évidence la probabilité de l'influence prépondérante des chlorures de sodium et de magnésium aux teneurs de l'eau de mer sur le signal du cuivre mesuré par spectrophotométrie d'absorption atomique sans flamme.

Pris séparément, le chlorure de sodium, non-sensible à l'hydrolyse provoque une interférence qui peut atteindre 80%. Cette interférence serait due à un départ du cuivre sous forme chlorure avant atomisation et à une stabilisation de ce composé en phase gazeuse en raison de la pression partielle du chlore. Il est possible d'éliminer cette interférence par addition de nitrate ou de sulfate à des concentrations ne permettant pas l'élimination totale du chlorure ce qui établit le rôle stabilisant de l'oxyde et du sulfure de sodium vis-à-vis du métal.

Le chlorure de magnésium, facilement hydrolysable, provoque une interférence qui, à une teneur de 5.10^{-2} M, atteint 85%. Elle peut être éliminée par une calcination à température comprise entre 600 et 800°C (hydrolyse) sans perte de cuivre. L'emploi de nitrate ou de sulfate à une concentration minimum de 5.10^{-2} M est également possible.

Enfin, la présence de sulfate de sodium au moment de l'atomisation à des concentrations supérieures à 5.10^{-3} M provoque une évolution remarquable de la forme du signal dont le pic est accentué et retardé.

REFERENCES

1 W. Slavin et G. R. Carnrick, Spectrochim. Acta, Partie B, 39 (1984) 271.
2 M. H. Massmann, Talanta, 29 (1982) 1051.
3 J. M. Harnly et J. A. Holcombe, Anal. Chem., 57 (1985) 1983.
4 W. Frech, E. Lundberg et A. Cedergren, Prog. Anal. At. Spectrosc., 8 (1985) 257.
5 B. Welz, S. Akman et G. Schlemmer, Analyst, 110 (1985) 459.
6 E. J. Czobik et J. P. Matousek, Anal. Chem., 50 (1978) 1.
7 S. G. Salmon et J. A. Holcombe, Anal. Chem., 54 (1982) 630.
8 R. E. Sturgeon, K. W. M. Siu et S. S. Berman, Spectrochim. Acta, Partie B, 39 (1984) 213.
9 F. Culkin, dans J. P. Riley (Ed.), Chemical Oceanography, 1st edn., Academic, London, 1965, p. 122.
10 M. Hoenig et R. Wollast, Spectrochim. Acta, Partie B, 37 (1982) 39.
11 D. A. Segar et A. Y. Cantillo, Adv. Chem. Ser., 147 (1975) 56.
12 A. D. Ediger, G. E. Peterson et J. D. Kerber, At. Absorpt. Newsl., 13 (1974) 61.
13 J. R. Montgomery et G. N. Peterson, Anal. Chim. Acta, 117 (1980) 397.
14 D. J. Churella et T. R. Copeland, Anal. Chem., 50 (1978) 309.
15 D. J. Hydes, Anal. Chem., 52 (1980) 959.
16 M. Tominaga, K. Bansho et Y. Umezaki, Anal. Chim. Acta, 169 (1985) 171.
17 H. M. Ortner, G. Schlemmer et B. Welz, Spectrochim. Acta, Partie B, 40 (1985) 959.
18 C. H. Chung, Anal. Chem., 56 (1984) 2714.
19 R. E. Sturgeon et S. S. Berman, Anal. Chem., 57 (1985) 1268.

20 S. L. Paveri-Fontana, G. Tessari et G. Torsi, Anal. Chem., 46 (1974) 1032.
21 W. M. Van der Broeke et L. de Galan, Anal. Chem., 49 (1977) 2176.
22 E. Schroll, Z. Anal. Chem., 198 (1963) 40.
23 Z. Slovak et B. Dočekal, Anal. Chim. Acta, 130 (1981) 203.
24 J. A. Krasowski et T. R. Copeland, Anal. Chem., 51 (1979) 1843.
25 J. P. Matousek, Prog. Anal. At. Spectrosc., 4 (1981) 247.
26 S. Yasuda et H. Kakiyama, Anal. Chim. Acta, 84 (1976) 291.
27 M. Suzuki et K. Ohta, Anal. Chim. Acta, 151 (1983) 401.
28 R. H. Eklund et J. A. Holcombe, Anal. Chim. Acta, 109 (1979) 97.
29 W. Slavin, G. R. Garnrick et D. C. Manning, Anal. Chem., 56 (1984) 163.
30 B. V. L'vov et G. N. Ryabchuk, Spectrochim. Acta, Partie B, 37 (1982) 673.
31 R. E. Sturgeon, K. W. M. Siu, G. J. Gardner et S. S. Berman, Anal. Chem., 58 (1986) 42.
32 J. Smeyers-Verbeke, Y. Michotte, P. Van den Winkel et D. L. Massart, Anal. Chem., 48 (1976) 125.
33 J. Smeyers-Verbeke, Y. Michotte et D. C. Massart, Anal. Chem., 50 (1978) 10.
34 K. Matsusaki, Anal. Chim. Acta, 141 (1982) 233.
35 B. V. L'vov, Spectrochim. Acta, Partie B, 33 (1978) 153.
36 Handbook of Chemistry and Physics, 48th edn., CRC, Cleveland, OH, 1967.
37 W. Frech, E. Lundberg et A. Cedergren, Can. J. Spectrosc., 30 (1985) 123.
38 J. Y. Cabon, A. Le Bihan et J. Courtot-Coupez, Anal. Lett., 19 (1986) 755.
39 K. H. Stern, J. Phys. Chem. Ref. Data, 1 (1972) 747.
40 J. P. Erspamer et T. M. Niemczyk, Anal. Chem., 54 (1982) 538.
41 T. Kantor et L. Bezur, J. Anal. At. Spectrosc., 1 (1986) 9.

Analytica Chimica Acta, 198 (1987) 103—111
Elsevier Science Publishers B.V., Amsterdam — Printed in The Netherlands

LA MATRICE EAU DE MER ET LE SIGNAL DU CUIVRE EN SPECTROMETRIE D'ABSORPTION ATOMIQUE SANS FLAMME
Partie 2: Proposition d'un Schéma Explicatif des Phénomènes Observés pour une Eau de Mer

J. Y. CABON et A. LE BIHAN*

Université de Bretagne Occidentale, UA CNRS 322 (Chimie, électrochimie et photochimie moléculaires), 6, Avenue V. Le Gorgeu, 29287 Brest-Cedex (France)

(Reçu le 27 novembre 1986)

SUMMARY

(Copper signals from seawater matrices in electrothermal atomic absorption spectrometry. Part 2: model for phenomena observed with sea water.)

A model to explain the variations of copper signals in seawater is proposed on the basis of the results of Part 1 of this study and data obtained by ashing simulated seawaters under different conditions. The model is confirmed by the results found with nitric or sulfuric acid as modifier. In this model, ashing at 800° C hydrolyses $MgCl_2$ to MgO, and the consequent formation of sodium sulfide from the matrix stabilizes the copper in the furnace. The addition of a small nitrate concentration (0.2 M) induces, when magnesium is present, a complementary decrease of the interference.

RESUME

Un schéma explicatif des variations du signal du cuivre dans l'eau de mer est proposé à partir des résultats de la première partie de l'étude et des données fournies par la calcination de milieux de composition proche de celle d'une eau de mer naturelle. Ce schéma est vérifié par l'étude de l'influence de l'addition des modificateurs acide nitrique et acide sulfurique. Il est proposé de considérer que la calcination à 800° C hydrolyse le chlorure de magnésium en oxyde de magnésium, ce qui provoque l'apparition de la matrice sulfate (sulfure) de sodium qui stabilise le métal. L'addition d'une faible quantité de nitrate (0,2 M) provoque, en la présence de magnésium, une atténuation complémentaire de l'interférence.

L'étude de l'influence des principaux composants de la matrice eau de mer et de la calcination sur le signal d'atomisation du cuivre et sur les absorptions non-spécifiques [1] nous a permis de proposer la prépondérance des interférences provoquées par les chlorures de sodium et de magnésium aux teneurs rencontrées dans l'eau de mer. L'influence stabilisatrice de l'oxyde ou du sulfure de sodium, s'ils sont présents au moment de l'atomisation a également été démontrée. A partir des données contenues dans cette étude, il est possible de considérer les variations des signaux spécifique et non-spécifique mesurés pour une eau de mer en fonction des traitements thermique ou chimique effectués et d'en proposer une interprétation. La com-

0003-2670/87/$03.50

position d'un mélange se comportant, vis-à-vis du cuivre et de la méthode d'analyse employée, comme une eau de mer naturelle découle en particulier de l'étude de la calcination. La validité de ce modèle est vérifiée lors de l'étude de l'influence des modificateurs sulfate et nitrate.

Afin de s'affranchir des phénomènes d'adsorption très sensibles en milieu neutre pour les métaux traces [2], nous avons systématiquement acidifié par de l'acide chlorhydrique (Suprapur) jusqu'à pH voisin de 1,5 [3] tous les milieux étudiés. Cet acide est éliminé de la matrice au séchage ainsi que le dioxyde de carbone provenant des carbonates et hydrogénocarbonates présents dans le milieu dans le cas d'une eau de mer naturelle. De ce fait le modèle que nous proposons exclut la contribution éventuelle des carbonates.

PARTIE EXPERIMENTALE

Les concentrations en cuivre et sels étudiés, le volume d'échantillon injecté et le débit de gaz utilisé ont été choisis de telle sorte que le signal du métal, tant en mode hauteur de pic qu'en mode intégration de surface, soit suffisamment important pour qu'un suivi de ses variations puisse être effectué, sans que les valeurs soient entachées d'erreurs importantes de corrections. Les courbes présentées dans la partie quantitative de l'étude correspondent aux variations de surface du massif d'atomisation qui sont nettement plus reproductibles que les hauteurs de pic plus sensibles à l'état de surface du four.

Les solutions de sels de sodium, magnésium et calcium (produits pour analyse) sont préparées par dilution dans de l'eau ultrapurifiée à l'aide du système MQ-Millipore alimenté en eau par le système Milliro-Millipore. Les acides utilisés sont des produits Suprapur (Merck).

Le spectromètre d'absorption atomique utilisé est un Perkin-Elmer Zeeman 3030 muni d'un passeur d'échantillons AS-60. La lampe au cuivre est une lampe Intensitron (15 mA).

Conditions d'atomisation

L'échantillon (10 μl) est introduit dans un four de graphite à revêtement pyrolytique (Perkin-Elmer). Le débit de gaz (azote Air-Liquide, qualité U) est fixé à 50 ml min^{-1}. Le séchage est réalisé à 120°C. Les signaux d'atomisation du cuivre et de volatilisation des matrices ont été observés à 324,7 nm en utilisant une vitesse de montée en température à 100°C s^{-1} soit à partir de la température de séchage, soit à partir de la température de calcination. Ces conditions ne correspondent pas aux conditions optimales de dosage mais permettent un meilleur suivi de l'évolution des massifs d'atomisation du cuivre en présence des diverse matrices.

Dans le cas de mesures quantitatives, la montée en température à 2700°C s'effectue en 1 s soit à partir de la température de séchage, soit à partir de la température de calcination considérée [1].

RESULTATS ET DISCUSSION

Influence de la calcination et interprétation

L'étude de l'influence de la température de calcination sur le signal d'atomisation du cuivre en présence de différents chlorures pris séparément est reportée dans la partie 1. Elle montre que seul le chlorure de magnésium est hydrolysé dans les conditions employées et que cette hydrolyse se traduit, dès lors qu'elle est totale, par l'élimination de l'interférence liée à ce composé. Une calcination à température trop élevée entraîne une perte de métal sous forme de Cu_3Cl_3 [4] associée à la volatilisation de le fraction de $MgCl_2$ qui n'a pas eu le temps d'être hydrolysée.

Afin de préciser les phénomènes apparaissant dans le cas d'une eau de mer, nous avons réalisé une étude de l'influence de la température de calcination sur deux milieux B et C (Tableau 1) se rapprochant par leur composition en ions majeurs de l'eau de mer naturelle et sur l'eau de mer acidifiée elle-même par l'acide chlorhydrique à pH 1,5. Les courbes traduisant les résultats obtenus en calcinant 50 s et en atomisant avec une montée rapide en température sont reportées sur la Fig. 1. Ces courbes présentent un maximum semblable à celui reporté pour $MgCl_2$ seul. Il est donc, pour ces

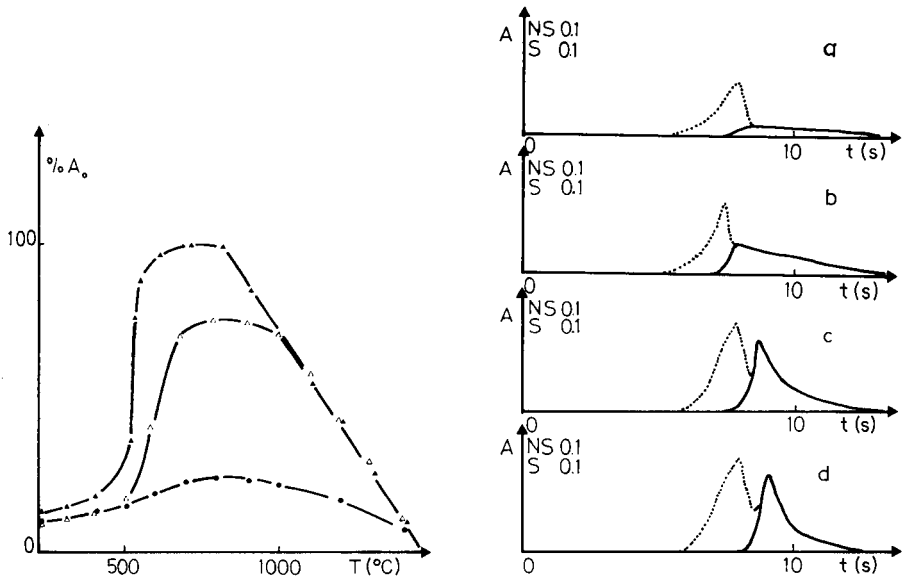

Fig. 1. Influence de la température de calcination (t = 50 s) sur la surface du pic d'atomisation du cuivre (10^{-6} M): (▲) $MgCl_2$ 0,053 M; (●) NaCl 0,47 M + $CaCl_2$ 0,01 M + $MgCl_2$ 0,053 M; (△) NaCl 0,47 M + $CaCl_2$ 0,01 M + $MgCl_2$ 0,053 M + Na_2SO_4 0,028 M; (△) eau de mer A.

Fig. 2. Signal d'atomisation du cuivre (10^{-6} M) (——) dans une eau de mer pour différents temps (t) de calcination à 800°C: (a) 0 s; (b) 10 s; (c) 20 s; (d) 50 s. (····) Matrice observée à 324,7 nm.

TABLEAU 1

Composition en ions majeurs des milieux étudiés (M)

Milieu	Na^+	Mg^{2+}	Ca^{2+}	Cl^-	SO_4^{2-}	K^+	HCO_3^-
0 eau de mer [5]	0,47	0,053	0,01	0,55	0,028	0,01	0,0024
A eau de mer acidifiée (après séchage)	0,47	0,053	0,01	0,55	0,028	0,01	—
B	0,47	0,053	0,01	0,55	—	—	—
C	0,47	0,053	0,01	0,55	0,028	—	—

mélanges et l'eau de mer, logique d'attribuer la présence de ces maximums à l'hydrolyse du chlorure de magnésium présent.

En l'absence de sulfate, l'interférence due aux chlorures de sodium et de magnésium reste importante quelle que soit la température de calcination. En l'absence de calcination la présence de sulfate n'a pas d'influence sur l'interférence mesurée. Le fait que le signal non-spécifique caractéristique de Na_2SO_4-Na_2S [6] n'apparaît pas en l'absence de calcination (Fig. 2) de l'eau de mer indique que ce composé n'existe pas dans le four au début de l'atomisation. Dans l'hypothèse que nous proposons, les ions sulfates présents sont, à ce moment, associés au calcium et au magnésium dans des composés non-volatiles jusqu'à une température supérieure à la température de volatilisation des chlorures de sodium et de magnésium. L'association du sulfate au calcium est quantitative tandis que l'association totale du sulfate au magnésium nécessite un excès de ce métal [6]. Il est envisageable qu'en raison de la faible solubilité du sulfate de calcium dans l'eau (pK_{so} = 5,82 [7]) ce produit qui est solide jusqu'à 1450°C, soit formé dès le séchage rendant indisponible ainsi dès ce stade 10^{-2} M de sulfate. La concentration de magnésium (0,053 M) suffit dans ce schéma, en l'absence de calcination, pour rendre indisponible à la vaporisation sous forme Na_2SO_4, les $1{,}8.10^{-2}$ M de sulfate restant. La calcination provoque l'hydrolyse du chlorure de magnésium en oxyde, solide jusqu'à 2800°C. Elle exclut de fait le magnésium du milieu et laisse donc disponible une quantité d'ion sulfate telle que le signal non-spécifique du sulfate de sodium apparaisse ainsi que le pic spécifique du métal (Fig. 2).

Outre l'évolution du signal non-spécifique, ce schéma explique convenablement l'élimination par la calcination de l'interférence liée à la présence de $MgCl_2$ et l'atténuation de l'interférence NaCl à laquelle se substitue l'interférence de Na_2SO_4. Il est donc possible de proposer d'écrire sans prétendre équilibrer les réactions ni indiquer si elles ont lieu en solution au cours du séchage ou en milieu sel fondu, qu'en l'absence de calcination:

$$Na^+ + Mg^{2+} + Ca^{2+} + Cl^- + SO_4^{2-} \rightarrow NaCl + CaSO_4 + MgCl_2 + MgSO_4$$

et en cas de calcination:

$$Na^+ + Mg^{2+} + Ca^{2+} + Cl^- + SO_4^{2-} \rightarrow NaCl + CaSO_4 + Na_2SO_4 + MgO$$

Il est à remarquer que le signal maximum de cuivre dans le cas de l'eau de mer acidifiée et des solutions B (chlorure seul) et C (chlorure et sulfate) n'est obtenu qu'à partir d'une calcination vers 800°C alors que dans le cas du chlorure de magnésium [1] ce maximum est obtenu vers 600° C. L'excès de chlorure présent dans ces milieux explique la plus grande stabilité du chlorure de magnésium.

La superposition (Fig. 1) des courbes correspondant aux milieux A et C (chlorure et sulfate) indique que du point de vue de la calcination l'eau de mer peut être en première approximation confondue avec le mélange C.

Addition de sulfate

L'addition de sulfate à une eau de mer en tant que modificateur se traduit comme dans le cas de l'halogénure de sodium seul [1] par une diminution rapide de l'interférence. Sur la Fig. 3, nous avons reporté l'évolution des massifs spécifiques et non-spécifiques à 324,7 nm pour différentes concentrations en sulfate (ajouté sous forme d'acide sulfurique) en l'absence de calcination. Ces signaux sont ceux obtenus en montée lente en température. Dès une addition de 3.10^{-2} M de sulfate, la forme caractéristique du pic d'atomisation du cuivre sous forme Cu_2S apparaît, elle se précise jusqu'à 9.10^{-2} M puis disparaît progressivement au fur et à mesure qu'augmente (voir Fig. 7 [1]), l'interférence liée aux concentrations en Na_2SO_4 plus importantes. On note également un retard à la sortie du massif d'atomisation du cuivre et un accroissement très important de la matrice provenant de la substitution de la matrice Na_2SO_4 à la matrice NaCl.

Les courbes de la Fig. 4 correspondent aux résultats obtenus en montée rapide par addition d'acide sulfurique au mélange B (chlorure seul) et à de l'eau de mer acidifiée (A), avec et sans calcination. En l'absence de calcination, l'évolution des courbes obtenues pour les deux milieux est similaire, le décalage remarqué correspond aux $2{,}8.10^{-2}$ M de sulfate présents initialement dans l'eau de mer. Quelle que soit la quantité d'acide sulfurique ajoutée, il n'est pas possible d'obtenir plus de 50% du signal maximum, valeur de l'interférence provoquée par le sulfate de sodium résultant. Le point d'inflexion des deux courbes correspond à une teneur en sulfate total voisine de 0,05 M ce qui est cohérent avec les résultats reportés dans la partie 1 [1] qui indiquent que l'interférence liée à la présence de chlorure de magnésium n'est éliminée que pour un rapport $[SO_4^{2-}]/[Mg^{2+}]$ voisin de 1.

Les courbes obtenues après calcination à 800°C confirment que la seule hydrolyse du chlorure de magnésium ne provoque qu'une faible atténuation de l'interférence mais qu'elle est un préalable indispensable à l'importante atténuation obtenue par la stabilisation du cuivre par le sulfate (sulfure). Il est remarquable que l'atténuation maximale de l'interférence (25% d'interférence résultante) corresponde à une concentration en sulfate voisine de 3.10^{-2} M: concentration naturellement présente dans une eau de mer.

Vis-à-vis de l'ensemble des résultats obtenus par addition de sulfate, il apparaît donc qu'il est dans ce cas aussi possible d'assimiler le comporte-

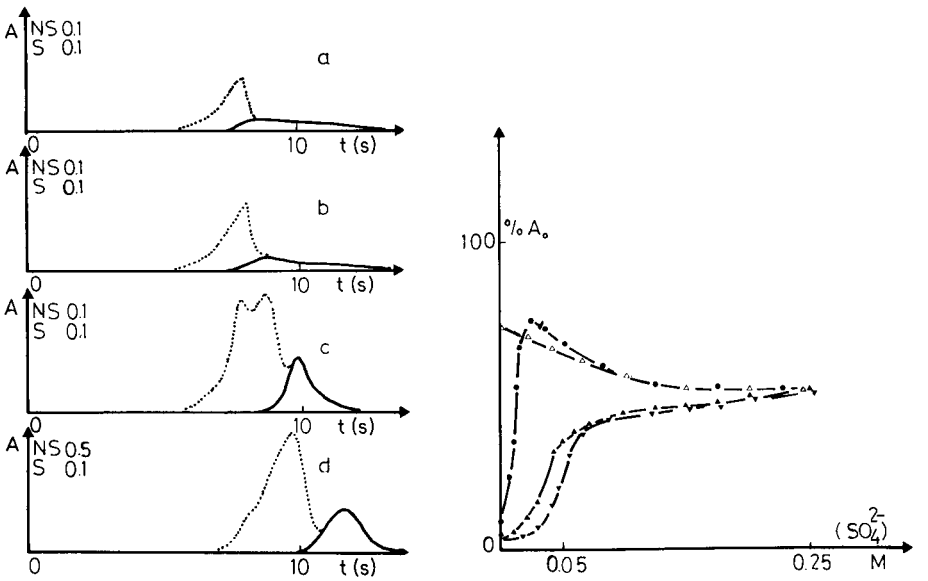

Fig. 3. Signal d'atomisation du cuivre (10^{-6} M) (—) dans une eau de mer pour différentes concentrations en H_2SO_4 : (a) 0; (b) 0,005 M; (c) 0,05 M; (d) 0,25 M. (. . . .) Matrice observée à 324,7 nm.

Fig. 4. Influence de la concentration en H_2SO_4 sur la surface du pic d'atomisation du cuivre (10^{-6} M) en milieu NaCl 0,47 M + $CaCl_2$ 0,01 M + $MgCl_2$ 0,053 M après calcination (•) ou non (▼), et en milieu NaCl 0,47 M + $CaCl_2$ 0,01 M + $MgCl_2$ 0,053 M + Na_2SO_4 0,028 M ou eau de mer A après calcination (△) ou non (▲).

ment de l'eau de mer à celui du mélange C (NaCl + $CaCl_2$ + $MgCl_2$ + Na_2-SO_4).

Addition de nitrate

L'effet de l'augmentation de la concentration en nitrate par addition d'acide nitrique dans une eau de mer est traduit par les courbes reportées sur la Fig. 5 qui représentent les signaux spécifiques et non-spécifiques observés à 324,7 nm en l'absence de calcination et en montée lente en température (100°C s^{-1}). Ces courbes montrent l'apparition du signal de forme caractéristique du cuivre en présence de sulfure de sodium nette dès une concentration de 0,1 M en nitrate, la hauteur du pic s'atténuant par la suite en même temps qu'apparaît à partir de 0,1 M un second pic, assez net vers 0,5 M. Ce dernier pic n'apparaît pas pour une eau de mer uniquement calcinée ou additionnée de sulfate. On note, comme dans le cas de l'addition de sulfate, que la sortie du massif d'atomisation du cuivre est retardée et que l'absorption de la matrice augmente en raison de l'apparition de la matrice Na_2SO_4 présente alors dans l'eau de mer et de la substitution de NaCl par $NaNO_3$ plus absorbant à cette longueur d'onde.

Sur le plan quantitatif, les courbes de la Fig. 6 correspondent à l'addition

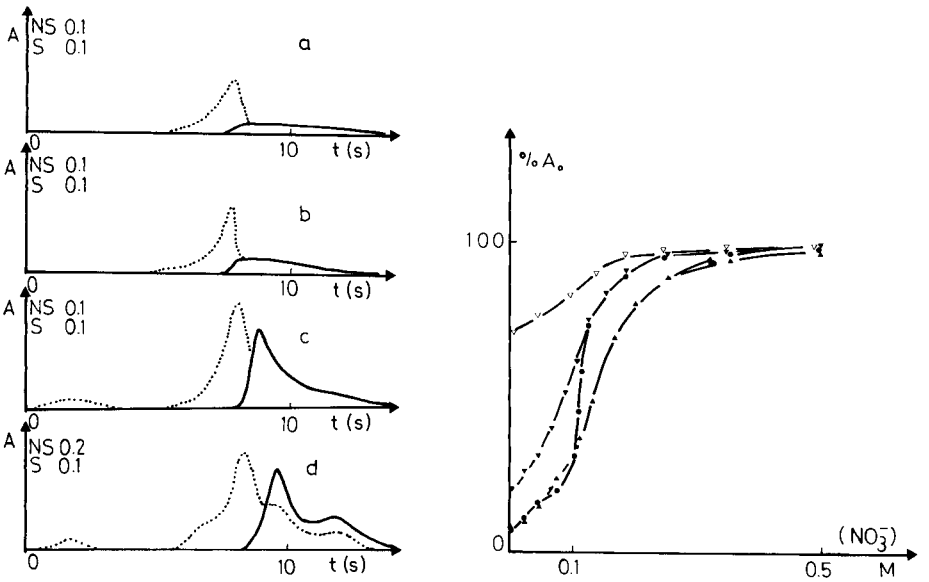

Fig. 5. Signal d'atomisation du cuivre (10^{-6} M) (—) dans une eau de mer pour différentes concentrations en HNO_3: (a) 0; (b) 0,01 M; (c) 0,1 M; (d) 0,5 M. (· · · ·) Matrice observée à 324,7 nm.

Fig. 6. Influence de la concentration en HNO_3 sur la surface du pic d'atomisation du cuivre (10^{-6} M) en milieu NaCl 0,47 M + $CaCl_2$ 0,01 M + $MgCl_2$ 0,053 M apres calcination (▼) ou non (▲), et en milieu NaCl 0,47 M + $CaCl_2$ 0,01 M + $MgCl_2$ 0,053 M + Na_2SO_4 0,028 M ou eau de mer A après calcination (▽) ou non (●).

d'acide nitrique dans l'eau de mer préalablement acidifiée par HCl et dans le milieu B, en montée rapide en température, avec ou sans calcination. Les courbes correspondant au milieu C ne sont pas reportées car pratiquement confondues avec celles traduisant l'influence du nitrate sur le signal de l'eau de mer acidifiée A, ce qui indique que dans ce cas aussi il est possible d'assimiler le comportement du milieu C à celui d'une eau de mer naturelle. Le décalage apparaissant entre les deux courbes qui correspondent au mélange B avec et sans calcination (suppression de l'interférence $MgCl_2$ par hydrolyse de $MgCl_2$) est de l'ordre de 0,08 M de nitrate, ce qui coïncide approximativement avec le rapport $[NO_3^-]/[Mg^{2+}]$ voisin de 2 dont nous avons montré la nécessité [1] pour l'élimination de l'interférence due à $MgCl_2$. Les deux courbes reportées pour l'eau de mer acidifiée par HCl indiquent qu'en l'absence de calcination l'addition de 10^{-1} M de nitrate permet d'accéder à des valeurs de l'absorbance proches de celles obtenues, en cas de calcination.

Pour les deux milieux, l'atténuation de l'interférence est comme dans le cas des halogénures pris séparément [1] très nettement supérieure à celle qui résulterait de la simple suppression de l'interférence due à NaCl. De plus, pour une concentration en nitrate supérieure à 3.10^{-1} M, la valeur de l'absor-

bance mesurée est, dans le cas de l'eau de mer et du mélange B, comprise entre 90 et 100% du signal maximum, ce qui répresente une atténuation de l'interférence du signal nettement plus importante que celle obtenue par calcination, même en présence de sulfate. Cette atténuation complémentaire n'existe pas en l'absence de magnésium. Il semble donc que l'addition de nitrate induise, lorsque le milieu contient du magnésium, une atténuation complémentaire de l'interférence que nous relions à l'apparition (Fig. 5) d'un deuxième pic d'atomisation du métal. La présence du magnésium et du nitrate entraîne dans ce cas un effet positif alors que nous avons montré (voir Fig. 8B [1]) que en présence de nitrate de magnésium (0,1 M), une perte de 20% de sensibilité est obtenue en l'absence de calcination, perte qui peut atteindre 50% si l'on calcine à 600° C.

Ceci amène à conclure que la présence du chlorure de sodium (0,47 M) dans la matrice empêche la formation du nitrate de cuivre dont la sublimation à basse température est la cause de l'interférence liée à la présence du nitrate de magnésium. Dès lors que le départ de métal sous forme $Cu(NO_3)_2$ est évité, la présence du composé résultant de la décomposition à chaud de $Mg(NO_3)_2$ en milieu chlorure A, au contraire, un effet stabilisant complémentaire. Il est possible que ce composé soit MgO mais aussi $MgCl_x$ envisagé par Erspamer et Niemczyk [8].

Sur un plan pratique, il apparaît que pour 10 μl d'eau de mer calcinée 50 s à 800°C en présence de 0,2 mol l^{-1} nitrate, on peut accéder à une atténuation pratiquement maximum de l'interférence, tout en évitant l'emploi de teneurs trop importantes en nitrate qui entraînent une rapide détérioration de la surface des fours. Dans ces conditions et en utilisant les conditions opératoires décrites pour une montée rapide, la sensibilité de la méthode est pour 10 μl d'échantillons injectés de: 1 $\mu g\ l^{-1}$ en mode lecture de pic (0,0044 A) et de 3 $\mu g\ l^{-1}$ (0,0044 A) en mode intégration de surface.

Les limites de détection sont dans les mêmes conditions de 1,5 $\mu g\ l^{-1}$ en mode lecture de pic, et de 3 $\mu g\ l^{-1}$ en mode intégration de surface.

Il n'est pas possible d'accéder dans ces conditions d'atomisation aux teneurs présentes dans une eau de mer non ou peu polluée (0,1–0,3 $\mu g\ l^{-1}$). L'augmentation du volume d'échantillon injecté peut être un moyen d'accès à cette gamme de concentration.

Conclusion

Les modifications du signal d'atomisation du cuivre et de la matrice mesurées en spectrométrie d'absorption atomique sans flamme, pour une eau de mer naturelle, sont explicables en considérant que ce milieu une fois légèrement acidifié par l'acide chlorhydrique se comporte comme un mélange de chlorure de sodium (0,47 M), Na_2SO_4 (0,028 M), $CaCl_2$ (0,01 M) et $MgCl_2$ (0,053 M). Les principaux interférents sont les chlorures de sodium et de magnésium, dont les effets peuvent être atténués ou éliminés par calcination, et addition de sulfate ou de nitrate. Ces derniers composés provoquent un retard du signal d'atomisation du cuivre en raison de la

présence des matrices sulfate de sodium (sulfure de sodium) ou nitrate de sodium. Le nitrate de magnésium en présence de chlorure de sodium entraîne une atténuation supplémentaire de l'interférence permettant d'accéder au signal maximum.

Enfin, une première application de cette étude permet d'atteindre avec un très faible ajout de nitrate une sensibilité de l'ordre de 1 $\mu g\ l^{-1}$ pour une injection de 10 μl d'eau de mer. Cette sensibilité est encore trop faible pour accéder aux teneurs présentes dans une eau de mer non polluée mais en se fondant sur les résultats de ce travail nous étudions l'injection de volumes d'échantillons plus importants pour améliorer la sensibilité atteinte.

REFERENCES

1 J. Y. Cabon et A. Le Bihan, Anal. Chim. Acta, 198 (1987) 87.
2 R. Massee, F. J. M. J. Maessen et J. J. M. De Goeij, Anal. Chim. Acta, 127 (1981) 181.
3 R. E. Pellenbarg et T. M. Church, Anal. Chim. Acta, 97 (1978) 81.
4 K. Matsusaki, Anal. Chim. Acta, 141 (1982) 233.
5 F. Culkin, dans J. P. Riley (Ed.), Chemical Oceanography, 1e edn. Academic, London, 1965, p. 122.
6 J. Y. Cabon, A. Le Bihan et J. Courtot-Coupez, Anal. Lett., 19 (1986) 785.
7 L. G. Sillen et A. E. Martell, Stability constants of metal-ion complexes, Special Publication No. 17, The Chemical Society, London, 1964.
8 J. P. Erspamer et T. M. Niemczyk, Anal. Chem., 54 (1982) 538.

Analytica Chimica Acta, 198 (1987) 113—123
Elsevier Science Publishers B.V., Amsterdam — Printed in The Netherlands

DIRECT DETERMINATION OF LEAD IN BLOOD BY ELECTROTHERMAL ATOMIC ABSORPTION SPECTROMETRY WITH L'VOV PLATFORM AND MATRIX MODIFICATION

CARLOS G. BRUHN*, JORGE M. PIWONKA, MAURICIO O. JERARDINO, GLADYS M. NAVARRETE and PAULINA C. MATURANA

Departamento de Análisis Instrumental, Facultad de Farmacia, Universidad de Concepción, P.O. Box 237, Concepción (Chile)

(Received 3rd November 1986)

SUMMARY

An electrothermal atomic-absorption procedure with the L'vov platform and a simple five- or ten-fold sample dilution with a matrix-modifier solution containing diammonium hydrogenphosphate, Triton X-100 and nitric acid, is described for the direct determination of relatively low levels of lead in heparinized blood. The graphite-furnace parameters and matrix-modifier composition are optimized. Sensitivity, imprecision, accuracy and detection limit are reported. Results obtained by standard addition for ten human blood samples (30—400 $\mu g\ l^{-1}$ lead) were confirmed by an extraction/flame atomic-absorption reference method. Differences in mean lead values ranged from 2 to 31 $\mu g\ l^{-1}$ with 5.1% mean relative difference. The mean relative standard deviations for consecutive and between-day determinations were 4.6 and 9%, respectively. Accuracy was verified by analyzing six bovine-blood standards certified for lead in the range 70—1100 $\mu g\ l^{-1}$; deviations of found concentrations from expected values ranged from 0 to 44 $\mu g\ l^{-1}$ with 4.3% mean relative error. Recovery experiments done with human blood gave 104% (90—121%) of the added lead. The method offers several advantages for routine application in comparison with the extraction/flame atomic-absorption procedure.

The determination of lead in blood is an important clinical screening procedure in studies of environmental pollution as well as occupational exposure. Besides other measurable indicators of lead uptake such as δ-aminolevulinic acid, free erythrocyte protoporphyrin, etc. [1], lead in whole blood is the most reliable indicator for recent exposure [2]. Increasing awareness about the depredations of lead at levels previously considered non-toxic has become apparent [3—5] and has indicated the necessity of evaluating baseline lead levels in blood from occupationally unexposed persons and consideration of their epidemiological significance.

Several atomic-absorption spectrometric procedures have been proposed for the determination of lead in blood (e.g., chelation/extraction [6], Delves cup [7], and electrothermal atomization [8, 9]). The characteristics of high sensitivity, simplicity and reduced sample-preparation time, as well as several matrix modification techniques [10, 11] proposed to reduce matrix and background interferences in combination with background correction, have

0003-2670/87/$03.50

made electrothermal atomization procedures the most widely used. The stabilized-temperature-platform technique [12] has further advantages in this determination. Nevertheless, the transfer and/or adaptation of methods to instrumentation with different characteristics remain unsolved.

This paper reports the development and evaluation of an electrothermal atomization procedure using the L'vov platform and a matrix modifier to determine lead in human blood by the standard-addition method in a relatively wide concentration range (30—400 $\mu g\ l^{-1}$). Sample preparation involved only a suitable dilution with a matrix-modifier diluent solution that contained diammonium hydrogenphosphate [10, 12], Triton X-100 [8] and nitric acid [5, 11]. Lead was determined in ten human samples from occupationally unexposed persons and also from persons with low degrees of occupational lead exposure. These results were confirmed by comparison with a reference method based on extraction and flame atomic absorption spectrometry (a.a.s.). The electrothermal a.a.s. procedure was tested for precision and accuracy with six bovine-blood standard samples obtained from a blood-lead proficiency testing program, and was also tested for recovery with human blood samples with known lead concentrations.

EXPERIMENTAL

Apparatus

Measurements were made with a Perkin-Elmer Model 380 atomic absorption spectrometer equipped with a deuterium arc background corrector, Perkin-Elmer HGA-400 graphite furnace and AS-40 autosampler accessories. A lead hollow-cathode lamp was used as the radiation source. Pyrolytically coated graphite tubes and pyrolytic graphite L'vov platforms were from Perkin-Elmer (Part 290-2310A and Part 290-2311B, respectively). Signals were recorded on a Beckman linear-log potentiometric recorder.

In the flame reference method, a 4-in. single-slot burner head and an air/acetylene flame were used. The flow rates were 1.1 l min^{-1} for acetylene and 19.5 l min^{-1} for air.

All glassware was cleaned with nonionic detergent, rinsed with distilled water, soaked in (1 + 9) nitric acid for 24 h, thoroughly rinsed with reagent-grade water (Milli-Q system, Millipore Corp.) and air-dried. Polypropylene and polyethylene vessels, and capped microcentrifuge tubes (Eppendorf 3810) were soaked in (1 + 9) hydrochloric acid for 24 h, rinsed with reagent-grade water, air-dried and stored in plastic bags until required. Only units free of lead were used. Disposable acid-soaked, 2-ml polystyrene cups (Perkin-Elmer) were used with the autosampling accessory.

Eppendorf micropipets of fixed and adjustable volumes were used. Pipet tips were soaked for 24 h in 20% nitric acid followed by several rinses with reagent-grade water before use.

Reagents and standards

All reagents were of analytical grade (Merck) except for nitric acid (Suprapur, Merck), heparin (Sigma) and Triton X-100 (Serva). Lead was removed from diammonium hydrogenphosphate and sodium citrate by chelating with ammonium pyrrolidinedithiocarbamate and extracting the complex into methyl isobutyl ketone [13] until no lead was detectable. The above Milli-Q water was used for all dilutions.

Six blood standards from the Center for Disease Control (CDC, Atlanta GA), which were bovine blood of certified lead content, were used to assess the accuracy and precision of the proposed procedure.

A standard solution (10 μg ml^{-1} in 0.028 M nitric acid) was prepared weekly by dilution of a 1000 μg ml^{-1} standard stock solution. An additional standard solution (250 μg l^{-1} in 0.028 M nitric acid) was prepared daily by dilution from the 10 μg ml^{-1} standard solution. Lead working solutions (10, 20, 40 and 60 μg l^{-1} and blank) were prepared in two sets, one having diammonium hydrogenphosphate (0.005 M), Triton X-100 (0.20%) and nitric acid (0.014 M) as matrix modifiers and the other, having a pooled human blood prepared from blood samples with very low lead content (Blood Bank, Concepción Clinical Regional Hospital) diluted 5-fold in the same matrix modifier. In the latter, the matrix-modifier diluent solutions were prepared successively with lead concentrations of 0, 12.5, 25, 50 and 75 μg l^{-1} and containing each, diammonium hydrogenphosphate (0.0063 M), Triton X-100 (0.25%) and nitric acid (0.0168 M).

Lead standards for the flame reference method were prepared as described previously [6], modified by the addition of 1 ml of 0.1 M sodium citrate to keep the pH at 7.4.

Procedures

Preparation of sample solutions. Adult blood samples were obtained from the Blood Bank of the Concepción Clinical Regional Hospital and from the Workers Hospital of the Chilean Security Association. The samples (20 ml) were obtained by venipuncture with disposable lead-free plastic syringes (Terumo-20 ml excentric syringes, Terumo Corp.), transferred immediately to heparinized lead-free polyethylene vessels and gently mixed. The blood samples and CDC blood standards were stored at 4°C and, prior to spectrometry, were thoroughly mixed until room temperature was reached. For blood samples containing <300 μg l^{-1} lead, a 5-fold dilution was needed: 200-μl aliquots of blood were diluted in microcentrifuge tubes with 800 μl of the matrix-modifier diluent solution containing lead concentrations of 0, 12.5, 25 and 50 μg l^{-1} as standard additions. Except for the studies of charring and atomization temperature which were done with this diluted blood, blood samples containing >300 μg l^{-1} were diluted 10-fold, to keep absorbance readings within the linear range of the calibration curve. For 10-fold dilution, 100-μl aliquots were diluted with 100 μl of water and 800 μl of the aforementioned matrix-modifier solutions. The microcentri-

fuge tubes were capped and shaken thoroughly by hand for 5 min and then centrifuged for 6 min at 12,000 rpm for good phase separation. The clear supernatant liquid was transferred to a clean autosampler cup for the measurement step. Blank samples were prepared by adding 20 ml of water to the heparinized lead-free polyethylene vessels following the same procedure as for preparing blood samples.

Electrothermal atomization procedure. Conditions were optimized, as suggested by the manufacturer, by using two sample solutions: the first, a solution of pooled human blood from occupationally exposed workers (395 $\mu g\ l^{-1}$ lead) diluted 5-fold in the matrix modifier, and the second, an equivalent solution spiked with 64 $\mu g\ l^{-1}$. To facilitate sample introduction into a platform, the injection port of the graphite tube was enlarged from 1.5 mm to 2.0 mm and sample aliquots were kept at 20 μl. In this way, no sample was lost to the tube walls and/or pipetted past the platform to one side.

The optimized conditions are listed in Table 1. A six-step heating program was used to avoid sample splattering during drying, to allow as steady and complete matrix removal as possible, and to facilitate platform cleaning and cooling to room temperature. A wavelength of 283.3 nm and a spectral slit width of 0.7 nm (Alt.) were used. The hollow-cathode lamp was run at 8 mA, and background-corrected absorption signals (peak-height mode) were measured with an integration time of 7 s.

Procedures for measurement. Calibration graphs and standard additions were applied in the electrothermal procedure. Standard additions were necessary for full compensation of sample matrix effects not matched by the composition of the standard solutions prepared without and with a human blood matrix. At least three replicate runs were done on each standard and sample solution within 1 h after solutions were prepared. After each furnace program run, the peak-height absorbance was measured from the display. The calibration and standard-addition graphs were prepared from mean values of peak-height absorbances. Peak areas were evaluated but not used because baseline blank values were not reproducible. Results were very dependent on integration time, being negative results in some cases as has been noticed by others [14] using deuterium-arc background correction.

Blank absorbances were consistently low and were subtracted by using the autozero function of the spectrometer. Calibration and standard-addition results were subjected to regression analysis to obtain slopes, intercepts and correlation coefficients.

For the flame reference method, standard additions and direct comparison with standard calibration curves were applied. No significant differences were observed.

TABLE 1

Graphite-furnace program for blood lead determination with the L'vov platform

Program step	Temp. (°C)	Ramp time (s)	Hold (s)	Argon[a] (ml min^{-1})
Drying (I)	130	5	5	300
Drying (II)	200	25	20	300
Charring	550	20	40	300[b]
Atomization[c]	1550	0[d]	6	40
Cleaning	2500	1	4	300
Cooling	20	1	13	300

[a]99.998% pure. [b]Miniflow (40 ml min^{-1}) after 55 s of charring. [c]Recorder "on" — 5 s. Read "on" — 1 s. [d]Maximum power heating mode.

RESULTS AND DISCUSSION

Charring and atomization temperatures

Drying, charring and atomization temperatures are not always transferable between instruments, and must be optimized on the basis of the sample matrix under study, the matrix modifier composition and the type of graphite tubes and platforms in use. A suitable charring temperature for diluted human blood without and with spiked lead was selected after a study of minimum and maximum temperatures allowed. In this study, an atomization temperature of 1600°C was used, and the minimum usable charring temperature was 450°C, as evaluated from a plot of charring temperature vs. absorbance at 280.3 nm without background correction (Fig. 1, curve a). For 5-fold diluted human blood without matrix modifier, the non-specific absorbance obtained in the 400—700°C range was >0.2; with matrix modifier it was <0.1. The maximum charring temperature before significant lead losses became apparent was 650°C, evaluated from a plot of charring temperature vs. absorbance at 283.3 nm with background correction (Fig. 1, curves b and c). A charring temperature of 550°C was chosen as a compromise to minimise lead losses. The matrix modifier permitted the use of a relatively higher charring temperature by 50—100°C, as compared to the use of either simple acid lead standards or diluted blood samples. Nevertheless, the selected charring temperature was significantly lower in comparison to previous reports in which the L'vov platform was used with matrix modification [13, 15].

In the atomization cycle, analyte evolution is shifted until the tube and gas temperatures are almost the same. Therefore, the matrix modifier reduces lead volatility and permits steady-state temperatures to prevail before the analyte is vaporized [16].

The dependence of the absorbance on the amount of diammonium hydrogenphosphate in the matrix modifier was investigated. Lead solutions

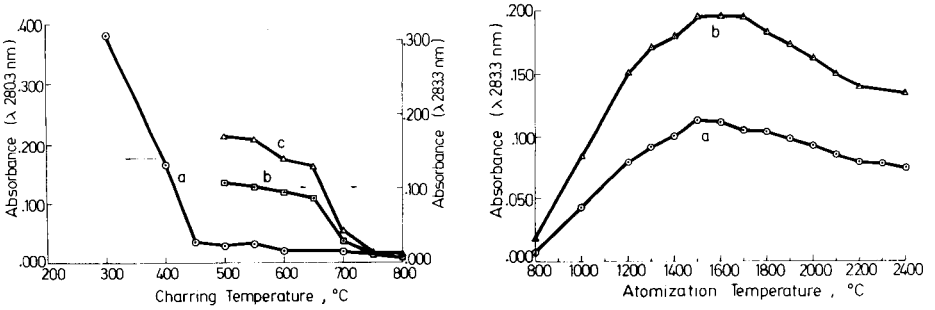

Fig. 1. Effect of charring temperature: (a) on non-specific background absorbance for pooled blood (5-fold dilution) in matrix modifier; (b) on lead absorbance for pooled blood (5-fold dilution) in matrix modifier; (c) on lead absorbance for pooled blood (5-fold dilution) in matrix modifier + 64 $\mu g\ l^{-1}$ lead.

Fig. 2. Effect of atomization temperature on lead absorbance: (a) pooled blood (5-fold dilution) in matrix modifier; (b) pooled blood (5-fold dilution) in matrix modifier + 64 $\mu g\ l^{-1}$ lead.

(60 $\mu g\ l^{-1}$) and blanks were prepared in the matrix modifier containing variable diammonium hydrogenphosphate concentrations in the 0.001—0.50 M range. Maximum sensitivity and minimum baseline distortion were obtained with a hydrogenphosphate concentration of 0.005 M. At higher concentrations (e.g., 0.10 M) the specific absorption increased above the level attained at 0.005 M; however, excessive smoke was produced during the atomization cycle and significant overcompensation was produced because of inadequate background correction. The signal enhancement observed for lead in the presence of diammonium hydrogenphosphate is consistent with the increase in thermal stability and higher peak absorption reported previously [17, 18]. The concentrations of Triton X-100 and nitric acid were kept as low as possible to avoid deleterious effects such as sample losses by foaming action during sample introduction to the platform (Triton X-100) and decrease in platform lifetime (nitric acid).

Optimum atomization was obtained at 1550°C (Fig. 2) for both solutions of pooled human blood diluted 5-fold in the matrix modifier without and with a lead spike of 64 $\mu g\ l^{-1}$, showing no difference in the atomization behavior between endogenous and exogenous lead. The atomization temperature was lower than in other reports [12, 13]. A short cleaning step at 2500°C avoided residue buildup even after 100—150 firings with the blood samples. However, after each sample was run by the standard-addition method, at least two blank firings were done to avoid any memory effects between samples. When a buildup of charcoal residue was detected through a loss of precision and/or sensitivity, the platform was removed and the residue was removed with the aid of a scalpel blade. The useful lifetime of the graphite tube and platform could be extended to about 400—450 determinations before replacement became necessary.

Calibration curves and standard additions

Replicate calibration curves for lead standards in the matrix modifier were compared with similar calibration curves obtained for diluted pooled blood spiked with known amounts of lead (10–60 $\mu g\ l^{-1}$) in the matrix modifier. The parameters for the regression equations, absorbance $A = (a \pm s_a)\, c + b \pm s_b$, S_{yx}, r and the reciprocal sensitivity are given in Table 2. Both calibration curves were linear from 0 to 60 $\mu g\ l^{-1}$ (0.0–1.20 ng injected mass); however, the slopes differed by about 20% and consequently the reciprocal sensitivities do not agree. The intercept was nearly indistinguishable from zero for curve I; for curve II, it corresponded to 5.2 ± 0.6 $\mu g\ l^{-1}$ lead. The criterion for detection was estimated from replicate measurements of blank solutions consisting of matrix modifier; the detection limit (3 × standard deviation of blanks) corresponded to 10 pg of lead by the standard calibration method. For blood, the detection limit was 36 pg of lead.

Apparently, the matrix modifier did not completely compensate for the depression of the absorbance signal in the diluted pooled human-blood sample. Considering the complex composition of whole blood, the difficulty of preserving heparinized human blood for long periods, and the need to circumvent errors from matrix-matched calibration graphs, the normal calibration method was discarded and the standard addition method with lead in the matrix modifier was adopted.

Imprecision

Ten replicate injections of two lead standard solutions (5 and 60 $\mu g\ l^{-1}$) in matrix modifier gave within-run relative standard deviations (r.s.d.) of 5.9 and 3.1%, respectively. When pooled blood in matrix modifier spiked with 40 $\mu g\ l^{-1}$ lead, and a 5-fold diluted blood solution sample containing 66 ± 5 $\mu g\ l^{-1}$ of endogenous lead were tested similarly, the within-run r.s.d. were 2.2 and 5.8%, respectively.

Table 3 shows the results of a study of imprecision in lead determinations by the standard addition method in three blood samples with low, medium

TABLE 2

Comparison of linear regression parameters and reciprocal sensitivity for the standard calibration curve in matrix modifier (I) and for the matrix-matched calibration curve (II)[a]

	$(a \pm s_a)$ (A ng^{-1})	$(b \pm s_b)$ (A)	S_{yx} (A)	r	Reciprocal sensitivity (pg/0.0044 A)
I	0.210 ± 0.006	0.0004 ± 0.0009	0.0043	0.9995	21
II	0.170 ± 0.005	0.0177 ± 0.0020	0.0012	0.9998	26

[a]Results are the average of ten independent batches.

TABLE 3

Imprecision of replicate blood lead determination with the L'vov platform

Mean ($\mu g\ l^{-1}$)	S.d. ($\mu g\ l^{-1}$)	Mean ($\mu g\ l^{-1}$)	S.d. ($\mu g\ l^{-1}$)
Within-day		*Between-day*	
46 (3)[a]	±3	52 (10)	±6
108 (6)	±5	118 (8)	±8
339 (3)	±9	645 (5)[b]	±51

[a]Number of determinations in parentheses. [b]TOX-EL 2 control blood, 634 $\mu g\ l^{-1}$ lead (569-699), A.R. Smith Lab., Los Angeles, U.S.A.

and high lead concentrations. The r.s.d. values ranged from 2.7 to 6.5% with a mean value of 4.6%; however, it depends on the lead concentration. This result is consistent with the reproducibility attained in replicate injections, suggesting that the imprecision for consecutive samples was not greatly influenced by factors such as mixing, dilution with the matrix modifier, or centrifugation to separate the lysed red cells and particulate matter. The centrifugation step provided a significant improvement in precision and was found crucial for the desired accuracy.

A study of between-day standard deviations of blood lead determinations, based on the variability over a 5-day period for three blood samples with low, medium and high lead concentrations, gave a mean r.s.d. of 9% (7.6—11.5%). Clotting degrades both precision and accuracy. Despite the relatively high r.s.d. values obtained in the day-to-day study, results were within the range of variability accepted by blood-lead proficiency programs.

Accuracy

To test the accuracy, lead was quantified in six bovine blood standards certified for lead. Four CDC blood standards were certified by isotope-dilution mass spectrometry (i.d.m.s.) and the other two by acid digestion and anodic stripping voltammetry or electrothermal a.a.s. [19—21].

A comparison between results by the proposed method and the certified results is given in Table 4. Deviations of the concentrations found from the expected values ranged from 0 to 44 $\mu g\ l^{-1}$ (mean relative percent error was 4.3%) and the 95% confidence interval ranged from about 6 to 48 $\mu g\ l^{-1}$ (mean r.s.d. was 4.5%). A least-squares fit of results obtained with the proposed method (y) vs. those by the reference method (x) yielded $y = (1.031 \pm 0.049)x + (0.079 \pm 0.034)$; $S_{yx} = 15.9$; $r = 0.9994$, showing good correlation between results by the two methods.

To test further the accuracy of the proposed method, recoveries were determined for three human blood samples spiked with different amounts of lead standards. The results (Table 5) show that recoveries varied from 90 to 121%, with a mean recovery of 104% over a concentration range of 32—162 $\mu g\ l^{-1}$.

TABLE 4

Comparison of blood lead results in CDC standards by proposed method with certified results

Sample	Concentration ($\mu g\ l^{-1}$)		n[b]	Error (%)
	Certified	Proposed method[a]		
DE4-A02	72[c]	68 ± 6	4	−5.6
DE4-C02	197[d]	205 ± 16	4	4.1
DE3-B02	304[c]	331 ± 22	4	8.9
DE3-D01	507[c]	522 ± 48	4	3.0
DE3-C01	709[c]	709 ± 20	6	0.0
DE3-D02	1104[d]	1148 ± 46	6	4.0

[a]Mean ± 95% confidence interval. [b]Number of independent determinations. [c]I.d.m.s. [d]Acid digestion and voltammetry or a.a.s.

TABLE 5

Recovery of lead in blood by electrothermal a.a.s. with L'vov platform

Mean ± s.d.	Lead concentration ($\mu g\ l^{-1}$)		Recovery (%)
	Added	Found	
32 ± 1	50	48	96
	110	119	119
	200	202 ± 21[a]	101 ± 11
76 ± 0	100	90	90
	200	200 ± 18[a]	100 ± 9
162 ± 17	67	68	102
	134	161	121

[a]Average of duplicates.

Comparative study of blood lead determination

Ten blood samples from adults with no known occupational exposure and with a low degree of occupational exposure were analysed in duplicate or triplicate by the flame atomic absorption reference method and by the proposed method. The results are shown in Table 6. Despite the low number of independent replicates, because of limitations in sample availability (6-ml aliquots are required in the flame method), the results are in good agreement. Again, a least-squares fit of results obtained by the proposed method (y) vs. those by the flame a.a.s. (x) showed good correlation: $y = (1.054 \pm 0.063)\ x - (0.025 \pm 0.020)$, $S_{yx} = 10.7$; $r = 0.9973$. On average, the accuracy is within the standard deviation of the method. Furthermore, whether the sample matrix is bovine or human blood, there are apparently no differences in sample homogeneity after the dilution with the matrix modifier and the centrifugation step used. For five samples processed in

TABLE 6

Comparison of results obtained for lead in blood by extraction/flame a.a.s. and the proposed electrothermal method

Sample	Lead conc. ($\mu g\ l^{-1}$)		Difference (%)	Sample	Lead conc. ($\mu g\ l^{-1}$)		Difference (%)
	Flame	Electro-thermal			Flame	Electro-thermal	
1	34 ± 8	36 ± 6	5.8	6	179 ± 9	194 ± 9	8.4
2	91 ± 6	95 ± 10	4.4	7[a]	248 ± 8	279 ± 6	12.5
3[a]	95 ± 6	103 ± 3	8.4	8	331 ± 10	360 ± 8	8.8
4[a]	113 ± 8	118 ± 3	4.4	9[a]	380 ± 11	389 ± 3	2.4
5	122 ± 12	112 ± 4	−8.2	10[a]	393 ± 16	408 ± 7	3.8

[a]Sample processed in triplicate.

triplicate, the proposed method provided significantly lower imprecision than the flame method (i.e., 2% vs. 4.7% r.s.d.).

The authors thank Dr. Joe Boone, Center for Disease Control, Atlanta, GA, for providing the bovine blood standards and information regarding the CDC Blood Lead Proficiency Testing Program, the Blood Bank of the Concepción Clinical Regional Hospital for providing blood samples of unexposed persons, Dr. Nelson Maureira (Laboratory for Labor Medicine of the Workers Hospital of the Chilean Security Association) for providing blood samples of workers occupationally exposed to lead, and the Dirección de Investigación, Universidad de Concepción for financial support (Proyecto 20.71.04).

REFERENCES

1 O. J. David, H. L. Wintrob and C. G. Arcoleo, Arch. Environ. Health, 37 (1982) 147.
2 World Health Organization, Recommended Health-based Limits in Occupational Exposure to Heavy Metals. Technical report series 647. World Health Organization, Geneva, 1980.
3 O. David, S. Hoffman, B. McGann, J. Sverd and J. Clark, Lancet, 2 (1976) 1376.
4 H. L. Needleman, C. Gunnoe, A. Leviton, R. Reed, H. Peresie, C. Maher and P. Barrett, N. Engl. J. Med., 300 (1979) 689.
5 M. Stoeppler, Spectrochim. Acta, Part B, 38 (1983) 1559.
6 L. J. M. Zinterhofer, P. I. Jatlow and A. Fappiano, J. Lab. Clin. Med., 78 (1971) 664.
7 H. T. Delves, Analyst, 95 (1970) 431.
8 F. J. Fernandez, Clin. Chem., 21 (1975) 558.
9 M. Stoeppler, K. Brandt and T. C. Rains, Analyst, 103 (1978) 714.
10 K. S. Subramanian and J. C. Meranger, Clin. Chem., 27 (1981) 1866.
11 D. J. Hodges and D. Skelding, Analyst, 108 (1983) 813.
12 D. C. Manning and W. Slavin, Appl. Spectrosc., 37 (1983) 1.
13 E. J. Hinderberger, M. L. Kaiser and S. R. Koirtyohann, At. Spectrosc., 2 (1981) 1.
14 B. Welz and G. Schlemmer, J. Anal. At. Spectrosc., 1 (1986) 119.
15 E. Pruszkowska, G. R. Carnrick and W. Slavin, At. Spectrosc., 4 (1983) 59.
16 W. Slavin, G. R. Carnrick, D. C. Manning and E. Pruszkowska, At. Spectrosc., 4 (1983) 69.

17 E. J. Czobik and J. P. Matousek, Talanta, 24 (1977) 573.
18 S. Smith and R. Schleicher, in T. Y. Kometani (Ed.), Advances in Graphite Furnace Atomic Absorption Spectrometry, The Franklin Institute Press, Philadelphia, 1978, p. 61.
19 J. Boone, T. Hearn and S. Lewis, Clin. Chem., 25 (1979) 389.
20 D. M. T. Dudley, Critique, Blood Lead Analysis 1981. U.S. Department of Health and Human Services, Public Health Service, Center for Disease Control, Atlanta, GA, 1982.
21 J. Boone, personal communication (1985).

Analytica Chimica Acta, 198 (1987) 125—144
Elsevier Science Publishers B.V., Amsterdam — Printed in The Netherlands

SAMPLING AND QUANTITATION OF LIPIDS IN AEROSOLS FROM THE REMOTE MARINE ATMOSPHERE[a]

EDWARD T. PELTZER* and ROBERT B. GAGOSIAN

Department of Chemistry, Woods Hole Oceanographic Institution, Woods Hole, MA 02543 (U.S.A.)

(Received 29th September 1986)

SUMMARY

A procedure is described for the determination of organic compounds in aerosols and rain from the remote marine atmosphere. Five classes of naturally occurring lipids (n-alkanes, wax esters, fatty alcohols, sterols, and fatty acids) were quantified in the samples. Air samples (4000—10 000 m^3) were collected on glass-fiber filters under automatic control. Rain samples (1—5 l) were collected on an event basis. Filter and rain samples were extracted with dichloromethane and the extracts were fractionated into discrete chemical classes by adsorption chromatography with silica gel. The fractions were derivatized (if necessary) and quantified by high-resolution glass-capillary gas chromatography (HRGC) and HRGC/mass spectrometry. A second filter extraction was required for quantitation of fatty acid salts. On-column injection of the fractions provided identification and quantification of a wide range of homologs within each compound class: C_{15}—C_{44} for n-alkanes, C_{39}—C_{62} for wax esters, and C_{13}—C_{36} for fatty alcohols and fatty acids. Internal standards were used to quantify recoveries and concentratins. Mean recoveries relative to the internal standards were 96.5% for C_{18}—C_{36} n-alkanes, 96.4% for C_{20}—C_{30} n-fatty acids, 92.5% for C_{14}—C_{30} n-fatty alcohols and 93.3% for cholesterol. The procedural blanks for the remote marine aerosol samples allow detection limits of 0.1—1.0 pg m^{-3} for most compounds. These values are lower than any other method used at coastal marine, rural or suburban sampling locations.

Characterization of trace amounts of organic compounds in the marine atmosphere is a problem distinctly different from the monitoring of organic pollutants in urban, suburban or rural continental areas. On the one hand, aliphatic and polycyclic aromatic hydrocarbons derived from petroleum and fossil fuel combustion are quantified in atmospheric samples from urban and suburban areas. On the other hand, biogenic lipids, in a variety of compound classes, may predominate in background aerosol samples from rural continental, seashore and coastal marine locations [1, 2]. It is the wide variety of compound classes contained in these lipid materials, and their concentrations which are orders of magnitude lower at remote marine locations, that present unique analytical problems.

Thus far, ten different classes of organic compounds have been detected in

[a]Woods Hole Oceanographic Institution Contribution No. 6307.

0003-2670/87/$03.50

aerosol samples from rural continental, seashore and marine sites. These so-called "background aerosols" were collected under clean-air conditions away from local sources of contamination and anthropogenic emissions. Normal alkanes have been most commonly determined [1—15], but isoprenoid hydrocarbons [1, 2] and a complex mixture of unresolved aliphatic petroleum hydrocarbons have also been found [5—7]. Other naturally derived lipid-type compound classes found in background aerosols are: fatty acids [7—13], terpenoid acids [1, 2], fatty alcohols [1, 2, 11—14] and sterols [11—14]. Some methods also included determinations of anthropogenic compounds such as polycyclic aromatic hydrocarbons [6, 15] and phthalate esters [16].

Sampling of atmospheric particulate matter for determination of organic compounds has been done primarily through the use of high-volume air samplers with glass-fiber filters. Simoneit [17] has also used nylon nets to sample large (>2 μM) particles in the eastern tropical Atlantic near the coast of Africa. Recently, size-fractionated aerosol samples have been collected [6, 13, 18, 19]. The concentration of particulate organic matter may also be affected by interactions with gas/vapor phase organic compounds. This may be especially true for aliphatic and aromatic hydrocarbons. Hahn [20], van Vaeck et al. [21] and Zafiriou et al. [22] have reviewed much of this work, with special emphasis on the gas and aerosol distribution of the n-alkanes.

This paper describes the sampling equipment, protocols, and procedures for extraction, fractionation, derivatization, and high-resolution glass-capillary gas chromatography (HRGC) used for the determination of five lipid compound classes in background aerosol and rain samples collected at remote marine locations (Enewetak Atoll, American Samoa and Northern New Zealand) as part of the SEA-AIR EXCHANGE program (SEAREX) [23]. Results from recovery experiments and aerosol samples are provided to evaluate critically the technique and demonstrate its applicability to background-level samples in remote marine locations.

EXPERIMENTAL

Automatic control of atmospheric sampling

The collection system was controlled automatically according to real-time meteorological parameters to sample only when "clean-air" conditions prevailed; and therefore, only the uncontaminated background aerosol was collected [23]. Relevant meteorological and chemical conditions were monitored continuously: wind speed, direction, condensation nuclei counts, precipitation, ozone and radon. Collection was stopped immediately whenever the local surface wind direction was not from the open sea, when the wind speed dropped below 5 knots, when the condensation nuclei count exceeded 750 particles cm^{-3}, when precipitation started or when either ozone or radon concentrations were outside the limits set for each site. Sampling began again only when all minimum conditions were met.

Sample collection

High-volume air sampler. A schematic diagram of the high-volume atmospheric sampler is shown in Fig. 1. The glass-fiber filter for collecting aerosol samples is mounted inside an all-metal frame. A 1/8-in. thick silicone rubber gasket was used between the glass-fiber filter frame and filter holder to prevent leakage of air. The aluminum polyurethane foam (PUF) plug cartridge (290-mm × 76-mm o.d., 3-mm wall) was held in place with three stainless steel tie-rods against silicone rubber O-rings. The check-valve had a stainless steel body and spring with a silicone rubber O-ring seal. This valve is used to prevent the back-diffusion of material from the pump and ducting into the sampler during non-pumping intervals. Two complete assemblies were mounted in individual, aluminum and 316 stainless-steel shelters outside the windward railing on the top level platform of a 20-m aluminum tower [24].

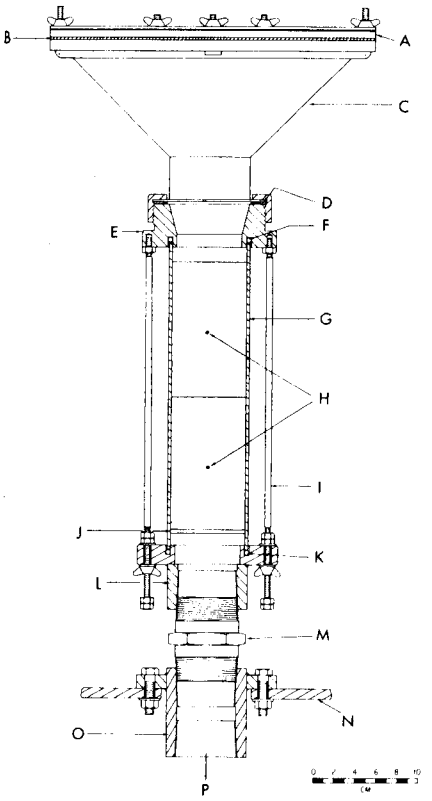

Fig. 1. High-volume air sampler: (A) glass-fiber filter frame; (B) silicone rubber gasket; (C) filter frame holder; (D) silicone rubber gasket; (E) top adaptor; (F) silicone rubber O-ring; (G) PUF-plug cartridge; (H) PUF-plug; (I) tie-rod; (J) perforated aluminum disc; (K) silicone rubber O-ring; (L) bottom adaptor; (M) check valve; (N) mounting plate in bottom of sampler shelter; (O) mounting adaptor; (P) air-flow through ducting to pump.

Each air sampler was connected to a Clements Cadillac Model HP33 blower-suction unit via 20 m of rigid aluminum tubing. Prior to sampling, the tubing was checked for leaks under maximum vacuum.

The sampler can be used for the collection of aerosol samples only or for the simultaneous collection of aerosol and gas phase samples. For aerosol sampling only, the aluminum cartridge is left empty. For gas-phase sampling two polyurethane foam plugs were placed inside the cartridge as an adsorbent. A perforated aluminum plate at the bottom of each cartridge prevents slippage of the foam plug into the check-valve. The PUF plug cartridge can be modified to hold Florisil (or any other granular adsorbent) by covering the perforated aluminum plate with a stainless-steel screen.

Sampling flow rates were determined for each high-volume pump by measuring the vacuum and pressure drop across a calibrated orifice installed in the vacuum line just upstream of the high-volume pump. The flow rates during sampling were adjusted to a preselected value by controlling the high-volume pump speed with a Variac; for glass-fiber filter only and cascade impactor samples 68 $m^3\ h^{-1}$ was used. Flow rates were measured and recorded twice each day.

Cascade impactor. A Sierra Instrument Model 235 five-stage high-volume cascade impactor was used. The impactor stages were attached to a modified glass-fiber filter frame so that an all-metal assembly was obtained. The impactor collection substrates and the backup glass-fiber filter contacted only aluminum or stainless steel. The impactor could be used with the high-volume air sampler described above or with a modified assembly which omitted the PUF plug cartridge. The cascade impactor sampler was mounted inside an all metal shelter and was automatically controlled.

Rain collector. The rain collector was constructed of two pieces: a stainless-steel mixing bowl (77.5-cm diameter) for collecting the rain, and a 55-gallon polyethylene drum for supporting the rain bowl and protecting the collecting flask and lab-jack from wind-driven rain during storms. A door in the side of the drum allowed access to the 5-l round-bottom flask used to contain the rain sample. An aluminum lid served to protect the rain-bowl from fugitive dust and/or dry fallout contamination during non-sampling intervals. Rain storms were tracked by radar and rain was collected on an event basis. The rain collector cover was removed just prior to the onset of rain and the bowl was rinsed with distilled water. The 5-l collecting flask was connected to the rain bowl as the first drops of rain began to fall and the upper level of the tower was evacuated for the duration of the storm. The rain collector was covered immediately after the rain stopped in order to limit contamination from sea spray. The 5-l flask containing the rain sample was then stoppered and carried to the field laboratory for subsampling and extraction.

Pre-extractions of sampling substrates

Because of the extremely low levels of naturally derived organic com-

pounds expected in background aerosol samples, the glass-fiber filters and cascade-impactor substrates were rigorously cleaned prior to use. For aerosol samples, 20 x 15-cm Gelman type A/E glass-fiber filters were used. For the cascade-impactor samples, 143 X 137-mm slotted glass-fiber filters (Sierra Instruments) were used.

The filters were Soxhlet-extracted for 16—20 h with 50/50 acetone/methanol, and twice more with dichloromethane. Filters were vacuum-dried and placed in clean glass jars with solvent-rinsed caps lined with aluminum foil for shipment to the sampling site. Two filters were used per sample: one for collecting the aerosol and one as a blank.

The glass-fiber filters were loaded into aluminum frames at the sampling site and carried from the laboratory to the tower top inside a thoroughly cleaned aluminum box. Solvent-extracted nylon gloves were worn when filter frames were handled. Blank filters were placed inside the shelter for the full duration of the sample. After sampling, the filters were stored frozen (ca. —10°C) in glass jars until required.

Glassware and reagents

Glass-distilled solvents (Burdick and Jackson) were used exclusively. Blanks on every individual bottle (1 gallon) of hexane (non-spectro grade) and dichloromethane were run prior to their use. Ethyl acetate and toluene were redistilled in an all-glass still (70-cm distillation column filled with Raschig rings) prior to use. Aluminum foil and all-metal sampling gear were rinsed with acetone then dichloromethane and oven-dried. All glassware was washed with 3% Micro (a surfactant) and water, rinsed thoroughly with tap then distilled water, acidic methanol (10 ml of 6 M HCl/500 ml of methanol), acetone and dichloromethane, and then oven-dried. Pipettes used for sample transfers were precleaned by Soxhlet extraction overnight with dichloromethane. All glassware was rinsed again with hexane or dichloromethane immediately before use. Double azeotropic distillation of concentrated hydrochloric acid was used to prepare 6 M HCl; acid of lower molarity was prepared by mixing the doubly-distilled 6 M azeotrope with water distilled from permanganate and then extracting three times with hexane. Boron trifluoride/methanol (14% w/v) was extracted three times with hexane and diluted with methanol to give a ca. 3% (w/v) BF_3/methanol solution before use.

Analytical methodology

A flowchart of the sample processing is shown in Fig. 2. Detailed stepwise procedures have been described [24]. Briefly, the samples were spiked with a mixture of internal-standard compounds (Table 1) and solvent-extracted with dichloromethane overnight (E1). The filters were then extracted a second time with hexane following acidification with 0.1 M HCl/methanol (E2). The dichloromethane extracts (E1) were fractionated by adsorption chromatography on silica gel (5% water) into discrete compound classes.

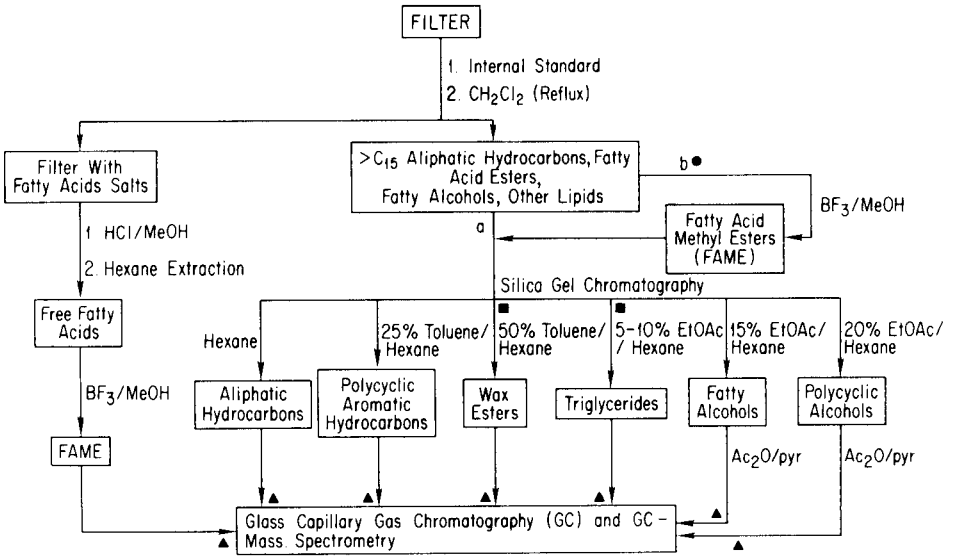

Fig. 2. Flowchart of analytical scheme. Path a or b is followed. For path a (aerosols), six fractions are collected. For path b (25% of rain extract), all wax esters and triglycerides are transesterified to FAME; five fractions are collected. (■) Fractions are combined as one fraction. (▲) Internal standards are added just prior to GC quantitation.

For rain samples, the dichloromethane extract was split: 75% was applied to the column directly; 25% was transesterified with BF_3/methanol prior to the column chromatography. The column was eluted with 25 ml of hexane (L1), 10 ml of hexane, 20 ml of 25% toluene in hexane (L2), 20 ml of 50% toluene in hexane (L3), 20 ml of 5% ethyl acetate in hexane, and 20 ml of 10% ethyl acetate in hexane (L4), 20 ml of 15% ethyl acetate in hexane (L5), 20 ml of 20% ethyl acetate in hexane (L6), and 30 ml of ethyl acetate and 30 ml of methanol (L7). Most fractions were used for high-resolution glass-capillary gas chromatography (HRGC) without derivatization. Fatty alcohols (L5) and sterols (L6) were derivatized with acetic anhydride, then purified by using the short-column silica gel chromatography procedure [25] prior to HRGC. The fatty acid salt fraction (E2) was derivatized with 3% BF_3/methanol and purified by using the short-column silica-gel chromatography procedure [24] prior to HRGC.

Combined high-resolution glass capillary gas chromatography/mass spectrometry (HRGC/MS) was used to verify peak identifications based on relative retention times and co-injections. Several glass-capillary columns were used during this work. Typically, n-alkane (L1), polycyclic aromatic hydrocarbon (L2), fatty acid methyl ester (FAME) (L3 + L4 or E2), fatty alcohol (L5) and sterol acetate (L6) fractions were quantified by using a surface-deactivated SE-52 (0.15 μm) glass capillary column (18—20 m × 0.32 mm i.d.) in a Carlo Erba Fractovap Model 2150 with a Grob-type air-cooled,

septumless, on-column injector. (See Grob [25] for column fabrication techniques.) The temperature program was: 2-min isothermal at 70°C, 5°C min^{-1} to 160°C, 3.5°C min^{-1} to 290°C, then hold at 290°C for 20 min. A Grob-type split/splitless injector was initially used for these fractions, but did not allow the determination of as high molecular-weight homologs as the on-column injector. Wax ester fractions (L3) were quantified on a SE-52 immobilized-film glass-capillary column (25 m × 0.32 mm i.d.) in a Carlo Erba Fractovap Model 4160 using the air-cooled, septumless, on-column injector. The temperature program was: on-column injection at 100°C, fast program to 180°C, 3 min at 180°C, then 3°C min^{-1} to 360°C, and 20 min at 360°C. Hydrogen was used as the carrier gas for both columns; linear gas velocities were 50 cm s^{-1} and 140 cm s^{-1}. Peak areas were measured using a Varian Vista Model 401 Chromatography Data System.

Electron-impact mass spectra were obtained using a Carlo Erba Fractovap Model 4160 gas chromatograph with on-column injector equipped with a fused silica capillary column (32 mm long × 0.32 mm i.d., DB-5, J&W Scientific) interfaced to a Finnigan Model 4505 quadrupole mass spectrometer. Mass spectra were recorded continuously with an Incos Model 2300 data system. Helium was used as the carrier gas; all spectra were obtained at 70 eV.

Two kinds of internal standards were used for each compound class. The quantitation standards were used to quantify the amount of each analyte found while the recovery standards were used to measure the percent recovery for the compound class. Compounds of the same class as those being measured but not normally found in the samples were used as recovery standards and were added to the samples just prior to the dichloromethane extraction (Table 1). Quantitation standards were compounds from a class other than the one being measured and were added to the individual fractions just prior to HRGC (Table 1).

Relative mass-response factors were determined for all compounds (standards and analytes) and the results were corrected accordingly. Compounds were quantified by the method of internal standards, then corrected for the measured percent recovery. Concentrations were calculated following blank subtraction.

RESULTS AND DISCUSSION

Sampling artifacts

The collection of atmospheric aerosols has the potential for introducing a variety of sampling artifacts. First, the filter may not be 100% efficient at collecting the particles of interest. The glass-fiber filters used in this study are rated as ⩾98% efficient for the collection of particles with radius ⩾0.015 μm [26]. Typically double filters have been used by several investigators

TABLE 1

Recovery and quantitation standards

Fraction	Compound class	Recovery standard	Quantitation standard
L1	hydrocarbons	3-methyltricosane	methyl nonadecanoate
L2	PAHs	fluorene-d_{10} *p*-terphenyl-d_{14}	n-octacosane
L3	wax esters	nonadecyl docosanoate	n-tetracontane
L4	triglycerides (NQ)[a]	—	—
L5	fatty alcohols	n-heptadecanol	n-octacosane
L6	sterols	n-heptadecanol	n-octacosane
L7	polar lipids (NQ)[a]	—	—
E2	fatty acid salts	3-methyloctadecanoic acid	n-octacosane

[a]Not quantified at this time.

(e.g., Duce et al. [27]) for the collection of aerosols. For n-alkanes and fatty alcohols, $\geqslant 95\%$ of the material was collected by the first filter [12]. Because these compound classes have the highest vapor pressure of all the compounds discussed in this report, it is considered that single filters are acceptable for the collection of atmospheric aerosols for the determination of lipid-class compounds.

The second problem in using glass-fiber filters for the collection of aerosols is the possible loss of material from the filter. This can result in lower estimates for the aerosol phase, as well as increased estimates for the gas phase if a gas-phase trapping device is installed serially behind the filter. Some of the problems associated with the use of serial particle and gas-phase samplers have been discussed by Junk and Jerome [28]. For example, one of the major processes they cite is the sublimation loss of loosely bound compounds from organic particles and their subsequent trapping by the serially-installed gas-phase collector. Van Vaeck et al. [21] have conclusively demonstrated that this occurs for coastal aerosols. Keller and Bidleman [29] have extensively addressed the problems of collecting gas-phase compounds with polyurethane foam plugs.

The third process affecting the collection of aerosols with glass-fiber filters involves the adsorption of gas-phase compounds onto the surface of the filter. For remote marine locations, the gas-phase concentrations are so low that except for the most reactive of compounds this process is probably negligible. Comparison of gas-phase and aerosol lipid compositions suggests that these are two distinct phases, and adsorption of the gas phase by the glass-fiber filter is minimal [12, 22]. Indeed, Zafiriou et al. [22] believe that the process proceeds in the other direction based on observations of hydrocarbons in rain.

The fourth process involves the interaction of trapped compounds with

reactive gases in the sampling stream. Not only are compounds lost by this process, but new ones are formed. This process is expected to be especially acute for the relatively reactive compounds containing double bonds. Thus, the polyunsaturated fatty acids are especially good candidates for this type of interaction with ozone, hydroxyl radicals, etc. Their lack of detection in aerosol samples may be evidence of this effect. Indeed we have evidence that this hypothesis is correct from initial results of samples collected only during daylight or night-time hours when the levels of OH are significantly different. Higher levels of polyunsaturated fatty acids were found at night. No significant difference was observed for the saturated compounds. Furthermore, several photo-oxidation products of unsaturated fatty acids have been found in remote marine aerosol samples [30, 31].

The fifth sampling artifact is connected with the comparison of two different types of aerosol samples. Because of the ability of rain to scavenge aerosols, rain samples can be considered a different type of "aerosol sample". Indeed, this is exactly what is done whenever a washout ratio (the ratio of the concentration of a substance in rain divided by its concentration in air) is calculated. However, there are significant differences between the temporal and spatial sampling characteristics of the two methods. Aerosol samples are typically collected over a period of several days at the base of the marine boundary layer. Rain samples are collected on a discrete-event basis lasting from tens of minutes to a few hours in duration while the rain scavenges aerosols from cloud base to ground level. Thus, already two distinctly different "aerosol" samples have to be considered. An additional factor to be considered is the possibility that gas-phase compounds can be adsorbed by rain drops. Clearly, the comparison of aerosol and rain samples is a complex situation and the reader is referred to Zafiriou et al. [22] where the subject is discussed in detail.

General blank problems

Efforts to achieve the lowest possible procedural blank led to several different schemes for cleaning the glass-fiber filters prior to sampling. Several methods are described in the literature including no treatment [14], combustion only [1, 2], solvent extraction only [8, 10, 18], or a combination of solvent extraction and combustion techniques [3, 4]. Our best results were achieved by extracting the filters overnight with 50/50 acetone/methanol followed by two overnight extractions with dichloromethane. After solvent extraction, the filters were dried at room temperature under vacuum. Vacuum-drying was found to be a cleaner process than drying inside a standard laboratory convection oven even when the filters were protected from dust during the latter process.

For most compound classes, solvent extraction alone is sufficient to clean the filters prior to sampling. However, the fatty acid salts are not removed by this process. Glass-fiber filters were combusted prior to solvent extraction in an effort to lower the blank for these compounds. The pro-

cedural blanks for the filters used in Samoa were compared (combusted vs. uncombusted). For the combusted filters the mean blank was 50% higher than for the uncombusted filters. Chesselet et al. [32] reported similar results when comparing the two processes for total organic carbon. Given that the combustion step tends to make the glass-fiber filters somewhat brittle and difficult to handle, solvent extraction alone was the precleaning method of choice. Recent preliminary experiments with the combustion of quartz-fiber filters at higher temperatures did not lower the fatty acid salt blank [33]. Under these conditions the quartz-fiber filters tended to shrink causing unknown effects on the effective pore size.

Although polyethylene bags have been used to store and transport glass-fiber filters by other workers [3, 4, 8, 23], it was found here that the polyethylene bags caused exceptionally high blanks. "Blank" filters stored in polyethylene bags contained twice the amount of dichloromethane-extractable organic matter as was found in the sample filters. Furthermore, gas chromatographic analysis of this extract yielded a large, broad, unresolved complex mixture with few discernible peaks. In contrast, transporting the filters in glass jars with foil-lined lids results in procedural blanks which are indistinguishable from blanks done immediately after the initial solvent clean-up extraction.

Compound class fractionation

An adsorption chromatographic procedure developed for the trace determination of organic compounds in marine sediments [34], plankton and oceanic particulate matter [35], was modified for the preseparation of lipids and waxes in marine aerosols. Four of the five compound classes of primary interest were completely resolved by this procedure and each was contained within a single fraction. These compound classes are: n-alkanes (L1), wax esters (L3), fatty alcohols (L5) and sterols (L6). The fifth compound class (fatty acids) was extracted from the glass-fiber filter with hexane (E2) following acidification of the filter with 0.1 M HCl in methanol. The free fatty acids contained in E2 were quantitatively separated from the neutral lipids by differential extraction because these compounds in their salt forms are essentially insoluble in the first extracting solvent, dichloromethane. For rain samples, the fatty acids were extracted along with the non-saponifiable lipids following the acidification of the rain sample and the sample was then split 3:1. The major portion was quantified as usual; the smaller portion was treated with BF_3/methanol yielding the methyl esters of the free fatty acids as well as those of esterified fatty acids contained in wax esters, triglycerides, etc., from transesterification.

High-resolution glass-capillary gas chromatography

The separation, identification and quantitation of the individual homologs within each compound class was accomplished by HRGC and HRGC/MS Actual chromatograms for sample and blank analyses are shown in Figs. 3—6

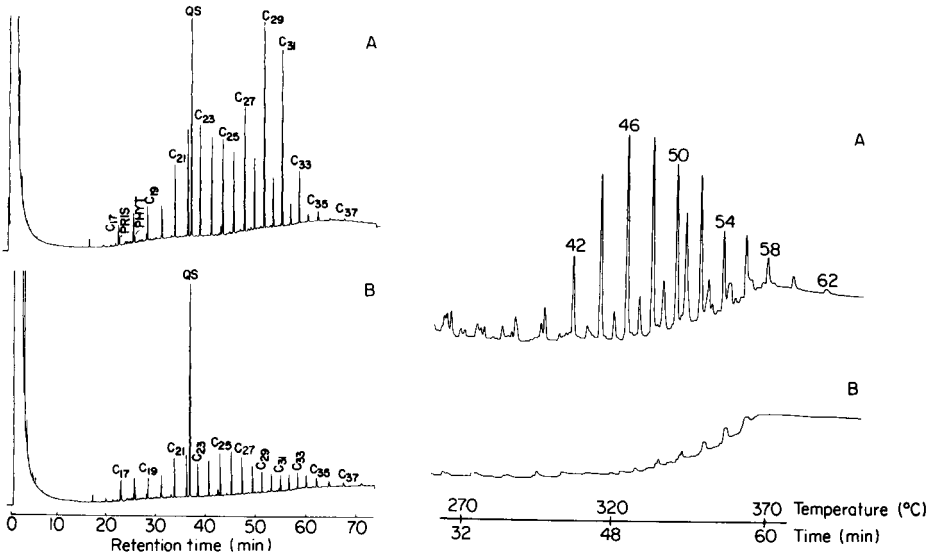

Fig. 3. High-resolution gas chromatogram of n-alkanes. (A) sample; (B) blank. QS, quantitation standard (methyl nonadecanoate); PRIS, pristane; PHYT, phytane.

Fig. 4. High-resolution gas chromatogram of wax esters: (A) sample; (B) blank. Numbers are total carbon atoms: alkyl + acyl moieties.

for the n-alkanes, wax esters, fatty alcohols (as acetates) and fatty acid salts (as methyl esters). All compound identities were confirmed by comparison of retention times and mass spectra with those for authentic standards (in no cases were spurious compounds found co-eluting with the major homologs). Splitless injection allowed identification and quantitation of C_{15}—C_{36} n-alkanes, C_{11}—C_{32} fatty alcohols (as acetates) and C_{11}—C_{32} fatty acids (as methyl esters). On-column injection expanded the analytical window to include C_{15}—C_{44} n-alkanes, C_{11}—C_{40} fatty alcohols (as acetates), C_{11}—C_{40} fatty acids (as methyl esters) and C_{39}—C_{62} wax esters. An in-depth discussion of the compounds found and their significance has been reported by Gagosian and co-workers [11—13, 19, 22, 36].

Recoveries

Compound recoveries by this method are very good, being quantitative for most compound classes. It is important to use inert, non-absorbing and non-contaminating materials for the storage and transfer of the samples. Additionally, the derivatization conditions for the fatty alcohol acetates and the fatty acid methyl esters were optimized. In trials with standard compounds, the yields (mean ± s.d.) for fatty alcohol acetylation with acetic anhydride were 93.8 ± 4.7%. The yields for fatty acid methylation were 100.3 ± 1.3% for saturated compounds and 94.4 ± 7.4% for unsaturated

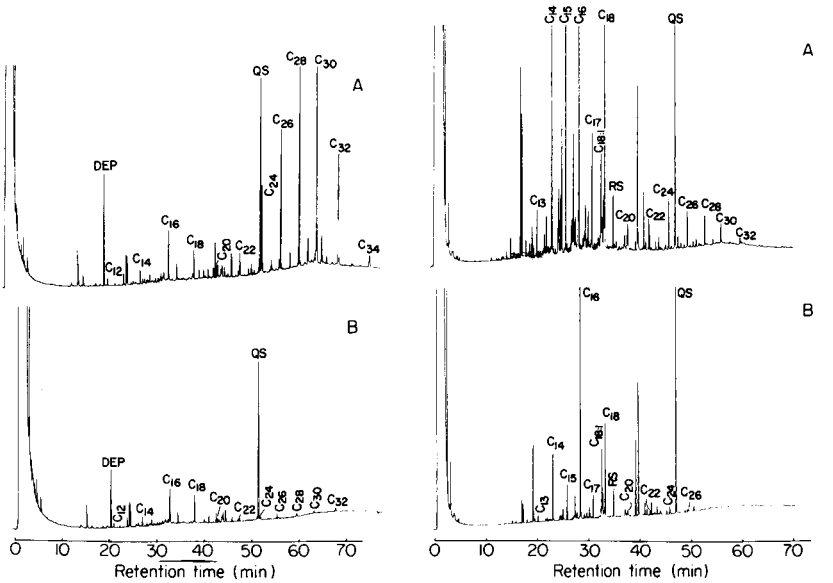

Fig. 5. High-resolution gas chromatogram of fatty alcohol acetates: (A) sample; (B) blank. Carbon numbers are chain lengths for underivatized alcohol. QS, quantitation standard (n-octacosane); DEP, diethyl phthalate.

Fig. 6. High-resolution gas chromatogram of fatty acid methyl esters: (A) sample; (B) blank. Carbon numbers are chain lengths for underivatized fatty acid. QS, quantitation standard (n-octacosane); RS, recovery standard (16-methyloctacosanoic acid as methyl ester).

ones. Transesterification yields for fatty acid esters (wax esters, steryl esters, or triglycerides) were 91.8 ± 4.8%.

Recoveries of the recovery standards measured for actual samples are listed in Table 2. For aerosol samples, recoveries ranged from 63% to 92% with 3-methyltricosane having the best recovery. For the rain samples, the recoveries were similar (54% to 91%); n-heptadecanol had the best recovery. The recoveries for the fatty acid standard were the lowest in both cases probably due to its highly surface-active nature. Considering the very low levels measured, these recoveries are quite good and reproducible (s.d. < 10%).

In cases for which recoveries are less than quantitative (95—99%), it is important to establish that the method does not discriminate between individual components of a specific compound class. This determination was made by analyzing a set of filters spiked with a series of known compounds from each compound class at levels equivalent to those found in atmospheric samples from remote marine locations. The four filters used for this experiment were prepared according to the standard method for pre-extracting filters prior to an atmospheric sampling experiment. Three filters

TABLE 2

Results for recovery standards used in Enewetak Atoll and American Samoa aerosol and rain samples

Standard	Recovery[a] (%)	
	Aerosol samples	Rain samples
3-Methyltricosane	91.5 ± 10.3	77.3 ± 8.4
n-Heptadecanol	88.8 ± 10.1	90.9 ± 7.5
3-Methyloctadecanoic acid	63.2 ± 11.0	54.3 ± 6.4

[a]Mean ± s.d. of 10 aerosol samples or 8 rain samples.

were spiked with 2 μl of a mixture of standard compounds containing 40 ng μl^{-1} of each compound. The mixture of standard compounds contained thirteen n-alkanes, ten fatty alcohols, ten fatty acid salts and two sterols to approximate the range of compounds found in a typical sample. The mixture of standard compounds also contained the three recovery standards at 50 ng μl^{-1} of each standard. A fourth filter was used as a blank and was spiked with a solution containing only the recovery standards. These filters were then processed according to the procedures outlined in the Experimental section. The results from the analyses are listed in Table 3. In contrast to the absolute recoveries of the recovery standards, the recoveries of the individual compounds relative to the recovery standards were essentially quantitative. The relative recoveries (mean ± s.d.) were: 96.5 ± 2.8% for the C_{18} to C_{36} n-alkanes, 92.5 ± 4.5% for the C_{14} to C_{30} fatty alcohols, 96.4 ± 5.3% for the C_{20} to C_{30} fatty acid salts, 93.3 ± 1.4% for cholesterol and 72.7 ± 2.0% for β-sitosterol. (Although the C_{12} to C_{18} fatty acids were added to the filter, the higher blank levels for these compounds precluded an accurate determination of their recoveries.)

Within each compound class, there is a carbon number below which the recoveries rapidly drop to zero, but above this carbon number there is very little discrimination between homologs. The losses at the low end are due to compound evaporation during sample processing, most likely during the nitrogen evaporation step. Above C_{20}, the recoveries are high, uniform and very reproducible. For individual homologs, the standard deviations for the three analyses ranged from ±0.1% to ±12.9%. The mean standard deviations for these analyses were 4.0% overall, 3.0% for the n-alkanes, 4.6% for the fatty alcohols and 5.3% for the fatty acid salts.

If the criterion for the low end for this analytical window is chosen as 80% recovery efficiency, then the lower limits for the method are C_{18} for the n-alkanes, C_{14} for the fatty alcohols and C_{14}—C_{16} for the fatty acid salts. If the criterion for the low end is chosen as 50% recovery efficiency, then smaller homologs can be determined. It is reasonable to assume that the relative recoveries will stay quantitative for the higher homologs beyond the limits of the standards used here, at least up to the upper limits of the gas

TABLE 3

Recoveries of individual compounds vs. recovery standards

Carbon no.	Recoveries[a] (10^{-2}%)		
	Hydrocarbons	Fatty alcohols	Fatty acid salts
	Recovery standard		
	3-Methyltricosane	n-Heptadecanol	3-Methyloctadecanoic acid
12	0.014 ± 0.019	0.527 ± 0.051	
14	0.117 ± 0.038	0.911 ± 0.129	
16	0.450 ± 0.035	0.862 ± 0.084	
18	0.871	0.951 ± 0.030	
20	0.909 ± 0.035	0.945 ± 0.011	0.975 ± 0.087
22	0.975	0.930 ± 0.018	
24	1.004 ± 0.060	0.961 ± 0.021	1.014 ± 0.056
26	0.939 ± 0.014	0.975 ± 0.044	1.012 ± 0.026
28	0.957 ± 0.013	0.920 ± 0.024	0.895 ± 0.036
30	0.961 ± 0.025	0.873 ± 0.044	0.922 ± 0.061
32	0.970 ± 0.001		
34	1.044 ± 0.030		
36	1.022 ± 0.055		
Cholesterol		0.933 ± 0.014	
β-Sitosterol		0.727 ± 0.020	
Mean ± s.d. for	0.965 ± 0.028 C_{18} to C_{36}	0.925 ± 0.045 C_{14} to C_{30}	0.964 ± 0.053 C_{20} to C_{30}

[a]Mean ± s.d. of 3 trials.

chromatographic procedure, because of the non-discriminating nature of on-column injection [37]. The relative recoveries for the wax esters were not determined because appropriate standards were not available. Because they are essentially non-volatile and "relatively inert", they probably have high recoveries similar to those of the hydrocarbons and fatty alcohols. These limits to the analytical window are listed in Table 4A; typical limits for the results reported here are listed in Table 4B.

The less-than-quantitative recoveries of the internal standards encountered during the recovery trials and during actual sample processing suggested that complete extraction of the compounds from the glass-fiber filters may not have been accomplished. In order to test this hypothesis and possibly to increase the recovery yields, some of the filters were extracted a second time by refluxing overnight in a second aliquot of dichloromethane prior to the acidic methanol/hexane extraction. This second extraction did not yield any detectable quantities of the neutral lipid compound classes. It is therefore concluded that a single overnight reflux with dichloromethane is sufficient, and that the losses observed for the internal standards are due to absorption or other effects and not due to incomplete extraction.

Dichloromethane is known to decompose slowly to hydrochloric acid.

TABLE 4

Carbon-number limits for the method

A. Analytical method

Compound class	Low end		High end	
	50% recovery	80% recovery	Splitless	On-column
n-Alkanes	C_{15}	C_{18} [a]	C_{36}	C_{44}
Wax esters	C_{12} [a]	C_{16} [a]	C_{42} [b]	C_{62}
Fatty alcohols	C_{12}	C_{14}	C_{32}	C_{36}—C_{40} [c]
Sterols[d]	Cholesterol	Cholesterol	β-sitosterol	β-sitosterol
Fatty acid salts	C_{12}	C_{14}	C_{32}	C_{36}—C_{40} [c]

B. Typical ranges of sample results

Compound class	Aerosol	Rain
n-Alkanes	C_{21}—C_{36} (C_{40})[e]	C_{15}—C_{36} (C_{40})[e]
Wax esters	C_{39}—C_{62}	C_{39}—C_{62}
Fatty alcohols	C_{14}—C_{32} (C_{36})[e]	C_{14}—C_{32} (C_{36})[e]
Sterols	Cholesterol, β-sitosterol	Cholesterol, β-sitosterol
Fatty acid salts	C_{13}—C_{32} (C_{36})[e]	C_{13}—C_{32} (C_{36})[e]

[a]Estimated. [b]Splitless injection of wax esters is not routinely used. [c]Estimated; authentic standards not available. [d]Sterol recovery not limited by volatility or GC injection method. [e]Numbers in parentheses are upper limits for on-column injection only.

This small amount of hydrochloric acid inadvertently introduced into the procedure may cause decomposition of the wax esters during the glass-fiber filter reflux step to form free fatty alcohols and fatty acids. In order to test this hypothesis and to compare the extraction efficiency of dichloromethane vs. hexane, duplicate samples were extracted. The two aerosol samples used were collected simultaneously under identical conditions at Enewetak Atoll. Wax ester hydrolysis was measured as the amount of n-nonadecanol formed from the hydrolysis of the wax ester internal standard, nonadecyl docosanoate; 3.2% decomposition of wax ester internal standard was found for the dichloromethane extract and 5.4% for the hexane extract. In either case, the amount of decomposition is very small and demonstrates that hydrolysis of wax esters is not a significant problem The measured concentrations of C_{21}—C_{36} n-alkanes, C_{13}—C_{32} fatty alcohols and C_{19}—C_{32} fatty acid salts for the two samples agreed within experimental error.

Filter and rain blanks

The gas chromatograph used had a detection limit of 0.05—0.1 ng. (This limit was conservatively estimated by multiplying the smallest acceptable peak height by the amount of compound required for a full-scale peak. Much smaller peak heights and areas could be detected and accurately

measured by the Vista 401-CDS but 0.5% full scale was selected as a conservative limit.) For a 5000-m^3 sample, this corresponds to a theoretical detection limit of 0.01—0.02 pg m^{-3}.

The procedures have been optimized so that approximately one-tenth of the sample is injected. With a maximum injection volume of 2.5 μl, sample volumes of 25 μl are required in order to inject ca. 10% of the sample. Sample volumes smaller than 25 μl are exceptionally difficult to handle.

With sample volumes of 25 μl, the point is reached at which the amount of the analyte in the procedural blanks becomes the limiting factor in further efforts to utilize the maximum sensitivity. The occurrence of the analytes in the procedural blanks was minimized by: (1) using the best grade of contamination-free solvents, (2) developing an elaborate glassware washing and solvent rinsing scheme, (3) scrupulously cleaning and rinsing all equipment prior to use, (4) thoroughly cleaning all sampling media, and (5) paying constant attention to the fact that only the best of laboratory anticontamination protocols are acceptable when working with samples. In order to maintain the lowest possible blank levels, each lot of hexane (non-spectro grade) and dichloromethane was tested prior to purchase, and each individual bottle from these lots was tested for contamination prior to use. Maximum allowable limits are 200 ng l^{-1} for the C_{21}–C_{36} n-alkanes with no individual n-alkane to exceed 25 ng l^{-1}, and 500 ng l^{-1} for phthalate esters with no individual phthalate to exceed 100 ng l^{-1}.

The mean blanks for samples collected during the SEAREX American Samoa field experiment will be used as representative of the blank levels found by this method (Table 5). In general, the blanks were very low, and in many cases they are the lowest procedural blanks for this type of analysis reported in the literature. Even so, for many of the compounds these blank levels are greater than the instrumental detection limits. Consequently, the limits of detection (LODs) and the limits of quantitation (LOQs) for these compounds are substantially above the theoretical limits. This limiting of detection by the background levels of the analytes in the procedural blanks is the primary reason why so much attention was given to reducing and eliminating contamination.

The detection limits for the specific compounds of interest were determined individually. According to the recommendations of the ACS Subcommittee on Environmental Analytical Chemistry [38], the LOD is 3 times the standard deviation above the blank. Likewise, the LOQ was recommended as 10 times the standard deviation above the blank. From our experience, the major source of each compound in the blank came from the extraction solvent. Very little if any material could be attributed to the glass-fiber filter or the glassware used in the procedure. Because the same bottle and amount of solvent were used for the extraction of a sample filter and its companion blank filter, there was very little variation between the amount of each compound measured in the blank and that contributed to the sample by the extraction solvent. However, because it was possible to extract only

TABLE 5

Mean blanks for Samoa aerosol and rain samples

Carbon no.	Average blank for aerosols[a] (pg m^{-3})			Average blank for rains[b] (ng l^{-1})		
	n-Alkanes	Fatty alcohols	Fatty acid salts	n-Alkanes	Fatty alcohols	Fatty acid salts
13	—	—	11	—	—	<0.3[c]
14	—	1.6	340	—	3.0	<0.3[c]
15	0.21	—	38	<0.1	—	<0.3[c]
16:0	0.43	5.6	323	<0.1	11.8	32.2
16:1	—	—	11	—	—	7.8
17	0.66	—	21	2.1	—	<0.3[c]
18:0	0.87	8.9	90	1.4	6.4	26.6
18:1	—	—	20	—	—	8.8
19	0.99	—	—	2.4	—	—
20	0.76	1.3	—	1.8	1.3	—
Mean ± s.d.	0.65 ± 0.26	4.4 ± 3.1	107 ± 132	1.3 ± 0.9	5.6 ± 4.0	8.4 ± 11.1
Median	0.71	3.6	30	1.6	4.7	3.5
19	—	—	2.1	—	—	<0.3[c]
20	—	—	4.2	—	—	6.7
21	0.80	0.10	<0.1[c]	1.8	<0.3[c]	<0.3[c]
22	0.73	0.62	7.2	3.0	0.5	20
23	0.73	<0.10[c]	1.1	5.6	<0.3[c]	<0.3[c]
24	0.91	0.25	8.1	11.0	0.3	20
25	0.87	<0.10	<0.1[c]	14.0	<0.3	<0.3[c]
26	0.91	0.36	2.5	14.3	0.3	6.7
27	0.87	<0.10[c]	<0.1[c]	10.3	<0.3[c]	<0.3[c]
28	0.68	0.80	<0.1[c]	7.5	2.1	<0.3[c]
29	0.70	<0.10[c]	<0.1[c]	5.4	<0.3[c]	<0.3[c]
30	0.55	0.42	<0.1[c]	2.6	2.0	<0.3[c]
31	0.48	<0.10[c]	<0.1[c]	1.9	<0.3[c]	<0.3[c]
32	0.38	0.10	<0.1[c]	1.2	<0.3[c]	<0.3[c]
33	0.31	—	—	0.9	—	—
34	0.26	—	—	<0.3[c]	—	—
35	0.25	—	—	<0.3[c]	—	—
36	0.22	—	—	<0.3[c]	—	—
Cholesterol		2.4			7.5	
β-Sitosterol		1.3			1.9	
Mean ± s.d.	0.60 ± 0.24	0.26 ± 0.23	1.9 ± 2.6	5.0 ± 4.8	0.6 ± 0.6	4.0 ± 7.3
Median	0.69	0.10	<0.1	2.8	<0.3	<0.3

[a]Calculated by dividing mean blank (ng) for 10 samples by nominal sample volume (5000 m^3). [b]Calculated by dividing mean blank for 6 samples (ng) by nominal sample volume (1 l). [c]The values given as less than a certain amount are estimated maximum concentrations; no detectable peaks were found.

four filters (sample or blank) per bottle of solvent, it was not possible to calculate the variability of the blank in a meaningful way with any kind of statistical treatment of the data. Instead, an estimate of the uncertainty was obtained by assuming that the mean of the standard deviations from the

analysis of the individual compounds in the recovery experiment (described previously) is representative of the variability of this method.

The uncertainties for the various compound classes are listed in Table 6. Each compound class is divided into two carbon-number ranges based on their biological source distribution, levels of occurrence and reproducibility of recovery. The lower carbon-number range is generally restricted to marine-derived compounds while the higher carbon-number range contains compounds of primarily terrestrial plant wax origin [39]. This division also corresponds to a difference in the uncertainty of the measurements. The marine-derived compounds, being lower in molecular weight, were the more volatile and the more difficult to determine. Hence, results for them tended to be more variable than for those of terrestrial origin. Thus, for each group of compounds the mean of the individual standard deviations as measured during the recovery experiment was used as the best approximation of the uncertainty of the result. These uncertainties (expressed as a percentage of the blank) then determine the limits of detection and quantitation. For simplicity, these limits were rounded to the nearest 5%. The actual limits used here are listed in Table 6 as a percentage of the blank. Then for each sample the limits for the individual compounds were calculated by simply multiplying the appropriate percentage times the procedural blank for that sample. The mean LODs are summarized in Table 7 for the American Samoa sample set. For the aerosol samples, the LODs for all compound classes, except the C_{13}–C_{18} fatty acid salts, were less than 1.0 pg m^{-3}. For the rain samples, the LODs ranged from 0.1 to 2.5 ng l^{-1}, again with the C_{13}—C_{18} fatty acid salts having the highest detection limits. These LODs are the lowest detection limits reported in the literature for any method (aerosol or rain) of this type, and they represent the cumulative results of an extensive effort in this laboratory to reduce and control sample contamination and procedural blanks.

The limits of quantitation used were approximately three times the limits of detection. For the aerosol samples, the LOQs for all compound classes, except the C_{13}—C_{18} fatty acid salts, were 0.07—2.6 pg m^{-3}. For the rain samples, the LOQs ranged from 0.1—8.4 ng l^{-1}. These limits, like the LODs,

TABLE 6

Analytical uncertainties, LODs and LOQs

Carbon no. range	n-Alkanes		Fatty alcohols		Fatty acid salts	
	C_{17}–C_{20}	C_{21}—C_{36}	C_{14}—C_{20}	C_{21}—C_{32}	C_{13}—C_{18}	C_{19}—C_{32}
Mean s.d.[a] (%)	3.5	2.8	6.1	2.5	N.M.	5.3
LOD (%)	10	10	20	10	30	15
LOQ (%)	35	30	60	25	100	50

[a]Based on 10 samples. LOD and LOQ are expressed as a percentage of the blank; N.M., not measured.

TABLE 7

Mean limits of detection for the American Samoa sample set[a]

	n-Alkanes	Fatty alcohols	Fatty acid salts
Aerosol samples (mean ± s.d., pg m^{-3})			
LMW[b]	0.07 ± 0.03	0.9 ± 0.6	32 ± 40
HMW[c]	0.06 ± 0.02	0.03 ± 0.02	0.3 ± 0.4
Rain samples (mean ± s.d., ng l^{-1})			
LMW[b]	0.13 ± 0.09	1.1 ± 0.8	2.5 ± 3.3
HMW[c]	0.5 ± 0.5	0.06 ± 0.06	0.62 ± 1.1

[a]Based on the results for 10 aerosol and 6 rain samples. [b]LMW, C_{15}—C_{20} for n-alkanes, C_{14}—C_{20} for fatty alcohols and C_{13}—C_{18} for fatty acid salts. [c]HMW, C_{21}—C_{36} for n-alkanes, C_{21}—C_{32} for fatty alcohols and C_{19}—C_{32} for fatty acid salts.

were very low and are the lowest values reported in the literature. Of the approximately 100 naturally occurring organic compounds chosen for study in remote marine aerosols, more than 90% were found at levels greater than or equal to the LOQ, and another 5% were found at levels exceeding the LOD but not the LOQ. A few compounds, notably the lower-molecular-weight n-alkanes and fatty alcohols, were not detected. For compounds with concentrations just above the LOQ, the uncertainty in the concentration is ±30% at the 99% confidence level. As the concentration increases above the LOQ, the uncertainty of the concentration approaches the uncertainty in the measurement of air volume (estimated as ±10%).

We thank Dr. Oliver Zafiriou for helping us to formulate the method; Ms. Gale Nigrelli and Dr. Stuart Wakeham for their comments and direction during the development of the silica gel and gas chromatography procedure; and Dr. Nelson M. Frew's assistance with the gas chromatography/mass spectrometric analyses. We thank Ms. Jane Alford for her work in the laboratory processing most of the Enewetak and American Samoa aerosol and rain samples. We are grateful to Mr. C. Snipes and W. Koga at Holmes and Narver, Inc., the staff of the University of Hawaii's Mid-Pacific Marine Laboratory at Enewetak, the Department of Energy, and Mr. Don Nelson and the staff at the National Oceanic and Atmospheric Administration, Global Monitoring for Climatic Change Observatory in American Samoa for major logistical support during the field work at these sites. This work was supported by the National Science Foundation, Ocean Sciences Division under NSF grants OCE 77-12914, OCE 81-11947, and OCE 84-06666 as part of the SEAREX program.

REFERENCES

1 B. R. T. Simoneit, Adv. Org. Geochem., 1979 (1980) 343.
2 B. R. T. Simoneit and M. A. Mazurek, Atmos. Environ., 16 (1982) 2139.

3 R. Eichmann, P. Neuling, G. Ketseridis, J. Hahn, R. Jaenicke and C. Junge, Atmos. Environ., 13 (1979) 587.
4 R. Eichmann, G. Ketseridis, G. Schebeske, R. Jaenicke, J. Hahn, P. Warneck and C. Junge, Atmos. Environ., 14 (1980) 695.
5 J. C. Marty, A. Saliot, P. Buat-Menard, R. Chesselet and K. A. Hunter, J. Geophys. Res., 84 (1979) 5707.
6 G. Broddin, W. Cautreels and K. Van Cauwenberghe, Atmos. Environ., 14 (1980) 895.
7 R. E. Cox, M. A. Mazurek and B. R. T. Simoneit, Nature, 296 (1982) 848.
8 W. R. Barger and W. D. Garrett, J. Geophys. Res., 75 (1970) 4561.
9 W. R. Barger and W. D. Garrett, J. Geophys. Res., 81 (1976) 3151.
10 L. van Vaeck, G. Broddin and K. Van Cauwenberghe, Environ. Sci. Technol., 13 (1979) 1494.
11 R. B. Gaosian, E. T. Peltzer and O. C. Zafiriou, Nature, 291 (1981) 312.
12 R. B. Gagosian, O. C. Zafiriou, E. T. Peltzer and J. B. Alford, J. Geophys. Res., 87 (1982) 11, 133.
13 J. K. Schneider and R. B. Gagosian, J. Geophys. Res., 90 (1985) 7889.
14 M. Barbier, D. Tusseau, J. C. Marty and A. Saliot, Oceanol. Acta, 4 (1981) 77.
15 W. Cautreels and K. Van Cauwenberghe, J. Chromatogr., 131 (1977) 253.
16 E. Atlas and C. S. Giam, Science, 211 (1981) 163.
17 B. R. T. Simoneit, Mar. Chem., 5 (1977) 443.
18 J. C. Marty and A. Saliot, Nature, 298 (1982) 144.
19 J. K. Schneider, R. B. Gagosian, J. K. Cochran and T. W. Trull, Nature, 304 (1983) 429.
20 J. Hahn, in T. J. Kneip and P. J. Lioy (Eds.), Aerosols: Anthropogenic and Natural, Sources and Transport, N.Y. Acad. Sci., New York, 1980, p. 359.
21 L. van Vaeck, K. Van Cauwenberghe and J. Janssens, Atmos. Environ., 18 (1984) 417.
22 O. C. Zafiriou, R. B. Gagosian, E. T. Peltzer, J. B. Alford and T. Loder, J. Geophys. Res., 90 (1985) 2409.
23 R. A. Duce, in M. Waldichak, G. Kullenburg and M. Orren (Eds.), Marine Pollutant Transfer Process, Elsevier, New York, 1983.
24 E. T. Peltzer, J. B. Alford and R. B. Gagosian, Methodology for Sampling and Analysis of Lipids in Aerosols from the Remote Marine Atmosphere, Woods Hole Oceanog. Inst. Tech. Rept. WHOI-84-9, Woods Hole, MA, 1984.
25 K. Grob, Making and Manipulating Capillary Columns for Gas Chromatography, Huethig, New York, 1986.
26 S. S. Butcher and R. J. Charlson, An Introduction to Air Chemistry, Academic, New York, 1972, p. 49.
27 R. A. Duce, R. Arimoto, B. J. Ray, C. K. Unni and P. J. Harder, J. Geophys. Res., 88 (1983) 5321.
28 G. A. Junk and B. A. Jerome, Am. Lab., Dec (1983) 16.
29 C. D. Keller and T. F. Bidleman, Atmos. Environ., 18 (1984) 837.
30 K. Kawamura and R. B. Gagosian, Nature, 325 (1987) 330.
31 K. Kawamura and R. B. Gagosian, private communication.
32 R. Chesselet, M. Fontugne, P. Buat-Menard, U. Ezat and C. E. Lambert, Geophys. Res. Lett., 8 (1981) 345.
33 K. Kawamura, private communication.
34 C. Lee, R. B. Gagosian and J. W. Farrington, Geochim. Cosmochim. Acta, 41 (1977) 985.
35 S. G. Wakeham, J. W. Farrington, R. B. Gagosian, C. Lee, H. DeBaar, G. E. Nigrelli, B. W. Tripp, S. O. Smith and N. M. Frew, Nature, 286 (1980) 798.
36 R. B. Gagosian, E. T. Peltzer and J. T. Merrill, Nature, 325 (1987) 800.
37 M. Galli and S. Trestianu, J. Chromatogr., 203 (1981) 193.
38 D. MacDougall, Anal. Chem., 52 (1980) 2242.
39 P. E. Kolattukudy (Ed.), Chemistry and Biochemistry of Natural Waxes, Elsevier, New York, 1976.

Analytica Chimica Acta, 198 (1987) 145—152
Elsevier Science Publishers B.V., Amsterdam — Printed in The Netherlands

DETERMINATION OF AMORPHOUS SILICA AND TOTAL SILICA IN PLANT MATERIALS

P. F. REAY* and W. D. BENNETT

Applied Biochemistry Division, Department of Scientific and Industrial Research, Private Bag, Palmerston North (New Zealand)

(Received 21st October 1986)

SUMMARY

Amorphous silica in plant material was dissolved with potassium carbonate solution, after nitric acid/hydrogen peroxide digestion. Total silica in plant material and some minerals was obtained after ashing and fusing in nickel crucibles with potassium hydroxide containing potassium tetraborate/nitrate. The relative standard deviation for determinations of silicon by these methods in plant material was <2% for plant material containing 2—2100 μmol Si g^{-1} (dry weight).

The silicon content of plants ranges from the trace level up to 1% and above [1—3], when silica deposits are present in cells and cell walls. The occurrence of these silica bodies has been frequently investigated and the amount estimated roughly [3, 4]. Silicon in plants has been determined by neutron activation analysis [5], by gravimetric techniques after ashing [6] and by spectrophotometry after ashing and fusing with sodium tetraborate in graphite crucibles [2]. The fusion procedures which are generally applied to geological samples for silicon analysis [7] do not require prior ashing. Here, a routine batch procedure with nickel crucibles is reported for the ashing and fusion of plant material containing a wide range of silica contents.

This procedure determines the total silicon, which includes silicate and silica present as dust and soil contamination. Silica is taken up from soil as silicic acid and then incorporated in the plant body as amorphous silica [8, 9] which can be determined separately from the extraneous silica and silicates [1]. This procedure [1] is modified to determine trace amounts of amorphous silica in plant material such as seeds. These two procedures are compared for plant material containing from <0.1 to 2100 μmol Si g^{-1} (dry weight), and for some selected soils and minerals.

EXPERIMENTAL

Equipment

Polystyrene test tubes, 15 × 100 mm, were used for the ion exchange of silicate solutions and for the spectrophotometric determination of silicon.

0003-2670/87/$03.50

Plant material was digested in 15 × 100-mm polypropylene test tubes, heated within 16 × 40-mm deep holes drilled into a cast aluminium block placed on a thermostatted electric frypan.

For dry ashing, the nickel crucibles (15-ml size) were placed on a stainless steel plate lying on a square 200 × 200-mm radiant cooking element (1 kW) controlled with a simmerstat. During fusions, the tapered crucibles were held in holes cut in an aluminium plate (2 mm thick) above a similar element, being inserted to half their height with the bottom 5 mm above the element. The temperature at the bottom of the crucibles was 400—420°C. The upper surface of the plate was cooled with cold water flowing through a single 6-mm diameter copper pipe held between the holes with copper saddles. During ashing and fusing, the crucibles were covered with an aluminium sheet held 150 mm above the crucibles.

A Pye-Unicam SP6 digital spectrophotometer was used with 1-cm quartz cuvettes.

Reagents

All solutions were prepared from deionized, glass-distilled water stored in polyethylene or polypropylene plastic containers and transferred with plastic pipettes. This water was also used for all washing operations. Reagents were analytical-reagent grade where available except for Aristar-grade potassium hydroxide, sodium hydroxide and potassium carbonate (BDH). Hydrogen peroxide was 50% (w/w) (BDH). For the assay of silicon [10], AnalaR sodium acetate trihydrate was used in place of the anhydrous salt for which the blank slowly increased after dissolving. Standard silicate solutions were prepared by diluting a silicon standard for atomic absorption spectrometry (BDH).

Ion-exchange resins (Dowex 50 and Amberlite IRA-93) were freed of silicate by heating with 1 M sodium hydroxide at 70°C overnight in polypropylene beakers. The resin was then washed with water until the effluent was neutral, heated with 1% (w/v) hydrofluoric acid at 70°C for 2 h, washed with distilled water, heated with 2 M hydrochloric acid at 70°C for 1 h, washed again, heated with 2 M sodium hydroxide at 70°C for 1 h, and washed again. Dowex 50 was converted to the hydrogen form with 2 M hydrochloric acid at room temperature and washed until the effluent was neutral. Amberlite IRA-93 was converted to the acetate form with 2% (v/v) acetic acid and washed with water until the pH of the effluent was greater than 3.0.

Preparation of plant material and soils

Potato tubers (*Solanum tuberosum*) were scrubbed under tap water, the skin was rubbed off under water and the intact tuber was freeze-dried. A longitudinal core (2 cm^2) was cut from the centre. French bean seeds (*Phaseolus vulgaris*) were shelled from clean green pods. Mature wheat (*Triticum aestivum*) caryopses were cut from both field-grown and glasshouse-grown plants. Wheat straw was cut from under the green leaf sheaths of

field-grown plants. Wheat awns were collected from mature, soil-grown plants in the glasshouse. White clover (*Trifolium repens*) and *Chrysanthemum mori* leaf blades were cut from plants grown in a glasshouse in peat/perlite potting mix. After collection, the leaves, stems and seeds were freeze-dried, ground in a small blade mill, and stored in polystyrene vials. Prior to decomposition, all the samples were dried in vacuum over phosphorus pentoxide.

Whatman cellulose powder (grade C-11) was soaked in 1 M sodium hydroxide for 2 days, then heated at 90°C for 2 h, washed with water, soaked for 2 days in 5% (v/v) hydrofluoric acid, washed again until the effluent was neutral, and finally dried in vacuum.

The recent alluvial soil (Manawatu silt loam [1]) and a buried volcanic ash (H_5 member of Hamilton Ash Formation [11]) were wet-sieved into three size fractions. The soil was suspended in water (2 g in 10 ml), sonicated for 15 min and wet-sieved on 100-μm nylon mesh; then the <100-mesh fraction was sieved on 50-μm nylon mesh. The three size fractions were air-dried, and then dried over phosphorus pentoxide prior to weighing.

Procedures

Total silicon. Nickel crucibles (15-ml capacity) were soaked in distilled water, dried at 100°C and heated on a hot plate at 400—500°C for 10 min to oxidize the surface. Then 0.4 ml of a solution of potassium nitrate (3% w/v) and potassium tetraborate (3.6% w/v) was evaporated to dryness in each crucibles at 100°C. Plant material (50—100 mg) was weighed into these crucible and ashed from 200 to 410°C until white, or for 2 h at most. Potassium hydroxide (0.4 g) was added and the crucibles were heated above the radiant element (see above) for 0.5 h at 400—420°C. After the crucibles were cool, 1 ml of water was added, and the crucibles were left for 5 min to dissolve the melt, heated at 70°C for 15 min and cooled. The solution was washed into a polystyrene test tube and diluted to 10.6 ml. The capped tubes were heated at 70°C for 1 h, cooled and centrifuged.

Soil and mineral samples were fused in 35-ml nickel crucibles, and the eventual solution was diluted to 80 ml in polystyrene containers.

Amorphous silica. Freeze-dried and ground plant material (50—100 mg) was weighed into polypropylene test tubes and digested with nitric acid (0.8 ml, 4.3 M) at 90°C for 2 h in the aluminium block. Then hydrogen peroxide (0.1 ml, 50% w/w) was added, heating was continued for 1 h, more hydrogen peroxide (0.4 ml per 100 mg of sample) was added and heating was continued for 2 h. Dimethylformamide (0.05 ml) and 0.03 ml of a solution of urea (30% w/v) and potassium dichromate (0.003% w/v) were then added, and the tubes were heated overnight and then until dry.

The residue was extracted with 56% (w/v) potassium carbonate solution: 0.4 ml for samples containing <5 μmol Si g^{-1} (dry weight), 0.5 ml for 5—20 μmol Si g^{-1}, 1 ml for 20—200 μmol Si g^{-1}, and 2.0 ml for 200—2500 μmol Si g^{-1}. The tubes were shaken for 0.5 h and then heated at 70°C for 3 h. The solutions were diluted to ca. 4.5 ml, vortexed, diluted to 10.6 ml, heated for

3 h at 70°C, mixed, stood overnight and centrifuged at 2000 g. Appropriate blanks were taken through the procedure.

Ion-exchange treatment of alkaline silicate solutions. Silicate solutions were diluted before ion exchange to contain less than 0.2 mmol Si l^{-1} in order to prevent silica polymerization. Solutions were diluted to either 4.5 ml or 10.6 ml in polystyrene test tubes. For 0.12—0.5 mmol of potassium carbonate or 0.25—1.0 mmol of potassium hydroxide, ca. 0.76 g of Dowex 50 (H^+-form, 200—400 mesh) was added; for less than these amounts, 0.3 g of Dowex 50 was added. The solutions were shaken for 1 h or longer, heated at 70°C for 0.5 h and shaken again for 0.5 h or longer. The solutions were then slightly acidic. Amberlite IRA-93 (acetate form; 0.28 g) was added, the tubes were shaken for 0.5 h, vortexed, then shaken for a further 3 h, vortexed again and centrifuged. The dilution of the solutions by water in the ion-exchange resins was evaluated by taking standard solutions through the procedure.

Determination of silicic acid. The molybdenum blue reaction (5-ml total volume) was conducted, as described by Smith and Milne [10], on up to 2.5 ml of the ion-exchanged solution containing <0.18 μmol of silicon.

RESULTS AND DISCUSSION

Amorphous and total silica in plant material

In contamination-free plant material, the amorphous silica found in plants was equal within experimental error to the total silica found (Table 1), over a range of silicon contents from <0.07 to 2100 μmol g^{-1} (dry weight). In wheat caryopses from the field, the total silica was slightly higher (1.25-fold) than the amorphous silica but caryopses are not totally enclosed within the palea and lemma. Wheat caryopses grown in a glasshouse had similar total and amorphous silica contents (Table 1). This proposed method for amorphous silica therefore includes all of the silica in plants in the results.

In the previous determination [1] of amorphous silica in mature bean and lupin seeds with acetic acid/peroxide digestion, a blue precipitate appeared after the addition of the molybdate reagent in the spectrophotometric assay. It was found that oxidation of the plant material with a modified Fenton's reagent [12] prevented precipitation in the spectrophotometric procedure.

After the digestion of ryegrass or wheat and drying of the residue at 90°C, dissolution of silica by the carbonate solution was incomplete unless urea and dimethylformamide, were included (Table 2). These compounds appear to prevent the residue from dehydrating. The addition of 50 mg of urea slightly reduced the recovery of silicon compared with 10 mg, but the addition of dimethylformamide also, gave complete recovery. In their presence, the dissolution of silica by 56% (w/v) potassium carbonate was increased by about 10% after heating for 3 h compared with 1 h, but was not further increased by heating for longer periods.

The ion-exchange procedure neutralized the extract, to ensure that spectrophotometry proceeded at the correct pH, and also removed phosphate

TABLE 1

The amorphous and total silicon found with the recommended procedures compared for some plant materials

Plant	Sample	Silicon found[a]		Significant difference[b]
		Amorphous	Total	
Field grown				
Wheat	Straw	422 ± 4.6	406 ± 5.1	*
Ryegrass	Leaf	156 ± 2.6	155 ± 2.0	ns
Wheat	Caryopsis	2.70 ± 0.081	3.20 ± 0.064	**
French bean	Seed	2.20 ± 0.031	2.26 ± 0.025	ns
Potato	Tuber	<0.07	<0.08	—
Glasshouse grown				
White clover	Leaf blade	18.27 ± 0.31	18.33 ± 0.21	ns
Chrysanthemum	Leaf	104.0 ± 1.0	102.0 ± 1.7	ns
Wheat	Caryopsis	0.59 ± 0.057	0.55 ± 0.046	ns
Wheat	Husk[c]	2042 ± 13	2084 ± 24	ns
Cellulose	Powder[d]	<0.07	<0.08	—

[a]Average μmol g^{-1} (dry weight), with standard deviation (n = 3). [b]ns, not significant for p = 0.05. *, significant for $p < 0.05$, **, significant for $p < 0.01$. [c]Lemma and palea. [d]Purified as in Experimental.

TABLE 2

The effect of adding urea and dimethylformamide (DMF) on the dissolution of amorphous silica in plant material

Sample (50 mg)	Si found (μmol g^{-1}, dry weight)					DMF (0.05 ml) with urea (10 mg)[a]
	No addition	DMF (0.05 ml)	Urea (mg)			
			5	10	50	
Ryegrass leaf	105	147	130	147	146	153
Wheat caryopsis	2.44	2.22	2.50	2.54	2.40	2.50

[a]Recommended procedure.

which interferes if present in excess [10]. Phosphate has been separated from silicate with anion-exchange resins [13] in the hydrogencarbonate form. With low concentrations of silicon (ca. 30 μmol l^{-1}), weakly basic resins in the hydroxide form adsorbed silicic acid from solution, as did the strongly basic Dowex 1 (hydroxide) (Table 3). Another batch of AG 3-X4 used earlier did not take up silicate [1]. The acetate form of the resins tested adsorbed silicate the least; IRA-93 in the acetate form did not significantly adsorb silicate (Table 3). After ion exchange of the extract or fusion solution, the phosphate content was <3 μmol l^{-1}, less than 1% of that originally present.

TABLE 3

Adsorption of silicic acid by anion-exchange resins (ca. 0.2 g) from 0.03 mmol l^{-1} silicate solution, mixed with Dowex 50 (H^+-form)

Anionic form	Silicic acid removed (%)			
	BioRad AG 3-X4A	Dowex 1-X8	Amberlite IRA-45	Amberlite IRA-93
Hydroxide	48	83	38	86
Borate	20	39	8	3
Acetate	12	3	3	1
Carbonate	39	18	18	2

The recovery of silicate standard solution added to clover leaf blades, potato tuber and to cellulose powder was complete and ranged from 97.5 to 102.9% (Table 4).

Selectivity of the procedure for amorphous silica. Silica in a recent alluvial soil, in a weathered allophane-rich soil, in sand and in some minerals was only slightly dissolved by the recommended procedure (Table 5). The size of soil particle separated by sieving had little effect on the amount of silica dissolved. Magnesium trisilicate was dissolved to a greater extent (about 16% of the total silicon) but this mineral is an unlikely contaminant of plants. Not all of the silicon in silica gel was found by this procedure (Table 5) because the amount was too large in relation to the volume of potassium carbonate. Only 4% of the silicon in celite, a diatomaceous silica, was dissolved. The procedure is essentially specific for amorphous silica which is the major form present in plants [8, 9].

Total silica determinations. Nickel crucibles, which resist molten alkali, were used because they are more resistant than platinum to the nitrate present in plants and are economical enough to use in batch procedures. After the dry ashing of ground lupin seeds in nickel crucibles, the ash was green from nickel. Adding alkaline salts directly to the plant material prevented attack of the nickel but often prevented complete ashing whereas coating the inside bottom of the crucible with potassium tetraborate and potassium nitrate (required for complete oxidation of carbon in the melt) prevented attack of the crucible during ashing. Heating, and thus oxidizing the crucibles before the ashing and fusion, was found to maintain a constant and low blank in the spectrophotometric procedure.

The quantity of alkali hydroxide required for complete dissolution of silica in minerals was assessed by fusing celite, magnesium trisilicate and the weathered volcanic ash soil with varying proportions of sodium hydroxide or potassium hydroxide. On a molar basis, sodium hydroxide and potassium hydroxide were found to be equally effective in dissolution of these minerals. At a ratio of between 30:1 and 60:1 (w/w) for potassium hydroxide, the recovery of silicon reached a plateau. After fusion of acid-washed sand with

TABLE 4

Recovery of silica from a silicate solution added to plant material (n = 3)

Sample	Amorphous Si (μmol)			Average recovery (%)
	Found in plant	Added	Found	
Clover leaf blade[a]	0.915	1.70	2.55	97.5
Potato tuber core[b]	<0.002	1.70	1.69	99.4
Cellulose powder[b]	<0.002	1.70	1.75	102.9

[a]50 mg. [b]100 mg.

TABLE 5

The extraction of silica from several minerals and two soils by the procedure for amorphous silica

Mineral (10 mg)	Amorphous silicon (μmol g^{-1})	Proportion of total silicon (%)
Sand	7.7	0.05
Kaolin	122	1.6
Perlite, commercial	404	3.3
Magnesium trisilicate	1440	16.0
Celite	560	4.0
Silica gel	13390	90.0
Silt loam		
Coarse fraction >100 μm	307	2.5
Medium fraction >50 μm	299	2.6
Fine fraction <50 μm	190	2.1
Volcanic ash soil[a]		
Coarse fraction >100 μm	22	0.4
Medium fraction >50 μm	17	0.3
Fine fraction <50 μm	17	0.3

[a]Allophane-rich [14].

potassium hydroxide, 16.3 mmol Si g^{-1} (n = 2) was found compared with the theoretical 16.6 mmol Si g^{-1}. On the presumption that plant material contains less than 10% (w/w) ash, then 0.4 g of KOH per fusion was adequate and was found to remain melted during the fusion.

Precision and sensitivity

The recommended procedures for amorphous and total silica had a relative standard deviation of <2% for the samples containing more than 2 μmol Si g^{-1} (dry weight) as shown in Table 1. The blank absorbance found with the greatest amount of potassium carbonate used in the amorphous silica

procedure was 0.006 (0.001 absorbance was the blank of the spectrophotometric reagent alone), and the blank absorbance for the fusion procedure was about 0.008. These values are equivalent to 0.07 and 0.09 μmol Si g^{-1} (dry weight), respectively.

The two procedures described here are suitable for determinations of either amorphous silicon in plants or total silicon in plant material over a wide range of silicon concentrations from 0.1 to at least 2100 μmol Si g^{-1} (dry weight). The selective dissolution of amorphous silica enables silica taken up by the plant to be determined free from contamination by dust and soil.

The authors thank B. Evans and P. J. Van Dingenen, Applied Biochemistry Division, DSIR, for developing and constructing the ashing, fusion equipment, and the aluminium heating blocks.

REFERENCES

1 P. F. Reay and C. Waugh, Plant Soil, 60 (1981) 435.
2 H. J. M. Bowen and A. Peggs, J. Sci. Food Agric., 35 (1984) 1225.
3 M. J. Hodson, A. G. Sangster and D. Wynn Parry, Ann. Bot. (London), 55 (1985) 649.
4 A. G. Sangster and D. W. Parry, in T. L. Simpson and B. E. Volcani (Eds.), Silicon and Siliceous Structures in Biological Systems, Springer, New York, 1981, p. 383.
5 J. D. Jones, P. B. Kaufman and W. L. Rigot, J. Radioanal. Chem., 50 (1979) 261.
6 F. C. Lanning and L. N. Eleuterius, Ann. Bot. (London), 56 (1985) 157.
7 G. J. S. Govett, Anal. Chim. Acta, 25 (1961) 69.
8 L. H. P. Jones and K. A. Handreck, Adv. Agron., 19 (1967) 107.
9 P. B. Kaufman, P. Dayanandan, C. I. Franklin and Y. Takeoka, Ann. Bot. (London), 55 (1985) 487.
10 J. D. Smith and P. J. Milne, Anal. Chim. Acta, 123 (1981) 263.
11 W. T. Ward, N.Z. J. Geol. Geophys., 10 (1967) 1105.
12 W. Kracke and K. Bunzl, Radiochem. Radioanal. Lett., 42 (1980) 77.
13 O. A. Ohlweiler, J. O. Meditsch, C. L. P. Silveira and S. Silva, Anal. Chim. Acta, 61 (1972) 57.
14 K. Wada, in J. D. Dickson and S. B. Weed (Eds.), Minerals in Soil Environments, Soil Science Society of America, Madison, WI, 1977, p. 603.

Analytica Chimica Acta, 198 (1987) 153—163
Elsevier Science Publishers B.V., Amsterdam — Printed in The Netherlands

CONFLUENT STREAMS IN FLOW INJECTION ANALYSIS

E. A. G. ZAGATTO*, B. F. REIS, M. MARTINELLI, F. J. KRUG, H. BERGAMIN F° and M. F. GINE

Centro de Energia Nuclear na Agricultura, Universidade de São Paulo, Caixa Postal 96, 13400 Piracicaba, São Paulo (Brazil)

(Received 21st November 1986)

SUMMARY

The addition of a confluent stream increases the mean length of the sample zone and simultaneously decreases the involved concentrations. Simple equations describing these effects under ideal mixing conditions are proposed. The effects of the confluent stream on the overall sample dispersion may be more or less compensated, depending on the decrease in the post-confluence dispersion. When this compensation is almost total, a paradoxical situation occurs, in which the recorded peak height becomes practically unaffected by variations in the flow rate of the merging stream. In this situation, the peak width approaches a limiting value which is independent of the injected volume and of the flow rate of the confluent stream. Limiting values for the peak width and for the mean length of the sample zone are postulated. When the post-confluence dispersion is negligible, the effects of the confluence appear in the recorded peak. The confluent stream addition reduces the overlap between successive sample zones. The site of the confluence may be an important dispersion factor. A saturation index is proposed and practical implications are discussed.

Concentration gradients are inherent in flow injection analysis, f.i.a. [1]. The exploitation of analyte concentration gradients has led to the development of valuable techniques such as merging zones [2, 3], zone sampling [4, 5], electronic dilution [1], kinetic assays [6], simultaneous determinations [7], selectivity measurements [8], etc. Also, pH gradients have been useful in some applications of f.i.a. [9]. However, the establishment of some undesirable gradients along the sample zone can impair the final measurement. The effects of gradients depend mainly on the differences in concentrations between the injected solution and its carrier stream, becoming less pronounced as the dispersion proceeds. In flow-injection systems characterized by large dispersion [1], the effects of gradients are reduced, so that measurements can usually be made without significant perturbation. In this situation, the introduction of a small volume of sample into the reagent carrier stream, according to the original concepts of f.i.a. [10, 11], usually presents no limitations.

With regard to systems with limited dispersion [1], two situations can be distinguished. In flow-injection procedures involving no chemical reactions,

0003-2670/87/$03.50

large sample volumes can be injected into a chemically inert carrier stream [12] with similar matrix composition as the sample. This reduces undesirable matrix concentration gradients, thus minimizing problems with the blank value [12]. The main functions of the sample carrier stream are then to feed the detection unit with processed samples and to promote wash-out of the system. This approach guarantees a more stable situation for the sensor. However, if reagents must be added, the single-line configuration [13] is not always feasible: the intercalation of a large sample plug into the reagent carrier stream may worsen the sensitivity [12]. The utilization of reagents becomes less efficient because, in the central portion of the sample zone, where it is most needed, its concentration is reduced. The mean available time for chemical reactions becomes significantly shorter than the mean sample residence time, as a certain time is required for the reagent to reach the central portion of the sample zone. In spectrophotometric single-line systems, the sensitivity can be limited by gradients of colour, turbidity and/or refractive index [12]; distorted and/or inverted peaks have often been reported [5, 14]. Some limitations of the single-line configuration have also been observed in routine analytical work with ion-selective electrodes. When large volumes of natural water samples are injected into the electrolyte/buffer carrier stream, the reduction of ionic strength at the central portion of the sample zone impairs the measurement.

These drawbacks are minimized in the confluence flow-injection systems proposed by Bergamin et al. [12]: the samples are introduced into chemically inert carrier streams, and reagents are added by confluence of streams. Such systems, improperly termed "high sensitivity systems" [15], present some advantages over the single-line systems [12]. Although confluence systems have been discussed in the literature, a systematic investigation of the effects of the confluent stream has not been reported previously. Studies of such effects are important in the design of flow-injection systems. This paper deals with the contribution of the confluent stream to sample dispersion, emphasizing the situations of limited and large dispersion. A confluence paradox is discussed, and the concepts of saturation index and w and σ limits are proposed.

EXPERIMENTAL

The flow-injection system was built as already described [5]. A Varian spectrophotometer (model 634) provided with a Hellma 178-OS flow cell (inner volume 80 μl; optical path 10 mm) was connected to a Radiometer REC61 recorder. The wavelength was set at 617 nm [5]. With such flow-through cuvettes, the effects of dead volume and response time could be considered negligible. The model system was based on use of a dye, as is commonly done to enable the measured signals to be referred directly to concentrations. In this situation, the recorded output truly represents the monitored concentration/time function. Averaging effects in spectrophotometry

are unavoidable, and all measurements reflect the mean concentrations of slices of the injected sample.

All solutions were prepared from analytical-grade chemicals and distilled/deionized water. The dye solutions used to simulate the sample were prepared by suitable dilutions of a 1000 mg l^{-1} bromocresol green (BCG) stock solution in 0.01 M sodium tetraborate with the same tetraborate solution. The tetraborate solution also served as carrier streams.

The flow-injection system of Fig. 1, including three manually operated commutators, was used to investigate the influence of the flow rate of the confluent stream. Dye solutions (15, 60, 150 mg l^{-1} BCG) simulating the sample were aspirated to fill the sampling loop. Switching the IC1 commutator intercalated the sample selected volume into its carrier stream (1.6 ml min^{-1}). At the confluence point, X, located 2 cm from the IC1 commutator, the confluent stream was added to the sample zone. The IC2 commutator was used to direct the confluent stream towards X, thus simplifying the modifications in flow rates. Thereafter, the sample zone was transported through the 100-cm long R1 reactor to the detector. Two distinct analytical path lengths were attained by switching the IC3 commutator which intercalated or removed an extra 300-cm R2 reactor into the path. In this investigation, the entire factorial experiment involving variations in sampling loops (2.5, 5, 10, 25, 50, 100 and 250 cm, corresponding to injected volumes of

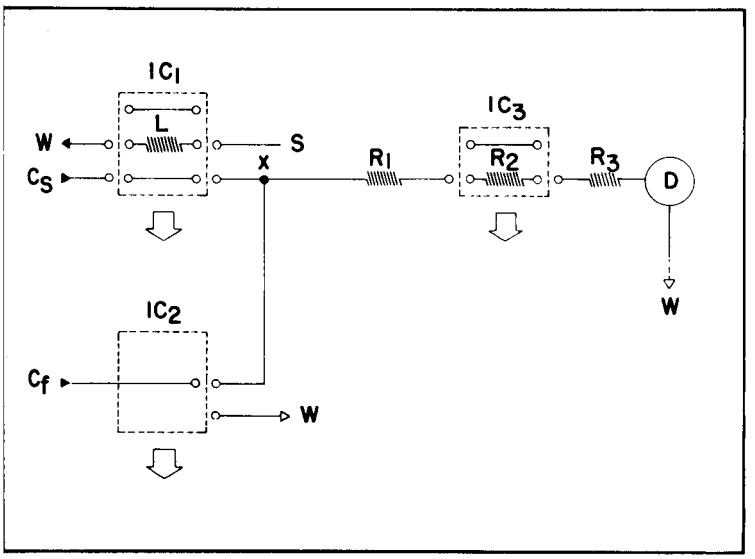

Fig. 1. Flow diagram of the system used to investigate the effect of the confluent stream flow rate: S, sample; L, sampling loop; Cs, sample carrier stream; Cf, confluent stream; R1 and R2, tubular helical reactors; R3 transmission line (20 cm); D, detector; W, waste; IC1, IC2 and IC3, commutators; X, confluence point. The components within the dashed lines are linked to the movable central bar of the commutators, the movement being indicated by the big arrows. The sites where pumping is applied are indicated by filled arrows.

about 13, 25, 50, 125, 250, 500 and 1250 μl, respectively), confluent stream flow rates (0.0, 1.6, 3.2, 4.8, 6.4 and 8.0 ml min^{-1}) and analytical path lengths was done in triplicate. For each situation, peak height (h) and peak width at half maximum (σ) were measured. Peak heights were expressed in relative units, as the ratios between the absorbances related to peak maximum and to the steady-state situation inherent in the "infinite" sample volume [5]. Peak widths were expressed in volume units (ml) in order not to be affected by variations in total flow rate through the detector.

The flow-injection system of Fig. 2, which involves sequential injections [16], was used to study the reduction of overlap between consecutive zones caused by the confluent stream addition. The sample (75 or 150 mg l^{-1} BCG) was aspirated to fill both the L1 (10 cm) and the L2 (20 cm) sampling loops, its excess being discarded. When the central sliding portion of the commutator was moved, the loops were intercalated into the same carrier stream, producing two sample zones initially separated by the 50-cm R1 reactor. The zones would overlap while being transported through the analytical path. In this experiment, the R2 reactor was either 100 or 300 cm long, and the sample carrier stream was pumped at 8.0 ml min^{-1} in absence of confluence, or at 1.6 ml min^{-1}, when the confluent stream flowing at 6.4 ml min^{-1} was added.

The flow-injection system of Fig. 3 was used to check the relevance of the point of addition of the confluent stream as a dispersion factor. Sectioned tubular reactors [17] were used as R1* and R2*, so that the position of the Y-connector required for the confluence could be modified at will. The IC2

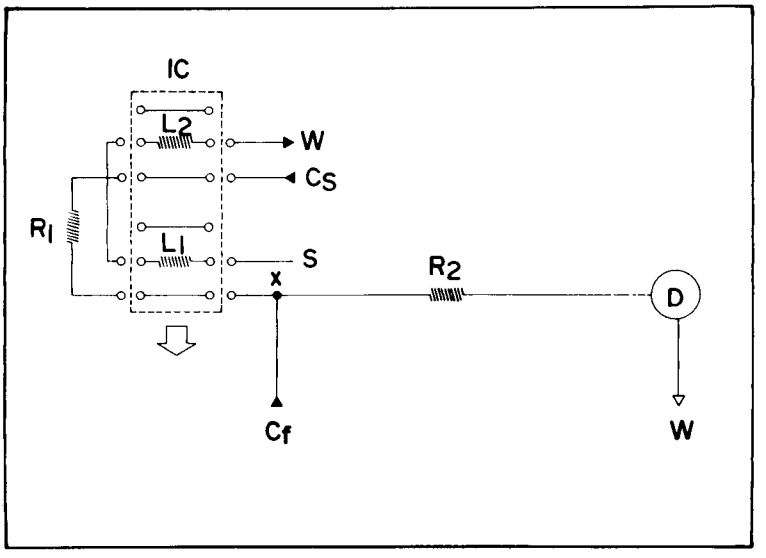

Fig. 2. Flow diagram of the system used to investigate the reduction in axial sample dispersion caused by the addition of the confluent stream. L1 and L2, sampling loops. Other symbols as in Fig. 1.

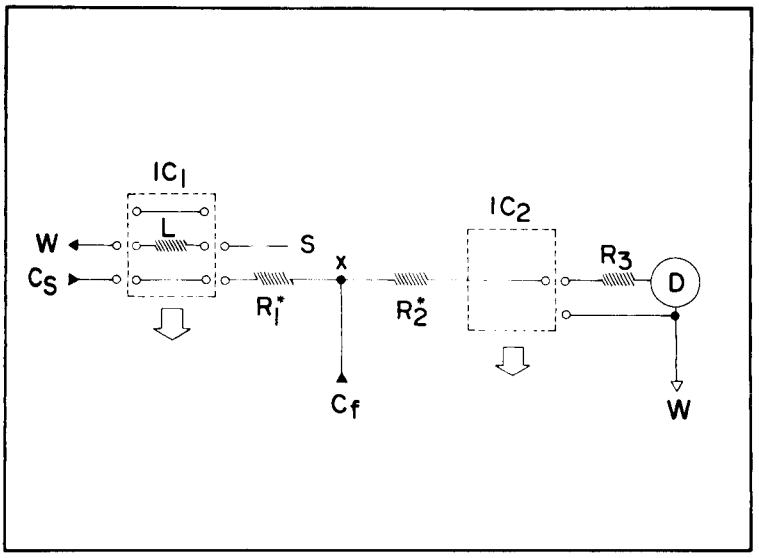

Fig. 3. Flow diagram of the system used to investigate the influence of the point of addition of the confluent stream. R1* and R2*, sectioned tubular helical reactors. Other symbols as in Fig. 1.

commutator permitted any manifold modifications to be easily accomplished without the inlet of air bubbles into the flow-through cuvette. In this experiment, the total length of R1* plus R2* was fixed as 150 cm, the length of the R3 transmission line was 20 cm and the flow rates of the carrier and confluent streams were 1.6 and 4.8 ml min^{-1}, respectively. The sampling loop was either 5 or 250 cm long: therefore, different sample concentrations (100 and 15 mg l^{-1} BCG) were required.

RESULTS AND DISCUSSION

Under ideal mixing conditions, the effects of the addition of a confluent stream can be described by the equations

$$[A'] = [A]\left\{\phi_{Cs}/(\phi_{Cs} + \phi_{Cf})\right\} \quad (1)$$

$$w' = w\left\{(\phi_{Cs} + \phi_{Cf})/\phi_{Cs}\right\} \quad (2)$$

where [A] and [A'] are the mean concentrations of species A in a very thin slice of fluid immediately before and after the confluence point; w and w' are the axial mean lengths of that fluid element associated with [A] and [A']; ϕ_{Cs} and ϕ_{Cf} are the flow rates of the sample carrier and the confluent solutions flowing through convergent conduits of identical geometry.

In practice, Eqn. 2 is not directly applicable for describing a sample zone passing through a confluence point because, for a cylindrical fluid element with significant volume, the $(w' - w)$ enlargement includes also continuous

increase of w as the fluid element is transported. In addition, the effects described by Eqns. 1 and 2 can be masked by the dispersion of the fluid element occurring before detection. As data associated with "infinite"-volume situations are independent of the post-confluence dispersion, they were used to validate Eqn. 1. Within the precision of measurement used, the expected and measured signals were identical. This conclusion can be also drawn from the data of curve c (Fig. 4B) because, with the 250-cm sampling loop, the injected volume can be considered as almost "infinite".

The experimental confirmation of Eqn. 2 is less trivial because the magnitude available from the recorded output is not the mean length of the sample zone (w); the peak width at half maximum (σ) is used. Post-confluence dispersion is unavoidable because the "infinite"-volume situation cannot be considered. However, when the 250-cm long sampling loop was used, the post-confluence dispersion was negligible, σ then becoming proportional to w. The addition of the confluent stream simultaneously increases w, hence σ (cf. Eqn. 2), and the total flow rate through the detector. This increase in flow rate determines the decrease in σ (expressed in time units) which compensates the increase in w at the confluence point only if Eqn. 2 is valid. As only slight variations in recorded peak width (usually <5%) were observed for widely varying confluent stream flow rates (cf. Fig. 5), the exactness of Eqn. 2 was confirmed.

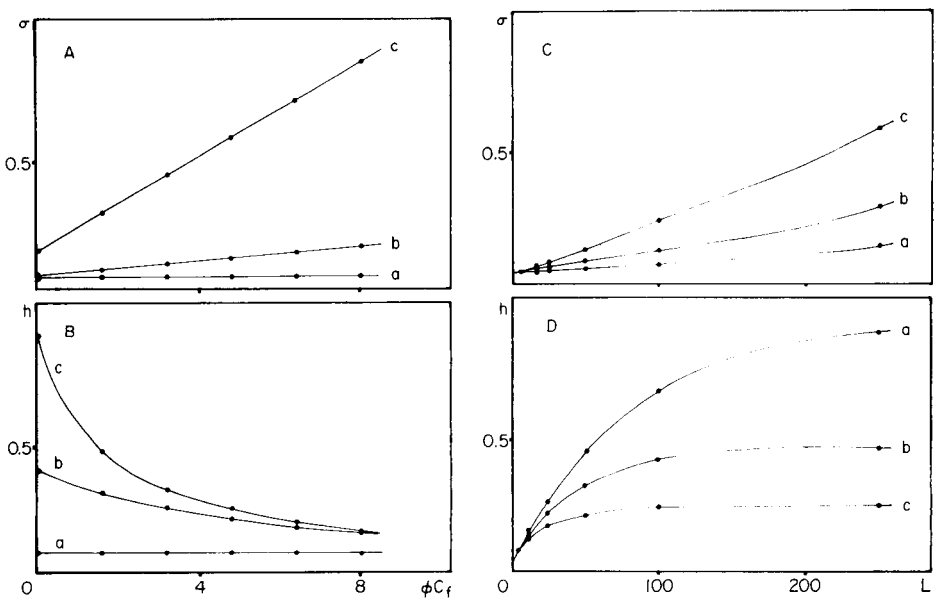

Fig. 4. Effects of the flow rate of the confluent stream (A, B) and of the length of the sampling loop (C, D) on σ (A, C) and h (B, D). The system in Fig. 1 was used with R2 removed from the analytical path. The peak width at half maximum, σ, is expressed in ml, and the peak height, h, in relative units (see text). In parts A and B, curves a, b and c correspond to loop lengths of 5, 50 and 250 cm, respectively. In parts C and D, curves a, b and c correspond to confluent stream flow rates of 0, 1.6 and 4.8 ml min^{-1}, respectively.

The effects described by Eqns. 1 and 2 are completely masked when the injected volume tends to zero. In this situation, the mean length of the sample zone at the detection unit approaches a limiting value, w^*, associated with σ^*. These limiting values are independent of the injected volume and of the confluent stream flow rate, being estimated by extrapolation of the curves of Fig. 4. It is important to emphasize that the σ^* value is predictable from the theoretical signal/time curves of Schifreen et al. [18] presented by Růžička and Hansen (p. 47 [15]). Also, when the first flow-injection/i.c.p. system was proposed, Jacintho et al. [19] noticed that, in situations of large dispersion, the time required for quantifying about 80% of the sample zone was less dependent on the injected volume. Similar observations were made by Vanderslice et al. [20] who pointed out that when the injected volume was less than 20% of the total volume of the analytical path, the peak width became only slightly dependent on the injected volume. This somewhat surprising phenomenon was also discussed by Painton and Mottola [21] and by Betteridge et al. [22]. Here, it was noticed that the σ^* value depends on the analytical path length: when the R2 reactor (Fig. 1) was placed into the analytical path, the σ^* value increased almost three-fold (Fig. 4C).

The existence of a limiting value for w should be postulated to explain why the overall sample dispersion becomes less dependent on the flow rate of the confluent stream when the injected volume tends to zero. In this situation, the addition of the confluent stream immediately after the sample injection dilutes the sample zone (cf. Eqn. 1) and simultaneously increases its mean length (cf. Eqn. 2). As a consequence of the increase in w, the post-confluence dispersion is reduced, thus compensating for the sample dilution at the confluence site. This compensation is almost total because, when the injected volume tends to zero, the same w^* value is attained at the detection unit, irrespective of the flow rate of the confluent stream (Fig. 4A). In this sense, the confluence site can be imagined as an injector port. The increase in the flow rate of the confluent stream is equivalent to a reduction in the "initial sample concentration" (cf. Eqn. 1) plus an increase in the "injected volume" (cf. Eqn. 2). As in this situation the peak height/injected volume function tends to become linear [14, 15], the increase in the "injected volume" determines an increase in peak height which compensates for the reduction of the "initial sample concentration". This compensation is a corollary of the validity of Eqns. 1 and 2. In this situation, the continuous increase of w occurring as the sample zone passes the confluence point is not important because, when the injected volume tends to zero, the value of w immediately after the injection becomes very small. Variations in total flow rate caused by the addition of the confluent stream were not considered because of their small relevance as a dispersion factor [14].

Figure 5 illustrates this apparently paradoxical situation, showing the negligible effect of a (1 + 4) confluence on the recorder output for a small sample (given suitable adjustment of chart speed). Although the total sample dispersion is affected by the confluence, the composition of the fluid element

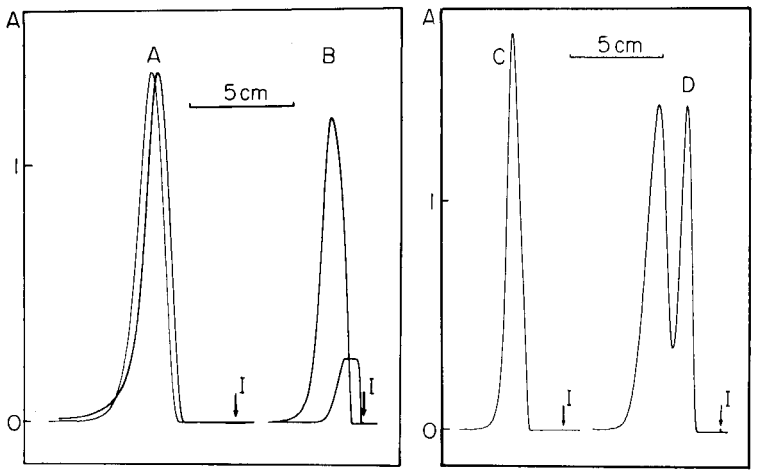

Fig. 5. Effects of the addition of confluent streams. The system of Fig. 1 was used for A and B, and that of Fig. 2 (with R2 = 300 cm) was used for C and D; I represents the instant of injection. (A) 5-cm sampling loop; R2 placed in the analytical path; 150 mg l^{-1} BCG as sample; the earlier peak, recorded at 2.5 cm min^{-1}, corresponds to the single-line manifold and the other, recorded at 12.5 cm min^{-1}, to the confluence system. (B) 250-cm sampling loop; 15 mg l^{-1} BCG sample; R2 removed from the analytical path; paper speed 5 cm min^{-1}; the earlier peak is obtained from the confluence system and the other from the single-line manifold. (C) Manifold without confluence; 75 mg l^{-1} BCG sample; paper speed 5 cm s^{-1}. (D) Manifold with confluence; 150 mg l^{-1} BCG sample; paper speed 5 cm s^{-1}.

associated with the peak maximum is strongly modified. Without confluence, the sample zone composition comprises only the sample and carrier solutions; in the confluence system, the volumetric fraction of the confluent solution in that fluid element is 80%. In applied flow-injection systems with confluent reagents, the analytical signal may be strongly dependent on the flow rate of the confluent stream.

These considerations on confluence systems should be taken into account in the design of flow-injection systems with large dispersion. The following rules can be derived: (1) adding the confluent stream near the injection port is not effective in promoting sample dispersion; (2) the concentrations and flow rates of the confluent streams should be compatible with those of the carrier stream (the utilization of too concentrated reagents at low flow rates should be avoided in order to improve the mixing conditions); (3) modifications of the injected volume of sample require a redimensioning of the flow rates and concentrations of the convergent streams; and (4) any variations in the composition of the main carrier stream caused by the confluent streams, which may alter the diffusive/convective processes must be considered.

In flow-injection systems with medium dispersion [1], the modifications in [A] and w at the confluence point (cf. Eqns. 1 and 2) are not fully compensated by the reduction of the post-confluence dispersion. In this case,

increasing the flow rate of the confluent stream increases both the height and width of the recorded peaks (Fig. 4). In situations with smaller injected volumes and lower flow rates of the confluent stream, hence smaller w' values, an increase in injected volume is reflected in a peak-height increase, only slight peak broadening being observed (Fig. 4A, B). For larger w' values, however, the dependence of the peak height on the injected volume is lessened, a more pronounced peak broadening being observed after increasing the injected volume and/or the flow rate of the confluent stream (Fig. 4A–D). As the w' value increases (by increasing the injected volume and/or the confluence-stream flow rate), the sample zone becomes less susceptible to post-confluence dispersion, the overall effect being analogous to saturation. A saturation index, I_S, is proposed here to quantify this effect.

$$I_S = (w'' - w^*)/w'' \tag{3}$$

where w'' is the length of the sample zone after the mean residence time. Although images of the sample zone have recently been obtained [17, 23], the w'' and w^* values are not readily available. For practical purposes, the saturation index I_S can be calculated as

$$I_S = (\sigma - \sigma^*)/\sigma \tag{4}$$

In this definition, the saturation index obviously refers only to the analyte zone at the detection unit. It can be noted that in the confluence paradox situation, I_S tends to zero and in flow-injection systems with medium dispersion, I_S increases with the injected volume and/or with the flow rate of the confluent stream. This should be considered in the design of flow-injection systems with medium dispersion: any increase in the flow rate of the confluent stream should be accompanied by a reduction of the injected volume. But the I_S value should be kept high when large time intervals are required for quantifying the processed sample.

The reduction of the post-confluence dispersion caused by the addition of a confluent stream is evident in Fig. 5C, D which refers to flow-injection systems with sequential injections [16]. The addition of the confluent stream minimizes the overlap between the consecutive zones established after the injection. When the R2 reactor length was 300 cm, total zone overlap was observed only in the single-line system (Fig. 5C). The individuality of the consecutive zones was better preserved when the R2 reactor length was only 100 cm and a high confluent flow rate was used. In this situation, the carry-over between the successive zones was less then 1%. The total overlap between the zones as shown in Fig. 5C leads to the conclusion that flow-injection systems with merging zones could be designed without confluence. Surprisingly, such systems seem not to be yet proposed. The addition of a confluent stream at high flow rate to minimize overlap between successive recently separated zones is common practice in gas chromatography. This stream addition into the dead volume existing before the detector provokes a signal attenuation but improves the resolution. It should be stressed that the effect of the confluence on the sampling frequency should be further investigated.

In flow-injection systems with limited dispersion, the modifications in [A] and w caused by confluence are clearly observed in the recorded outputs (Fig. 4), as already discussed. The increase in the saturation index with the flow rate of the confluent stream becomes more pronounced (cf. Fig. 5B). It is interesting to note that, as this flow rate increases, the volumetric fraction of the sample carrier stream in the fluid element associated with the analytical signal (peak maximum) becomes less significant. Increasing the flow rate of the confluent stream is also an alternative approach to achieving the sample "infinite"-volume situation.

The effects of the confluence are always those described by Eqns. 1 and 2, more or less masked by the post-confluence dispersion, which depends on w'. As w' is linked to w (cf. Eqn. 2), and as the mean length of the sample zone undergoes a continuous increase during the transport of the sample zone, it can be concluded that the site of the confluence point can be an important dispersion factor. This is evident from Fig. 6, which indicates also that the relevance of the confluence site as a dispersion factor depends on the injected volume. When large volumes are concerned, the continuous increase in w before the confluence point is not pronounced, so that the effect of the position of the confluence in the overall sample dispersion is not relevant. But for very small sample volumes the increase in w before the confluent stream addition is of utmost relevance. In this situation, increasing

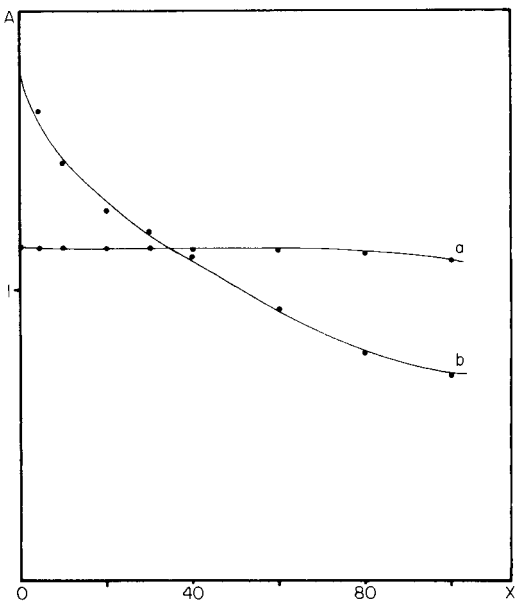

Fig. 6. Effect of the position of the confluence addition on the peak height. The system described in Fig. 3 was used. X is the distance (cm) between the injector and the confluence connector. Curves a and b correspond to loop lengths of 5 and 250 cm and to BCG concentrations of 100 and 15 mg l^{-1}, respectively.

the distance between the confluence connector and the injection port increases the overall sample dispersion (Fig. 6) and the saturation index. The following guidelines for design can then be derived. First, if the sample concentration must be preserved, large injected volumes should be used and the confluent stream, at low flow rate, should be added as near to the injection port as possible. Secondly, if large sample dilution is required, small injected volumes should be used and the confluent stream, at high flow rate, should be added as far from the injection port as possible.

Partial support of this project by CNPq (Conselho Nacional de Desenvolvimento Cientifico e Tecnologico) and by FINEP (Financiadora de Estudos e Projetos) is greatly appreciated. The authors express their gratitude to Mrs. D. Athie for her kind assistance with the manuscript and to M. A. Z. Arruda for critical comments.

REFERENCES

1 J. Růžička, Philos. Trans. R. Soc. London, Ser. A, 305 (1982) 645.
2 H. Bergamin F°, E. A. G. Zagatto, F. J. Krug and B. F. Reis, Anal. Chim. Acta, 101 (1978) 17.
3 J. Mindegaard, Anal. Chim. Acta, 104 (1979) 185.
4 B. F. Reis, A. O. Jacintho, J. Mortatti, F. J. Krug, E. A. G. Zagatto, H. Bergamin F° and L. C. R. Pessenda, Anal. Chim. Acta, 123 (1981) 221.
5 F. J. Krug, H. Bergamin F° and E. A. G. Zagatto, Anal. Chim. Acta, 179 (1986) 103.
6 P. Linares, M. D. Luque de Castro and M. Valcárcel, Talanta, 33 (1986) 889.
7 J. Ruz, A. Rios, M. D. Luque de Castro and M. Valcárcel, Fresenius' Z. Anal. Chem., 322 (1985) 499.
8 E. H. Hansen, J. Růžička, F. J. Krug and E. A. G. Zagatto, Anal. Chim. Acta, 148 (1983) 111.
9 D. Betteridge and B. Fields, Anal. Chem., 50 (1978) 654.
10 J. Růžička and E. H. Hansen, Anal. Chim. Acta, 78 (1975) 145.
11 K. K. Stewart, P. E. Hare and G. H. Beecher, Anal. Biochem., 10 (1976) 167.
12 H. Bergamin F°, B. F. Reis and E. A. G. Zagatto, Anal. Chim. Acta, 97 (1978) 427.
13 J. Růžička, E. H. Hansen and E. A. G. Zagatto, Anal. Chim. Acta, 88 (1977) 1.
14 M. Valcárcel and M. D. Luque de Castro, Analisis por Inyeccion en Flujo, Pub Monte de Piedad y Dpto de Quimica Analitica, Cordoba, Spain, 1984.
15 J. Růžička and E. H. Hansen, Flow Injection Analysis, Wiley, New York, 1981.
16 E. A. G. Zagatto, M. F. Gine, E. A. N. Fenandes, B. F. Reis and F. J. Krug, Anal. Chim. Acta, 173 (1985) 289.
17 E. A. G. Zagatto, O. Bahia F° and H. Bergamin F°, Anal. Chim. Acta, 193 (1987) 309.
18 R. S. Schifreen, D. A. Hanna, L. D. Bowers and P. W. Carr, Anal. Chem., 49 (1977) 1932.
19 A. O. Jacintho, E. A. G. Zagatto, H. Bergamin F°, F. J. Krug, B. F. Reis, R. E. Bruns and B. R. Kowalski, Anal. Chim. Acta, 130 (1981) 243.
20 J. T. Vanderslice, K. K. Stewart, A. G. Rosenfeld and D. J. Higgs, Talanta, 28 (1981) 11.
21 C. C. Painton and H. A. Mottola, Anal. Chim. Acta, 154 (1983) 1.
22 D. Betteridge, W. C. Cheng, E. L. Dagless, P. David, T. B. Goad, D. R. Deans, D. A. Newton and T. B. Pierce, Analyst, 108 (1983) 1.
23 J. T. Vanderslice, A. G. Rosenfeld and G. R. Beecher, Anal. Chim. Acta, 179 (1986) 119.

Analytica Chimica Acta, 198 (1987) 165—172
Elsevier Science Publishers B.V., Amsterdam — Printed in The Netherlands

COMPARISON OF IMMOBILIZED ENZYME REACTORS FOR FLOW-INJECTION SYSTEMS

ROBERT Q. THOMPSON*, HIDONG KIM and CHARLES E. MILLER
Chemistry Department, Oberlin College, Oberlin, OH 44074 (U.S.A.)
(Received 26th January 1987)

SUMMARY

Straight, coiled, beaded, and packed-bed reactors containing immobilized glucose oxidase or L-(+)-lactate dehydrogenase were compared in terms of reaction rate, sensitivity, sample throughput, and sample dispersion. The enzymes were covalently attached to the inside walls of 5.0-cm long, 1.12-mm i.d. nylon tubes, and the resulting reactors were tested in a flow-injection system. The beaded enzymatically-active reactors (BEARs) were filled with solid glass beads of 0.5-mm or 1.0-mm diameter. Reactors with the larger beads had 2—4 times the activity, twice the sensitivity, and better throughput than the open reactors; they also minimized the physical and chemical contributions to dispersion. Packed-bed reactors were superior in the lactate determination, but the beaded reactors were better for the determination of glucose. With BEARs containing 1.0-mm beads, glucose was determined in the range 10—800 μM with a conversion efficiency of 0.056 mol of product per mole of substrate; for lactate, the range was 8—64 μM with a conversion efficiency of 0.13 mol mol^{-1}.

Sample dispersion is a necessary evil in flow-injection systems because it is required for single-line mixing of reagents and concomitantly causes a decrease in analytical sensitivity. While advantage has been taken of dispersion for pseudo-titrations [1] and for zone sampling [2], in general, maximal mixing with minimal sample broadening is most desired. This goal is most closely approached through the use of single-bead string reactors (SBSRs), first introduced by Reijn et al. [3]. In beaded reactors, laminar flow is disrupted, mixing is enhanced, and dispersion is small and almost independent of flow rate [4]. Furthermore, the pressure drop is much less than in packed-bed reactors, and samples that might clog packed beds are not a problem with SBSRs.

Many recent reports have dealt with single-bead string reactors. Several have described aspects of sample dispersion in beaded reactors [4—6], including dispersion caused by homogeneous chemical reactions [7], and another paper compared open, beaded, and air-segmented reactors [8]. Few reports, however, have dealt in detail with the combination of SBSRs and heterogeneous chemical reactors, such as immobilized enzyme reactors. Because the kinetics of open-tubular reactors are influenced by the rate of radial transport of substrate and because more material is directed toward

0003-2670/87/$03.50

the tube wall in SBSRs, the marriage of enzymes and beads has much potential. The apparent activity and sensitivity of a beaded enzymatically-active reactor (BEAR) should be greater than that of an open-tubular reactor because the beaded reactor provides a higher rate of mass transport. Of course, enzyme could also be bound to the glass beads to improve further the reactor activity, but only the first step was taken in this work so that a more direct comparison between open and beaded reactors could be made. The use of SBSRs with enzyme-coated beads has been reported [9, 10].

Open, coiled, and two beaded-type reactors were compared by using the enzymes, glucose oxidase (E.C. 1.1.3.4) and L-(+)-lactate dehydrogenase (E.C. 1.1.1.27), to determine glucose and lactate, respectively. Packed-bed reactors were also prepared and tested for comparison of sensitivities. Glucose oxidase catalyzes the oxidation of glucose to gluconic acid and hydrogen peroxide, and lactate dehydrogenase catalyzes the reaction of lactate with β-NAD to form pyruvate and β-NADH. Glucose oxidase has a fairly large turnover number ($1200\ s^{-1}$) [11], and, therefore, the kinetics of the immobilized form are considerably influenced by mass transfer. In contrast, lactate dehydrogenase has a slowest step (dissociation of product) rate constant of only $50\ s^{-1}$ [12], and, thus, is less influenced by radial transport of substrates. Earlier work with these enzymes immobilized in a stopped-flow system supports these statements about the influence of mass transport [13, 14]. In this flow injection study, the reaction rate, sensitivity, sample throughput, and dispersion effects were measured for each reactor type at constant reactor length, sample volume, and volumetric flow rate. Recommendations for efficient reactor design are made.

EXPERIMENTAL

Reagents

Solutions were prepared in deionized water. Standards were prepared from solid D-(+)-glucose (Aldrich Chemical Co.), solid L-(+)-lactic acid (Grade L-1, Sigma Chemical Co.), and a 30% stock hydrogen peroxide solution (Fisher Scientific). A 0.05 M, pH 6.5, phosphate buffer served as the carrier stream for glucose and a 2.00 mM solution of β-nicotinamide adenine dinucleotide (NAD) in pH 9.6 buffer was used in the lactate studies. The latter buffer was prepared from solid tris(hydroxymethyl)aminomethane (Tris), hydrazine sulfate, and ethylenediaminetetraacetic acid, disodium salt (all from Sigma). Details of buffer preparation can be found elsewhere [13]. Standard solutions of the reduced form of NAD (NADH) were prepared by dissolving the solid (Sigma) in pH 9.6 Tris buffer. The enzymes, glucose oxidase (Type X) and bovine-muscle L-lactate dehydrogenase (LDH, Type X), both from Sigma, were used as received.

Enzyme reactors. Enzyme was immobilized in 1.12-mm i.d., 40 cm long, nylon 66 tubing (Universal Plastics, Seattle, WA) as described earlier [15]. The nylon was activated with 0.1 M triethyloxonium tetrafluoroborate in dichloromethane (Fluka Chemical Co.), a spacer molecule (1,4-diaminobutane, Aldrich) was added, and the enzyme was linked to the aminated nylon via

glutaraldehyde (Aldrich). The amount of enzyme bound was 10—20 μg cm^{-1} of tubing. Reactors (5 cm long) were cut from the prepared tubing, and four segments with relative activities between 0.9 and 1.0 were retained. The relative activities were measured by injection of a single standard into each reactor, and all final results were normalized to these values. One reactor was used directly, one was coiled to a diameter of 1.0 cm, one was filled with 0.5-mm diameter solid glass beads (BEAR 1), and the last was filled with 1.0-mm diameter solid glass beads (BEAR 2). The borosilicate glass beads (Propper Manufacturing, Long Island City, NY) varied in diameter as much as 15% from the nominal values and were aspirated into the nylon tubes with deionized water. Squeezed teflon tubing was added to each end of the enzyme reactors to prevent loss of the glass beads. Table 1 gives a full description of the design parameters for each of the reactors. The coiled reactors had the same values as the open ones.

Packed-bed reactors were prepared by attaching enzyme to aminopropyl porous glass chips (Sigma) and then packing the glass into 1.0-cm long, 1.12-mm i.d. nylon tubes. Glass (50 mg) was treated with 1% (w/v) glutaraldehyde in pH 10.0 carbonate buffer for 5 min, rinsed thoroughly with deionized water, and then treated with enzyme solution for 30 min. A 2.0 mg ml^{-1} solution of glucose oxidase in pH 6.5 phosphate buffer and the LDH suspension as sold by Sigma were used in the final step.

Instrumentation. The flow-injection system included a Rainin Rabbit peristaltic pump, which forced carrier and sample through the system at rates of 0.75 and 0.54 ml min^{-1}, respectively, and a pneumatically-actuated, six-way injection valve (Cheminert), controlled with an Apple II-Plus computer

TABLE 1

Design parameters for reactors

Parameter	Symbol	Units	Reactor Type		
			Open	BEAR 1	BEAR 2
Reactor length	L	cm	5.0	5.0	5.0
Reactor diameter	d_r	cm	0.112	0.112	0.112
Bead diameter	d_b	cm	—	0.050	0.10
Aspect ratio[a]	ρ	—	—	0.45	0.90
Number of beads	n	—	—	325	52
Total volume	V_t	10^{-2} cm^3	4.9	4.9	4.9
Void volume	V_o	10^{-2} cm^3	4.9	2.8	2.2
Void fraction[b]	ϵ	—	1.00	0.57	0.45
Sample volume	V_s	10^{-2} cm^3	5.5	5.5	5.5
Injection parameter[c]	α	—	1.1	2.0	2.5
Volumetric flow rate	F	10^{-2} cm^3 s^{-1}	1.25	1.25	1.25
Linear flow rate	v_f	cm s^{-1}	1.3	2.2	2.8
Reaction time	t_r	s	3.9	2.2	1.8

[a] $\rho = d_b/d_r$. [b] $\epsilon = V_o/V_t$. [c] $\alpha = V_s/V_o$.

containing an ADALAB interface board (Interactive Microware, State College, PA), which introduced 55-μl samples into the carrier stream. Connecting the valve to the enzyme reactor and the reactor to the detector were 20-cm lengths of 0.8-mm i.d. teflon tubing. The amount of peroxide generated in the glucose oxidase reactors was detected amperometrically (Model LC-3 amperometric detector, Bioanalytical Systems). A constant potential of +0.5 V was applied between platinum working and steel auxiliary electrodes, and a Ag/AgCl reference electrode completed the thin-layer, flow-through cell. In the lactate experiments, the fluorescence of NADH was monitored with an Ames Fluoro-colorimeter (Miles Laboratories) equipped with a 9-μl flow cell (Aminco) and optical filters (primary, 360-nm bandpass; secondary, 400-nm long-pass cutoff plus a 10% neutral density filter). Detector output was traced on a strip-chart recorder.

Procedures

To find the values for the physical dispersion of each system, the signal resulting from the injection of 10 μM H_2O_2 or 5 μM NADH was compared to the signal when the corresponding solution served as the carrier stream. Next, the four different reactors (without enzyme) were, in turn, placed in the flow stream to measure their effect on the physical dispersion. Finally, reactors containing enzyme were incorporated into the flow system, standard solutions (10—800 μM glucose or 8—64 μM lactate) were injected in triplicate, and peak heights and widths were measured. The sampling rate for the glucose study was 60 h^{-1} and for the lactate work it was 45 h^{-1}. The duty cycle of the valve was 50%. All reagents and reactors were at room temperature during these studies.

RESULTS AND DISCUSSION

Reaction rates

The area of each peak generated by sample injection was estimated by multiplying the peak height by the peak width at half-height. The peak areas should be accurate to ±10% because the peaks were fairly symmetrical with little tailing, and area values should be nearly independent of dispersion. Because peak area was proportional to the total amount of product formed, an approximate initial reaction rate for each enzyme-catalyzed reaction could be calculated by dividing area by residence time in the reactor. Table 2 lists the relative peak areas obtained for the sets of glucose oxidase and lactate dehydrogenase reactors. There was no significant difference in the activities of the open and coiled reactors, showing that coiling short reactors like the ones used here does not affect the overall reaction rate. The beaded glucose oxidase reactors, however, did show a significant increase in peak area. Taking into account the smaller residence times in these reactors, the reaction rates were 2.8 and 3.8 times the rate in an open tube for BEAR 1 and BEAR 2, respectively. The increased efficiency was due in part to the increased linear flow rate through the mass transport-controlled reactors. It is known that the apparent activity of open-tubular reactors increases with $v_f^{1/3}$ [16] and

TABLE 2

Relative peak area, sensitivity, and sample throughput for the different reactor types

Reactor	Glucose oxidase			Lactate dehydrogenase		
	Relative peak area[a]	Sensitivity[b]	Throughput[c]	Relative peak area[a]	Sensitivity[b]	Throughput[c]
Open	1.0	0.025	80	1.0	0.075	60
Coiled	1.0	0.029	100	1.1	0.087	65
BEAR 1	1.6	0.050	115	0.21	0.029	100
BEAR 2	1.8	0.056	120	1.0	0.13	100
Packed-bed	0.5	0.0098	100	4.1	0.50	100

[a]Peak areas for injections of 100 μM glucose or 48 μM lactate. [b]Peak-height based, moles of product produced per mole of sample. [c]Injections per hour, based on peak separation equal to 1.6 times the peak width at half-height.

recent work in this laboratory has revealed a $v_f^{1/4}$ dependence for beaded glucose oxidase reactors. Reaction rates may also have been increased because the beaded reactors, especially BEAR 2, directed much of the flowing solution along the tube walls, increasing the contact between substrate and enzyme.

The LDH reactors showed very different results, owing to enzyme control of the reaction rate; BEAR 2 had a rate only 2.3 times higher than the open form, and BEAR 1 had a lower rate. The loss of apparent activity was due to physical blocking of the enzyme and loss of the protein during the packing procedure. Figure 1 illustrates the effect of first packing and then unpacking a LDH open-tubular reactor with solid glass beads. It appears that the 0.5-mm beads scraped against the tube wall and released much of the enzyme, while the 1.0-mm beads, because of the tight fit, glided into and out of the tube on the thin film wetting the walls. The glucose oxidase reactors were not as affected by this physical process because of greater control of the kinetics by mass transport. Mottola [17] reported a similar decrease in activity with beaded reactors. He packed solid glass beads (aspect ratio = 0.77) into a glass tube coated with penicillinase and measured peak areas that were only one-third of those obtained with an open-tubular penicillinase reactor. It appears that the aspect ratio is a crucial factor in the design of beaded reactors.

Packed-bed reactors were limited to a length of 1 cm because of excessive back-pressure with longer reactors. The very large surface area of the tiny, porous glass chips allowed much more LDH to be immobilized, and so the reaction rate was more than ten times as large as the open-tube rate. However, immobilization of glucose oxidase was not as effective, and the peak area of the packed-bed reactor was only about one-third of the BEAR 2 value. The small residence time in the packed-bed reactor also contributed to its low conversion efficiency. Packed-bed reactors are not always better than other flow-through reactor types, rather the comparison depends on the enzyme characteristics and enzyme loading.

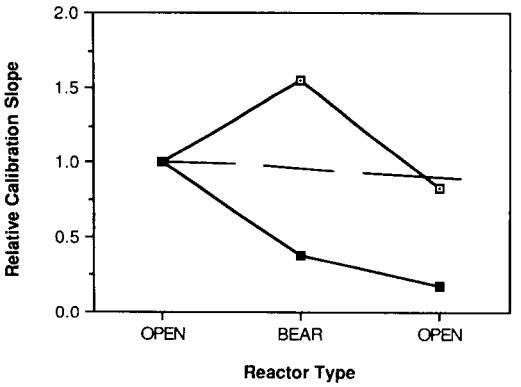

Fig. 1. Effect of packing (Open → BEAR) and then unpacking (BEAR → Open) open-tubular immobilized enzyme reactors. Beads of 1.0-mm diameter (□) and beads of 0.5-mm diameter (■) were used to fill the reactors. The broken line shows the change in reactor activity of an undisturbed beaded reactor during the same time.

Sensitivity

The average peak height produced by injection of each of five standards was compared to the concentrations of these standards by linear regression. The calculated slope (peak height units per μM) was divided by the peak height units produced per μM product concentration (H_2O_2 or NADH) to give the sensitivity. The value calculated for each reactor is given in Table 2. Despite similar peak areas, the coiled reactors showed better sensitivity because peak broadening was less than in open, straight reactors. Both BEAR 2 reactors had almost double the sensitivity of the open form, while the BEAR 1 reactors showed improvement for glucose but lower sensitivity for lactate, as expected from the discussion of peak areas. The sensitivity of the packed-bed reactors also followed the relative peak areas. The linear range of the glucose determination was not explored, but earlier results [10] indicated that the upper limit would be about 10 mM, or about one tenth of the Michaelis constant (K_m) for glucose. Mass-transport control is indicated. The linear range of the lactate determination extends only to about 0.060 mM, or 0.03 K_m. This limit is more characteristic of aqueous, enzyme-controlled kinetics than immobilized enzyme kinetics where mass transport plays an important role.

Sample throughput, precision and reactor stability

Table 2 also lists the sample throughput for each of the tested reactors. These values were calculated by stipulating an 80% return to baseline between peaks, i.e., peak separation equals 1.6 times the peak width at half-height. The BEAR 2 reactors again showed the best characteristic; in this case, the highest sample throughput was 25—60% higher than the throughput of the open reactors.

The precision of repeated injections of the same standard into the reactors was uniformly excellent. For example, five injections of 0.048 mM lactate

into a BEAR 2 reactor yielded a relative standard deviation of less than 1%. The stability of the immobilized enzyme was good and did not vary significantly between reactors. Measurements over a week with each of the glucose oxidase reactors fluctuated but showed no definite trend.

Sources of sample dispersion

The dispersion parameter, D, as proposed by Růžička and Hansen [18], was evaluated for each of the reactors in this study. Physical dispersion and sample broadening caused by mixing of sample and carrier streams, were measured by incorporating in the flow system reactors without bound enzyme. The ratios of the signals obtained with 10 μM H_2O_2 or 5 μM NADH as carrier vs. the signals with these solutions as sample gave the values for D_{phys} listed in Table 3. In general, the dispersion with and without a reactor was not significantly different because the reactor was such a small part of the flow system. The reason for the substantial increase in D_{phys} for the open glucose oxidase and coiled LDH reactors was not apparent. It is also interesting to note the difference in the values for the glucose and lactate systems. The most likely reason for the increased D_{phys} in the lactate case is the larger molecular weight of the product, NADH, and its much smaller diffusion coefficient compared to that of hydrogen peroxide.

With active reactors in place, increased peak width was clearly noticeable, especially for the open and coiled reactors. This added contribution to broadening of the sample zone was measured by calculating D_{chem} from D_{total} and D_{phys} as suggested by Mottola [19] in his homogeneous kinetics work. Mottola's method was modified so that the reactors were compared on the basis of equal product formation, rather than equal sample concentration. This eliminates the effect of different reactor activities, and sheds light instead on the rate of movement of sample and product through the enzyme layer and sample-enzyme interactions. Table 3 lists the dispersion values measured for each of the reactors, except the packed-bed reactors. Sample concentrations that gave equal areas were calculated, and peak heights for

TABLE 3

Effects of reactor type and enzyme reaction on dispersion and standard deviation (s.d.) of peak

Reactor	Glucose oxidase					Lactate dehydrogenase				
	D_{phys}	Conc.[a] (μM)	D_{total}	D_{chem}	S.d. (s)	D_{phys}	Conc.[a] (μM)	D_{total}	D_{chem}	S.d. (s)
None	3.3	—	3.3	0.0	6.6	4.3	—	4.3	0.0	9.7
Open	3.8	290	5.8	2.0	12.2	4.5	35	7.6	3.1	16.6
Coiled	3.2	290	5.3	2.1	10.0	4.7	29	7.2	2.5	16.0
BEAR 1	3.3	180	5.1	1.8	8.8	4.4	162	4.8	0.4	10.5
BEAR 2	3.2	160	4.8	1.6	8.3	4.3	34	4.7	0.4	10.5

[a]Concentration of glucose (or lactate) which gives an area equal to that of 10 μM H_2O_2 (or 5 μM β-NADH).

these concentrations were obtained from the calibration statistics. The total dispersion was then calculated in the normal fashion, and D_{chem} equalled the difference between the total and the physical dispersion. The values of D_{chem} for the glucose oxidase reactors were nearly constant, decreasing only slightly in going from open to beaded reactors, whereas chemical dispersion decreased dramatically in the beaded LDH reactors compared to the open forms. The reason for this difference is unclear.

The standard deviations in time units of the flow-injection peaks were calculated from measurements of the peak widths at half-height. The values for the glucose oxidase reactors were smaller on the whole than those for the LDH reactors, paralleling the physical dispersion measurements. Within each set of reactors, the standard deviations followed a trend also seen in the D_{total} values, i.e., the beaded reactors gave smaller values than their open counterparts.

Beaded enzymatically-active reactors provide the advantages of improved sensitivity and decreased sample dispersion, which in turn allows higher sample throughput. These advantages were shown for 5-cm reactors and would be even more significant for the longer reactors most often used in biochemical analyses. The enhanced properties were most associated with beaded reactors having a large aspect ratio, and so, for best results, open tubular immobilized-enzyme reactors should be filled with beads of a diameter equal to about 90% of the tube diameter. In addition, the influence of the heterogeneous kinetics on the dispersion was found to be significant and deserves further study.

This material is based upon work supported by the National Science Foundation under Grant No. CPE-8412299 and by the W. M. Keck Foundation which awarded a fellowship to R. Q. T. to pursue this and other work.

REFERENCES

1 J. Růžička, E. H. Hansen and H. Mosbaek, Anal. Chim. Acta, 92 (1977) 235.
2 B. F. Reis, A. O. Jacintho, J. Mortatti, F. J. Krug, E. A. G. Zagotto, H. Bergamin Fº and L. C. R. Pessenda, Anal. Chim. Acta, 123 (1981) 221.
3 J. M. Reijn, W. E. van der Linden and H. Poppe, Anal. Chim. Acta, 123 (1981) 229.
4 J. M. Reijn, W. E. van der Linden and H. Poppe, Anal. Chim. Acta, 126 (1981) 1.
5 J. M. Reijn, H. Poppe and W. E. van der Linden, Anal. Chim. Acta, 145 (1983) 59.
6 S. M. Ramasamy and H. A. Mottola, Anal. Chem., 54 (1982) 283.
7 J. M. Reijn, H. Poppe and W. E. van der Linden, Anal. Chem., 56 (1984) 943.
8 C. J. Patton and S. R. Crouch, Anal. Chim. Acta, 179 (1986) 189.
9 R. Granasekaran and H. A. Mottola, Anal. Chem., 57 (1985) 1005.
10 R. Q. Thompson, Ph.D. Thesis, Michigan State University, 1982, p. 150.
11 V. Linek, P. Benes, J. Sinkule, O. Holocek and V. Maly, Biotechnol. Bioeng., 22 (1980) 2515.
12 P. D. Boyer (Ed.), The Enzymes, Vol. XI, Academic, New York, 1975, p. 271.
13 R. Q. Thompson and S. R. Crouch, Anal. Chim. Acta, 144 (1982) 155.
14 R. Q. Thompson and S. R. Crouch, Anal. Chim. Acta, 159 (1984) 337.
15 R. Q. Thompson, C. S. Mandoke and J. P. Womack, Anal. Lett., 18 (1985) 93.
16 T. T. Ngo and K. J. Laidler, Biochim. Biophys. Acta, 377 (1975) 317.
17 H. A. Mottola, Anal. Chim. Acta, 145 (1983) 27.
18 J. Růžička and E. H. Hansen, Flow Injection Analysis, Wiley, New York, 1981, p. 16.
19 H. A. Mottola, Anal. Chem., 53 (1981) 1713.

Analytica Chimica Acta, 198 (1987) 173—181
Elsevier Science Publishers B.V., Amsterdam — Printed in The Netherlands

SIMULTANEOUS MULTI-ELEMENT ANALYSIS FOR TRACE METALS IN SEA WATER BY INDUCTIVELY-COUPLED PLASMA/ATOMIC EMISSION SPECTROMETRY AFTER BATCH PRECONCENTRATION ON A CHELATING RESIN

CHU JIA CHENG[a], TASUKU AKAGI and HIROKI HARAGUCHI*

Department of Chemistry, Faculty of Science, The University of Tokyo, 7-3-1, Hongo, Bunkyo-ku, Tokyo 113 (Japan)

(Received 9th December 1986)

SUMMARY

Batch treatment with Chelex-100 resin was investigated for preconcentration of trace metals in sea water followed by determination by inductively-coupled plasma atomic emission spectrometry. The preconcentration conditions such as resin weight, stirring time, and amount of ammonium acetate buffer solution were carefully examined for effective multi-element preconcentration from sea water. The resin weight could be decreased to 0.5 g (dry weight) for 1 l of sea water, which was much less than that required in the column method, and a preconcentration factor of 100 was achieved. Al, Ti, V, Mn, Fe, Co, Ni, Cu, Zn, Y, Mo, Cd and Pb in sea water were measured with good precision. The detection limits ranged from 6 to 180 ng l^{-1}. The time required for one sample by the batch method was only 3 h.

Recently, inductively-coupled plasma/atomic emission spectrometry (ICP/AES) has been recommended for measurements of trace metals in sea water [1—5]. The concentrations of most trace elements in sea water are generally low compared with their detection limits by ICP/AES [2] and the salts in sea water at high concentrations often provide serious problems in such analyses. Thus, preconcentration techniques such as liquid/liquid extraction [1] and coprecipitation [2, 3] by which trace elements can also be separated from matrix salts, have often been used for sample preparation in sea water analysis.

Column preconcentration on a chelating resin has also been applied to sea water analysis prior to ICP/AES [4, 5]. Various metals are successfully separated from matrix salts [6—8] although adsorption of salts on the resin must be carefully avoided for preconcentration of several elements from sea water [4]. Column preconcentration, however, has several drawbacks. It takes about a day to treat 1 l of sample. The preconcentration factor is often limited, because the relatively large amount of the resin in the column requires a large volume of acid solution for elution of analytes.

---

[a]Present address: The Water Transportation Research Institute, Ministry of Communication, 12 Bei Huan Xi Road, Beijing, China.

0003-2670/87/$03.50

Isozaki et al. [9] used a batch method with Chelex-100 resin to concentrate trace copper from natural waters, including sea water [9]; 0.4 g of chelating resin per l of sample was used. However, only copper was studied, which has the largest stability constant with Chelex-100 [7]. Thus it was necessary to establish whether such a batch technique can be applied to simultaneous multi-element preconcentration of trace metals in sea water prior to simultaneous multi-elemental determination by ICP/AES. It is shown that 13 elements can be determined satisfactorily.

EXPERIMENTAL

Chemicals and equipment

Chemicals of analytical reagent or ultrapure grade and sub-boiling distilled water were used. Chelex-100 resin (200—400 mesh; Bio-Rad) was purified as described previously [4]. Artificial sea water, used in the recovery tests, was prepared as reported by Kester et al. [10]; 100 $\mu g\ l^{-1}$ each of Al, Mn, Fe and Zn, and 50 $\mu g\ l^{-1}$ each of Ti, V, Co, Ni, Cu, Y, Mo, Cd, and Pb were added when necessary.

A Plasma Atom Comp MK. II inductively-coupled plasma atomic emission spectrometer (Jarrell-Ash) was used for simultaneous multi-element determination of trace metals. The operating and experimental conditions are shown in Table 1 (the analytical wavelengths are given in Table 5). The pH meter used was an Orion Ionalyzer 401A.

Recommended preconcentration procedure

Into exactly 1 l of sea water, 0.5 g of Chelex-100 resin (dry weight) and 10 ml of 1 M ammonium acetate buffer solution (pH 6) were added. The pH of the solution was adjusted to 6 with 1 M acetic acid or 1 M ammonia. The solution was stirred with a magnetic stirrer for 2 h. The resin was collected on a glass filter, and was washed with 30 ml of 1 M ammonium acetate buffer (pH 6) and 15 ml of pure water. The analyte elements adsorbed on the resin were desorbed with 7 ml of 2 M nitric acid, and the solution was made up to 10 ml with pure water, thus, giving a 100-times preconcentration. The solution was analyzed by ICP/AES, under the conditions shown in Table 1.

TABLE 1

Instrumental components and operating conditions for the Jarrell-Ash Plasma Atomcomp Mk. II

RF frequency	27.12 MHz	Nebulizer	Cross-flow type
RF power	1.1 kW	Polychromator	Pashen-Runge type (75 cm focal length)
Argon flows (l min^{-1})			
Coolant	15	Grating	2400 grooves mm^{-1}
Auxiliary	0.5	Reciprocal linear dispersion	0.54 nm mm^{-1} at 270 nm
Carrier	1.0		
Observation height	17 mm above work coil	Entrance slitwidth	25 μm
		Exit slitwidth	50 μm

RESULTS AND DISCUSSION

pH dependence of recoveries of various analyte elements from sea water

The matrix elements of sea water (Na, Ca, Mg) at high concentrations often provide severe interference in the ICP measurement. Thus it is desirable to separate them from analyte elements as completely as possible. Elements such as calcium and magnesium in sea water, however, are to some extent adsorbed on the chelating resin [6]. It was reported that ammonium acetate buffer could remove calcium and magnesium adsorbed on the resin [4], but it sometimes caused loss of analyte [5]. In order to investigate the influence of ammonium acetate buffer on the recoveries of analyte elements in sea water, the pH dependences of the recoveries of these elements were examined under the following experimental conditions; (a) pure water was used as the test solution and acetate buffer treatment was not included; (b) pure water was used as the test solution but the resin was washed with 30 ml of 1 M ammonium acetate buffer (pH 6) after preconcentration; (c) the artificial sea water was used as the test solution and the resin was washed with the ammonium acetate buffer (pH 6) after preconcentration. The recoveries of 13 elements (Al, Ti, V, Mn, Fe, Co, Ni, Cu, Zn, Y, Mo, Cd, Pb) was evaluated in the pH range 3—8. The weight of resin used was 0.75 g (dry weight) and the stirring time was 2 h.

Figure 1 shows the pH dependences of recoveries for Al, Mo, Ni and Mn. Generally, the dependences were similar to those obtained by the column method [4]. Most of the elements showed higher recoveries at higher pH, while the recoveries of elements forming oxoanions such as molybdenum and vanadium were poorer at higher pH. Comparing the recoveries from

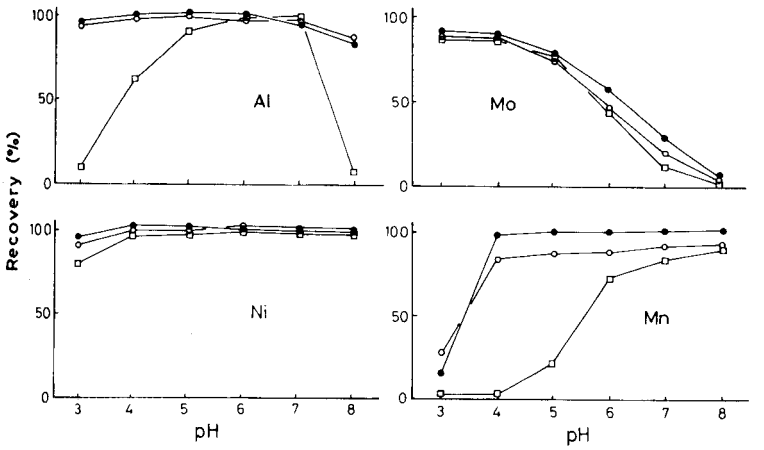

Fig. 1. pH dependences of recoveries for Al, Mo, Ni and Mn. (Resin weight 0.75 g; stirring time 2 h; 10 ml of 2 M HNO_3 for desorption.) Curves: (●) pure aqueous solution as sample, resin not washed with buffer solution; (○) pure aqueous solution as sample, resin washed with 30 ml of 1 M ammonium acetate buffer (pH 6); (□) artificial sea water as sample, resin washed with 30 ml of 1 M ammonium acetate buffer (pH 6).

method (a) with those from method (b), losses of some analytes by the buffer treatment were observed. Some copper and iron have been reported to be lost by the buffer treatment [5]. The recoveries of Al, Co, Ni, Cu, Zn, Y, Mo, Cd and Pb were not decreased by treatment with the buffer solution, but those of Ti, Mn and Fe were. Comparison of the results of experiments (a) and (c) indicates that the recoveries of Al, Mn, Zn, Y, Cd and Pb became less when matrix salts at high concentrations were present, but Ti, V, Fe, Co, Ni, Cu and Mo did not show any changes in recovery in the presence of matrix salts. It should be noted that titanium and iron, which were partly lost in the buffer treatment, did not show any deterioration in recovery in the presence of matrix salts. Moreover, molybdenum and vanadium, which gave lower recovery at high pH, did not show any decrease in recovery in the presence of matrix salts. These results suggest that calcium and magnesium may interfere with the adsorption of Al, Mn, Zn, Y, Cd and Pb onto the resin by competitive reaction with the resin.

In the analysis of natural sea water, experimental procedure (c) was used for sample treatment. As mentioned above, the recoveries of analytes and the concentrations of matrix elements retained on the resin varied with pH. Therefore, the experimental conditions, especially the pH, had to be a compromise between the different groups of analytes. Eight elements (Al, Ni, Cu, Co, Zn, Cd, Y and Pb) gave recoveries of more than 90% at pH 6; the recovery of manganese was ca. 70%. In order to concentrate Fe, Ti, Mo, and V efficiently, pH 3 is recommended.

Optimization of resin weight and stirring time

Resin weight and stirring time in the batch treatment can influence the partition of analyte elements between the resin and the solution. It is supposed that a longer stirring time requires a smaller amount of resin for collection of analytes. In order to minimize contamination, a smaller amount of resin and a shorter stirring time are preferable. In addition, considering contamination from the eluent, a small amount of resin is again desirable. The recoveries of analytes at pH 6 were examined by changing the resin weight and stirring time independently. In this experiment, 30 ml of ammonium acetate buffer was used for washing the resin.

The results obtained for aluminium are shown in Fig. 2. As expected, the recovery was better when larger resin weights and longer stirring times were used. Similar results were obtained for Mn, Co, Ni, Cu, Zn, Y, Cd and Pb. It was found that at least 0.3 g of the resin and a 1-h stirring time were necessary for quantitative preconcentration of aluminium. A similar examination was also made at pH 3 for Ti, V, Fe and Mo. A resin weight of 0.45 g and a 2-h stirring time are recommended for efficient preconcentration of these elements from sea water.

The optimum conditions of resin weight and stirring time for preconcentration of each element examined at pH 3 and 6 are summarized in Table 2. On the basis of these results, a resin weight of 0.5 g and a stirring time of

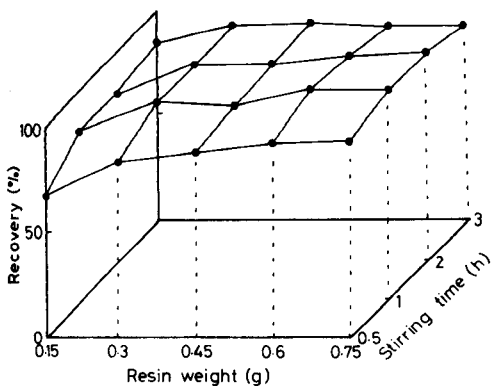

Fig. 2. Optimization of preconcentration of aluminium as functions of resin weight and stirring time. Conditions: batch treatment at pH 6, resin washed with 30 ml of 1 M ammonium acetate buffer (pH 6), 10 ml of 2 M nitric acid for desorption.

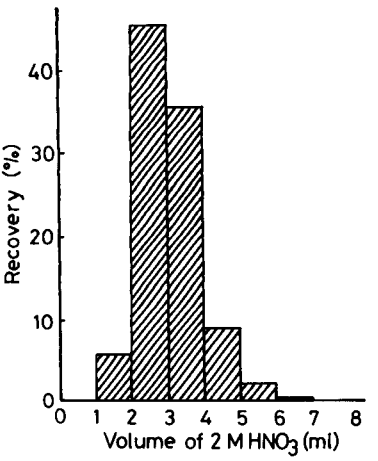

Fig. 3. Elution profile of copper from chelating resin with 2 M nitric acid. Conditions: 0.5 g of resin, batch treatment at pH 6 with stirring for 2 h, resin washed with 30 ml of 1 M ammonium acetate buffer (pH 6).

TABLE 2

Optimum conditions for preconcentration of trace elements by the batch method[a]

Metal	pH	Resin weight (g)	Stirring time (h)	Recovery (%)	Metal	pH	Resin weight (g)	Stirring time (h)	Recovery (%)
Al	6	0.30	1.0	93.5	Cu	6	0.15	0.5	97.6
Ti	3	0.45	2.0	92.5	Zn	6	0.30	0.5	95.2
V	3	0.45	2.0	93.2	Y	6	0.45	1.0	91.3
Mn	6	0.45	2.0	69.6	Mo	3	0.45	2.0	89.2
Fe	3	0.45	2.0	95.5	Cd	6	0.30	0.5	91.2
Co	6	0.15	0.5	94.1	Pb	6	0.75	3.0	92.5
Ni	6	0.15	0.5	93.9					

[a]After batch treatment the resin was washed with 30 ml of 1 M ammonium acetate (pH 6). Desorption was with 10 ml of 2 M nitric acid. The resin weights and stirring times are the minimum needed to give the recoveries shown.

2 h are recommended in order to preconcentrate many elements simultaneously, although the pH should be changed depending on the elements.

Removal of matrix elements by ammonium acetate buffer solution

It is known that matrix salts at high concentrations cause several problems such as spectral interference and clogging of the nebulizer in the ICP

measurement. In such cases, treatment of the resin with ammonium acetate buffer solution has been used to remove the matrix salts [4]. However, when an excess of the buffer is used for washing the resin, loss of analyte elements is often observed [5]. Thus the volume of the ammonium acetate buffer solution should be minimized. The concentrations of Ca, Mg, Na and K retained on 0.5 g of the resin from 1 l of sea water are given in Table 3. As can be seen, the concentrations of Ca, Mg, Na and K in the final solution decreased with increasing volume of the wash solution. The concentrations in 30 ml of the buffer solution were low enough to avoid interferences from the matrix salts in sea water [4]. Therefore, for natural seawaters, 30 ml of buffer is recommended for washing. In the column method, more than 100 ml of buffer solution was required to remove matrix elements effectively because of the larger amount of resin used [4]. The smaller volume of buffer solution in the batch method compared to the column method is obviously preferable.

Desorption of analytes by nitric acid

Figure 3 shows the progress of the removal of copper from the resin in 1-ml fractions of 1 M nitric acid. The copper was removed within the first six 1-ml fractions. Other elements examined gave almost the same desorption pattern. Thus, in the present batch method, analyte elements on the resin were desorbed with 7 ml of the nitric acid. In the column method, a larger amount (25 ml) of the nitric acid was required because of the larger amount of the resin used [4]. A preconcentration factor of more than 100 was easily obtainable without evaporation in the batch method.

Analytical parameters

The recoveries of metals spiked in 1 l of artificial sea water by the batch method are summarized in Table 4. At pH 6, the recoveries of Al, Co, Ni, Cu, Zn, Y and Cd were more than 90%, and those of Pb and Mn were 85 and 72%, respectively. The low recoveries of Pb and Mn may be due to residual

TABLE 3

Concentration ($\mu g\ ml^{-1}$) of Na, Mg, K and Ca in the 10 ml of solution after washing the resin with different volumes of 1 M ammonium acetate buffer (pH 6)[a]

Element	Volume of buffer (ml)					
	0	10	20	30	40	50
Na	56	0.8	0.8	0.8	0.8	0.8
Mg	760	35.0	18.7	6.4	4.2	0.5
K	6	0.3	0.3	0.3	0.2	0.2
Ca	430	42.8	13.3	4.5	3.8	0.6

[a]Artificial seawater (1 l) was treated with 0.5 g of chelating resin at pH 6 with stirring for 2 h, and matrix elements were finally desorbed with 10 ml of 2 M nitric acid.

TABLE 4

Recoveries of analyte elements from 1 l of artificial sea water by batch preconcentration[a]

Metal	pH	Added (μg)	Recovery[b] (%)	Metal	pH	Added (μg)	Recovery[b] (%)
Al	6	100.2	99.1 (2.0)	Ni	6	51.3	101.6 (0.9)
Ti	6	50.0	58.4 (8.4)	Cu	6	51.5	94.5 (1.5)
	3	50.0	96.4 (1.1)	Zn	6	102.7	101.4 (1.0)
V	6	50.1	28.9 (5.9)	Y	6	52.8	90.4 (0.8)
	3	50.1	95.9 (1.7)	Mo	6	46.4	25.1 (5.6)
Mn	6	101.4	72.0 (3.1)		3	46.4	88.8 (2.3)
Fe	6	102.2	62.7 (8.3)	Cd	6	50.5	96.2 (0.7)
	3	102.2	100.5 (0.4)	Pb	6	48.4	85.6 (1.3)
Co	6	50.3	100.6 (1.2)				

[a]After the batch treatment (resin weight 0.5 g, stirring time 2 h), the resin was washed with 30 ml of 1 M ammonium acetate (pH 6), and the analytes were eluted with 7 ml of 2 M nitric acid. [b]Mean with relative standard deviation (in parentheses) of 4 separate determinations.

matrix salts and/or removal with buffer. At pH 6, recoveries of Ti, V, Fe and Mo were less than 60%. As discussed previously, the recoveries of Ti and Fe were decreased by buffer treatment, and the poor recoveries of V and Mo were due to their oxoanion forms at this pH. Better recoveries of 89—100% were obtained at pH 3.

Reproducibilities of the recoveries at pH 6 were in the range 0.5—3% for all the elements except Ti, V, Fe and Mo, for which better reproducibilities were obtained at pH 3.

In Table 5, blank values for the whole preconcentration procedure and detection limits are given along with the analytical wavelengths used. The blank for each element was estimated by applying the same procedure to 200 ml of sub-boiling distilled water and was converted to the concentration corresponding to 1 l of sample. The analytical detection limits were calculated by dividing the instrumental detection limit by the preconcentration factor. The instrumental detection limits were defined as the analyte concentrations corresponding to three times the standard deviation of the background emission intensities for pure water. The blank values for Ti, Mn, Co, Ni, Cu, Y, Mo, Cd and Pb were lower than or close to the analytical detection limits. For V, Fe and Zn, correction for the blank values was essential in sea water analysis.

The analytical results for sea water collected at coastal areas of Tokyo Bay and Hiroshima Bay are shown in Table 6. These samples were stored at pH 2 after addition of hydrochloric acid and filtered through Nuclepore filters prior to the preconcentration treatments. For the water from Tokyo Bay, preconcentration was done at pH 6. The results for Ti, V and Mo are not shown in the Table, because of the poor recoveries at pH 6. The relative

TABLE 5

Analytical wavelengths, detection limits, and blanks for the batch preconcentration method

Element	Wavelength (nm)	Detection limit ($\mu g\ l^{-1}$)	Blank ($\mu g\ l^{-1}$)	Element	Wavelength (nm)	Detection limit ($\mu g\ l^{-1}$)	Blan (μg l
Al	308.2	0.18	0.34	Cu	324.7	0.01	0.02
Ti	334.9	0.006	0.01	Zn	213.8[a]	0.02	0.13
V	292.4	0.04	0.12	Y	371.0	0.006	<0.00
Mn	257.6	0.008	<0.008	Mo	202.0	0.03	<0.03
Fe	238.2	0.02	0.06	Cd	228.8[a]	0.03	<0.03
Co	228.6	0.03	<0.03	Pb	220.3	0.15	<0.15
Ni	231.6[a]	0.1	<0.1				

[a]Second-order lines were used.

TABLE 6

Analytical results for sea waters

Metal	Tokyo Bay		Hiroshima Bay
	Conc. ($\mu g\ l^{-1}$)	R.s.d. (%)	Conc.[a] ($\mu g\ l^{-1}$)
Al	2.01	6	90.4 (93.9)
Ti	—[b]		2.44[c] (2.48)
V	—[b]		1.31[c] (3.32)
Mn	3.55	5	5.64 (5.73)
Fe	4.63	5	69.8 (67.1)
Co	0.12	14	0.36 (0.15)
Ni	1.08	5	0.73 (0.45)
Cu	0.36	5	1.01 (1.08)
Zn	1.76	3	5.29 (4.79)
Y	0.05	16	0.10 (—[d])
Mo	—[b]		9.11[c] (9.32)
Cd	0.05	1	0.06 (0.04)
Pb	0.64	14	5.18 (5.03)

[a]The values in parentheses were obtained by the column method reported previously [4]. [b]Not determined because of the poor recovery at pH 6. [c]Preconcentration at pH 3. [d]Not determined.

standard deviations for the results were less than 6% except for Co, Y, and Pb. The poor precisions for these three elements is probably due to their low concentrations (less than 10 times analytical detection limits).

The results for sea water samples from Hiroshima Bay in Japan Inland Sea obtained by the batch method were compared to those obtained by the column method. The concentrations of the analytes except for Co, Ni and Zn obtained by the two methods were in good agreement.

Conclusions

Chelex-100 resin, which gave excellent results for the preconcentration of trace elements from sea water by the column method, is also satisfactory for preconcentration by a batch method. Compared with the column method, the volume of ammonium acetate buffer required for resin washing, and the amount of acid required for retrieval were significantly decreased in the batch method, allowing more convenient experimentation and less contamination. Furthermore, a larger preconcentration factor can be achieved. Thus the concentrations of Al, Ti, V, Mn, Fe, Co, Ni, Cu, Zn, Y, Mo, Cd and Pb at levels lower than $\mu g\ l^{-1}$ in sea water could be determined with good precision. The present method should be applicable in the routine analysis of sea water, including open sea water.

REFERENCES

1 C. W. McLeod, A. Otsuki, K. Okamoto, H. Haraguchi and K. Fuwa, Analyst, 106 (1981) 419.
2 T. Akagi, K. Fuwa and H. Haraguchi, Anal. Chim. Acta, 177 (1985) 139.
3 T. Akagi, M. Matsui, Y. Nojiri and H. Haraguchi, Appl. Spectrosc., 39 (1985) 662.
4 J. C. Chu, T. Akagi and H. Haraguchi, Bull. Chem. Soc. Jpn., 58 (1985) 3229.
5 R. E. Sturgeon, S. S. Berman, J. A. H. Desaulniers, A. P. Mytytiuk, J. W. McLaren and D. S. Russell, Anal. Chem., 52 (1980) 1585.
6 K. Kawabuchi, M. Kanke, T. Muraoka and M. Yamauchi, Bunseki Kagaku, 25 (1976) 213.
7 E. W. Davey and A. E. Soper, in T. R. P. Gibbs, Jr. (Ed.), Analytical Methods in Oceanography, Adv. Chem. Ser., Am. Chem. Soc., Washington, DC, 1975, p. 147.
8 T. M. Florence and G. E. Batley, Talanta, 24 (1977) 151.
9 A. Isozaki, N. Soeda and S. Utsumi, Bull. Chem. Soc. Jpn., 54 (1981) 1364.
10 D. R. Kester, I. W. Duedall, D. N. Connors and R. M. Pytkowicz, Limnol. Oceanogr., 12 (1967) 176.

Analytica Chimica Acta, 198 (1987) 183—189
Elsevier Science Publishers B.V., Amsterdam — Printed in The Netherlands

DETERMINATION OF THE MAJOR Δ^9-TETRAHYDROCANNABINOL METABOLITE IN URINE BY HIGH-PERFORMANCE LIQUID CHROMATOGRAPHY AND PHOTODIODE ARRAY DETECTION

D. BOURQUIN and R. BRENNEISEN*
Institute of Pharmacy, University of Berne, Baltzerstr. 5, CH-3012 Berne (Switzerland)
(Received 11th December 1986)

SUMMARY

A procedure for quantifying urinary 11-nor-Δ^9-tetrahydrocannabinol-9-carboxylic acid (THC-COOH), the primary metabolite of Δ^9-tetrahydrocannabinol, is presented. Urine samples with cannabinol as internal standard undergo alkaline hydrolysis, followed by a clean-up on short bonded-phase extraction columns. The extracts are separated by high-performance liquid chromatography on a C_8 reversed-phase column with acetonitrile/aqueous phosphoric acid as mobile phase. Detection is done with an on-line high-speed spectrophotometer (photodiode array detector). The improvement of peak identification and the validation of peak identity is demonstrated by u.v. spectra scanned from 200 to 350 nm, three-dimensional spectrochromatograms and contour plots. A linear relationship is observed between the peak height ratio of THC-COOH vs. internal standard and the concentration of THC-COOH (r = 0.9995). The sensitivity is as good as that of a single-channel u.v. detector. The detection limit is 10 ng ml^{-1} THC-COOH. The method was used to confirm THC-COOH in 100 urine specimens, which were cannabinoid-positive in an immunoassay drug screening. All specimens were confirmed as positive, with 30—280 ng ml^{-1} THC-COOH.

Δ^9-Tetrahydrocannabinol (THC) is the main psychomimetic constituent of *Cannabis sativa*, the most abused psychotropic drug of the world. To detect THC metabolites, e.g., the major metabolite 11-nor-Δ^9-tetrahydrocannabinol-9-carboxylic acid (THC-COOH) [1—3], in biological matrices after smoking or oral ingestion of cannabis products, immunoassays are used as rapid screening tests. The commonest methods in the field of socio-medical and forensic urine drug control are enzyme-multiplied immunoassay techniques (EMIT) [4—7] and radioimmunoassays (r.i.a.) [5, 8, 9]. As these tests are not specific, positive results should be validated by a reliable alternative method with comparable sensitivity but different analytical principle. Many confirmatory techniques have been developed, including thin-layer chromatography (t.l.c.) [5, 6, 10—13], gas chromatography (g.c.) [14—16], gas chromatography/mass spectrometry (g.c./m.s.) [5, 7, 16—21] and high-performance liquid chromatography (h.p.l.c.) [16, 22—24].

In a previous communication [25], the authors reported a sensitive procedure which enables THC-COOH to be quantified down to the low ng ml^{-1}

0003-2670/87/$03.50

level with h.p.l.c. and electrochemical detection. In this paper a method is described for quantifying urinary THC-COOH by using a simple bonded-phase adsorption clean-up, h.p.l.c. and computer-aided high-speed spectrophotometry (photodiode array detection). This type of detector has already been applied in analyses for psychotropic drugs [26, 27], and it was the aim of this work to check the efficiency of photodiode array detection in the field of analytical toxicology.

EXPERIMENTAL

Apparatus and chemicals

The h.p.l.c. system consisted of an Altex 420 controller/programmer, two Altex 110A pumps, a pulse-dampener, a Rheodyne 71-25 injection valve with 20-μl loop, a Hewlett-Packard 1040A high-speed spectrophotometric detector system (photodiode array detector) and a 3390A integrator. An Uvikon LCD-725 digital spectrophotometer (Kontron) and a Shimadzu Chromatopac C-R1A integrator were used to compare the sensitivity of the photodiode array detector and a conventional single-channel u.v. detector. Separation was done at room temperature on a 250 × 4.6 mm i.d. column, packed with Spherisorb 5-μm octyl (C_8) (Phase Separations) by using a slurry technique [28]. The mobile phase was 68.5% (v/v) acetonitrile/31.5% aqueous 50 mM phosphoric acid at a flow rate of 1.5 ml min^{-1}. The eluent was degassed for 10 min in an ultrasonic bath under reduced pressure and during use with a constant flow of helium.

All chemicals were of analytical or h.p.l.c. grade, purchased from Fluka and Merck; Bond Elut-THC columns (500 mg, bonded-phase silica gel) were from Analytichem International (Harbor City, CA). 11-Nor-Δ^9-tetrahydrocannabinol-9-carboxylic acid (THC-COOH) was provided by Research Triangle Institute, NC, and cannabinol by Supelco.

Urine screening

Most of the authentic urine specimens were obtained from pharmacies and health and rehabilitation centers which participated in a socio-medical program against drug abuse. The urines were screened for the presence of cannabinoids by the EMIT-st cannabinoid urine assay (Syva Co., Palo Alto, CA). The cutoff calibrator of this test contains 100 ng ml^{-1} 11-nor-Δ^8-THC-9-carboxylic acid (Δ^8-THC-COOH). Samples which gave an ultraviolet response equal to or higher than the calibrator response were interpreted as positive and confirmed by the h.p.l.c./photodiode array method.

Extraction and clean-up procedure

To 10 ml of urine (blank, spiked or EMIT-st positive), 30 μl of a methanolic 90 μg ml^{-1} solution of cannabinol (internal standard) and 2 ml of 10 M potassium hydroxide were added. After hydrolyzing on a magnetic stirrer at 50°C for 20 min, the urine was then adjusted to pH 5—6 with concentrated

hydrochloric acid. The sample clean-up was done on a Bond Elut-THC column according to the manufacturer's directions but with the following modifications: before eluting with two 750-μl aliquots of acetonitrile, the column was dried under vacuum for 5 min. The first aliquot was allowed to percolate through the column without vacuum; the second was aspirated slowly under vacuum. The combined eluates were concentrated to about 500 μl under a stream of nitrogen and 10—15 μl was injected into the h.p.l.c. Quantitation was done by measuring the peak heights of THC-COOH and cannabinol at 211 nm (attenuation: 0.02 absorbance).

RESULTS AND DISCUSSION

In human urine, most of THC-COOH is excreted as ester-linked glucuronide [1, 23, 29, 30]. Therefore an alkaline hydrolysis step has to be done before the clean-up procedure to obtain the total amount of free, unconjugated THC-COOH. The standardized urine clean-up can be done efficiently and rapidly by using short solid-phase extraction columns. As demonstrated in Fig. 1 for the chromatogram of a blank urine extract, most of potentially interfering endogenous background can be eliminated. The broad peak eluting between 14 and 16 min is an obligate endogenous compound observed in every urine specimen. The THC-COOH and the internal standard cannabinol have the same recovery, 90% in each case (cf. Table 1), despite the structural difference of one carboxyl group. Cannabinol is a naturally occurring degradation product of THC, formed under influence of air, light and heat (smoking). It is a typical cannabinoid of old, stored cannabis products [28]. However, it is mainly excreted in the feces, only 8% being found in the urine, almost entirely as acidic metabolites [31]. With the proposed method, no unchanged cannabinol could be detected in EMIT-st positive urines, which were used without adding internal standard to evaluate the chromatographic system. The urine extracts are stable over several months when stored at −20°C. As described previously [25], the same extracts can also be used with or without a further concentration step for alternative confirmation methods, such as g.c./m.s. and t.l.c.

The chromatographic system used in the method with electrochemical detection [25], C_{18} reversed-phase material and methanol/aqueous acetic acid, was not suitable for use with the photodiode array detector because endogenous, very late eluting (>30 min) compounds were not detected electrochemically but were u.v.-positive, and because the absorption of the mobile phase was very high at 211 nm. With C_8 material and acetonitrile/aqueous phosphoric acid as mobile phase, the run-time was shortened to 15—16 min with sufficient separation of THC-COOH, internal standard and endogenous substances, as well as good peak shape and symmetry (Figs. 1—3). The chromatographic system showed excellent stability with little drift in retention times over the course of a working day (±0.1 min).

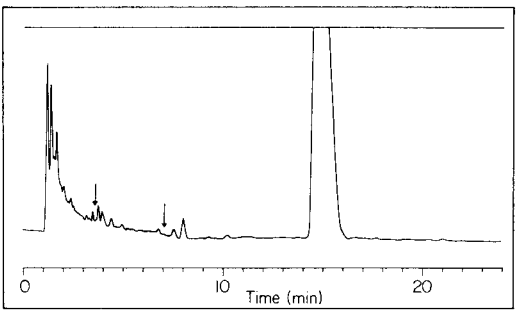

Fig. 1. Chromatogram of a cleaned-up blank urine at 211 nm. Chromatographic conditions as described under Experimental.

TABLE 1

Linearity, recovery, precision and detection limit of the described method for THC-COOH

Linearity (n = 7)		*Precision ($\bar{x}$, r.s.d.; n = 5)*	
slope	107.46 ± 1.01	30 ng ml^{-1} spiked sample	28.7 ng ml^{-1}, 3.5%
intercept	−5.99 ± 1.34	100 ng ml^{-1} spiked sample	100.2 ng ml^{-1}, 2.8%
correlation coefficient	0.9995		
Recovery (n = 5)	90 ± 5%	*Detection limit*	
		relative	10 ng ml^{-1}
		absolute[a]	5 ng

[a]Cleaned-up sample concentrated to about 200 µl, 15 µl injected.

The recognition of metabolites can be very difficult if they are present in low concentrations and in variable complex matrix. The application of a computer-aided high-speed spectrophotometer (photodiode array detector) represents a significant improvement for peak assignation and identification. Figure 2 shows the chromatogram and on-line u.v. spectra of a cleaned-up spiked urine sample. As demonstrated by Fig. 3, THC-COOH (peak 1) can be identified in an EMIT-st positive urine from the retention time and the characteristic u.v. spectrum over the range of 200—350 nm by comparison with the data for the THC-COOH standard shown in Fig. 2. The identical nature of the THC-COOH and internal standard peaks was further demonstrated by the coincident up-slope, apex (maximum) and down-slope spectra. The three-dimensional data plot shown in Fig. 3 (spectrochromatogram) represents the spectra of THC-COOH and cannabinol on the z-(wavelength, λ) and y-(absorbance, A) axis and the elution profile within 5-min segment (time, t) of the chromatogram. With the selected projection angle of 30°, the small peak adjacent to the intense peak of THC-COOH is entirely obscured whereas in the corresponding (λ, t) contour map it is visualized by skewed isoabsorptive contour lines in the wavelength domain of THC-COOH (Fig. 4). The time intervals for the spectrochromatogram in Fig. 3 and the contour map in Fig. 4 are the same (3.0—7.2 min).

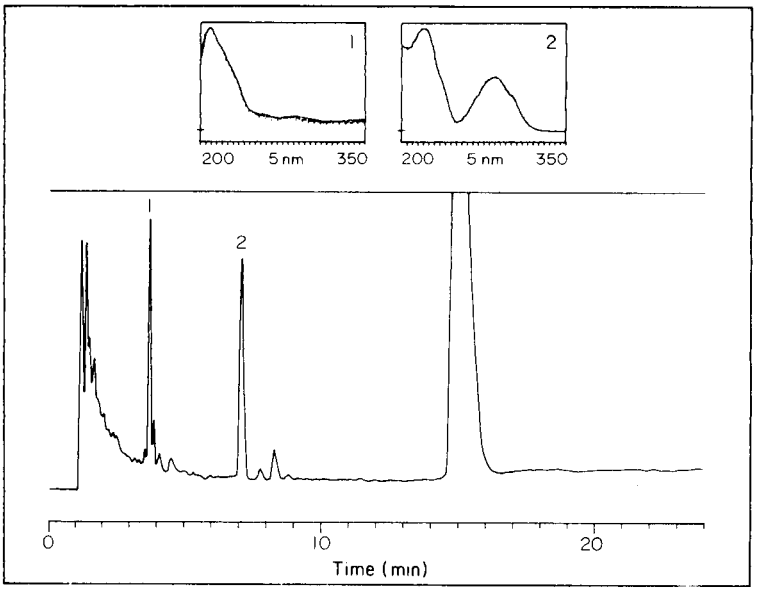

Fig. 2. Chromatogram and on-line u.v. spectra of a cleaned-up urine spiked with 100 ng ml^{-1} THC-COOH and 270 ng ml^{-1} cannabinol. Peaks: (1) THC-COOH; (2) cannabinol.

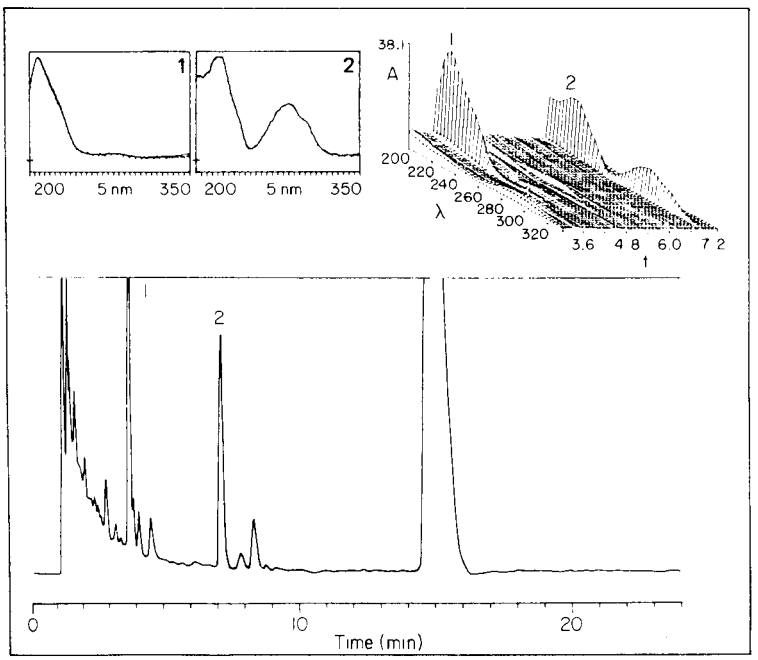

Fig. 3. Chromatogram, on-line u.v. spectra and three-dimensional spectrochromatogram of a cleaned-up EMIT-st positive urine (156 ng ml^{-1}). Peaks as in Fig. 2.

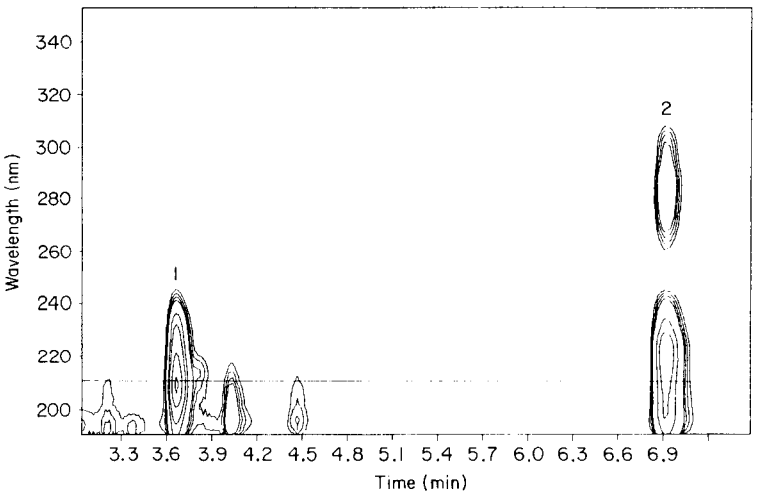

Fig. 4. Isoabsorption contour map of a 5-min segment of the chromatogram shown in Fig. 3. Contour intervals: 0.006, 0.007, 0.008, 0.009, 0.015, 0.02, 0.03, 0.04 absorbance. Peaks as in Fig. 2. The horizontal line marks the detection wavelength (211 nm).

The optimum wavelength of detection for sensitive THC-COOH quantitation was 211 nm, measured by the photodiode array detector. The internal standard cannabinol has two absorption maxima at 221 and 285 nm. The sensitivity obtained by using the photodiode array detector was directly compared with that of a conventional single-channel h.p.l.c. detector by placing the detectors in series. At a signal-to-noise ratio of 5:1, both detection systems showed about the same detection limit (Table 1), provided that the cleaned-up urine sample was further concentrated to 200—250 μl. With electrochemical detection [25], the minimal detectable amount of THC-COOH was 5 ng ml^{-1}.

The calibration graph was obtained by using a blank pooled urine spiked with 30—250 ng ml^{-1} THC-COOH and 270 ng ml^{-1} internal standard. The samples were analyzed by the procedure described under Experimental. A linear relationship was found between the peak-height ratio of THC-COOH vs. internal standard and the concentration of THC-COOH (Table 1). The precision of the method in the high and low THC-COOH concentration range was measured by analyzing five replicates of two blank urine samples spiked with 100 and 30 ng ml^{-1} (Table 1).

With the h.p.l.c./photodiode array detector method all of 100 EMIT-st positive urine specimens could be confirmed as THC-COOH positive. The chromatogram of an EMIT-st positive urine is shown in Fig. 3. The THC-COOH content varied between 30 and 280 ng ml^{-1} of urine; THC-COOH contents far below the cut-off calibrator concentration of 100 ng ml^{-1} Δ^8-THC-COOH can be explained by the fact that an EMIT immunoassay may cross-react with other polar metabolites, e.g., polycarboxylic acids or hydroxylated

carboxylic acids [32, 33], and/or urine compounds unrelated to cannabinoids [14].

REFERENCES

1 M. E. Wall and M. Perez-Reyes, J. Clin. Pharmacol., 21 (1981) 178s.
2 R. L. Hawks, in R. L. Hawks (Ed.), The Analysis of Cannabinoids in Biological Fluids, NIDA Research Monograph No. 42, U.S. Department of Health and Human Services, Washington, DC, 1982, p. 125.
3 M. M. Halldin, S. Carlsson, S. L. Kanter, M. Widman and S. Agurell, Arzneim.-Forsch., 32 (1982) 764.
4 B. Riesselmann, Dtsch. Apoth. Ztg., 121 (1981) 2078.
5 D. L. Frederick, J. Green and M. W. Fowler, J. Anal. Toxicol., 9 (1985) 116.
6 C. A. Sutheimer, R. Yarborough, B. R. Hepler and I. Sunshine, J. Anal. Toxicol., 9 (1985) 156.
7 L. J. McBurney, B. A. Bobbie and L. A. Sepp, J. Anal. Toxicol., 10 (1986) 56.
8 B. Law, P. A. Mason, A. C. Moffat and L. J. King, J. Anal. Toxicol., 8 (1984) 14.
9 C. E. Cook, H. H. Seltzman, V. H. Schindler, C. R. Tallent, K. M. Chin and C. G. Pitt, in R. L. Hawks (Ed.), The Analysis of Cannabinoids in Biological Fluids, NIDA Research Monograph No. 42, U.S. Department of Health and Human Services, Washington, DC, 1982, p. 19.
10 S. L. Kanter, L. E. Hollister and M. Musumeci, J. Chromatogr., 234 (1982) 201.
11 S. L. Kanter, L. E. Hollister and J. U. Zamora, J. Chromatogr., 235 (1982) 507.
12 K. K. Kaistha and R. Tadrus, J. Chromatogr., 237 (1982) 528.
13 J. A. Vinson and D. J. Lopatofsky, J. Anal. Toxicol., 9 (1985) 6.
14 J. D. Whiting and W. W. Manders, J. Anal. Toxicol., 6 (1982) 49.
15 M. A. ElSohly, E. S. Arafat and A. B. Jones, J. Anal. Toxicol., 8 (1984) 7.
16 L. Karlsson and C. Roos, J. Chromatogr., 306 (1984) 183.
17 R. L. Foltz, P. A. Clarke, B. J. Hidy, D. C. K. Lin, A. P. Graffeo and B. A. Petersen, in J. A. Vinson (Ed.), Cannabinoid Analysis in Physiological Fluids, ACS Symposium Series No. 98, American Chemical Society, Washington, DC, 1979, p. 59.
18 L. Karlsson, J. Jonsson, K. Aberg and C. Roos, J. Anal. Toxicol., 7 (1983) 198.
19 M. Hanke and G. Megges, Z. Rechtsmed., 90 (1983) 105.
20 G. R. Nakamura, W. J. Stall, R. G. Masters and V. A. Folen, Anal. Chem., 57 (1985) 1492.
21 U. Lemm, J. Tenczer and H. Baudisch, J. Chromatogr., 342 (1985) 393.
22 M. A. ElSohly, H. N. ElSohly, A. B. Jones, P. A. Dimson and K. E. Wells, J. Anal. Toxicol., 7 (1983) 262.
23 B. Law, P. A. Mason, A. C. Moffat and L. J. King, J. Anal. Toxicol., 8 (1984) 19.
24 B. L. Posey and S. N. Kimble, J. Anal. Toxicol., 8 (1984) 234.
25 D. Bourquin and R. Brenneisen, J. Chromatogr., 414 (1987) 187.
26 R. Brenneisen and S. Geisshüsler, Pharm. Acta Helv., 60 (1985) 290.
27 R. Brenneisen and S. Borner, Pharm. Acta Helv., 60 (1985) 302.
28 R. Brenneisen, Pharm. Acta Helv., 59 (1984) 247.
29 R. L. Foltz, K. M. McGinnis and D. M. Chinn, Biomed. Mass Spectrom., 10 (1983) 316.
30 P. L. Williams and A. C. Moffat, J. Pharm. Pharmacol., 32 (1980) 445.
31 M. E. Wall, D. R. Brine and M. Perez-Reyes, in M. C. Braude and S. Szara (Eds.), The Pharmacology of Marihuana, Raven Press, New York, 1976, p. 93.
32 M. M. Halldin, L. K. R. Andersson, M. Widman and L. E. Hollister, Arzneim.-Forsch., 32 (1982) 1135.
33 M. M. Halldin, M. Widman, C. V. Bahr, J.-E. Lindgren and B. R. Martin, Drug Metab. Dispos., 10 (1982) 297.

Analytica Chimica Acta, 198 (1987) 191—196
Elsevier Science Publishers B.V., Amsterdam — Printed in The Netherlands

COMPARISON OF LIGANDS FOR THE RECOVERY OF TRACE ALUMINIUM(III) BY ANION-EXCHANGE

CORRADO SARZANINI*, MARIA CARLA GENNARO, VALERIO PORTA and EDOARDO MENTASTI

Department of Analytical Chemistry, University of Turin, Via P. Giuria 5, 10125 Turin (Italy)

(Received 11th June 1986)

SUMMARY

The preconcentration of aluminium(III) traces in the form of anionic complexes on an anion-exchanger is described. The ligands used to form anionic complexes are hydroxide, sulphosalicylic acid, chromotropic acid and 2-(4-sulphophenyl)-1,8-dihydroxynaphthalene-3,6-disulphonic acid. Recoveries were evaluated under different conditions and in the presence of potential interferences (surfactants, inorganic salts, organic anions). The experimental behaviour is compared with that which can be predicted from the computed distribution of the different species. The results show that chromotropic acid is superior for the recovery and preconcentration of Al(III).

The suitability of sulphonated chelating agents coupled with anion-exchangers for the separation and preconcentration of metal ions has been discussed in several papers [1—8]. The method is based on interaction of sulphonic groups not involved in metal chelation with the active sites of the resin and may be applied via two different techniques: (i) selected ligands are added to the solution of the metal adjusted to the proper pH, and then the complex is eluted through the column containing the exchanger; or (ii) the metal solution is eluted through the resin which is preloaded with chelating agent. In a previous paper [9] these techniques were compared for the pyrocatechol violet complex and here the behaviour of different ligands with the same anion-exchange resin and Al(III) are considered. A series of ligands, namely the hydroxide ion, 3-carboxy-4-hydroxybenzene-sulphonic acid (5-sulphosalicylic acid, SSA), 1,8-dihydroxynaphthalene-3,6-sulphonic acid (chromotropic acid, CTA) and 2-(4-sulphophenyl)-1,8-dihydroxynaphthalene-3,6-disulphonic acid (SPADNS), was tested for Al(III) by using the first technique, which was earlier shown to be the more satisfactory [9]. The results of recovery of each complex were compared with those predicted by a theoretical model of species distribution obtained with a computer program [10].

0003-2670/87/$03.50

EXPERIMENTAL

Reagents

Chromotropic, sulphosalicylic and salicylic acids (Merck) and SPADNS (Fluka) were all certified ACS reagents. A 0.05 M stock solution was prepared from each compound. Metal ion solutions were prepared by diluting an Al(III) stock solution (1000 mg l^{-1}, Merck). The anion-exchange resin used was Bio-Rad AG-MP-1 macroporous resin (100—200 mesh, chloride-form). The resin was converted to the OH^- form with 1 M sodium hydroxide for the aluminate method (see below). High-purity water obtained from a Millipore Milli-Q water system was used throughout. All other reagents were of analytical grade.

Equipment and techniques

Aluminium concentrations were evaluated by d.c. argon plasma atomic emission spectrometry (Spectraspan IV, SMI, Andover, MA) at 369.15 nm, where the detection limit of Al(III) is 5—10 ng ml^{-1}. Calibration was done with reference to standards reproducing the sample solution matrix.

Thermostatted (water-jacketed) borosilicate glass columns (8 mm i.d., 30 cm high) were used. The columns were packed by adding a slurry of the resin in water until the height of the resin bed was 3—5 cm (1.0 g of wet resin). A rotary vacuum pump with a by-pass flowmeter ensured a constant flow of solutions within the range 5—10 ml min^{-1}.

Glassware, polyethylene and polypropylene laboratory materials were cleaned and washed as in earlier procedures [11].

The stock solution (0.5 ml, 25 μmol) of SSA or CTA, or 4.0 ml (200 μmol) of SPADNS was added to aqueous solutions (100.0—1000.0 ml) containing 1.00—0.01 ng ml^{-1} aluminium(III). These solutions were passed through the resin adjusted to the same pH. The column was then washed and the metal was recovered by elution with hydrochloric acid into a 10.0-ml volumetric flask. The optimum acidity for total elution of the metal was established for each ligand, as shown in Table 1. A slightly modified version of the technique was used when the ligand considered was hydroxide; the resin was first converted by 1.0 M sodium hydroxide to the hydroxylated form and preconditioned with water for subsequent experiments.

RESULTS AND DISCUSSION

The species distribution in aqueous solutions of aluminium(III) containing the investigated ligands was computed with the aid of an iterative program, at different pH values, by using published stability constants corrected for ionic strength [12—14]. The results were compared with the experimental recoveries obtained for anionic species on a macroporous anion-exchange resin. The experiments done without organic ligands were intended to identify the effectiveness of hydroxide on the one hand, and on the other

TABLE 1

Optimal acidity for elution of Al(III) for each ligand

Ligand	HCl (M)	Al(III) recovery (%)	Ligand	HCl (M)	Al(III) recovery (%)
CTA	0.15	94.8 ± 2.1	SPADNS	0.5	62.9 ± 4.1
	0.17	98.1 ± 3.6		1.0	97.8 ± 1.9
	0.20	97.7 ± 2.5		1.5	99.2 ± 1.6
	0.22	100.0 ± 1.5		2.0	99.9 ± 0.6
SSA	1.0	95.0 ± 1.6	OH	1.0	98.5 ± 1.6
	3.0	99.1 ± 1.0			

hand, the effect of inorganic species such as $Al(OH)_4^-$ on the experiments performed at higher pH values in the presence of the organic ligands.

Figure 1 shows that the recovery of the metal closely follows the species distribution as a function of OH^- and that $Al(OH)_4^-$ furnishes a good recovery. To avoid any doubt about possible retention of $Al(OH)_3$, which may affect the results, some experiments were done by filtering the samples on 0.45-μm filters at the appropriate pH before the elution. These experiments demonstrated that the recovery is not due to precipitate retention. To optimise the recovery obtained with the hydroxide ligand and taking into account the different affinity of the resin for Cl^- and OH^-, the resin was converted to the OH^- form by passage of 100.0 ml of 1 M sodium hydroxide. Under these conditions, a recovery of 98% was obtained (see Fig. 1).

The metal recovery (Figs. 2 and 3) shows an overall behaviour which parallels the values of the stability constants of each ligand with Al(III). However, the theoretical species distribution is not followed exactly for the Al(III) recovery; there are discrepancies for each ligand. For CTA, the experimental and calculated curves (see Fig. 2) coincide, following the Al-CTA species concentration up to a recovery of 80%, but then a constant value is shown until pH 9.0 is reached at which a total recovery of 100% is obtained. This behaviour is similar for all the organic ligands, but for SSA and SPADNS between pH 8 and 9, a contribution of $Al(OH)_4^-$ must be considered in order to justify the higher experimental recovery obtained. This was confirmed by the preconcentration experiments (see below).

The experimental recovery obtained in the case of Al(SSA) (M:L, 1:1) is lower than expected from the theoretical computation (see Fig. 3A). This may be explained by taking into account the nature of the molecule involved, in which the global charge is zero. Thus ionic retention is probably also due to an adsorption phenomenon. The greatest discrepancy between the amount of anion species that can be bound on the resin and the experimental recovery is shown by Al-SPADNS complexes (Fig. 3B). In fact, at pH higher than 4.0, the metal recovery is 90% while the computations predict about zero.

As described in earlier papers [1, 15], retention greater than expected

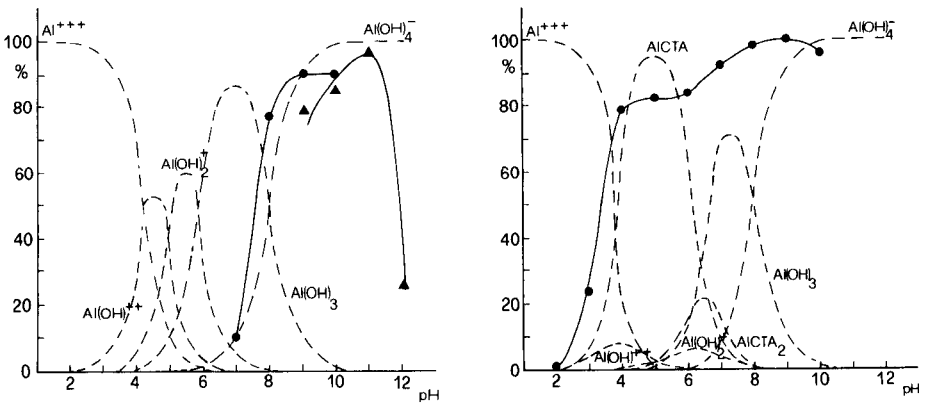

Fig. 1. Distribution of Al-OH species (---) and experimental percentage recovery of Al(III) (——) as a function of pH: (●) exchanger in Cl^--form; (▲) exchanger in OH^--form.

Fig. 2. Distribution of aluminium/chromotropic acid (CTA) complexes (---) and experimental percentage recovery of Al(III) (——).

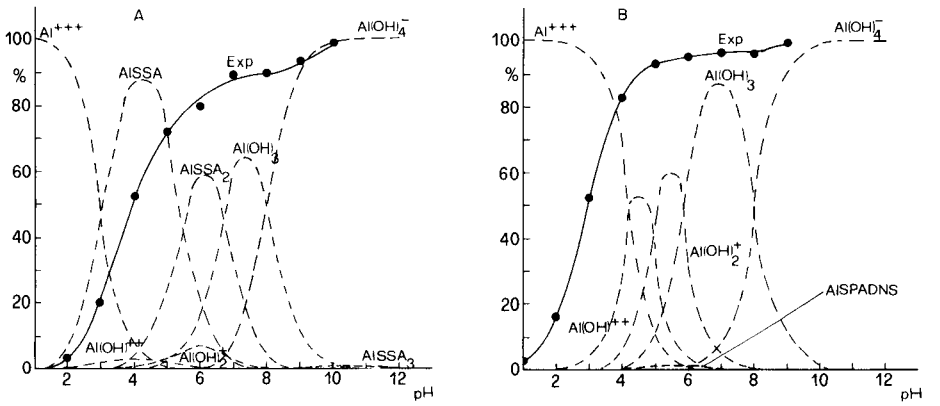

Fig. 3. Distribution of aluminium/ligand complexes (---) and experimental percentage recovery (——). Ligand: (A) sulphosalicylic acid (SSA); (B) SPADNS.

is common for aromatic ligands which show a π-electron interaction with the matrix of the resin [16].

Table 2 shows the yields for the investigated systems in the presence of surfactants and organic and inorganic competing ligands. These experiments were done to evaluate the suitability of the methods for natural systems. Similar behaviour was found for CTA and SPADNS (see Table 2) which are characterized by the same chelating groups and show similar stability constants. However, the experiments at high ionic strength (0.5 M NaCl) are surprising if one takes into account the computed species distribution. In fact, at 0.1 M sodium chloride with SPADNS the recovery is 99%, whereas

TABLE 2

Effect of interfering agents on percentage Al(III) recovery
(Conditions: 1.0 mg l^{-1} metal; volume 100.0 ml; pH 9 for SSA and CTA, pH 6.5 for SPADNS)

Interferent	Amount added (mg l^{-1})	Al(III) recovery (%)			
		CTA	SSA	SPADNS	OH
Sodium dodecyl sulphate	5.0	92.6 ± 2.8	94.3 ± 0.6	88.9 ± 0.8	99.4 ± 1.6
	50.0	72.1 ± 2.2	94.7 ± 2.2	94.0 ± 1.4	97.0 ± 1.3
Poly(ethyleneglycol)[a]	5.0	88.6 ± 1.1	96.6 ± 2.2	87.8 ± 0.3	100.4 ± 0.5
	50.0	85.9 ± 0.5	96.3 ± 0.6	89.1 ± 0.3	98.2 ± 1.8
Cetyltrimethyl ammonium bromide	5.0	81.0 ± 1.5	98.2 ± 0.6	90.4 ± 0.1	99.4 ± 0.9
	20.0	*[b]	*[b]	88.0 ± 1.9	94.0 ± 3.0
Salicylic acid	3.5	95.3 ± 1.8	97.4 ± 0.3	92.1 ± 1.5	—
	17.3	102.7 ± 1.2	92.9 ± 0.9	87.7 ± 0.1	—
	276.2	92.6 ± 1.4	85.3 ± 1.5	98.5 ± 0.4	—
K_2HPO_4	100.0	101.0 ± 1.0	99.1 ± 1.0	84.4 ± 1.4	—
	200.0	99.6 ± 1.2	98.7 ± 0.7	78.8 ± 1.1	—
	500.0	102.0 ± 2.0	99.8 ± 1.1	90.8 ± 1.4	—
NaCl	0.1 M	28.9 ± 6.5	24.2 ± 3.9	99.1 ± 0.8	4.8 ± 0.7
	0.5 M	11.8 ± 0.6	6.7 ± 0.7	93.8 ± 0.1	0.9 ± 0.2

[a]Molecular weight 6000. [b]*, under these conditions, separation of insoluble products occurs.

for CTA it is only 24%. The same discrepancy can be observed for the recovery obtained by using sulphosalicylic acid.

The results obtained in preconcentration experiments are shown in Table 3. These experiments were done, except for SPADNS, with the ligand concentration at the same value as that in previous evaluations so that the resulting ligand/metal ratio increased. In the case of SPADNS, the quantity was limited to 5.0 ml of stock solution to avoid saturation of the resin. The decreased values of Al(III) recovery obtained for SSA and CTA, (76.3 and 91.6%, respectively) can be explained if one considers that the same experiments done with hydroxide furnished a recovery of only 5.0%. The decreased

TABLE 3

Percentage recovery of Al(III) by preconcentration
(Conditions: 10.0 μg l^{-1} Al; volume 1000 ml; pH 9 for SSA and CTA, pH 6.5 for SPADNS)

Ligand	Al(III) recovery[a] (%)	Ligand	Al(III) recovery[a] (%)
CTA	91.6 ± 2.2	SPADNS	53.5 ± 1.5
SSA	76.3 ± 2.6	OH	5.3 ± 1.2

[a]Mean and average error of 3 experiments.

aluminium recovery can thus be attributed to $Al(OH)_4^-$ for all the ligands used.

It can be concluded that, among the ligands considered, CTA is the most suitable for preconcentration of Al(III). In addition, the preconcentration procedure used here (i.e., addition of the ligand to the sample before elution) is the simplest procedure, because it does not involve lengthy resin-loading steps. The excess of ligand used is completely retained by the resin, so that, after the described procedure, the aqueous effluent is not only free of aluminium but also does not contain the added ligand.

After each experiment, the resin can be cleaned and reactivated in a rather lengthy procedure. However, the amount of resin used for each experiment (1 g, wet weight) is small so that the cost is minimal even if no recovery is attempted.

The preconcentration factor obtained is around 10—100-fold, which provides more accurate determinations of the metal in the recovered solution. Under these conditions, quantitative recoveries were obtained with a ligand which shows a $\log \beta_1 > 15$ (i.e., chromotropic acid) and the procedure has the advantage that any relevant matrix effect from the sample is removed; the results obtained for samples containing surfactants and other salts such as phosphate or chloride illustrate this point.

REFERENCES

1 J. E. Going, G. Wesemberg and G. Andrejat, Anal. Chim. Acta, 81 (1976) 349.
2 D. G. Berge and J. E. Going, Anal. Chim. Acta, 123 (1981) 19.
3 K. Brajter and E. Olbrych-Sleszynska, Talanta, 30 (1983) 355.
4 M. Nakayama, M. Chikuma and H. Tanaka, Talanta, 29 (1982) 503.
5 K. S. Lee, W. Lee and D. W. Lee, Anal. Chem., 50 (1978) 255.
6 M. Otha and K. Ohzeki, Bull. Chem. Soc. Jpn., 57 (1984) 3571.
7 C. Sarzanini, E. Mentasti, M. C. Gennaro and C. Baiocchi, Ann. Chim. (Rome), 73 (1983) 385.
8 C. Sarzanini, E. Mentasti, M. C. Gennaro and E. Marengo, Anal. Chem., 57 (1985) 1960.
9 C. Sarzanini, E. Mentasti, V. Porta and M. C. Gennaro, Anal. Chem., 59 (1987) 484.
10 S. Sammartano, personal communication, Analytical Chemistry Institute, University of Messina, Messina, Italy.
11 D. P. H. Laxen and R. H. Harrison, Anal. Chem., 53 (1981) 345.
12 A. E. Martell and R. H. Smith, Critical Stability Constants, Vol. 3, Plenum, New York, 1975.
13 D. D. Perrin, Stability Constants of Metal-Ion Complexes, Part B, Organic Ligands, Pergamon, New York, 1979.
14 S. P. Mushran, Om Prakash, U. C. Srivastava and S R. Kusshwara, Analusis, 8 (1975) 571.
15 K. Brajter and E. Dabek-Zlotorzynska, Talanta, 33 (1986) 149.
16 D. M. Ordemann and H. F. Walton, Anal. Chem., 48 (1976) 1728.

Analytica Chimica Acta, 198 (1987) 197—206
Elsevier Science Publishers B.V., Amsterdam — Printed in The Netherlands

DECREASED ASCORBATE SENSITIVITY WITH NAFION-COATED CARBON FIBRE ELECTRODES IN COMBINATION WITH COPPER(II) IONS FOR THE ELECTROCHEMICAL DETERMINATION OF ELECTROACTIVE SUBSTANCES IN VIVO

PETER HULTHE*, BARBRO HULTHE[a], KENN JOHANNESSEN and JÖRGEN ENGEL

Department of Pharmacology, P.O. Box 33031, Gothenburg University, S-400 33 Gothenburg (Sweden)

(Received 19th November 1986)

SUMMARY

A Nafion coating is applied on voltammetric carbon fibre electrodes. This treatment lowered the sensitivity to ascorbate and 3,4-dihydroxyphenylacetic acid (DOPAC), and increased that for dopamine. Electrochemical oxidation with a 70-Hz, 3-V, anodic triangular-wave voltage was used for pretreatment before the Nafion coating. The inclusion of copper ions in the Nafion film further decreased the sensitivity to ascorbic acid, but did not significantly affect the sensitivity to dopamine or DOPAC. In-vitro equilibration with a buffer of appropriate copper concentration is recommended for pretreatment of carbon fibre electrodes before their use in in-vivo voltammetry.

In the electrochemical determination of neurotransmitters and their metabolites in vivo, it is always necessary to take the endogenous ascorbate level into account. In the extracellular space of the rat brain, values of ascorbic acid above 200 μM have been reported [1]. A corresponding figure for dopamine, for example, is 20 nM [2]. As the potential for the first ascorbic acid oxidation step is below that of dopamine and its major metabolite 3,4-dihydroxyphenylacetic acid (DOPAC), a contribution from the ascorbic acid oxidation current will increase the background current when these compounds are determined. Uncertainty will therefore arise in the determination of the absolute values of the species studied. In the case of fluctuations in the ascorbic acid level, severe analytical problems may result. This situation creates a demand for electrodes with a high immunity to ascorbic acid.

The advantage of using carbon fibres, compared to other materials such as graphite paste, as the electrode material for the in-vivo determinations of neurochemically interesting substances is well documented [3]. It has also been shown that an electrochemical pretreatment of the carbon fibre will

[a]Department of Analytical and Marine Chemistry, Gothenburg University, S-412 96 Gothenburg, Sweden.

0003-2670/87/$03.50

produce an increase in resolution between ascorbic acid and catechols [4]. In recent work, a Nafion coating on carbon paste electrodes has been shown to suppress markedly the current arising from oxidation of ascorbic acid. It is assumed that Nafion, which is a cation-exchanger material, will allow the passage of positively charged ions to the electrode surface, but hinder that of anionic and neutral species [5]. A difference in ion-exchange selectivity for different compounds is the probable explanation [6]. In a 200 μM ascorbic acid solution, buffered to pH 7.4, the sensitivity to ascorbic acid compared to dopamine is shown to be below 1/200 for the Nafion-coated graphite paste electrode, measured chronoamperometrically [5]. With thicker layers, the sensitivity to ascorbic acid is even lower. A limiting effect is the tendency of particularly thick layers to impair the responsiveness of the electrode [5].

It is well known that the oxidation of ascorbic acid is catalytically enhanced by the presence of copper(II) ions. Even very small amounts of copper(II) have a significant effect [7]. The copper(II)-catalyzed oxidation of ascorbic acid by oxygen involves two steps; ascorbic acid is first oxidized by copper(II) ions, and the copper(I) produced is then oxidized back to copper(II). It has been shown that oxygen rapidly oxidizes ascorbic acid if traces of copper(II) are present [8]. It has also been shown [9] that copper(II) ions rapidly attach to carbon paste electrodes containing a cation-exchanger resin.

In the present work, a further improvement of the electrochemically-treated carbon fibre electrode is presented. A coating with a thin layer of Nafion increased the sensitivity to dopamine, and decreased that to ascorbic acid and DOPAC, as was previously reported for carbon paste [5]. Nafion-treated carbon fibre electrodes were prepared, and the sensitivity to ascorbic acid, DOPAC and dopamine was tested before and after dipping in a copper(II) solution. The presence of copper ions in the Nafion film further lowered the sensitivity to ascorbate.

EXPERIMENTAL

Chemicals

Chemicals for the preparation of electrodes were: solid Nafion (35—60 mesh, Fluka), Nafion, 5% (w/w) in alcoholic solutions (Aldrich Chemical Company), dimethyl sulphoxide (DMSO), copper sulphate and copper(II) acetate. Other chemicals were ascorbic acid, dopamine hydrochloride and DOPAC (Sigma), 2,9-dimethyl-2,7-diphenyl-1,10-phenanthroline (bathocuproine; Merck), potassium dihydrogenphosphate, sodium hydroxide, and sodium chloride. Ascorbic acid and all the inorganic chemicals were of analytical-reagent grade.

All voltammetric experiments were done with a 0.1 M phosphate buffer solution. Sodium chloride was added to give a chloride concentration of 125 mM, which is equivalent to the extracellular chloride concentration

[10]. The pH was adjusted to 7.4 by adding sodium hydroxide. The copper concentration in the buffer solution was determined spectrophotometrically by extraction with bathocuproine to 0.05 μM.

Buffer solutions were deaerated prior to use by purging with purified nitrogen for 15 min. The surfaces of the solutions were then flushed with nitrogen and kept isolated from the surrounding air during voltammetry.

Electrodes

The working electrodes were fabricated from carbon fibres [11] of the type MODMOR II, 12 μm diameter, not surface treated (Morganite Modmor, London). The fibres were cut to 1-mm length and were electrochemically treated [4] with 70-Hz, triangular-wave, +3 V (vs. Ag/AgCl) in the phosphate buffer for 20 s, followed by 1.5 V d.c. for another 20 s. The electrodes were then rinsed in distilled water and dried for 10 min at 60°C.

The following Nafion treatment was done either with the commercially available alcoholic solution (5%), or with a laboratory-prepared saturated solution of granulated Nafion in DMSO. When the alcoholic solution was used, the electrode was horizontally inserted 5—10 times into a drop of solution, hanging from a pipette. After each insertion, the electrode was allowed to dry for at least 10 s. The final thickness of the Nafion layer depends on the dipping technique. The length of time that the hanging drop is exposed to solvent evaporation is often more critical than the number of insertions. The highest Nafion concentration will be on the surface of the hanging drop, where solid phase will also participate eventually.

The Nafion solution in DMSO was prepared by gently refluxing an excess of solid Nafion for 30 min in DMSO. This solution was more difficult to use than the alcoholic solution, because it had less wetting capacity for the carbon fibre. The best results were obtained when the solution was used near its boiling point. The fibre was inserted into a heated drop, hanging from a pipette under a microscope. After the fibre had been dried by gentle air-blowing for some minutes, the process was repeated. Between 10 and 20 insertions were usually required. As the results obtained with the two methods did not differ significantly, the alcoholic Nafion solution was used in all later work.

For the copper treatment, the electrode was immersed for 2 s in a drop of 0.79 mM copper(II) acetate solution, pH 6, and then rinsed in distilled water for 1 s.

The reference electrode was cut from Teflon-insulated fine silver wire (0.2 mm). A length of 5 mm was stripped, and the bare silver was then electrically oxidized in 1 M HCl to produce an even layer of silver chloride. A suitable time was 4—5 min. The auxiliary electrode was prepared from a bare 0.2-mm platinum wire.

Instrumentation

Linear-scan voltammetry was used. The scan rate was 100 mV s^{-1}. The

potential of the working electrode between the scans was maintained at the starting potential of the scan. The time lapse between scans (1 or 3 min) was kept constant.

The voltammetric instrument (Bio-Analytical Systems, Model DCV-5) was slightly modified for computer-controlled function. A Z-80 desk-top computer (Luxor ABC-806) was used as controller and a program for conducting linear scans was written. In order to increase the signal/noise ratio, a program part allowing a point-by-point subtraction of a previously recorded voltammogram was developed [12]. The highest available precision was 0.1 pA/digit, and the shortest sampling time 0.1 mS. In this work, the sensitivity was generally set to 25 pA/digit and the sampling time to 20 mS.

Procedures

Evaluation of a suitable resting potential. Electrochemically treated (EC), or electrochemically- and Nafion-treated (ECN) electrodes were prepared. Some of the ECN electrodes were also treated with copper(II) (ECNCu). In order to evaluate an appropriate resting potential, potentials between −100 and 0 mV were tested. A resting time of 1 min was chosen.

Equilibration time after the copper(II) treatment. Repetitive scanning was done in solutions of 200 μM ascorbate in the phosphate buffer with the EC and ECN electrodes. When steady signals were obtained (10 to 15 scans), the electrode was removed from the cell vessel and treated with copper(II). The electrode was then returned to the ascorbic acid solution, and scanning was continued until stable readings were observed. Series with 1 and 3 min between scans were run in deaerated and undeaerated solutions.

Calibration curves for dopamine, DOPAC and ascorbic acid and evaluation of sensitivity. Calibration curves were obtained in deaerated and undeaerated phosphate buffer solutions. EC, ECN and ECNCu carbon-fibre electrodes were used. Separate calibrations were obtained with dopamine, DOPAC and ascorbic acid by adding increasing amounts of the oxidizable substance to the buffer. The background-corrected currents were used to calculate the regression coefficients for each calibration.

Experiments with bathocuproine as a carrier material for copper ions on the electrode surface. In order to study the observed effect of copper ions with a carrier material other than Nafion, the copper(I) salt of a highly selective complexing agent for copper was used (bathocuproine). A 3-mm diameter disc-shaped glassy carbon electrode was used. A portion (100 μl) of a 1:1 acetone/dichloromethane solution of bathocuproine (0.1 mg ml^{-1}) was placed on the electrode surface by means of a pipette and was allowed to evaporate at room temperature. The electrode was then immersed in a solution of 0.1 mM copper sulphate, 0.1 mM ascorbic acid and 0.1 M sodium chloride. This preparation produces a thin layer of the $(bathocuproine)_2$/-copper(I) chloride complex on the electrode [13].

Determination of the sensitivity to ascorbic acid relative to dopamine and DOPAC. The method for evaluating the relative electrode sensitivities

mainly follows the work by Gerhardt et al. [5]. Scanning, 0—512 mV, was done in the deaerated buffer solution. After the current had stabilized (15—20 repetitive scans), DOPAC was added, to give a final concentration of 2 μM. After 3—5 scans had been recorded, and the oxidation curves coincided, ascorbic acid (AA) was added to the solution to a final concentration of 200 μM. Another 3—5 scans were recorded. Dopamine was then added to give a final concentration of 1 μM, and when stable signal conditions were established (after 15—20 scans), the electrode responses were calculated. The peak potential for dopamine was measured for each individual electrode. For DOPAC, the oxidation current peak is rather flat with the linear method; its maximum is around 250 mV. The i (buffer)-corrected i(DOPAC) at 250 mV was calculated (i, oxidation current). Then the i(DOPAC)-corrected i(AA) signal was evaluated at 250 mV, and at the dopamine (DA) peak potential (120—180 mV). Finally the i(AA)-corrected i(DA) signal was taken at the dopamine peak potential. The i(AA)/i(DA), with correction for difference in molarity, at the dopamine peak potential (the AA/DA response) was then calculated.

The AA/DOPAC response at 250 mV was evaluated by an analogous procedure.

RESULTS AND DISCUSSION

The treatment with Nafion gives rise to a pronounced decrease in oxidation current for ascorbic acid and DOPAC at the carbon fibre electrode (Table 1). The dopamine signal, however, increases markedly. This has also been shown with the carbon paste electrode [5, 14]. The electrochemical pretreatment before the Nafion coating gives a good initial increase in sensitivity for dopamine. With this fibre, the response to DOPAC is slightly increased and the response to ascorbic acid is decreased. The most important effect of the electrochemical treatment is, however, a gain in reproducibility combined with shorter equilibration times in the sample solution. In addition to these features, it was noticed that the electrochemical treatment seems to facilitate smooth coating with Nafion.

When a Nafion-coated electrode is exposed to the sample solution, an equilibrium in copper concentration between the Nafion film and the solution is established, the equilibration time depending on the diffusion rates for the ions involved. Copper ions will occupy places in the exchanger lattice, together with other cations from the sample. Constants for the partition in Nafion between copper(I) and copper(II) and alkali metal ions are not available at present.

If a Nafion-coated electrode is transferred from one solution to another, the sensitivity to ascorbic acid may change, depending on a difference in the concentration of copper ions or of other cations involved in the parti-

TABLE 1

Sensitivities to ascorbic acid, dopamine and DOPAC, given as the slopes of the linear calibration plots. (Five additions each experiment, oxidation current for dopamine at 160—180 mV, and for DOPAC and ascorbic acid at 250—320 mV.)

Compound	Response (pA/μM)[a]		
	EC	EC/Naf	EC/Naf/Cu
Ascorbic acid	1070	33	17
DOPAC	1490	148	145
Dopamine	2180	2410	2320

[a]EC, electrochemically treated; Naf, Nafion-covered; Cu, copper-dipped (0.79 mM), after equilibration.

tioning with copper ions within the film. Stabilization of the sensitivity for ascorbic acid will be reached in time (Fig. 1).

Optimization of the resting potential between scans with the copper-treated electrode

The surface of a carbon fibre electrode which has been subjected to only electrochemical treatment has insufficient ion-exchange capability to bind the quantities of copper ions required to affect the sensitivity to ascorbic acid. If such an electrode is first covered with Nafion, immersion in copper acetate solution (0.79 mM for 1—2 s) will produce a further electrode modification. With a newly prepared electrode, a peak around 0 mV will occur with a scan starting from —100 mV, and a resting time of 1 min (Fig. 2). With a less-negative starting potential, the peak declines in magnitude, and at about —50 mV it disappears. It seems clear that the observed oxidation maximum originates from the oxidation of copper(I) to copper(II) during the scan. During the time between scans, copper(II) will be reduced if the resting potential is low enough. A new oxidation peak will then occur during the next scan, when copper(I) is oxidized at the electrode. With chemically-reduced copper(I) ions in the Nafion layer, which will probably be the case if the electrode is placed in an ascorbic acid solution, copper(II) will be formed during the resting period before the next scan. This indicates the need for a high resting potential if the copper(II)-catalyzed discrimination against ascorbic acid is to be maintained. Another reason to keep the potential above —50 mV is the avoidance of a possible current from the oxidation of copper(I), which may interfere in the determination of dopamine (Fig. 2). With a resting potential near or slightly above 0 mV, ascorbic acid is oxidized between the scans; this decreases the influence of ascorbic acid [12], but does not affect the determination of dopamine or DOPAC.

When a newly copper-treated electrode is used in an ascorbic acid solution, the oxidation current for ascorbic acid will be only 10—30% of its

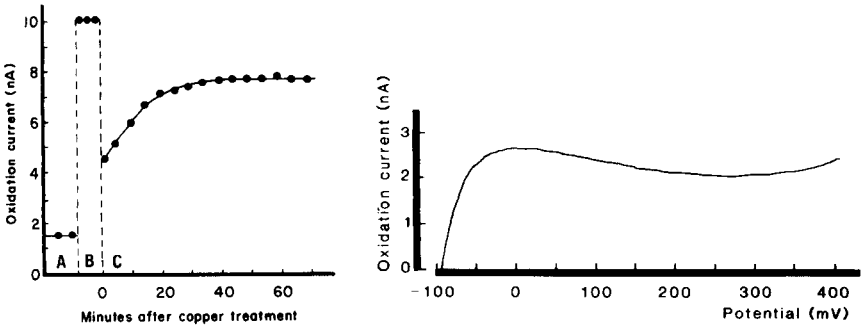

Fig. 1. Oxidation current vs. time for a Nafion-treated carbon fibre electrode: (A) in buffer solutions; (B) in 200 μM ascorbic acid; (C) in 200 μM ascorbic acid, after immersing the electrode in a copper solution (0.79 mM).

Fig. 2. Voltammogram obtained from a Nafion-treated carbon fibre electrode after dipping in copper solution (0.79 mM). Linear voltammetry from —100 mV to 412 mV in buffer solution. One minute between scans.

earlier value (Fig. 1). After a certain time of equilibration, the ascorbic acid signal reaches a constant, higher level. Stabilization is likely to depend mainly on the stripping of an excess of copper ions from the Nafion film into the sample solution. A constant sensitivity to ascorbic acid will be reached when there is an equilibrium in copper concentration between the ion-exchanger and the aqueous phase. The amount of metal transferred to the solution from the Nafion layer changes the copper concentration only marginally, and may be assumed to be negligible.

Calibration curves

Linear calibrations for ascorbic acid, DOPAC and dopamine were obtained with differently treated electrodes. It was observed that reliable dopamine readings from Nafion-treated carbon fibre electrodes required longer stabilization times than for DOPAC and ascorbic acid, indicating enrichment of dopamine in the Nafion film. A similar, but much weaker, effect was observed with DOPAC. No difference in sensitivity was observed for dopamine before and after copper treatment of the electrode. For DOPAC, a minor decrease in sensitivity was seen. Figure 3 shows oxidation curves for the phosphate buffer, ascorbic acid and dopamine. The slopes of calibration curves for differently treated electrodes are compared in Table 1.

The shapes of the oxidation waves for dopamine, DOPAC and ascorbic acid, as obtained with the ECNCu electrode, were not changed by the copper treatment. This indicates that copper ions do not mediate the electron transfer during oxidation at the electrode surface.

Experiments with bathocuproine as a carrier material for copper ions on the electrode surface.

With linear-scan voltammetry over 0—512 mV, a marked relative discrimination against ascorbic acid was reached compared to dopamine, following

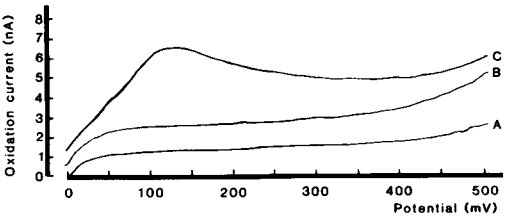

Fig. 3. Oxidation current for the Nafion-treated electrode, after equilibration in the sample solution: (A) only buffer; (B) 100 μM ascorbic acid; (C) 100 μM ascorbic acid, 1 μM dopamine.

the (bathocuproine)$_2$/copper(I) treatment (Table 2). Depending on layer thickness, probably caused by screening of the electrode from the solution by the isolating (bathocuproine)$_2$/copper(I) complex, the treatment also yielded a lowered sensitivity to dopamine. The pronounced discrimination against ascorbic acid is probably due to small amounts of copper(II) ions close to the electrode, involved in the equilibration with copper(I) in the bathocuproine complex phase. It is likely that dissolved oxygen oxidizes copper(I) back to copper(II) in undeaerated samples. As the same effect was obtained even in deaerated samples, it is likely that copper(I) is slowly oxidized back to copper(II) by the electrode, during the time between scans (1 min). No peak was observed, however, with cyclic voltammetry in deaerated solutions, which could explain the oxidation of copper(I) to copper(II).

Copper in the brain

The copper concentration in mammal serum is highly variable, averaging about 14 μM [15]. The main part of this is firmly protein bound as ceruloplasmin, but 5—20% is "direct-reacting" copper, available for reaction with complexing agents like dithizone and diethyldithiocarbamate. Assuming that the extracellular fluid in the rat brain contains a corresponding copper concentration, the "free" copper level is 0.7—2.7 μM. With so high a copper level in the extracellular fluid, it is not possible to disregard the effect of catalysis on the electrochemical determination of ascorbate. Since ascorbate is a powerful agent for the reduction of copper(II) to copper(I) and the ascorbate concentration is at least one order of magnitude higher than that of the "free" copper, the main "free" copper content is likely to be in the monovalent oxidation state.

The practical use of Nafion-treated carbon fibre electrodes

Electrodes with a 15—30% ascorbic acid/DOPAC (0.5—1.5% ascorbic acid/dopamine) response were regarded as usable for in-vivo experiments with the linear-scan voltammetric method, for monitoring mainly DOPAC. After calibration, the electrodes were placed in the phosphate buffer solution with the copper concentration additionally raised to 1.78 μM. The

TABLE 2

Sensitivity to dopamine and ascorbic acid for a glassy carbon electrode before and after the treatment with (bathocuproine)$_2$/copper(I) chloride

Working electrode	Sensitivity (nA/μM)[a]		
	DA	AA	AA/DA
Untreated GC	62.2	30.0	0.482
Treated GC	12.8	0.958	0.075

[a]DA, dopamine; AA, ascorbic acid.

ultimate lowering of the response to ascorbic acid was 10—50% after an equilibration time of 1 h. The electrodes were then taken out of the buffer solution and stored dry.

If the ascorbic acid/dopamine response is lower than 1% before the equilibration with copper, a thick coating is indicated. The diffusion time for compounds within the Nafion layer still does not affect the determination of dopamine and DOPAC with linear-scan voltammetry at 100 mV s^{-1}, but the sensitivity to DOPAC begins to decline. It is possible to prepare electrodes responding well below 0.01% in the ascorbic acid/dopamine ratio. For use with the linear-scan method in vivo, these electrodes were found to produce insufficient responses to both DOPAC and dopamine. Electrodes found to be too thickly or too thinly coated with Nafion were again subjected to the Nafion treatment step. When these electrodes were washed in a fresh drop of Nafion solution, the old Nafion layer dissolved. A new coating could then be prepared, as previously described.

Conclusions

The use of a cation-exchanger as a thin film on the surface of carbon fibre electrodes as a discriminator for uncharged and negatively charged compounds is promising. The use of copper as an electrocatalyst for ascorbic acid in combination with the ion-exchanger appears substantially to improve this selectivity.

When Nafion-coated carbon fibre electrodes are prepared for in-vivo use, it is recommended that they be stored for some time (1—2 h) in a buffer containing copper and other ions at concentrations approximating those in the extracellular fluid. The time for equilibration between the electrode surface and the extracellular fluid will then be shorter, and the ascorbic acid discrimination will thus be established more quickly.

Some effort should be made to find an ion-exchanger suitable for the attachment to carbon fibre, and with a partition coefficient for copper, as compared to other cations, higher than that of Nafion.

When dopamine is to be determined in vivo, a technique with a higher resolution capability than linear-scan voltammetry should be used, such as one of the pulse methods.

This work was supported by the Swedish Medical Research Council (4247) Leo Research Foundation and the Tercentenary Fund of the Bank of Sweden. The authors gratefully acknowledge the helpful comments and criticism of Dr. Lennart Svensson, Dr. David Dyrssen and Dr. Barry Snape.

REFERENCES

1 P. M. Kovach, A. G. Ewing, R. L. Wilson and R. M. Wightman, J. Neurosci. Meth., 10 (1984) 215.
2 F. G. Gonon, F. Navarre and M. J. Buda, Anal. Chem., 56 (1984) 573.
3 T. E. Edmonds, Anal. Chim. Acta, 175 (1985) 1.
4 F. G. Gonon, C. M. Fombariet, M. J. Buda and J. F. Pujol, Anal. Chem., 53 (1981) 1386.
5 G. A. Gerhardt, A. F. Oke, G. Nagy, B. Moghaddam and R. N. Adams, Brain Res., 290 (1984) 390.
6 G. Nagy, G. A. Gerhardt, A. F. Oke, M. E. Rice, R. N. Adams, R. B. Moore III, M. N. Szentirmay and C. R. Martin, J. Electroanal. Chem., 188 (1985) 85.
7 T. Shigematsu and M. Munakata, Bull. Inst. Chem. Res. Kyoto Univ., 48 (1970) 198.
8 E. V. Shtamm, A. Purmalis and Yu. I. Skurlatov, Zh. Fiz. Khim., 48 (1974) 1454.
9 J. Wang, B. Greene and C. Morgan, Anal. Chim. Acta, 158 (1984) 15.
10 H. A. Harper, V. W. Rodwell and P. A. Mayes, Review of Physiological Chemistry, 16th edn., Lange Medical Publications, Los Altos, CA, 1977, pp. 534—535.
11 C. A. Marsden, M. P. Brazell and N. T. Maidment, in C. A. Marsden (Ed.), Measurement of Neurotransmitter Release In Vivo, Wiley, Chichester, 1984, pp. 127—151.
12 R. D. O'Neill, M. Fillenz and W. J. Albery, J. Neurosci. Meth., 8 (1983) 263.
13 P. Hulthe, Analyst, 95 (1970) 351.
14 M. E. Rice, A. F. Oke, C. W. Bradberry and R. N. Adams, Brain Res., 340 (1985) 151.
15 H. A. Harper, V. W. Rodwell and P. A. Mayes, Review of Physiological Chemistry, 16th edn., Lange Medical Publications, Los Altos, CA, 1977, p. 586.

Analytica Chimica Acta, 198 (1987) 207—222
Elsevier Science Publishers B.V., Amsterdam — Printed in The Netherlands

COMPUTERIZED CONDUCTOMETRIC DETERMINATION OF STABILITY CONSTANTS OF COMPLEXES OF CROWN ETHERS WITH ALKALI METAL SALTS AND WITH NEUTRAL MOLECULES IN POLAR SOLVENTS

D. Ph. ZOLLINGER[a], E. BULTEN, A. CHRISTENHUSZ, M. BOS and W. E. VAN DER LINDEN*

Laboratory for Chemical Analysis, Department of Chemical Technology, Twente University of Technology, P.O. Box 217, 7500 AE Enschede (The Netherlands)

(Received 1st November 1986)

SUMMARY

A computerized conductometric procedure for the determination of stability constants of the complexes of crown ethers (15-crown-5, benzo-15-crown-5 and 12-crown-4) with alkali metal salts in polar solvents is described, based on a microcomputer-controlled titration system. For the control of the experiments from software, a modular computer program was written in FORTH computer language. The procedure is especially suitable for the study of 1:2 metal ion/ligand complexes, which occur frequently with the compounds used. For the study of the interaction between crown ethers and neutral molecules, an indirect procedure is outlined.

Crown ethers and related compounds are capable of forming complexes with many metal salts, with organic salts (such as organic ammonium, arenediazonium and guanidinium salts) and with many (neutral) organic molecules. For the determination of the (thermodynamic) stability of these complexes, a large variety of methods and procedures has been reported; these have been reviewed [1]. In this laboratory, a polarographic procedure has been developed for the computerized determination of stability constants of CE-complexes with (alkali) metal salts and neutral compounds in polar solvents [2, 3].

The conductance of an electrolyte solution depends on the number and nature of the ionic species present in the solution. In view of the fact that crown ethers form complexes with a variety of cations, and with the assumption that the mobility of the free cations is different from their complexes, conductometry is a technique that can be applied to the study of complexation of cations by crown ethers. For neutral species, the technique cannot be applied as such. An indirect procedure, however, is a possible alternative for the study of the interaction between crown ethers and these species.

---

[a]Present address: Sandoz AG, Abt. QSP, Postfach, 4002 Basle (Switzerland).

0003-2670/87/$03.50

In this paper, the development of a microcomputer-controlled conductometric titration system is described, together with the possible applications of the system to the study of complexation of cations. An indirect procedure for the study of the interaction between neutral species and crown ethers is outlined as well.

Determination of the stability constants

For the conductometric determination of stability constants (or ion-pair association or dissociation constants), the standard procedure involves the measurement of the (specific) conductance of an electrolyte solution as a function of ionic strength or electrolyte concentration. From these measurements, the equivalent conductance (at infinite dilution) and the degree of association between anions and cations can be evaluated by means of the equations describing the conductance of electrolyte solutions in terms of inter-ionic effects, for example the Onsager equation [4] or an extended form of this equation (see, e.g. ref. 5).

In the case of complexation of ionic species by crown ethers that have no acidic and/or basic substituents, it is possible to evaluate the interaction between the species involved by studying the equivalent conductance of the salt solution as a function of the ligand concentration. Therefore, the solutions containing a completely dissociated metal salt and a variable concentration of the crown compound can be regarded as a mixed electrolyte with a common anion at constant ionic strength. In this approach, no corrections for the inter-ionic effects on ionic mobility are necessary, assuming that any changes in interactions are negligible when the solvated cation is converted to the complex with the crown ether. Taking into consideration the possible effects of cations with different mobilities on the mobility of the common anion, some correction term might be necessary. However, these corrections are likely to be very small [6] and can also be neglected.

A second advantage of this approach is the fact that no indifferent salt has to be added in order to obtain constant ionic strength. Therefore, the experiment can be done with diluted systems, thereby minimizing the formation of ion-pairs in solvents of lower dielectric constant.

If only one complex is formed and if the equivalent conductivity of the complex salt MLX_n can be determined experimentally, the stability constant of the complex can be calculated directly from the observed (specific) conductance value and the total concentrations of M and L. This applies only to those cases in which it is possible to measure the conductance of the solution at such excess ligand concentrations L_T that it can be assumed that the concentration of the metal ion M^{n+} is negligibly small, i.e., for stable complexes and/or at large ratio of L_T/M_T. This approach has been used by several authors (see, e.g. refs. 7—16). If more than one complex species is formed, or if the equivalent conductivity of the complex species ML_i cannot be determined experimentally, a general least-squares procedure has to be applied in order to obtain the desired parameters.

The interaction between crown ethers and uncharged species (e.g., urea) can only be studied by means of an indirect procedure. This procedure is similar to the indirect polarographic one described previously [2, 3]. First, the conductometric properties of an indicator system have to be studied. From the conductometric study of the interaction between the indicator compound and the crown compound L, the equivalent conductivity and stability constants of the complex between M and L are evaluated as outlined above (Fig. 1A). Next, the influence of addition of the neutral guest species, U, to a solution of the metal salt M in presence of an arbitrary, but fixed amount of L is investigated. As a result of the (assumed) interaction between U and L, M is displaced from the complex and the observed conductivity will change in the direction of the conductance of the free metal salt. Usually, this will result in an increase of the observed conductance (Fig. 1B). From this change in conductance upon addition of the neutral compound U, the stability constant of the complex between U and the ligand L can be evaluated.

Computer programs for data-acquisition and data-handling

For the over-all control of the experiment and for the calculation of stability constants from the conductance data, two different computer programs were developed.

Computer program for control of the experiment. The experiment was controlled entirely from software by means of a program KONDAT, written in FORTH (FysForth version 03). Some words defined for the control of polarographic experiments (described earlier [3]) were used in this program, while other words were developed specifically for the control of the conductometric experiments.

After the input of some experimental parameters from the keyboard (i.e., the concentrations of metal salt and titrant as well as the total volume of

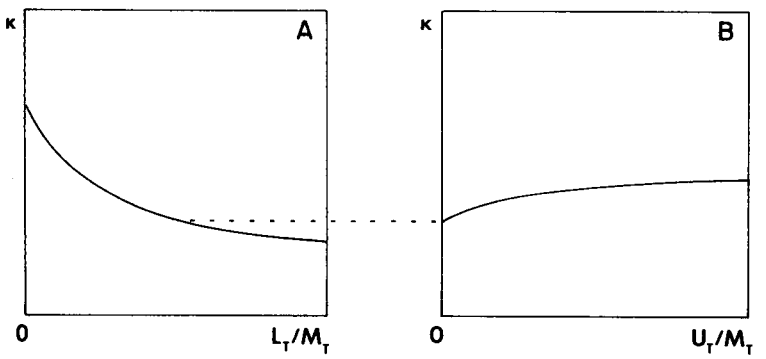

Fig. 1. Indirect conductometric procedure for the determination of stability constants: (A) determination of K_1; (B) determination of K_B (cf. Table 1). Specific conductance as a function of the analytical concentration of L or U. M, metal salt; L, crown ether; U, neutral guest species (in competition with M).

titrant to be added to the metal salt solution), data acquisition and storage take place automatically. This task is performed by the apparatus described previously [3]. After each addition of titrant to the metal salt solution, a delay period of 90 s is allowed for mixing and obtaining temperature equilibrium. Next, the conductance of the solution is measured as soon as the observed signal (as obtained from the ADC) has attained a stable level. The input parameters and all the experimental data are recorded on disk in a format that allows the data to be used by both FysForth and Pascal programs.

Computer program for evaluation of the data. For the evaluation of the conductometric data, a non-linear least-squares curve-fitting program KONFIT was developed. The program, written in Pascal, is based on the iterative adjustment of the calculated values of the specific conductance to the observed conductance values by using a modified Simplex procedure [17]. Adjustable parameters are both the stability constants and the equivalent conductivities of all the species present, but the user has the option of excluding any parameter from the refinement procedure. Because the selected mathematical model is only applicable to experiments that are done at constant ionic strength, complexes of the type M_nL were not taken into consideration and only the systems given in Table 1 were used. In the case of models III and IV, the stability constants K_1 and K_2 of the metal/crown ether complexes were incorporated in the program as non-adjustable.

The experimental data are read from the data files created by the FORTH program KONDAT. Input parameters for the program are the initial values for the N parameters to be refined and the step size for the first simplex, which decides the initial surface area in the $(N + 1)$-dimensional space to be evaluated. The use of Simplex algorithms minimizes the chance of divergence of the refinement procedure, but it is possible that the optimum found is

TABLE 1

Mass-balance equations used in computer program KONFIT for evaluation of conductometric data[a]

Model	Reactions		Stability constants	Mass-balance equations
I	M + L	ML	$K_1 = (ML)/(M)(L)$	$M_T = (M) + (ML)$ $L_T = (L) + (ML)$
II	M + L	ML	$K_1 = (ML)/(M)(L)$	$M_T = (M) + (ML) + (ML_2)$
	ML + L	ML_2	$K_2 = (ML_2)/(ML)(L)$	$L_T = (L) + (ML) + 2(ML_2)$
III	M + L	ML	$K_1 = (ML)/(M)(L)$	$M_T = (M) + (ML)$
	U + L	UL	$K_B = (UL)/(U)(L)$	$U_T = (U) + (UL)$ $L_T = (L) + (ML) + (UL)$
IV	M + L	ML	$K_1 = (ML)/(M)(L)$	$M_T = (M) + (ML) + (ML_2)$
	ML + L	ML_2	$K_2 = (ML_2)/(ML)(L)$	$U_T = (U) + (UL)$
	U + L	UL	$K_B = (UL)/(U)(L)$	$L_T = (L) + (UL) + (ML) + 2(ML_2)$

[a] U is the guest species in competition with M.

TABLE 2

Solutions of the mass-balance equations given in Table 1 in terms of the free ligand concentration [L]

Model	Solution
I	$K[L]^2 + [L](1 + K(M_T - L_T)) - L_T = 0$
II	$K_1K_2[L]^3 + [L]^2(K_1(1 + K_2(2M_T - L_T))) + [L](1 + K_1(M_T - L_T) - L_T = 0$
III	$K_1K_B[L]^3 + [L]^2(K_1 + K_B + K_1K_B(U_T + M_T - L_T)) + [L](1 + K_1(M_T - L_T) + K_B(U_T - L_T)) - L_T = 0$
IV	$K_1K_2K_B[L]^4 + [L]^3(K_1K_2(K_B(2M_T + U_T - L_T) + 1) + K_1K_B) + [L]^2(K_1(K_B(M_T + U_T - L_T) + K_2(2M_T - L_T) + 1) + K_B) + [L](K_1(M_T - L_T) + K_B(U_T - L_T) + 1) - L_T = 0$

only a local optimum [18, 19]. Therefore it is a standard procedure to repeat the fitting procedure once or twice with different starting values and different initial step sizes in order to test if the true optimum is found.

The mass-balance equations of Table 1 can be solved in order to obtain equations for the free ligand concentration [L] (Table 2). For models II–IV, the free ligand concentrations [L] were calculated by means of a Newton–Raphson procedure. Once the value of [L] had been obtained, the concentrations of all the other species involved were calculated from the corresponding equations given in Table 1, by using the estimated values of the stability constants at the current iteration step of the program. The refinement of the parameters is continued until the sum-of-squares of the residuals between calculated and observed values of the conductance for all experimental points is minimized. The output of the program KONFIT comprises the refined parameters, the sum-of-squares and the standard deviation of the data as well as the distribution of the species.

EXPERIMENTAL

Chemicals and instrumentation

12-Crown-4 (Janssen), 15-crown-5, benzo-15-crown-5 and dibenzo-24-crown-8 (all from Merck) were used as obtained. 18-Crown-6 (Merck) was purified from the acetonitrile complex as described by Gold and Rice [20]. Alkali metal chlorides were dried at reduced pressure (3.33 kPa) and a temperature of 323 K for 24 h and stored over phosphorus pentoxide. Double-distilled water was used throughout the experiments. Methanol (Merck) was of analytical-reagent grade (water content 0.05%). Guanidinium hydrochloride (Merck, zur Synthese) was recrystallized from water. All other chemicals were of at least analytical-reagent grade and were used as received.

A Philips PW-9509 conductivity meter was used (accuracy 0.15% full scale

deflection), together with a Philips PW-9510/60 measuring cell; the cell constant (0.85 cm^{-1}) was evaluated by using aqueous solutions of potassium chloride. For the addition of titrant solutions, a Radiometer Autoburette ABU-12a, total volume 2.5 or 25.0 ml, was used. Additions to the titration vessel were done at constant volume increments of 0.01 or 0.1 ml, respectively. The accuracy of the buret is 0.1%. The titration vessel with the conductivity cell was kept at 298 ±0.1 K by using a Tamson thermostat.

The recorder output of the conductivity meter was connected to a Basis 108 microcomputer through a 12-bit ADC [3].

Procedure

Purified nitrogen was passed through an aqueous solution of tetramethylammonium hydroxide in order to remove CO_2 and then through a washing-bottle containing the solvent to be used before it was led into the titration vessel. Nitrogen was passed over the salt solution in this vessel for 30 min in order to remove CO_2 before the experiment was started. No special precautions were taken to exclude the influence of moisture on the water content of the solvent used.

Titrant solutions were prepared by dissolution of the sample into a salt solution of the same concentration as present in the titration vessel at the start of the experiment, in order to keep the ionic strength constant during the experiment. The solution in the titration vessel was mixed by means of a magnetic stirrer.

RESULTS AND DISCUSSION

Complexation of alkali metal ions

As a first evaluation of the procedure, the complexation of potassium chloride by 18-crown-6 in water was studied. Upon addition of the crown to the solution of the potassium salt, a decrease of the equivalent conductance

TABLE 3

Complexation of potassium chloride by 18-crown-6 in water. Comparison of manual and computerized method; equivalent conductivities of free and complex salt and logarithmic value of stability constant at 298 K

Method	Λ_{MX} [Ω^{-1} m^2 eq^{-1}]	Λ_{MLX} [Ω^{-1} m^2 eq^{-1}]	log(K)
Manual (n = 5)			
Range	151.2—153.7	102.2—111.9	2.05—2.18
Mean	152.2	107.5	2.12
S.d.	1.2	3.5	0.05
Computerized (n = 5)			
Range	151.3—152.0	109.2—112.1	2.08—2.12
Mean	151.7	110.6	2.10
S.d.	0.3	1.2	0.02

κ was observed, which can be regarded as the effect of the lower mobility of the complex species in comparison with the free potassium ion. The conductometric data were evaluated by means of the program KONFIT based on model I. In Table 3, the results are given for the computerized procedure in comparison to a manual one. It can be seen that the precision of the computerized procedure is better than that of the manual one. The value for the stability constant of the potassium/18-crown-6 complex is in good agreement with literature data [21]. The value for the equivalent conductivity of the free metal salt is slightly larger than the values reported in the literature (for potassium chloride in water at 298 K, this value is 149.86). This was found to be the case for some other systems as well, but no explanation can be given.

Next, the complexation of the sodium and potassium ion by benzo-15-crown-5 in a solvent mixture of methanol and water (7:3 w/w) was studied. This system was chosen in view of the fact that Izatt et al. [22] had reported 1:2 complexation for the potassium ion (a 'sandwich' type of complex in which the metal ion is surrounded by two crown ether molecules) with the stability constant for the 1:2 complex more than 10 times greater than the value of K_1. Moreover, relatively little quantitative data on this type of complexation could be found in the literature [21, 23–26]. The techniques used in these studies were potentiometry [22, 24, 25], calorimetry [22, 23] and NMR spectroscopy [26]. Ungaro et al. [27] studied the complexation of sodium and potassium by 4′-substituted benzo-15-crown-5 derivatives in acetone by means of conductometry; the existence of 1:2 complexes with the potassium ion was discussed in qualitative terms only. In other papers on

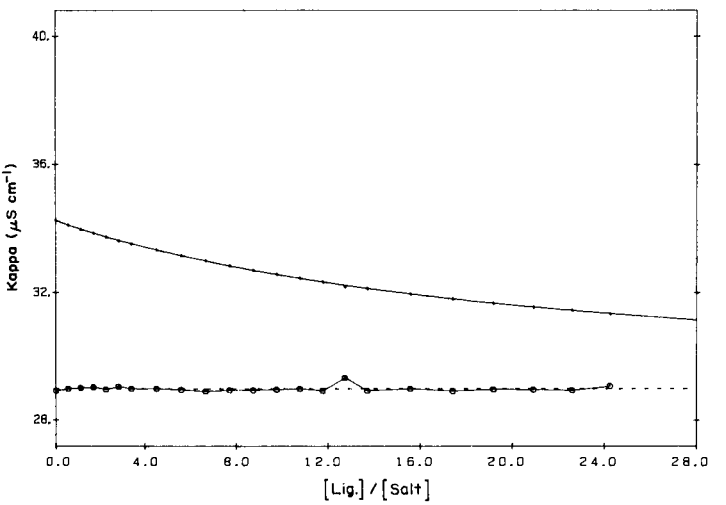

Fig. 2. Conductance of a solution of sodium chloride (0.508×10^{-3} M) in methanol as a function of the concentration of benzo-15-crown-5, showing the experimental points and the calculated curve (upper curve). Deviation between observed and calculated conductance values for the 1:1 model is indicated by the lower curve (enlarged).

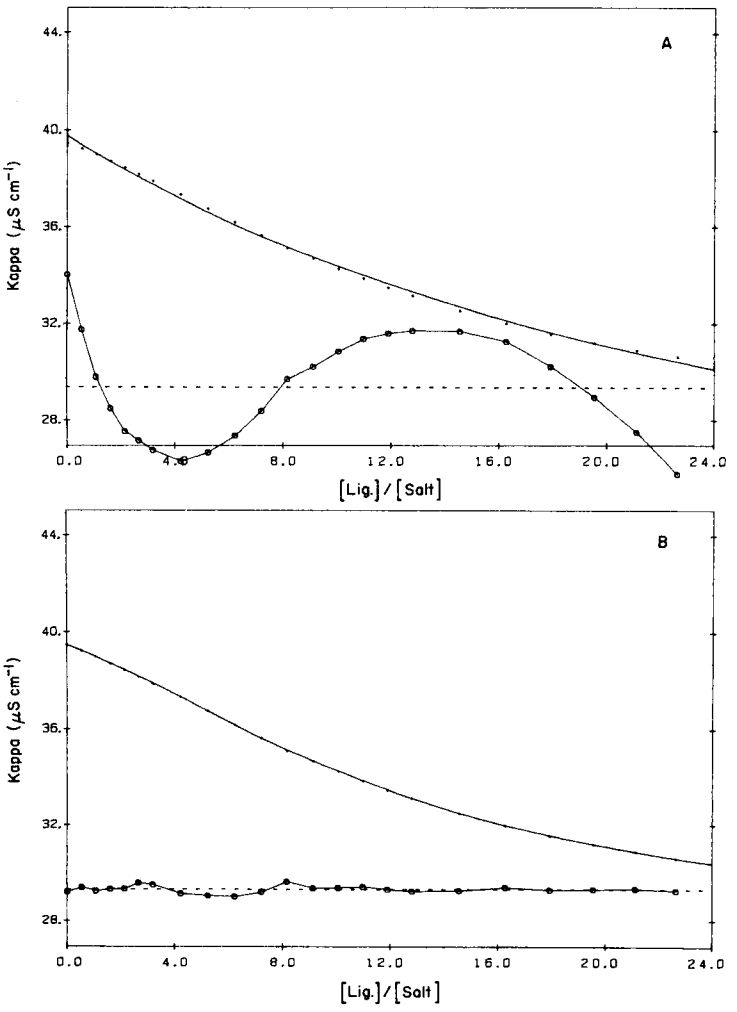

Fig. 3. Conductance of a solution of potassium chloride (0.524×10^{-3} M) in methanol as a function of the concentration of benzo-15-crown-5. The upper (calculated) curve is given with the experimental data points. The lower curves (enlarged) show the deviation between observed and calculated conductance values for the 1:1 model (A) and the 1:2 model (B).

the conductometric study of complexation of alkali metal ions with small crown ethers [12, 13, 28, 29], the formation of 1:2 complexes was discussed in qualitative terms only or not at all.

The conductance of the solutions of sodium and potassium chloride as a function of the concentration of benzo-15-crown-5 in 70% methanol is represented in Figs. 2 and 3. The upper curve in each frame is the calculated curve; the lower curve shows the difference between observed and calculated values. A good fit was obtained with model I in the case of the sodium ion

(Fig. 2). For the potassium ion, however, a characteristic 'deviation plot' was obtained when the data were evaluated according to model I (Fig. 3A), whereas a good fit was obtained by using model II (Fig. 3B). The difference between the 'goodness of fit' for models I and II can be grasped from the calculated standard deviation of the data, but the graphical representation as given in Figs. 2 and 3 is very helpful in this respect. The calculated values of the stability constants and equivalent conductivities of the complex species for the sodium and potassium salts and the other alkali metal chlorides are given in Table 4.

The most remarkable fact is the strong tendency for sandwich complex formation for the potassium ion compared to the other alkali metal ions. Sandwich-type complexes have been reported in the literature for different metal salts with crown ethers having a small cavity such as the 12-crown-4 and 15-crown-5 derivatives, both in the solid state and in solution. As can be

TABLE 4

Stability constants and equivalent conductivities (Λ) of alkali chloride complexes with benzo-15-crown-5 and 15-crown-5 in methanol/water (7:3) at 298 K

Cation	[Salt] (mM)	Λ_{MX}	Λ_{MLX}	Λ_{ML_2X}	$\log(K_1)$	$\log(K_2)$
Benzo-15-crown-5						
Li	0.797	54.8	<50	—	<0.4	—
Na	0.508	67.5	56.7	—	1.97	—
K	0.524	76.0	59.4	52.9	1.97	2.40
Rb	0.516	78.4	65.0	50.5	1.77	1.96
Cs	0.508	79.1	69.0	46.0	1.66	1.02
	0.798	78.5	66.2	44.3	1.55	1.13
15-Crown-5						
Li	0.797	54.8	52.1	—	1.02	—
Na	0.508	67.9	59.4	—	2.32	—
K	0.524	77.0	70.0	55.0	2.79	2.04
Rb	1.138	75.6	71.5	50.0	2.81	1.83
Cs	0.798	78.4	75.4	55.0	2.49	1.48
	1.007	77.9	70.8	52.9	2.22	1.35

TABLE 5

Alkali metal ion diameters and cavity sizes of crown ethers (from ref. 30)

Metal ion	Radius (Å)	Crown ether	Radius (Å)
Li	1.36	14-crown-4	1.2—1.5
Na	1.90	15-crown-5	1.7—2.2
K	2.66	18-crown-6	2.6—3.2
Rb	2.94	21-crown-7	3.4—4.3
Cs	3.34		

seen from the data in Table 5, the potassium ion is too large for the cavity of 15-crown-5. Therefore, the formation of 1:2 complexes is not unexpected. In contrast with this finding, for the larger rubidium and cesium ions the relative amount of 1:2 complexation is less prominent. (Recently, it has been established that cesium picrate, like the sodium salt and unlike the potassium salt, forms a 1:1 complex with benzo-15-crown-5 [31].) Moreover, the sodium ion, which should fit exactly into the cavity of the 15-crown-5 ring, can form a 'sandwich' type of complex with benzo-15-crown-5 if the anion present has unfavourable coordinating properties (see, e.g. ref. 32). Hence it can be concluded that the size/fit concept, often used to explain the selectivity of the crown ethers towards complexation of alkali metal ions, by itself provides insufficient ground for a more quantitative explanation of the observed tendency towards 1:2 stoichiometry.

The stability constants for the alkali metal complexes with the unsubstituted 15-crown-5 (in the same solvent mixture) are also given in Table 4. By comparison with the complexes of the benzo derivative, these complexes are more stable. The ratio of K_1/K_2 is larger for the potassium and rubidium ion and somewhat smaller for the cesium ion. The lower stability of the complexes of the substituted crown ether can be explained by the fact that the catecholic oxygen atoms of the benzo-crown are less basic than the other oxygen atoms in the ring of the crown ether. Moreover, the presence of the benzo group reduces the flexibility of the molecule, thereby diminishing the possible wrapping of the crown around the (partially desolvated) cation in the (sandwich) complex.

The interaction between the alkali metal ions and 12-crown-4, 15-crown-5 and benzo-15-crown-5 was also investigated in pure methanol; the results are presented in Table 6. In comparison with the methanol/water mixture, the complexes of 15-crown-5 and benzo-15-crown-5 are more stable in methanol, while the ratio of K_1/K_2 is larger in methanol than in the methanol/water mixture (except for the complexes of 15-crown-5 with K^+ and Cs^+). The stability of the lithium complexes is very small, even for 12-crown-4. Apparently the solvation of this ion more than balances the binding forces of the crown ethers in these solvents.

From the values of the equivalent conductivities of the free metal ions and their complexes with 12-crown-4, 15-crown-5 and benzo-15-crown-5, the (relative) size of the ionic species can be calculated from the equation

$$r_i = 0.82/\lambda_i^0 \eta$$

where λ_i^0 and η represent the limiting ion conductance and the viscosity of the solvent, respectively [33]. The Stokes radii of the alkali metal ions in water, methanol and methanol/water (7:3) are presented in Table 7. The limiting ionic conductance values for the methanol/water mixture were calculated from the observed equivalent conductance values and the Onsager equation. (For this purpose, the values for the dielectric constant and the viscosity of this solvent mixture were taken as 47.1 and 1.19 cP, respectively.)

TABLE 6

Stability constants and equivalent conductivities of alkali chloride complexes with benzo-15-crown-5, 15-crown-5 and 12-crown-4 in methanol at 298 K

Cation	[Salt] (mM)	Λ_{MX}	Λ_{MLX}	Λ_{ML_2X}	log (K_1)	log (K_2)
Benzo-15-crown-5						
Li	0.561	89.4	89.4	—	—[a]	—
Na	0.515	94.6	90.4	—	2.94	—
	1.029	89.6	84.8	84.6	2.94	2.14
K	0.535	101.4	91.4	86.0	2.96	3.20
					2.68	2.70
Rb	0.516	103.3	87.4	83.1	2.68	2.70
	1.017	102.4	89.3	81.5	—	—
Cs	0.472	108.3	85.1	—	2.20	—
	0.796	108.2	85.2	82.7	2.21	1.53
	1.000	105.3	81.3	80.7	2.15	1.34
15-Crown-5						
Li	0.561	89.3	99.6	—	1.21	—
Na	0.515	94.6	94.6	—	—[a]	—
K	1.089	98.3	90.2	85.8	3.38	2.62
Rb	0.516	105.6	89.4	88.9	2.88	2.23
Cs	0.796	107.5	94.1	87.1	2.78	1.74
	1.001	105.3	93.1	85.6	2.81	1.90
12-Crown-4						
Li	1.028	79.6	—	—	<0.0	—
Na	1.029	89.4	89.2	85.2	2.05	1.73
K	1.047	98.5	92.8	83.9	1.73	0.86
Rb	1.086	100.4	94.4	81.7	1.65	0.87
Cs	0.796	107.4	102.2	82.6	1.60	0.74
	1.001	105.2	100.6	84.0	1.65	0.90

[a]No change in conductance was observed.

TABLE 7

Calculated Stokes radii of free alkali metal ions in water, methanol and methanol/water (7:3) at 298 K

Metal	Stokes radius (Å)		
	Water	Methanol/ water	Methanol
Li	2.38	3.6	3.75
Na	1.84	2.3	3.29
K	1.25	1.8	2.82
Rb	1.18	1.7	2.65
Cs	1.19	1.7	2.43

From Table 7, it can be concluded that the Li^+ and Na^+ ions are more strongly solvated than the other alkali metal ions while, apart from the lithium ion, there is a preferential solvation by the water molecules in the methanol/water mixture.

This can also be concluded from the differences between the equivalent conductivities of the alkali metal ion complexes in methanol and the methanol/water solvent mixture (compare Table 4 with Table 6). In methanol, the differences between the equivalent conductivities of the free metal ions and their complexes are smaller than those in the methanol/water mixture. This suggests that replacement of methanol molecules by the crown ether molecule has a smaller effect on the radius of the complex than the removal of water molecules. It can also be concluded from the data on the equivalent conductivities of the complex species that in the 1:1 complexes of the alkali metal ions with the small crown ethers used, the solvation shell is not completely removed. The equivalent conductivities of the 1:1 complexes of 12-crown-4 and 15-crown-5 differ relatively little from the values of the free cations, whereas the values for the 1:2 complex are significantly lower. Moreover, these latter values are very much the same for all the alkali metal ions (with the exception of the lithium ion) for a certain crown compound. Finally, the equivalent conductivities for the 1:2 complexes of 12-crown-4 are lower than those for 15-crown-5, suggesting that in the latter complexes, the solvation shell is removed to a larger extent than in the case of 12-crown-4.

In Tables 8 and 9, the stability constants of the complexes of 12-crown-4, 15-crown-5 and benzo-15-crown-5 with the alkali metal ions in methanol (and in methanol/water, 7:3) are summarized and compared with literature values. It can be seen that not all data are in good agreement, especially with regard to the values of the stability constant for the ML_2 complexes. This may be caused by the fact that different techniques have been used for the determination of the stability constants. With potentiometric procedures, for example, it is impossible to work with a large excess of ligand, in particular in those cases in which rather stable complexes are being formed ($\log K \geqslant 3$). Therefore, the relative amount of the ML_2 complex is small and the determination of the value of K_2 is subjected to a large uncertainty (as reported by Michaux and Reisse, for instance [24]). This is also the case for determinations by means of calorimetry; the values reported by Buschmann [46], for example, tend to be high. It is clearly desirable to evaluate the methods and procedures used by the different authors, carefully and critically in order to rate the results reported at their true value.

Complexation of urea

The interaction between urea and some crown ethers was studied by means of the indirect procedure described above. In water, the addition of urea to a solution containing potassium chloride and a 5-fold excess of 18-crown-6 resulted in a very small increase of the observed equivalent conductance of

TABLE 8

Comparison of present and literature values of the stability constants (log K_1 and log K_2) of alkali metal salt complexes with 12-crown-4, 15-crown-5 and benzo-15-crown-5 in methanol at 298 K

Crown	Li		Na			K			Rb			Cs		
	K_1	Ref.	K_1	K_2	Ref.	K_1	K_2	Ref.	K_1	K_2	Ref.	K_1	K_2	Ref.
12C4	<0	TW[a]	2.0	1.7	TW	1.7	0.9	TW	1.6	0.9	TW	1.6	0.8	TW
	<1	26	1.7	—	35	1.74	—	35						
	~0[b]	34	1.47	2.28	24	1.59	0.56	24						
			2.1	1.7	26	1.7	0.7	26						
			1.41	2.20	36	1.58	0.15	36						
15C5	1.2	TW	—[c]		TW	3.4	2.6	TW	2.9	2.2	TW	2.8	1.8	TW
	1.23[b]	34	3.25		37	3.61	1.3	24				2.18		38
			3.24		35	3.59		39				1.89	1.2	40[d]
			3.14	2.4	24	3.77	2.71	38				2.62		41
			3.48		38	3.63	2.45	42[e]						
			3.39		43[d]	3.86	2.21	43[d]						
			3.30		41	3.35	2.65	41						
			3.30	1.44	36	3.1	2.9	48						
			3.27		44	3.34	2.21	36						
			3.31		45	3.34		45						
			3.43	2.40	46	3.43		44						
			3.42	2.77	46	3.85	2.48	46	4.07	2.47	46	3.58	2.53	46
B15C5	—[c]	TW	2.9	2.1	TW	3.0	3.2	TW	2.7	2.7	TW	2.2	1.4	TW
	1.23	43[d]	3.38		43[d]	2.90	2.75	43[d]				1.91		47
			3.05		48	2.8	3.15	48				2.03		49
			2.97		3				2.90	2.45	3			
			3.37		47									
			2.87		50									
			3.12		51									
			3.03	2.42	46	3.93	2.57	46	3.97	2.55	46	3.52	2.68	46

[a]This work. [b]Temperature = 300 K. [c]Not determined (no change in conductance was observed). [d]Found by differential vapour-pressure osmometry. [e]Found by a polarographic method.

TABLE 9

Comparison of present and literature values of the stability constants (log K_1 and log K_2) of alkali metal salt complexes with 15-crown-5 and benzo-15-crown-5 in methanol/water (7:3) at 298 K

Crown	Li	Na	K		Rb		Cs		Ref.
	K_1	K_1	K_1	K_2	K_1	K_2	K_1	K_2	
15C5	1.0	2.3	2.8	2.0	2.8	1.9	2.3	1.4	This work
		2.21—2.65							37
B15C5	0.4	2.0	2.0	2.4	1.8	2.4	1.6	1.1	This work
		1.99	1.5	2.65	1.8	1.97	1.70		52

the solution. This can be explained by the interaction between urea and the crown ether, because addition of urea to a solution containing only the potassium salt did not have any effect on the conductance. The change in the conductance value observed in the presence of the crown ether, however, was too small to calculate the stability constant of the crown ether/urea complex.

In methanol, no change in conductance was observed upon addition of urea when the sodium/benzo-15-crown-5 couple was used as the indicator system, indicating that the interaction between urea and this crown ether is absent or very weak. For 18-crown-6 and dibenzo-24-crown-8, the difference between the equivalent conductivities of the free metal salt and its 1:1 complex with the crown ether was too small to be used for the indirect procedure. Therefore, it was decided to look for an alternative indicator compound. The guanidinium ion is a suitable species for this purpose because it can be considered as a charged analogue of the urea molecule. (Moreover, the complexation of guanidinium salts in solution has been studied by different authors [53, 54] and the crystal structure of the solid complexes of guanidinium salts with some crown ethers has been elucidated [55, 56].)

When guanidinium hydrochloride served as the indicator compound, it was possible to calculate the stability constant of the urea/18-crown-6 complex in methanol. This value was very small ($\log K = 0.4 \pm 0.1$), but in agreement with results of the polarographic experiments [1, 2]. It was not possible to study the interaction between urea and dibenzo-24-crown-8 by using the guanidinium ion as indicator; the specific conductance of a solution of the guanidium ion in methanol changed only very little on addition of the crown ether and no reproducible value of the stability constant could be calculated.

Conclusions

The conductometric study of the complexation of metal salts by crown ethers provides a suitable means for determining the stability constants of these complexes. Moreover, additional information concerning the solvation and size of the free and complex species in solution can be obtained from the equivalent conductivities of the species involved.

In principle, it is possible to study the interaction between crown ethers and uncharged compounds by means of an indirect procedure. For this purpose, the availability of a suitable indicator system is a major prerequisite.

REFERENCES

1 D. Ph. Zollinger, Ph.D. Thesis, Twente University of Technology, Enschede, The Netherlands, 1986.
2 D. Ph. Zollinger, M. Bos, A. M. W. van Veen-Blaauw and W. E. van der Linden, Anal. Chim. Acta, 161 (1984) 83.
3 D. Ph. Zollinger, M. Bos, A. M. W. van Veen-Blaauw and W. E. van der Linden, Anal. Chim. Acta, 167 (1985) 89.

4 L. Onsager, Phys. Zeit., 28 (1927) 277.
5 R. M. Fuoss and R. M. Jarret, J. Phys. Chem., 89 (1985) 3167.
6 G. S. Kell and A. R. Gordon, J. Am. Chem. Soc., 81 (1959) 3207.
7 E. Shchori, J. Jagur-Grodzinski, Z. Luz and M. Shporer, J. Am. Chem. Soc., 29 (1971) 7133.
8 D. F. Evans, S. L. Wellington, J. A. Nadis and E. L. Cussler, J. Sol. Chem., 1 (1972) 499.
9 R. Ungaro, B. El Haj and J. Smid, J. Am. Chem. Soc., 98 (1976) 5198.
10 K. Ono, K. H. Konami and K. Murakami, J. Phys. Chem., 83 (1979) 2665.
11 Y. Takeda, Bull. Chem. Soc. Jpn., 53 (1980) 1720; 54 (1981) 3133; 56 (1983), 866, 3600; 58 (1985) 1259, 1315.
12 Y. Takeda, H. Yano, M. Ishibashi and H. Isozumi, Bull. Chem. Soc. Jpn., 53 (1980) 72.
13 Y. Takeda, Bull. Chem. Soc. Jpn., 55 (1982) 2040.
14 H. Awano, K. Ono and K. Murakami, Bull. Chem. Soc. Jpn., 56 (1983) 1715.
15 N. Morel-Desrosiers, N. and J.-P. Morel, Nouv. J. Chim., 8 (1984) 269.
16 Y. Takeda, Y. Ohyagi and S. Akabori, Bull. Chem. Soc. Jpn., 57 (1984) 3381.
17 M. S. Caceci and W. P. Cacheris, Byte, 9 (1984) 340.
18 A. Gustavsson and J.-E. Sundkvist, Anal. Chim. Acta, 167 (1984) 1.
19 D. Betteridge, A. P. Wade and A. G. Howard, Talanta, 32 (1985) 709, 723.
20 H. S. Gold and M. R. Rice, Talanta, 29 (1980) 637.
21 H. K. Frensdorff, J. Am. Chem. Soc., 93 (1971) 600.
22 R. M. Izatt, R. E. Terry, B. L. Haymore, L. D. Hansen, N. K. Dalley, A. G. Avondet and J. J. Christensen, J. Am. Chem. Soc., 98 (1976) 7620.
23 J. D. Lamb, R. M. Izatt, C. S. Swain and J. J. Christensen, J. Am. Chem. Soc., 102 (1980) 475.
24 G. Michaux and J. Reisse, J. Am. Chem. Soc., 104 (1982) 6895.
25 G. W. Gokel, D. M. Goli, C. Minganti and L. Echegoyen, J. Am. Chem. Soc., 105 (1983) 6786.
26 E. Amble and E. Amble, Polyhedron, 2 (1983) 1083.
27 R. Ungaro, B. El Haj and J. Smid, J. Am. Chem. Soc., 98 (1976) 5198.
28 M. Della Monica, A. Ceglie and A. Agostiano, Electrochim. Acta, 28 (1983) 529.
29 H. Richman, Y. Harada, E. M. Eyring and S. Petrucci, J. Phys. Chem., 89 (1985) 2373.
30 E. Weber and F. Voegtle, Top. Curr. Chem., 98 (1981) 1.
31 K. Venkatasubramanian, K. Joshi, N. S. Poonia, W. R. Montfort, S. R. Ernst and M. L. Hackert, J. Inclusion Phenom., 3 (1985) 453.
32 D. G. Parsons, M. R. Truter and J. N. Wingfield, Inorg. Chim. Acta, 14 (1975) 45.
33 H. S. Harned and B. B. Owen, The Physical Chemistry of Electrolyte Solutions, 3rd. edn., Reinhold, New York, 1958, p. 283.
34 A. J. Smetana and A. I. Popov, J. Sol. Chem., 9 (1980) 183.
35 G. W. Gokel, D. M. Goli, C. Minganti and L. Echegoyen, J. Am. Chem. Soc., 105 (1983) 6786.
36 T. Miyazaki, S. Yanagida, A. Itoh and M. Okahara, Bull. Chem. Soc. Jpn., 55 (1982) 2005.
37 D. M. Dishong and G. W. Gokel, J. Org. Chem., 47 (1982) 147.
38 J. D. Lamb, R. M. Izatt, S. W. Swain and J. J. Christensen, J. Am. Chem. Soc., 102 (1980) 475.
39 R. M. Izatt, N. . E. Izatt, B. E. Rossiter, J. J. Christensen and B. L. Haymore, Science, 199 (1978) 994.
40 B. Jebbink, D. Ph. Zollinger and M. Bos, unpublished results.
41 R. B. Davidson, R. M. Izatt, J. J. Christensen, R. A. Schultz, D. M. Dishong and G. W. Gokel, J. Org. Chem., 49 (1984) 5080.
42 D. Ph. Zollinger, A. M. W. van Veen, M. Bos and W. E. van der Linden, unpublished results.

43 R. Nijland, D. Ph. Zollinger and M. Bos, Unpublished results.
44 Y. Nakatsuji, T. Nakamura and M. Okahara, Chem. Lett., (1982) 1207.
45 I. Ikeda, H. Emura, S. Yamamura and M. Okahara, J. Org. Chem., 47 (1982) 5150.
46 H.-J. Buschmann, Chem. Ber., 118 (1985) 2746.
47 G.-H. Luo, M.-C. Shen, X.-M. Zhuge, A.-B. Dai, G.-Y. Lu and H.-W. Hu, Acta Chim. Sin., 41 (1983) 877.
48 D. G. Parsons, M. R. Truter and J. N. Wingfield, Inorg. Chim. Acta, 47 (1980) 81.
49 Y. Takeda, Bull. Chem. Soc. Jpn., 55 (1982) 2040.
50 D. E. Fenton, D. Parkin and R. F. Newton, J. Chem. Soc., Perkin Trans., (1981) 449.
51 H. Piekarski, S. Taniewska-Osinska and J. F. Biernat, Inorg. Chim. Acta, 124 (1986) 115.
52 R. M. Izatt, R. E. Terry, D. P. Nelson, Y. Chan, D. J. Eatough, J. S. Oradshaw, L. D. Hansen and J. J. Christensen, J. Am. Chem. Soc., 98 (1976) 7626.
53 J. M. Lehn, P. Vierling and R. C. Hayward, J. Chem. Soc., Chem. Commun. (1979) 296.
54 J. A. A. de Boer, J. W. H. M. Uiterwijk, J. Geevers, S. Harkema and D. N. Reinhoudt, J. Org. Chem., 48 (1983) 4821.
55 J. W. H. M. Uiterwijk, S. Harkema, D. N. Reinhoudt, K. Daasvatn, H. J. den Hertog Jr. and J. Geevers, Angew. Chem., 94 (1982) 462.
56 T. B. Stolwijk, P. D. J. Grootenhuis, P. D. van der Wal, E. J. R. Suedholter, D. N. Reinhoudt, S. Harkema, J. W. H. M. Uiterwijk and L. Kruise, J. Org. Chem., 51 (1985) 4891.

Analytica Chimica Acta, 198 (1987) 223—229
Elsevier Science Publishers B.V., Amsterdam — Printed in The Netherlands

MATHEMATICAL TREATMENT OF CONCENTRATION PROFILES AND ANODIC CURRENT OF AMPEROMETRIC MULTILAYER ENZYME ELECTRODES

THOMAS SCHULMEISTER

Central Institute for Molecular Biology, Academy of Sciences of the German Democratic Republic, Robert-Roessle-Str. 10, 1115 Berlin-Buch (German Democratic Republic)

(Received 25th August 1986)

SUMMARY

Formulae are presented for explicit solutions of partial differential equations describing the transient behaviour of concentration profiles and the anodic current in amperometric multilayer enzyme electrodes. The mathematical treatment is based on reaction/diffusion models with irreversible first-order catalytic reactions. Numerical results are presented to demonstrate the feasibility of the given formulae. The expression for the anodic current is used to fit kinetic parameters to measured current/time data.

One-layer models of enzyme electrodes have been investigated for the stationary operational mode and for kinetic measurements [1—6]. However, sensors based on composite enzyme membranes are increasingly used [7—10]. The present paper deals with a mathematical model for an amperometric product-sensitive multilayer electrode. On the basis of explicit formulae for the transient behaviour of concentration profiles in separated layers, a method is derived for describing the dynamics of multilayer arrangements. The approach is also valid for potentiometric enzyme electrodes.

THEORY

An electrode consisting of l layers with a single enzyme is considered. For each layer, it is assumed that the enzyme is homogeneously distributed and immobilized. The irreversible enzyme reactions

$$S \xrightarrow{k_i} P \quad (i = 1, \ldots l)$$

are assumed to depend linearly on the substrate concentration. If a one-dimensional diffusion model is used, the transient behaviour of substrate, S, and product, P, can be described by a system of reaction/diffusion equations:

$$\partial S_i/\partial t = D_{S_i}\partial^2 S_i/\partial r^2 - k_i S_i \tag{1}$$

$$\partial P_i/\partial t = D_{P_i}\partial^2 P_i/\partial r^2 + k_i S_i \tag{2}$$

where r is a point in the membrane ($0 \leqslant r \leqslant d_i$; $i = 1, \ldots l$) and time $t \geqslant 0$. Here, $S_i(r, t)$ and $P_i(r, t)$ denote the concentrations of substrate and product

0003-2670/87/$03.50

in the ith layer, respectively, and d_i is the thickness of this layer; the diffusion coefficients and kinetic parameters are denoted by D_{S_i}, D_{P_i} and k_i, respectively. These equations are solved for each layer with respect to local time and space variables, i.e., the corresponding solutions have to be combined to obtain formulae for the whole multilayer model.

At the layer interfaces separating two media, the solutions have to satisfy the boundary conditions

$$S_i(d_i, t) = S_{i+1}(0, t) = S_i^*(t)$$

$$P_i(d_i, t) = P_{i+1}(0, t) = P_i^*(t)$$

for $(i = 1, \ldots l - 1)$ and $t \geqslant 0$. It should be noted that the above-defined boundary functions S_i^* and P_i^* are unknown. It is assumed that the product is not present in the well-stirred bulk solution. At the start of the measurement, substrate and product are not present in the enzyme electrode layers. Therefore, the boundary and initial conditions are

$$S_1(0, t) = S_0; P_1(0, t) = 0$$

$$S_i(0, t) = S_{i-1}^*(t); P_i(0, t) = P_{i-1}^*(t) \quad (i = 2, \ldots, l) \text{ for } t > 0$$

$$S_i(d_i, t) = S_i^*(t); P_i(d_i, t) = P_i^*(t) \quad (i = 1, \ldots, l - 1)$$

$$(\partial S_l/\partial t)(d_l, t) = 0; P_l(d_l, t) = 0 \quad \text{for } t > 0$$

$$S_i(r, 0) = 0; P_i(r, 0) = 0 \quad (i = 1, \ldots, l) \text{ for } 0 \leqslant r \leqslant d_i$$

where S_0 stands for the bulk concentration of the substrate.

Conversion of mass at the layer interfaces requires

$$D_{S_i}(\partial S_i/\partial t)(d_i, t) = D_{S_{i+1}}(\partial S_{i+1}/\partial t)(0, t) \tag{3}$$

$$D_{P_i}(\partial P_i/\partial t)(d_i, t) = D_{P_{i+1}}(\partial P_{i+1}/\partial t)(0, t) \quad (i = 1, \ldots, l - 1) \text{ for } t > 0 \tag{4}$$

Equations 1 and 2 cannot be solved explicitly because the boundary functions are unknown. To overcome this problem Eqns. 3 and 4 are used to calculate polygonal approximations of $S_i^*(t)$ and $P_i^*(t)$. An equidistant subdivision of the considered time interval, T_{end}, into m time steps is constructed: $T = T_{\text{end}}/m$. A grid of quantities, $S_{i,j}$ and $P_{i,j}$ which represent the approximations $S_i^b(t)$ and $P_i^b(t)$ of $S_i^*(t)$ and $P_i^*(t)$, respectively, is thus obtained. The subscript i indicates the number of the corresponding boundary function, and j stands for the number of the time step (see Fig. 1). With this approximation linear initial and boundary conditions are obtained with

$$S_{0,j} = S_0; P_{0,j} = 0 \quad (j = 0, \ldots, m)$$

$$S_{l,j} = S_{l-1,j}; P_{l,j} = 0 \quad (j = 0, \ldots, m)$$

$$S_{i,0} = 0; P_{i,0} = 0 \quad (i = 1, \ldots, l - 1)$$

The other values will be calculated as follows. Let $\tilde{S}_{i,j}(r, t)$ denote the solution of Eqn. 1 with the approximated linear initial and boundary conditions

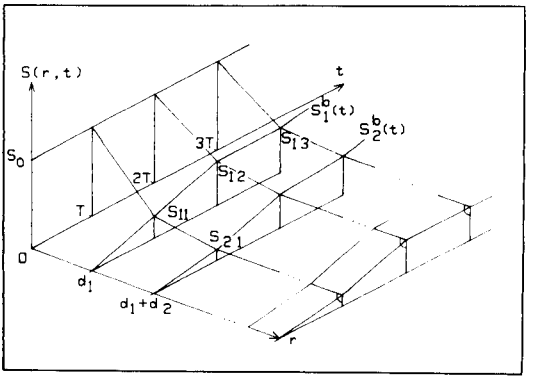

Fig. 1. Schematic diagram of the polygonal approximation of the interface functions $S_i^*(t)$ for the substrate S. The unknown values $S_{i,j}$ can be calculated successively and represent the solution of the system of partial differential equations (1). The same algorithm is used for the product P.

defined by the values $S_{i-1,j-1}$, $S_{i-1,j}$, $S_{i,j-1}$ and $S_{i,j}$. This solution $\tilde{S}_{i,j}(r, t)$ is a multilinear function with respect to the four corner values [11]. Starting from $j = 0$, i.e., with $t = 0$ in each layer, there are two known values ($j = 0$) and two unknown ones ($j = 1$). The same is valid for the product. Hence, differentiation of $S_{i,j}$ and $P_{i,j}$ with respect to r (at $r = 0$ and d_i) changes Eqns. 3 and 4 to a system of $2(l-1)$ linear equations with $2(l-1)$ variables. The solution of this system, $S_{i,1}$ and $P_{i,1}$ ($i = 1, \ldots, l-1$), yields the values for the next step, in which $S_{i,2}$ and $P_{i,2}$ ($i = 1, \ldots, l-1$), are calculated and so on. In other words, the concentration profiles have to be approximated successively for $j = 1, 2, \ldots$ because the values $S_{i,j}$, $P_{i,j}$ ($i = 1, \ldots, l-1$) of the jth time-step are needed to calculate the $(j+1)$th profiles.

The $(l-1)$ linear inhomogeneous equations which arise from Eqn. 3 can be solved separately. When the values so obtained for $S_{i,j}$ are inserted into Eqn. 4 ($i = 1, \ldots, l-1$), another system of $l-1$ linear equations is obtained, this time with respect to $P_{i,j}$ ($i = 1, \ldots, l-1$). Both systems have tridiagonal coefficient matrices and can be solved by fast Gaussian elimination [12].

The formulae $\tilde{S}_{i,j}(r, t)$ and $\tilde{P}_{i,j}(r, t)$ are given in the Appendix. There are two special cases. For the first layer and the first time-step the boundary value is $S_{0,0} = S_0$, but the initial condition requires $S_{0,0} = 0$ (cf. Fig. 1). Therefore, modified formulae are obtained for $\tilde{S}_{1,1}$ and $\tilde{P}_{1,1}$. Further, because of the no-flux boundary condition for S at the sensor, special formulae have to be derived for the solutions $\tilde{S}_{l,j}$ and $\tilde{P}_{l,j}$ ($j = 1, \ldots, m$) in the lth layer. All solutions can be obtained by using the above-cited formulae for inhomogeneous heat-conduction problems [11].

To obtain a good approximation of the considered problem, a sufficiently small value of T must be chosen. Furthermore, each layer must be subdivided

into thin sublayers (all with the same diffusion coefficients and kinetic parameters). This increases the number of layers, l, but involves only a little additional numerical work because the coefficients in the systems of linear equations do not vary within one layer. Moreover, these coefficients are identical for equidistant time-steps and have to be calculated only for the first time-step.

For fixed i, the values $S_{i,j}$ and $P_{i,j}$ represent concentration profiles at the time jT. The corresponding anodic current is

$$i(jT) = nFAD_{P_l}(P_{l-1,j}/d_l) \tag{5}$$

where n, F, A are the number of electrons involved in the electrochemical oxidation or reduction of the product, the Faraday number and the electrode surface area, respectively. It can be shown by induction that all quantities $S_{i,j}$, $P_{i,j}$ and the anodic current depend linearly on the bulk concentration value, S_0.

RESULTS AND DISCUSSION

To demonstrate the proposed approach, a multilayer model was fitted to current/time data obtained from a commercial glucose analyzer (see Table 1 [6]). The membrane arrangement used there consisted of three layers; an enzyme membrane was enclosed by two identical dialysis membranes. This three-layer model was investigated with different additional restrictions which resulted from the consideration of known electrode parameters (i.e., the known thickness of the dialysis membranes or the measured ratio of the

TABLE 1

Least-squares fits, F, of three-layer models to the current/time data reported earlier (Table 1 [6]). The thickness of the enzyme layer and the kinetic parameter are denoted by d_{enz} and k, respectively. For all layers, the calculated ratio of the diffusion coefficients of hydrogen peroxide and glucose in hydrophilic gel membranes [6] was used: $D_{H_2O_2} = 2.46\, D_{gluc}$; time-step $T = 0.1$

Model[a]	$D_{gluc,2}$ ($mm^2\ s^{-1}$)	$D_{gluc,1}$ ($mm^2\ s^{-1}$)	d_{enz} (mm)	d_{dial} (mm)	k (s^{-1})	F (nA^2)
I	1.18	1.98	0.038	0.03	6.40	2.35
II	1.30	1.30	0.022	0.029	3.29	2.40
III	1.27	1.27	0.016	0.03	3.13	2.42
IV	1.52	—	0.094	—	0.94	2.52
V	1.53	—	0.094	—	0.95	2.35

[a]Restrictions used: (I) fixed thickness of the dialysis membrane, $d_{dial} = 0.03$ mm; (II) identical diffusion coefficients of glucose in enzyme layer, $D_{gluc,2}$, and dialysis membrane, $D_{gluc,1}$; (III) restrictions (I) and (II). Comparison models: (IV) test model with identical layers of thickness $d_{dial}/150$ (i.e., $l = 150$); (V) solution of the corresponding one-layer model [6]. Note that all fits were made with assumptions on experimental parameters, not with known values.

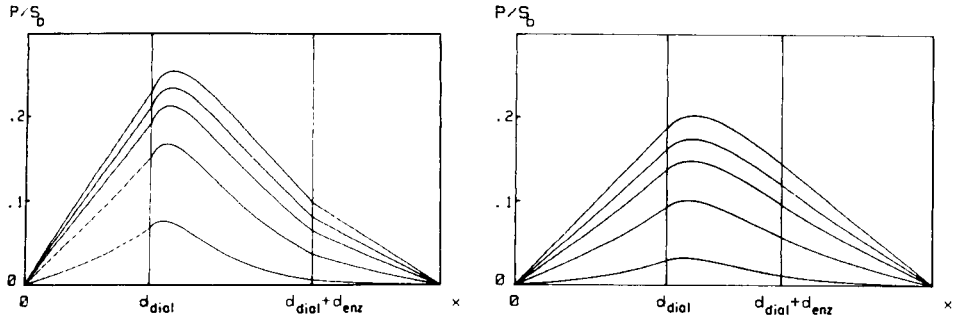

Fig. 2. Calculated concentration profiles for the product, P, in model (I) (left) and model (II) (right) of Table 1. The profiles were obtained for t = 1.5, 3, 4.5, 6 and ∞s (from below). The figures illustrate the influence of the model restrictions used.

diffusion coefficients). The results given in Table 1 show that the three-layer models yield very good fits and may be preferable to one-layer models (Fig. 2). The proposed method can be implemented on a personal computer.

The same data-fit problem was used to demonstrate the accuracy of the derived method, by comparison of a multilayer model consisting of 150 identical enzyme layers with the one-layer model reported earlier [6]. The solutions showed excellent correspondance.

The derived model generalizes the earlier one-layer approach [6]. The transient behaviour of multilayer reaction/diffusion systems, usually investigated by extensive numerical algorithms, can be calculated by using explicit formulae.

The proposed approach can be simplified to the stationary measuring principle or be extended to bi-enzyme electrodes. By changing the boundary conditions of the product at the sensor to no-flux conditions, the method might also be applied to potentiometric enzyme electrodes.

APPENDIX

The linear parabolic differential Eqn. 1 with linear initial and boundary conditions can be solved separately. When the solution is inserted into Eqn. 2, the arising inhomogeneous differential equation can be solved to obtain multilinear expressions with respect to the corner values $S_{i,j}$ and $P_{i,j}$:

$$\tilde{S}_{i,j}(r, t) = C_1 S_{i-1,j} + C_2 S_{i,j} + C_3 S_{i-1,j-1} + C_4 S_{i,j-1} \tag{A1}$$

$$\tilde{P}_{i,j}(r, t) = C_5 P_{i-1,j} + C_6 P_{i,j} + C_7 S_{i-1,j} + C_8 S_{i,j} + C_9 P_{i-1,j-1} + C_{10} P_{i,j-1} + C_{11} S_{i-1,j-1} + C_{12} S_{i,j-1} \tag{A2}$$

where

$$C_m(r, t) = L_m(r, t) + \frac{2}{\pi} \sum_{n=1}^{\infty} \{\sin [(n\pi r)/\mathrm{d}]/n\} B_q(t) \tag{A3}$$

for (q = 1, . . . 12) with

$$B_1(t) = (-tk^2 - twk - w + wM)/[T(w + k)^2]$$

$$B_3(t) = [k(k + w)(t - T) + w + (Tk^2 + Tkw - w)M]/[T(k + w)^2]$$

$$B_5(t) = -(1 - N)/Tv$$

$$B_7(t) = kw[M/(k + w)^2 - N/v^2]/\{T(v - k - w)] - kw(v + k + w)/[v^2(k + w)^2T] + kwt/Tv(k + w)\}$$

$$B_9(t) = (1 - N)/Tv$$

$$B_{11}(t) = kw[v + k + w + Tv(k + w)]/[v^2(k + w)^2T] - kwt/[Tv(k + w)] + k[Tk(k + w) - w]M/[(v - k - w)(k + w)^2T] + k[w + (w - v)Tv] \times N/[Tv^2(v - k - w)]$$

$$B_q(t) = -(-1)^n B_{q-1}(t) \quad (q = 2, 4, 6, 8, 10, 12)$$

where $w = D_S(n\pi/d)^2$, $v = D_P(n\pi/d)^2$, $M = \exp[-(k + w)t]$ and $N = \exp(-vt)$; and $L_1(r, t) = L_5(r, t) = (1 - r/d)t/T$, $L_2(r, t) = L_6(r, t) = tr/(Td)$, $L_q(r, t) = 0$ $(q = 3, 4, 7, 8, 11, 12)$, $L_9(r, t) = (1 - r/d)(1 - t/T)$, and $L_{10}(r, t) = (1 - t/T)r/d$. For convenience, the index i is omitted at D_s, D_P, k and d, respectively.

The formulae for $\tilde{S}_{1,1}$, $\tilde{P}_{1,1}$, $\tilde{S}_{l,j}$ and $\tilde{P}_{l,j}$ can be evaluated in an analogous way:

$$\tilde{S}_{1,1}(r, t) = \hat{C}_1 S_0 + \hat{C}_2 S_{11}$$

$$\tilde{P}_{1,1}(r, t) = \hat{C}_6 P_{11} + \hat{C}_7 S_0 + \hat{C}_8 S_{11}$$

with

$$\hat{B}_1 = (-k - wM)/(k + w)$$

$$\hat{B}_2 = (-1)^n[kt(k + w) + w - wM]/[T(k + w)^2]$$

$$\hat{B}_6 = (-1)^n(1 - N)/Tv$$

$$\hat{B}_7 = kw\{[1/v(k + w)] + N/[v(v - k - w)] - M/[(k + w)(v - k - w)]\}$$

$$\hat{B}_8 = (-1)^n kw\{(v + k + w)/[v^2(k + w)^2] - t/[v(k + w)] - M/[(k + w)^2(v - k - w)] + N/[v^2(v - k - w)]\}/T$$

and $\hat{L}_1 = 1 - r/d$, $\hat{L}_2 = \hat{L}_6 = \hat{L}_8 = rt(dT)$, and $\hat{L}_7 = 0$.

For the layer on the sensor side:

$$\tilde{S}_{l,j}(r, t) = \check{C}_1 S_{l-1,j} + \check{C}_3 S_{l-1,j-1}$$

$$\tilde{P}_{l,j}(r, t) = \check{C}_5 P_{l-1,j} + \check{C}_7 S_{l-1,j} + \check{C}_9 P_{l-1,j-1} + \check{C}_{11} S_{l-1,j-1}$$

with more complex terms

$$\check{C}_1(r, t) = t/T + (4/\pi) \sum_{m=0}^{\infty} \frac{\sin\left(\frac{2m + 1}{2} \pi \frac{r}{d}\right)}{2m + 1} \{[(M - 1)u - (k + u)kt]/[T(k + u)^2]\}$$

$$\check{C}_3(r, t) = 1 - t/T + \frac{4}{\pi} \sum_{m=0}^{\infty} \frac{\sin\left(\frac{2m + 1}{2} \pi \frac{r}{d}\right)}{2m + 1} \{[-u + kT(k + u)]M + [k(t - T)(k + u) + u]/[T(k + u)^2]\}$$

$$\check{C}_5(r, t) = (1 - r/d)t/T - \frac{2}{\pi} \sum_{n=1}^{\infty} \frac{\sin\left(\frac{n\pi r}{d}\right)}{n} \{(1 - N)/Tv\}$$

$$\check{C}_7(r,\,t) = \frac{2k}{\pi}\sum_{n=1}^{\infty}\sin\left(\frac{n\pi r}{d}\right)\Big\{(-1)^n\,\frac{4}{\pi}\sum_{m=0}^{\infty}\Big[\frac{(-1)^{m+1}}{(k+u)(2m+1)}\,\frac{4n}{4n^2-(2m+1)^2}$$
$$\times\,[-u((1-N)/v-(P-N)/(v-k-u))]/[T(k+u)]-[t/v-(1-N)/v^2]k/T\Big]$$
$$+\,[1-(-1)^n][t/v-(1-N)/v^2]/Tn\Big\}$$

$$\check{C}_9(r,\,t) = (1-r/d)(1-t/T)+\frac{2}{\pi}\sum_{n=1}^{\infty}\frac{\sin\left(\frac{n\pi r}{d}\right)}{n}\,[(1-\mathrm{N})/Tv]$$

$$\check{C}_{11}(r,\,t) = \frac{2k}{\pi}\sum_{n=1}^{\infty}\Big(\sin\Big)\frac{n\pi r}{d}\Big\{(-1)^n\,\frac{4}{\pi}\sum_{m=0}^{\infty}\Big[\frac{(-1)^{m+1}}{(k+u)(2m+1)}\,\frac{4n}{4n^2-(2m+1)^2}$$
$$\times\,[-k+u/T(u+k)]\,[(1-N)/v-(P-N)/(v-k-u)]+[t/v-(1-N)/v^2]k/T\Big]$$
$$+\,[1-(-1)^n]\,[(1-N)/v-[t/v-(1-N)/v^2]/Tn]\Big\}$$

with $u = D_S(2m+1)^2\pi^2/(4d^2)$ and $P = \exp\,[-(k+u)t]$.

REFERENCES

1 W. J. Blaedel, T. R. Kissel and R. C. Boguslaski, Anal. Chem., 44 (1972) 2030.
2 P. W. Carr and L. D. Bowers, Immobilized Enzymes in Analytical and Clinical Chemistry, Wiley, New York, 1980.
3 J. J. Kulys, Enzyme Microb. Technol., 3 (1981) 344.
4 M. A. Arnold and G. A. Rechnitz, Anal. Chem., 52 (1980) 977.
5 M. Cordonnier, F. Lawny, D. Chapot and D. Thomas, FEBS Lett., 59 (1975) 263.
6 Th. Schulmeister and F. Scheller, Anal. Chim. Acta, 170 (1985) 279.
7 C. Bertrand, R. R. Coulet and D. C. Gautheron, Anal. Chim. Acta, 126 (1981) 23.
8 D. Pfeiffer, F. Scheller, M. Jänchen, K. Bertermann and H. Weise, Anal. Lett., 13 (1980) 1179.
9 R. Renneberg, D. Pfeiffer, F. Scheller and M. Jänchen, Anal. Chim. Acta, 134 (1982) 359.
10 A. Bergel and M. Comtat, Anal. Chem., 56 (1984) 2904.
11 M. N. Özisik, Heat Conduction, Wiley, New York, 1980, p. 223.
12 A. A. Samarskij and E. S. Nikolaev, Metody rešenija setočnych uravnenij (in Russian), Nauka, Moskva, 1978, pp. 73—83.

Analytica Chimica Acta, 198 (1987) 231–237
Elsevier Science Publishers B.V., Amsterdam — Printed in The Netherlands

REDUCTIVE STRIPPING CHRONOPOTENTIOMETRY FOR SELENIUM IN BIOLOGICAL MATERIALS WITH A FLOW SYSTEM

H. ESKILSSON and C. HARALDSSON*

Department of Analytical and Marine Chemistry, Chalmers University of Technology and University of Gothenburg, Gothenburg S-412 96 (Sweden)

(Received 3rd October 1986)

SUMMARY

Reductive stripping chronopotentiometry in a flow system is used for determination of selenium in mussels and NBS bovine liver after acid digestion. The automated flow system contains a thin-layer cell with a mercury film electrode. In the deposition step, mercury(II) selenide is formed on the mercury film surface; the stripping step involves reduction to mercury and hydrogen selenide. This reduction is done in a separate solution of almost saturated calcium chloride, which eliminates interferences from oxygen so that solutions need not be deoxygenated. The detection limit is 0.14 $\mu g\ l^{-1}$ selenium at a deposition time of 120 s.

Several papers published in recent years [1–9] have dealt with stripping voltammetric determinations of selenium(IV) in the batch mode at a hanging mercury drop electrode (HMDE). Adeloju et al. [3] determined selenium in biological materials by differential-pulse cathodic stripping voltammetry (DPCSV) after ion-exchange separation of selenium from the acid digest; both a rotating gold disk electrode and a HMDE were used and $<1\ \mu g\ l^{-1}$ selenium could be determined. Kavel and Umland [10] developed a flow-through cell with a hanging mercury drop electrode for determination of selenium and tellurium. The supporting electrolyte is changed after the deposition step thus avoiding interferences.

The plating reaction is considered to involve reduction of selenium(IV) to mercury(II) selenide at a potential more negative than −0.05 V vs. Ag/AgCl [1–4, 11]. Stripping occurs when the potential is swept in the negative direction and the mercury(II) selenide is reduced to mercury and hydrogen selenide. Both the formation of mercury(II) selenide

$$H_2SeO_3 + 4H^+ + Hg + 4e^- \rightarrow HgSe + 3H_2O$$

and the stripping process

$$HgSe + 2H^+ + 2e^- \rightarrow H_2Se + Hg$$

are pH-dependent and favoured by an acidic medium. This is an advantage for the determination of selenium in acid-digested materials. In previously

0003-2670/87/$03.50

reported procedures, the sample had to be deoxygenated prior to voltammetry. This is time-consuming and the suggested techniques are difficult to automate. In the present work, therefore, the selenium determination was adapted to a flow system with a mercury film electrode by using an approach similar to that for the determination of nickel and cobalt by reductive stripping chronopotentiometry [12]. The automated flow technique is simple and the detection limits obtained are good enough for most studies on biological materials. An advantage of having a flow cell is that a separate solution can be used for the stripping process. This stripping solution can be designed to suit a special situation when stripping in the sample solution is unfavourable; for example, because of poor separation between metals with similar stripping potentials [13] or a need for increased sensitivity, which can be achieved by decreasing the stripping rate through a change of electrolyte [14].

EXPERIMENTAL

Electrochemical cell and flow system

The thin-layer flow cell (Fig. 1) consists of a glassy carbon electrode (2 mm diameter) pressure-fitted into a teflon cylinder. The flow channel with the working electrode is separated from the reference electrode compartment by a porous plug (zirconium dioxide) and the counter electrode is placed in the outlet flow channel. The flow channel (2 × 6 mm) is cut out in a polyethylene spacer (0.1 mm thick). The reference electrode is a Radiometer K4040 calomel electrode (SCE) and the counter electrode is a platinum tube (0.3 mm internal diameter).

The flow system consists of an Altex 401 valve with six different inlets and one outlet and a Gilson Minipuls 2 peristaltic pump which sucks solutions through the cell. A flow rate of 2 ml min^{-1} is used in all of the measurement steps.

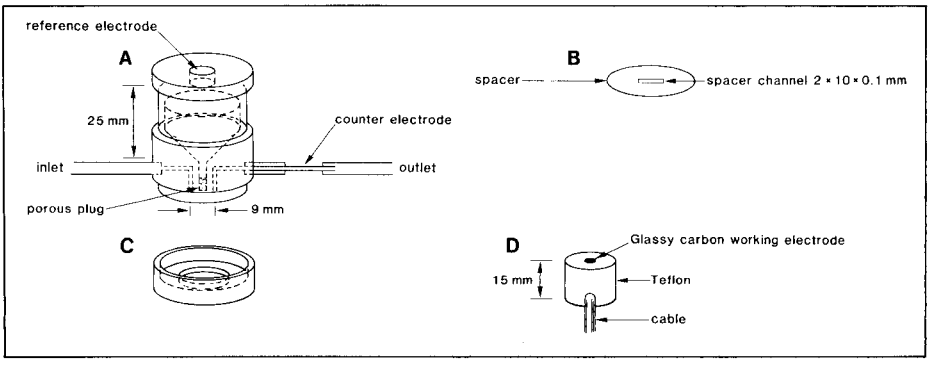

Fig. 1. Flow cell: (A) perspex reference compartment with inlet and outlet flow channels; (B) spacer; (C) perspex holder which locks the spacer in the right position and is screwed to the upper part; (d) pressure-fitted glassy carbon electrode. The cell is held together by a screw-clamp.

Instrumentation

A PDP 11/24 computer equipped with an ADF-01 interface and a DR11-C interface was used for data acquisition and to control the various measurement steps. The potential of the working electrode in the electrochemical flow cell is controlled with a potentiostat which is directed from the D/A converter on the ADF-01 interface in the computer. A constant reducing current is provided from a 4.5-V battery and a variable (1−10 MΩ) load resistance. The potentiostat counter-balances the current from the battery during the deposition period and the reducing current starts to go through the working and the counter electrodes as soon as the potentiostatic circuitry has been disconnected. The potential of the working electrode versus the SCE during the reduction is sampled with the A/D converter on the ADF-01 interface, which is buffered by an operational amplifier with a high input impedance (LF356). The data-acquisition rate can be varied between 2.5 kHz and 100 kHz. The whole measurement sequence and the Altex valve are controlled via relays with TTL signals from a DR11-C interface.

The collected potential/time data are transferred to dt/dE form and presented as a dt/dE vs. E plot (Fig. 2) in order to make the signal more easily interpreted [11].

The stripping time (size of the signal) for the selenium(IV) is evaluated, after a calculated background subtraction, from the number of potential readings between two potential boundaries defining the signal. These potentials could be preprogrammed or calculated with a peak-finding algorithm.

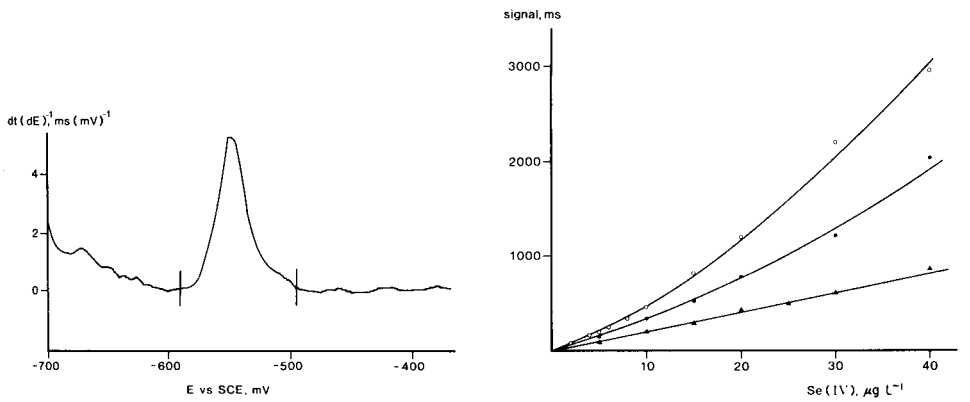

Fig. 2. Signal from the reduction of HgSe. The sample is an acid-digest of freeze-dried mussel containing 7 µg l^{-1} Se(IV). Deposition time 40 s, deposition potential −0.35 V vs. SCE, reducing current 0.8 µA, and data-acquisition rate 2.5 kHz. The size of the signal is 170 ms.

Fig. 3. Calibration graphs obtained with different deposition times: (○) 80 s; (●) 40 s; (▲) 20 s. Conditions: standard solutions in 0.5 M HCl with 1 mg l^{-1} Cu; deposition potential −0.35 V, reducing current 0.8 µA, data-acquisition rate 2.5 kHz; flow rate 2 ml min^{-1}; electrode area 3.14 mm^2.

Reagents

Standard stock solutions of mercury(II) and copper(II) (1 g l^{-1} in 0.2 M nitric acid) and selenium(IV) (1 g l^{-1} in 1 M hydrochloric acid) were prepared from Titrisol ampoules (Merck) and doubly-distilled water. Selenium(IV) standard solutions (10 and 1 mg l^{-1}) in 2 M hydrochloric acid were prepared weekly and gently boiled in a water bath before storage in stoppered glass flasks to avoid oxidation of selenium(IV) to selenium(VI). Almost saturated calcium chloride solutions (5.1 M) were prepared from calcium chloride dihydrate (Merck) dissolved in doubly-distilled water. Analytical-grade reagents were used.

Procedures

Pressurized digestion. The sample (ca. 0.2 g) of biological material (mussel tissue or bovine liver) is weighed into the teflon container of the digestion bomb (Perkin-Elmer Autoclave-3) and 10 ml of concentrated nitric acid is added. Digestion is done for 45 min at 140°C. After the vessel has cooled, 5 ml of 35% hydrogen peroxide is added and the digestion is continued at 140°C for 30 min. The cap is then removed and the mixture is evaporated at 140°C for 2—3 h, i.e., nearly to dryness. Finally, Se(VI) is reduced to Se(IV) by dissolving the residue in 10 ml of 5 M hydrochloric acid, transferring to a test tube and heating in a boiling water bath for 1 h. Before measurement, the sample is diluted 10—20 times with doubly-distilled water, after copper(II) and hydrochloric acid have been added to give final concentrations of 1 mg l^{-1} and ca. 0.5 M, respectively.

Electroanalytical determination. The operational sequence consists of five different steps controlled by the computer. A fresh mercury film is plated for each measuring cycle in a solution of 0.001 M Hg^{2+} in 3.5 M calcium chloride acidified to 0.5 M with hydrochloric acid. Starting at —0.5 V vs. SCE for 20 s, the plating potential is made more negative in steps of − 0.15 V each 20 s, ending with a potential of —0.95 V vs. SCE for 20 s before the change to sample solution. The selenite in the sample is reduced to mercury(II) selenide at —0.35 vs. SCE for 20—240 s depending on the Se(IV) concentration. The stripping of the mercury(II) selenide to form hydrogen selenide is done in a separate solution (5.1 M calcium chloride) by constant-current reduction with simultaneous recording of the mercury-film electrode potential. The change to this solution is done 15 s before the reduction starts. When the reduction of HgSe is complete, the mercury film is removed by oxidation of the mercury at 0.0 V vs. SCE in a triiodide solution (0.005 M iodine in 1 M potassium iodide) for 20 s. Rinsing is done with a 0.1 g l^{-1} sodium thiosulphate solution in 1:1 water/ethanol at 0.0 V vs. SCE for 10 s. Finally, doubly-distilled water is passed through the cell at —0.1 V vs. SCE until the next measurement. Each measurement is repeated twice and the selenium(IV) concentration is evaluated either from a standard curve or by standard additions. For the standard curve, solutions are prepared by diluting a 10 mg l^{-1} Se(IV) stock standard solution with hydrochloric acid at the same concentration as the sample and adding 1 mg l^{-1} Cu(II) to the solution.

RESULTS AND DISCUSSION

Deposition potential and electrolysis time

The deposition potentials used in cathodic stripping voltammetric determinations of selenium reported in acidic media range from −0.2 to −0.7 V vs. SCE [1—6, 8—10]. A deposition potential of −0.35 V vs. SCE was selected for this work because good sensitivity and reproducibility of the selenium signal was achieved. Less negative potentials (e.g., −0.25 to 0.0 V vs. SCE) gave less reproducible results and decreased signals. One inconvenience of using less negative potentials would be the increased risk of calomel formation on the mercury surface.

Short electrolysis times down to 20 s were preferred because of the decreased consumption of sample solution and saving of time. Electrolysis times shorter than 20 s gave less reproducible signals, and electrolysis times longer than 240 s for very low concentrations of selenium did not significantly improve the signal. In samples containing surface-active species, a short electrolysis time is preferred because there is less interference on the selenium signal from adsorption on the mercury film surface.

A fresh mercury film must be plated on the glassy carbon electrode before each new electrolysis. It was found that if the same film was used for several measurements without renewal, the size of the signal decreased after a few measurements. The reason for this was not investigated in detail, but is most likely a chemical change or damage of the film. A small increase in the signal size was seen when mercury(II) was added to the sample solution, but a complete renewal of the mercury film for each measurement cycle was found to be the best approach.

A suitable supporting electrolyte was hydrochloric acid (0.1—1 M) as reported for cathodic stripping voltammetry [2, 3]. In this electrolyte, good signals were obtained and it was also convenient to use hydrochloric acid because it is used for the prior reduction of selenium(VI) to the electroactive selenium(IV) in the sample solution.

Deoxygenation is not necessary when a separate stripping solution consisting of almost saturated calcium chloride (5.1 M) is used because the solubility of oxygen in 5.0 M $CaCl_2$ is only 18 μM at 25°C, compared with 50 μM in water. The rate of oxygen reduction at the working electrode cannot effectively compete with the reduction of HgSe on the electrode surface; this is due to the combined effect of the low oxygen solubility and the low diffusion rate of oxygen in this viscous solution. The pH of different batches of calcium chloride was found to vary from 3 to 6. If the pH of the 5.1 M calcium chloride was above 5, ascorbic acid crystals were added to make the pH about 3. This is important when very low concentrations have to be detected because a decrease of the pH of the stripping solution moves the signal to a more positive potential where it is less affected by the background signal.

Linear range and detection limit

The linear range depends on the electrolysis time. High concentrations of selenium(IV) in a sample which requires standard additions for calibration

need only short plating times in order to stay within the linear range of the plot. An increase in the slope of the standard curves is seen for increasing selenium concentrations (Fig. 3). The signal seems to increase linearly up to a point where the product of deposition time (s) and concentration ($\mu g\ l^{-1}$) equals 720 with a reducing current of 0.8 μA and with the present cell design and flow rate. Similar behaviour has been reported previously [1] although the reason for this is not clear. Addition of copper to the sample increases the signal and the linear range to some extent but the influence of copper on the signal is not as great as reported [1—3, 6, 7, 9] with the hanging mercury drop electrode.

The detection limit was estimated from measurements on a sample containing 1 $\mu g\ l^{-1}$ selenium(IV), 1 mg l^{-1} copper(II) and 0.5 M hydrochloric acid, the plating potential being —0.35 V vs. SCE for 120 s. The average signal for 17 measurements was 245 ms with a standard deviation of 35 ms. This indicates a detection limit (1 σ) of 0.14 $\mu g\ l^{-1}$ selenium(IV) at a plating time of 120 s. The total time for one measurement cycle is 245 s.

Determination of selenium in natural samples

For the determination of the selenium concentration in organic samples such as mussels and bovine liver (NBS SRM 1571), the pressurized digestion technique described above was used. The diluted digest was used directly. The results obtained for selenium in mussels were in reasonable agreement with the results obtained by atomic absorption spectrometry after hydride generation (Table 1).

Pressurized digestion was chosen for sample decomposition because some materials needed effective digestion in order to release selenium in the ionic form and to decrease possible interference from organic matter. The bomb digestion also eliminates the possibility of losing selenium during the decomposition. Normally the digested sample was diluted 10—20 times in order to decrease possible interferences from the matrix (e.g., adsorption on the mercury film).

Heavy metals present in the samples did not have any serious effect on the selenium signal. A small increase in the selenium signal was obtained by addition of copper(II). At 1 mg l^{-1} copper(II), the precision was improved and

TABLE 1

Results obtained for selenium in biological samples

Sample	Selenium(IV)[a] ($\mu g\ kg^{-1}$)	
	Proposed method	Hydride generation
Freeze-dried mussels	1870 ± 60	2040
Bovine liver[b]	980 ± 90	—

[a]Mean and standard deviation for 5 separate determinations. [b]Certified value, 1100 ± 100 $\mu g\ kg^{-1}$.

the linear range of the selenium standard addition curve was increased. The signal did not change on further addition of copper up to 6 mg l^{-1} and 1 mg l^{-1} was regarded as appropriate. A greater copper influence on the selenium signal has been reported in several papers when the determination was done by DPCSV at the HMDE. The effect of the copper addition is explained as the formation of an intermetallic compound with selenium, Cu(Hg)Se, which could change both the potential and the size of the signal [1–3, 6, 7, 9].

Conclusions

Reductive stripping chronopotentiometry with a mercury film electrode in a flow system is a possible technique for determination of selenium(IV) at low μg l^{-1} concentrations. Biological materials can be analyzed for selenium after acid digestion. The technique has no serious interferences if organic material present in the sample is decomposed. This makes it possible to use a standard curve for evaluation of the concentration. The use of a separate stripping solution eliminates the need for sample deoxygenation before the measurement.

We thank David Dyrssen and Daniel Jagner for valuable discussions. The computer system was financed by the Knut and Alice Wallenberg foundation.

REFERENCES

1 U. Baltensperger and J. Hertz, Anal. Chim. Acta, 172 (1985) 49.
2 S. B. Adeloju, A. M. Bond and H. C. Hughes, Anal. Chim. Acta, 148 (1983) 59.
3 S. B. Adeloju, A. M. Bond, M. H. Briggs and H. C. Hughes, Anal. Chem., 55 (1983) 2076.
4 Huang Bi-xia, Z. Han-chang, P. Guo-gang, Y. Fang, Z. Shen-chun and Y. Hong, Anal. Lett., 18 (1985) 279.
5 G. Jarzabek and Z. Kublik, Anal. Chim. Acta, 143 (1982) 121.
6 G. Henze, Mikrochim. Acta, Part II, (1981) 343.
7 G. P. Bound and S. Forbes, Analyst, 103 (1978) 176.
8 B. L. Dennis, J. L. Moyers and G. S. Wilson, Anal. Chem., 48 (1976) 1611.
9 G. Henze, P. Monks and G. Tölg, Fresenius' Z. Anal. Chem., 295 (1969) 1.
10 H. Kavel and F. Umland, Fresenius' Z. Anal. Chem., 316 (1983) 386.
11 G. D. Christian, E. C. Knoblock and W. C. Purdy, Anal. Chem., 35 (1963) 1129.
12 H. Eskilsson, C. Haraldsson and D. Jagner, Anal. Chim. Acta, 175 (1985) 79.
13 L. Andersson, D. Jagner and M. Josefson, Anal. Chem., 54 (1982) 1371.
14 H. Eskilsson and D. R. Turner, Anal. Chim. Acta, 161 (1984) 293.

Analytica Chimica Acta, 198 (1987) 239—244
Elsevier Science Publishers B.V., Amsterdam — Printed in The Netherlands

STUDY OF IRON AND TITANIUM COMPLEXES WITH PROPYLENEDIAMINETETRAACETIC ACID BY DIFFERENTIAL PULSE POLAROGRAPHY
Determination of Iron and Titanium in Portland Cements

L. HERNÁNDEZ*, A. ZAPARDIEL, J. A. PÉREZ-LÓPEZ and E. BERMEJO
Department of Analytical Chemistry, Autonoma University, 28049 Madrid (Spain)
(Received 30th December 1986)

SUMMARY

Differential pulse polarography is used to study the iron(III) and titanium(IV) complexes with propylenediaminetetraacetic acid (PDTA). The complexes produce reduction peaks at −0.09 V and −0.32 V (vs. Ag/AgCl/3 M KCl), respectively, at pH 4.5. This is used for a simultaneous, precise determination of iron and titanium. The detection limits in aqueous solutions were 5.0×10^{-7} M for iron and 3.0×10^{-7} M for titanium and linear calibrations were obtained in the range 4.0×10^{-6}—6.0×10^{-4} M in both cases. Correct results were obtained for iron trioxide (ca. 2%) and titanium dioxide (ca. 0.3%) in Portland cements, with relative standard deviations of about 3% and 6%, respectively.

Portland cements contain Fe_2O_3 and TiO_2, among other components, as a result of the manufacturing process. Iron trioxide, which is present in higher proportion than titanium dioxide, is widely used as a melting agent in cement manufacture; the content of Fe_2O_3 affects cement hardening and improves resistance to various aggressive agents, especially sulphates. The content of titanium dioxide, as well as other minor components, affects the water resistance and setting of the cement. In official analytical schemes, iron trioxide is determined by titration with dichromate or EDTA and titanium dioxide spectrophotometrically by formation of the complex with hydrogen peroxide [1, 2]. Recently, other spectrophotometric procedures have been used [3—5] as well as atomic absorption spectrometry [6, 7], inductively-coupled plasma emission spectrometry [8], other spectrometries [9—11] and other titrimetric methods [12, 13].

Very few polarographic methods [14] have been developed for the Fe_2O_3 and TiO_2 determinations. The aim of this study was to set up a method based on differential pulse polarography for the simultaneous determination of iron and titanium by forming complexes with PDTA.

EXPERIMENTAL

Apparatus and reagents

Polarographic curves were recorded with a Metrohm Polarecord E506 in conjunction with an E505 polarographic stand equipped with a mechanical

0003-2670/87/$03.50

drop timer. The system included a dropping mercury working electrode, an Ag/AgCl/3 M KCl reference electrode and a vitreous carbon rod as auxiliary electrode.

Unless indicated otherwise, the differential pulse mode was used with a 50 mV pulse amplitude, a 10 mV s^{-1} scan rate and a drop time of 1 s.

Solutions were deaerated by passing a slow stream of nitrogen through the cell for 10 min. The polarographic cell was maintained at 20°C.

All chemicals used were of analytical grade.

Stock titanium sulphate solution (2.50×10^{-3} M) was prepared by treating 0.2000 g of pure titanium dioxide, dried previously at 105—110°C, with 5 g of ammonium sulphate and 10 ml of concentrated sulphuric acid. The mixture was heated until titanium dioxide was totally dissolved and the solution was transferred to a 1-l calibrated flask and diluted to the mark with sulphuric acid (1 + 19).

Stock iron(III) nitrate solution (0.0985 M) was prepared by dissolving the salt in water. The solution was standardized gravimetrically as iron(III) oxide [15].

Stock disodium propylenediaminetetraacetate (PDTA) solution (0.5000 M) was prepared by dissolving propylenediaminetetraacetic acid in water and adding sodium hydroxide to pH 4.5. PDTA was synthesized by the procedure of Dwyer and Garvan [16], and then dried at 110°C so that it can be considered a pure reagent [17, 18].

Diluted standard solutions of the reagents were prepared from the stock solutions. All aqueous solutions were prepared with Milli-Q and Milli-Ro (Millipore) purified water.

Procedures

The complex formation was studied by running differential pulse polarograms of deoxygenated solutions (25 ml) containing iron(III) and titanium(IV) of various concentrations and an excess of PDTA (0.05 M).

For the determination of iron and titanium in Portland cement, 0.5000 g of the cement was accurately weighed in a clean platinum dish and 20 ml of concentrated (48%) hydrofluoric acid and 2.5 ml of concentrated sulphuric acid were added. The dish was heated on a sand bath until most of the hydrofluoric acid had evaporated, then it was allowed to cool and a further 2 ml of hydrofluoric acid was added. The dish was again heated on the sand bath until all of the hydrofluoric acid and water had evaporated. The dish was allowed to cool, the content was dissolved in sulphuric acid (1 + 19) and the solution was diluted to 500 ml. A 5-ml aliquot was taken and, after addition of 0.75 g of PDTA and sodium hydroxide to pH 4.5, was diluted with water to 25 ml. This solution was placed in the polarographic cell and deoxygenated, and the differential pulse polarogram was recorded.

The number of electrons involved was determined by the microcoulometric method described by Meites [19], in a modified cell equipped with a mercury drop electrode, a platinum point auxiliary electrode and a Ag/

AgCl/3 M KCl reference electrode. A controlled reduction potential of −0.65 V was applied to a 5×10^{-4} M titanium(IV) solution containing 0.05 M PDTA at pH 4.5.

RESULTS AND DISCUSSION

The differential pulse polarograms obtained for solutions containing iron(III), titanium(IV) and PDTA at pH 4.5 showed two well-defined reduction peaks, one at −0.09 V for the iron(III) complex and one at −0.32 V for the titanium(IV) complex (Fig. 1). The peak potentials and peak currents of these reduction peaks were found to vary with pulse amplitude, drop time and pH. The way in which drop time, temperature and concentration influenced the peak current, as well as cyclic voltammograms, showed that the current for the complexes is controlled by diffusion, which is in accordance with a previous study of the iron-PDTA complex [14].

Differential pulse polarograms of the iron(III) and titanium(IV) complexes solutions were recorded at various drop times (0.4—2.5 s), pulse amplitudes (15—110 mV) and scan rates (2—12 mV s^{-1}). Optimum values were obtained at drop time 1 s, pulse amplitude 50 mV and scan rate 10 mV s^{-1}. It was observed that the peak current was independent of scan rate whereas the peak potential shifted slightly towards more negative values as the scan rate increases. The height of the peak increased linearly with drop time and pulse amplitude up to 60 mV.

The differential pulse polarograms for the iron(III) and titanium(IV) complexes with PDTA were investigated at various pH values. Results are shown in Fig. 2 (E_p vs. pH) and Fig. 3 (i_p vs. pH). It can be seen from Fig. 3 that an increase in PDTA concentration causes an increase in the pH range where the titanium complex is stable. Thus, the peak current of the titanium-PDTA complex begins to decrease at pH > 3.5 with 2.5×10^{-3} M PDTA but at pH > 7.0 with 0.05 M PDTA. However, when the ligand concentration is increased, no results are obtained at low pH values, because of PDTA precipitation. The iron-PDTA complex is stable over a wide range of pH, and is not affected by an excess of ligand. Results cannot be obtained at pH values higher than 7 because of the proximity of the mercury oxidation wave. The variation in peak potential caused by pH changes shows that, while the peak potential remains unchanged for the iron-PDTA complex over the whole pH range tested, it decreases for the titanium-PDTA complex at pH ⩾ 3.4 according to $E_p = 0.216 - 0.120$ pH ($r = 0.9995$).

At pH 4.5, the peak separation was found to be 240 mV which is adequate for a simultaneous determination. Thus the use of PDTA as chelating agent and supporting electrolyte is adequate.

Previous studies by d.c. polarography [14] established that the iron-PDTA complex has a 1:1 stoichiometry. Studies by differential pulse polarography on 1×10^{-4} M titanium solutions containing different PDTA concentrations at pH 4.5 showed this complex also to have a 1:1 stoichiometry (Fig. 4).

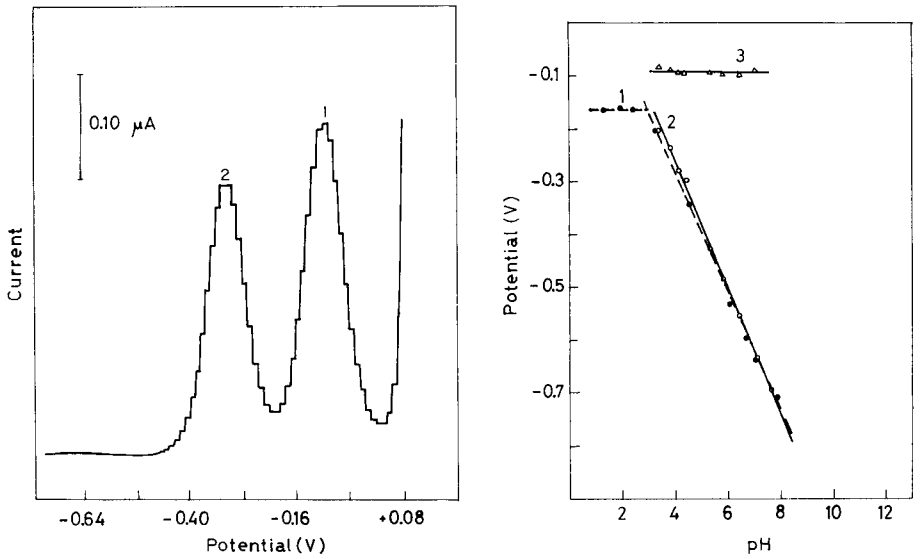

Fig. 1. Differential pulse polarogram for the iron(III) (peak 1) and titanium(IV) (peak 2) complexes with PDTA at pH 4.5. Conditions: 1.07×10^{-4} M iron(III), 1.07×10^{-4} M titanium(IV), 0.05 M PDTA; drop time 1 s, pulse amplitude 50 mV, scan rate 10 mV s^{-1}.

Fig. 2. Effect of pH on peak potentials: (1) 1.0×10^{-4} M titanium(IV), 2.5×10^{-3} M PDTA, 0.1 M KNO_3; (2) 5.0×10^{-5} M titanium(IV), 0.05 M PDTA; (3) 2.0×10^{-4} M iron(III), 0.05 M PDTA. Other conditions as in Fig. 1.

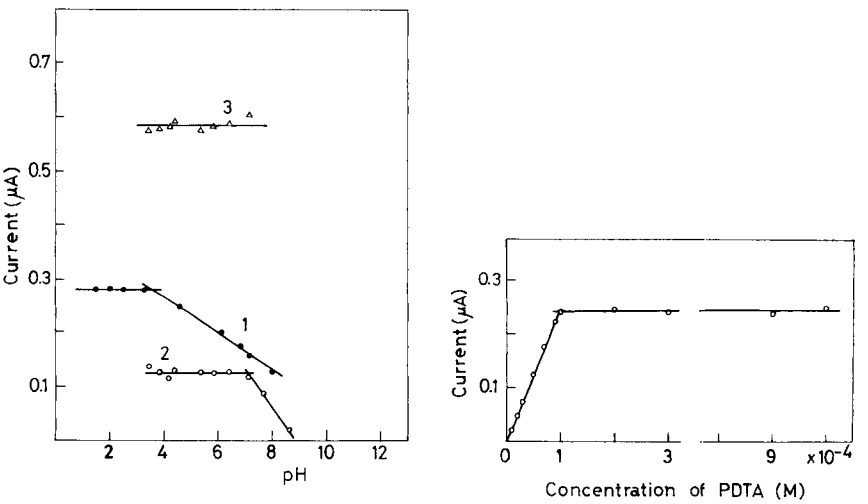

Fig. 3. Influence of pH on peak currents. Solutions and conditions as in Fig. 2.

Fig. 4. Influence of PDTA concentration on peak current in the titanium(IV)-PDTA complex for 1.0×10^{-4} M titanium(IV) at pH 4.5. Other conditions as in Fig. 1.

Results obtained for different concentrations of iron(III) and titanium-(IV) in 0.05 M PDTA indicated that for concentrations from 4.0×10^{-6} M to 6.0×10^{-4} M, the peak currents were linearly proportional to concentration:

$i_p(\mu A) = -0.001 + 2594\,C$ ($r = 0.9998$) for the iron(III)-PDTA complex

$i_p(\mu A) = 0.000 + 2393\,C$ ($r = 0.9999$) for the titanium(IV)-PDTA complex.

Results of the microcoulometric procedure at controlled potential indicated that in the electrode reduction process of the titanium-PDTA complex one electron is involved, just as for the reduction of the iron-PDTA complex [14]. The reduction of the titanium-PDTA complex was found to be reversible according to the procedure outlined by Birke et al. [20]; the peak half-width of 96 mV indicated the reversibility of the system. A similar result was obtained for the iron complex [14].

Given the reversibility of the titanium-PDTA reduction and the fact that the slope of the plot of peak potential vs. pH is -0.120 V pH^{-1}, which means that two protons are involved in the electrode process, the most likely electrode mechanism for pH $\geqslant$ 3.4 is

$$TiOL^{2-} + 2H^+ + e^- \rightleftharpoons TiL^- + H_2O$$

where L represents PDTA.

Simultaneous determination of iron and titanium in Portland cements

The most abundant components in Portland cements did not show any polarographic response within the potential range used in the electrochemical study of the iron(III)-PDTA and titanium(IV)-PDTA complexes, thus a simultaneous determination of iron and titanium was attempted for such cements. Because most ions present in the cement sample solution will form complexes with PDTA, the complexing agent has to be present in a large excess. A study of the influence of PDTA concentration on peak current values indicated that a realistic determination could be achieved by using a 25-fold excess of PDTA with respect to iron and titanium.

An ordinary calibration can be used but if the iron concentration in the cement is significantly higher than that of titanium, it is recommended to use the standard addition method for the determination of the latter.

Detection limits were 5×10^{-7} M for iron and 3.3×10^{-7} M for titanium.

Results obtained with five determinations on each sample are summarized in Table 1 and are compared with those obtained by reference methods. Comparison of the results shows the close agreement of the values obtained by the two methods; relative standard deviations were better than 3.2% for iron and 6.2% for titanium, indicating the acceptable reproducibility of the proposed method. On comparing the two mean values at the $\alpha = 0.05$ level of significance for eight degrees of freedom, no significant difference was found.

TABLE 1

Determination of iron and titanium in Portland cements

Cement	Titanium dioxide content (%)			Iron trioxide content (%)		
	Certified	Reference method [1, 2]	Proposed method[a]	Certified	Reference method [1, 2]	Proposed method[a]
BCS 372	0.33	0.31	0.31 (6.2)	2.49	2.50	2.47 (3.2)
P-450	—	0.38	0.38 (5.3)	—	2.42	2.39 (3.1)
P-450	—	0.35	0.34 (5.8)	—	1.78	1.76 (2.7)

[a]Mean with relative standard deviation (%), based on five determinations, in parentheses.

The method should be applicable to iron and titanium determinations in other materials, as long as they do not contain ions capable of producing reduction waves with peak potentials close to those of the iron and titanium complexes with PDTA.

The authors thank the Eduardo Torroja Institute in Madrid, for the provision of samples of Portland cements.

REFERENCES

1 R. C. 75, Pliego de Prescripciones Técnicas Generales para la Recepción de Cemento, Public Works Ministry, Madrid, 1975.
2 J. Calleja, J. Fernandez Pavis and F. Trivino, Método complexométrico para el análisis rápido de cemento Portland, Monografía No. 233 del Instituto Eduardo Torroja de la Construcción y del Cemento, Consejo Superior de Investigaciones Científicas, Madrid, 1963.
3 F. Salinas, J. L. Martinez-Vidal and J. Gonzalez-Parra, An. Quim., 82 (1986) 190.
4 F. Salinas, J. J. Berzas and A. Espinosa Mansilla, Bull. Soc. Chim. Belg., 94 (1985) 719.
5 P. Rodriguez, A. J. Suto and A. N. Tavares, Cem.-Hormigon, 54 (1983) 1025.
6 I. A. Voinovitch and M. Druon, Analusis, 14 (1986) 87.
7 J. Zivkovic, Cement (Zagreb), 23 (1983) 8.
8 B. Casetta and A. Giaretta, At. Spectrosc., 6 (1985) 144.
9 V. N. Maksimov, Tsement, 1 (1986) 20.
10 K. S. Harchand, R. Kumar and K. Chandra, Cem. Concr. Res., 14 (1984) 170.
11 N. A. Eissa, M. Y. Hasaan, H. A. Sallam and S. H. Salah, J. Mater. Sci. Lett., 3 (1984) 262.
12 M. E. A. Tapia and R. L. Ochoa, Bol. Soc. Quim. Peru, 49 (1983) 149.
13 H. J. Wierig and H. Winkler, Zem.-Kalk-Gips, 37 (1984) 308.
14 L. Hernàndez, A. Zapardiel, J. A. Pérez López and E. Bermejo, An. Quim., 82 (1986) 322 (and references therein).
15 F. Bermejo Martinez, Química Analítica General, Cuantitativa e Instrumental, Santiago de Compostela, Spain, 5th edn., Vol. 1, 1974, p. 278.
16 F. P. Dwyer and L. Garvan, J. Am. Chem. Soc., 81 (1959) 2855.
17 S. Vicente-Pérez, L. Hernández and J. Rosas, Studia Chemica, 5 (1974) 63.
18 S. Vicente-Pérez, L. Hernández and J. Vicente, Química e Industria, 20 (1974) 954.
19 L. Meites, Polarography Techniques, Wiley, New York, 2nd edn., 1965, pp. 138, 532.
20 R. L. Birke, M. M. Kim and M. Strassfeld, Anal. Chem., 53 (1981) 852.
21 A. J. Bard and L. R. Faulkner, Electrochemical Methods Fundamentals and Applications, Wiley, New York, 1980, p. 190.

Analytica Chimica Acta, 198 (1987) 245—257
Elsevier Science Publishers B.V., Amsterdam — Printed in The Netherlands

THE INFLUENCE OF UNCOMPENSATED SOLUTION RESISTANCE ON THE DETERMINATION OF STANDARD ELECTROCHEMICAL RATE CONSTANTS BY CYCLIC VOLTAMMETRY, AND SOME COMPARISONS WITH A.C. VOLTAMMETRY

DAVID F. MILNER and MICHAEL J. WEAVER*
Department of Chemistry, Purdue University, West Lafayette, IN 47907 (U.S.A.)
(Received 19th February 1987)

SUMMARY

A digital simulation analysis is presented of the deleterious effects of uncompensated solution resistance, R_{us}, on the evaluation of standard rate constants, k^s_{ob}, by cyclic voltammetry. The results are expressed in terms of systematic deviations of "apparent measured" rate constants, $k^s_{ob}(app)$, evaluated in the conventional manner without regard for R_{us}, from the corresponding actual values, $k^s_{ob}(true)$, as a function of R_{us} and other experimental parameters. Attention is focused on the effects of altering the electrode area and the double-layer capacitance on the extent of the deviations between $k^s_{ob}(app)$ and $k^s_{ob}(true)$, and on comparisons with corresponding simulated results obtained from phase-selective a.c. impedance data. The extent to which $k^s_{ob}(app) < k^s_{ob}(true)$ for small R_{us} values was found to be similar for the cyclic and a.c. voltammetric techniques. The latter method is, however, regarded as being preferable under most circumstances in view of the greater ease of minimising, as well as evaluating, R_{us} for a.c. impedance measurements. The influence of solution resistance on k^s_{ob} measurements with microelectrodes and without iR compensation is also considered.

In recent years cyclic voltammetry has been utilized to determine standard electrochemical rate constants, k^s, for a great number of redox couples under widely varying conditions. The rate constants have been most commonly derived from the cyclic voltammograms by using the Nicholson-Shain type of analysis [1, 2], although other methods have also been used [3—8]. Particularly given the common and sometimes indiscriminate use of cyclic voltammetry for this purpose, it is important to ascertain clearly the range of system properties and measurement conditions over which the observed rate parameters are indeed valid. This is of particular concern when relatively large rate constants must be evaluated, because the effect of even small positive amounts of uncompensated resistance, R_{us}, can easily be misinterpreted as slow electrode kinetics under these conditions [1]. In addition to the deleterious influence of solution resistance, measurement non-idealities associated with the effects of potentiostat bandwidth and double-layer charging current also need to be considered.

0003-2670/87/$03.50

Digital simulations of cyclic voltammograms of varying complexity have been performed for as long as cyclic voltammetry has been used for evaluating k^s for quasireversible systems [1, 2, 9]. These simulations have primarily been of the "idealised" form [9] in which no instrumental or electrochemical artifacts, such as those arising from R_{us}, the double-layer capacitance C_{dl}, or finite amplifier bandwidths, are considered to affect the cell response. Although significant attention has been given to the development of algorithms which account for the influence of R_{us} on the cyclic voltammograms [10, 11], surprisingly little effort has been directed towards providing analyses which enable the experimentalist readily to deduce the consequences for the reliable measurement of k^s. A significant difficulty is that the solution resistance distorts cyclic voltammograms in a manner qualitatively similar to that of sluggish electrode kinetics [1]. This can produce considerable uncertainty in evaluating the latter in the presence of the former, especially for moderate or large values of k^s ($>10^{-2}$ cm s^{-1}). While it is common to use positive-feedback compensation to minimise R_{us}, it is extremely difficult to reduce R_{us} to zero without severely distorting the potential-time ramp applied to the cell [12, 13].

Digital simulations have been used recently to examine the combined influences of uncompensated solution resistance and other measurement non-idealities on the determination of k^s by means of alternating current (a.c.) impedance techniques [14, 15]. For this purpose, it was found useful to distinguish between "apparent" observed rate constants, k^s_{ob}(app), that are obtained for a given instrument and measurement conditions by means of the conventional analysis assuming such non-idealities to be absent, and the desired actual ("true") value of the rate constant, k^s_{ob}(true). The extent of the systematic deviations between k^s_{ob}(app) and k^s_{ob}(true) was examined as a function of R_{us} and the magnitude of k^s_{ob}(true) in order to provide means by which the reliability of the k^s_{ob}(app) values could be diagnosed, and to enable the extent of the corrections to k^s_{ob}(app) arising from the presence of measurement non-idealities to be determined [14, 15].

In this paper, the results of a similar digital simulation study aimed at assessing the reliability of k^s_{ob}(app) values obtained by using cyclic voltammetry are summarised. Of particular interest is the extent to which the presence of uncompensated solution resistance provides an effective upper limit to the reliable evaluation of k^s_{ob}(true) for a given set of measurement conditions, and how this limit for cyclic voltammetry compares to that for corresponding a.c. impedance measurements. Simulation parameters are chosen to correspond to a range of conditions appropriate to typical aqueous and non-aqueous media. The effect of varying the electrode area is considered, including conditions appropriate for microelectrodes.

SIMULATION PROCEDURES

The digital simulations of cyclic voltammograms were of two types. For those instances in which the effect of C_{dl} was not considered, the method

of Nicholson [10] was used, while those for which this influence was included were finite difference simulations similar to those described by Feldberg [9].

The values of the various system parameters used in the simulations were selected to be representative of those commonly encountered for redox couples in non-aqueous solvents as well as aqueous media. The ranges of R_{us} values chosen (<50 Ω) are based on the minimum values that have generally been obtained in studies utilising common commercial potentiostats, such as the PAR 173/179 system (vide infra). The reactant (and product) diffusion coefficient was taken to be 1×10^{-5} cm^2 s^{-1}, the electrochemical transfer coefficient was assumed to be 0.5, the number of electrons transferred, n, was one, and the reactant concentration was 1 mM unless otherwise noted. The voltammetric sweep rate was set at 20 V s^{-1} unless specified otherwise.

The general procedure involved simulating cyclic voltammograms for a suitable range of system input parameters, including k^s_{ob}(true) and R_{us} values, and extracting "apparent observed" rate constants, k^s_{ob}(app), from the simulated voltammetric curves in the same fashion as is conventional for experimental data. For simplicity, this involved evaluating k^s_{ob}(app) from the difference between the cathodic and anodic peak potentials, ΔE_p in the manner prescribed by Nicholson [1].

When necessary, simulations were performed under "ideal" conditions (i.e., for R_{us}, C_{dl} = 0) to generate more complete ΔE_p data and thereby avoid any interpolation errors encountered by using data from Nicholson's Table 1 [1]. Strict adherence was also paid to the potential scan limits specified for the validity of the Nicholson relation [1].

All simulation programs were written in FORTRAN-77 and executed on a DEC LSI 11-73 microcomputer under the RSX11-M operating system.

RESULTS AND DISCUSSION

Origins of distortion of cyclic voltammograms from uncompensated solution resistance

Before examining systematically the extent to which the presence of R_{us} can lead to systematic differences between k^s_{ob}(app) as determined by cyclic voltammograms and the required k^s_{ob}(true) values, it is useful to clarify the origins of the underlying distortions in the current/potential profiles. Under most conditions, the solution resistance will be incompletely compensated by the positive-feedback circuitry so that R_{us} will be positive. The presence of R_{us} will yield a net ohmic potential drop, iR_{us}, through the solution in proportion to the current, i. Because the current peaks for the negative- and positive-going potential sweeps have opposite signs, the measured cathodic-anodic peak separation, ΔE_p, will clearly be larger for positive R_{us} than the "ideal" case, where R_{us} = 0.

An additional, less obvious, source of distortion arises from the fact that when $R_{us} \neq 0$, only the time derivative of the overall cell potential, dE_{cell}/dt,

will be held constant during the voltammetric scan, rather than the corresponding derivative of the double-layer potential, dE_{dl}/dt, as is required for the exact applicability of the usual cyclic voltammetric treatment. As a consequence, dE_{dl}/dt will vary with E_{cell} so as to distort the measured ΔE_p still further in the presence of R_{us}. This is illustrated in Fig. 1, which shows simulated i-E_{cell} and $(dE_{dl}/dt)/E_{cell}$ traces for a negative-going potential sweep, with $(dE_{cell}/dt) = 100\ V\ s^{-1} = v$ (sweep rate). The electrode area, A, is taken as 0.2 cm^2, R_{us} as 50 ohms, and C_{dl} as 20 $\mu F\ cm^{-2}$. The magnitude of dE_{dl}/dt is such that it is less negative when the current is decreasing (Fig. 1B). This "acceleration" of the effective sweep rate in the vicinity of the current peak contributes to larger ΔE_p values than in the absence of uncompensated solution resistance.

The non-faradaic current, i_{nf}, resulting from non-zero C_{dl} values will also contribute to this distortion. This is because i_{nf} enhances the total current throughout the voltammogram, and therefore enlarges ΔE_p more than when $R_{us} = 0$. This capacitive contribution to ΔE_p, $\Delta(\Delta E_p)$, can be determined approximately from $\Delta(\Delta E_p) = 2C_{dl}R_{us}v$, where v is the applied potential scan rate (dE_{cell}/dt). However, the precise influence of C_{dl} on ΔE_p will be more complex, not only because C_{dl} is usually potential-dependent, but also because the scan rate in this relation should really be identified with (dE_{dl}/dt) rather than with (dE_{cell}/dt).

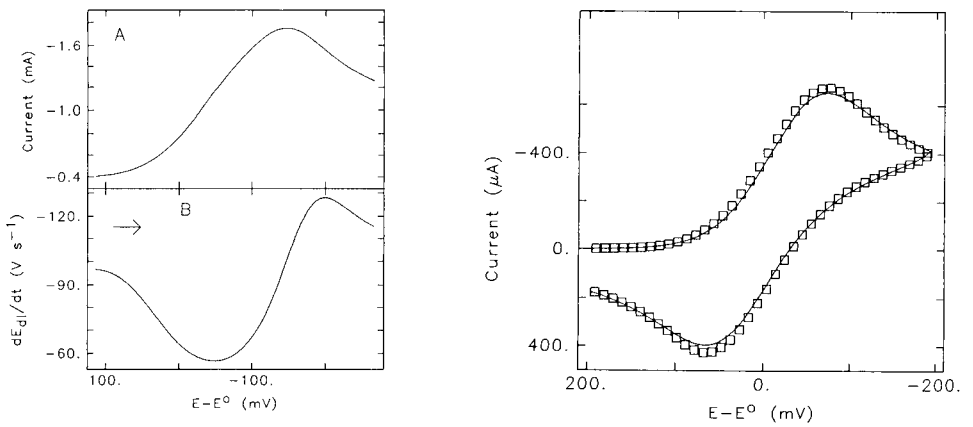

Fig. 1. Comparison between a simulated current/potential curve for a linear-sweep voltammogram (A) and the corresponding time derivative of the potential across the double layer, dE_{dl}/dt (B). Simulation conditions are: reactant concentration C_b = 1 mM; electrode area A = 0.2 cm^2, diffusion coefficient $D = 1 \times 10^{-5}\ cm\ s^{-1}$; sweep rate v = 100 $V\ s^{-1}$, uncompensated resistance R_{us} = 50 Ω, double-layer capacitance C_{dl} = 20 $\mu F\ cm^{-2}$, true standard rate constant, $k^s_{ob}(true) = \infty$.

Fig. 2. Illustrative comparison of the simulated effects of uncompensated solution resistance and finite electrode kinetics on cyclic voltammograms. Solid trace is for C_b = 1 mM, v = 20 $V\ s^{-1}$, $C_{dl} = 0$, $D = 1 \times 10^{-5}\ cm\ s^{-1}$, A = 0.2 cm^2, $R_{us} = 0$, and $k^s_{ob}(true) = 0.04\ cm\ s^{-1}$. Squares are obtained for the same conditions, but for R_{us} = 50 Ω and $k^s_{ob}(true) = \infty$.

Influence of varying the uncompensated solution resistance on the cyclic voltammetric determination of k^s_{ob}

It is well known that the presence of R_{us} can lead to large systematic errors in the determination of k^s_{ob}, because increasing R_{us} or decreasing k^s_{ob} both lead to greater ΔE_p values under a given set of experimental conditions [1]. A common procedure is to "fit" the experimental current/potential curves to corresponding simulated curves obtained for a set of input parameters and trial k^s_{ob} values until the best match is obtained, see e.g., ref. 16. Although this procedure is in a sense preferable to the examination of ΔE_p values alone, it is not always obvious that obtaining a "good fit" of the simulated to the experimental data is due to the correctness of the choice of k^s_{ob} rather than to an incorrect choice of other system variables, especially R_{us}.

The crux of the problem is that the diagnosis of ΔE_p values greater than the "reversible" limit (i.e., for $k^s_{ob} \rightarrow \infty$), $(59/n)$ mV at 25°C, as arising purely from the presence of "finite" (i.e., measurable) k^s_{ob} values rather than at least partly from $R_{us} > 0$ is far from straightforward. For example, Fig. 2 shows a pair of simulated voltammograms, the points corresponding to $k^s_{ob} = 0.04$ cm s^{-1} and $R_{us} = 0$, and the solid trace referring to $k^s_{ob} = \infty$ and $R_{us} = 50$ ohm. (The latter value is chosen here because it approximates the magnitude of R_{us} that can be anticipated in many non-aqueous media [17, 18]). The close similarity in the two curves, in addition to the almost identical ΔE_p values, clearly make the evaluation of k^s_{ob} values even as small as 0.04 cm s^{-1} fraught with difficulty unless R_{us} is known accurately, or preferably diminished substantially below 50 Ω. Although it is common to examine the dependence of ΔE_p on the sweep rate in order to evaluate k^s_{ob}, this procedure provides little or no diagnosis for the dominant presence of finite electrode kinetics rather than R_{us} because both show a similar ΔE_p-v dependence [1]. This is illustrated in Fig. 3, which shows plots of ΔE_p against v for the same conditions as in Fig. 2. The resistance-dominated and the kinetics-dominated plots are almost indistinguishable. Clearly, then, substantial systematic errors in the evaluation of k^s_{ob}, so that $k^s_{ob}(\text{app}) < k^s_{ob}(\text{true})$, can occur for analyses of this type unless R_{us} is known accurately.

In principle, a distinction between resistive dominated and kinetically-dominated ΔE_p behavior can be obtained by varying the bulk reactant concentration, C_b, while holding all other parameters fixed [17]. As shown in Fig. 4, if the sweep-rate-dependent ΔE_p is dominated by R_{us}, then ΔE_p should increase roughly linearly with C_b, whereas ΔE_p will be independent of C_b if the ΔE_p response is dominated by sluggish kinetics, at least if these are first order so that k^s_{ob} is independent of C_b. This approach, however, is often not practical. In circumstances in which either positive-feedback *iR* compensation and/or a Luggin probe is used to minimise R_{us}, it is usually very difficult to maintain precisely the same R_{us} values on successive measurements using solutions of varying reactant concentration. Moreover, the presence of non-faradaic current leads to some influence of R_{us} on ΔE_p even when $C_b \rightarrow 0$ (Fig. 4). Consequently, it is difficult to use this procedure to

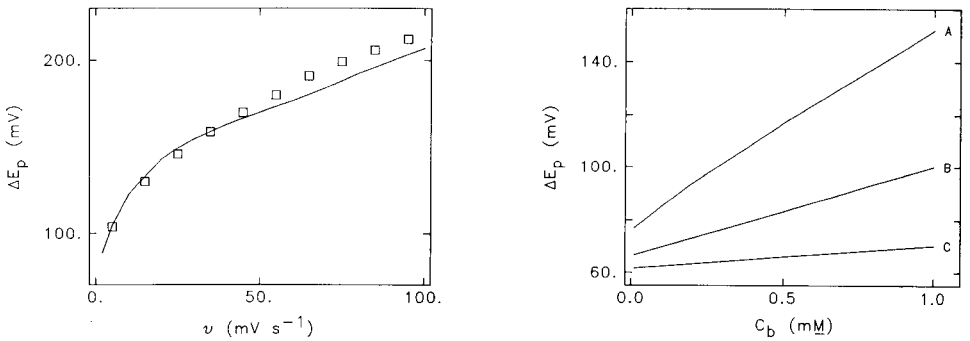

Fig. 3. Illustrative comparison of the simulated effects of uncompensated solution resistance (□) and finite electrode kinetics (—) on cyclic voltammetric potential peak separations, ΔE_p, as a function of sweep rate, v. Simulation conditions as in Fig. 2.

Fig. 4. Dependence of cyclic voltammetric peak separation, ΔE_p, on reactant concentration, C_b, in the presence of uncompensated solution resistance, R_{us}. R_{us} values (Ω): (A) 50; (B) 20; (C) 5. Other simulation conditions are: k^s_{ob}(true) = ∞, v = 20 V s^{-1}, C_{dl} = 20 μF cm^{-2}, $D = 1 \times 10^{-5}$ cm^2 s^{-1}, A = 0.2 cm^2.

diagnose the influence of R_{us} on the cyclic voltammograms except under relatively favorable circumstances.

It is therefore apparent that an accurate knowledge of R_{us} is a prerequisite for the reliable determination of k^s_{ob} by means of cyclic voltammetry. As noted above, digital simulations have previously been used to examine deviations between k^s_{ob}(true) and k^s_{ob}(app) as a function of R_{us} for a.c. impedence measurements, where k^s_{ob}(app) is determined from the conventional analysis that assumes that R_{us} = 0 [14, 15]. Such relationships enable estimates of k^s_{ob}(true) to be obtained from measured k^s_{ob}(app) values if R_{us} is known, as well as providing an upper limit to the k^s_{ob}(app) values for which meaningful kinetic information can be extracted.

Examples of such relationships obtained for cyclic voltammetry are shown in Fig. 5(a, b) in the form of plots of log k^s_{ob}(app) versus R_{us} for various k^s_{ob}(true) values (∞, 1.0 and 0.1 cm s^{-1}). The k^s_{ob}(app) values were obtained from the ΔE_p values for simulated cyclic voltammograms by using the Nicholson analysis [1] and ignoring the influence of R_{us}. Complete coincidence between these k^s_{ob}(true) values and the corresponding k^s_{ob}(app) values in these plots is only observed when R_{us} = 0. A sweep rate of 20 V s^{-1} is used in these simulations, although similar results were obtained over the range $1 \leqslant v \leqslant 100$ V s^{-1}. The remaining conditions in Fig. 5(a, b) are also identical, except that the electrode area is changed from 0.2 to 0.02 cm^2 in Fig. 5(b). Results similar to those in Fig. 5(a, b) were also obtained when a smaller C_{dl} value of 2 μF cm^{-2} was used (Fig. 5c).

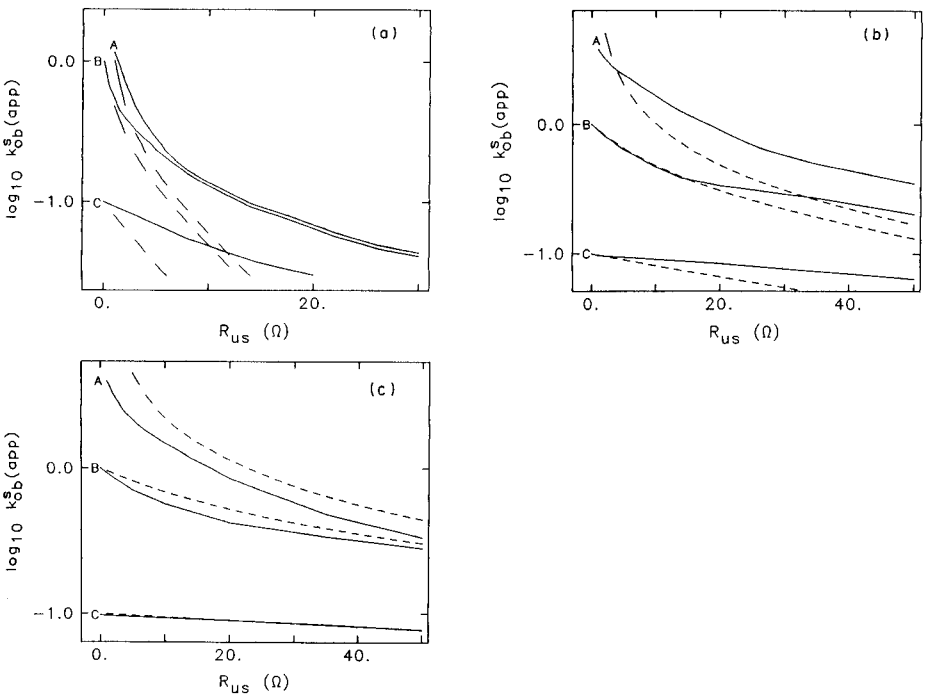

Fig. 5. (a) Plots of log k^s_{ob}(app), where k^s_{ob}(app) is the "apparent" rate constant extracted from simulated cyclic voltammograms (——) or a.c. voltammograms (— — —) assuming R_{us} = 0, against R_{us} for various values of the actual ("true") rate constant, k^s_{ob}(true). Curves A, B, and C are for k^s_{ob}(true) = ∞, 1, and 0.1 cm s^{-1}, respectively. Other simulation conditions are C_b = 1 mM, C_{dl} = 20 μF cm^{-2}, A = 0.2 cm^2, D = 1 × 10^{-5} cm^2 s^{-1}. The cyclic-voltammetric sweep rate is 20 V s^{-1}, and the a.c. impedance data are for frequencies between 100 and 500 Hz (see text for further details). (b) Plots as for (a) but with A = 0.02 cm^2. (c) Plots as for (a) but with C_{dl} = 2 μF cm^{-2}.

From Fig. 5(a) it can be seen that for an electrode area of 0.2 cm^2, a significant distinction between a completely reversible reaction [i.e., where k^s_{ob}(true) = ∞] and that for which k^s_{ob}(true) = 1 cm s^{-1} is only possible for very small R_{us} values (⩽3 Ω). In other words, the k^s_{ob}(app) values are independent of k^s_{ob}(true) under these conditions, being virtually indistinguishable for larger R_{us} (Fig. 5a), so that no meaningful kinetic data can be extracted if k^s_{ob}(true) ⩾1 cm s^{-1}. It is also evident that if R_{us} is larger than about 10 Ω, no value for k^s_{ob}(app) could be obtained that is larger than about 0.1 cm s^{-1}, a frequently reported value (e.g. [18]). Furthermore, the avoidance of substantial descrepancies between k^s_{ob}(app) and k^s_{ob}(true) when the latter approaches 1 cm s^{-1} requires that only extremely small uncompensated resistances be present. For example, in order to evaluate a k^s_{ob}(true) value of 1 cm s^{-1} to 50% accuracy [i.e. to obtain k^s_{ob}(app) > 0.5 cm s^{-1} under these conditions] it is required that R_{us} be less than 2 Ω.

Comparing Fig. 5(a) and (b) shows that decreasing the electrode area improves this unfavorable situation somewhat. Thus, for an electrode area of 0.02 cm^2 (Fig. 5b) there is a clear experimental distinction between k^s_{ob}(app) values corresponding to k^s_{ob}(true) values of ∞ and 1 cm s^{-1} (curves A and B) even for moderate R_{us} values (ca. 20 Ω), indicating that some kinetic information would be contained in experimental data gathered under these circumstances. Nevertheless, the k^s_{ob}(app) values in curve B fall markedly below k^s_{ob}(true) under these conditions, so that the corrections necessary to extract the latter from the former are still substantial. The errors involved in evaluating smaller k^s_{ob}(true) values, around 0.1 cm s^{-1}, are relatively small because then k^s_{ob}(app) $\simeq$ k^s_{ob}(true), even for $R_{us} \leqslant 40$ ohm (Fig. 5b). This diminished influence of R_{us} with decreasing electrode area is, however, slightly misleading because the effective solution resistance will increase under these conditions, yielding probable increases in R_{us}.

Comparisons with the influence of uncompensated solution resistance on rate constants determined with a.c. impedance measurements

Given that a.c. voltammetry, particularly involving phase-selective impedance measurements, provides the commonest means of evaluating k^s_{ob} other than cyclic voltammetry, it is of interest to compare quantitatively the extent to which the utility of these two techniques is impaired by the presence of uncompensated resistance. There is ample reason, however, to expect the nature and extent of the influences of R_{us} upon these two techniques to be significantly different. In the a.c. voltammetric experiment with a stationary electrode, the principal effect of R_{us} is to force the phase of the a.c. potential waveform across the double layer to differ from that applied by the potentiostat, yielding errors in the apparent phase angle of the current. While the presence of R_{us} also forces the magnitude of the a.c. potential waveform across the double layer to differ from that controlled by the potentiostat, this is of little consequence because it is generally only the phase angle, rather than the magnitude of the current which is of relevance to the evaluation of standard rate constants.

The error introduced into the evaluation of k^s_{ob} by a.c. voltammetry therefore depends principally on the combined influence of R_{us} and the double-layer capacitance, and is diminished with decreasing electrode area to the extent that the total capacitance is also decreased. The effects of R_{us} on cyclic voltammetry have distinctly different origins, as discussed above. Although the extent of the error in evaluating k^s_{ob} with cyclic voltammetry also decreases with the electrode area, this arises primarily as a result of the decreased total current flowing through the cell.

As a consequence, it was decided to compare simulated values of k^s_{ob}(app) obtained from phase-selective a.c. impedance as well as cyclic voltammetry by using conventional data analyses for the following three conditions: (1) electrode area A = 0.2 cm^2, C_{dl} = 20 μF cm^{-2}; (2) A = 0.02 cm^2, C_{dl} = 20 μF cm^{-2}; (3) A = 0.02 cm^2, C_{dl} = 2 μF cm^{-2}. The first two cases span the

range of areas commonly encountered with these two techniques, while the second and third cases cover the typical range of capacitance values. The frequency range taken for the a.c. voltammetric data was between 100 and 500 Hz, the analysis utilising the frequency-dependence of the quadrature to in-phase current ratio, I_Q/I_I (see [15] for simulation details). The resulting plots of log k^s_{ob} vs. R_{us} obtained with a.c. voltammetry for these three cases are shown as the dashed curves in Fig. 5(a—c), to be compared with the corresponding results given for cyclic voltammetry.

For the large (0.2 cm^2) electrode (Fig. 5a), the degree to which k^s_{ob}(app) falls below k^s_{ob}(true) for a given R_{us} value is more marked for a.c. voltammetry than for cyclic voltammetry. Under the specific conditions prescribed by these simulations, the degree of error induced in k^s_{ob}(app) by ignoring solution resistance effects, and therefore the extent of the corrections required to extract k^s_{ob}(true) from k^s_{ob}(app), is smaller for cyclic voltammetry than for a.c. voltammetry. However, for the smaller (0.02 cm^2) electrode having the same double-layer capacitance per unit area (20 $\mu F\ cm^{-2}$), the log k^s_{ob}(app)-R_{us} curves obtained for the two techniques are more similar (Fig. 5b). Moreover, the substitution of a smaller double-layer capacitance (Fig. 5c) yields slightly superior log k^s_{ob}(app)-R_{us} curves for a.c. compared with cyclic voltammetry.

These examples therefore suggest that roughly similar errors are introduced into cyclic and a.c. voltammetric measurements of k^s_{ob} under "typical" conditions in the presence of at least small amounts of uncompensated resistance. However, consideration of other factors clearly favor the latter technique for this purpose. Most importantly, it is crucial to minimise the value of the uncompensated resistance. This can be achieved relatively readily in the a.c. experiment because a small-amplitude waveform having relatively low frequencies ($\leqslant$2000 Hz) is used. In contrast, in the cyclic voltammetric experiment, the abrupt change in the time derivative of the potential which occurs when the scan direction changes is equivalent to the sudden injection of high-frequency "noise", which will result in a dampened oscillation ("ringing") of the current. The avoidance of severe distortion in the *i-E* profile for the return scan therefore normally requires the presence of significant uncompensated resistance (more than a few ohms).

In addition, the accurate estimation of R_{us} for a given level of electronic resistance compensation in the a.c. impedance experiment is relatively straightforward, either by evaluating the quadrature and in-phase currents at potentials well separated from the a.c. voltammetric wave or by a.c. measurements in conjunction with a dummy-cell arrangement [14, 15]. (The same procedures could, of course, be used to estimate R_{us} for a given set of experimental conditions, including the resistance compensation setting, used in a cyclic voltammetric experiment.) An alternative approach to evaluate R_{us} is to select a redox couple which under the measurement conditions used is known to exhibit k^s_{ob}(true) $\rightarrow \infty$, so that the measured response is necessarily dominated by R_{us} [19]. Although this method has obvious merits,

the selection of such a redox couple requires careful consideration [19, 20]. In our experience, using a variety of potentiostats of commercial and in-house design, it is difficult either to measure or to minimise R_{us} even for a.c. impedance measurements to much less than about 5 Ω in typical non-aqueous media. The corresponding minimum R_{us} values attainable in cyclic voltammetric experiments are often substantially larger.

Another advantage of the phase-selective impedance approach is that a distinction between apparent electrochemical irreversibility brought about by the presence of uncompensated resistance rather than by finite electrode kinetics can be made by examining the dependence of the (I_Q/I_I) ratio upon the a.c. frequency, ω [15]. If the former factor is predominant, then the slope of the (I_Q/I_I)-$\omega^{1/2}$ plot will increase with increasing ω, rather than be independent of ω as will be the case when electrode kinetics controls this response [15]. This diagnostic situation can be contrasted with the inability, noted above, to achieve a ready distinction between the dominant presence of R_{us} and finite electrode kinetics by varying the sweep rate in cyclic voltammetry.

Some considerations for microelectrodes

The virtues of using microelectrodes of especially small dimensions, having radii down to (or below) 1 μm for electrochemical measurements have recently been explored extensively, including preliminary applications to electrode kinetics [21—24]. An advantage of such small electrode areas is that the faradaic current decreases with the square of the electrode radius whereas the effective solution resistance only increases in inverse proportion to the radius [21]. Clearly, then, in the absence of iR compensation, the deleterious influence of solution resistance will be dramatically reduced by using microelectrodes rather than conventional electrodes. This advantage is, however, offset somewhat by the iR compensation that is much more readily applied with larger electrodes.

Figure 6 shows illustrative plots of log k^s_{ob}(app) versus log k^s_{ob}(true) obtained from simulated cyclic voltammograms for several conditions that are typically encountered with microelectrodes. A sweep rate of 1000 V s^{-1} was chosen because similar values are typically used with microelectrodes and it is sufficiently rapid to avoid influences from spherical diffusion even at the small electrodes considered here. For the 1-μm electrode, the R_{us} values of 1×10^5, 7×10^5, and 4×10^6 Ω correspond to solution-specific resistances, ρ, of 20, 140, and 800 Ω cm, respectively, obtained from the relation [25] $R_s = \rho/4r$ where r is the radius of a disk electrode, because in the absence of iR compensation, R_{us} will equal the solution resistance, R_s. These values were chosen because they are appropriate for concentrated aqueous electrolytes [26] and for 0.1 M electrolytes in acetonitrile and dichloroethane, respectively [18]. While there is reasonable agreement between k^s_{ob}(app) and k^s_{ob}(true) for curves A and B, at least up to $k^s_{ob} \approx 10$ cm s^{-1}, indicating the virtual absence of R_{us} effects up to this point, for curve

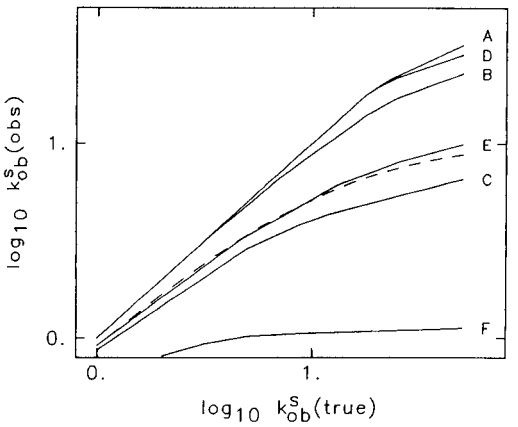

Fig. 6. Illustrative relationships between k^s_{ob}(app) and k^s_{ob}(true) for some typical conditions encountered in cyclic voltammetry with microelectrodes. Curves A—C and D—F are for 1.0- and 5-μm diameter electrodes, respectively. Solution resistance (Ω) conditions: (A) $R_{us} = 10^5$ (ρ = 20 Ω cm); (B) $R_{us} = 7 \times 10^5$ (ρ = 140 Ω cm); (C) $R_{us} = 4 \times 10^6$ (ρ = 800 Ω cm); (D) $R_{us} = 2 \times 10^4$ (ρ = 20 Ω cm); (E) $R_{us} = 10^5$ (ρ = 140 Ω cm); (F) $R_{us} = 7 \times 10^5$ (ρ = 800 Ω cm). Other simulation conditions: C_b = 1 mM, υ = 1000 V s^{-1}, C_{dl} = 20 μF cm^{-2}, $D = 1 \times 10^{-5}$ cm^2 s^{-1}. The dashed curve is from a simulation corresponding to curve E, but obtained for a.c. impedance data (a.c. frequencies of 100—500 Hz).

C substantial deviations are observed even for markedly smaller rate constants. This illustrates the need to consider resistive effects in the evaluation of large k^s_{ob} values even with extremely small microelectrodes when electrolytes with relatively high resistance are used.

When a 5-μm diameter microelectrode, such as is frequently applied in cyclic voltammetric experiments [21—24], was used under the same conditions as the 1-μm diameter electrode, reasonable concordance between k^s_{ob}(app) and k^s_{ob}(true) was obtained for $k^s_{ob} \leqslant 10$ cm s^{-1} in the least resistive media (curve D). However, the results obtained for conditions corresponding to typical non-aqueous media (curves E and F) are substantially inferior. Indeed, curve F (5-μm electrode in dichloroethane) shows that k^s_{ob}(app) $\ll k^s_{ob}$(true) at least for k^s_{ob}(true) > 1 cm s^{-1}; i.e., the ΔE_p values are determined almost entirely by solution resistance effects under these conditions.

Figure 6 also contains a comparative log k^s_{ob}(app)-log k^s_{ob}(true) trace obtained for the conditions of curve E, but with a.c. rather than cyclic voltammetry in the fashion described above. As for the behavior noted above for the larger electrodes, the influence of solution resistance on the a.c. and cyclic voltammetric response is similar. Similar behavior for these two techniques was also obtained for the other conditions considered in Fig. 6.

Conclusions

The foregoing considerations demonstrate that the deleterious influence of uncompensated solution resistance imposes a severe and sometimes

unexpected limitation on the magnitude of standard rate constants that can be evaluated by means of cyclic voltammetry. In order to extract meaningful k^s_{ob} values from this technique, it is clearly imperative to obtain reliable estimates of R_{us} for the measurement conditions used, and to demonstrate that R_{us} is sufficiently small so that k^s_{ob}(app) approximates k^s_{ob}(true). The observation of k^s_{ob}(app) values that approach the limiting value dictated by the known uncompensated resistance (i.e., those corresponding to k^s_{ob}(true) $\rightarrow \infty$) provides a clear signal that the desired electrode kinetics are not measurable under the conditions used. Given a reliable knowledge of R_{us}, desired k^s_{ob}(true) values can still be evaluated in the intermediate case of partial kinetic-resistive control from the k^s_{ob}(app) values by using the appropriate k^s_{ob}(app)-k^s_{ob}(true) relation extracted from digital simulations.

Although the extent of the systematic errors in k^s_{ob}(app) values obtained by cyclic and a.c. voltammetry are surprisingly similar for typical R_{us} values, the latter technique would seem to exhibit clear advantages for the evaluation of fast electrode kinetics under most conditions. This stems both from the ability to minimise and evaluate R_{us} better with a.c. impedance measurements, and from the diagnosis of dominant resistive effects from the observation of nonlinear (I_Q/I_I) vs. $\omega^{1/2}$ plots.

As has already been well documented [21—24], the use of cyclic voltammetry with microelectrodes offers real advantages for evaluating standard rate constants. However, even under these conditions, the influence of cell resistance can provide a serious impediment to the evaluation of k^s_{ob} values greatly in excess of 1 cm s^{-1}, especially for high-resistance media and in the absence of iR compensation. It therefore would appear that k^s_{ob} values evaluated by any of these approaches, expecially for moderately fast reactions ($k^s_{ob} \geqslant 0.1$ cm s^{-1}) should be regarded with some skepticism in the absence of due consideration of solution resistance effects.

This work was supported by the Office of Naval Research.

REFERENCES

1 R. S. Nicholson, Anal. Chem., 37 (1965) 1351.
2 R. S. Nicholson and I. Shain, Anal. Chem., 36 (1964) 706.
3 J. M. Saveant and D. Tessier, J. Electroanal. Chem., 65 (1975) 57.
4 J. M. Saveant and D. Tessier, J. Electroanal. Chem., 77 (1977) 225.
5 K. B. Oldham, J. Electroanal. Chem., 72 (1976) 371.
6 P. E. Whitson, H. W. VandenBorn and D. H. Evans, Anal. Chem., 45 (1973) 1298.
7 B. Aalstad and V. D. Parker, J. Electroanal. Chem., 122 (1981) 183.
8 B. Speiser, Anal. Chem., 57 (1985) 1390.
9 S. W. Feldberg, in A. J. Bard (Ed.), Electroanalytical Chemistry — A Series of Advances, Vol. 3, M. Dekker, New York, 1969, p. 199.
10 R. S. Nicholson, Anal. Chem., 37 (1965) 667.
11 W. T. DeVries and E. Van Dalen, J. Electroanal. Chem., 10 (1965) 183.
12 D. Garreau and J.-M. Saveant, J. Electroanal. Chem., 86 (1978) 63.
13 D. F. Milner, Ph.D. thesis, Purdue University, 1987.
14 D. F. Milner and M. J. Weaver, J. Electroanal. Chem., 222 (1987) 21.

15 D. F. Milner and M. J. Weaver, J. Electroanal. Chem., 191 (1985) 411.
16 D. A. Corrigan and D. H. Evans, J. Electroanal. Chem., 106 (1980) 287.
17 V. D. Parker in A. J. Bard (Ed.), Electroanalytical Chemistry — A Series of Advances, Vol. 14, M. Dekker, New York, 1986, p. 1.
18 K. M. Kadish, J. Q. Ding and T. Malinski, Anal. Chem., 56 (1984) 1741.
19 T. Gennett and M. J. Weaver, Anal. Chem., 56 (1984) 1444.
20 G. E. McManis, M. N. Golovin and M. J. Weaver, J. Phys. Chem., 90 (1986) 6563.
21 J. O. Howell and R. M. Wightman, Anal. Chem., 56 (1984) 524.
22 J. O. Howell and R. M. Wightman, J. Phys. Chem., 88 (1984) 3915.
23 M. I. Montenegro and D. Pletcher, J. Electroanal. Chem., 200 (1986) 371.
24 A. M. Bond, T. L. E. Henderson and W. Thormann, J. Phys. Chem., 90 (1986) 2911.
25 J. Newman, J. Electrochem. Soc., 113 (1966) 501.
26 J. F. Chambers, J. Phys. Chem., 62 (1958) 1136.

Analytica Chimica Acta, 198 (1987) 259—269
Elsevier Science Publishers B.V., Amsterdam — Printed in The Netherlands

DYNAMIC POLARIZATION OF LIPID BILAYERS AS A SPECIAL CASE IN THE ELECTROCHEMISTRY OF LIQUID/LIQUID INTERFACES

CHRISTOPHER J. BENDER and H. T. TIEN*

Department of Physiology (Giltner Hall), Michigan State University, East Lansing, MI 48824-1101 (U.S.A.)

(Received 15th December 1986)

SUMMARY

Dynamically obtained current/voltage curves of bilayer lipid membranes partitioning a solution of lipophilic ions are compared with the results of the type expected in a voltammetry experiment involving ionic transport across a liquid/liquid interface. Lipophilic ions yielding "voltammograms" analogous to reversible and irreversible voltammograms (in conventional electrochemical systems) are reported. Also reported are examples of ions which yield what may be analogous to a masked response, a phenomenon known in the literature of liquid/liquid interfaces. Although the behavior of the two systems is similar, there exist differences in the interpretation of the voltammograms and suggestions are offered for an energetic and mechanistic interpretation of the membrane voltammogram.

In many electrophysiological systems, the membrane constitutes a partition between two aqueous electrolyte phases and may act as a conduit for the passage of charge (i.e., ions, although conceivably electronic transport is possible in some situations) from one aqueous phase to the other. In this regard the electrochemical cell, defined by the membrane, bathing electrolyte solutions, and measuring electrodes (cf. Fig. 1), is similar to an electrochemical cell defined by the interface between two immiscible electrolyte solutions. These latter systems have been the subject of numerous investigations which have been reviewed in their own right [1, 2]. The focus of the electrochemistry of the interface between immiscible solutions (often called ITIES systems in the electrochemistry literature) is the transfer of charge across the interfacial boundary; a process which is very much akin to the usual electronic charge transfer process of the metal/electrolyte interface, with the exception that ions are the mobile charge carrier of ITIES electrochemical cells.

Because an ion must cross a region defined by the bilayer lipid membrane (BLM) when current appears, there is an analogy between the membrane cell and the ITIES cell. It might therefore be expected that a cell as described in Fig. 1 might be amenable to the methods of study used to characterize the interface between two immiscible electrolyte solutions. Many aspects of the considerations necessary when examining the electroanalytical chemistry of

0003-2670/87/$03.50

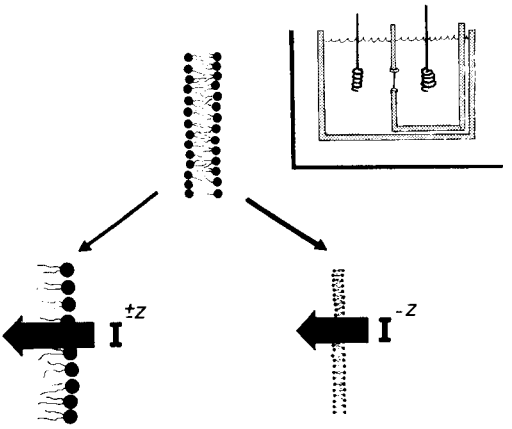

Fig. 1. The membrane-divided electrochemical cell and its representation as a liquid/liquid charge-transfer process, showing microscopic-ion transport into the organic membrane phase and microscopic-ion transport into the separated aqueous phase.

membranes have already been treated extensively [3—5], therefore this paper concerns the application of only one technique, namely voltammetry, to the study of charge transport across membranes.

Cyclic voltammetry is a method very well suited to the study of charge transfer in ITIES systems. The basic experiment consists of modulating an imposed potential in a controlled (usually linear) fashion, and recording the current response which is indicative of thermodynamic (i.e. energetic and kinetic) properties of the charge-transfer process [1, 6, 7]. Liberman and Topaly [8] performed an experiment involving the dynamic polarization of a membrane, and only minimal theoretical consideration [9] has been concerned with the results and its implications concerning ion transport. More recently, cyclic voltammetry has been applied [4, 5] to the system of modified bilayers in an effort to examine electronically conducting BLMs. In this paper the cyclic voltammetry of an electrochemical cell defined by a bilayer lipid membrane which partitions electrolyte solutions containing lipophilic ions is considered, and the results are examined as a possible extension of the generalized study of immiscible electrolyte solutions.

EXPERIMENTAL

The apparatus is modeled after a very simple two-electrode system and is composed of a triangular waveform generator which controls the potentials at all vertices of the potential sweeps and the polarization rate (accurate within a range 10—10 000 mV s^{-1}). The measuring circuit consists of a high-impedance electrometer in parallel with the cell and a picoammeter in series with the cell. The cell was enclosed in a Faraday cage and noise generated by external sources (r.f. and line) was typically less than 1 pA, whereas internal noise was generally of the order of 1 pA.

Calomel electrodes were used in a membrane chamber/cell originally described by Tien [4]. These cells suffer from the disadvantage that they may be polarized when made to carry significant currents (approx. 1 μA), therefore care was taken to ensure that current flow was kept well below this selected upper bound. This condition was readily achieved by moderating the concentrations of lipophilic ions.

Tetraphenylborate (TPB) (Aldrich Gold Label; sodium salt) was used as a representative lipophilic anion without further purification. Tetrabutylammonium tetraphenylborate was prepared by a co-precipitation of tetraphenylboron sodium and tetrabutylammoniumchloride from doubly distilled water. Other lipophilic ions were chosen for their tendency to adhere to the membrane surface, i.e., Gentian violet and Janus green B (Chem Service), as well as cross the membrane. These latter dyes were of interest because it was hoped that by interaction with the membrane, an irreversible (in the Nernstian sense) charge-transfer process could be observed [10]. The supporting electrolyte solution was 0.1 M KCl/20 mM 4-morpholineethanesulfonic acid (MES) or 2-[tris(hydroxymethyl)-methylamino]-1-ethanesulfonic acid (TES) buffer (Sigma) adjusted to pH 5.5 or 7.5, respectively. Stirring with magnetic bars in each chamber was interrupted during the voltammetric experiment (i.e., while applying potential). The membranes were formed by injecting a lecithin solution (24 mg of lecithin per ml of 3:1 dodecane/butanol) on to the hydrophobic support.

RESULTS AND DISCUSSION

Voltammetric response

A cyclic voltammogram obtained as a function of applied transmembrane potential is illustrated in Fig. 2 for the tetraphenylborate anion. It was found that when the midpoint potential of the voltammogram (i.e., the midpoint between the peaks obtained on the forward and reverse scans) was evaluated, the open-circuit potential was invariably the result obtained. This result is to be expected if one is correct in assuming that the process of ion transfer is associated with an equilibrium $C_i \rightleftharpoons C_o$ across the membrane, where the subscripts i and o refer to the arbitrary designation of inner and outer chambers, respectively. Therefore, if C denotes the concentration of ion in a given chamber, the open-circuit potential is of the magnitude $RT/nF \ln (C_o/C_i)$, and would correspond to that potential where the current equals zero. On this basis, one can define a membrane overpotential, η_m, as the difference between the applied potential and the open-circuit potential as determined by the ratio of ion concentrations in the inner and outer chambers:

$$\eta_m = V_{appl} - (RT/nF) \ln (C_o/C_i) \quad (1)$$

This definition immediately permits one to make an analogy between the membrane electrochemical cell and electrode cells as regards equilibrium and the notion of overpotential. Given this notion of overpotential for this

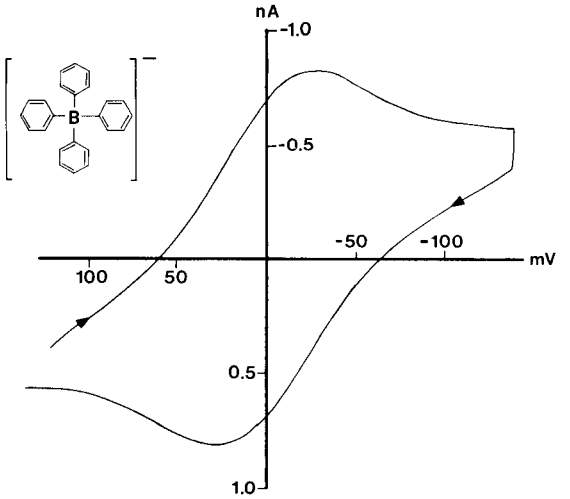

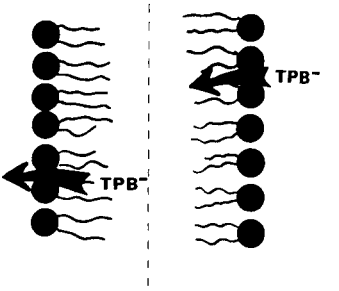

Fig. 2. Voltammogram of membrane-divided cell containing 10^{-6} M tetraphenylborate. Membrane polarization (scan) rate is 10 mV s^{-1}. Background electrolyte: 0.1 M KCl/20 mM MES buffer (pH 5.5). Voltammogram of background electrolyte yields a flat featureless profile in the potential range ±200 mV. The open circuit potential (caused by inherent mismatching of the SCEs) is −2.5 mV, hence the slight shift of symmetry to negative values; the voltammogram is symmetrical about −3 mV.

Fig. 3. The membrane as a thin-layer charge-transfer region. Under an applied voltage and current flux there occur two interfacial charge-transfer processes within a small distance parallel to the direction of charge flow. The analogous redox voltammetric cell would have a thin layer of solution containing an electroactive species interposed between the cathode and anode.

electrochemical cell, it can be reported that in the case of tetraphenylborate, the voltammogram (Fig. 2) possesses peaks at +17 mV and −17 mV and therefore a peak separation of 34 mV. Ordinarily the peak separation of a voltammogram is taken to correspond to the quantity RT/nF or ca. $59/n$ mV for a reversible process. The observed value of 34 mV would imply that $n = 2$ (i.e., that tetraphenylboron was a dianion) which is not realistic because tetraphenylboron is univalent as can be readily verified by a Nernst plot.

Although the above-mentioned inter-relationship between peak separation and equivalents of charge transferred is originally derived from a theoretical treatment of electrical processes at metal electrodes [11], it is unlikely that the observed discrepancy may be attributed to the ionic nature of the charge-transfer process in the membrane system. This statement may be inferred from the results of ITIES systems in which it has been demonstrated [1] that the ionic charge-transfer process between immiscible phases is equivalent to redox processes at electrodes. Moreover, the theoretical studies of de Levie and co-workers [12—14] make it seem appropriate to subject the membrane electrochemical cell to the same criteria as ITIES systems.

Rather than the nature of the electrochemical process, what may in fact provide an explanation of the discrepancy between observed and predicted peak separation is the physical dimension of the organic phase (i.e., the membrane). In a conventional ITIES experiment, ion transfer occurs between two separate bulk phases, whereas in the membrane cell, the immiscible phase is in reality a very thin organic layer between two bulk aqueous electrolyte phases. Under conditions of current flow, in an ITIES cell there exists a net flux of ion movement from one phase to another; in the case of a thin bilayer membrane separating two aqueous phases, there is simultaneous flux of ions into and out of the membrane (cf. Fig. 3). The situation in the membrane cell may be likened to a thin layer of electrolyte sandwiched between electrolyte "electrodes" capable of imparting ions as charge equivalents. The thin-layer voltammetric model is well known in the literature of electrode processes and perhaps the membrane might be deemed an example of thin-layer ITIES.

A thin-layer electrode process does not typically exhibit the $59/n$ mV separation between peaks because of the physical dimensions of the cell. Instead, for a reversible process the peak separation in a voltammetric experiment performed in a thin-layer cell is zero. Peak separation in these cells occurs for irreversible systems and increases as the rate of charge transfer decreases [6]. Another factor which influences the peak separation of a thin-layer voltammogram and in addition affects the shape of the peak is the so-called transfer coefficient which is a measure of the symmetry of the energy barrier to the process. As this transfer coefficient increases (on a scale of 0 to 1), the peaks separate and broaden asymmetrically (one peak broadens, the other sharpens).

Reversibility in a Nernstian sense is often assessed by examining the response of the voltammetric profile as the scan rate (denoted by v) is varied [11]. Reversible behavior is indicated by a linear relationship between the peak height and the square root of the scan rate, while the peak potential remains invariant. Both of these criteria are met by the charge-transfer process involving the tetraphenylborate ion (Fig. 4). From these data, it becomes apparent that the membrane electrochemical cell will not fit neatly into a simple descriptive explanation of an irreversible thin-layer process or a reversible electrode-like ITIES process.

The peak height is also linearly dependent upon the concentration of charge transferred (i.e. ions or electroactive molecules). In the membrane cell, there exists a linear dependence of peak height on the tetraphenylborate concentration over the range $1\text{—}4 \times 10^{-6}$ M. Interestingly, the individual peaks obtained on the forward and reverse scans can be independently varied by altering the concentration of ion on one side of the membrane or the other. This effect is accompanied by what appears to be a shift in peak potentials; however, this shift in potential may be attributed to the concurrent change in the open circuit potential when the concentrations are varied. When this Nernstian potential is subtracted from the applied potential

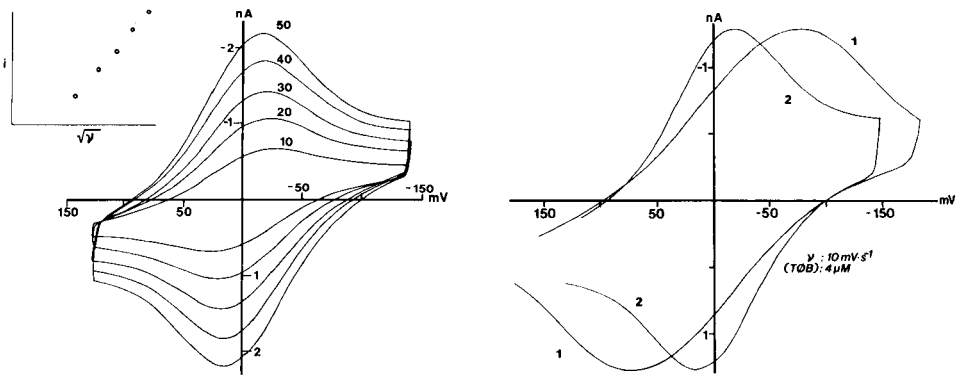

Fig. 4. Voltammogram of tetraphenylborate as the polarization rate is varied. Experimental conditions are identical to those cited in Fig. 2, except for the polarization rate which is indicated on the corresponding voltammogram in units of mV s^{-1}.

Fig. 5. Voltammograms obtained during the formation of the lipid bilayer (10 mV s^{-1}, 4×10^{-6} M TPB). Voltammogram 1 corresponds to a membrane during its "colored" phase of formation, and therefore a kinetically slower rate of transport compared to that of the thinner bilayer membrane characterized by voltammogram 2.

a true "membrane overvoltage" is obtained, and voltammograms recorded for all concentration gradients thereby agree with respect to peak potentials.

Nature of the charge-transfer process

As yet, the underlying mechanism responsible for the observed voltammetric response has not been mentioned. The occurrence of a peak in a voltammetric experiment is caused by a mass transport-limiting process. In the previous section and in Fig. 2, it is shown that transmembrane ion transport and current flux requires ion movement from aqueous to organic layers and from the organic to aqueous layers. The question then becomes; which of these steps limits the mass transport. The demonstrated dependence of individual peak height on lipophilic ion concentration in a given chamber of the cell implies that the rate-limiting step may be the transfer from the aqueous to the organic membrane phase. If the converse were true, it is unlikely that the peak heights would be subject to independent variation.

The nature of the rate-limiting step might also be argued based on earlier results discussed by LeBlanc [9] and de Levie and co-workers [12—16] who have demonstrated the concentration dependence of ion transport. The static current/voltage (i/V) curves of membrane cells containing lipophilic ions were shown to change in shape as the concentration of the lipophilic ion was varied. At low concentrations, the shape of the i/V curve could be described as diffusion-limited and had the form of the so-called current-overpotential equation [6]. At higher concentrations, the i/V curve acquired a shape with no limiting current, i.e., the shape depicted by the Butler-Volmer

equation. LeBlanc [9] stated that the changes in ionic concentration enabled the system to shift from diffusion-limited kinetics to space-charge-limiting kinetics. The only condition necessary for the occurrence of Butler-Volmer kinetics is that there be no mass-transport effect and merely requires that there be no appreciable difference between surface and bulk ion concentrations. Space-charge-limiting processes inherently assume the lack of a mass-transport effect. The theoretical work of de Levie et al. [12—16] illustrated the effect of charge concentration at the surface upon the kinetics of the charge-transfer process and the resultant shape of the static i/V curve.

In the experiments reported here and the results depicted in Figs. 2 and 4, concentrations of the lipophilic ion were maintained at the low concentration end of the kinetic-effect range, thereby ensuring that a diffusion-controlled process was occurring. As the concentration was increased, the voltammetric peaks became poorly resolved as the voltammogram became increasingly dominated by the Butler-Volmer predicted shape. At approximately 10^{-4} M concentrations of tetraphenylboron, the kinetics are almost entirely of the Butler-Volmer predicted shape and the effect may simply be said to be due to the limited current-carrying capacity of the membrane in comparison to the aqueous phase, hence the loss of the mass transport-limiting nature of the process.

In ordinary voltammetry of electrodic or ionic charge transfer on interfaces, the energetics of the process can be inferred from the peak potentials. In the former system, the midpoint potential of the cyclic voltammogram corresponds to the redox potential of the electroactive species, whereas for an ITIES system, the midpoint potential is related to the equilibrium phase distribution of the ion, i.e., the partition coefficient [17]. In the situation in which the membrane separating aqueous phases is polarized, however, the symmetry of the cell dictates that the midpoint potential equals zero (or the open-circuit voltage) and therefore interpretation of the voltammogram in terms of the energetic aspects of the charge-transfer process is more difficult for the membrane cell. It may become necessary to derive energetic information from the peak potentials themselves rather than the midpoint potentials.

It is possible to imagine that there might coexist two physical properties governing the energetics of the charge-transfer process, and therefore the observed peak potentials. The most obvious of these properties concerns the physicochemical aspects of the interaction of the ion with the membrane phase, namely, the equilibrium phase distribution of the ion and the aqueous electrolyte solution, and whether the ion adsorbs onto the membrane surface. However, a perhaps more subtle factor which may strongly influence the energetics of ion transport is the physical size of the membrane. The possible importance of this factor may be inferred from the experimental results of Benz and co-workers [18, 19] who demonstrated the rate dependence of ion transport on membrane thickness. A theoretical model derived from the Born charging equation predicts that the relative rates of ion transport across membranes of differing thicknesses (denoted by d and d') is given [18] by

$$k/k' = \exp\{-h[(1/d') - (1/d)]\} \quad (2)$$

where k and k' denote the rate constants of ion transport of membranes with thicknesses d and d', and h is a constant which depends on the properties of the membrane formation solvent (dielectric constant, etc.). This suggests some correlation with those results cited in the nature of a thin-layer voltammetric experiment which concern the dependence of peak position upon the rate constant of the charge-transfer process. The observation of a direct functional dependence of voltammetric peak potential upon the thickness of the membrane might be expected. Experiments on membrane systems such as those described by Pickar and Benz [18] and Dilger and Benz [20] would be ideally suited for the establishment of this relationship; however, a crude illustration of this type of experiment will be reported here and adequately demonstrates the dependence of peak position upon membrane thickness.

Figure 5 depicts two voltammograms obtained during the formation phase of a bilayer membrane. The voltammogram characterized by peaks with a relatively large separation (curve 1) corresponds to an experiment performed during the colored phase of membrane formation, i.e., when the membrane is somewhat thicker than a bilayer. The other voltammogram (curve 2) is the previously reported result obtained for the same system in which the membrane has attained the "black" bilayer state. Continuous cycling of the potential during the membrane-formation process yields a gradual shift in peak potential towards that finally attained at the bilayer state.

Irreversible behavior

Nicholson and Shain [11] outlined several criteria for evaluating the extent of irreversibility for an electrode process, and their criteria can be simply described as the converse of what was cited above as the characteristics of irreversible behavior. The typical voltammogram of an irreversible process has a peak separation far greater than RT/nF and a profile with features that may vary with scan rate (i.e., increase of peak separation with increased scan rate). Gavach et al. [21] established that for ionic charge transfer across a liquid/liquid interface there exists a response identical to that observed in conventional irreversible processes at electrodes.

Excluding the RT/nF factor in the description of the tetraphenylborate system and the relation to thin-layer voltammetry, the transport of this ion is reversible at scan rates below 500 mV s^{-1}. Irreversible ion transfer might be predicted for ions which adsorb onto the lipids (i.e., the surface) of the membrane, and any number of ionic dyestuffs ordinarily used in biological staining procedures might be excellent candidates for a search of irreversible behavior. Figures 6 and 7 exemplify the irreversibility of some dyestuffs, as these voltammograms obtained from cells containing Gentian violet and Janus green B possess peak separations far in excess of the RT/nF separation which would be predicted. Furthermore, the peak separation increases markedly as the scan rate increased. These data are in agreement with a

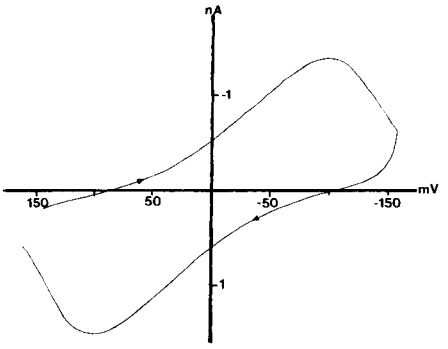

Fig. 6. Voltammogram of Janus green B.

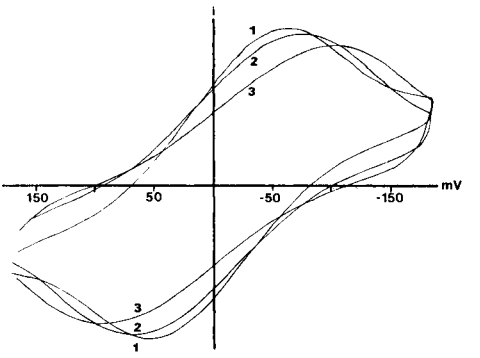

Fig. 7. Voltammograms of Gentian violet at different polarization rates: (1) 10 mV s^{-1}; (2) 35 mV s^{-1}; (3) 80 mV s^{-1}. The current scale was arbitrarily set on the various scans in order to juxtapose the voltammograms and best exemplify the changing peak potentials.

predicted irreversible response as derived from the theoretical interpretations of Nicholson and Shain [11]. It seems reasonable to suggest that these data are analogous to the ITIES experiments reported by Gavach et al. [21] and in part constitute a class of compounds for which interfacial charge transfer across the membrane is decidedly irreversible in the Nernstian sense.

Other ions

Ions other than those reported above were used in further experiments in search of a voltammetric response; however "peaked" voltammograms similar to those observed for tetraphenylborate were not obtained for many ions ordinarily considered lipophilic. For example, ions such as iodide, tetraalkylammonium ions, and tetraphenylarsonium all failed to yield a response similar to that illustrated in Fig. 2 and instead elicited a response characteristic of the Butler-Volmer equation. There seemed to be no concentration dependence in the nature of the profile; decreasing the ion concentration failed to alter the kinetic description of the voltammetric response.

These results prompted an investigation of the possibility that a carrier-mediated process was involved in the tetraphenylboron and dye systems. The voltammogram of tetraphenylboron was not affected by variation of the Na^+ concentration nor by replacement of Na^+ with tetrabutylammonium cation. Likewise, removal of the buffer had no effect, nor did a change in the supporting electrolyte. However, when iodine was added to a cell containing iodide as the lipophilic anion such that triiodide formation occurred, a diffusion-limited voltammetric response developed. The voltammogram of the triiodide system was irreversible in the same sense that those of the dyestuffs were irreversible. Whether the triiodide system is acting as an iodide exchanger or simply represents different transport kinetics of I_3^- is unclear.

Perusal of the literature of the electrochemistry of liquid/liquid interfaces indicates that for some ions a similar type of behavior has been observed [1].

Koryta and Vanysek [17] reported that some semihydrophobic ions yield an increase in conductance when added to an ITIES cell, yet possess no voltammetric response in the sense that there is no characteristic profile. The authors attributed this effect to an interplay between the rates of transfer of the ion under study and the supporting electrolyte; namely, a masking effect caused by co-transport of ions. In the membrane cell, such a mechanism is unlikely because usually the supporting electrolyte does not cross the membrane at an appreciable rate. The increased current upon addition of potassium iodide to a membrane bathing solution of potassium chloride cannot simply be attributed to an increase in the ratio of anion concentration in the membrane to that in the phase.

The results seem to imply that for some reason the current is kinetically limited by ion movement across the membrane, possibly at the stage where mechanistically the ion must shed its solvation sphere and change phases. At some point, however, a kinetic effect arising from competition between rates of membrane transport and K^+/Cl^- passage across the salt-bridge junction will have to be ruled out. This latter prospect may be assessed by altering the present cell to one in which four electrodes are used. This would eliminate the calomel electrodes from the current-carrying portion of the circuit.

CONCLUSION

The stated aim of this investigation was to establish whether there exists any evidence that would indicate an analogy between the electrochemical response of liquid/liquid interfaces and the interface defined by an ultrathin lipid membrane. Results indicate that such an analogy can be made although there it is unclear as to whether a thin-layer or bulk-electrode approach is best suited to the membrane system. Furthermore, there exists as yet only circumstantial evidence implicating the energetic and kinetic dependencies of peak potentials and the shape of the voltammogram. Finally, there also appears to be a dependence of the observed kinetics (based on the nature of the voltammetric response) upon ionic concentration and the ion itself.

Behavior indicative of both reversible and irreversible charge transfer is observed and there appears to be some correlation between this behavior and known aspects of lipid—ion interactions. These data lend credence to the suggestion that there exists an analogy between the electrochemistry of membranes and generalized electrode processes because similarities have been demonstrated between the electrochemical responses of these systems. Although the relationship of the voltammogram to the thermodynamic properties of the cell (e.g., the membrane/water partition of the ion, double-layer effects, thickness, etc.) is still uncertain, it is hoped that the dyes in particular will aid in this evaluation because their partition properties can be measured by spectroscopic means.

No data are yet available which resolve the dilemma posed by the results obtained with iodide and the tetraalkylammonium salts, nor is it certain

which (if indeed either) type of data is anomalous. The membranes are not easily amenable to conventional electrochemical procedures such as controlled potential electrolysis (a functionally cross-linked membrane may overcome the limited lifetime of the present membranes), therefore a mechanism proposed on present data is necessarily vague. Substantial research is still needed on the experimental and theoretical aspects of this phenomenon.

The authors gratefully acknowledge the support received from NIH (GM-14971) and ONR (N00014-85-K-0399). Thanks are due to Theresa Hubbard for typing.

REFERENCES

1 J. Koryta, Ions, Electrodes and Membranes, Wiley, New York, 1982.
2 P. Vanysek, Electrochemistry of Liquid/Liquid Interfaces, Springer-Verlag, Berlin, 1985.
3 H. T. Tien, Bilayer Lipid Membranes: Theory and Practice, M. Dekker, New York, 1974.
4 H. T. Tien, J. Electroanal. Chem., 174 (1984) 299.
5 H. T. Tien, J. Electroanal. Chem., 211 (1986) 19.
6 A. J. Bard and L. Faulkner, Electrochemical Methods, Wiley, New York, 1980, Chap 6.
7 K. Vetter, Electrochemical Kinetics, Academic Press, New York, 1967.
8 E. A. Liberman and V. P. Topaly, Biochim. Biophys. Acta, 163 (1968) 125.
9 O. H. LeBlanc, Biochim. Biophys. Acta, 193 (1969) 350.
10 H. T. Tien and J. Kutnik, Photobiochem. Photobiophys., 7 (1984) 319.
11 R. S. Nicholson and I. Shain, Anal. Chem., 36 (1964) 706.
12 R. de Levie and H. Moriera, J. Membrane Biol., 9 (1972) 241.
13 R. de Levie and N. G. Seidah, H. Moriera, J. Membrane Biol., 10 (1972) 171.
14 R. de Levie and N. G. Seidah, J. Membrane Biol., 16 (1974) 1.
15 R. de Levie, N. G. Seidah and H. Moriera, J. Membrane Biol., 16 (1974) 17.
16 R. de Levie, N. G. Seidah and D. Larkin, J. Electroanal. Chem., 49 (1974) 153.
17 J. Koryta, P. Vanysek, Adv. Electrochem. Electrochem. Eng., 12 (1981) 115.
18 A. D. Pickard and R. Benz, J. Membrane Biol., 44 (1978) 353.
19 R. Benz and B. F. Grislin, J. Membrane Biol., 40 (1978) 293.
20 J. P. Dilger and R. Benz, J. Membrane Biol., 85 (1985) 181.
21 C. Gavach, P. Seta and F. Henry, Bioelectrochem. Bioenerg., 1 (1974) 329.

Analytica Chimica Acta, 198 (1987) 271—275
Elsevier Science Publishers B.V., Amsterdam — Printed in The Netherlands

Short Communication

SPECTROPHOTOMETRIC DETERMINATION OF COPPER(II) WITH CARBON DISULFIDE, A SECONDARY AMINE AND TRITON X-100

KENJIRO HAYASHI*, YOSHIAKI SASAKI, SHOJI TAGASHIRA and KOJI HIRATA

Department of Chemistry, Faculty of Science, Yamaguchi University, Yoshida, Yamaguchi-shi 753 (Japan)

(Received 19th August 1986)

Summary. Copper(II) is determined by non-extractive spectrophotometry as a complex of butylene dithiocarbamate formed in situ by reaction between carbon disulfide and pyrrolidine in aqueous Triton X-100 medium. This method is similar to that with butylene dithiocarbamate as starting material in the sense of simplicity, sensitivity, precision and accuracy. Pyrrolidine is the best of seven secondary amines tested in this way for copper determinations.

Dialkyl and alkylene dithiocarbamates have been widely used in analytical chemistry as chelating agents for heavy metal ions [1]. Most of the metal chelates are sparingly soluble in water but soluble in organic solvents, and there are many papers on the liquid/liquid extraction of metal ion with dithiocarbamate, especially the diethyl and butylene derivatives [2, 3].

It has been shown that the addition of Triton X-100 (*p*-(1,1,3,3-tetramethylbutyl)phenoxypolyoxyethylene glycols, containing an average of 9.5 oxyethylene units per molecule) causes the solubilisation of the metal dithiocarbamates in aqueous medium [4]; the chelates are dissolved into the micelles of Triton X-100. This phenomenon has been utilised for the non-extractive spectrophotometry of tellurium [4, 5], iron [6], osmium [7] and copper [8] with butylene dithiocarbamate (1-pyrrolidinecarbodithioate).

Dithiocarbamates are unstable in solution, and especially in acidic solutions [9], so that their solutions must be prepared daily. However, dithiocarbamates can be formed easily and rapidly by reaction between carbon disulfide and the relevant secondary amine in an alkaline Triton X-100 solution. This communication deals with a study of the spectrophotometric determination of copper(II) as its dithiocarbamate complex by using carbon disulfide and secondary amine as the starting materials.

Experimental

Reagents. A stock solution (9.896 mM) of copper(II) was prepared by dissolving copper metal (99.999%) in dilute nitric acid, evaporating it to dryness, and then dissolving the residue in 0.5 M sulfuric acid. A carbon disulfide solution (0.1 M) was prepared by diluting carbon disulfide with 10%

0003-2670/87/$03.50

(v/v) Triton X-100 solution. Secondary amine solutions were prepared by diluting the amine with water or the Triton X-100 solution (for dipropylamine and dibutylamine which were insoluble in water).

General procedure. A portion of ammonia buffer solution was transferred to a 25-ml measuring cylinder equipped with a stopper. Secondary amine, Triton X-100 and carbon disulfide solutions were successively added, and the total volume of the solution was made up to 18 ml with water. The solution was shaken and the cylinder was allowed to stand for 2—3 min. A suitable amount of copper(II) solution was added, then hydrochloric acid or sodium hydroxide solution was added (if necessary) and the solution was diluted to 20 ml with water. After mixing, the absorbance of the solution was measured in 1-cm quartz cells.

Results and discussion

Absorption spectra. The absorption spectra for each amine system were similar in shape to those of the copper(II) complex of corresponding dithiocarbamate. Each had an absorption maximum at a wavelength in the range 428—443 nm. As shown in Fig. 1, the spectrum and molar absorptivity (ϵ) at 440 nm for the pyrrolidine system were identical with those of butylene dithiocarbamato complex of copper [8]. The formation of the dithiocarbamate by the above-mentioned procedure was thus confirmed.

Effects of experimental variables. The effects of pH and concentrations of components on the absorbance for 5×10^{-5} M copper(II) were investigated. The optimum conditions for each amine system and some analytical characteristics are summarised in Table 1.

Figure 2 shows the effect of pH on the formation of the dithiocarbamate reagent in the pyrrolidine system as an example. All other systems gave similar results. The absorbance decreased rapidly with decreasing pH below

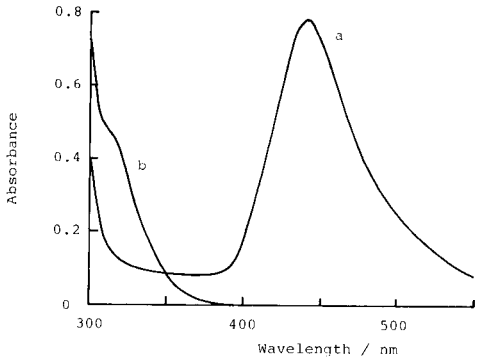

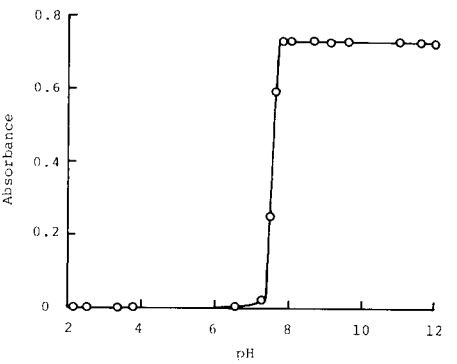

Fig. 1. Absorption spectra: (a) 5×10^{-5} M copper(II) complex with 0.03 M pyrrolidine and 5 mM carbon disulfide in 2% Triton X-100 solution; (b) reagent blank.

Fig. 2. Effect of the pH used for ligand formation on the absorbance (440 nm) of 5×10^{-5} M copper(II) in the presence of 0.03 M pyrrolidine and 5 mM carbon disulfide.

TABLE 1

Optimum conditions and some properties for the determination of 5×10^{-5} M copper(II) with carbon disulfide and a secondary amine

Optimum conditions	Amine						
	Dimethyl-	Diethyl-	Dipropyl-	Dibutyl-	Pyrrolidine	Piperidine	Morpholine
Amine (mM)	>36	>9.6	>4.5	>3.0	>18	>2.5	>6.8
CS_2 (mM)	>2.6	>2.1	>0.52	>0.52	>1.0	>1.0	>0.52
Triton X-100 (% v/v)	0.5—4.0	1.5—12.5	1.0—13.0	1.0—13.8	0.5—3.0	0.5—3.0	0.5—8.0
pH (ligand)[a]	7.9—12.0	7.8—12.0	7.9—12.0	7.7—12.0	7.7—12.0	7.9—12.0	7.0—12.0
pH (chelation)[a]	0.8—13.0	1.0—13.0	1.5—13.0	1.8—13.0	0.5—13.0	0.8—13.0	1.5—13.0
Stability[b] (h)	<1	<3	<3	<3	<1	<2	<3
pK_a (amine)	10.87	10.98	11.00	11.25	11.11	11.12	8.33
λ_{max} (nm)	443	438	437	436	440	437	428
ϵ[c]	8.80×10^3	1.17×10^4	1.24×10^4	1.27×10^4	1.54×10^4	1.23×10^4	1.32×10^4

[a]These pH values relate to formation of the ligand and formation of the chelate, respectively. [b]Stability of the absorbance after chelation. [c]Molar absorptivity (l mol^{-1} cm^{-1}) at λ_{max}.

the lower limit of the optimum pH range. This lower limit was roughly dependent on the pK_a value of the amine, which indicates that the acid form of the amine is inactive.

The stability of the color formed was poor outside the optimum range of Triton X-100 concentrations and turbidity also appeared at low concentration of Triton X-100. The lower limits of the optimum ranges for other factors probably depend on the balance between the instability (acid decomposition) of dithiocarbamate in acidic medium and the thermodynamic stability of the copper complex formed.

Determination of copper with the pyrrolidine system. Further experiments were done only on the determination with the pyrrolidine system because this system gave the highest molar absorptivity, and because it was possible to compare it directly with the butylene dithiocarbamate method reported previously [8].

TABLE 2

The effect of diverse ions on the determination of 63 μg of copper

Ion	Added as	Amount added (mg)	Absorbance	Ion	Added as	Amount added (mg)	Absorbance
—	—	—	0.762	Pb^{2+}	$Pb(NO_3)_2$	1.0	0.724
			0.753			2.1	0.700
			0.750[a]	Sn^{4+}	$SnCl_4$	8.0	0.733
			0.744[b]			20	0.714
Cl^-	NH_4Cl	71	0.760	Mn^{2+}	$MnCl_2$	0.38	0.760
		360	0.782			0.94	0.850
SO_4^{2-}	$(NH_4)_2SO_4$	670	0.760			1.9	0.764[a]
PO_4^{3-}	Na_2HPO_4	170	0.761			2.8	Turbidity[a]
CH_3COO^-	CH_3COONa	790	0.760	Cd^{2+}	$Cd(NO_3)_2$	0.006	0.720
CN^-	KCN	0.04	0.757			0.022	0.693
		0.20	0.732			1.1	0.745[a]
Na^+	NaCl	230	0.760			2.2	Turbidity[a]
Mg^{2+}	$MgSO_4$	11	0.726	Fe^{3+}	$FeNH_4(SO_4)_2$	2.8	0.780
		100	0.747[b]			8.4	0.822
Zn^{2+}	$ZnCl_2$	0.038	0.718			31	0.765[a]
		9.6	0.738[b]			61	Turbidity[a]
Al^{3+}	$AlCl_3$	1.1	0.765	Co^{2+}	$CoSO_4$	0.42	0.717
		2.2	0.847			2.1	0.921
		11	0.756[b]			2.1	0.745[a]
		22	Turbidity[b]			4.2	0.701[a]
Ni^{2+}	$NiCl_2$	0.20	0.773				
		0.30	0.830				

[a]With EDTA (6.3×10^{-4} M) added. [b]With EDTA (2.5×10^{-2} M) added.

TABLE 3

Results on synthetic samples[a]

Other metal ions (mg)	Cu added (μg)	Cu found[b] (μg)
Zn^{2+} (1.9), Cd^{2+} (0.22), Mn^{2+} (0.19), Fe^{3+} (0.15), Co^{2+} (0.042)	62.9	61.7 ± 0.2
	25.2	24.5 ± 0.1
Zn^{2+} (0.96), Cd^{2+} (0.11), Mn^{2+} (0.095), Fe^{3+} (0.076), Co^{2+} (0.021)	62.9	62.1 ± 0.2
	25.2	24.5 ± 0.2

[a]EDTA (2.5×10^{-2} M) was added as masking agent. [b]Mean and standard deviation (n = 5).

The calibration graph at 440 nm was linear over the range 2—120 μg of copper(II) under the conditions of 0.03 M pyrrolidine, 5 mM carbon disulfide, 2% Triton X-100 and pH 10 for the process of ligand formation, with pH 9—10 for the complex formation. The relative standard deviation was 1.4% (10 runs) for 63 μg of copper(II).

The effects of diverse ions are shown in Table 2. As with the butylene dithiocarbamate method, zinc(II), nickel(II), manganese(II), cadmium(II) and cobalt(II) interfered seriously but could be masked in moderate amounts by the addition of EDTA. Copper in synthetic samples was determined with excellent results (Table 3).

Compared with the earlier method, this method was similar in terms of simplicity, sensitivity, precision and accuracy.

REFERENCES

1 K. L. Cheng, K. Ueno and T. Imamura (Eds.), Handbook of Organic Analytical Reagents, CRC Press, Boca Raton, FL, 1982, p. 389.
2 G. H. Morrison and H. Freiser, Solvent Extraction in Analytical Chemistry, Wiley, New York, 1957, p. 180.
3 J. Stary, The Solvent Extraction of Metal Chelates, Pergamon, Oxford, 1964, p. 155.
4 K. Hayashi, Y. Sasaki, M. Nakanishi and S. Ito, Bunseki Kagaku, 19 (1970) 1673.
5 K. Hayashi and K. Ito, Bunseki Kagaku, 20 (1971) 1550.
6 K. Hayashi, Y. Sasaki and K. Ito, Bunseki Kagaku, 21 (1972) 1338.
7 K. Hayashi, K. Ito and M. Ochi, Bunseki Kagaku, 24 (1975) 156.
8 K. Hayashi, H. Doukan and A. Yamamoto, Bunseki Kagaku, 27 (1978) 405.
9 S. Tagashira, Anal. Chem., 55 (1983) 1918.

Analytica Chimica Acta, 198 (1987) 277—280
Elsevier Science Publishers B.V., Amsterdam — Printed in The Netherlands

Short Communication

AN IMPROVED NEPHELOMETRIC METHOD FOR THE DETERMINATION OF SMALL AMOUNTS OF THIOSULFATE IN AQUEOUS SAMPLES

ROBERTO ARUGA* and ENNIO CAMPI

Department of Analytical Chemistry, University of Turin, via Giuria 5, 10125 Turin (Italy)

(Received 2nd October 1986)

Summary. The procedure is based on decomposition of thiosulfate, with formation of sulfur, in the presence of 0.5 mol l^{-1} nitric acid. Thiosulfate is determined in the range 15—100 mg l^{-1}, with a relative standard deviation of 5.4% and a mean relative error of 3.2%. These data are of the same order of magnitude as those obtained for the earlier silver/1,10-phenanthroline method. The present method has the advantage of being almost completely free from interferences; the only interference observed (sulfide) is easily eliminated.

A nephelometric determination of thiosulfate in aqueous samples was recently described [1]; thiosulfate was precipitated with bis(1,10-phenanthroline)silver(I) cation from an aqueous ethanolic medium. The method was valid for 3—70 mg l^{-1} thiosulfate, which is of the same order (and even better, in some cases) as that of the iodimetric techniques generally suggested for thiosulfate. However, although various interfering species can be easily eliminated (e.g., metal ions by use of a cation-exchange resin), interferences of anions such as iodide and thiocyanate remained [1].

In the nephelometric method proposed here, advantage is taken of the fact that thiosulfate decomposes in acidic medium with formation of sulfur suspensions. Nitric acid was chosen as the acid, as precipitation of other cationic or anionic species present in the sample is unlikely when this acid is added.

Experimental

Reagents and solutions. The chemicals and distilled water were as reported previously [1]. Sodium salts of anions and acetates of cations were used in interference studies (C. Erba RPE and Merck products).

Precipitant solution (A). Polyvinylpyrrolidone (6.25 g) was dissolved in 690 ml of 65% nitric acid. The solution was diluted to 1 l with water, to give a final nitric acid concentration of 10 mol l^{-1}.

Standard solution of thiosulfate (B). Exactly 17.84 ml of 0.1 N sodium thiosulfate was diluted to 200 ml with water (final concentration 1000 mg l^{-1} $S_2O_3^{2-}$).

0003-2670/87/$03.50

Equipment and instrument calibration. A commercial HF-DRT-1000 nephelometer (HF Instruments, Bolton, Canada) was used. Fuller details on the instrumentation and the calibration procedure were reported previously [1].

Procedures. For calibration, known amounts of the thiosulfate standard solution (B) were placed in 50-ml volumetric flasks (the concentration of thiosulfate after dilution to the final volume should be between 15 and 100 mg l^{-1}). Then 2.50 ml of precipitant solution A was added, so that a final concentration of 0.5 mol l^{-1} of nitric acid was obtained. After dilution to 50 ml with water, the suspension was kept for one night (17 h) at 20—22°C, and then the turbidity was measured. The turbidity values as a function of the thiosulfate concentration gave the calibration graph (see below).

For the determination of thiosulfate, a known volume (47.5 ml) of sample containing 15—100 mg l^{-1} thiosulfate was treated as above. The thiosulfate content was evaluated from the parameters of the calibration plot.

Results and discussion

Ten determinations were done for each of twelve concentrations of thiosulfate. The mean turbidity values (in FTU) plotted as a function of the thiosulfate concentrations (in mg l^{-1}) gave a curve with the equation $Y = 6.4 \times 10^{-3} X^2 + 0.35 X - 4.8$. The reproducibility (relative standard deviation, *RSD*) and accuracy (relative error) of the method were evaluated in the usual way [2]. All the values are reported in Table 1.

TABLE 1

The nephelometric determination of thiosulfate with nitric acid in aqueous samples[a]

Thiosulfate taken (mg l^{-1})	Turbidity (FTU)	Thiosulfate found (mg l^{-1})	*RSD* (%)	Relative error (%)
15.7	3.2 ± 0.4	17.3 ± 0.6	3.5	+10
21.0	6.3 ± 0.7	22.5 ± 0.7	3.2	+7.1
26.2	8.5 ± 1	25.8 ± 1.5	5.9	−1.5
31.5	12.6 ± 1	31.5 ± 1.1	3.5	0
36.7	15 ± 2	34.6 ± 1.7	5.0	−5.7
42.0	20 ± 3	41 ± 3	7.3	−2.4
52.5	31 ± 5	52 ± 5	9.6	−0.9
63.0	40 ± 4	61 ± 3	4.9	−3.2
73.5	60 ± 5	77 ± 3	3.9	+4.7
84.0	71 ± 6	85 ± 6	7.0	+1.2
94.5	85 ± 9	94 ± 8	8.5	−0.5
105.0	101 ± 3	104 ± 2	1.9	−0.9
			Mean 5.4	Mean 3.2

[a]The uncertainty of the measured values is expressed as the estimated standard deviation for 10 separate determinations.

Optimization of the procedure. At nitric acid concentrations lower than that proposed above (0.5 mol l^{-1}), the turbidity values obtained were lower for the same concentration of thiosulfate. This is probably connected with slower precipitation of sulphur when insufficient acid is present [3, 4]. Some tests with similar concentrations of hydrochloric acid instead of nitric acid showed poorer reproducibility of the turbidity data. The specified quantity of polyvinylpyrrolidone (used as suspension stabilizer) was shown to be the best; when its concentration was higher than that recommended, turbidity values were lower. Arsenious acid was also tested, in order to increase the speed of formation of the suspension, because it is known to exert a catalytic action on the thiosulfate decomposition [5]. However, arsenious acid proved useless because, with quantities corresponding to 150—300 mg l^{-1} arsenic, yellow-brown suspensions with poor light-scattering properties were obtained; the coloration was probably due to arsenic sulfides.

Interferences. It is unlikely, in general, that other ionic species in the sample will produce precipitates on addition of nitric acid, but a retarding action on the thiosulfate decomposition (together with lower turbidity of the suspension) is possible. Precipitation of sulfur by the decomposition of thiosulfate can be delayed by the presence of certain heavy metals, such as cadmium (which is also strongly complexed by thiosulfate), or by thiocyanate [6, 7]. No interferences on the thiosulfate determination were found in the presence of cadmium acetate (up to 150 mg l^{-1} Cd) or in the presence of sodium thiocyanate (up to 15 mg l^{-1} SCN^-). Thiocyanate interfered seriously in the nephelometric method with 1,10-phenanthroline and silver [1] but with the new procedure, errors were caused only when $\geqslant$20 mg l^{-1} thiocyanate was present. The decomposition of thiosulfate is retarded by glycerol and ethanol, but only at high concentrations [7]. In the case of sulfide, at the lowest concentration studied (5 mg l^{-1} sulfide) then was a clear interference on the turbidity values obtained for 52 mg l^{-1} thiosulfate. But the interference of sulfide was eliminated simply by treating the sample with a zinc carbonate suspension [1, 8].

Conclusions

Comparison of the present method with the previous 1,10-phenanthroline/silver method shows that the present method is less sensitive and precise (15—100 mg l^{-1} thiosulfate with mean *RSD* 5.4% and mean relative error 3.2% compared to 3—70 mg l^{-1} with mean *RSD* 2.6% and mean relative error 2.5%). The present method has, however, a sensitivity of the same order (and even better, in some cases) as the iodimetric methods generally suggested for thiosulfate [1, 9], and is virtually free from interferences other than sulfide, which is easily eliminated.

REFERENCES

1 R. Aruga and E. Campi, Anal. Chim. Acta, 182 (1986) 207.
2 Standard Methods for the Examination of Water and Wastewater, American Public Health Association, Washington, DC, 1975.

3 R. E. Kirk and D. F. Othmer, Encyclopedia of Chemical Technology, Vol. 22, Wiley, New York, 1983, p. 976.
4 M. C. K. Jablczynski and M. Z. Warszawska-Rytel, Bull. Soc. Chim. Fr., 39 (1926) 409.
5 F. Foerster and G. Stühmer, Z. Anorg. Allg. Chem., 206 (1932) 1.
6 P. Pascal (Ed.), Traité de Chimie Minérale, Vol. II, Masson, Paris, 1932, p. 162.
7 G. Gaillard, Comptes Rendues, 140 (1905) 652.
8 J. H. Karchmer and J. W. Dunahoe, Anal. Chem., 20 (1948) 915.
9 M. A. V. Devanathan, Q. Fernando and P. Peries, Anal. Chim. Acta, 16 (1957) 292.

Analytica Chimica Acta, 198 (1987) 281—286
Elsevier Science Publishers B.V., Amsterdam — Printed in The Netherlands

Short Communication

EXTRACTION-SPECTROFLUORIMETRIC DETERMINATION OF CADMIUM WITH DIETHYLDITHIOCARBAMATE AND CALCEIN IN NON-AQUEOUS MEDIA

JOSE AZNAREZ*, JAVIER GALBAN, CARMELO DIAZ and JOSE M. RABADAN

Department of Analytical Chemistry, Faculty of Sciences, University of Zaragoza, Zaragoza (Spain)

(Received 1st September 1986)

Summary. Cadmium (7—80 ng ml^{-1}) is extracted with diethyldithiocarbamate into chloroform from aqueous media, at pH 11—12 and the fluorescent complex is developed by addition of a calcein solution in dimethylformamide. The method is applied to the determination of cadmium in waste waters, high-purity metals and zinc ores.

Reagents synthesized from fluorescein (eosin and erythrosin) have been used for the fluorimetric determination of cadmium. The good fluorescent properties of these reagents, however, are offset by their poor chelating properties. For that reason, it has been necessary to use them in conjunction with ion-association complex formation in an organic solvent [1]. Alternatively, iminodiacetic groups may be incorporated into the fluorescein-type molecule, so that its reactivity is increased but its fluorescent properties remain. Many reagents, such as calcein [2], have been synthesized on this basis. Various other reagents have also been used for the determination of cadmium. These and the fluorescein derivatives are summarized in Table 1. These reagents either have good sensitivity and poor selectivity, so it is necessary to use a preseparation step (ion exchange [2, 5] or liquid/liquid extraction [6, 15]), or their sensitivity is poor, although they are reasonably selective.

In this work, cadmium is extracted with diethyldithiocarbamate into chloroform, followed by formation of a fluorescent complex by addition of calcein in dimethylformamide (DMF), to form a fluorescent complex in the organic phase. The method permits the determination of 7—80 ng ml^{-1} cadmium in the presence of large concentrations of other ions, and is applied to the determination of cadmium in zinc ores, pure aluminium and waste waters.

Experimental

Apparatus. A Shimazdu RF-510 spectrofluorimeter with 1-cm quartz cells, a Kotterman mechanical shaker and a Salvix thermostatted bath were used.

0003-2670/87/$03.50

TABLE 1

Some fluorimetric methods for cadmium

Reagent	Determination medium	Optimum pH	λ_{ex} (nm)	λ_{em} (nm)	Linear range ($\mu g\ ml^{-1}$)	Ref.
5-Sulpho-8-quinolinol	H_2O	7.5			0.02—0.8	3,4
8-Mercaptoquinoline	H_2O/EtOH/DMF (1:1:1)	2.5	365	534		5
	$CHCl_3$	14[a]	365	515	0.05—1.5	6
Dibromofluorescein/1,10-phenanthroline	$CHCl_3$/acetone (1:1)	9[a]	536	580	0.01—0.2	7
Eosin/cobalt(II)/1,10-phenanthroline	$CHCl_3$	8.5[a]	530	570	0.05—1.0	8
Indoeosin/cobalt(II)/1,10-phenanthroline	$CHCl_3$	8.5[a]	530	570	0.05—1.0	8
Calcein	H_2O	13.3	490	520	0.002[b]	2
2-Pyridyl ketone-2-quinolylhydrazone	H_2O	3	469	555	0.01—0.56	9
	H_2O/EtOH (1:4)	11	465	545	0—0.09	10
Methylsalicylidenedithiocarbazide	H_2O/DMF (1:1)		350	470	0—7	11
	H_2O		340	460	0—7	12
p-Chlorobenzyl-(2-hydroxy-1-naphthylidene)dithiocarbazide	H_2O/DMF (1:1)		470	520	<1.10	13
Dicarboxymethylaminomethyldihydro-*trans*-stilbene	H_2O	8	360	440	0.02—0.1	14
8-*p*-Tosylaminoquinoline	Dimethyl ketone	11[a]	360	515	0.02—0.1	15

[a]Extraction pH. [b]Detection limit.

Reagents and solutions. All chemicals used were of analytical-reagent grade. A 300 $\mu g\ ml^{-1}$ cadmium stock solution was prepared by dissolving cadmium metal in concentrated nitric acid and diluting with water to 1 l. A 10 $\mu g\ ml^{-1}$ solution was prepared by diluting the stock solution with water immediately before use. A 2% (w/v) sodium diethyldithiocarbamate (DDTC) solution in water was prepared daily. Likewise, an 0.03% (w/v) calcein solution and an aqueous 50% (v/v) pyridine solution were prepared daily. The phosphate buffer (pH 11) was prepared from 0.05 M disodium hydrogenphosphate and 0.1 M sodium hydroxide.

Procedure. Place in a 100-ml beaker an appropriate amount of finely ground zinc ore or aluminium metal sample (0.1—0.7 g, depending on the cadmium content of the sample). Add 5 ml of concentrated hydrochloric acid and warm carefully, until total evolution of hydrogen sulphide is achieved. Add 1 ml of concentrated nitric acid and boil for 5 min. Allow the beaker to cool, and dilute the solution to 100 ml with distilled water in a volumetric flask. Pipette a portion of the sample (water or zinc ore or aluminium metal solution) containing up to 8 μg of cadmium into a 100-ml separating funnel. Add 1 ml of 1 M potassium cyanide, 1 ml of DDTC solution and phosphate buffer to bring the solution to pH 11—12. Add 10 ml of chloroform and extract the cadmium by mechanical shaking for 2 min. Allow the phases to separate. Pipette exactly 1 ml of the chloroform extract. Add 1 ml of pyridine/DMF solution and 2 ml of calcein solution, and dilute to

10 ml in a volumetric flask with DMF. After 15 min, measure the emission intensity at 535 nm, with excitation at 519 nm. Prepare a blank solution in the same way, but free from added cadmium. Calibrate with aqueous solutions containing 1—8 μg of cadmium.

Results and discussion

Extraction reagent and solvents. DDTC, ammonium pyrrolidinedithiocarbamate (APDC), cupferron, iodide and dithizone were used for cadmium extraction before its spectrofluorimetric determination. Calcein in several non-aqueous solvents (DMF, ethanol, methyl isobutyl ketone (MIBK), chloroform, diethyl ether) was added to the extracts. The results are shown in Table 2. The best results were obtained with DDTC as extractant and DMF as non-aqueous solvent. The iodide/diethyl ether extraction system also gave good results. For determination of 30 μg of cadmium by extraction with DDTC into chloroform, the best conditions were found to be 0.2% (w/v) DDTC and pH 11—12 (phosphate buffer solution).

The influence of t-butylamine and pyridine on the cadmium/calcein complex formation in DMF was studied (Fig. 1). The butylamine produced changes in excitation and emission spectra, and also lower responses than DMF alone. Pyridine in low concentrations improved the sensitivity and

TABLE 2

Reagents used for cadmium extraction and spectral characteristics in several organic media after extraction into chloroform

Reagent	Solvent	λ_{ex}[a] (nm)	λ_{em}[a] (nm)	Intensity[b]	
				Complex	Reagent
DDTC	$CHCl_3$	468	522	67.5	41.8
	Ethanol	493	515	149.0	122.4
	MIBK	475	525	162.4	80.7
	DMF	519	535	69.2	24.6
Dithizone	$CHCl_3$	509	529	3.5	146.5
	Ethanol	511	531	2.7	104.2
	DMF	526	545	97.7	80.2
Cupferron	$CHCl_3$	473	525	12.9	12.9
	Ethanol	475	524	93.0	92.9
	DMF	473	525	90.2	90.2
Iodide	$CHCl_3$	465	512	34.6	53.5
	Ethanol	469	515	72.5	74.5
	MIBK	467	516	50.4	38.6
	DMF	508	532	12.0	3.8
Iodide[c]	Diethyl ether	467	521	82.2	48.0
	Ethanol	471	518	104.0	102.0
	MIBK	470	515	66.0	70.0
	DMF	470	535	22.4	23.0
APDC	DMF	516	532	79.0	64.0

[a]Most sensitive wavelength. [b]Arbitrary units. [c]Diethyl ether extraction.

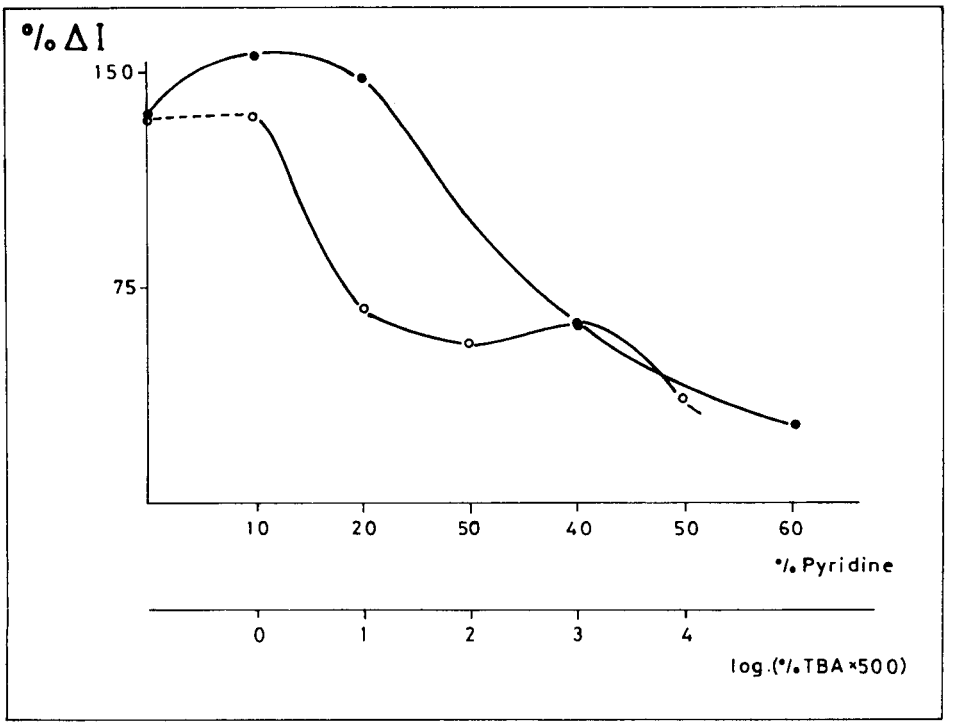

Fig. 1. Change in $\%\Delta I$ of the cadmium/calcein complex on base addition: (•) pyridine; (○) t-butylamine (TBA). (2.67×10^{-7} M cadmium, 2.67×10^{-6} M calcein). $\%\Delta I$ = 100 (intensity complex — intensity calcein)/intensity calcein).

precision of the emission without changing the fluorescence and excitation spectra. The best results were obtained with 10% (v/v) pyridine in DMF, and this was used throughout the present work.

The influence of ethanol and acetic acid on the emission of the cadmium/calcein complex in DMF was also studied. Concentrations of acetic acid higher than ca. 0.001% (v/v) decreased the responses and modified the complex and reagent emission and excitation spectra. Concentrations of ethanol above 20% (v/v) also decreased the responses to cadmium.

Calibration precision and interferences. At 535 nm, the wavelength of maximum emission of the cadmium/calcein complex in DMF, the calcein solution also emits (Fig. 2) and therefore the calcein concentration must be kept to a minimum. For that reason, a 10-fold molar excess of calcein was considered as optimum. Under these conditions, the complex was formed after less than 15 min and its emission remained constant for at least 60 min.

Over the range 7—80 ng ml^{-1} cadmium in the final solution, the fluorescence intensity increased linearly with increasing cadmium concentration. The relative standard deviation for seven replicate determinations of 30 ng ml^{-1} cadmium was 5.0%.

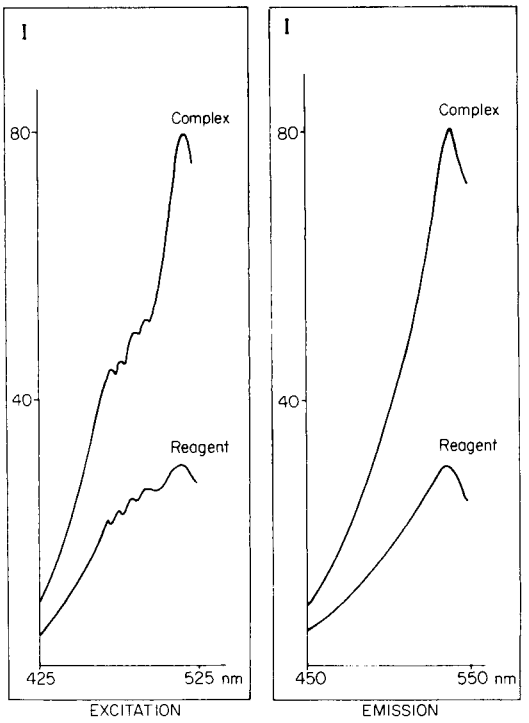

Fig. 2. Emission and excitation spectra of cadmium/calcein complex and calcein alone. (Concentrations as in Fig. 1).

TABLE 3

Tolerance limits for the determination of 0.3 μg of cadmium

Interferent	Tolerance limit (μg)	Interferent	Tolerance limit (μg)
Tartrate, PO_4^{3-}, Al^{3+}	11 000	Zn^{2+}	0.3
CN^-, S^{2-}	8000		300[a]
F^-, BO_3^{3-}	4000	Fe^{2+}	1.0
Acetate, Cl^-	1200		70[b]
Ca^{2+}, Ba^{2+}, Sr^{2+}, Mg^{2+}, Hg^{2+}	1000	Co^{2+}	1.0
Cr^{3+}, Sn^{2+}	60		15[a]
Pb^{2+}	1.5	Cu^{2+}, Ni^{2+}	—
			15[b]

[a]With addition of potassium cyanide as in Procedure. [b]With potassium cyanide and 0.5 M sodium fluoride (1 ml) added.

The effects of several elements most frequently associated with cadmium in ores and other samples were studied. The tolerance limits for the determination of 0.3 μg of cadmium are shown in Table 3.

Applications. Two waste-water samples were analyzed for cadmium. The cadmium contents found were 0.96 and 1.32 $\mu g\ ml^{-1}$; recoveries of 0.3 μg of cadmium added to the samples were about 96%.

The method was applied to the determination of cadmium in ores and synthetic samples and high-purity aluminium. Two certified zinc ores kindly supplied by Sociedad Española del Cinc, Canadian blende (61.84% Zn, 2.14% Fe, 0.50% Cd) and Bolivian blende (56.11% Zn, 7.19% Fe, 0.20% Cd), were analyzed and gave accurate results, as did a sample of aluminium metal (Merck, Ref. 1057). The results obtained are shown in Table 4.

TABLE 4

Results for the determination of cadmium in ores and aluminium

Sample	Cadmium (%)		Sample	Cadmium (%)	
	Certified	Found[a]		Certified	Found[a]
Canadian blende	0.50	0.50 (2.1)	Bolivian blende	0.20	0.21 (3.0)
A[b]	0.075	0.070 (3.3)	B[c]	0.060	0.055 (3.8)
Aluminium	—	0.0041 (4.3)			

[a]Mean of six replicate determinations with relative standard deviation (%) in parentheses. [b]A: 15% Canadian blende + 70% ZnS + 15% Fe_2O_3. [c]B: 30% Bolivian blende + 55% ZnS + 15% Fe_2O_3.

REFERENCES

1 P. R. Haddad, Talanta, 1 (1977) 24.
2 A. J. Heffley and B. Jaselkis, Anal. Chem., 46 (1974) 2036.
3 Y. Nishikowa, K. Hiraki, K. Morishige and T. Katagi, Jpn. Analyst, 26 (1977) 365; Anal. Abstr., 34 (1978) 1B15.
4 K. Hiraki, K. Morishige and Y. Nishikawa, Anal. Chim. Acta, 97 (1978) 121.
5 M. Shibata and H. Kakiyuma, Jpn. Analyst, 26 (1977) 640; Anal. Abstr., 34 (1978) 4H28.
6 K. Watanabe and K. Kawagaki, Jpn. Analyst, 23 (1974) 1356; Anal. Abstr., 29 (1975) 2B59.
7 K. P. Stolyarov and V. V. Firyulina, Zh. Anal. Khim., 33 (1978) 2102; Anal. Abstr., 36 (1979) 6B40.
8 M. A. Matreets and D. P. Scherbor, Zh. Anal. Khim., 26 (1971) 823; Chem. Abstr., 75 (1971) 41093z.
9 J. J. Laserna, A. Navas and F. Garcia Sanchez. Anal. Lett., Part A, 14 (1981) 833.
10 F. Garcia Sanchez, A. Navas and M. Santiago, Anal. Chim. Acta, 167 (1985) 217.
11 I. Kasa and J. Korosi, Period Polytech. Chem. Eng., 17 (1973) 241; Chem. Abstr., 80 (1974) 43707e.
12 I. Kasa and J. Korosi, Magy. Kem. Foly., 80 (1974) 151; Chem. Abstr., 81 (1974) 20527c.
13 I. Kasa and G. Bajnoczky, Period Polytech. Chem. Eng., 18 (1974) 289; Chem. Abstr., 83 (1975) 2159w.
14 B. Budesinsky and T. S. West, Analyst, 94 (1969) 182.
15 T. Vesiene and B. Paicinskyte, Liet. TSR Mokslu Akad. Darb. Ser. B, 6 (1972) 115; Chem. Abstr., 79 (1973) 61184r.

Analytica Chimica Acta, 198 (1987) 287—292
Elsevier Science Publishers B.V., Amsterdam — Printed in The Netherlands

Short Communication

ENHANCED LUMINESCENCE OF THE EUROPIUM/TERBIUM/ THENOYLTRIFLUOROACETONE/1,10-PHENANTHROLINE/ SURFACTANT SYSTEM, AND ITS ANALYTICAL APPLICATION

YANG JING-HE*, ZHU GUI-YUN and WU BO

Department of Chemistry, Shandong University, Jinan, Shandong (Peoples' Republic of China)

(Received 2nd October 1986)

Summary. The enhanced luminescence of europium in a thenoyltrifluoroacetone/1,10-phenanthroline/Triton X-100 system in the presence of terbium is studied. The sensitivity is increased by two orders of magnitude, giving a detection limit of 1×10^{-13} M. The optimized procedure is applied to the determination of europium in lanthanide oxide samples.

During a study of the europium/thenoyltrifluoroacetone (TTA)/1,10-phenanthroline (phen)/surfactant fluorescence system [1], fluorescence enhancement was observed when La^{3+}, Tb^{3+}, Gd^{3+}, Lu^{3+} and Y^{3+} were added. Of these, terbium increases the intensity by 1—2 orders of magnitude. This phenomenon has also been observed as an interference in another complex fluorescence system [2], but was not investigated. In the present communication, this enhancement effect is investigated in detail. It can be used for the determination of ultratrace amounts of europium.

Experimental

Reagents. Standard solutions (1.00×10^{-3} M) of lanthanides were prepared by dissolving the oxides (99.9%) in dilute hydrochloric acid. Working solutions were prepared by dilution with distilled water. Aqueous 1.0×10^{-3} M solutions of TTA and 1,10-phenanthroline were used. The concentrations of aqueous non-ionic surfactant solutions were 1% (w/w); the others were 0.1% (w/w). The buffer solution was 0.3 M ammonium acetate. All the reagents used were of analytical grade.

Apparatus. An RF-540 spectrofluorimeter (Shimadzu, Japan) was used.

Procedure. To a 25-ml test tube, solutions were added in the following order: standard solutions of Eu^{3+} and Tb^{3+}, surfactant solution, buffer solution, and TTA and 1,10-phenanthroline solutions. The mixture was diluted to 25 ml with distilled water and allowed to stand for 25 min. The fluorescence intensity was measured in a 1-cm quartz cell at excitation and emission wavelengths of 371 nm and 612 nm, respectively.

0003-2670/87/$03.50

Results and discussion

The excitation and emission spectra of the systems investigated are shown in Fig. 1. The Tb/TTA/phen/Triton X-100 system has four emission peaks, one at 548 nm (Tb^{3+}) and three at 582 nm, 592 nm and 612 nm (Eu^{3+}) arising from traces of Eu^{3+} in the Tb_4O_7 used to prepare the solutions. The excitation and emission spectra of Eu/TTA/phen/Triton X-100 in the presence and absence of terbium are similar to each other, and show the emission spectra of Eu^{3+}. The maximum excitation wavelength is 371 nm; the maximum emission wavelength is 612 nm. However, the intensity of the Eu/Tb/TTA/phen/Triton X-100 system is 1—2 orders of magnitude stronger than that of the system without terbium.

The effect of terbium concentration on the intensity of the europium system is shown in Fig. 2. For 1×10^{-7} M Eu^{3+} the intensity reaches a maximum at 2×10^{-5} M Tb^{3+}, whereas in the range 1×10^{-8}—1×10^{-10} M Eu^{3+}, the maximum intensity occurs in the range 1—2×10^{-5} M Tb^{3+}. Figure 3 shows the effect of pH on the fluorescence intensity in the presence and absence of terbium. The greatest intensity occurs over the pH range 5.0—9.0 in the presence of terbium compared to only 5.5—7.0 in the absence of terbium. The type of buffer also affects the fluorescence intensity. Under the general conditions used for Fig. 3 at pH 7, ammonium acetate and hexamine/hydrochloric acid buffers gave the same intensity but ammonia/ammonium chloride reduced the intensity (by 15%) and citrate and phosphate buffers

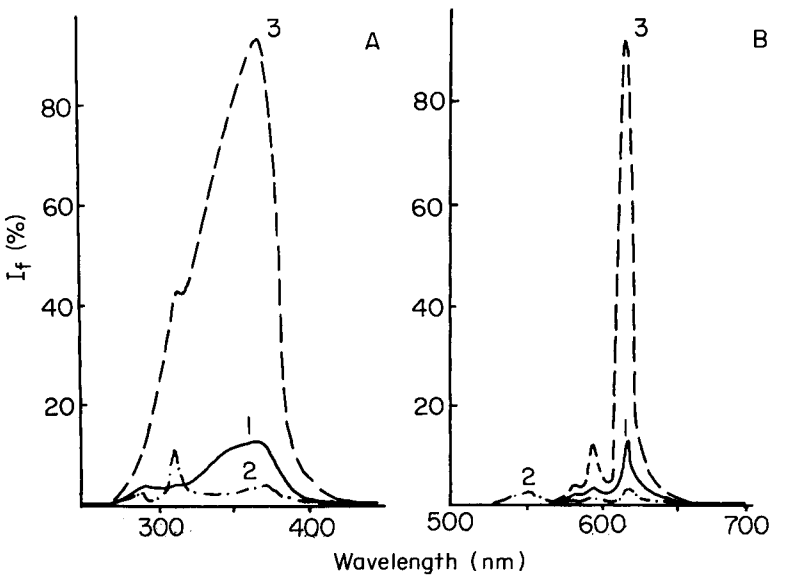

Fig. 1. Fluorescence spectra: (A) excitation; (B) emission. (1) Eu/TTA/phen/Triton X-100 (coordinate ×4); (2) Tb/TTA/phen/Triton X-100; (3) Eu/Tb/TTA/phen/Triton X-100. Conditions: 1.0×10^{-7} M Eu^{3+}, 2.0×10^{-5} M Tb^{3+}, 1.0×10^{-4} M TTA, 1.0×10^{-4} M phen, 3×10^{-2} M ammonium acetate, 5×10^{-2}% Triton X-100.

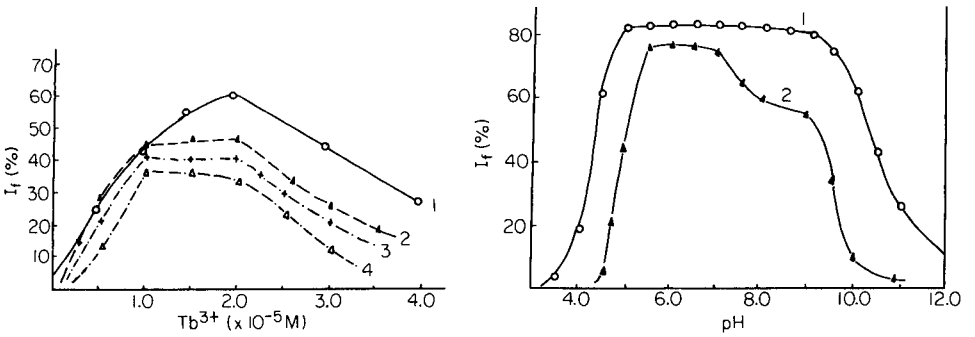

Fig. 2. Effect of terbium concentration. Europium concentration: (1) 1.0×10^{-7} M; (2) 1.0×10^{-8} M; (3) 1.0×10^{-9} M; (4) 1.0×10^{-10} M. Conditions: 1.0×10^{-4} M TTA, 1.0×10^{-4} M phen, 3×10^{-2} M ammonium acetate, 5×10^{-2}% Triton X-100.

Fig. 3. Effect of pH: (1) Eu/Tb/TTA/phen/Triton X-100 system; (2) Eu/TTA/phen/Triton X-100 system. Conditions: 1.0×10^{-7} M Eu^{3+}, 2.0×10^{-5} M Tb^{3+}, 1.0×10^{-4} M TTA, 1.0×10^{-4} M phen, 5×10^{-2}% Triton X-100.

quenched the fluorescence completely. Thus ammonium acetate (at $>10^{-3}$ M) was chosen for further use. The effects of TTA and 1,10-phenanthroline concentrations on the intensity of the europium/terbium system were examined. The concentration ranges that gave greatest intensity were 7×10^{-5}—1.3×10^{-4} M for TTA and $>3 \times 10^{-5}$ M for 1,10-phenanthroline.

The sensitizing effects of different types of surfactant were examined. Both non-ionic and anionic surfactants have a sensitizing effect, Triton X-100 and Tween-20 giving the greatest enhancement (Table 1). This is similar to the sensitizing effect of surfactants on the fluorescence of the Eu/TTA/phen system [1]. Amphoteric surfactants have a slight quenching effect but this is less marked than on the Eu/TTA/phen system. Cationic surfactants can quench the fluorescence of the Eu/TTA/phen system but had little effect on the system studied here. Triton X-100 was selected; its optimum concentration range is 2.0—9.0×10^{-2}% (w/w).

The fluorescence intensity of the europium/terbium system is a linear function of the europium concentration in the range 1×10^{-8}—1×10^{-11} M under the recommended conditions. The sensitivity is thus two orders of magnitude better than that of the Eu/TTA/phen/Triton X-100 system. The detection limit (signal/noise = 2) is 1.0×10^{-13} M, which is about four orders of magnitude less than that of the Eu/TTA/phen/Triton X-100 system.

The effects of other lanthanides and other ions on the intensity of the Eu/Tb system were studied. At 1.0×10^{-9} M europium, the highest permissible concentrations of other lanthanides (i.e., causing <2% relative error in the intensity) were as follows: 4×10^{-8} M La; 8×10^{-8} M Ce (or thorium); 2×10^{-8} M Pr; 7×10^{-8} M Nd; 4×10^{-8} M Ho; 5×10^{-8} M Er, Tb or Y; 9×10^{-8} M Yb or Lu; 10×10^{-8} M Sm; and 20×10^{-8} M Gd or Dy. Larger

TABLE 1

Effect of surfactants (conditions as in Fig. 3)

Surfactant	Concentration range ($\times 10^{-2}$%, w/w)	I_f[a]
Triton X-100	2.0—9.0	224
Tween-20	1.0—5.0	197
OP-20	1.0—28	173
Polyoxyethylene lauryl ether	0.5—12	167
Sodium dodecyl sulfonate	0.1—2.8	168
Sodium dodecylbenzene sulfonate	0.3—3.0	144
Cetyltriethylammonium bromide	1.0—5.0	108
Cetylpyridinium chloride	0.2—0.4	104
N,N-Dimethyl-*N*-chlorocetylammonium acetate	3.0—10.0	81
N,N-Dimethyl-n-bromocetylammonium acetate	0.2	55

[a]Intensity of Eu/Tb/TTA/phen in water is taken as 100.

concentrations decreased the intensity. Therefore, the standard addition method was applied for the determination of europium in samples containing other lanthanides. The results obtained for synthetic mixtures and commercial oxides (Table 2) show that the procedure is suitable for the determination of traces of europium in such oxides.

Enhancement mechanism. Figure 2 shows that there is no constant mole ratio between Eu^{3+} and Tb^{3+} in the Eu/Tb/TTA/phen/Triton X-100 system. Figure 4 shows that the absorption spectrum of this system is similar to that of the system without terbium. These results show that terbium does not form a new compound with Eu/TTA/phen/Triton X-100. It should also be noted that the enhancement effect occurs only in an aqueous phase in the presence of surfactants and not in organic solvents (e.g., benzene, n-butanol, cyclohexane and tributyl phosphate). It is likely therefore that Eu/TTA/phen and Tb/TTA/phen are both formed and dissolve in the Triton X-100 micelles with the two complexes in close contact.

The excited singlet states of TTA in these complexes undergo a radiationless transition to their triplet states. Europium can be excited both by intramolecular energy transfer, as suggested by Crosby et al. [3], from the excited triplet state of TTA in the Eu/TTA/phen complex and by intermolecular energy transfer from the excited triplet state of TTA in the Tb/TTA/phen complex. Because the concentration of the terbium complex is much greater than that of the europium complex in the Triton X-100 solution, each Eu/TTA/phen molecule is surrounded by many Tb/TTA/phen molecules, and the fluorescence of the europium complex is considerably enhanced. Triton X-100 also plays an important part in the dissolution of both complexes and their protection against collision with solvent (water) molecules, which would cause loss of energy.

TABLE 2

Determination of europium by the standard addition method

Rare earth oxides (weight %)			Eu_2O_3 found (weight %)[a]
Synthetic samples			
La_2O_3 19.52	CeO_2 19.67	Pr_2O_3 19.77	
Nd_2O_3 20.15	Sm_2O_3 20.88	Eu_2O_3 0.015	0.013 ± 0.003
Tb_4O_7 11.67	Gd_2O_3 12.00	Dy_2O_3 12.34	
Ho_2O_3 12.50	Er_2O_3 12.63	Tm_2O_3 12.73	0.014 ± 0.002
Yb_2O_3 12.99	Lu_2O_3 13.11	Eu_2O_3 0.012	
La_2O_3 6.68	CeO_2 6.73	Pr_2O_3 6.77	
Nd_2O_3 6.90	Tb_4O_7 7.67	Gd_2O_3 7.90	
Dy_2O_3 8.11	Ho_2O_3 8.21	Sm_2O_3 7.14	0.071 ± 0.002
Er_2O_3 8.30	Tm_2O_3 8.37	Yb_2O_3 8.54	
Lu_2O_3 8.61	Eu_2O_3 0.07		
Commercial oxides			
Tb_4O_7	(99.99)		0.003
La_2O_3	(99.99)		0.004
CeO_2	(99.9)		0.014
Pr_2O_3	(99.9)		0.021
Nd_2O_3	(99.9)		0.027
Dy_2O_3	(99.9)		0.010

[a]Mean ± std. dev. (n = 6).

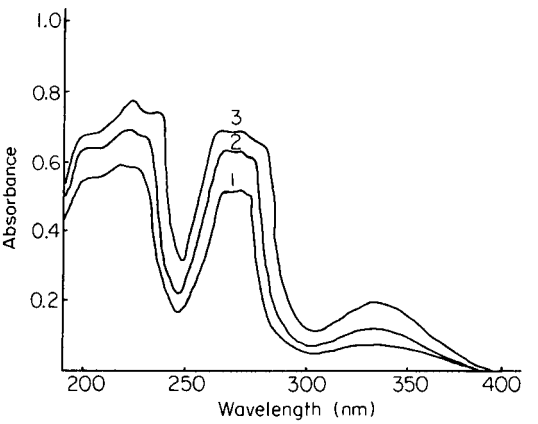

Fig. 4. Absorption spectra: (1) Eu/TTA/phen/Triton X-100 system; (2) Tb/TTA/phen/Triton X-100 system; (3) Eu/Tb/TTA/phen/Triton X-100 system. Conditions: 1.0×10^{-7} M Eu^{3+}, 2.0×10^{-5} M Tb^{3+}, 1.0×10^{-4} M TTA, 1.0×10^{-4} M phen, 3×10^{-2} M ammonium acetate, 5×10^{-2}% Triton X-100.

REFERENCES

1 Yang Jing-he, Zhu Gui-yun, Xue Jing-hua and Zhang Xin-yong, Proceedings of Second Academic Discussion of Photometry of The Chinese Chemical Society, Vol. 3, Jinan, 1984, p. 5.
2 E. V. Melentieva, N. S. Poluektov and L. I. Kononenko, Zh. Anal. Khim., 22 (1967) 187.
3 G. A. Crosby, R. E. Whan and R. M. Alire, J. Chem. Phys., 34 (1961) 744.

Analytica Chimica Acta, 198 (1987) 293—296
Elsevier Science Publishers B.V., Amsterdam — Printed in The Netherlands

Short Communication

SPECTROPHOTOMETRIC DETERMINATION OF CHROMIUM(VI) AS DICHROMATE AFTER EXTRACTION WITH THE PENTAMETHYLENE-BIS(TRIPHENYLPHOSPHONIUM) CATION

D. THORBURN BURNS*, D. CHIMPALEE and P. F. HAGAN

Department of Analytical Chemistry, The Queen's University, Belfast BT9 5AG (Northern Ireland)

(Received 30th January 1987)

Summary. Chromium(VI) (0—100 μg) can be determined spectrophotometrically at 365 nm after its extraction as pentamethylene-bis(triphenylphosphonium) dichromate into 1,2-dichloroethane. The system is applied to the determination of chromium in a range of steels.

Although there are excellent sensitive and selective spectrophotometric methods for most common metals, this is not true for metalloids, non-metals or anions in general [1] or oxoanions in particular [2]. For the extraction of the dichromate ion, several onium cations have been examined [3—10], of which the triphenylselenonium [7], trioctylmethylammonium [8], tetraphenylarsonium [9] and 1-naphthylmethyltriphenylphosphonium [10] cations have been applied to the determination of chromium in steels. The present communication reports the use of the pentamethylene-bis-(triphenylphosphonium) cation as an ion-pairing extractant for dichromate and application of the system to the determination of chromium in steels, after oxidation of chromium(III) to chromium(VI) by permanganate.

Experimental

Apparatus. Pye Unicam SP8-400 and SP6-550 u.v./visible spectrophotometers were used for recording absorption spectra and for routine absorbance measurements, respectively, in matched 1-cm quartz cells.

Reagents and solutions. Pentamethylene-bis(triphenylphosphonium) bromide (Lancaster Synthesis) was used as supplied. Analysis for carbon and hydrogen indicated that the material was reasonably pure. A stock 0.5% (w/v) solution was prepared in water. A stock aqueous 1000 μg ml^{-1} chromium(VI) solution was prepared from potassium dichromate (AnalaR, dried to constant weight at 140°C). A stock aqueous 500 μg ml^{-1} chromium(III) solution was prepared from chromium(III) potassium sulphate dodecahydrate (AnalaR, > 99%). More dilute solutions of chromium(VI) and chromium(III) were prepared as required. All other reagents were of analytical grade, and twice-distilled water was used throughout.

0003-2670/87/$03.50

General procedure. Place an aliquot (5 ml) containing about 50 μg of chromium(VI) in a 100-ml separating funnel. Add 5 ml of 0.5 M sulphuric acid and 5 ml of the 0.5% pentamethylene-bis(triphenylphosphonium) bromide solution. Extract twice with 4-ml portions of 1,2-dichloroethane. Filter the organic phase into a 10-ml volumetric flask and dilute to volume with 1,2-dichloroethane. Cover the flask with aluminium foil to protect the contents from light. Measure the absorbance at 365 nm against a reagent blank.

Procedure for steel samples. For samples containing 3–6% chromium, such as high-speed tool steels, dissolve accurately weighed 0.1-g samples in 10 ml of 20% (v/v) sulphuric acid in 250-ml conical flasks by warming. Add 1 ml of concentrated nitric acid and simmer gently until all the carbides are decomposed. Add 2 ml of (1 + 1) sulphuric acid and evaporate carefully to fumes. Cool. Add 50 ml of water and warm to dissolve the soluble salts. Cool and if necessary filter through a Whatman No. 40 filter paper into a 100-ml (or larger or smaller depending on the chromium content) volumetric flask. Wash the residual solids (silica, tungstic acid) with a small volume of hot (1 + 99) sulphuric acid followed by water and dilute to volume. Mix well and dilute (1 + 4). Transfer a 5-ml aliquot to a 100-ml beaker, add 1 ml of (1 + 1) sulphuric acid, 1 ml of 1% (w/v) potassium permanganate solution, and 5 ml of water. Heat the solution on a steam bath for 20 min, cool to room temperature, and transfer quantitatively to a 100-ml separating funnel. Add 5% (w/v) sodium nitrite solution dropwise with swirling to destroy the excess of permanganate and add 2 further drops (avoid introducing an uncontrolled excess of sodium nitrite). Add 5 ml of 0.5% reagent solution immediately the permanganate colour has disappeared and extract with 1,2-dichloroethane as in the general procedure. Measure the absorbance of the extract at 365 nm as above.

Prepare a calibration graph over the range 0–100 μg of chromium by using aliquots of standard chromium(III) solution, oxidizing with permanganate and proceeding as for steel samples. For samples containing 0.1–1% chromium increase the sample weights to 0.3–0.5 g.

Examination of the main experimental variables

A variety of solvents including alcohols, ketones, esters, ethers, and chlorinated and aromatic hydrocarbons, was examined for extraction efficiency of 50 μg of chromium as in the general procedure, absorbances being measured against the pure solvents. Of the liquids examined only chloroform, dichloromethane and 1,2-dichloroethane extracted the dichromate ion-pair, and the last solvent gave the greatest apparent molar absorptivity (at 365 nm).

The absorbance of extracts was found to be independent of the sulphuric acid concentration over the range 0.1–2.0 M, and 0.5 M was adopted for use. The absorbance of extracts increased with increase of amount of ion-pairing reagent up to a constant value. A convenient amount of reagent, in the plateau region, is specified in the general procedure. The extracts, when protected from light, were stable for at least 5 h.

The composition of the ion-pair was established spectrophotometrically by Job's method of continuous variation [11] and by the mole ratio method [12] to be $[(C_6H_5)_3P(CH_2)_5P(C_6H_5)_3]\ Cr_2O_7$.

Results and discussion

A linear calibration graph was obtained over the range 0—100 μg of chromium(VI) at 365 nm (apparent molar absorptivity = 1.38×10^3 l mol^{-1} cm^{-1}). For the determination of 50 μg of chromium, the relative standard deviation was 0.49% (10 results).

The possible interferences of a number of cations and anions were checked for 50 μg of chromium(VI) under the conditions of the general procedure. Iron(III) at a weight ratio of 1200:1, acetate, citrate, tartrate, sulphate, nitrate, and hydrogenphosphate at 500:1, and vanadate, fluoride, calcium, aluminium, ammonium, lead, manganese(II), copper(II), cobalt(II), zinc and nickel at 200:1 were without significant effect (±3%). The only ions of interest in steel analysis which interfered were manganese(VII), molybdenum(VI) and tungsten(VI). The interference from manganese(VII) was overcome by addition of 5% sodium nitrite. Tungsten(VI) was removed during the dissolution of the steels and molybdenum(VI) could be removed by extraction of its chloro complex into 10 ml of 1:1 (v/v) diethyl ether/carbon tetrachloride followed by addition of 0.1 M silver sulphate to mask the chloride. For the steels examined, it was not necessary to extract molybdenum(VI).

Permanganate was used for the oxidation of chromium(III) to chromium(VI) and the excess of permanganate was selectively decomposed by addition of sodium nitrite. It was necessary to avoid an uncontrolled addition of sodium nitrite because this caused slight positive errors (e.g., a 5-drop excess of 5% sodium nitrite solution after destruction of the pink colour gave a positive 2.5% error at 50 μg Cr(VI)). Nitrite was preferred to azide for reduction of permanganate because such positive errors were lower. The results of the interference and masking studies are summarized in Table 1.

TABLE 1

Effect of diverse ions on the determination of dichromate (50 μg Cr)

Ion[a]	Ion/Cr(VI) (w/w)	Absorbance change (%)	Ion[a]	Ion/Cr(VI) (w/w)	Absorbance change (%)
Oxalate	500	−6	WO_4^{2-}	100	+30
	250	0		5	0
ClO_4^-	500	−100	MoO_4^{2-}	500	+24
	1	0		50	0
Cl^-	500	−12		500[c]	0
	5	0	MnO_4^-	2	+50
	500[b]	0		1	0
				200[d]	0

[a]Added as sodium or potassium salts. [b]In the presence of silver sulphate. [c]After extraction of the chloro complex with 1:1 (v/v) diethyl ether/carbon tetrachloride. [d]After addition of sodium nitrite.

TABLE 2

Analysis of steel samples

BCS Steel	Chromium in steel (% w/w)		
	Certified	Certified range	Found[d]
435/1[a]	0.14	0.13—0.15	0.14 ± 0.01
214/2[b]	0.09	0.08_5—0.09_5	0.09 ± 0.01
219/3[b]	0.76	0.75—0.76	0.78 ± 0.02
408[b]	0.09	0.08_5—0.09_5	0.09 ± 0.01
410/1[b]	1.34	1.32—1.35	1.34 ± 0.01
220/2[c]	5.12	5.07—5.17	5.09 ± 0.08
241/2[c]	5.35	5.29—5.40	5.32 ± 0.03
482[c]	4.09	4.06—4.14	4.06 ± 0.05
483[c]	3.21	3.17—3.26	3.20 ± 0.04
485[c]	4.15	4.11—4.18	4.14 ± 0.04

[a]Unalloyed. [b]Low alloy. [c]Highly alloyed steel. [d]Mean ± 95% confidence limits for 5 replicates.

The results for the determination of chromium in British Chemical Standard steel samples (Table 2) are in excellent agreement with certificate values. The confidence limits are somewhat narrower than the previous method [10] which used azide to remove the excess of permanganate and extraction with the 1-naphthylmethyltriphenylphosphonium cation. Interferences are considerably less than in single-phase methods for chromate. The method described does not require additions of iron to prepare the calibration graph [13] and is tolerant to vanadium.

REFERENCES

1 C. A. Watson, Analyst, 111 (1986) 1353.
2 D. T. Burns, Anal. Proc., 19 (1982) 355.
3 R. Bock and C. Hummel, Z. Anal. Chem., 198 (1963) 176.
4 R. Bock and J. Jainz, Z. Anal. Chem., 198 (1963) 315.
5 R. Bock and E. Grallath, Z. Anal. Chem., 222 (1966) 283.
6 J. Hála, O. Navrátil and V. Nechuta, J. Inorg. Nucl. Chem., 28 (1966) 553.
7 M. Zeigler and K. D. Pohl, Z. Anal. Chem., 204 (1964) 413.
8 J. Adam and R. Přibil, Talanta, 18 (1971) 91.
9 N. K. Baishya and G. Baruah, J. Indian Chem. Soc., 59 (1982) 389.
10 D. T. Burns and S. Kheawpintong, Anal. Chim. Acta, 177 (1985) 253.
11 P. Job, Ann. Chim. (Paris), 9 (1928) 113.
12 J. H. Yoe and A. L. Jones, Ind. Eng. Chem., Anal. Ed., 16 (1944) 111.
13 Methods for the Sampling and Analysis of Iron, Steel and other Ferrous Alloys, British Standards Institution, 1970.

Analytica Chimica Acta, 198 (1987) 297—302
Elsevier Science Publishers B.V., Amsterdam — Printed in The Netherlands

Short Communication

INDIRECT DETERMINATION OF FLUORIDE IN WATERS WITH LANTHANUM ALIZARIN COMPLEXONE AND INDUCTIVELY-COUPLED PLASMA EMISSION SPECTROMETRY

AKIRA MIYAZAKI* and KENJI BANSHO

National Research Institute for Pollution and Resources, 16-3, Onogawa, Yatabe, Tsukuba, Ibaraki 305 (Japan)

(Received 11th August 1986)

Summary. Fluoride is determined indirectly by measurement of the La II 333.75-nm line in the lanthanum/alizarin complexone/fluoride complex. The ternary complex is extracted into hexanol containing *N,N*-diethylaniline and the extract is introduced directly into the plasma. Related to water samples, the detection limit (3σ, concentration factor 5) is 0.59 ng ml^{-1} fluoride, calibration is linear up to 1.2 $\mu g\ ml^{-1}$ and the relative standard deviation for 0.04 $\mu g\ ml^{-1}$ is 2.6%. Alkali, alkali earth elements and most anions do not interfere. The method is applied in the analysis of river water, coastal seawater and drinking water.

Inductively-coupled palsma emission spectrometry (i.c.p.e.s.) has been widely used to quantify traces of various elements, but its direct use for fluorine is limited by poor sensitivity. Windsor and Denton [1] reported a 1-mg detection limit for the 685.60-nm F I line. Later, Fry et al. [2] examined 56 i.c.p. excited, nonresonance atomic fluorine lines and achieved an approximate 3000-fold improvement in the detection limit. Both these papers were concerned with the intoduction of gaseous samples or application to gas chromatography. No papers have been published so far on the determination of trace amounts of fluoride in aqueous samples by argon i.c.p.e.s.

Several indirect methods including spectrophotometry [3, 4], atomic absorption spectrometry [5—8] and molecular emission cavity spectrometry [9] have been reported for the determination of fluoride. In this communication, a new method is reported for the indirect determination of fluoride based on the i.c.p.e.s. measurement of lanthanum in the well-known lanthanum/alizarin complexone/fluoride (La—AC—F) complex. The complex in aqueous solution is extracted into hexanol containing *N,N*-diethylaniline and the emission intensity of the La II 333.75-nm line is measured. The method is rapid and applicable to determination of ng ml^{-1} levels of fluoride in water.

0003-2670/87/$03.50

Experimental

Apparatus. The i.c.p. spectrometer used was the Jarrell-Ash AtomComp 96-975. The emission intensity of the La line was measured with the 50-cm monochromator (Jarrell-Ash 82-025, N+1 channel) attached to the instrument. The operating conditions for the plasma and monochromator are described in Table 1.

Reagents. A stock solution (1000 μg ml^{-1}) of fluoride was prepared by dissolving dried analytical-reagent grade sodium fluoride in water. Working standards were prepared by appropriate dilution of the stock solution. Lanthanum/alizarin complexone (La—AC) solution was prepared by a standard method [10]; 1 l of the solution (pH 4.4) contained 0.192 g of alizarin complexone [(3,4-dihydroxy-2-anthraquinonyl)methyliminodiacetic acid], 41 g of sodium acetate trihydrate, 24 ml of acetic acid, 400 ml of acetone, and 0.163 g of lanthanum oxide.

Two acetate buffer solutions (pH 4.4) were used [11]. Buffer A contained 110 g of sodium acetate trihydrate and 98 ml of acetic acid, diluted to 1 l with water. Buffer B contained 65 g of sodium acetate trihydrate and 55 ml of acetic acid, diluted to 1 l with water. Distilled/deionized water was used throughout. All other chemicals used were of analytical grade.

Procedure. A 50-ml sample was transferred to a 100-ml separatory funnel and 4 ml of buffer A and 6 ml of La—AC solution were added. After 15 min, the La—AC—F complex was extracted into 10 ml of a 4% (v/v) *N,N*-diethylaniline solution in hexanol by shaking for 6 min. After at least 5 min for phase separation, the aqueous phase was discarded. The organic phase was washed with 3 ml of buffer B by shaking for 2 min. After phase separation (ca. 2 min), the aqueous phase was discarded and the La II 333.75-nm emission intensity was measured while the extract was sprayed. A calibration graph was prepared by using the above extraction for 50-ml portions of appropriate working standard solutions.

Results and discussion

Selection of organic solvents and amines. The La—AC—F complex can be extracted into organic solvents containing amines [11—13]. For the spectrophotometric determination of fluoride, Hirano et al. [11] reported that isoamyl alcohol containing *N,N*-diethylaniline offered the best sensitivity.

TABLE 1

Instrumental operating conditions

Grating	1180 line mm^{-1}	Argon flow rates	
Slit widths	50 μm	coolant	18 l min^{-1}
Integration time	20 s	auxiliary	0.8 l min^{-1}
Operating power	1.8 kW	carrier	0.6 l min^{-1}
Observation height above load coil	16 mm		

Table 2 gives the signal-to-background ratios (S/B) for i.c.p.e.s. measurements of the La II 333.75-nm line in various organic solvents containing amine. Although isoamyl alcohol containing methylaniline offered the best S/B among the solvents tested, the sensitivity with this solution was about 40% lower than that for hexanol containing *N,N*-diethylaniline. Moreover, the volume of isoamyl alcohol extract decreased about 10% compared with that of hexanol extract, because of their different solubilities in water. *N,N*-Diethylaniline in hexanol, which offered the best sensitivity and the second highest S/B, was therefore selected.

Optimization of conditions. For i.c.p.e.s. measurements of lanthanum in aqueous solution, Winge et al. [14] reported that the best six wavelengths, 333.75, 379.48, 408.68, 412.32, 398.85 and 379.08 nm, offered almost the same detection limits. In hexanol containing amine, the La II 379.47 and 379.08-nm lines were not useful because of the interference from CN bands. The other four lines provided detection limits similar to those obtained for aqueous solution, and the La II 333.75-nm line was used. The five parameters (forward power to the coil, observation height and gas flow rates) in Table 1 were optimized by using a univariate search based on S/B measurements.

The effect of the *N,N*-diethylaniline concentration is shown in Fig. 1A. The net signal intensity for lanthanum was almost constant up to 8% (v/v) but the emission intensity of the blank increased above 4% (v/v), probably because the amount of excess La—AC dissolved in hexanol increases with increasing amine concentration. Consequently, the 4% (v/v) concentration was chosen. As shown in Fig. 1B, the net signal intensity of sample solutions increased with increasing volumes of La—AC solution up to 6 ml; this volume was selected to avoid excessive blank intensities. The net signal intensity was independent of the volume of buffer A up to 4 ml, but decreased thereafter because of poorer conditions for formation of the complex, as in the spectrophotometric method [11]. Shaking times of 2—10 min for the extraction did not affect the results.

TABLE 2

Effects of organic solvents containing amine on signal/background (S/B) ratios[a]

Amine	Solvent	S/B	Amine	Solvent	S/B
N,N-Diethylaniline	Hexanol	12.8	*o*-Toluidine	Hexanol	12.2
	Isoamyl alcohol	8.7		Isoamyl alcohol	10.3
	Amyl alcohol	4.0		Amyl alcohol	6.7
Methylaniline	Hexanol	8.4	Aniline	Hexanol	12.2
	Isoamyl alcohol	15.5		Isoamyl alcohol	10.3
	Amyl alcohol	11.6		Amyl alcohol	14.4

[a]The La—AC—F complex could not be extracted with di-isobutyl ketone or xylene containing *N,N*-diethylaniline, methylaniline, *o*-toluidine or aniline. Signal/background ratios were poor (ca. 0.2) with tri-n-octylamine in any of the solvents mentioned.

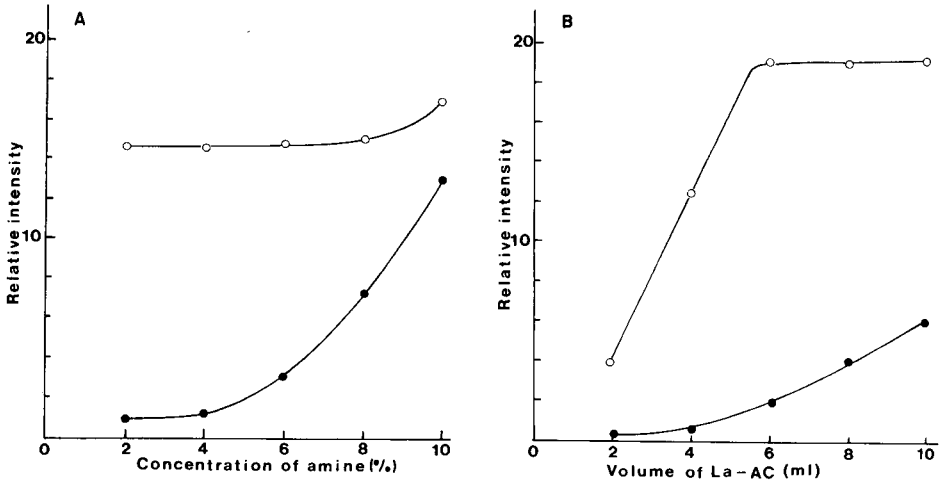

Fig. 1. Effect of *N,N*-diethylaniline concentration (A) and volume of La—AC solution (B): (○) net signal intensity; (●) blank intensity.

Calibration, precision and interferences. The detection limit, defined as the concentration of fluoride equivalent to three times the standard deviation (3σ) of the background signal was 0.59 ng ml^{-1}, when a 50-ml water sample and 10 ml of hexanol containing *N,N*-diethylaniline were used. The limit of determination (10σ) was 2.0 ng ml^{-1}. For the spectrophotometric determination with isoamyl alcohol containing *N,N*-diethylaniline, the limit of determination was 25 ng ml^{-1} [11]. The proposed method is therefore more sensitive than the conventional spectrophotometric method. The good detection limit is attributed not only to the preconcentration of the complex by extraction, but also to the good sensitivity of i.c.p.e.s. for lanthanum. The relative standard deviation (n = 10) of the complete procedure for 2 μg of fluoride was 2.6%. The calibration graph was linear from the detection limit to at least 1.2 μg ml^{-1} (60 μg) of fluoride.

The effects of diverse ions for 10 μg of fluoride are shown in Table 3. No interference was caused by 20 μg of any ion except aluminium, which formed hexafluoroaluminate. Boron, cadmium and Cr(VI) were permissible in 10-fold amounts. If necessary, Cd, Co, Cu, Fe, Ni, Pb and Zn were removed by extraction with ammonium pyrrolidine dithiocarbamate (APDC) in di-isobutyl ketone at pH 4.4 [15] prior to addition of La—AC solution. There was no interference from 100-fold amounts of the following ions; Li, Na, K, Mg, Ca, Sr, Ba, Ag, Hg, Mn(II), As(III), Se(IV), PO_4^{3-}, Cl^-, Br^-, I^-, NO_3^-, SO_4^{2-} and NH_4^+.

Erosion of plasma torch and nebulizer spray chamber. In measurements of fluoride, the plasma torch and nebulizer spray chamber made of silicate may be eroded. Wavelength scans in the vicinity of the Si I 251.61-nm line for blanks and sample (Fig. 2) showed that erosion by fluoride is negligible. No problem occurred even when the same torch was used for 1 year.

TABLE 3

Effect of diverse ions on recoveries of 10 μg of fluoride

Other ion	Amount added (μg)	Recovery (%)	Other ion	Amount added (μg)	Recovery (%)	Other ion	Amount added (μg)	Recovery (%)
None	—	100	Cu	20	103	Sb	20	102
Al	10	103		100	58		100	64
	20	60	Fe(III)	20	96	Se	20	103
B	100	99		100	88		100	64
	1000	90	Ge	20	108	Sn	20	102
Cd	100	96		100	83		100	83
	1000	91	Mo	20	98	Ti(III)	20	96
Co	20	96		100	41		100	45
	100	73	Ni	20	98	V	20	97
Cr(VI)	100	95		100	69		100	74
	1000	82	Pb	20	102	Zr	20	104
				100	87		100	83

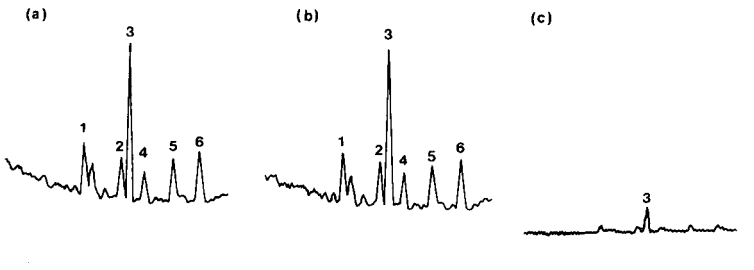

Fig. 2. Wavelength scans to check the erosion of the plasma torch and nebulizer/spray chamber: (a) hexanol blank; (b) sample extract; (c) water. (1) Si, 250.7 nm; (2) Si, 251.4 nm; (3) Si, 251.6 nm; (4) Si, 251.9 nm; (5) Si, 252.4 nm; (6) Si, 252.9 nm.

TABLE 4

Determination of fluoride in waters

Sample	F (ng ml^{-1})	
	I.c.p.e.s.	Spectrophotometry
River water A	3.0	—[a]
B	33	32
C	172	170
Sea water D	960[b]	980
E	1280[b]	1270
Drinking water F	120	120
G	108	110

[a]Not detected. [b]These samples were analyzed by i.c.p.e.s after 5-fold dilution.

Applications. When 1.0—7.0 μg of fluoride was added to 50 ml of lake water, which itself contained 0.1 μg ml^{-1} fluoride, the recoveries ranged from 97 to 100%. The values obtained by the proposed method for river water, coastal seawater and drinking water (Table 4) are in good agreement with those obtained by the spectrophotometric method [11]. Samples A and B are unpolluted river waters from the northern part of Japan. Samples F and G are drinking waters collected in our laboratory. As suggested by Greenhalgh and Riley [16], the values for the seawater were multiplied by 1.040 to compensate for salt error.

The results summarized here demonstrate that the i.c.p.e.s. measurement of lanthanum in La—AC—F extracted into hexanol containing *N,N*-diethylaniline is useful for the indirect determination of fluoride in water and is significantly more sensitive than conventional spectrophotometry. Cerium and praseodymium which form similar complexes with alizarin complexone and fluoride would also be applicable.

REFERENCES

1 D. L. Windsor and M. B. Denton, J. Chromatogr. Sci., (1979) 492.
2 R. C. Fry, S. S. Northway, R. M. Brown and S. K. Hughes, Anal. Chem., 52 (1980) 1716.
3 APHA, AWWA, WPCA, Standard Methods for the Examination of Water and Wastewater, 15th edn., p. 332 (1980).
4 L. Lenarczyk, Z. Marczenko and M. Jarosz, Mikrochim. Acta, Part III, (1984) 485.
5 A. M. Bond and T. A. O'Donnell, Anal. Chem., 40 (1968) 560.
6 B. Gutshe, H. Kleinoeder and R. Herrmann, Analyst, 100 (1975) 192.
7 C. C. Fong and C. O. Huber, Spectrochim. Acta, Part B, 31 (1976) 113.
8 B. Gutche, K. Rudigeran and R. Herrmann, Spectrochim. Acta, Part B, 30 (1975) 441.
9 M. Burguera, A. Townshend and S. L. Bogdanski, Anal. Chim. Acta, 117 (1980) 247.
10 Japanese Industrial Standard, Testing Methods for Industrial Wastewater, K0102, p. 102 (1986).
11 S. Hirano, H. Fujinuma and T. Kasai, Bunseki Kagaku, 15 (1966) 1339.
12 R. J. Hall, Analyst, 88 (1963) 76.
13 W. Lei, K. Fujiwara and K. Fuwa, Anal. Sci., 2 (1986) 213.
14 R. K. Winge, V. A. Fassel, V. J. Peterson and M. A. Floyd, Inductively Coupled Plasma-Atomic Emission Spectrometry, An Atlas of Spectral Information, Elsevier, Amsterdam, p. 273, 1985.
15 A. Miyazaki, A. Kimura, K. Bansho and Y. Umezaki, Anal. Chim. Acta, 144 (1982) 213.
16 R. Greenhalgh and J. P. Riley, Anal. Chim. Acta, 25 (1961) 179.

Analytica Chimica Acta, 198 (1987) 303—308
Elsevier Science Publishers B.V., Amsterdam — Printed in The Netherlands

Short Communication

ATOMIC ABSORPTION SPECTROMETRIC DETERMINATION OF TRACE COPPER IN WATER BY SORPTION ON AN ION-EXCHANGE RESIN AND DIRECT ATOMIZATION OF THE RESIN

TAKEO TAKADA* and TOSHIO KOIDE

Department of Chemistry, College of Science, Rikkyo (St. Paul's) University, Nishi-Ikebukuro, Toshima-ku, Tokyo 171 (Japan)

(Received 23rd September 1986)

Summary. Traces of copper ions are sorbed on a cation-exchange resin, and a copper-loaded resin bead is inserted directly into a graphite furnace for atomic absorption spectrometry. The procedure is used for the determination of copper (>2 pg ml^{-1}) in tap and various distilled waters.

The concentrations of many metal ions are low in tap and distilled waters. The determination of these metal ions requires the use of procedures with very low detection limits. For this reason, preconcentration methods have been of interest for many years. Atomic absorption spectrometry with electrothermal atomization is very useful for the determination of many metals in various waters, but preconcentration of some metals is necessary. One of the techniques currently used to preconcentrate metals is ion exchange. After collection, the metals are eluted and the atomic absorption is measured directly on the eluate [1—4]. This method, however, can require a relatively large volume of eluent which leads to decreased sensitivity, and also to high blank values unless the reagents have been carefully purified.

Direct determination of the metals on the resin by graphite-furnace atomic absorption spectrometry (a.a.s.) would provide many advantages. No sample dilution occurs, and addition of reagents and further separation are unnecessary. The risks of introducing contaminants in the time-consuming decomposition of resin samples are removed. Some papers, however, have pointed out that the problems of sample homogeneity, the need for repeated microweighing, the possibility that non-specific absorption of radiation during atomization may exceed the maximum compensating capacity of the background corrector, and the relatively slow rates of analysis, have prevented this technique from being widely acceptable [5].

Previous studies on the determination of trace metals by direct atomization of metals adsorbed on ion-exchange resins with an electrothermal atomizer, have shown the theoretical basis of this method [6]. The purpose

0003-2670/87/$03.50

of the present work was to investigate this technique further, and evaluate its applicability in the routine analysis of water samples.

Experimental

Apparatus. The Nippon Jarrell-Ash atomic absorption spectrometer, model AA-8500, was equipped with a FLA-10 furnace atomizer, and a Hamamatsu Photonics copper hollow-cathode lamp. Commercial pyrolytically-coated graphite tubes (Nippon Jarrell-Ash) were used after modification. This was necessary because the low precision of absorbance measurements was mainly due to random location of the resin particle in the graphite tube and sputtering of the resin during heating. Therefore a small crater (1.2 mm diameter) was drilled at the center of the bottom of the inside wall of the tube, into which the resin particle was placed. Plastic forceps and a small glass funnel were used for inserting the particle into the crater. This sample handling procedure gave the highest precision. A Toyo Kagaku Sangyo synchro-stirrer SYM-6 with rotation meter and thermostat TB-6 were used.

Reagents and preparation of ion-exchange resin. Stock solutions of copper (1000 μg ml^{-1}) were prepared by dissolving 0.1000 g of pure metal (99.9999% pure) in a slight excess of nitric acid, evaporating to dryness, dissolving the residue in a small amount of 1 M hydrochloric acid, transferring the solution into a 100-ml volumetric flask and making up to the mark with the same acid. This solution was diluted, as required, with ultra-pure water. The pH of the working solution was adjusted with hydrochloric acid. The hydrochloric acid was Wako Super Special grade. Ultra-pure water was prepared by sub-boiling distillation of deionized, doubly-distilled water.

The strong acid cation-exchange resin Amberlite IR-120B gave good adsorption and ashing characteristics [6], and was used in these experiments. The resin was sieved to obtain uniform 16—20 mesh fractions; in this way it was possible to achieve dry resins with a mean particle size of 0.85 mm and weight of about 0.6 mg. If the resin bead is too large, it can be difficult to decompose completely during the ashing stage, and also sometimes causes a background signal during atomization.

Ion-exchange resins were treated with large amounts of ultra-pure water, small amounts of 1 M hydrochloric acid and small amounts of 3 M hydrochloric acid, and washed with small amounts of ultra-pure water until free from any acid reaction. The resins were stored on a watch glass in a glass "desiccator" containing water instead of a drying agent, thus avoiding breakage of dry resin particles on swelling in the sample solution.

Procedures

Ten resin beads were placed in a beaker containing 50 ml of the sample or blank solution previously adjusted to an appropriate pH with hydrochloric acid and heated to 80°C. The magnetic stirrer was switched on. After a specified time, the resin particles were removed to a watch glass and dried for 30 min at 95°C. One of the copper-loaded beads was put into the graphite

tube, and the peak absorbance of the element under test was measured. The FLA-10 control unit settings and nitrogen flow rate that were found to give optimal recovery of copper, without background interference from resin ash, are shown in Table 1.

Results and discussion

Effect of pH on adsorption behavior. The relationship between pH and copper atomic absorption signal was investigated with 51-ml samples containing 2 ng ml^{-1} copper and ten resin beads. The adsorption behavior of copper depended greatly on the pH (Fig. 1). At pH 2—5.5, copper(II) is sorbed efficiently on the resin, but less sorption is observed below pH 2, and there is no appreciable sorption from 1—6 M acid. With the solution at pH 2, continued stirring for 24 h produced no variation in pH; therefore pH 2 was selected for use.

Choice of stirring temperature and time. An ion-exchange reaction proceeds through several steps; the diffusion steps are slow and control the overall rate. However, regardless of which type of diffusion controls the process, rapid exchange is favored by a high temperature. Further, in a batchwise operation, the overall rate is affected by the speed of stirring of the solution. Therefore, the effects of solution temperature and stirring time were investigated. The results are shown in Fig. 2.

The absorbance increases slowly with increase in stirring time at 30°C. An enhancement of the signal with increase in temperature was observed over the whole range of temperature studied. However, at 80°C, the absorbance was increased sharply when the stirring time was increased to 4 h; an almost constant signal was obtained above 4 h. Thus, the temperature and stirring time were found to be critical, and the time required to establish equilibrium at room temperature was very long. The minimum time at 80°C was 5—6 h, so this solution temperature was chosen.

Effect of amount of resin used and solution volume. The effect of the amount of resin put into the solution was studied for 0.3 ng ml^{-1} copper in 50 ml of solution at pH 2.0 and 80°C. The plots of absorbance vs. the reciprocal of the number of resin beads for various stirring times are shown in Fig. 3. These results suggest that the copper absorbance is directly proportional to the reciprocal of the amount of resin in the solution when equilibrium is reached. So the linear range depends upon the stirring time.

TABLE 1

Recommended operating conditions

Mean particle size of resin	0.85 mm
Mean particle weight of resin	0.6 mg
Drying current and time	32 A, 20 s
Ashing current and time	60 A, 30 s
Atomizing current and time	220 A, 6 s
Nitrogen gas flow rate	3.0 l min^{-1}
Wavelength	324.7 nm

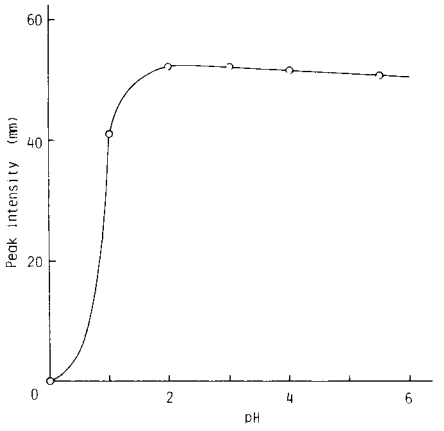

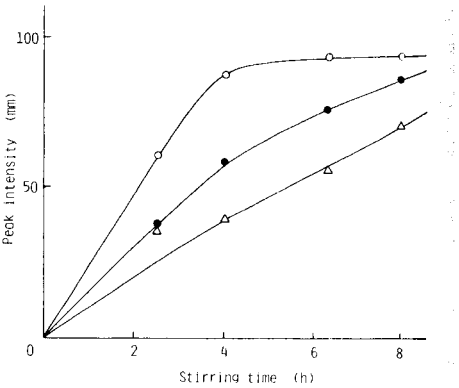

Fig. 1. Effect of pH on the sorption of Cu(II) on the ion-exchange resin. Conditions: 2.0 ng Cu(II) ml^{-1}; 51.0 ml of solution; 10 resin beads put into solution; stirring time 1 h; stirring temperature 21°C.

Fig. 2. Variation of atomic absorption peak height with stirring temperature and time. Solution temperature: (△) 30°C; (●) 55°C; (○) 80°C. Conditions: 0.3 ng Cu(II) ml^{-1}; solution volume 50.0 ml; pH 2.0; 10 resin beads.

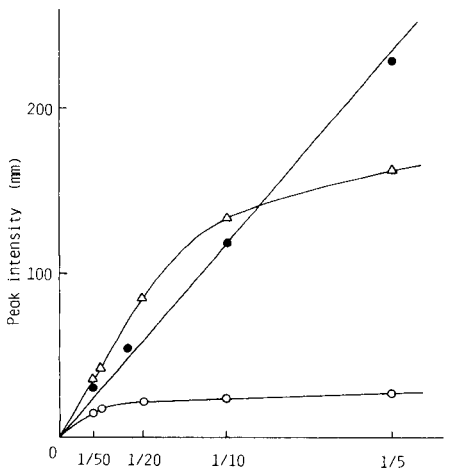

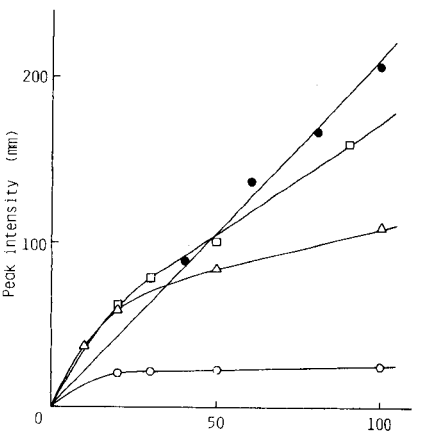

Fig. 3. Variation of atomic absorption peak height with the reciprocal of the number of resin beads (50—5) added to the solution, and with stirring time. Stirring time: (○) 1 h; (△) 5 h; (●) 24 h. Conditions: 0.3 ng Cu(II) ml^{-1}; solution volume 50.0 ml; pH 2.0; solution temperature 80°C; only one bead is inserted for a.a.s.

Fig. 4. Variation of atomic absorption peak height with solution volume and stirring time. Stirring time: (○) 1 h; (△) 5 h; (□) 10 h; (●) 24 h. Other conditions: 0.3 ng Cu(II) ml^{-1}; pH 2.0; 10 resin beads; solution temperature 80°C.

The absorbance should be directly proportional to the total volume of the solution used, at equilibrium. For various stirring times, the effect of variation in the volume of solution was measured (Fig. 4). The slope increases greatly with the stirring time, and sufficient stirring time is necessary in order to obtain a linear relationship.

Application to various waters. The samples were acidified with hydrochloric acid to pH 2 immediately after sampling. Ten resin beads in the hydrogen form were added to 50 ml of the sample solution previously heated to 80°C. The mixture was stirred for 10 min for tap and singly-distilled water, 30 min for doubly-distilled water and 120 min for sub-boiling purified water, in the thermostat. The stirring times were chosen from a practical point of view to minimize the total time needed. The resin was then processed as described above.

To confirm the accuracy of the method, direct and standard addition methods can be used. Concentration ranges for the standard additions were 2—6 ng ml^{-1} for tap and singly-distilled waters, 0.5—1.5 ng ml^{-1} for doubly-distilled water and 0.01—0.04 ng ml^{-1} for sub-boiling purified water, respectively. The direct calibration results were based on four replicate measurements of four standards. Although equilibrium was not attained under these conditions, the calibration plot was linear. Table 2 summarizes the precision data obtained with the direct and standard methods, under the above conditions. Results obtained by the two methods agreed within 5%. The mean relative standard deviations were 4.1% for the direct method and 3.4% for the standard addition method. Under the conditions described above, the sensitivity based on readings in the linear range, i.e. the characteristic concentration giving 0.004 absorbance, was ca. 2 pg ml^{-1}.

Conclusions

The procedure has the following characteristics. The sensitivity for copper under the recommended conditions is 2 pg ml^{-1} for 1% absorption. The

TABLE 2

Results of copper determinations in several kinds of water[a]

Sample	Direct method			Standard addition method		
	Range (ng ml^{-1})	Mean (ng ml^{-1})	R.s.d. (%)	Range (ng ml^{-1})	Mean (ng ml^{-1})	R.s.d. (%)
Tap water	2.2—2.4	2.3	2.9	2.1—2.3	2.2	3.5
Singly-distilled water	0.87—0.91	0.90	3.1	0.89—0.92	0.91	1.2
Doubly-distilled water	0.39—0.43	0.41	3.9	0.38—0.42	0.40	3.5
Sub-boiling purified water	0.03_5—0.04_8	0.04	6.4	0.03_8—0.04_5	0.04	5.5

[a]Five samples were tested in each case.

sensitivity could be increased either by increasing the sample volume, or decreasing the amount of ion-exchange resin used. Uniform resin particles can readily be obtained, so that the troublesome repeated weighings accompanying a direct insertion of a solid sample can be omitted, and sample homogeneity is not a problem.

REFERENCES

1 J. F. Pankow and G. E. Janauer, Anal. Chim. Acta, 69 (1974) 97.
2 J. Korkisch and A. Sorio, Anal. Chim. Acta, 76 (1975) 393.
3 J. Korkisch, L. Gödl and H. Gross, Talanta, 22 (1975) 289.
4 K. M. Kingston, I. L. Barners, T. J. Brady, T. C. Rains and M. A. Champ, Anal. Chem., 50 (1978) 2064.
5 F. J. Langmyhr, Analyst, 104 (1979) 993.
6 T. Takada, H. Okano, T. Koide, K. Fujita and K. Nakano, J. Chem. Soc. Jpn., Chem. Indust. Chem., (1981) 13.

Analytica Chimica Acta, 198 (1987) 309—314
Elsevier Science Publishers B.V., Amsterdam — Printed in The Netherlands

Short Communication

DETERMINATION OF LEAD AND NICKEL IN ANIMAL BONE BY MICROWAVE-INDUCED PLASMA ATOMIC EMISSION SPECTROMETRY WITH SAMPLE INTRODUCTION BY ELECTROTHERMAL VAPORIZATION

NEIL W. BARNETT[a]

Department of Instrumentation and Analytical Science, UMIST, P.O. Box 88, Manchester M60 1QD (Great Britain)

(Received 12th November 1986)

Summary. Sulphuric/nitric acid digestion of the bone precedes introduction of the diluted digest into a helium microwave-induced plasma via a tantalum electrothermal vaporizer. Atomic emission is measured at the Ni I 352.454-nm and Pb I 405.781-nm lines. Detection limits (aqueous solution) are 1.1×10^{-10} g Ni and 8×10^{-11} g Pb. The technique was applied to the analysis of IAEA H-5 animal bone reference material.

Nickel and lead in the International Atomic Energy Agency's Animal Bone reference material (IAEA H-5) have been determined by several instrumental techniques. The provisionally accepted values [1] are 3.1 $\mu g\ g^{-1}$ for lead, with a 95% confidence interval of 2.5—3.7 $\mu g\ g^{-1}$, and 1.5 $\mu g\ g^{-1}$ (0.7—2.3 $\mu g\ g^{-1}$) for nickel. Thus H-5 was considered to be a suitable standard for the assessment of the capability of electrothermal vaporization for sample introduction into a microwave-induced plasma (MIP), which is reported in this communication.

Lead has previously been determined by electrothermal vaporization into an atmospheric-pressure helium MIP system [2—5] and nickel has been determined by a similar sample introduction procedure into an argon MIP [6, 7]. Only two of these reports were concerned with real samples. Bauer and Natusch [4] used a quartz induction furnace to determine lead in atmospheric particulates and Aziz et al. [7] applied a graphite-tube furnace to determine minor and trace elements, including nickel, in biological reference materials. Vaporizer materials were tungsten [2], graphite [3, 5—7] and quartz [4]. Whereas lead was determined successfully with either metallic or non-metallic atomizers, only graphite has been used for nickel. McIntyre et al. [8] showed that tantalum was not a suitable material for an electrothermal atomizer for nickel or cobalt because of its interaction with these elements

[a]Present address: Department of Environmental Sciences, Plymouth Polytechnic, Drake Circus, Plymouth, Devon, PL4 8AA, Great Britain.

at elevated temperatures. Fricke et al. [6] also reported this interaction. Kirkbright and Snook [9] demonstrated the use of a chemically active halocarbon atmosphere around a graphite-rod vaporization device, connected to an inductively-coupled plasma, to prevent the formation of refractory carbides. In the present investigation, an active atmosphere of trifluoromethane (0.1% v/v) in helium was used to alleviate the problem of the tantalum/nickel reaction. Both nickel and lead were determined by the introduction of portions of acid-digested animal bone samples into a helium MIP operated at atmospheric pressure.

Experimental

Equipment. The system used has been described [10] for the determination of iodine in high-purity hydrochloric acid. The specifications of the instrumental components are listed in Table 1.

Samples were dissolved in Kjeldahl flasks (25 ml) on an Isopad digestion bank (Nelson Scientific). Sample solution was delivered to the tantalum ribbon by a SGE model 15A-5V microsyringe/pipette (0—15 μl) with disposable PTFE tips. All the volumetric apparatus was soaked in a solution (5% v/v) of Decon 90 for 24 h, thoroughly rinsed in water and soaked in (1 + 9) nitric

TABLE 1

Description and specifications of the major instrumental components

Instrumental component	Description and specifications[a]
Microwave generator and reflected power meter	Microtron 200 MkII, 2450 MHz/200 W, (EMS, Wantage).
Microwave cavity	TM_{010} type in silver plated copper as described by Beenakker [11]. (EMS, Wantage).
Monochromator	D330, 300 mm focal length Czerny-Turner mount with a 1200 line mm^{-1} plane grating blazed at 300 nm with reciprocal linear dispersion of 2.57—2.40 nm mm^{-1} in the range 200—600 nm. F/5.5 aperture. (Hilger Analytical).
Optical arrangement	Cavity and monochromator mounted on the same optical bar. Plasma viewed axially and imaged 1:1 into the entrance slit by a fused silica lens 40 mm diameter and 70 mm focal length.
Readout system	6256B PMT (EMI Electronics) and 476R power supply (Brandenburg) with a Model 3000. 250 ms/fsd chart recorder (Oxford Instruments).
Electrothermal vaporizer and power supply	Tantalum (99.9%) foil. 25 × 8 × 0.125 mm (Goodfellow Metals, Cambridge). 100 A/12 V transformer controller for an A3370 electrothermal atomizer (Shandon Southern Instruments) [10].
Helium flow control	R-2-15-D volume flow controllers (Brooks Instruments, Netherlands).
Discharge tube	Fused silica tubes, 6 mm o.d. × 2 mm i.d. (Heraeus Silica and Metals, Merseyside).

[a] All companies are located in Great Britain unless otherwise indicated.

acid. When the equipment was required, it was removed from this acid and rinsed with water. The anti-bumping granules were also washed in the dilute nitric acid, rinsed with water and dried at 150°C overnight prior to storage in an acid-washed container.

Reagents and solution preparation. The sulphuric acid (1.835—1.840 g l^{-1}) and nitric acid (1.412—1.417 g l^{-1}) were Aristar grade and the lead nitrate (99.5% pure) was AnalaR grade (BDH). Nickel wire (99.9% pure; Goodfellow Metals, Cambridge) was used to prepare the nickel standard solutions. Singly distilled water was used throughout. The helium and the Freon 23 helium mixture (0.1% v/v) were obtained from British Oxygen Company. Stock solutions of nickel and lead (1000 mg l^{-1}) were prepared as described by Dean and Rains [12] from nickel wire and lead nitrate. Working standards were prepared from these stock solutions by serial dilution. The H-5 sample was obtained from the International Atomic Energy Agency, Vienna, as a (30-g) in a screw-cap polypropylene vial.

Sample pretreatment and calibration procedure. All samples and solid reagents were transferred by means of glass spoons and spatulas to minimize the risk of contamination [13]. Portions of H-5 (1000 ± 0.1 mg) were weighed directly into Kjeldahl flasks (25 ml), each of which contained four anti-bumping granules. At this stage standard additions of nickel or lead were made to the respective flasks by adding 1-ml aliquots of the appropriate working standards. The samples were digested by heating with 1.0 ml of sulphuric acid and 5.0 ml of nitric acid was added dropwise. After the digests had cooled to ambient temperature, 1 ml of water was added carefully to each digest and the solution was swirled to mix. The diluted digests (which included a fine white residue) were quantitatively transferred into 5-ml volumetric flasks and diluted to volume with water from a Pasteur pipette. After the white insoluble matter had settled, 15 μl of the diluted digest was placed on the tantalum ribbon for introduction to the MIP. Standard additions similar to those made to H-5 samples were made to a set of digestion reagent blanks. These solutions were treated exactly as described above.

Optimization of instrumental parameters

A 0.1% (v/v) Freon 23 in helium mixture was used as the carrier/plasma gas. A satisfactory three-stage heating program was achieved by use of the A3370 transformer (12 V, 100 A) and tantalum filament for the determination of nickel and lead at low power settings for the dry and ash controls, viz., 0.5 for 90 s for drying, 1.0 for 70 s for ashing, followed by 3.0 (Pb) or 3.5 (Ni) for 3 s for vaporization. During initial experiments with the tantalum filament vaporizer, the plasma discharge tube was disconnected from the vaporization chamber while the sample was dried and ashed; the chamber was then re-connected to the discharge tube prior to initiation of the plasma and subsequent sample vaporization. This procedure resulted in poor reproducibility because the MIP was switched on and off every 3 min or so, so that the plasma never stabilized. This disconnection was then found to be

unnecessary as the plasma was not extinguished by the evolved vapours produced during the first two stages of the heating program. The background emission intensity rose appreciably during the dry and ash cycles, but returned to its initial level before the vaporization cycle commenced. The plasma also tolerated entrained air; removal and replacement of the sample introduction port did not extinguish the MIP. A small reproducible signal was observed when the vaporization cycle was initiated without any sample on the filament. This was attributed to the pulse of hot helium entering the discharge as has been observed by other workers [14, 15] who used tantalum filament vaporization to introduce samples into the MIP or ICP.

The helium plasma gas flow rate, based on previous experience [10] that 200—300 ml min^{-1} of helium gave the highest signal intensity, was chosen to be 250 ml min^{-1}. The forward power to the cavity was maintained at 130 W for all experiments with a resultant reflected power reading of 17 W. Both power readings did not vary significantly over periods in excess of 6 h provided that the helium flow rate remained constant. The analyte wavelengths chosen were Ni I 352.454 nm [13] and Pb I 405.781 nm [16]. The entrance and exit slits on the monochromator were set at 25 μm which corresponded to a spectral band-pass of 0.06 nm. The photomultiplier tube was operated at 1.2 kV and the output was fed directly to the chart recorder.

The sample introduction volume was kept constant at 15 μl; this volume could be delivered reproducibly and was suitable for the shallow V-shaped depression in the tantalum ribbon, which was made with a screwdriver blade located centrally on the tantalum ribbon supported by a wooden block.

Results and discussion

Aqueous standards were used to evaluate the 2σ detection limits at 352.454 nm and 405.781 nm for nickel and lead, respectively. No analytically useful signals for nickel were recorded without the use of Freon 23 in the plasma gas, as predicted by earlier workers [6, 8]. The use of 0.1% (v/v) Freon 23 increased the background emission at the wavelength monitored and the discharge became blue/green. The presence of halocarbons in the MIP severely limited the useful life of the silica discharge tube, owing to the high reactivity of fluorine-containing species generated in the plasma from the Freon 23.

Measurements on aqueous standards gave linear calibration graphs with equations $y = 2.49x + 0.18$ for lead ($r = 0.99988$, 5 points) and $y = 2.14x + 0.37$ for nickel ($r = 0.99978$, 6 points) where x is the analyte mass (ng) and y is the emission intensity in mm of chart paper (20 cm f.s.d. = 20 mV). The 2σ detection limits were 1.1×10^{-10} g Ni and 8×10^{-11} g Pb (10 consecutive blank determinations). These detection limits are compared with some previously reported values in Table 2. It is noteworthy that the detection limits for lead vary over five orders of magnitude even when the same wavelength is used. This probably arises because one result was obtained for aqueous standards [2] and the other for environmental samples [4]. While

TABLE 2

Comparison of detection limits obtained for lead and nickel

Plasma gas	Element and spectral wavelength (nm)	Vaporizer material	Detection limit (g)	Ref.
Helium	Pb I 217.000	Tungsten microarc	5.6×10^{-13}	2
Helium	Pb I 283.305	Graphite cup	7×10^{-12}	3
Helium	Pb I 217.000	Quartz induction furnace	1×10^{-8}	4
Helium	Pb I 261.418	Graphite cup	2.5×10^{-11}	5
Argon	Pb I 405.781	Tantalum filament	3×10^{-10}	6
Helium	Pb I 405.781	Tantalum filament	8×10^{-11}	This study
Argon	Ni I 232.003	Graphite cup	1×10^{-10}	6
Argon	Ni I 341.376	Graphite cup	3.8×10^{-9}	7
Helium	Ni I 352.454	Tantalum filament	1.1×10^{-10}	This study

no improvement in the aqueous standard detection limits for either nickel or lead was achieved here, the detection capability was adequate for analyses of real samples.

After the standard additions, the H-5 digests and digestion blanks were analyzed for nickel and lead. Linear graphs were obtained in each instance. The nickel content of H-5 was found to be 1.3 $\mu g\ g^{-1}$ by the standard addition procedure and 2.0 $\mu g\ g^{-1}$ by calibration with the digested standards. The lead content was found to be 3.7 $\mu g\ g^{-1}$ by both calibration regimes. These nickel and lead values fall within the 95% confidence interval of the IAEA provisional certificate of analysis [1]. The slope of the nickel calibration graph for solutions of H-5 digest was 1.54 times that in the absence of H-5, a phenomenon similar to that observed for the analysis of digested IAEA milk samples [13]. Possibly some concomitant material in both bone and milk enhanced the nickel emission at Ni I 352.454 nm. Such a difference was not observed for the lead calibration slopes.

The results show the feasibility of the use of an electrothermal vaporizer and MIP system for the determination of traces of some elements in bone. The two elements determined reflected the versatility of this means of sample introduction and the plasma source with respect to quite different physicochemical and spectrochemical properties. It is intended to use an extraction/preconcentration step with dithizone in chloroform similar to

that used on the IAEA milk analysis programme [13]. This may eliminate the need for a halocarbon atmosphere in the vaporization chamber because the nickel would be present as the dithizonate and therefore less prone to interaction with tantalum. Other benefits may be improved detection limits and avoidance of standard additions.

REFERENCES

1 R. M. Parr, International Atomic Energy Agency, Animal Bone (H-5) Provisional Certificate of Analysis, Vienna, 1982.
2 A. T. Zander and G. M. Hieftje, Anal. Chem., 50 (1978) 1257.
3 C. I. M. Beenakker, P. W. J. M. Boumans and P. J. Rommers, Philips Tech. Rev., 39 (1980) 65.
4 C. F. Bauer and D. F. S. Natusch, Anal. Chem., 53 (1981) 2020.
5 M. Zerezghi, K. J. Mulligan and J. A. Caruso, Anal. Chim. Acta, 154 (1983) 219.
6 F. L. Fricke, O. Rose and J. A. Caruso, Anal. Chem., 47 (1975) 2018.
7 A. Aziz, J. A. C. Broekaert and F. Leis, Spectrochim. Acta, Part B, 37 (1982) 381.
8 N. S. McIntyre, M. G. Cook and D. G. Boase, Anal. Chem., 46 (1974) 1983.
9 G. F. Kirkbright and R. D. Snook, Anal. Chem., 51 (1979) 1983.
10 N. W. Barnett and G. F. Kirkbright, J. Anal. At. Spectrom., 1 (1986) 337.
11 C. I. M. Beenakker, Spectrochim. Acta, Part B, 31 (1976) 483.
12 J. A. Dean and T. C. Rains, in R. Mavrodineanu (Ed.), Procedures Used at the National Bureau of Standards to Determine Selected Trace Elements in Biological and Botanical Materials, NBS Special Publication 492, Washington, 1977, p. 254.
13 N. W. Barnett, L. S. Chen and G. F. Kirkbright, Anal. Chim. Acta, 149 (1983) 115.
14 J. W. Carnahan and J. A. Caruso, Anal. Chim. Acta, 136 (1982) 261.
15 D. E. Nixon, V. A. Fassel and R. N. Knisely, Anal. Chem., 46 (1974) 210.
16 G. M. Greenway, Ph.D. Thesis, University of Manchester, 1986.

Analytica Chimica Acta, 198 (1987) 315—318
Elsevier Science Publishers B.V., Amsterdam — Printed in The Netherlands

Short Communication

SYNERGIC EXTRACTION OF COBALT(II) WITH MIXTURES OF 4-METHYL-*N*-8-QUINOLINYLBENZENE SULPHONAMIDE AND NEUTRAL ORGANOPHOSPHORUS COMPOUNDS

J. M. CASTRESANA* and M. P. ELIZALDE
Depto Química (Analítica), Univ. Pais Vasco, Aptdo 644, 48080 Bilbao (Spain)
M. AGUILAR
Depto Química, E.T.S.I.I.B., Univ. Politécnica de Cataluña, Barcelona (Spain)
M. COX
Division of Chemistry, The Hatfield Polytechnic, Hatfield, Hertfordshire (Great Britain)
(Received 20th August 1986)

Summary. The distribution equilibria of cobalt(II) with 4-methyl-*N*-8-quinolinylbenzene sulphonamide in the presence of tributylphosphate or trioctylphosphine oxide dissolved in toluene were studied as a function of hydrogen ion concentration and the concentration of the organophosphorus compounds. Evaluation of the extraction data made it possible to deduce the stoichiometry of the extracted species, determine their corresponding extraction constants and quantify the synergic effect.

The commercial chelating extractant LIX-34 [1] has been tested as a component in synergic mixtures involving carboxylic or organophosphoric acids or neutral donors [2, 3]. However, neither the composition of the extracted species nor the values of the extraction constants has been determined. 4-Methyl-*N*-8-quinolinylbenzenesulphonamide was chosen here as a model compound of similar structure to that of the active component in LIX-34, in order quantitatively to investigate the synergic effects on the extraction of cobalt(II) in the presence of tributylphosphate (TBP) or trioctylphosphine oxide (TOPO). Some chemical properties of the reagent including protolytic and distribution equilibria and interaction constants with the neutral donors have been previously reported [4, 5].

Experimental

Reagents. 4-Methyl-*N*-8-quinolinylbenzenesulphonamide was synthesized and purified as described previously [6]. All the other chemicals were analytical-grade quality and used without further purification.

Procedure. Aqueous solutions (10 cm^3) containing different total cobalt(II) nitrate concentrations (ranging from 2.0×10^{-4} to 1.0×10^{-3} mol dm^{-3}) in 0.1 mol dm^{-3} potassium nitrate were shaken mechanically at 293 ± 2 K for at least 90 min. with an equal volume of organic solutions containing

0003-2670/87/$03.50

1.0×10^{-2} mol dm^{-3} of the chelating reagent and different concentrations of the organophosphorus compounds dissolved in toluene. After centrifugation, the equilibrium H^+ concentration was measured potentiometrically and the metal content in both phases determined by atomic absorption spectrometry (a.a.s.) after stripping the extracted cobalt into 0.5 mol dm^{-3} sulphuric acid. Organic phases were previously pre-equilibrated with cobalt-free solutions otherwise of the same composition as those used for the distribution measurements. All the data which did not fulfill the mass balance for cobalt within 5% were rejected.

Results and discussion

The extraction of cobalt(II) from nitrate medium with 4-methyl-*N*-8-quinolinylbenzenesulphonamide (HR) and the neutral donors (S) can be represented by the following general equilibrium:

$$Co^{2+} + r\,NO_3^- + p\,HR_{org} + q\,S_{org} \rightleftharpoons Cd(NO_3)_r R_p S_{q,org} + p\,H^+ \quad (1)$$

characterized by the stoichiometric extraction constant K_{rpq}.

Therefore, the distribution coefficient of the metal ion, D, can be expressed as:

$$D = \sum_r \sum_p \sum_q K_{rpq}\,\alpha_{Co}^{-1}\,[NO_3^-]^r [HR]_{org}^p [S]_{org}^q [H^+]^{-p} \quad (2)$$

where α_{Co} is the side-reaction coefficient of the metal ion related to the formation of nitrate complexes in the aqueous phase. The absence of polynuclear extracted metal complexes implied by Eqn. 1 was experimentally proved because the values of D did not vary with the total cobalt concentration.

Plots of log D vs. pH for the two systems studied are shown in Fig. 1. Straight lines of slope close to 2 (ranging from 1.8 to 1.9) were found for all the concentrations used, which indicates values of $p = 2$ and $r = 0$ as stoichiometric coefficients of the main extracted complexes. Ascending curves having limiting slope values, q, of 0 and 1, as the ones shown in Fig. 2 for the HR—TOPO system, were obtained in the plots of log $D - 2$ log $[HR]_{org} = f(\log [S]_{org})$ at different constant pH values. This leads to the conclusion that the main extracted species have the stoichiometry CoR_2 and CoR_2S, which are predominant at low and high neutral donors concentrations, respectively. The concentrations of HR and S used in the plots were calculated from the mass balance of the reagents, taking into account the interaction constants for the formation of 1:1 adducts between the extractants in the organic phase [5].

Graphical values of the corresponding extraction constants K_{020} and K_{021} were obtained by following a curve-fitting method [7], from the differences in both axes between the experimental functions log $D - 2$ log $[HR]_{org} = f(\log [S]_{org})_{pH}$ and the theoretical $\log(1 + X) = f(\log X)$ in the position of best fit. Figure 2 shows the superimposition of the functions in the system HR—TOPO.

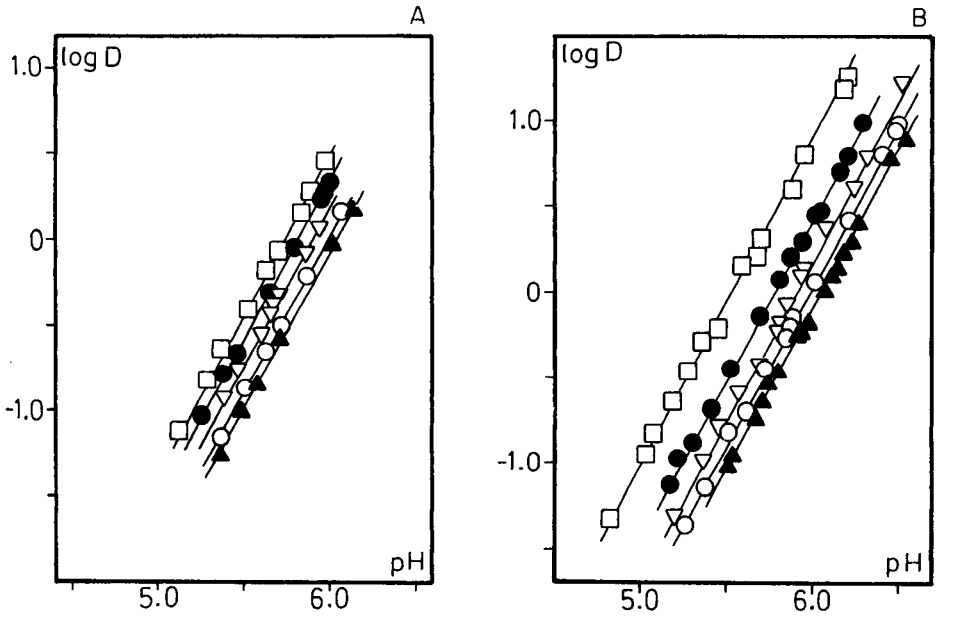

Fig. 1. log D vs. pH at different total TBP or TOPO concentrations. C_{HR} = 1.0×10^{-2} mol dm^{-3}; C_{Co} = 5×10^{-4} mol dm^{-3}. (A) C_{TBP} (mol dm^{-3}): (□) 7.8×10^{-1}, (●) 4.5×10^{-1}; (▽) 2.2×10^{-1}; (○) 8.3×10^{-2}; (▲) 3.9×10^{-2}. (B) C_{TOPO} (mol dm^{-3}): (□) 1.0×10^{-1}; (●) 2.5×10^{-2}; (▽) 1.0×10^{-2}; (○) 5.0×10^{-3}; (▲) 2.0×10^{-3}.

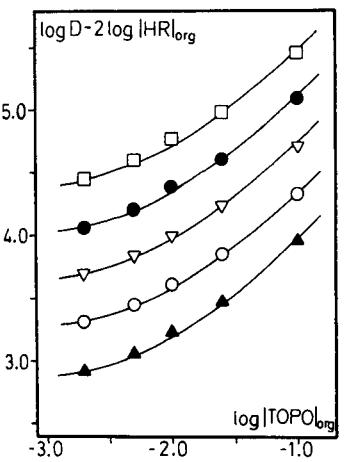

Fig. 2. Positions of best fit between the experimental function log D — $2\log|HR|_{org}$ = $f(\log |TOPO|_{org})$ and the theoretical $\log(1 + X) = f(\log X)$ at different pH values for the extraction with the mixture HR-TOPO. pH: (□) 6.3; (●) 6.1; (▽) 5.9; (○) 5.7; (▲) 5.5.

TABLE 1

Stoichiometric equilibrium constants for the extraction of cobalt(II) in the systems Co/HR-TBP and Co/HR-TOPO

System	Method	CoR_2 $\log K_{020}$	$Co(NO_3)R$ $\log K_{110}$	CoR_2S	
				$\log K_{021}$	$\log \beta_{ad}$
Co/HR-TBP	Graphical	−8.0	—	−7.2	0.8
	LETAGROP	−8.1 ± 0.2	−5.1 ± 0.3	−7.2 ± 0.1	0.9
Co/HR-TOPO	Graphical	−8.1	—	−6.0	2.1
	LETAGROP	−8.2 ± 0.1	−5.2 ± 0.3	−6.0 ± 0.1	2.2

The synergic effect of the mixtures was quantified through the values of the equilibrium constants for the adduct formation in the organic phase

$$CoR_{2,org} + S_{org} \rightleftharpoons CoR_2S_{org} \quad (3)$$

derived from K_{020} and K_{021} according to $\beta_{ad} = K_{021}/K_{020}$.

The subsequent numerical treatment by means of the LETAGROP-DISTR program [8], showed that the inclusion in the graphically derived model of the mixed species $Co(NO_3)R$ improves the fit and eliminates systematic errors. Although the ratio of the mixed complex in the extracts always remains low, its presence can account for the deviations to lower values than 2 of the slopes of the plots of log D vs. pH. Such a species has been postulated in the extraction of copper(II) from nitrate or chloride media with 8-sulphonamidequinoline derivatives [9, 10].

Table 1 collects the values of the stoichiometric constants obtained by both graphical and numerical methods. The larger synergic effect found in the presence of TOPO is in agreement with its greater capacity for the displacement of water molecules from the coordination sphere of the metal ion.

REFERENCES

1 M. J. Virnig, Proc. Int. Solvent Extraction Conf. ISEC'77, Toronto, CIM Special Vol. 21, 1979, p. 535.
2 Y. C. Hoh, N.P. Chou and W. K. Wang, Ind. Eng. Chem. Process Des. Dev., 21 (1982) 12.
3 I. L. Dukov and S. Guy, Hydrometallurgy, 8 (1982) 77.
4 S. Ide, T. Yoshida, S. Matsuno, M. Tagaki and K. Ueno, Anal. Chim. Acta, 149 (1983) 235.
5 J. M. Castresana, M. P. Elizalde, M. Aguilar and M. Cox, Chem. Scr., 26 (1986) 319.
6 J. M. Castresana, M. P. Elizalde, M. Aguilar and M. Cox, Chem. Scr., 25 (1985) 300.
7 F. J. C. Rossotti and H. Rossotti, The Determination of Stability Constants, McGraw-Hill, New York, 1961.
8 D. H. Liem, Acta Chem. Scand., 25 (1971) 1521.
9 G. Sandström, L. Hummelstedt and M. Hangström, Ion Exchange and Solvent Extraction, Society of Chemical Industry Symposium, 1982.
10 J. M. Castresana, J. L. Aparicio, M. P. Elizalde, M. Aguilar and M. Cox, Hydrometallurgy, 15 (1986) 363.

Analytica Chimica Acta, 198 (1987) 319—324
Elsevier Science Publishers B.V., Amsterdam — Printed in The Netherlands

Short Communication

DIFFERENTIAL-PULSE POLAROGRAPHIC DETERMINATION OF SULPHATE AFTER REDUCTION TO HYDROGEN SULPHIDE

M. A. AL-HAJJAJI

Chemistry Department, Faculty of Applied Sciences & Engineering, Umm Al-Qura University, Makkah Al-Mukarramah (Saudi Arabia)

(Received 21st January 1987)

Summary. Sulphate (0—80 μg) is reduced by heating with a mixture of hydriodic acid, formic acid and red phosphorus, the gas is swept by nitrogen into 1 M sodium hydroxide and sulphide is quantified by differential pulse polarography from the peak at —0.76 V vs. Ag/AgCl. None of the ions investigated interfered except those capable of reduction to hydrogen sulphide.

The reduction of sulphate to hydrogen sulphide and the subsequent removal and determination of this gas provides a means for the separation and selective determination of sulphate [1—3]. A wide range of reducing agents has been proposed for the complete reduction of sulphate which include various mixtures containing hydriodic acid [4], titanium/phosphoric acid [5], chromium(II)/phosphoric acid [6] and tin(II)/strong phosphoric acid [7]. A two-step digestion apparatus has been proposed to ensure the complete conversion of sulphate to hydrogen sulphide [8] by mixtures of hydriodic acid, sodium hypophosphite and acetic anhydride. The analysis can be finished by titrimetry [5, 9, 10], spectrophotometry [1—3] or with ion-selective electrodes [11, 12]. The most sensitive procedure is the methylene blue spectrophotometric method, which has many defects such as fading of the colour with time, restricted range and low sulphate recovery from nitrogenous compounds, attributed to the formation of volatile materials that interfere with the formation of methylene blue. A silver sulphide electrode was used [11] to detect hydrogen sulphide produced by the reduction of sulphate with a mixture of hydriodic and hypophosphorous acids. A cadmium ion-selective electrode was used [12] for the potentiometric titration of hydrogen sulphide obtained by the reduction of sulphate with a mixture of hydriodic acid, sodium hypophosphite and acetic acid.

Sulphate is not reducible at the dropping mercury electrode, so indirect polarography has long been applied for the determination of the ion based on its ability to react with or to displace polarographically active ions. Sulphate was precipitated as lead sulphate and redissolved in ammonium chloride solution and the lead wave recorded [13]. Barium was applied in a similar

0003-2670/87/$03.50

fashion [14]. The displacement of polarographically active chromate [15] and chloranilate [16] from their insoluble barium salts by sulphate has also been utilized. In this communication, polarography is used to determine sulphate after its reduction to hydrogen sulphide.

Experimental

Apparatus. A Metrohm Polarecord Model 506 polarograph was used to record all differential pulse polarograms at 0.8 s drop time. Other conditions were as described previously [17]. Polarograms were recorded starting at −0.6 V unless otherwise mentioned (50 mV pulse height). All potentials quoted are measured against a silver/silver chloride electrode in saturated potassium chloride.

Reagents. The chemicals used were of analytical-reagent grade. A reducing mixture consisting of 15 g of red phosphorus, 100 ml of hydriodic acid and 75 ml of 90% formic acid, was prepared as described elsewhere [3]. The mixture was heated to boiling in an apparatus similar to that shown in Fig. 1 but with a 250-ml round-bottomed flask and the gases were swept with nitrogen into the polarographic cell containing 20 ml of deoxygenated (nitrogen-purged) 1 M sodium hydroxide. The digestion was continued until no sulphide peaks were obtained at −0.76 V (90—120 min). This mixture retained its activity for about 10 days and could be regenerated when necessary. Sulphur-free rubber tubing (boiled in dilute sodium hydroxide and washed) was used. The ground-glass joint lubricant used was treated with a

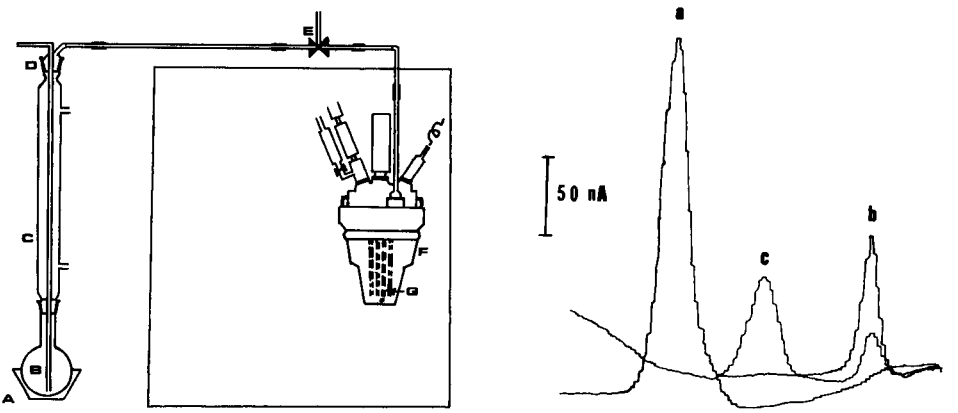

Fig. 1. Digestion apparatus connected to the polarographic cell: (A) heating mantle; (B) digestion vessel (50 ml); (C) condenser; (D) nitrogen bubbler; (E) two-way tap; (F) polarographic cell; (G) outlet for swept hydrogen sulphide.

Fig. 2. Polarograms of absorbed hydrogen sulphide obtained from the reduction of 40 μg of sulphate: (a) in 1 M sodium hydroxide; (b) as (a) but at pH 3.6; (c) as (b) but spiked with 20 μg of sulphite.

mixture of hydriodic and hypophosphorus acids, boiled for 45 min [3], washed and stored.

Method. Aqueous samples (≤2 ml) or finely ground solids (30 mesh, ca. 1 g) were mixed with 4-ml portions (using a glass pipette) of the reducing mixture in the reaction vessel shown in Fig. 1. The reaction mixture was heated to boiling for 10 min (20 min for solids) while bubbling with nitrogen at 50 ml min^{-1}. The gas was passed into the polarographic cell as above and the polarograms were recorded at 5 mV s^{-1}.

Optimization

As the reduction of sulphate is time-dependent, the effect of nitrogen flow through sodium hydroxide (1 M) containing 2 μg ml^{-1} sulphide was evaluated. The peaks decreased slightly (2%) after 20 min bubbling at 100 ml min^{-1} and 7% after 50 min (Table 1). Air oxidation was ruled out because of the high purity of the nitrogen used which was further scrubbed in a train consisting of vanadium(II)/zinc amalgam mixture and alkaline pyrogallol solution. The use of a mixture of sodium hydroxide (1 M), EDTA (0.2 M) and ascorbic acid (0.2 M) [18] as a supporting electrolyte (so-called sulphur antioxidant buffer solution, SAOB II [18]) gave similar results to sodium hydroxide. This precluded air oxidation and the decrease in peak heights was therefore attributed to slight volatilization.

The effect of nitrogen flow rate (50, 100, 200 and 400 ml min^{-1}) on the recovery of hydrogen sulphide from the reduction of 40 μg of sulphate, using a 10-min reaction time was also investigated. There was no increase in sensitivity when higher flow rates were applied, so a 50 ml min^{-1} flow rate was used in subsequent experiments.

To investigate the effect of sodium hydroxide concentration, 20 ml of 1 M, 2 M or 3 M sodium hydroxide was used as collector and supporting electrolyte for the determination of 8 μg ml^{-1} sulphide. The peaks did not shift but decreased in height by 40% as the concentration of the alkali increased from 1 to 3 M. Therefore 1 M sodium hydroxide was subsequently used to absorb the evolved hydrogen sulphide. The effect of reduction time is shown in Table 2. A 10-min reaction time was enough for maximum recovery. However when finely ground solid samples that contained traces of sulphate were analyzed, 20 min was necessary for complete reduction.

TABLE 1

Effect of time of nitrogen flow (100 ml min^{-1}) on the peak height of sulphide (2 μg ml^{-1} in the polarographic cell)

Time (min)	1	10	30	35
Peak height (nA)	440	431	416	408

TABLE 2

Effect of reduction time on response to 40 μg of sulphate at 100 ml min^{-1} nitrogen

Time (min)	10	20	30	40	50	60
Peak height (nA)	235	232	227	216	211	203

Results and discussion

The polarographic activity of sulphide was observed as early as 1934 [19]. The anodic wave produced was attributed to the formation of mercury(II) sulphide. The current was proportional to the ion concentration below 10^{-4} M. Differential pulse polarography was later applied to the determination of sulphide in the paper industry [18] and to the degradation products of cephalexin [20]; normal pulse polarography may also be used with advantage [21].

The possibility of sulphur dioxide production during the reduction of sulphate was suggested by thermodynamic evaluation [8], so two reducing mixtures in series were proposed to ensure complete reduction to hydrogen sulphide. Because of the inherent selectivity of polarography towards some sulphur anions [18], it was possible to investigate whether sulphur dioxide was obtained when only one reducing mixture was used. After the sulphide peak had been recorded, the solution was acidified with acetic acid to pH 3.6 and polarographed again. Figure 2 shows that only one peak was observed, at −0.34 V, which corresponds to residual hydrogen sulphide in the acid solution. When this solution was spiked with 20 μg of sulphite, it gave a peak at −0.57 V [18]. So no detectable quantities of sulphur dioxide were produced during the reduction of sulphate when the single reducing mixture was used.

The use of a gas washing trap [8] increased the time needed for full recovery of hydrogen sulphide. This may be attributed to the slight solubility of the gas in the solution used (0.1 M hydrochloric acid) and to the slower nitrogen flow rate used (50 ml min^{-1}). Hydriodic acid, formic acid or phosphine gas did not seem to interfere with the method as no iodine can be produced in the inert atmosphere; so no gas washing trap was necessary.

Linear calibration graphs were obtained for the range 0—80 μg sulphate (in 2.0 ml of aqueous solution). The relative standard deviation of the slopes of these graphs (on 10 different days) was 3.4%. The r.s.d. for the determination of 40 μg of sulphate (n = 10) was 1.9%. The effect of 15 ions on the determination of 40 μg of sulphate is shown in Table 3. All ions capable of hydrogen sulphide production interfered seriously, as in the previous method [8]. Other known interferents such as nitrate and nitrite did not do so. The method was applied for the determination of sulphate in pure chemicals. The results are shown in Table 4.

The method has the inherent selectivity of the reduction method in addition to the ease, sensitivity and economy of the polarographic finish without the need for special reagents other than the reducing mixture. The inert

TABLE 3

Effect of diverse ions on the determination of sulphate (40 μg) (10 min reduction time)

Ion	Amount (μg)	Sulphate found[a] (μg)	Relative error (%)	Ion	Amount (μg)	Sulphate found[a] (μg)	Relative error (%)
SO_3^{2-}	40	73.0	82.4	NO_3^-	100	39.0	−2.6
SCN^-	40	62.1	55.3	PO_4^{3-}	100	39.7	−0.8
$S_2O_3^{2-}$	20	71.0	77.5	SeO_4^{2-}	100	40.1	0.2
$NH_2SO_3^-$	40	65.1	62.8	Ba^{2+}	100	38.7	−3.3
$R{-}SO_3^-$[b]	40	73.0	82.5	Ca^{2+}	100	39.1	−2.3
F^-	100	39.0	−2.5	Pb^{2+}	100	39.5	−1.3
MoO_4^{2-}	100	41.0	2.5	Sr^{2+}	100	38.9	−2.7
NO_2^-	100	39.3	−1.7				

[a]Mean of two measurements. [b]Benzenedodecyl sulphonate, taken as 40 μg SO_3.

TABLE 4

Application to the analysis of pure chemicals as solids or solutions

Chemical	Sample digested (g)	Sulphate found[a] (μg)	Maximum reported[b] (%)	Sulphate found (%)
H_3BO_3	0.4[c]	72.1	0.040	0.0180 ± 0.0003
	0.4	73.2	0.040	0.0183 ± 0.0005
$Na_4P_2O_7$	0.8	45.4	0.005	0.00568 ± 0.00011
KCl	2.0[c]	19.6	0.001	0.00098 ± 0.00002

[a]Mean of four measurements. [b]As reported by manufacturer. [c]Digested in the solid form.

atmosphere during the reduction and measurement, the strongly alkaline medium and the relatively short time needed for the recording of the polarograms (1.5 min) minimized the loss of hydrogen sulphide through oxidation or volatilization. The method was readily applied directly to some solid samples.

The author acknowledges the skilful technical assistance of Mr. Ahmed Abo El-Majd.

REFERENCES

1 G. D. Patterson Jr., in D. F. Boltz and J. A. Howell (Eds.), Colorimetric Determination of Nonmetals, 2nd edn., Wiley-Interscience, New York, 1978, p. 491.
2 F. D. Snell, Photometric and Fluorometric Methods of Analysis (Nonmetals), Wiley-Interscience, New York, 1981, p. 456.
3 W. J. Williams, Handbook of Anion Determination, Butterworths, London, 1979, p. 547.
4 L. Gustafsson, Talanta, 4 (1960) 227, 236.

5 P. G. Quartermain and A. G. Hill, Analyst, 85 (1960) 211.
6 V. A. Zinchenko and N. M. Gertseva, Zh. Anal. Khim., 22 (1967) 1080.
7 T. Kiba and I. Kishi, Bull. Chem. Soc. Jpn., 30 (1957) 44.
8 J. B. Davis and F. Lindstrom, Anal. Chem., 44 (1972) 524.
9 E. E. Archer, Analyst, 81 (1956) 181.
10 J. M. Murphy and G. A. Sergeant, Analyst, 99 (1974) 512.
11 S. R. Porter and A. P. Runnacles, Anal. Chim. Acta, 94 (1977) 449.
12 D. Chakraborti and F. Adams, Z. Anal. Chem., 298 (1979) 397.
13 R. Baranowski and Z. Gregorowicz, Chem. Anal. (Warsaw), 10 (1965) 125.
14 S. W. Bishara, Microchem. J., 15 (1970) 211.
15 J. Mayer, E. Hluchan and E. Abel, Anal. Chem., 39 (1967) 1460.
16 R. E. Humphery and C. E. Laird, Anal. Chem., 43 (1971) 1895.
17 M. A. Al-Hajjaji, Anal. Chim. Acta, 157 (1984) 31.
18 D. L. Noel, Tappi, 61 (1978) 73.
19 J. Ravenda, Collect. Czech. Chem. Commun., 6 (1934) 453.
20 A. G. Fogg, N. M. Fayad and C. Burgess, Anal. Chim. Acta, 110 (1979) 107.
21 J. A. Turner, R. H. Abel and R. A. Osteryoung, Anal. Chem., 47 (1975) 1343.

Analytica Chimica Acta, 198 (1987) 325—328
Elsevier Science Publishers B.V., Amsterdam — Printed in The Netherlands

Short Communication

POTENTIOMETRIC TITRATION OF MILLIGRAM AMOUNTS OF ORGANIC ACIDS WITH AN INTERFACIAL VOLTAIC CELL FOR END-POINT DETECTION

WEN MENG-LIANG and WANG CHANG-YI

Department of Chemistry, Yunnan University, Kunming, Yunnan (People's Republic of China)

(Received 9th September 1986)

Summary. A small interfacial (antimony scratch) cell is shown to be satisfactory for indicating end-points in microtitrations of 28 organic acids, as well as pharmaceutical preparations. The method is simple and rapid and end-points are sharp. Recoveries were 98.0—101.9% for sample weights of 0.6—4 mg.

Various alkaloids have been determined by potentiometric titration in non-aqueous media, with a small cell for end-point detection [1, 2]. Carboxylic acids are conventionally titrated in aqueous or non-aqueous media to a potentiometric end-point, for which a glass or antimony indicating electrode is used with a saturated calomel or glass reference electrode. Pharmaceutical preparations have been analyzed in this way [3]. In this communication, the interfacial (antimony scratch) cell is used to indicate the end-point of such potentiometric titrations. Results obtained for five pharmaceutical preparations were in good agreement with those obtained by standard methods [4]. The method is simple, rapid and precise for samples in the 0.6—4.0 mg range. It is suitable for various acids of natural and pharmaceutical interest.

Experimental

Equipment and reagents. The apparatus was the same as recently described [2]. Chloroform, acetone, benzene, absolute ethanol and tetrahydrofuran were of analytical-reagent grade.

Standard solutions (0.01 M) of hexadecyltrimethylammonium hydroxide or tetraethylammonium hydroxide in the appropriate organic solvent were prepared in 100-ml volumetric flasks. The solutions were standardized against standard benzoic acid in the conventional manner. A 0.01 M solution of sodium hydroxide in deionized water was standardized against standard potassium hydrogen phthalate.

Procedure for pure organic acids. Weigh accurately 0.5—2.5 mg of the acid and transfer to a 5 ml or 10 ml vessel, depending on sample size. Add 3 or 5 ml of organic solvent or deionized water, insert the interfacial cell and stir

0003-2670/87/$03.50

the solution. While stirring magnetically, titrate with 0.01 M hexadecyltrimethylammonium hydroxide (or tetraethylammonium hydroxide or sodium hydroxide) in the appropriate medium, adding equal increments (100 μl) from a microliter syringe. Calculate the end-point from the second derivative; 0.500—2.000 ml of the titrant is usually consumed in the titration.

Procedure for acetylsalicylic acid in aspirin or APC tablets. Grind one tablet to a fine powder, add 15 ml of absolute ethanol and stir magnetically for 15 min. Filter the solution and dilute to 25.00 ml with ethanol. Dilute a 1.00 ml aliquot to 10.00 ml with absolute ethanol. Pipette to a 1-ml portion of this solution into the titration vessel and add 3—5 ml of acetone. Place the interfacial cell in the solution and titrate with 0.01 M tetraethylammonium hydroxide in benzene.

Procedure for 4-[(dipropylamino)sulfonyl]-benzoic acid in probenecid tablets. Finely powder one tablet, add 5 ml of acetone and stir magnetically for 15 min. Filter and dilute the solution to 25.00 ml with acetone. Dilute a 1.00-ml aliquot to 5.00 ml with acetone. To 1.00 ml of this solution, add 3—5 ml of acetone and titrate with 0.01 M tetraethylammonium hydroxide in benzene.

Procedure for 5-(aminosulfonyl)-4-chloro-2-[(2-furanylmethyl)amino]-benzoic acid in furosemide tablets. Finely powder one tablet, add 5 ml of acetone and stir magnetically for 20 min. Filter the solution and dilute to 10.00 ml with acetone. Treat a 1-ml aliquot as described for probenecid tablets.

Procedure for glutamic acid in tablets. Stir one finely ground tablet with 15 ml of deionized water for 20 min. Filter and dilute to 25.00 ml with deionized water. Dilute a 1.00 ml aliquot to 10.00 ml with deionized water, mix a 1.00 ml portion with 3—5 ml of water and titrate with aqueous 0.01 M sodium hydroxide.

Results and discussion

The end-points were fairly sharp. For example, in the titration of 5 ml of 1.86×10^{-3} M salicylic acid in acetone with standard 8.90×10^{-3} M hexadecyltrimethylammonium hydroxide, the potential jump was about 60 mV at the end-point. The results obtained for various organic acids and pharmaceutical preparations are shown in Tables 1 and 2. Sample solutions were prepared in acetone unless otherwise mentioned. For the pharmaceutical preparations, comparative results were obtained by standard procedures [3, 4]. As can be seen, agreement was good.

This work was supported by the Science Fund of the Chinese Natural Sciences.

TABLE 1

Results obtained for organic acids by titration with tetraethylammonium hydroxide (TEAH) or hexadecyltrimethylammonium hydroxide (HTAH) solution

Compound	Titrant	Weight (mg)		Recovery (%)	Compound	Titrant	Weight (mg)		Recovery (%)
		Taken	Found				Taken	Found	
Picric acid	TEAH	3.052	3.027	99.2	*p*-Phthalic acid[a]	TEAH	0.596	0.594	99.7
		1.995	1.990	99.7			0.911	0.908	99.7
		2.661	2.650	99.6			2.146	2.150	100.2
Picrolonic acid	TEAH	1.869	1.903	101.8	Propionic acid	TEAH	1.444	1.436	99.5
		1.453	1.472	101.3			1.767	1.767	100.0
		1.446	1.440	99.6			1.833	1.831	99.9
Oxalic acid	HTAH	1.275	1.280	100.4	Stearic acid[b]	TEAH	2.399	2.353	98.1
		1.517	1.509	99.5			2.413	2.410	99.9
		2.499	2.450	98.0			1.985	1.980	99.8
Salicylic acid	HTAH	1.287	1.300	101.0	Arachidic acid[b]	TEAH	1.999	2.007	100.4
		0.937	0.927	98.9			2.051	2.046	99.8
		2.496	2.450	98.2			3.519	3.581	101.8
Aspirin	TEAH	1.365	1.358	99.5	Butyric acid	TEAH	2.122	2.136	100.7
		2.176	2.147	98.7			2.272	2.233	98.3
		1.927	1.923	99.8			2.513	2.514	100.0
o-Iodobenzoic acid	TEAH	1.680	1.677	99.8	Isobutyric acid	TEAH	1.702	1.699	99.8
		2.222	2.216	99.7			1.634	1.613	98.7
		2.262	2.253	99.6			1.324	1.323	99.9
Citric acid	TEAH	1.402	1.386	98.9	Acetic acid	TEAH	0.606	0.603	99.5
		2.382	2.421	101.6			0.780	0.781	100.1
		2.065	2.068	100.2			0.862	0.868	100.7
Hippuric acid	HTAH	1.214	1.226	101.0	Cinnamic acid[b]	TEAH	1.484	1.481	99.8
		1.232	1.212	98.4			1.957	1.953	99.8
		1.251	1.231	98.4			1.685	1.688	100.2
m-Trifluoro-methyl benzoic acid	HTAH	1.404	1.386	98.7	Phenylacetic acid[b]	TEAH	1.582	1.573	99.4
		1.763	1.762	99.8			1.531	1.560	101.9
		1.626	1.631	100.3			1.354	1.375	101.5
p-Chloro-benzoic acid	HTAH	1.182	1.183	100.1	Succinic acid	TEAH	1.913	1.911	99.9
		1.199	1.214	101.3			2.091	2.086	99.8
		1.834	1.828	99.7			1.573	1.566	99.6
p-Bromo-benzoic acid	HTAH	1.686	1.678	99.5	Oleanonic acid	TEAH	3.261	3.250	99.7
		1.704	1.705	100.1			3.699	3.695	99.9
		1.999	1.997	99.9			3.692	3.687	99.9
Amygdalic acid	HTAH	1.512	1.514	100.1	Glutamic acid[c]	NaOH	2.125	2.133	100.4
		0.889	0.881	99.1			1.438	1.450	100.8
		1.369	1.365	99.7			2.143	2.131	99.4
3,5-Dinitro-benzoic acid	HTAH	1.978	1.986	100.4	Tartaric acid[c]	NaOH	1.362	1.340	98.4
		1.988	1.990	100.1			1.164	1.165	100.1
		1.233	1.233	100.0			1.030	1.028	99.8
Chloroacetic acid	HTAH	0.573	0.572	99.8	Ascorbic acid[c]	NaOH	1.866	1.865	99.9
		0.870	0.869	99.9			1.188	1.183	99.6
		0.808	0.807	99.9			1.541	1.534	99.6

[a]Sample in tetrahydrofuran. [b]Sample in chloroform. [c]Sample in deionized water.

TABLE 2

Results for pharmaceutical preparations

Tablet	Acid content (mg/tablet)		
	Proposed method	Pharmacopoeia method	Nominal
Acetylsalicylic acid	498.4	497.4	500
	496.1	497.7	
	497.0	495.8	
Acetylsalicylic acid (composite)	223.1	228.2	220
	226.3	228.1	
	228.7	228.9	
Probenecid	241.6	243.9	250
	245.7	243.4	
	243.8	247.0	
Furosemide	19.0	18.6	20
	19.3	18.9	
	19.4	19.0	
Glutamic acid[a]	330.6	331.0	300
	328.3	330.8	
	332.1	331.6	

[a]Aqueous sample solution.

REFERENCES

1 B. Waligóra and M. Paluch, Anal. Chim. Acta, 132 (1981) 229.
2 Wang Chang-yi, Zhang Dong-hua, Guo Yong-li, Zhong Hui-min and Wen Meng-liang, Anal. Chim. Acta, 196 (1987) 299.
3 The Pharmacopoeia of the People's Republic of China, Part II, 1985, pp. 5, 52, 171, 191.
4 The Pharmacopoeia of the People's Republic of China, Part II, 1977, p. 386.

Analytica Chimica Acta, 198 (1987) 329—341
Elsevier Science Publishers B.V., Amsterdam — Printed in The Netherlands

Book Reviews

J. J. Katz, G. T. Seaborg and L. R. Morss (Eds.), *The Chemistry of the Actinide Elements, 2nd edn.* Chapman and Hall, London, 1986, *Vol. 1* (ISBN 0-412-10550-0). xii + 886 pp. + indexes. *Vol. 2* (ISBN 0-412-27370-5). xii + 788 pp. + indexes. Price £95.00 per vol.

This is the second edition of Katz and Seaborg's classic textbook on the chemistry of the actinide elements first published in 1957. In the thirty years that have elapsed since then, a great deal of work has been done on the chemistry of these elements, and further elements have been discovered. A second edition is therefore timely.

The new edition retains the general structure of the first edition, but the text has been greatly expanded and completely rewritten by 33 contributors, mostly from the U.S.A. The first 65% of the book describes the actinide elements in turn; the chapter on transeinsteinium elements also includes post-actinide elements. Most accounts are about 50 pages long, but those of uranium and plutonium cover 274 and 388 pp. respectively. The second part of the book looks at comparative aspects of the actinide elements (spectra and electronic structures, thermodynamic, magnetic and metallic properties, structural and solution chemistry, and organometallic compounds). There is a concluding chapter on future elements, and appendices on nuclear properties. Each volume carries an author index and a subject index to the whole book.

These volumes will be welcomed by all those who need a knowledge of the chemistry of the actinides, including those involved in their analysis, speciation and toxicology. The treatment is thorough, authoritative and up-to-date (references up to 1985). However analytical chemistry is included in only one of the chapters (neptunium). It must be considered a grave defect to omit a subject of such crucial importance to all aspects of the nuclear industry.

P. G. Nelson

B. Fried and J. Sherma, *Thin-Layer Chromatography. Techniques and Applications, 2nd edn.* M. Dekker, New York, 1986 (ISBN 0-8247-7609-7). xiv + 394 pp. Price $74.75.

This is Vol. 35 in the series of monographs "Chromatographic Science" (the 1st edition was Vol. 17). The book is divided into two major parts, general practices of TLC and applications based on compound types. Following a brief introduction and history the mechanism and theoretical aspects are dealt with in detail as are sample preparation and classical and modern instrumental aspects such as HPTLC, overpressurised TLC and state-of-the-art densitometry. The applications reviewed are of particular interest to biologists

and biochemists amongst others, covering lipids, amino acids, carbohydrates, natural pigments, vitamins, nucleic acid derivatives, steroids and teperinoids and pharmaceuticals. Some excellent teaching experiments are described in full.

Overall, an excellent well illustrated practically orientated text, with a detailed overview of current TLC equipment world-wide, and up-to-date literature coverage. A worthy successor to the first edition.

D. T. Burns

B. W. Rossiter and J. F. Hamilton (Eds.), *Physical Methods of Chemistry, 2nd edn.* Wiley-Interscience, New York, 1986, Vol. I *Components of Scientific Instruments and Applications of Computers to Chemical Research* (ISBN 0-471-0803409). xiv + 834 pp. Vol. II *Electrochemical Methods* (ISBN 0-471-08027-6). xiv + 904 pp. Price £143.00 per vol.

This is a continuation of a series of books started by A. Weissberger in 1945 entitled "Physical Methods of Organic Chemistry", which in due course became part of a broader series, "Techniques of Organic Chemistry", which by 1970 was succeeded by the all embracing "Techniques of Chemistry".

In the space available and with a single reviewer it is not possible to review in detail the diverse topics included in Volume I which include: "Electronics" (A. M. Ferguson and L. F. Phillips, p. 111), "Foundations of Vacuum Technology" (H. Adam, p. 191), "Generation, Detection and Control of Optical Radiation" (M. Hercher and H. J. Caulfield, p. 59), "Techniques for Handling Air Sensitive and Toxic Materials" (H. J. Gysling and A. L. Thunberg, p. 115), "Microcomputer Architectures in Chemical Research" (P. R. Rony, p. 116), "Discrete (Digital) Modelling and Control" (P. R. Rony, p. 82), "Chemical Structure Handling by Computer" (J. Figueras, p. 88), and finally "Computer Aided Synthesis Design" (P. Gund and D. R. Hoff, p. 31).

The principal audience the writers were urged to aim at was intelligent scientists, technically trained but inexperienced in the topic to be discussed. The material is therefore all at a serious postgraduate level. The sections with which your reviewer is reasonably familiar were found to fit this remit, e.g. the optics sections bring together much useful material not easily found in the technical literature by chemists.

Volume II is more cohesive in content and is in effect a stand-alone text of modern electroanalytical techniques. The first chapter is an overview "Choosing and Performing an Electrochemical Experiment" (W. E. Geiger and M. Dale Hawley, p. 52), followed by more specialised sections, "Potentiometry: Oxidation Reduction, pH Measurements, and Ion-Selective Electrodes" (T. R. Kissel, p. 137), "Voltammetry with Stationary and Rotated Electrodes" (Z. Galus, p. 82), "Cyclic Voltammetry, AC Polarography, and Related Techniques" (E. R. Brown and J. R. Sandifer, p. 160), "Controlled-Potential Electrolysis and Coulometry" (L. Meites, p. 91), "Chronoamperometry, Chronocoulometry and Chronopotentiometry" (R. W. Murray, p. 65),

"Spectroelectrochemistry" (R. L. McCreery, p. 71), "Conductance and Transference Determinations" (M. Spiro, p. 134) and lastly but by no means the least important topic "Polarography" (A. A. Vicek, J. Volke, L. Pospisil and R. Kalvoda, p. 90). Overall a well written and scholarly work giving a well balanced view of the subject area.

Both volumes are beautifully printed and well illustrated as they should be since the volumes are expensive acquisitions unless one or more sections match your current specific study requirements.

D. T. Burns

D. Schuetzle and R. Hammerle (Eds.), *Fundamentals and Applications of Chemical Sensors.* ACS Symposium Series 309, Washington, DC, 1986 (ISBN 0-8412-0973-1). x + 394 pp. Price $89.95 ($74.95 in the U.S.A. and Canada).

This book is a collection of twenty-three papers that were presented at the 1984 International Chemical Congress of Pacific Basin Societies on the fundamentals and applications of a variety of chemical sensors. There are five sections: general discussions, gas sensors, sensors for liquids and solids, environmental sensors, and biosensors, of which the section on gas sensors contains nearly half of the presentations. The papers have been submitted in camera-ready form and were subjected to the normal reviewing process. The quality of the diagrams and the clarity of the typefaces used is good and there is a detailed general index.

The types of sensor described are based predominantly on electrochemical transducers, although there is some discussion of infra-red techniques. The majority of gas sensors utilize solid state semiconductor devices, e.g. tin oxide, zinc oxide and zirconium oxide, either in the pure form or doped with noble metals such as palladium to improve sensitivity. The predominant development in other application areas appears to be the use of modified electrodes, e.g. microbial sensors for process control and enzyme electrodes for blood glucose monitoring.

In general, the presentations are much more concerned with the fundamental processes involved in the mode of action of chemical sensors than with their application, and this is a reflection on the current state of development of such devices. Nevertheless, this book is a useful reference source which also highlights the analytical potential of sensors.

P. J. Worsfold

C. J. McNeal (Ed.), *Mass Spectrometry in the Analysis of Large Molecules.* Wiley, New York, 1986 (ISBN 0-471-91262-X). ix + 221 pp. Price £24.00.

The rapid development in the versatility of mass spectrometry over the past few years has been nowhere more evident than in the analysis of large

biomolecules. The key to this development has been the separate, but synergic development of new ionization methods and the instrumentation capable of measuring the large ions formed. As recently as 1979, the mass limit of a top-of-the-range spectrometer was less than 2000 daltons, whereas the equivalent instrument today is capable of analyzing masses in excess of 10 000 daltons. It is therefore appropriate that the Third Texas Symposium on Mass Spectrometry held in April 1986, the proceedings of which are published in this volume, should take as its theme "Success and Failure at *m/z* 10 000 and beyond".

The nature of a forum such as this precludes a comprehensive review of the subject. Nevertheless, this volume reflects the present state of the art in many of the foremost laboratories (mostly American) involved in the development of methods for the mass spectrometric analysis of large molecules. Of the thirteen invited or submitted contributions, six describe the application of different ionization techniques, principally fast atom bombardment/SIMS and ^{252}Cf-plasma desorption, to the analysis of large biomolecules. Four papers concentrate on developments in mass spectrometric techniques, including tandem mass spectrometry and Fourier transform mass spectrometry, and three are devoted to a consideration of the mechanistic processes underlying the desorption of molecules by particle bombardment. A good balance has therefore been achieved between the interests of the mass spectrometrists and the biochemists, making this volume a useful addition to many mass spectrometry laboratories, as well as providing an overview of possible applications for potential users of these techniques.

C. S. Creaser

A. M. Krstulovic (Ed.), *Quantitative Analysis of Catecholamines and Related Compounds.* Ellis Horwood, Chichester, 1986 (ISBN 0-85312-824-3). 384 pp. Price £47.50.

The Editor states in his Preface that "This book was written with the idea of informing its readers about the current state of the art in methodologies for catecholamine analysis, with critical examination of their relative advantages and disadvantages." He then presents ten different chapters, by different authors, dealing with a general introduction to the biochemistry of neurotransmitters and a discussion of a number of techniques for the separation and determination of catecholamines and their metabolites in a variety of biological samples.

The short (11 pp.) introductory chapter on the biochemistry of neurotransmitters contains 104 references, four of which are from the 1980s, the most recent being 1981. This is followed by a chapter on gas-liquid chromatography which highlights the practical side of the technique (i.e. column selection, injection techniques, detection modes, derivative formation etc.) and gives a few applications. Chapter III begins with a brief introduction to GC/MS followed by a substantial number of applications. There are many (121) references at the end of this chapter, most being from the 1980s.

Chapter IV on HPLC is so long (180 pp.) that it is divided into seven sub-sections, each written by different authors. Following an excellent discussion on the fundamentals of HPLC and a brief sub-section on sample handling and preparation for LC and electrochemical assay, there are two sub-sections dealing with the electrochemical detection (EC) of catecholamines and related compounds. The second of these focuses on dual-electrode EC applied to micro-HPLC. Another sub-section is concerned with the assay of enzymes of catecholamine metabolism, using either EC or fluorescence for the determinative step. The last two sub-sections deal with fluorescence detection applied to reverse-phase LC and automated HPLC, respectively. Chapter V deals with radioenzymatic assay of catecholamines, VI with immunoassay, including RIA, of catecholamines, and VII with the RIA of Chromogranin A, the major soluble protein co-stored and co-released with catecholamines from their sympathoadrenal storage vesicles. The final three chapters discuss immunofluorescence assays applied to histochemistry, fluorescence determination of catecholamines, and tissue analysis, using many of the methods detailed in earlier chapters.

As with any multiple-author book there is often unevenness between chapters, and in the case of Chapter IV, within a chapter. Furthermore, whenever many authors are writing in a rather narrow subject area, opportunities abound for a certain amount of duplication. Both of these criticisms can be levelled at this book. In addition, there are numerous typographical errors, particularly in the reference sections. Nevertheless, there is so much useful information to be found here that this book is highly recommended for those embarking on the analysis of catecholamines.

William C. Purdy

Allen J. Bard, Roger Parsons and Joseph Jordan (Eds.), *Standard Potentials in Aqueous Solutions*. M. Dekker, New York, 1985 (ISBN 0-8247-7291-1). xii + 834 pp. Price $29.95 (personal subscription).

This book fills one of the greatest needs in chemical data compilation, the assembly in a single book of up-to-date, critically selected values of standard electrode potentials. Such a text has not been available since the last revision of Latimer's celebrated collection in 1952. After such a long time, the assembly of such data has been an enormous task, but was undertaken by Commissions I.3 (Electrochemistry) and V.5 (Electroanalytical Chemistry) of IUPAC. The potentials of the half-reactions of all elements are arranged in chapters comprising related elements, with considerable discussion of chemical and electrochemical features included, together with other thermodynamic data (especially ΔH°, ΔG° and S°). These chapters are preceded by introductory material by Prof. R. Parsons, covering symbols, units, conventions, standard state, calculations, a discussion and tabulation of single electrode potentials, and the relationship of electrode potentials to other

physicochemical properties. The book concludes with an extensive author index. There is no doubt that this is a book of great value to the scientific community, that has been prepared with great care, and is a most worthy successor to Latimer.

Alan Townshend

J. C. Giddings, E. Grushka, J. Cazes and P. R. Brown (Eds.), *Advances in Chromatography, Vol. 25.* M. Dekker, New York, 1986 (ISBN 0-8247-7546-5). xvii + 391 pp.

It is an indication of the dominance of liquid chromatography that all the eight articles in this volume discuss aspects of HPLC and in doing so demonstrate the wide application and interest in this technique from biochemistry to physical chemistry.

Tomlinson and Hafkenscheid review the use of HPLC for the estimation of physicochemical properties, with particular emphasis on the prediction of partition coefficients for QSAR studies. The next two chapters concentrate on the methodology of HPLC. Firstly de Galan and Billiet review the use of iterative methods for mobile phase optimization and the criteria used to guide the search. The problems of interfacing FT-IR to HPLC are then reviewed by Griffiths and Conroy, who demonstrate the advantages of methods in which the eluent is eliminated before spectroscopic examination.

In an extensive review, Sander and Wise report their investigations into the selectivity of reversed-phase HPLC for the separation of the polycyclic aromatic hydrocarbons, and examine the relationship between different methods for the preparation of the stationary phase and the separation of closely related hydrocarbons.

The remaining four chapters review the application of liquid chromatography to the separation of different groups of analytes. The separation of the oxo-acids of phosphorus is reviewed by Ramsey. Nakano reports the HPLC analysis of the biochemically and pharmacologically important oxypurines and related compounds. Hanai considers advances since 1970 in the separation of carbohydrates, and McCluer, Ullman and Jungalwala survey the separation of glycosphingolipids and phospholipids.

Roger M. Smith

I. S. Krull (Ed.), *Reaction Detection in Liquid Chromatography. Chromatographic Science Series Vol. 34.* M. Dekker, New York, 1986 (ISBN 0-8247-7579-1). x + 377 pp.

Post-column derivatization by chemical, photochemical or enzymatic means, can provide more selective and sensitive detection for liquid chromatography than is possible with direct detection methods, e.g., refractive index,

uv/visible spectrophotometry. This particular volume in the Chromatographic Science Series gives a comprehensive account of all aspects of post-column derivatization, with a strong emphasis on practical considerations. The possibility of using flow injection procedures to investigate potential post-column reactions is also alluded to by several authors.

There are seven chapters, each written by specialists in their field, and all are well written, clearly presented and include up-to-date references. There are two general chapters on physical and chemical aspects of post-column derivatization, and five chapters dealing with particular modes of derivatization, namely inorganic solution-phase reactions, enzyme reactions, solid-phase reactors, ion pairing and photochemical derivatization. In each case design details for the post-column reaction devices are given, together with results from several applications.

This volume is therefore recommended as an excellent overview and practical guide to post-column derivatization and should achieve its stated aim of stimulating interest and activity in this particular aspect of liquid chromatography.

P. J. Worsfold

M. Dressler, *Selective Gas Chromatographic Detectors. Journal of Chromatographic Library, Vol. 36.* Elsevier, Amsterdam, 1986 (ISBN 0-444-42488-1). xiii + 319 pp. Price Dfl. 195.00.

This book describes all selective detectors used in combination with gas chromatography. For each detector, the principle on which operation is based, design, the effects of operating conditions, and application are reviewed. The book starts with definitions of some basic terms then discusses, in separate chapters, alkali flame ionization detectors, flameless alkali-sensitized detectors, the hydrogen-atmosphere FID, photoionization systems, chemiluminescence detectors, the electrolytic conductivity detector, electron capture detectors, the ion mobility method, and miscellaneous detectors (including GC with AAS, MS and FTIR). The performance of each detector is assessed mostly in terms of selectivity, sensitivity, noise and minimum detectability, very frequently summarizing performances in convenient tabular form. The book contains copious references up to 1984 and ends with a subject index (which is too brief to be particularly helpful). The camera-ready copy print quality is adequate.

The book emphasizes simple systems (GC/FTIR and GC/MS are treated in just 9 pages) and requires prior knowledge of GC including the rudiments of the common detectors. The author aimed to collect and collate information on the various selective detectors, and this aim has been fulfilled. A wealth of information, and an almost bewildering array of facts, is presented, largely without critical comment. The English is quirky in places and there are a few errors. In effect, the book is a comprehensive collection of data — it

reviews rather than *teaches*. I would use this book only at postgraduate level because of the lack of didactic style. However, the book has considerable value to the GC user in the laboratory: the detailed accounts of the effects of working conditions on performance of operation can act virtually as a laboratory manual. The book will be most helpful as an extended review in laboratories using, or considering use of, a broad range of selective detectors.

M. E. Rose

R. P. W. Scott, *Liquid Chromatography Detectors. Journal of Chromatography Library, Vol. 33.* Elsevier, Amsterdam, 1986 (ISBN 0-444-42610-8). xvi + 271 pp. Price Dfl. 175.00/$64.75.

Since the appearance of the first edition of this book in 1977, detectors for liquid chromatography (LC) have developed rapidly. A far wider range is available, and the design of all detectors has had to change to accommodate the faster separations and narrower peaks that can be achieved today. This entirely revised second edition deals first with some basic features of detection systems (sensitivity, linearity, noise, dispersion etc.) and connections to the chromatography column. This is followed by two chapters describing detectors based on bulk properties (refractive index, electrical conductivity, dielectric constant etc.) and solute properties (uv/visible absorption, fluorescence, electrochemical properties, AAS etc.), and others on multifunctional detectors (curiously combined with derivatization and vacancy chromatography) and on combinations with NMR, MS and IR for structure determination. Finally, there are useful chapters on data acquisition and processing, detector selection, and practical hints on detector operations and other aspects of LC. There are some omissions, of which chemiluminescence detection is notable. The index is rather brief, and more examples of the applications of each detection would have been welcomed, but overall it gives a timely overview of a rapidly developing area.

Alan Townshend

W. Geary, *Radiochemical Methods — Analytical Chemistry by Open Learning (ACOL).* Wiley, Chichester, 1986 (ISBN 0-471-91118-6) (paper). xix + 229 pp. Price £9.95. (ISBN 0-471-91117-8) (cloth). Price £28.00.

The importance of radioanalytical methods has declined since the halcyon 1950s. Nevertheless their inclusion in the repertoire of "Analytical Chemistry by Open Learning" (ACOL) is welcome. The text is fresh and lively, the topics are interesting and the self-assessment questions are well presented and challenging (detailed model answers are given). Dr. Geary has largely succeeded in compressing radiochemistry, nuclear chemistry, health physics and biological applications into a unit suitable for a degree or diploma course.

The introductory chapter is comprehensive and concise, but omits the neutrino and the three-body nature of beta decay. Chapter 2 deals with the preparation and availability of radioactive materials. Geiger counting is covered at some length in Chapter 3, but insufficient attention is paid to the quenching process and to dead time. The short section on semiconductor detectors is particularly clear for a topic with which students often have descriptive and visual difficulty. A surprising omission in the "Statistics of Counting" section is the "Chi-squared" test. Liquid scintillation counting is outlined, but it would have been appropriate to mention the problem of quenching which has exercised instrument designers for 25 years. Radiation protection and control is neatly covered.

Chapter 4, "Radiochemical Methods", is the centrepiece of the book. The direct measurement of natural radioactivity, the use of tracers to investigate precipitation and liquid-liquid extraction processes, isotope dilution analysis and activation analysis are all covered, but simple radiometric analysis is not mentioned. An interesting feature is the reproduction of three published papers.

The criticisms made are not meant to detract from a valiant effort to gather many strands of a diverse subject into a single, relatively short, distance-learning text. As such, it is excellent and, if the ACOL scheme is successful, the book should be widely read.

C. G. Taylor

R. M. Harrison and R. Perry (Eds.), *Handbook of Air Pollution Analysis, 2nd edn.* Chapman and Hall, London, 1986 (ISBN 0-412-24410-1). xxii + 634 pp. Price £42.50.

The first edition of this handbook was published in 1977 with the aim of providing a comprehensive working knowledge of the theory and practice of air pollution analysis. The second edition follows a similar pattern, with several authors updating their original material, but with additional contributions on subjects of general interest (air pollution meteorology and chemistry) and topical areas of application (physicochemical speciation techniques and rainwater analysis). The emphasis is on the analysis for particular species in the atmosphere, e.g., metals, nitrogen and sulphur compounds, hydrocarbons and carbon monoxide and halogen compounds, but there are also chapters describing special techniques for atmospheric analysis such as remote sensors, particular areas of application, (e.g. rainwater) and subjects of general interest which include sampling techniques and quality assurance.

Each of the contributions is notable for the attention to detail in the text, the clarity of the diagrams and the list of references. Thus this book is not particularly suitable as a general introduction to air pollution analysis, but it is recommended as a comprehensive and practical manual.

P. J. Worsfold

A. Gomez, R. Leschber and P. L'Hermite, *Sampling Problems for the Chemical Analysis of Sludge, Soils and Plants.* Elsevier, Amsterdam, 1986 (ISBN 1-85166-049-6). vi + 94 pp. Price £18.00.

This book is based predominantly on eight review papers presented at a Commission of the European Community's Round Table seminar held in Bordeaux, France, in November 1985, and culminates with general conclusions about the sampling techniques for sludges, soils and plants. In the introduction, Leschber explains that the objective of the special workshop was to collect together practical experience of participants. The authors, therefore, have illustrated their individual presentations largely with first-hand experience. The reader is often left wondering, however, who exactly they were writing for. As an account of proceedings of a meeting, the book is adequate, but anyone who bought it hoping for a clear and concise practical guide to field sampling would undoubtedly be disappointed. If you look carefully, useful background information on spatial and temporal variability of samples and on contamination may be extracted from some of the contributions. Unfortunately the reader is often left to decide on the significance of the points raised, or how particular sampling strategies have been arrived at.

In some places, especially perhaps in the statistically-based papers, many readers will find the liberal use of specialist jargon irritating. Linguistically the book would have benefited from more rigorous editing, because at times the poor grammar and typographical errors become rather obtrusive. One redeeming feature is the price, which is not unreasonable, bearing in mind that the camera-ready copy is adequate and the text contains several monochrome photographs.

Malcolm S. Cresser

J. H. Kennedy, *Analytical Chemistry: Principles, 1st edn.* Harcourt Brace Jovanovich, Orlando, FL, 1984 (ISBN 0-15-502700-X). xi + 753 pp. Price £12.50.

This book has been published in conjunction with a book called "Analytical Chemistry: Practise", written by the same author. The book, which is aimed at American undergraduates, is divided into two parts: the first section covers traditional classical principles and statistics and the second concentrates on principles of instrumental methods.

At the beginning of the book the concept of the total analytical process from sampling to evaluation of results is stressed and statistical methods are discussed. This is followed by chapters on classical quantitative chemical analysis that include many worked examples. Unfortunately for European students, although SI units are mentioned briefly, most of the worked examples use rather unfamiliar units and expressions, such as formality and

meq. This problem arises throughout the book, and although the electrochemical section uses the IUPAC convention for the Nernst equation, the calculations in that section use "formal potentials".

The instrumental section covers the main techniques of spectroscopy, electrochemistry and chromatography. These sections are generally up-to-date and the theoretical aspects of each topic are simply but thoroughly explained with the aid of clear diagrams. The aspect of quantitative analysis which is stressed in the rest of the book, however, is somewhat neglected in the instrumentation section. This is most apparent in the chapter on chromatography where no mention is made of internal standards and the only worked example assumes that each component of the mixture gives the same molar response in the detector. Useful computer programs in BASIC are included in the appendix.

Gillian M. Greenway

C. S. Giam and H. J.-M. Dou, *Strategies and Advanced Techniques for Marine Pollution Studies: Mediterranean Sea.* Springer-Verlag, Berlin, 1986 (ISBN 3-540-16083-3). xiii + 475 pp. Price DM 190.

This volume is a record of the proceedings of a NATO Advanced Study Institute held at Beaulieu-sur-Mer, France, in 1984. It is a camera-ready collection of 27 papers primarily involved with the measurement and effects of hydrocarbon pollution in the marine environment. The papers cover a variety of subject areas, ranging from the publication statistics of marine chemistry, through the measurement of hydrocarbon pollution, to ultrastructural alterations in the digestive gland of mussels exposed to crude oil. It is inevitable in a book of this form that the included papers are of variable quality, but it is difficult to escape the feeling that, with the great emphasis being placed on the measurement of organic pollutants, the book might have been improved by the omission of some of the contributions. If it were not for the occasional mistake in the index, some of the odd entries would lead one to believe that it had been computer generated from the titles of the articles. After about page 440, the system completely breaks down and cannot be used.

These criticisms aside, many of the articles are of high quality and will be of great interest to those involved in the measurement of trace organics in the marine environment. Anyone contemplating the purchase of the volume should however be aware that the title is not an accurate reflection of the contents, and that there are few references to be found in it to studies of the Mediterranean Sea.

Alan Howard

S. Fleischer and B. Fleischer (Eds.), *Methods in Enzymology*. Academic Press, Orlando, FL, 1986, *Vol. 125* (ISBN 0-12-182025-4). 788 pp. Price $85.50/£71.00. *Vol. 126* (ISBN 0-12-182026-2). 832 pp. Price $85.00/£71.00.

These volumes are subtitled "Biomembranes" and are the first in a sequence dealing with topics falling into this broad area of research. Volumes 125 and 126 are concerned with methods of studying transport into bacteria, mitochondria and chloroplasts but also include articles on the generation, measurement and utilization of the proton electrochemical gradient in these systems. The subjects covered reflect the great influence in this area of Mitchell's theories of energy-coupling for membrane-associated activities such as oxidative phosphorylation, photophosphorylation and transport processes.

Volume 125 contains a section concerned with membrane isolation and characterization, e.g. on the use of alkyl glycosides such as octyl glucoside and lauryl maltoside to solubilize membrane-bound proteins and reconstitute these into phospholipid vesicles. Examples of the application of these techniques are given in articles dealing with the reconstitution of transport systems derived from bacteria, notably the lactose and other sugar transport systems of *Escherichia coli*. These articles form part of a section entitled "Bacterial Transport". The scope of this section is extensive with detailed descriptions of studies in a range of transport systems for protons, amino acids and metal ions found in bacteria. A related section entitled "Membrane Assembly, Mutation and Cloning Strategy" reflects the impact of modern genetic techniques on the study of membrane-bound processes. Articles describing the application of new genetic techniques for the isolation of mutants defective in sugar transport systems, and the use of gene-fusion techniques to study transport proteins in bacteria are highly informative. The remaining section in Volume 125 deals with transport into mitochondria and chloroplasts and includes a series of articles describing the application of fluorescent techniques and also NMR and ESR to the study of the adenine nucleotide translocator.

Volume 126 contains seventy-four articles concerned with topics falling into two major areas. One of these concerns electron transfer reactions and is presented in three sections. The first of these deals with techniques for the study of cytochrome oxidase activities isolated from sources including mitochondria and bacteria. As with many of the contributions concerned with transport processes (Volume 125), the articles in this section reflect the increased use of the extraction and reconstitution approach based on phospholipid vesicles or planar lipid bilayers. The second section describes similar studies of cytochrome bc_1 complexes while the third section deals with a range of electron transfer complexes mainly isolated from bacteria. The second major area deals with studies of reversible ATP synthases (membrane-bound ATPases). Again the impact of reconstitution techniques and, in the contributions based on microbial systems, the application of modern genetic techniques is evident. A series of thirteen articles deals with mechanistic studies of ATP synthase, including contributions describing the application of isotopes, photoaffinity labels and monoclonal antibodies.

The contributions in both volumes are, in most cases, highly detailed and would appear to be adequate for use in the laboratory. Although many of the procedures and techniques described are probably specific to the system under investigation, the articles presented in these two volumes provide a welcome source of useful and timely information for research workers in this area.

M. Midgley

ANALYTICA CHIMICA ACTA, VOL. 198 (1987)

AUTHOR INDEX

INFORMATION FOR AUTHORS

ailed "Information for Authors" was published in Vol. 190, No. 2, pp. 375–378. A free reprint is available from the tors or from:

evier Editorial Services Ltd., Mayfield House, 256 Banbury Road, Oxford OX2 7DH (Great Britain)

pes of contribution. The journal welcomes original research papers, short communications and reviews. iews are written by invitation of the editors, who welcome suggestions for subjects. Short communications are ially complete descriptions of limited investigations, and should generally not exceed six printed pages. Preliminary mmunications of important urgent work can be printed within four months of submission, if the authors are pared to forgo proofs.

nuscripts. The preferred language of the journal is English, but French and German manuscripts are also eptable. For authors whose first language is not English, French or German, linguistic improvement is provided as t of the normal editorial processing. Authors should submit three copies of the manuscript in double-spaced typing one side of the paper only, with a margin of 4 cm, on pages of uniform size. If any variety of machine copying is d (e.g. xerox), authors should ensure that all copies are easily legible and that the paper used can be written on h both ink and pencil. Authors are advised to retain at least one copy of the manuscript. Manuscripts should be ceded by a sheet of paper carrying (a) the title of the paper, (b) the name and full postal address of the person to om proofs are to be sent, (c) the number of pages, tables and figures.

ormation on the *submission of papers* is given on the inside front cover.

mmary. Research papers and reviews begin with a Summary (50–250 words) which should comprise a brief tual account of the contents of the paper, with emphasis on new information. Short communications and liminary communications require summaries, which should not exceed 50 words. Uncommon abbreviations, ion and reference numbers must not be used. The Summary should be suitable for use by abstracting services hout rewriting. Papers in French or German require a Résumé or Zusammenfassung preceded by a Title and mmary in English; authors are encouraged to provide translations where necessary.

roduction. The first paragraphs of the paper should contain an account of the reasons for the work, any essential torical background (as briefly as possible and with key references only) and preliminary experimental work.

ures. Figures should be prepared in black waterproof drawing ink on drawing or tracing paper of the same size as t on which the manuscript is typed. One original (or sharp glossy print) and two photostat (or other) copies are uired. Attention should be given to line thickness, lettering (which should be kept to a minimum) and spacing on s of graphs, to ensure suitability for reduction during printing. Axes of a graph should be clearly labelled, along the s, and outside the graph itself.

figures should be numbered with Arabic numerals, and require descriptive legends. Explanatory information should placed not in the figure, but in the legend, which should be typed on a separate sheet of paper. Simple straight-line phs are not acceptable, because they can readily be described in the text by means of an equation or a sentence. ims of linearity should be supported by regression data that include slope, intercept, standard deviations of the pe and intercept, standard error, and the number of data points; correlation coefficients are optional.

otographs should be glossy prints and be as rich in contrast as possible; colour photographs cannot be accepted. In neral, line diagrams are more informative and less liable to dating than photographs of equipment, which are refore not usually acceptable.

mputer outputs for reproduction as figures must be good quality on blank paper, and should preferably be mitted as glossy prints.

menclature, abbreviations and symbols. In general, the recommendations of the International Union of Pure d Applied Chemistry (IUPAC) should be followed, and attention should be given to the recommendations of the alytical Chemistry Division in the journal *Pure and Applied Chemistry* (see also *IUPAC Compendium of Analytical menclature*, 1978).

ferences. The references should be collected at the end of the paper, numbered in the order of their appearance in text (*not* arranged alphabetically), and typed on a separate sheet.

the list of references, the following forms should be adopted.

urnals

W. Lund and M. Salberg, Anal. Chim. Acta, 76 (1975) 131.

M. McDaniel, A. D. Shendrikar, K. D. Reizneir and P. W. West, Anal. Chem., 48 (1976) 2240.

e title of the journal must be abbreviated as in the Bibliographic Guide for Editors and Authors.

oks

D. D. Perrin, Masking and Demasking of Chemical Reactions, Interscience–Wiley, New York, 1970, p. 188.

S. Hofmann, in G. Svehla (Ed.), Wilson and Wilson's Comprehensive Analytical Chemistry, Vol. 9, Elsevier, Amsterdam, 1979, p. 89.

les of papers are unnecessary. Citations of reports which are not widely available (e.g., reports from government earch centres) should be avoided if possible. Authors' initials should not be used in the text, unless real confusion uld be caused by their omission. If the reference cited contains three or more names, only the first author's name lowed by et al. (e.g., McDaniel et al.) should be used in the text; but the reference list must contain the initials and mes of *all* authors.

Experimental Design: A Chemometric Approac

by **S. N. Deming,** *University of Houston, Houston TX, and* **S. L. Morgan,** *University of South Carolina, Columbia, SC, USA*

(Data Handling in Science and Technology, 3)

One of the greatest needs in all areas of competitive research and development is an efficient approach to experimentation. To be effective scientists, engineers or managers, individuals today require a clear understanding of the principles of experimental design. This book – unlike most current textbooks – approaches experimental design from the point of view of the experimenter, rather than that of the statistician. It provides a *practical* approach to experimental design and allows the reader to obtain the required information in the minimum number of experiments.

The book introduces the reader to the fundamentals of experimental design. Systems theory, response surface concepts, and basic statistics serve as a basis for the further development of matrix least squares and hypothesis testing. The effects of different experimental designs and different models on the variance-covariance matrix and on the analysis of variance (ANOVA) are extensively discussed. Applications and advanced topics (such as confidence bands, rotatability, and confounding) complete the text. Numerous worked examples are presented.

The clear and practical approach adopted by the authors makes the bo applicable to a wide audience. It will appeal particularly to those with a practical need (scientists, engineers, managers, research workers) who hav completed their formal education but who still need to know efficient ways carrying out experiments. It will also an ideal text for advanced undergraduate and graduate students following courses in chemometrics, da acquisition and treatment, and design experiments.

Contents: 1. System Theory. 2. Respon Surfaces. 3. Basic Statistics. 4. One Experiment. 5. Two Experiments. 6. Hypothesis Testing. 7. The Variance-Covariance Matrix. 8. Three Experiments. 9. Analysis of Variance (ANOVA) for Linear Models. 10. A Ten-Experiment Example. 11. Approximating a Region of a Multifactor Response Surface. 12. Additional Multifactor Concepts and Experimental Designs. Appendices: Matrix Algebra. Critical Values of t. Critical Values of F, {a} = 0.05.

1987 about 294 pages; US $ 109.75 / Dfl. 225.00;
ISBN 0-444-42734-1

ELSEVIER THE SCIENCE PUBLISHER
P. O. BOX 211 • 1000 AE AMSTERDAM • THE NETHERLANDS
P. O. BOX 1663 • GRAND CENTRAL STATION • NEW YORK • NY 10163